THE JOURNAL
OF
CHEMICAL PHYSICS

VOLUME 33, NUMBER 1 JULY, 1960

Madelung Constants of the Cubic Perovskite Structures

F. G. FUMI AND M. P. TOSI
Istituto di Fisica Teorica, Università di Pavia, Pavia, Italy

(Received October 5, 1959)

A proof is given of a simple linear relation between the Madelung constant, referred to the lattice parameter a, of a cubic perovskite structure ABX_3 with the ionic charges in the ratio $+z:+(3-z):-1$ and the corresponding Madelung constants for the NaCl, CsCl, and Cu_2O structures.

IT has recently been pointed out[1] that the numerical value of the Madelung constant, referred to the lattice parameter a, for the cubic perovskite structure ABX_3 in which the charges of the ions A, B, and X are in the ration $1:2:-1$ is related to the numerical values of the corresponding Madelung constants for the Cu_2O structure and for the CsCl structure as follows:

$$\alpha_a(A^{+1}B^{+2}X_3^{-1}) = 2\alpha_a(Cu_2O) - 4\alpha_a(CsCl). \quad (1)$$

We give here a simple proof of a generalized form of Eq. (1) valid also for the cubic perovskite structures with different ionic charge ratios, such as those considered by Templeton.[2] This will emphasize the general applicability of the method that we used to prove the two independent linear relations between the Madelung constants for the NaCl, CsCl, zincblende, and CaF_2 structures.[3] The method is based on the decomposition of the electrostatic potential in an ionic crystal into the sum of the electrostatic potentials due to the simple Bravais lattices of the structure, each neutralized by a uniform distribution of charge.

Let us consider a cubic perovskite structure ABX_3 with the ionic charges in the ratio $+z:+(3-z):-1$ and let us take the charge of the X ion as equal to -1 even if this results in a nonintegral value for z, against the customary convention. The Madelung constant of this structure, referred to the lattice parameter a, can be expressed through the electrostatic potential of the structure $\Phi_{ABX_3}(r_p)$ at the ionic positions r_p in the unit cell as follows:

$$\alpha_a(A^{+z}B^{+(3-z)}X_3^{-1}) = -\tfrac{1}{2}a[z\Phi_{ABX_3}(A^{+z}) + (3-z)\Phi_{ABX_3}(B^{+(3-z)}) - 3\Phi_{ABX_3}(X^{-1})]. \quad (2)$$

The electrostatic potential $\Phi_{ABX_3}(r_p)$ can in turn be written as a sum of the electrostatic potentials due to the "neutralized" simple cubic lattices which compose the structure. The pertinent equations are

$$\Phi_{ABX_3}(A^{+z}) = z\bar{\psi}(000) - 3\psi(\tfrac{1}{2}\tfrac{1}{2}0) + (3-z)\psi(\tfrac{1}{2}\tfrac{1}{2}\tfrac{1}{2}) \quad (3)$$

$$\Phi_{ABX_3}(B^{+(3-z)}) = (3-z)\bar{\psi}(000) - 3\psi(\tfrac{1}{2}00) + z\psi(\tfrac{1}{2}\tfrac{1}{2}\tfrac{1}{2}) \quad (4)$$

$$\Phi_{ABX_3}(X^{-1}) = -\bar{\psi}(000) + (3-z)\psi(\tfrac{1}{2}00) + (z-2)\psi(\tfrac{1}{2}\tfrac{1}{2}0). \quad (5)$$

Here $\psi(xyz)$ stands for the electrostatic potential in a "neutralized" simple cubic lattice of positive unit charges with lattice parameter a at the point xa, ya, za of the unit cube, and $\bar{\psi}(000)$ stands for the electrostatic self-potential of the same lattice. The use of the Hund identity,[4] $\bar{\psi}(000) = 3\psi(\tfrac{1}{2}00) + 3\psi(\tfrac{1}{2}\tfrac{1}{2}0) + \psi(\tfrac{1}{2}\tfrac{1}{2}\tfrac{1}{2})$, yields finally

$$\alpha_a(A^{+z}B^{+(3-z)}X_3^{-1}) = -\tfrac{1}{2}a[(6z^2-12z+18)\psi(\tfrac{1}{2}00) + (6z^2-24z+42)\psi(\tfrac{1}{2}\tfrac{1}{2}0) + 12\psi(\tfrac{1}{2}\tfrac{1}{2}\tfrac{1}{2})]. \quad (6)$$

We can, however, replace the three independent dimensionless potentials $a\psi(\tfrac{1}{2}00)$, $a\psi(\tfrac{1}{2}\tfrac{1}{2}0)$, and $a\psi(\tfrac{1}{2}\tfrac{1}{2}\tfrac{1}{2})$ in Eq. (6) by the three independent Madelung constants for the NaCl, CsCl, and Cu_2O structures by means of the following equations[3]:

$$6a\psi(\tfrac{1}{2}00) = \alpha_a\,(NaCl) - 2\alpha_a\,(CsCl) \quad (7)$$

$$6a\psi(\tfrac{1}{2}\tfrac{1}{2}0) = -\alpha_a\,(NaCl) \quad (8)$$

$$6a\psi(\tfrac{1}{2}\tfrac{1}{2}\tfrac{1}{2}) = \alpha_a\,(NaCl) + 6\alpha_a\,(CsCl) - 2\alpha_a\,(Cu_2O). \quad (9)$$

We arrive then at the formula

$$\alpha_a(A^{+z}B^{+(3-z)}X_3^{-1}) = (1-z)\alpha_a\,(NaCl) + (z^2-2z-3) \times \alpha_a\,(CsCl) + 2\alpha_a\,(Cu_2O). \quad (10)$$

[1] G. C. Benson and F. van Zeggeren, J. Chem. Phys. **26**, 1083 (1957).
[2] D. H. Templeton, J. Chem. Phys. **23**, 1826 (1955).
[3] F. G. Fumi and M. P. Tosi, Phil. Mag. **2**, 284 (1957).
[4] F. Hund, Z. Physik **94**, 11 (1935).

Copyright © 1960 by the American Institute of Physics

Of course the same relation holds also between the Madelung constants of these structures referred to the lattice parameter a multiplied by any numerical factor. Equation (10) contains as special cases both Eq. (1) and the relations connecting the Madelung constant of the cubic perovskite structure with the 1:2:—1 ionic charge ratio to the Madelung constant of a cubic perovskite structure with a different charge ratio, as given by Templeton.[2] In particular, we see at once that the Madelung constant of the cubic perovskite structure with ionic charges $+3$, $+3$, and -2, measured in units of their largest common factor as customary, is given by

$$\alpha_a(A^{+3}B^{+3}X_3^{-2}) = 4\alpha_a(A^{+1}B^{+\frac{3}{2}}X_3^{-1}) = 4\alpha_a(A^{+1}B^{+2}X_3^{-1}) - 2\alpha_a\,(\mathrm{NaCl}) + \alpha_a\,(\mathrm{CsCl}).$$

The utility of equations such as Eq. (6) and Eq. (10) lies of course in avoiding *ab initio* calculations of the Madelung constants of complex ionic structures. In this connection it is of interest to note that the method used here and in footnote 3 can be used also to establish linear relations between general lattice sums of two-body central interactions over any composite structures having common Bravais lattice. Applications of the method to lattice sums of r^{-n} interactions over cubic structures have recently been presented by Naor.[5]

ACKNOWLEDGMENTS

The authors are glad to acknowledge their indebtedness to Dr. P. Naor and Dr. G. C. Benson for informative and stimulating correspondence.

[5] P. Naor, Z. Krist. **110**, 112 (1958).

THE JOURNAL OF CHEMICAL PHYSICS VOLUME 33, NUMBER 1 JULY, 1960

Note on Secondary Isotope Effects in Reaction Rates

MAX WOLFSBERG*

Physical Chemistry Laboratory, Oxford University, Oxford, England

(Received December 1, 1959)

It is shown that secondary kinetic isotope effects, for all isotopes with the possible exception of hydrogen isotopes, are expected to be small unless the force constants involving the isotopically substituted positions are considerably different in the transition state from those in the reactant. Cases involving secondary hydrogen isotope effects are investigated in detail for certain model reactions. It is concluded that hydrogen isotope effects do not constitute an exception to the above rule.

INTRODUCTION

THE object of this note is to present some calculations with respect to isotope effects to be expected on chemical rates in cases where the isotopically substituted atoms are not directly involved in the bond breaking or in the bond forming of the reaction. Such isotope effects are referred to as secondary isotope effects. The calculations were carried out within the framework of the transition state theory.

The ratio of isotopic rate constants is given in the harmonic approximation by[1]

$$k_1/k_2 = (\nu_{1L}^{\ddagger}/\nu_{2L}^{\ddagger})\,(\textstyle\prod_K f_K/f^{\ddagger})\,[1+\tfrac{1}{24}(\,|\,u_{1L}^{\ddagger}\,|^2 - |\,u_{2L}^{\ddagger}\,|^2)] \quad (1)$$

where

$$f_K = (s_{1K}/s_{2K})\prod_i^{3N-6}(u_{2iK}/u_{1iK}) \times \exp[(u_{1iK}-u_{2iK})/2]\frac{[1-\exp(-u_{1iK})]}{[1-\exp(-u_{2iK})]}$$

and

$$f^{\ddagger} = (s_1^{\ddagger}/s_2^{\ddagger})\prod_i^{3N-7}(u_{2i}^{\ddagger}/u_{1i}^{\ddagger}) \times \exp[(u_{1i}^{\ddagger}-u_{2i}^{\ddagger})/2]\frac{[1-\exp(-u_{1i}^{\ddagger})]}{[1-\exp(-u_{2i}^{\ddagger})]}.$$

The symbol $\ddagger$ refers to the transition state; the product $\prod_K$ runs over all species of substrate molecules in the rate equation; the symbols s are symmetry numbers; $u=h\nu c/kT$ with ν the vibrational frequency in cm^{-1}; u_L and ν_L refer to that vibrational frequency of the transition state which is calculated to be imaginary

* National Science Foundation Senior Postdoctoral Fellow 1958–1959. Permanent address: Chemistry Department, Brookhaven National Laboratory, Upton, Long Island, New York.

[1] See for instance J. Bigeleisen and M. Wolfsberg in *Advances in Chemical Physics*, edited by I. Prigogine (Interscience Publishers, Inc., New York, 1958), Vol. I, pp. 15–76. $\Delta u_i = u_{1i} - u_{2i}$.

(or zero); the subscripts 1 and 2 refer to the isotopic species, with 1 always the lighter species. The product in the definition of f_K is taken over the $3N-6$ (in a linear molecule over the $3N-5$) normal vibrations of the molecule. In the definition of f^*, the product is only taken over the real bound vibrations of the transition state.

For small u and small Δu, Eq. (1) becomes[1]

$$k_1/k_2=\nu_{1L}^*/\nu_{2L}^*[1+(1/24)(|u_{1L}^*|^2-|u_{2L}^*|^2)]\times[1+(1/24)\sum^{3N-6}(u_{1i}^2-u_{2i}^2)-(1/24)\sum^{3N-7}(u_{1i}^{*2}-u_{2i}^{*2})]$$
$$=\nu_{1L}^*/\nu_{2L}^*[1+(1/24)\sum^{3N-6}(u_{1i}^2-u_{2i}^2)-(1/24)\sum^{3N-6}(u_{1i}^{*2}-u_{2i}^{*2})] \quad (2)$$

since u_L^* is imaginary. The simplifying assumption (which does not affect the subsequent argument) has been made that there is only one isotopically substituted substrate species. Equation (2) may be simplified by the use of the sum rule of Decius and Wilson[2]

$$4\pi^2\sum_i^{3N-6}(\nu_{1i}^2-\nu_{2i}^2)=\sum_j^{3N}(m_{1j}^{-1}-m_{2j}^{-1})a_{jj}. \quad (3)$$

Here the a_{jj}'s are the diagonal force constants for Cartesian displacement coordinates and the m_j's are the masses of the respective atoms. One then obtains

$$k_1/k_2=\nu_{1L}^*/\nu_{2L}^*[1+(1/24)(\hbar c/kT)^2\times\sum_i^{3N}(m_{1i}^{-1}-m_{2i}^{-1})(a_{ii}-a_{ii}^*)]. \quad (4)$$

If the Cartesian diagonal force constants of the isotopically substituted atom remain the same in the transition state as in the reactant molecule(s), Eq. (4) reduces to

$$k_1/k_2=\nu_{1L}^*/\nu_{2L}^* \quad (5)$$

which is just the equation for the isotope effect in the classical approximation. Thus the first quantum correction to the secondary isotope effect vanishes if the diagonal Cartesian force constants of the isotopically substituted atom remain the same in the transition state as in the reacting molecule. For most isotopic substitution, excepting hydrogen, the condition of small Δu is fulfilled while the condition of small u may not be fulfilled. When the condition of small u is not fulfilled, the differences of higher even powers of u than the second have to be taken into account in evaluating Eq. (2).[3] The use of higher order sum rules[4] analogous to Eq. (3) convinces one that the deviation of the secondary isotope effect from the classical one is small for all isotopes with the possible exception of hydrogen (where the values of u are too large to use the foregoing method), if the larger Cartesian force constants involving the isotopically substituted position remain the same in the transition state as in the normal molecule. If one finds larger ratios than expected on the basis of Eq. (5), such isotope effects must then be the result of having changed the Cartesian force constants of the isotopically substituted atoms in the transition state, and this effect may be taken as an indication that this has happened.

In the present note, some secondary hydrogen isotope effects will be calculated for carbon-hydrogen systems in order to gain some feeling of how one should interpret experimentally found isotope effects in such systems. Only a few "model" reactions have been chosen and any generalizations based on these suffer from the weakness of the models and from their paucity. In all the models which involve C_2H_4, C_2H_6, and CH_2 it has been assumed that the diagonal and the larger off-diagonal Cartesian force constants of the "secondary" hydrogen atoms keep the same value in the transition state as in the normal molecule. Actually the work has not been carried out in Cartesian coordinates but it is easy to see that none of the force constant changes undertaken change diagonal or large off-diagonal Cartesian force constants. The changes in the bending force constants in CH_2 are an exception and do, indeed, cause some such changes. Moreover, all these models involve one bond break, and the normal mode in the transition state which corresponds to the decomposition path is the motion which moves the two fragments apart.

CALCULATIONS

A. Ethylene

The relative rates of C—C bond rupture in ethylene and in perdeutero ethylene were considered. For the normal molecule the force constants of Crawford and co-workers[5a] were used. In the activated state, the C—C stretching force constant as well as the force constants corresponding to cross terms with the C—C stretching motion were set equal to zero. All other force constants, including bending force constants, were taken to be the same in the transition state as in the normal molecule. This prescription makes the normal

[2] J. C. Decius and E. B. Wilson, Jr., J. Chem. Phys. **19**, 1409 (1951). It may be noted that the validity of this rule, which follows from the fact that the sum of the eigenvalues of a matrix is equal to the trace of the matrix, is not affected by the presence of an imaginary frequency.

[3] J. Bigeleisen in *Proceedings of the International Symposium on Isotope Separation*, edited by Kistemaker, Bigeleisen, and Nier (North-Holland Publishing Company, Amsterdam, 1958), p. 148.

[4] See reference 3.

[5] (a) B. L. Crawford, Jr., J. E. Lancaster, and R. G. Inskeep, J. Chem. Phys. **21** 678 (1953). (b) R. L. Arnett and B. L. Crawford, Jr., J. Chem. Phys. **18**, 118 (1950).

TABLE I. Ethylene frequencies.

	C_2H_4 (cm^{-1})	C_2D_4	$C_2H_4^{\ddagger}$	$C_2D_4^{\ddagger}$
ν_1	3316.3 (−37.31)[c]	2417.6 (−19.83)[c]	3295.8 (−37.08)[c]	2361.4 (−19.03)[c]
ν_2	1624.5	1521.0	0	0
ν_3	1343.3	984.8	1524.5	1138.6
ν_5	3361.2 (−37.8)[c]	2476.9 (−20.5)[c]	3361.2[a] (−37.8)[c] 3265.1[b] (−36.7)[c]	2476.9[a] (−20.5)[c] 2335.3[b] (−18.8)[c]
ν_6	1231.0	1010.1	1231.0[a] 866.8[b]	1010.1[a] 683.5[b]
ν_8	942.2	774.4	942.2[a] 907.3[b]	774.4[a] 731.6[b]

case A[a] $\frac{1}{2}(\Sigma\nu_{iH}-\Sigma\nu_{iD}-\Sigma\nu_{iH}^{\ddagger}+\Sigma\nu_{iD}^{\ddagger})=20.8\ cm^{-1}$[d]

case B[b] $\frac{1}{2}(\Sigma\nu_{iH}-\Sigma\nu_{iD}-\Sigma\nu_{iH}^{\ddagger}+\Sigma\nu_{iD}^{\ddagger})=8.9\ cm^{-1}$[d]

[a] $r_{C\text{-}C}^{\ddagger}=r_{C\text{-}C}$.
[b] $r_{C\text{-}C}^{\ddagger}=1.33\,r_{C\text{-}C}$.
[c] Correction to zero point energy due to anharmonicity, calculated in the manner of Crawford *et al.*, reference 5.
[d] Anharmonicity correction taken into account.

mode corresponding to decomposition be the motion which takes the two $CH_2(CD_2)$ groups apart. The changing force constants affect the a_{1g} vibrations of ethylene, ν_1, ν_2, ν_3, which therefore have to be recalculated. If all the bond distances remain the same in the transition state as in the normal molecule, none of the other frequencies change. If, on the other hand, the C—C bond distance in the transition state is different from that in the normal molecule, the b_{1g} (ν_5, ν_6) and the b_{2g} (ν_8) frequencies also have to change since the rotations of the whole molecule belong to these representations. The effect of this change of bond distance is probably not as significant from a general point of view as the effect due to the changing a_{1g} frequencies since the former effect depends on the actual lengthening of the C—C distance assumed. A corresponding statement applies to all the present calculations, and results are therefore always presented for no changes in bond distances in the transition state and only sometimes for change in the bond distance of the bond to be broken. The calculations of frequencies were carried out by means of the FG matrix method as described by Arnett and Crawford.[5b] The calculations of the transition state frequencies present no special difficulties with the given recipe for force constants and bond distances. The calculated frequencies are shown in Table I together with the important zero point energy differences. The calculations of rate constant ratios were carried out with the use of Eq. (1). When there is no change in bond distance, the term $\prod^{3N-6}\nu_{1i}^{\ddagger}/\nu_{2i}^{\ddagger}\prod^{3N-6}\nu_{2i}/\nu_{1i}$ contributes nothing to the effect because of the Teller-Redlich product rule; when there is a change in bond distance, only those frequencies contribute to the ratio which change just because of the change in bond distance. One finds (at 300°K) with no change in C—C bond distance

$$k_1/k_2=1.11$$

while with a lengthening in the transition state of the C—C bond distance to 1.33 r_{Normal},

$$k_1/k_2=1.12.$$

B. Ethane

Again the relative rates of C—C bond break in the normal and in the perdeutero compounds were considered. For the normal molecule the force constants of F. Stitt[6] were used. In the transition state the C—C stretching force constant as well as the force constants corresponding to cross terms with the C—C stretching motion were again set equal to zero. All other force constants were taken to be the same in the transition state as in the normal molecule. At constant C—C bond distance, the changing force constants affect only the a_{1g} vibrations ν_1, ν_2, ν_3. A changing C—C bond distance would affect other vibrations, but this calculation was not carried out. The effect of changing the C—C distance on the relative rates is expected to be similar to the effect in ethylene. The calculated frequencies, together with the important zero point energy differences, are shown in Table II. One finds at 300°K, with no change in C—C bond distance

$$k_1/k_2=1.14.$$

C. Methylene

Calculations were carried out to find the relative rates of hydrogen (H) carbon bond rupture in CH_2

[6] F. Stitt, J. Chem. Phys. **7**, 297 (1939). The potential III (configuration D_{3d}) was used.

TABLE II. Ethane frequencies.

	C_2H_6 (cm^{-1})	C_2D_6	$C_2H_6^\ddagger$	$C_2D_6^\ddagger$
ν_1	2887.0	2087.1	2882.3	2071.4
ν_2	1372.6	1139.1	1431.1	1091.9
ν_3	1005.1	838.2	0	0

$\frac{1}{2}(\Sigma\nu_{iH}-\Sigma\nu_{iD}-\Sigma\nu_{iH}^\ddagger+\Sigma\nu_{iD}^\ddagger)=25.1\ cm^{-1}$

and CHD. The relevant C—H stretching force constant, as well as the force constants which correspond to cross terms between this C—H stretching motion and other motions, were set equal to zero in the transition state. The calculations were carried out both for a linear CH_2 molecule and for a bent CH_2 molecule (with an angle of 120°).

(*a*) *Linear* CH_2

The carbon hydrogen stretching force constant and the stretching interaction force constant in the normal molecule were taken from those found by Crawford *et al.*[5] for C_2H_4. The bending frequency in the normal molecule was taken to be 1450 cm^{-1}. Calculations were also carried out using larger C—H_1, C—H_2 stretching, interaction force constants in the normal molecule

TABLE III. Linear methylene molecule.

A. Stretching frequencies

$2V=F_1\Delta r_1^2+F_2\Delta r_2^2+2F_{12}\Delta r_1\Delta r_2$

Normal molecule $F_1=F_2$ $\times10^5$ dyne/cm	F_{12} dyne/cm	Zero point energy difference $(H-D)$ between normal molecules minus zero point energy difference between transition states (cm^{-1})	Contribution to k_1/k_2
6.1262	0.0429[a]	1.5	1.007
6.1262	0.2145	1.7	1.008
6.1262	0.61262	1.8	1.009

B. Bending frequency

Force constant normal molecule	Force constant transition state	Zero point energy difference $(H-D)$ between normal molecules minus zero point energy difference between transition states (cm^{-1})	Contribution to k_1/k_2
d	d[b]	0.0	1.00
d	d[c]	−12.6[d]	0.98
d	$0.25d$[c]	34.8[d]	1.20
d	$0.0625d$[c]	58.5[d]	1.28

[a] From ethylene one obtains $F_1=F_2=6.1262$, $F_{12}=0.0429$.
[b] $r_1/r_2=1$ in transition state.
[c] $r_1/r_2=1.33$ in transition state.
[d] The bending frequency of the normal CH_2 molecule was taken to be 1450 cm^{-1}. The zero point energy differences here refer only to the bending frequency.

TABLE IV. Frequencies of bent methylene molecule ($\alpha=120°$).

	HCH (cm^{-1})	HCD	$HCH^\ddagger$		$HCD^\ddagger$	
ν_1	3396.7	2443.3	3343.2[a]	3343.8[b]	2450.3[a]	2451.1[b]
ν_2	1484.6	1310.7	1509.2[a]	1334.4[b]	1331.7[a]	1129.6[b]
ν_3	3287.8	3344.6	0		0	

case A[a] $\frac{1}{2}(\Sigma\nu_{iH}-\Sigma\nu_{iD}-\Sigma\nu_{iH}^\ddagger+\Sigma\nu_{iD}^\ddagger)=0.05\ cm^{-1}$

case B[b] $\frac{1}{2}(\Sigma\nu_{iH}-\Sigma\nu_{iD}-\Sigma\nu_{iH}^\ddagger+\Sigma\nu_{iD}^\ddagger)=-13.5\ cm^{-1}$

[a] $r_1/r_2=1$ in transition state.
[b] $r_1/r_2=1.33$ in transition state.

If the C—H distance of the breaking bond is the same in transition state as in the normal molecule, the bending frequency does not change in going from the normal molecule to the transition state (provided the relevant force constant remains unchanged). Calculations have been made both with the bond distance the same in the transition state and with variations in this bond distance. In addition calculations have been carried out with lower bending force constants in the transition state than in the normal molecule. In Table III are listed the relevant differences in zero point energies, for various cases, of stretching and of bending frequencies and also the contributions of stretching and of bending frequency changes to k_1/k_2.

(*b*) *Bent* CH_2

Again the force constants were taken from those determined for C_2H_4 by Crawford *et al.* In Table IV are listed the frequencies and the relevant zero point energy differences. One obtains with no change in the C—H distance in the transition state

$$k_1/k_2=1.002$$

while with a lengthening of the C—H bond to 1.33 times its normal value, one finds

$$k_1/k_2=0.97.$$

DISCUSSION

The results, with no change in the Cartesian diagonal or large off-diagonal force constants of the isotopic positions in the transition state, are summarized in

TABLE V. Calculated isotope effects.

Reactant	No. of D's	k_1/k_2 $r_{breaking}=r_{normal}$	k_1/k_2 $r_{breaking}=1.33\ r_{normal}$
$H_2C—CH_2$	4	1.11	1.12
$H_3C—CH_3$	6	1.14	
CH_2 (linear)	1	1.007	0.99
CH_2 (bent)	1	1.002	0.97

Table V. It is seen that the isotope effect per deuterium atom is small for all the models. Suppose that one observed an isotope effect on a rate larger than about 3% per deuterium atom where the isotopically substituted hydrogen is attached to the carbon where a bond is being broken or made during the reaction. If one feels justified in generalizing from the present model cases, one might then say that this result means that the values of the diagonal or large off-diagonal force constants of the substituted hydrogen are not the same in the transition state as in the reacting species. Such a conclusion would be quite important. Most workers in the field have indeed interpreted their results on this basis. If the substituted hydrogen is yet further removed from the locus of the reaction, one expects even greater validity for the conclusion.

The conclusion which we have reached here depends largely on the fact that the differences between the zero point energies (or between the sums of the frequencies) of the isotopic species are very much the same in the postulated transition states as in the reacting molecules. There is of course an interesting relationship involving sums of squares of frequencies which has already been mentioned at the beginning of this note. One can also obtain relationships for higher powers of the frequencies. There is little doubt that the effect here observed follows also from some rigorous or approximate sum rule. No large effort has been made as yet to determine this sum rule although one should undertake to do this. The important matter for the present is that, by making the indicated changes in the observed force constants (which do actually correspond to making some changes in off-diagonal Cartesian force constants of the isotopic atoms), only fairly small isotope effects have been calculated.

Sizable secondary isotope effects must be explained then in terms of sizable changes of the force constants of isotopic positions in the transition state with respect to the normal molecule. A change in the stretching force constant involving the atom can obviously be used to explain large secondary isotope effects and this has been done by Bigeleisen and Wolfsberg.[1] The calculations on the linear methylene molecule show that one can obtain quite nonnegligible secondary isotope effects by reasonable changes of bending force constants in the transition state. Changes in torsional force constants of the carbon skeleton can also give rise to sizable secondary isotope effects. Thus the torsional oscillation in ethylene contributes a factor of 1.41 to the ratio of the partition functions of C_2H_4 and C_2D_4 from the difference of zero point energies. In ethane, the factor $e^{\frac{1}{2}\Delta u_i}$ for the trosional oscillation is equal to 1.20. Therefore other force constants besides the stretching ones may be of importance in calculating secondary isotope effects.[7] Future calculations should be made to determine changes in force constants on the basis of observed secondary isotope effects.

It may be mentioned that the conclusions which have been reached here about kinetic isotope effects also apply to equilibrium isotope effects.

ACKNOWLEDGMENTS

The author would like to express his gratitude to Mr. R. P. Bell for his hospitality and for many stimulating discussions. He is also very grateful to the U.S. National Science Foundation for the award of a fellowship.

[7] No detailed consideration has been given to the possibility that sizable secondary hydrogen isotope effects might arise from large changes in anharmonicity constants.

Lattice Vibrations in Alkali Halide Crystals. II. Potassium and Rubidium Halides; Cesium Fluoride*

ARNOLD M. KARO

Lawrence Radiation Laboratory, University of California, Livermore, California

(Received December 7, 1959)

Vibrational frequency distributions for the potassium and rubidium halides and for cesium fluoride have been evaluated on the basis of the Born lattice theory by the use of Blackman's numerical sampling method. Both room-temperature and extrapolated 0°K parameters have been used in the calculation. Specific heats, the corresponding Debye characteristic temperatures, and the moments of the distributions have been obtained directly from the frequencies. Comparison is made with experimental data and with other theoretical work.

I. INTRODUCTION

IN this paper the vibrational frequency distributions of the potassium and rubidium halides and cesium fluoride are examined in some detail. From knowledge of the frequency spectra a number of thermodynamic properties of these substances can be obtained theoretically; here, most attention is given to the specific heat. The lithium and sodium halide spectra have been discussed extensively in a previous paper[1] (hereafter referred to as I), and the present paper has been organized to give a consistent presentation of the data. In the following sections frequent references to I are given for details of the calculation.

The basis of the calculation is the Born Model[2] in the form used by Kellermann.[3] Long-range Coulomb forces are summed over the ionic lattice, and the short-range repulsive interactions are assumed to be central and restricted to nearest neighbors. These short-range interactions are introduced into the equations of motion by means of the compressibility rather than through explicit use of the experimental elastic constants.

The calculation for each of the alkali halides has been carried out with two sets of parameters: one set obtained from room-temperature (RT) data and another set obtained from measurements near, or extrapolations to, 0°K. Values for these parameters are given in Table I. The evaluation of the two distribution functions allows us to make an appropriate comparison of either low-temperature or room-temperature experimental data with the theoretical results. There is an intermediate range of temperatures in which neither of the two limiting cases can strictly apply. Here the experimental data should fall between the computed values. In any event some answer is given to the question of just how much small changes in the values of the parameters can be expected to affect the results.

The frequencies were evaluated at 48 evenly distributed points in a properly chosen one forty-eighth portion of the reciprocal lattice cell (one forty-eighth of the first Brillouin Zone, Fig. 1 of paper I). This represents over 6000 frequencies sampled throughout the reciprocal cell. Although this number of frequencies is really too few to give the precise behavior of the branches and peaks in the spectra, the general behavior is probably quite accurate. Further details of the calculation are discussed in I.

II. CALCULATION OF THE ELASTIC CONSTANTS

The elastic constants were obtained from the coupling coefficients occurring in the equations of motion. The results are given in Table II where experimental values for three potassium and two rubidium salts are also listed. The calculated elastic constants are seen to agree quite well with experiment. Experimentally, the Cauchy relation (for the NaCl structure, $c_{12}=c_{44}$) holds very well for these halides, suggesting that the repulsive and attractive interactions are effectively approximated by central forces. The restriction in the Kellermann model to central force interactions implies that this

TABLE I. Values of the lattice constants and compressibilities at absolute zero and room temperature.

Substance	0°K[a] $r_0(10^{-8}$ cm)	0°K[a] $\beta(10^{-12}$cm^{2}d$^{-1})$	Room temperature $r_0(10^{-8}$cm)[b]	Room temperature $\beta(10^{-12}$cm^{2}d$^{-1})$[c]
KF	2.648	3.10	2.665	3.30
KCl	3.117	5.26	3.139	5.63
KBr	3.266	6.17	3.293	6.70
KI	3.492	7.75	3.526	8.54
RbF	2.796	3.86	2.815	4.1
RbCl	3.246	6.21	3.270	6.65
RbBr	3.399	7.35	3.427	7.94
RbI	3.627	8.70	3.663	9.57
CsF	2.983	3.94	3.004	4.25

[a] M. Born and K. Huang, *Dynamical Theory of Crystal Lattices* (Oxford University Press, New York, 1954), Table 16, p. 54.

[b] R. W. G. Wyckoff, *Crystal Structures* (Interscience Publishers, Inc., New York), Vol. I, Table III.

[c] M. Born and K. Huang, *Dynamical Theory of Crystal Lattices* (Oxford University Press, New York, 1954), Table 9, p. 26.

* The research reported in this document was performed under the auspices of the U. S. Atomic Energy Commission.

[1] A. M. Karo, J. Chem. Phys. **31**, 1489 (1959).

[2] M. Born, *Atomtheorie des festen Zustandes* (J. B. Teubner, Berlin, 1923); M. Born and M. Goeppert-Mayer, *Handbuch der Physik* (Springer-Verlag, Berlin, 1933), Vol. 24, Part 2.

[3] E. W. Kellermann, Trans. Roy. Soc. (London) **238**, 513 (1940); Proc. Roy. Soc. (London) **A178**, 17 (1941).

TABLE II. Calculated and experimental elastic constants (10^{11} d cm^{-2}).

	Calc[a]						Exptl[b]					
	c_{11} (0°K)	c_{11} (RT)	c_{12} (0°K)	c_{12} (RT)	c_{11}[c]	c_{12}[c]	c_{11} (0°K)	c_{11} (RT)	c_{12} (0°K)	c_{12} (RT)	c_{44} (0°K)	c_{44} (RT)
KF	6.40	5.90	1.64	1.59	6.1	1.6	...	...	...	...	...	...
KCl	4.00	3.67	0.85	0.83	3.9	0.8	4.832	4.032	0.54	0.66	0.663	0.629
KBr	3.45	3.11	0.71	0.68	3.5	0.7	4.18	3.46	0.56[d]	0.58	0.525	0.505
KI	2.79	2.47	0.54	0.52	3.1	0.5	3.38	2.71	0.22	0.45	0.368	0.364
RbF	5.14	4.75	1.32	1.28	5.4	1.3	...	...	...	...	...	...
RbCl	3.38	3.10	0.72	0.70	3.6	0.7	...	...	...	...	...	...
RbBr	2.88	2.61	0.60	0.58	3.2	0.6	...	3.17	...	0.42	...	0.388
RbI	2.52	2.24	0.46	0.45	2.8	0.4	...	2.56	...	0.31	...	0.287
CsF	5.58	5.08	1.02	0.99	5.1	1.0	...	...	...	...	...	...

[a] By the Cauchy relation, $c_{12}=c_{44}$.
[b] M. H. Norwood and C. V. Briscoe, Phys. Rev. **112**, 45 (1958) (KCl, KI); J. K. Galt, Phys. Rev. **73**, 1460 (1948) (KBr); D. I. Bolef and M. Menes, Bull. Am. Phys. Soc. Ser. II, **4**, 427 (1959) (RbBr, RbI).
[c] K. S. Krishnan and S. K. Roy, footnote 4.
[d] Measured at 138°K.

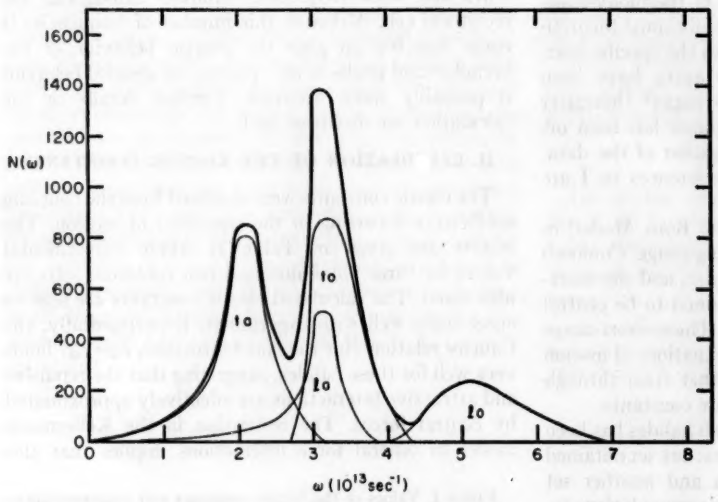

FIG. 1. Vibrational frequency distribution for KF.

model should be especially suitable for substances in which the Cauchy relation is fulfilled. The remarkably good agreement shown, for example, in Table VIII, appears to bear this out. The results given in Table IX for the rubidium halides do not compare as well with experiment. For these heavier ions polarization is expected to be quite significant, and anharmonic terms in the oscillatory motion of the ions also become important at lower temperatures.

Comparison is also made in Table II with the elastic constants evaluated by Krishnan and Roy[4] (KR) from the velocities of propagation of the acoustic modes. The agreement in all cases can be considered satisfactory.

[4] K. S. Krishnan and S. K. Roy. Proc. Roy. Soc. (London) A210, 481 (1952).

III. FREQUENCY DISTRIBUTIONS

Details of the numerical sampling procedure have been given in I. The frequency range in each case was divided evenly into 20 intervals and the number of frequencies falling within each interval was determined. Classification of the frequencies as belonging to the acoustic or optical branch of the spectrum was carried out as before. A further classification of the frequencies as longitudinal or transverse was also made; although, as pointed out in I, this division is not, in general, strictly proper for a nonisotropic lattice. The analysis was done graphically and used 37 vectors in the reciprocal lattice, so that each frequency was checked from two to four times in making the classification.

The smoothed frequency distributions for RT parameters are shown in Figs. 1 through 9. In smoothing the

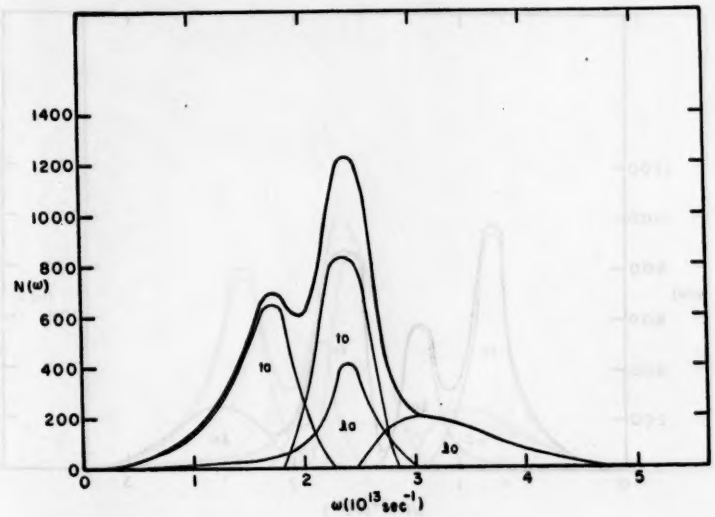

FIG. 2. Vibrational frequency distribution for KCl.

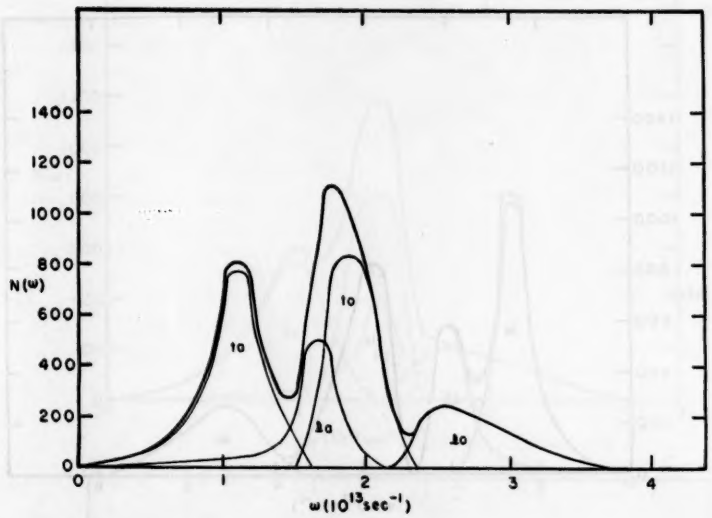

FIG. 3. Vibrational frequency distribution for KBr.

histograms, use was made of the fact that the areas associated with the optical and acoustic transverse modes are equal and are twice the areas corresponding to the longitudinal modes. In addition, in several cases where there appeared to be unusual statistical fluctuations due to a large number of frequencies falling near the limits of an interval range, the intervals were shifted by thirds to allow a recount. The total distribution curves were obtained by summing the smoothed subdistributions. The vertical scale represents the number of counts within the frequency interval.

The general behavior of the distribution curves corresponds to that found earlier for the lithium and sodium halides. For the lithium halides a reexamination of the distribution functions indicates that the maximum of the transverse optical branch perhaps should be increased from 50 to 100 counts in each case. The total picture which emerges for the complete set of alkali halides shows consistent trends in the structure of the distribution functions as the mass ratios, compressibilities, and lattice parameters change.

We have seen previously that the optical and acoustic branches gradually separate, as expected, for large mass ratios until a definite gap appears in the spectrum. On the other hand, when the masses are nearly equal, specifically for NaF, KCl, and RbBr, there is maximum overlap of the longitudinal acoustic and the transverse optical branches resulting in a

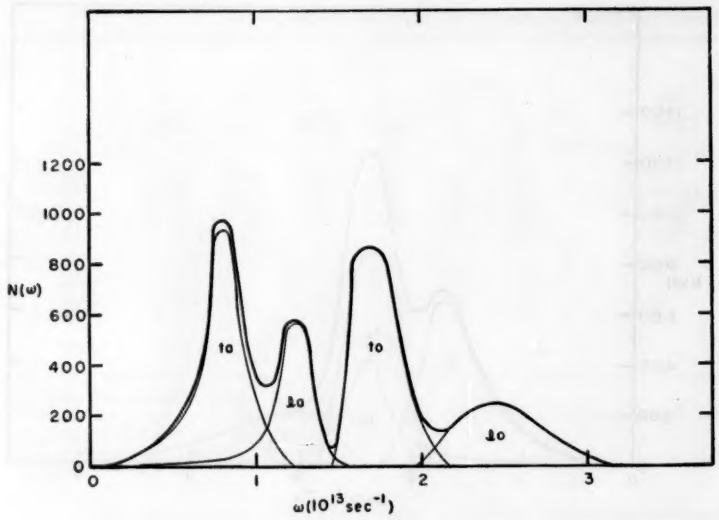

FIG. 4. Vibrational frequency distribution for KI.

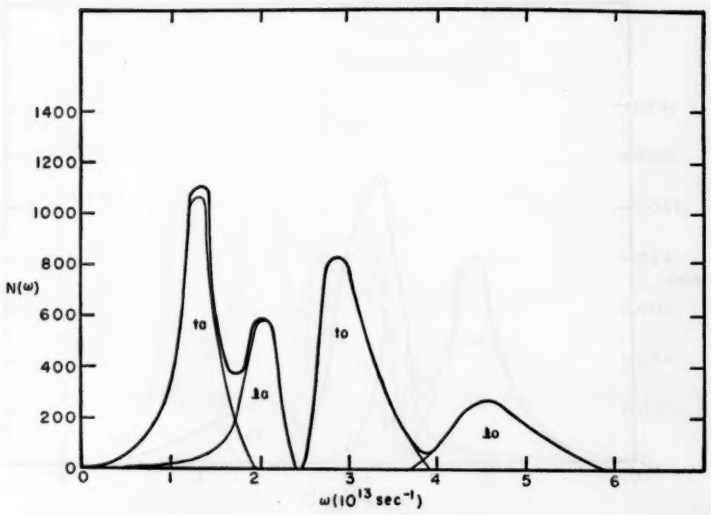

FIG. 5. Vibrational frequency distribution for RbF.

characteristically high central peak for these substances. The spectrum for NaCl is quite similar. Although the masses of the ions are not equal, the compressibility is nearly twice that of NaF. This is a partially compensating effect which tends to decrease the optical and acoustic frequencies in such a manner that the optical branch is shifted toward the acoustic branch.[5]

Another feature that was noted for the lithium and sodium halides and that is now seen to apply throughout the alkali halides, is the behavior of the longitudinal acoustic and optical branches and the transverse acoustic branch. As the mass ratio increases, the width of these branches decreases and there is a consequent increase in the height of the spectra. The width of the transverse optical branch is affected in a similar manner, although the peak height does not appear to be as sensitive to the mass ratio. The tail of the longitudinal optical branch, extending to higher frequencies, has been associated with long-range Coulomb forces.[6] Equally characteristic of the alkali halide spectra is the long forward tail of the longitudinal acoustic branch. This feature can be readily ascribed to the rapid increase in

[5] A study of the spectrum for the face-centered cubic modification of NH_4I, in which a large gap appears between the acoustic and optical branches, has shown that as β increases the gap decreases. At the same time there appears to be a slight decrease in the width of the acoustic branch as compared to a slight increase in the width of the optical branch.

[6] M. Blackman, *Handbuch der Physik* (Springer-Verlag, Berlin, 1955), Vol. VII, Part 1.

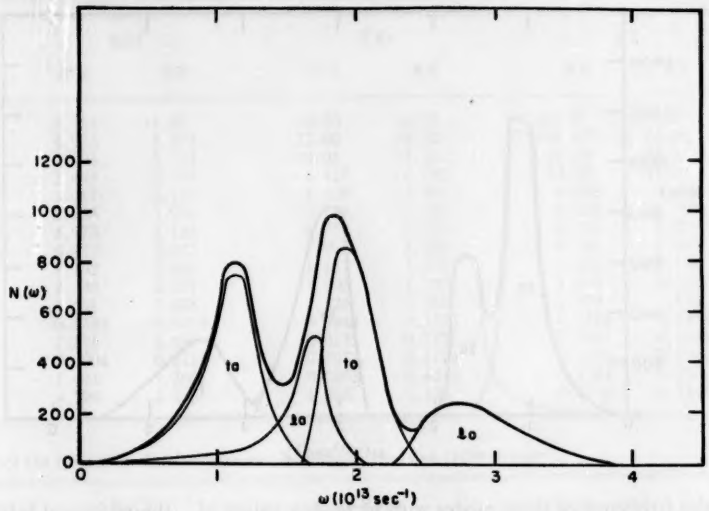

FIG. 6. Vibrational frequency distribution for RbCl.

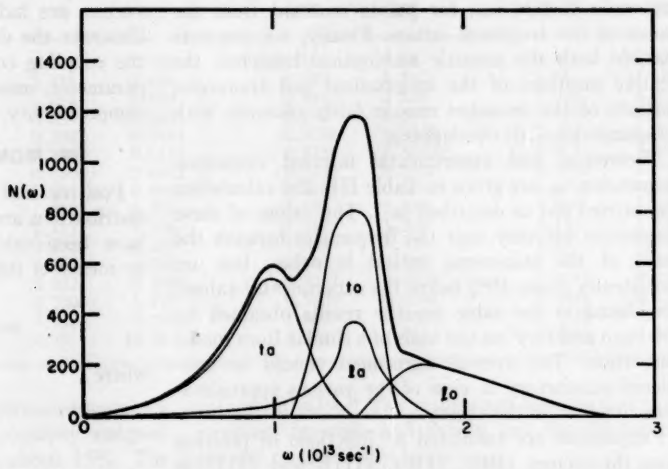

FIG. 7. Vibrational frequency distribution for RbBr.

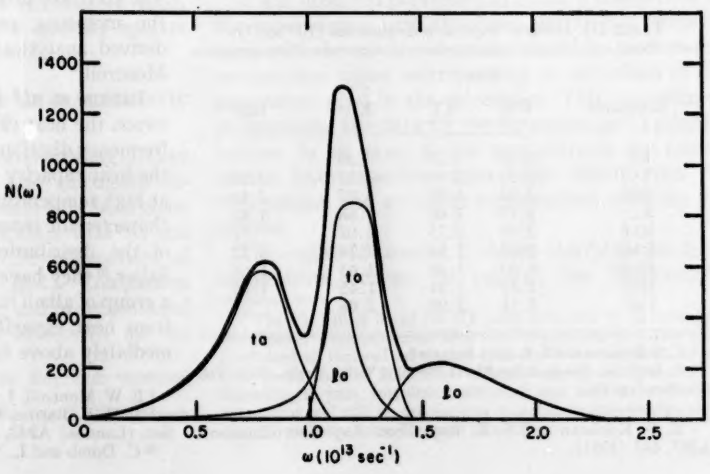

FIG. 8. Vibrational frequency distribution for RbI.

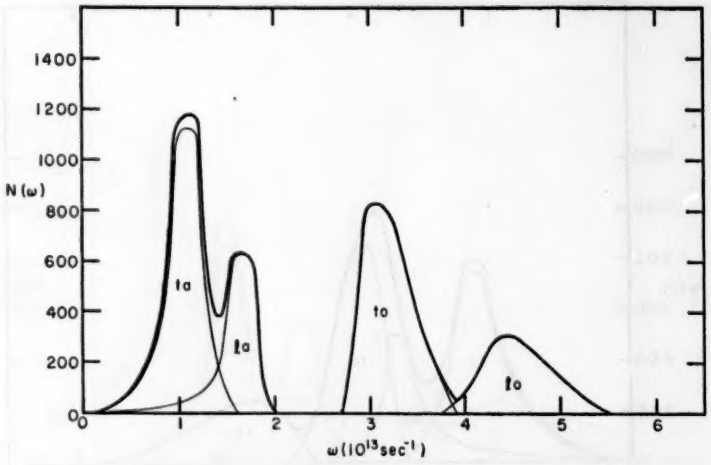

FIG. 9. Vibrational frequency distribution for CsF.

the frequency of these modes with increasing values of the wave vector; i.e., for points outward from the center of the reciprocal lattice. Finally, we can note that, in both the acoustic and optical branches, the relative positions of the longitudinal and transverse portions of the branches remain fairly constant with comparatively little overlapping.

Theoretical and experimental infrared dispersion frequencies, ω_0, are given in Table III. The calculation was carried out as described in I. The values of these frequencies are very near the frequencies beneath the peaks of the transverse optical branches, but are consistently about 10% below the experimental values. Also listed in the table are the results obtained by Krishnan and Roy[7] on the basis of a similar Born model calculation. The over-all agreement should be considered satisfactory in view of the various approximations involved in the theory.

Frequencies are tabulated as functions of position along the vectors (100), (110), (111), and (11$\bar{1}$) in the reciprocal lattice in Tables AI through AIII. The vectors are indicated in Fig. 1 of I. These examples illustrate the dependence of the frequencies, through the coupling coefficients, on the wave vector, lattice parameter, masses of the ions (and mass ratio), and compressibility.

TABLE III. Infrared dispersion frequencies (10^{13} sec^{-1}).

Substance	Calc 0°K	Calc RT	Calc KR[a]	Obs[b]
KF	3.45	3.29	3.39	...
KCl	2.52	2.40	2.51	2.67
KBr	2.03	1.91	2.07	2.13
KI	1.78	1.66	1.88	1.85
RbF	2.88	2.75	3.02	...
RbCl	2.03	1.94	2.14	2.22
RbBr	1.50	1.42	1.63	1.65
RbI	1.33	1.24	1.45	1.45
CsF	3.14	2.98	2.95	...

[a] K. S. Krishnan and S. K. Roy, footnote 7.
[b] G. Liebfried, *Handbuch der Physik* (Springer-Verlag, Berlin, 1955), Vol. VII, Part 1, p. 223.

[7] K. S. Krishnan and S. K. Roy, Proc. Roy. Soc. (London) **A207**, 447 (1951).

IV. MOMENTS OF THE DISTRIBUTION

Positive and negative moments of the frequency distributions are given in Tables IV–VI. The moments have been calculated directly from the frequencies by means of the equation

$$\mu_n = \int \omega^n N(\omega) d\omega = \sum_i \omega_i^n N_i$$

where

$$\int N(\omega) d\omega = \sum_i N_i = 1.$$

The converse process of determining the spectra from the moments, particularly when the latter can be derived analytically, has been discussed in detail by Montroll.[8]

Barron *et al.*[9] have discussed the relationship between the heat capacity and a direct expansion of the frequency distribution at low temperatures and between the heat capacity and the moments of the distribution at high temperatures. Using an expansion of the Debye characteristic temperature in terms of the even moments of the distribution in a form given by Domb and Salter,[10] they have evaluated several even moments for a group of alkali halides. The moments were determined from heat capacity measurements in the region immediately above $\theta_D/6$. A comparison is made in Table

[8] E. W. Montroll, J. Chem. Phys. **10**, 218 (1942); **11**, 481 (1943).
[9] T. H. K. Barron, W. T. Berg, and J. A. Morrison, Proc. Roy. Soc. (London) **A242**, 478 (1957).
[10] C. Domb and L. Salter, Phil. Mag. **43**, 1083 (1952).

TABLE IV. Moments of the frequency distributions for the potassium halides (10^{12n+m} sec^{-n}).

		KF		KCl		KBr		KI	
n	m	0°K	RT	0°K	RT	0°K	RT	0°K	RT
−6	−1	1.427	1.672	9.712	11.21	58.20	68.91	275.8	333.8
−5	−1	1.010	1.152	4.935	5.573	22.06	25.50	81.07	95.68
−4	−1	0.8594	0.9553	3.004	3.322	10.01	11.30	28.54	32.83
−3	−1	0.9885	1.073	2.493	2.702	6.127	6.752	13.39	14.98
−2	−1	1.625	1.721	3.017	3.198	5.406	5.797	8.901	9.650
−1.5	−1	2.347	2.453	3.755	3.928	5.755	6.075	8.235	8.767
−1	−1	3.615	3.724	4.973	5.128	6.558	6.805	8.219	8.579
−0.5	−1	5.876	5.965	6.917	7.025	7.908	8.058	8.788	8.983
0.5	0	1.772	1.745	1.492	1.469	1.317	1.292	1.203	1.176
1	0	3.254	3.159	2.288	2.217	1.795	1.728	1.519	1.452
1.5	0	6.174	5.913	3.591	3.428	2.523	2.385	1.999	1.870
2	1	1.207	1.141	0.5759	0.5419	0.3644	0.3383	0.2724	0.2496
3	1	5.003	4.626	1.571	1.439	0.8151	0.7327	0.5497	0.4846
4	2	2.276	2.065	0.4604	0.4124	0.1973	0.1724	0.1204	0.1026
5	2	11.16	9.970	1.441	1.266	0.5093	0.4343	0.2794	0.2309
6	2	58.12	51.14	4.790	4.136	1.386	1.156	0.6778	0.5446

TABLE V. Moments of the frequency distributions for the rubidium halides (10^{12n+m} sec^{-n}).

		RbF		RbCl		RbBr		RbI	
n	m	0°K	RT	0°K	RT	0°K	RT	0°K	RT
−6	0	1.430	1.667	6.174	7.149	22.61	26.55	74.41	88.65
−5	0	0.7029	0.7982	2.331	2.641	6.792	7.787	18.18	21.19
−4	0	0.4146	0.4593	1.054	1.169	2.444	2.738	5.324	6.065
−3	0	0.3219	0.3483	0.6397	0.6944	1.199	1.313	2.120	2.359
−2	0	0.3446	0.3638	0.5547	0.5881	0.8586	0.9168	1.237	1.337
−1.5	0	0.4015	0.4185	0.5847	0.6117	0.8224	0.8652	1.075	1.142
−1	0	0.5051	0.5195	0.6606	0.6812	0.8385	0.8681	0.9980	1.040
−0.5	0	0.6851	0.6949	0.7922	0.8046	0.8981	0.9141	0.9778	0.9989
0.5	0	1.564	1.542	1.320	1.299	1.149	1.129	1.059	1.036
1	0	2.605	2.532	1.812	1.756	1.357	1.309	1.155	1.106
1.5	0	4.579	4.393	2.574	2.457	1.640	1.556	1.291	1.210
2	0	8.421	7.979	3.769	3.546	2.024	1.889	1.475	1.354
3	1	3.158	2.927	0.8731	0.8000	0.3267	0.2958	0.2041	0.1802
4	1	13.05	11.87	2.200	1.970	0.5661	0.4994	0.3021	0.2576
5	1	57.56	51.41	5.923	5.196	1.047	0.9028	0.4740	0.3921
6	1	265.5	233.2	16.79	14.46	2.052	1.736	0.7833	0.6307

VII between these experimentally determined moments and the theoretical values. The uncertainty assigned to the experimental values of μ_6 is about 15%. The agreement shown in Table VII is remarkably good, the moments obtained from the 0°K and RT spectra often bracketing the experimental values.

V. HEAT CAPACITIES AND DEBYE CHARACTERISTIC TEMPERATURES

The heat capacities and the corresponding Debye characteristic temperatures were also calculated directly from the frequencies. Expressions have been given in I. Heat capacities are listed in Tables VIII–X, and the Debye characteristic temperature as functions of temperature are shown in Figs. 10–12. Comparison with the experimental work of Berg and Morrison[11] and with Clusius *et al.*[12] shows good agreement for the potassium salts.[13] The results are less satisfactory for rubidium bromide and iodide, but the discrepancies are not unexpectedly large.

It was observed previously in I that a comparison of the experimental heat capacities and Debye temperatures with the calculated values should be made in the temperature region corresponding to the values of the parameters used in the calculation. This is confirmed in examining the data for the potassium and rubidium halides. In all cases at low temperatures the experimental heat capacities agree more closely with the 0°K column and at higher temperatures with the RT column.

The region of crossing is shown clearly in the θ_D vs temperature curves. In general, the experimental

[11] W. T. Berg and J. A. Morrison, Proc. Roy. Soc. (London) **A242**, 467 (1957).

[12] K. Clusius, J. Goldmann, and A. Perlick, Z. Naturforsch. **4/**, 424 (1949).

[13] The C_V values listed for KF were obtained by assuming, in the absence of experimental data, the temperature variation of the coefficient of thermal expansion between room temperature and 0°K to be that of KCl. The exceptionally good agreement is, therefore, in part, fortuitous; although one anticipates that the agreement will still be satisfactory when more information about the thermal expansion becomes available.

TABLE VI. Moments of the frequency distribution for cesium fluoride (10^{13n+m} sec^{-n}).

n	m	0°K	RT
−6	0	4.937	5.676
−5	0	1.949	2.206
−4	0	0.9234	1.027
−3	0	0.5733	0.6250
−2	0	0.4880	0.5191
−1.5	0	0.5089	0.5338
−1	0	0.5790	0.5983
−0.5	0	0.7241	0.7364
0.5	0	1.520	1.494
1	0	2.514	2.427
1.5	0	4.439	4.214
2	0	8.231	7.685
3	1	3.106	2.813
4	2	1.262	1.112
5	2	5.361	4.608
6	3	2.351	1.974

points cross from the lower 0°K curve to the upper RT curve in the temperature region between 50° and 120°K. This is the temperature range which one might have expected, *a priori*, to separate the region where 0°K parameters are appropriate from the region at higher temperatures where room temperature parameters may be used.

The Debye temperatures become very sensitive to small changes in the heat capacity when the normal modes are nearly fully excited. This occurs below room temperature for the heavier alkali halides. In addition, there are contributions to the experimental heat capacity due to anharmonic terms and other effects. Although these contributions are not yet exceptionally large, as can be seen from the tables of heat capacities, they are sufficient to have a pronounced effect on the Debye temperatures. This effect is shown as a rapid drop in θ_D values at higher temperatures.

TABLE VII. Comparison of theoretical and experimental moments.

	μ_2 (10^{27} sec^{-2})			μ_4 (10^{54} sec^{-4})			μ_6 (10^{81} sec^{-6})		
	calc (0°K)	calc (RT)	exptl[a]	calc (0°K)	calc (RT)	exptl[a]	calc (0°K)	calc (RT)	exptl[a]
NaCl[b]	0.909	0.856	0.865	1.250	1.127	0.982	2.355	2.058	1.354
NaI[b]	0.460	0.424	0.391	0.402	0.348	0.290	0.453	0.372	0.326
KCl	0.576	0.542	0.570	0.460	0.412	0.429	0.479	0.414	0.363
KBr	0.364	0.338	0.362	0.197	0.172	0.193	0.139	0.116	0.129
KI	0.272	0.250	0.272	0.120	0.103	0.118	0.068	0.054	0.063

[a] Barron *et al.*, footnote 9.
[b] Calculated values are taken from I.

TABLE VIII. Theoretical and experimental heat capacities for the potassium halides (C_V in cal $mole^{-1}$ deg^{-1}).

	KF			KCl			KBr			KI		
T	0°K	RT	exptl[a]	0°K	RT	exptl[b]	0°K	RT	exptl[b]	0°K	RT	exptl[b]
5	0.00	0.00	...	0.00	0.00	0.01	0.02	0.02	0.02	0.04	0.05	0.06
10	0.02	0.02	...	0.06	0.07	0.08	0.18	0.21	0.23	0.46	0.52	0.58
15	0.09	0.10	...	0.25	0.27	0.30	0.67	0.75	0.78	1.38	1.52	1.58
20	0.25	0.27	0.28	0.63	0.69	0.71	1.46	1.60	1.60	2.50	2.70	2.71
25	0.51	0.56	0.55	1.20	1.31	1.30	2.42	2.62	2.54	3.63	3.88	3.79
30	0.88	0.96	0.92	1.92	2.07	1.99	3.42	3.66	3.51	4.68	4.96	4.79
35	1.34	1.44	1.39	2.72	2.90	2.73	4.38	4.64	4.43	5.62	5.91	5.62
40	1.85	1.99	1.89	3.53	3.74	3.56	5.27	5.53	5.30	6.44	6.72	6.33
45	2.40	2.56	2.44	4.31	4.53	4.32	6.05	6.31	6.09	7.15	7.42	7.10
50	2.96	3.14	3.02	5.03	5.26	5.05	6.73	6.98	6.76	7.75	8.00	7.81
60	4.06	4.27	4.16	6.30	6.51	6.31	7.84	8.05	7.87	8.69	8.90	8.75
70	5.07	5.28	5.15	7.30	7.50	7.35	8.66	8.85	8.73	9.37	9.55	9.43
80	5.96	6.16	6.05	8.10	8.27	8.16	9.27	9.43	9.33	9.87	10.02	9.91
90	6.72	6.91	6.83	8.72	8.87	8.79	9.74	9.88	9.80	10.24	10.37	10.28
100	7.37	7.55	7.49	9.21	9.35	9.31	10.10	10.21	10.15	10.52	10.63	10.57
120	8.39	8.54	8.50	9.93	10.03	10.06	10.60	10.69	10.68	10.92	11.00	10.95
140	9.13	9.25	9.27	10.40	10.48	10.52	10.93	10.99	11.02	11.17	11.23	11.22
160	9.67	9.77	9.77	10.73	10.79	10.84	11.15	11.20	11.26	11.34	11.38	11.37
180	10.07	10.16	10.16	10.96	11.02	11.09	11.30	11.34	11.42	11.45	11.49	11.49
200	10.38	10.46	10.46	11.13	11.18	11.24	11.42	11.45	11.54	11.54	11.57	11.59
220	10.62	10.69	10.69	11.26	11.30	11.39	11.50	11.53	11.64	11.60	11.63	11.67
240	10.81	10.87	10.88	11.37	11.40	11.49	11.57	11.59	11.72	11.65	11.68	11.73
260	10.97	11.01	11.00	11.45	11.47	11.56	11.62	11.64	11.80	11.69	11.71	11.79
280	11.09	11.13	11.09	11.51	11.53	...	11.66	11.68	...	11.72	11.74	...
300	11.19	11.23	11.19	11.56	11.58	...	11.69	11.71	...	11.75	11.76	...

[a] E. F. Westrum, Jr., and K. S. Pitzer, J. Am. Chem. Soc. **71**, 1940 (1949).
[b] W. T. Berg and J. A. Morrison, footnote 11.

TABLE IX. Theoretical and experimental heat capacities for the rubidium halides (C_V in cal mole^{-1} deg^{-1}).

	RbF		RbCl		RbBr			RbI		
T	0°K	RT	0°K	RT	0°K	RT	exptl[a]	0°K	RT	exptl[a]
5	0.01	0.01	0.02	0.02	0.04	0.04	...	0.07	0.08	...
10	0.09	0.10	0.20	0.22	0.37	0.41	0.57	0.67	0.75	1.25
15	0.39	0.42	0.72	0.78	1.24	1.36	1.39	1.95	2.15	2.21
20	0.91	0.98	1.53	1.64	2.51	2.71	2.48	3.51	3.79	3.51
25	1.55	1.65	2.48	2.64	3.86	4.11	3.80	4.99	5.29	5.06
30	2.23	2.35	3.46	3.65	5.11	5.37	5.05	6.23	6.53	6.33
35	2.90	3.04	4.40	4.61	6.18	6.43	6.20	7.24	7.51	7.42
40	3.55	3.70	5.26	5.47	7.07	7.30	7.13	8.03	8.28	8.22
45	4.17	4.33	6.03	6.24	7.79	8.00	7.87	8.66	8.88	8.83
50	4.74	4.91	6.70	6.90	8.38	8.57	8.52	9.16	9.35	9.37
60	5.78	5.95	7.79	7.97	9.27	9.42	9.43	9.89	10.03	10.26
70	6.67	6.83	8.61	8.76	9.87	9.99	10.01	10.37	10.48	10.61
80	7.41	7.57	9.22	9.36	10.30	10.40	10.45	10.70	10.79	10.92
90	8.03	8.17	9.69	9.81	10.61	10.69	10.78	10.94	11.02	11.17
100	8.54	8.68	10.05	10.15	10.84	10.91	11.05	11.12	11.18	11.37
120	9.34	9.45	10.57	10.64	11.15	11.20	11.42	11.35	11.40	11.60
140	9.90	9.99	10.90	10.95	11.35	11.39	11.68	11.50	11.53	11.71
160	10.30	10.38	11.12	11.17	11.48	11.51	11.82	11.60	11.62	11.77
180	10.60	10.66	11.28	11.32	11.57	11.59	11.90	11.66	11.68	11.81
200	10.83	10.88	11.40	11.43	11.64	11.65	...	11.71	11.73	11.87
220	11.00	11.05	11.49	11.51	11.68	11.70	...	11.75	11.76	11.89
240	11.07	11.18	11.55	11.58	11.72	11.74	...	11.78	11.79	11.91
260	11.25	11.28	11.61	11.63	11.75	11.76	...	11.80	11.81	11.93
280	11.33	11.36	11.65	11.67	11.78	11.79	...	11.81	11.82	11.94
300	11.41	11.43	11.68	11.70	11.79	11.80	...	11.83	11.84	...

[a] Clusius, *et al.*, footnote 12.

The relationship of this drop to vibrational anharmonicity has been considered in some detail by Barron *et al.*[9]

The behavior of the theoretical Debye temperature curves is consistent with previous work. The temperature range below 10° or 15°K is not adequately described, in large part because of the small number of frequencies evaluated. As discussed previously, we expect the temperature variation to be proportional to the mass ratio, and the results show that this occurs. The curves for NaF, KCl, and RbBr are comparatively flat after an initial decrease with temperature. However, the simple Born model used here is such that only a smooth, gradual rise to some high-temperature limiting value can result.

The limiting values of the Debye temperature at 0°K and at high temperatures were determined as before from the compressibilities and computed elastic con-

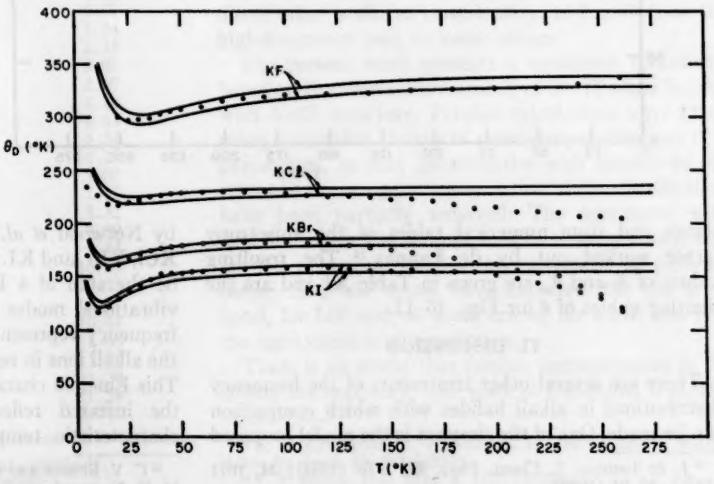

FIG. 10. Debye characteristic temperatures as functions of temperature for the potassium halides. Upper and lower curves are for 0°K and RT parameters, respectively. Experimental values are indicated by filled and empty circles.

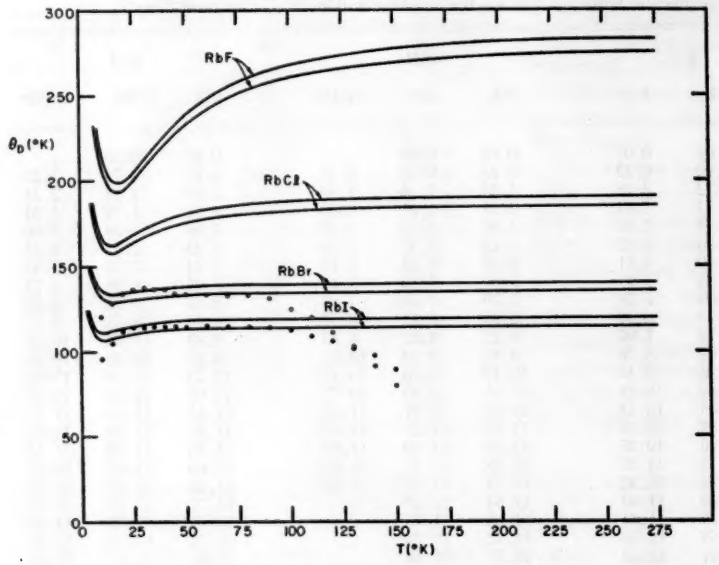

FIG. 11. Debye characteristic temperatures as functions of temperature for the rubidium halides. Upper and lower curves are for 0°K and RT parameters, respectively. Experimental values are indicated by filled and empty circles.

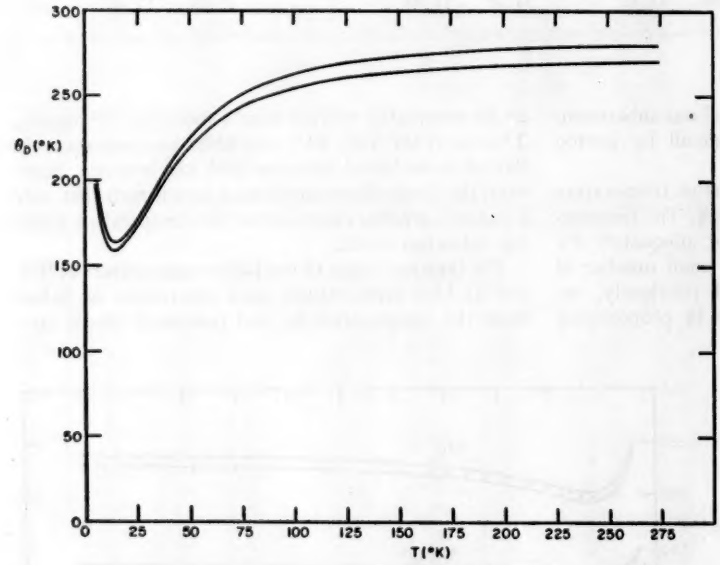

FIG. 12. Debye characteristic temperatures as functions of temperature for cesium fluoride. Upper and lower curves are for 0°K and RT parameters, respectively.

stants and from numerical tables of the anisotropy factor worked out by de Launay.[14] The resulting values of θ_0 and θ_∞ are given in Table XI and are the limiting values of θ for Figs. 10–12.

VI. DISCUSSION

There are several other treatments of the frequency distributions in alkali halides with which comparison can be made. One of the simplest is the model proposed by Norwood *et al.*[15] which they have applied to LiF, KCl, KBr, and KI. The vibrational spectrum is taken to be the sum of a Debye distribution representing the vibrational modes of the halide ions and an Einstein frequency representing the independent oscillations of the alkali ions in regions surrounded by the halide ions. This Einstein characteristic temperature is taken to be the infrared reflection frequency, and the Debye characteristic temperature is obtained from elastic-

[14] J. de Launay, J. Chem. Phys. **22**, 1676 (1954); **24**, 1071 (1956); **30**, 91 (1959).

[15] C. V. Briscoe and C. F. Squire, Phys. Rev. **106**, 1175 (1957); M. H. Norwood and C. V. Briscoe, Phys. Rev. **112**, 45 (1958).

constant data with the assumption that the halide ions occupy the entire volume of the crystal. Previous work[16] has shown that in many cases one obtains the most accurate two-term fit to the lattice heat capacity curves below room temperature with a Debye term and an Einstein term which is in almost exact agreement with the limiting lattice frequency, and which therefore nearly corresponds to that used by Norwood *et al.* However, their model is not based on any fitting procedure or parameter adjustment, so that the agreement with experiment which they find indicates some truth to their picture. In addition, for the potassium salts this model also shows improvement as the ratio of the ionic radii increases. From the frequency distributions shown here, it can be seen that the choice of the infrared reflection frequency to represent three vibrational degrees of freedom corresponds to representing the whole optical branch by a single frequency near the maximum of the transverse optical distribution. Assigning two degrees of freedom to this Einstein function and adding another Einstein term with a characteristic frequency near the maximum of the longitudinal optical branch would be a somewhat better approximation to the true situation. The Debye portion of the spectrum represents an averaging of the acoustic branches of the distribution. We have noted before that a single Debye term might well approximate the low-frequency part of the distribution.

Another recent calculation has been reported by Oliphant[17] using Houston's approximation to determine the frequency spectra for LiF, KCl, and KI. Long-range Coulomb interactions are not included in this treatment. There is some similarity between these spectra and those determined from the Kellermann model, mainly in the appearance of maxima at about the same values of the frequencies. It was noted, however, that the results of this method, as far as the specific heat is concerned, are not necessarily better than the results given by the simpler model of Norwood *et al.*

Of considerably interest is the recent work carried out by Lundqvist *et al.*[18] on the lattice vibrations and specific heats of KCl and NaCl at low temperatures. In their treatment the Born model was extended to include a modified Coulomb interaction, i.e., an effective charge was introduced into the potential; and to include, in addition, polarization by considering the lattice to be formed from point dipoles. Both effects, particularly polarization, shift the frequencies to lower values. This shift is quite large near the high frequency part of the spectrum.

Further work along this line has been carried out by J. R. Hardy[19] for NaCl, allowing for the deformability of the ions. He has considered the polarizability separately, and then has included deformation dipoles on the negative ions when they are displaced with respect to their nearest neighbors. The frequency distribution is altered considerably, with a shift of the high-frequency part to lower values.

The present work presents a consistent treatment, based on the simple Born model, of the 17 alkali halides with NaCl structure. Parallel calculations were made using reasonable choices of room-temperature and 0°K parameters, so that uncertainties with respect to the extent of the temperature variation of the distributions have been partially removed. The agreement with experiment for the sodium halides is satisfactory, and for the potassium halides the agreement is, perhaps, better than one would have expected. On the other hand, for LiF and, to some extent, for RbBr and RbI the agreement is disappointing.

There is no doubt that further improvements in the theory are necessary. The work of Lundqvist *et al.* and

TABLE X. Theoretical heat capacities for cesium fluoride (C_V in cal mole^{-1} deg^{-1}).

T	0°K	RT
5	0.01	0.01
10	0.19	0.21
15	0.70	0.77
20	1.44	1.54
25	2.21	2.33
30	2.92	3.05
35	3.55	3.69
40	4.13	4.28
45	4.66	4.83
50	5.16	5.34
60	6.08	6.27
70	6.88	7.07
80	7.56	7.75
90	8.15	8.32
100	8.64	8.80
120	9.40	9.53
140	9.94	10.05
160	10.34	10.43
180	10.63	10.71
200	10.85	10.92
220	11.02	11.08
240	11.16	11.20
260	11.26	11.30
280	11.35	11.38
300	11.42	11.45

TABLE XI. Limiting values of the Debye characteristic temperature (°K).

Substance	θ_0	θ_∞
KF	337	333
KCl	243	230
KBr	181	181
KI	140	156
RbF	231	279
RbCl	179	186
RbBr	144	135
RbI	118	115
CsF	188	273

[16] A. M. Karo and C. C. Stephenson (unpublished).
[17] C. Oliphant, Phys. Revs. **115**, 296 (1959).
[18] S. O. Lundqvist, V. Lundström, E. Tenerz, and I. Waller, Arkiv för Fysik **15**, 193 (1959).
[19] J. R. Hardy, Phil. Mag. **4**, 1278 (1959).

Hardy, although based on approximate theory, indicates the importance of taking into full account effective charges, polarization, and other aspects of the fact that the ions are indeed deformable. In all of the treatments discussed in this section the repulsive interactions between second-nearest neighbors have been neglected. For the lithium halides, where the radii of the halide ions are two to three times the radius of the lithium ion, these interactions cannot properly be disregarded. In these salts the contributions to the overlap energy from first and second neighbors are comparable.[20] For the heavier alkali halides the neglect of the next nearest neighbors is probably less serious, and for these compounds inclusion of polarization could be far more important.

When refinements in lattice theory are being investigated, it would be very instructive to include, for example, LiF, NaCl, and RbI, as test cases. These present most of the problems arising in ionic lattices as well as one example where the simple Born treatment works quite well.

[20] M. Born and K. Huang, *Dynamical Theory of Crystal Lattices* (Oxford University Press, New York, 1954), p. 32.

ACKNOWLEDGMENTS

The author is indebted to Mr. Robert Carpenter and to Miss Harriet Terry for programing and computing assistance during the later stages of this investigation.

APPENDIX A

TABLE AI. Potassium halide frequencies as a function of position in the reciprocal lattice (10^{13} sec^{-1}).

$p_x p_y p_z$:		1000	200	400	600	800	1000	111	222	333	444	555	220	440	660	333	442	551	660	77$\bar{1}$
KF	*la*	0.00	1.11	2.08	2.81	3.19	3.27	0.92	1.82	2.68	3.42	3.78	1.47	2.59	3.06	2.68	2.92	3.04	3.06	3.15
	lo	6.85	6.68	6.21	5.62	5.13	4.96	6.76	6.51	6.13	5.67	5.42	6.59	5.85	4.76	6.13	5.84	5.35	4.76	4.53
	ta	0.00	0.58	1.11	1.53	1.81	1.90	0.56	1.09	1.54	1.88	2.02	0.85	1.77	2.06	1.54	1.74	2.01	2.06	1.99
	ta	0.00	0.58	1.11	1.53	1.81	1.90	0.56	1.09	1.54	1.88	2.02	0.94	1.81	2.69	1.54	1.80	2.22	2.69	2.77
	to	3.29	3.32	3.39	3.49	3.57	3.61	3.26	3.19	3.08	2.96	2.89	3.17	2.93	3.04	3.08	2.94	2.91	3.04	3.25
	to	3.29	3.32	3.39	3.49	3.57	3.61	3.26	3.19	3.08	2.96	2.89	3.35	3.54	3.95	3.08	3.30	3.63	3.95	3.98
KCl	*la*	0.00	0.84	1.59	2.18	2.55	2.66	0.66	1.31	1.95	2.56	3.05	1.07	1.93	2.42	1.95	2.15	2.31	2.42	2.40
	lo	4.58	4.45	4.09	3.62	3.18	3.00	4.52	4.33	4.03	3.63	3.20	4.39	3.84	2.98	4.03	3.81	3.44	2.98	2.73
	ta	0.00	0.40	0.77	1.08	1.28	1.35	0.42	0.83	1.20	1.52	1.75	0.59	1.28	1.68	1.20	1.31	1.64	1.68	1.53
	ta	0.00	0.40	0.77	1.08	1.28	1.35	0.42	0.83	1.20	1.52	1.75	0.74	1.44	2.02	1.20	1.46	1.73	2.02	2.23
	to	2.40	2.42	2.45	2.49	2.52	2.53	2.38	2.31	2.19	2.02	1.84	2.30	2.03	2.05	2.19	2.03	1.87	2.05	2.61
	to	2.40	2.42	2.45	2.49	2.52	2.53	2.38	2.31	2.19	2.02	1.84	2.43	2.50	2.59	2.19	2.32	2.48	2.59	2.73
KBr	*la*	0.00	0.63	1.17	1.58	1.77	1.80	0.49	0.96	1.42	1.81	2.00	0.79	1.41	1.67	1.42	1.56	1.65	1.67	1.68
	lo	3.60	3.51	3.25	2.93	2.67	2.60	3.56	3.43	3.23	2.99	2.85	3.47	3.07	2.52	3.23	3.08	2.82	2.52	2.43
	ta	0.00	0.28	0.57	0.78	0.93	0.97	0.32	0.62	0.88	1.08	1.16	0.43	0.93	1.16	0.88	0.95	1.16	1.16	1.09
	ta	0.00	0.28	0.57	0.78	0.93	0.97	0.32	0.62	0.88	1.08	1.16	0.55	1.03	1.42	0.88	1.04	1.17	1.42	1.50
	to	1.91	1.93	1.96	2.00	2.04	2.05	1.90	1.85	1.78	1.70	1.66	1.84	1.69	1.73	1.78	1.69	1.66	1.73	1.85
	to	1.91	1.93	1.96	2.00	2.04	2.05	1.90	1.85	1.78	1.70	1.66	1.94	2.02	2.19	1.78	1.89	2.05	2.19	2.17
KI	*la*	0.00	0.49	0.90	1.19	1.30	1.31	0.37	0.74	1.07	1.33	1.44	0.61	1.07	1.23	1.07	1.17	1.22	1.23	1.22
	lo	3.07	3.00	2.81	2.58	2.41	2.36	3.04	2.95	2.81	2.67	2.60	2.97	2.68	2.28	2.81	2.70	2.50	2.28	2.22
	ta	0.00	0.23	0.43	0.59	0.69	0.73	0.25	0.48	0.67	0.80	0.85	0.33	0.69	0.86	0.67	0.72	0.85	0.86	0.81
	ta	0.00	0.23	0.43	0.59	0.69	0.73	0.25	0.48	0.67	0.80	0.85	0.43	0.77	1.03	0.67	0.78	0.86	1.03	1.09
	to	1.66	1.68	1.72	1.76	1.80	1.82	1.66	1.63	1.59	1.55	1.53	1.62	1.53	1.59	1.59	1.54	1.54	1.59	1.67
	to	1.66	1.68	1.72	1.76	1.80	1.82	1.66	1.63	1.59	1.55	1.53	1.69	1.79	1.98	1.59	1.68	1.84	1.98	1.98

TABLE AII. Rubidium halide frequencies as a function of position in the reciprocal lattice (10^{13} sec^{-1}).

$p_x p_y p_z$:		000	200	400	600	800	1000	111	222	333	444	555	220	440	660	333	442	551	660	77$\bar{1}$
RbI	*la*	0.00	0.76	1.40	1.85	2.03	2.06	0.63	1.23	1.78	2.19	2.35	1.00	1.72	1.94	1.78	1.92	1.96	1.94	1.96
	lo	5.72	5.61	5.29	4.91	4.62	4.51	5.67	5.52	5.30	5.09	4.99	5.55	5.06	4.32	5.30	5.11	4.75	4.32	4.18
	ta	0.00	0.40	0.75	1.02	1.18	1.24	0.38	0.73	1.01	1.20	1.26	0.58	1.14	1.29	1.01	1.14	1.26	1.29	1.28
	ta	0.00	0.40	0.75	1.02	1.18	1.24	0.38	0.73	1.01	1.20	1.26	0.64	1.19	1.69	1.01	1.15	1.42	1.69	1.73
	to	2.75	2.79	2.89	3.02	3.13	3.18	2.75	2.73	2.70	2.68	2.67	2.69	2.63	2.79	2.70	2.65	2.68	2.79	2.92
	to	2.75	2.79	2.89	3.02	3.13	3.18	2.75	2.73	2.70	2.68	2.67	2.83	3.11	3.63	2.70	2.91	3.27	3.63	3.67
RbCl	*la*	0.00	0.62	1.15	1.54	1.72	1.74	0.48	0.96	1.40	1.77	1.94	0.79	1.39	1.63	1.40	1.53	1.61	1.63	1.64
	lo	3.71	3.61	3.36	3.05	2.81	2.74	3.66	3.54	3.34	3.13	3.01	3.57	3.19	2.65	3.34	3.20	2.94	2.65	2.55
	ta	0.00	0.30	0.57	0.78	0.92	0.97	0.31	0.61	0.86	1.04	1.11	0.43	0.92	1.12	0.86	0.93	1.11	1.12	1.07
	ta	0.00	0.30	0.57	0.78	0.92	0.97	0.31	0.61	0.86	1.04	1.11	0.54	0.99	1.38	0.86	1.01	1.15	1.38	1.46
	to	1.94	1.96	2.00	2.05	2.09	2.11	1.93	1.89	1.83	1.76	1.73	1.88	1.74	1.80	1.83	1.75	1.73	1.80	1.91
	to	1.94	1.96	2.00	2.05	2.09	2.11	1.93	1.89	1.83	1.76	1.73	1.97	2.07	2.28	1.83	1.94	2.12	2.28	2.27
RbBr	*la*	0.00	0.50	0.94	1.29	1.51	1.58	0.39	0.77	1.15	1.51	1.81	0.63	1.14	1.43	1.15	1.27	1.36	1.43	1.41
	lo	2.70	2.62	2.41	2.13	1.87	1.76	2.66	2.55	2.38	2.14	1.87	2.59	2.26	1.75	2.38	2.25	2.03	1.75	1.60
	ta	0.00	0.24	0.46	0.63	0.75	0.80	0.25	0.49	0.71	0.90	1.05	0.35	0.76	1.00	0.71	0.77	0.96	1.00	0.91
	ta	0.00	0.24	0.46	0.63	0.75	0.80	0.25	0.49	0.71	0.90	1.05	0.44	0.85	1.19	0.71	0.87	1.03	1.19	1.32
	to	1.42	1.43	1.45	1.47	1.49	1.50	1.41	1.37	1.30	1.20	1.08	1.36	1.20	1.21	1.30	1.20	1.10	1.21	1.35
	to	1.42	1.43	1.45	1.47	1.49	1.50	1.41	1.37	1.30	1.20	1.08	1.44	1.48	1.53	1.30	1.37	1.47	1.53	1.55
RbI	*la*	0.00	0.42	0.79	1.08	1.23	1.25	0.32	0.63	0.93	1.21	1.38	0.52	0.94	1.16	0.93	1.06	1.11	1.16	1.17
	lo	2.24	2.18	2.00	1.77	1.58	1.53	2.21	2.13	1.99	1.81	1.68	2.15	1.89	1.50	1.99	1.88	1.71	1.50	1.44
	ta	0.00	0.19	0.36	0.50	0.60	0.63	0.21	0.42	0.60	0.75	0.83	0.28	0.60	0.81	0.60	0.64	0.77	0.81	0.74
	ta	0.00	0.19	0.36	0.50	0.60	0.63	0.21	0.42	0.60	0.75	0.83	0.37	0.72	0.94	0.60	0.73	0.83	0.94	1.04
	to	1.24	1.25	1.27	1.29	1.30	1.31	1.23	1.20	1.14	1.06	1.01	1.19	1.06	1.07	1.14	1.04	1.01	1.07	1.15
	to	1.24	1.25	1.27	1.29	1.30	1.31	1.23	1.20	1.14	1.06	1.01	1.26	1.29	1.35	1.14	1.20	1.29	1.35	1.32

TABLE AIII. Cesium fluoride frequencies as a function of position in the reciprocal lattice (10^{13} sec^{-1}).

$p_x p_y p_z$:	000	200	400	600	800	1000	111	222	333	444	555	220	440	660	333	442	551	660	77$\bar{1}$
la	0.00	0.67	1.22	1.56	1.66	1.66	0.51	0.99	1.41	1.71	1.82	0.83	1.41	1.57	1.41	1.52	1.58	1.57	1.55
lo	5.32	5.22	4.97	4.67	4.46	4.39	5.28	5.17	5.01	4.87	4.82	5.19	4.81	4.23	5.01	4.87	4.57	4.23	4.13
ta	0.00	0.30	0.57	0.77	0.90	0.94	0.34	0.65	0.89	1.05	1.11	0.44	0.90	1.11	0.89	0.94	1.11	1.11	1.06
ta	0.00	0.30	0.57	0.77	0.90	0.94	0.34	0.65	0.89	1.05	1.11	0.59	1.02	1.31	0.89	1.03	1.11	1.31	1.39
to	2.98	3.02	3.10	3.21	3.30	3.34	2.98	2.97	2.95	2.93	2.93	2.94	2.89	3.02	2.95	2.91	2.93	3.02	3.13
to	2.98	3.02	3.10	3.21	3.30	3.34	2.98	2.97	2.95	2.93	2.93	3.05	3.28	3.70	2.95	3.12	3.41	3.70	3.72

Isotope Effects on Reaction Rates and the Reaction Coordinate

MAX WOLFSBERG*

Physical Chemistry Laboratory, Oxford University, Oxford, England

(Received December 28, 1959)

The high temperature limit of the reaction rate isotope effect is discussed. The Slater approach is compared in this respect to the transition state theory approach. There is no essential disagreement between the two approaches. The Slater assumption with respect to this limit for simple bond rupture represents a special case, however, and is not necessarily correct.

THE high temperature limit of the ratio of the reaction rates of isotopic species is found, in the framework of the transition state theory, to be[1]

$$k_1/k_2=\nu_{1L}/\nu_{2L}, \tag{1}$$

where ν_L is the imaginary (or zero) frequency which results when one solves the vibrational problem at the transition state. The factor ν_{1L}/ν_{2L} is also necessary in order to calculate isotope effects at any temperature. In many instances, it is quite easy to estimate the magnitude of the other relevant factors so that a reliable estimate of ν_{1L}/ν_{2L} is quite important.

N. B. Slater[2] has investigated the classical theory of unimolecular rates at high pressures. The model used is that the molecule decomposes whenever a given coordinate q reaches a critical extension q_0. He obtains for the isotope effect at the high temperature limit

$$k_1/k_2=\nu_1/\nu_2, \tag{2}$$

where ν may be defined as the ratio of all $3N-6$ frequencies of the normal molecule to the $3N-7$ frequencies obtained when no motion is permitted to take place along q.

Further consideration of Slater's factor ν shows that its mass dependence is exactly that which is to be expected for a frequency which has q as its normal coordinate. Now the frequency ν_L in the transition state theory corresponds to a normal mode Q_L. One finds for the transition state $3N-7$ other normal modes which correspond to real bound motion. Thus motion along Q_L is the motion which corresponds to decomposition and, if the coordinates are properly defined, $Q_L(x_1,\cdots)$ larger than zero corresponds to reaction while $Q_L(x_1,\cdots)$ less than zero corresponds to no reaction, independent of the values of any of the other coordinates (if there are no "anharmonicities"). $x_1,\cdots$ are the Cartesian displacement coordinates of the atoms in the transition state. If one is dealing with a decomposition process involving essentially one molecule and uses the displacement coordinates of the normal molecule, then $Q_L(x_1',\cdots)>Q_{t.s.}$ corresponds to decomposition. Here $Q_{t.s.}$ is the numerical value of $Q_L(x_1',\cdots)$at the transition state and $Q_L(x_1',\cdots)$ is expressed in Cartesian displacement coordinates $x_1',\cdots$ of the original molecular species. Thus $Q_L(x_1',\cdots)$ is Slater's coordinate q and $Q_{t.s.}$ is its critical extension q_0.

The result has thus been obtained that the critical coordinate q which should be used in Slater's theory is just the normal coordinate corresponding to unbound motion which one obtains when solving the vibrational problem at the position of the transition state. Thus, there is no essential disagreement between transition state theory and Slater's theory here except for the following. In transition state theory, the force constant for the motion Q_L is determined from the potential energy surface at the transition state, while in Slater's approach the "force constant" corresponding to ν is the ratio of the value of the determinant of all the force constants of the normal molecule to the value of the minor of the force constant corresponding to q. If the coordinate Q_L or q were isotope independent, this fact would make no difference as far as the high temperature limit of the isotope effect is concerned; but Q_L is usually isotope dependent.

For the case of simple bond rupture of the bond between the atoms A and B in a molecule, Slater[2] defined q as x_A-x_B. The isotope effect is then found to be

$$k_1/k_2=(\mu_2/\mu_1)^{\frac{1}{2}} \tag{3}$$

where the μ's refer to the reduced mass of the AB diatomic molecule $\mu=M_AM_B/M_A+M_B$. This value has been used for ν_{1L}/ν_{2L} quite often in the past in the calculation of isotope effects. Suppose that the AB bond is broken in R—A—B—R′. The above q corresponds to a normal mode of decomposition in which the AB bond is lengthened simultaneous with AR and BR′ bond shortening. On the other hand, if the force constant of the A—B bond is much smaller in magnitude than the internal force constants of AR and BR′, then the normal mode of decomposition will be the one which takes the centers of mass of AR and BR′ apart, and the mass dependence of the frequency will be the inverse

* National Science Foundation Senior Postdoctoral Fellow, 1958–1959. Permanent address: Chemistry Department, Brookhaven National Laboratory, Upton, Long Island, New York.

[1] See, for instance, J. Bigeleisen and M. Wolfsberg, in *Advances of Chemical Physics*, Edited by I. Prigogine (Interscience Publishers, Inc., New York, 1958), Vol. I, pp. 15–76.

[2] N. B. Slater, Proc. Roy. Soc. (London) **A194**, 112 (1948).

square root of the reduced mass of the two fragment masses (i.e., $\mu = M_{AR}M_{BR}'/M_{AR}+M_{BR}'$). This latter case may be thought of as the case of simple bond rupture and the corresponding mass dependence for ν_{1L}/ν_{2L} has been proposed by Bigeleisen and Wolfsberg.[1] These authors have also considered calculations of the isotope effect in the decarboxylation of malonic acid using either of the two "extreme" values of ν_{1L}/ν_{2L} discussed here. The reader is referred to the quoted article for this discussion. *In general, however, the determination of ν_{1L}/ν_{2L} requires a knowledge of the potential energy surface.*

ACKNOWLEDGMENTS

The author is very grateful to Mr. R. P. Bell for stimulating discussion and for his kind hospitality at Oxford. Stimulating discussion with Dr. J. Bigeleisen and Dr. F. S. Klein is also thankfully acknowledged. The author is also grateful to the National Science Foundation for the award of a fellowship.

THE JOURNAL OF CHEMICAL PHYSICS VOLUME 33, NUMBER 1 JULY, 1960

A One-Center Wave Function for the Methane Molecule*†

ANTONY F. SATURNO‡ AND ROBERT G. PARR§

Department of Chemistry, Carnegie Institute of Technology, Pittsburgh, Pennsylvania

(Received January 22, 1960)

Slater orbitals, centered on the carbon nucleus and having variable orbital exponents and principal quantum numbers, are used to construct electronic wave functions for the ground state of the methane molecule of the form

$$\Psi = C_1(s^2s^{*2}p^6) + C_2(s^2s^{*2}p^5d) + C_3(s^2s^{*}fp^6) + C_4(s^2s^{*2}p^5f') + C_5(s^2s^{*2}p^5g).$$

Values for the five linear coefficients, the seven orbital exponents, and the seven principal quantum numbers are determined by the variational method. The total molecular energy obtained from a one-term wave function of this form is −39.50 a.u.; the five-term result is −39.80 a.u.; the experimental nonrelativistic energy is −40.51 a.u. Comparison with a similar calculation for the neon atom indicates that most of the residual error is in correlation energy, and it favors the high value for the heat of sublimation of carbon.

I. INTRODUCTION

THIS paper approaches the absolute, purely theoretical calculation of the physical properties of the methane molecule.

The method employed is expansion of the molecular electronic wave function in a set of one-electron atomic-like functions centered at the carbon atom, Slater orbitals of nonintegral principal quantum number and variable orbital exponent.[1] This method already has been applied to the hydrogen molecule,[2] and this type of orbital has also been used to describe the electronic structure of atoms.[3] Work with a one-center expansion method continues in other laboratories,[4–7] and recent research on the united atom viewpoint on molecular structure also is relevant.[8,9]

Strangely, of the multitude of papers that have been written about the electronic structure of the methane molecule, only three appear even comparable with the present work in accuracy and scope, those of Bernal,[10] Koide, Sekiyama and Nagashima,[11] and Mills.[12]

II. METHOD

Methane, or CH_4, is assumed to have the shape of a regular tetrahedron, the four protons each a distance

* Supported in part by research grants from the National Science Foundation, the Petroleum Research Fund of the American Chemical Society, and the Alfred P. Sloan Foundation.

† Based on part of a thesis submitted by Antony F. Saturno in partial fulfillment of the requirements for the degree of Doctor of Philosophy, Carnegie Institute of Technology, 1959.

‡ Present address: Department of Chemistry, University of Tennessee, Knoxville, Tennessee.

§ Alfred P. Sloan Fellow.

[1] R. G. Parr and H. W. Joy, J. Chem. Phys. **26**, 424 (1957).

[2] H. W. Joy and R. G. Parr, J. Chem. Phys. **28**, 448 (1958), where other references to various other calculations using one-center methods may be found.

[3] A. F. Saturno and R. G. Parr, J. Chem. Phys. **29**, 490 (1958).

[4] H. Z. Hartmann, Z. Naturforsch. **2a**, 489 (1947); Z. Physik. Chem. **15**, 108 (1958); **19**, 29 (1959).

[5] R. Gaspar, Acta Phys. Hung. **7**, 151, 447 (1957); R. Gaspar and I. Tamassy-Lentei, *ibid.* **9**, 105 (1958); Ann. Physik. **2**, 208 (1958); E. Kapuy, Acta Phys. Hung. **9**, 245, 445 (1959).

[6] T. C. Chen, J. Chem. Phys. **29**, 347, 356 (1958).

[7] S. Hagstrom and H. Shull, J. Chem. Phys. **30**, 1314 (1959).

[8] W. Bingel, J. Chem. Phys. **30**, 1250, 1254 (1959).

[9] C. Wulfman, J. Chem. Phys. **31**, 381 (1959).

[10] M. J. M. Bernal, Proc. Phys. Soc. (London) **A66**, 514 (1953). See also C. Carter, Proc. Roy. Soc. (London) **235A**, 321 (1956).

[11] S. Koide, H. Sekiyama, and T. Nagashima, J. Phys. Soc. Japan **12**, 1016 (1957); see also R. K. Nesbet, J. Chem. Phys. **32**, 1114 (1960).

[12] I. Mills, Mol. Phys. **1**, 99 (1958).

$R=\sqrt{3}S$ from the carbon nucleus.[13] Cartesian axes bisecting HCH angles are chosen, such that the Cartesian coordinates of the four protons are (S, S, S), $(S, -S, -S)$, $(-S, S, -S)$, $(-S, -S, S)$. The Cartesian coordinates of an electron at a distance r from the carbon nucleus are written as xr, yr, and zr.

If the protons were not localized in this way but were smeared out over the surface of a sphere of radius R,[14] the molecule in its ground state would have a spherically symmetric electronic wave function. A good approximation to its electronic wave function then would be provided by a simple neonlike description, namely,

$$\Phi=(s\bar{s}s^*\bar{s}^*p_x\bar{p}_xp_y\bar{p}_yp_z\bar{p}_z). \tag{1}$$

This is a single normalized Slater determinant, built from spin functions α and β (indicated, respectively, by no bar and a bar) and normalized atomic orbitals centered on the carbon nucleus,

$$s=N_sr^{n_s-1}\exp(-\zeta_sr),$$
$$s'=N_{s'}r^{n_{s'}-1}\exp(-\zeta_{s'}r),$$
$$s^*=(s'-Ss)/(1-S^2)^{\frac{1}{2}},\qquad S=\int ss'dv,$$
$$p_x=N_pr^{n_p-1}\exp(-\zeta_pr)[\sqrt{3}x],$$
$$p_y=N_pr^{n_p-1}\exp(-\zeta_pr)[\sqrt{3}y],$$
$$p_z=N_pr^{n_p-1}\exp(-\zeta_pr)[\sqrt{3}z],$$
$$N=(2\zeta)^{n+\frac{1}{2}}[4\pi(2n)!]^{-\frac{1}{2}}=N(\zeta,n). \tag{2}$$

The wave function of Eq. (1) depends parametrically on six quantities: n_s, ζ_s; $n_{s'}$, $\zeta_{s'}$; n_p, ζ_p.

The actual wave function of methane is not spherically symmetrical. It will have the spherical term of Eq. (1) as an important component, but it must contain additional terms which give tetrahedral symmetry to the electronic distribution. The most important of these are the following[15]:

$$\Phi_2=6^{-\frac{1}{2}}[(s\bar{s}s^*\bar{s}^*p_x\bar{d}_{yz}p_y\bar{p}_yp_z\bar{p}_z)+(s\bar{s}s^*\bar{s}^*d_{yz}\bar{p}_xp_y\bar{p}_yp_z\bar{p}_z)$$
$$+(s\bar{s}s^*\bar{s}^*p_x\bar{p}_xp_y\bar{d}_{zz}p_z\bar{p}_z)+(s\bar{s}s^*\bar{s}^*p_x\bar{p}_xd_{zz}\bar{p}_yp_z\bar{p}_z)$$
$$+(s\bar{s}s^*\bar{s}^*p_x\bar{p}_xp_y\bar{p}_yp_z\bar{d}_{xy})+(s\bar{s}s^*\bar{s}^*p_x\bar{p}_xp_y\bar{p}_yd_{xy}\bar{p}_z)], \tag{3}$$

$$\Phi_3=2^{-\frac{1}{2}}[(s\bar{s}s^*\bar{f}_{xyz}p_x\bar{p}_xp_y\bar{p}_yp_z\bar{p}_z)+(s\bar{s}f_{xyz}\bar{s}^*p_x\bar{p}_xp_y\bar{p}_yp_z\bar{p}_z)], \tag{4}$$

$$\Phi_4=6^{-\frac{1}{2}}[(s\bar{s}s^*\bar{s}^*p_x\bar{f}_{x(5z^2-3)}p_y\bar{p}_yp_z\bar{p}_z)$$
$$+\text{five other determinants}], \tag{5}$$

$$\Phi_5=6^{-\frac{1}{2}}[(s\bar{s}s^*\bar{s}^*p_x\bar{g}_{yz(7z^2-1)}p_y\bar{p}_yp_z\bar{p}_z)$$
$$+\text{five other determinants}]. \tag{6}$$

TABLE I. Wave functions for the integral-n spherical model of methane.[a-c]

R	1.90	2.00	2.0665	2.10
n_s	1.0000	1.0000	1.0000	1.0000
ζ_s	5.6280	5.6674	5.6882	5.6980
$n_{s'}$	2.0000	2.0000	2.0000	2.0000
$\zeta_{s'}$	1.5002	1.4793	1.4667	1.4609
n_p	2.0000	2.0000	2.0000	2.0000
ζ_p	1.3250	1.2852	1.2617	1.2501
E (total)	−39.4148	−39.4273	−39.4731	−39.4214
Q[d]	6.713	6.888	7.004	7.060

[a] Wave function of Eq. (1), integral n values assumed as listed.
[b] See text, footnote 13.
[c] All quantities subject to error in last digit listed.
[d] See text.

TABLE II. Wave functions for the nonintegral-n spherical model of methane.[a-c]

R	2.00	2.05	2.10
n_s	0.9865	0.9867	0.9868
ζ_s	5.5783	5.5940	5.6106
$n_{s'}$	2.1420	2.1429	2.1440
$\zeta_{s'}$	1.5638	1.5520	1.5401
n_p	1.6380	1.6390	1.6410
ζ_p	1.0760	1.0652	1.0542
E (total)	−39.5029	−39.5055	−39.5034
Q[d]	6.810	6.909	6.998

[a] Wave function of Eq. (1), n values determined variationally.
[b] See text, footnote 13.
[c] All quantities subject to error in last digit listed.
[d] See text.

TABLE III. Five-term wave functions for methane, at $R=2$.[a,b]

	Integral-n[c]	Nonintegral-n[d]
n_s	1.0000	0.9865
ζ_s	5.6714	5.5763
$n_{s'}$	2.0000	2.1420
$\zeta_{s'}$	1.4793	1.5641
n_p	2.0000	1.6380
ζ_p	1.2859	1.0767
n_d	5.0000	4.5310
ζ_d	2.3823	2.1948
n_f	8.0000	8.5000
ζ_f	3.9332	4.1761
$n_{f'}$	9.0000	9.0850
$\zeta_{f'}$	4.2068	4.2531
n_g	10.0000	9.3300
ζ_g	4.6600	4.3400
E (total)	−39.74120	−39.80386

[a] See text, footnote 13.
[b] All quantities subject to errors in last two digits listed.
[c] Wave function of Eq. (8), integral n values assumed as listed. See Tables IV and VI for linear parameters and matrix elements.
[d] Wave function of Eq. (8), n values determined variationally. See Tables V and VII for linear parameters and matrix elements.

[13] Unless otherwise indicated, all quantities in this paper are in atomic units: length in units of $a_0=0.52917\times10^{-8}$ cm, energies in units of $e^2/a_0=27.210$ ev, charges in units of e.

[14] This "atom puff" has the symmetry of the united atom but is energetically much more similar to the actual molecule than is the united atom itself. The considerable qualitative successes of "united atom" treatments of molecular structure may be due to these facts. An investigation exploiting the concept of the atom puff is planned.

[15] Group theory may be used to determine the neonlike configurations which mix under the tetrahedral symmetry. Thus f_{xyz} belongs to the representation A_1 of T_d, just like s and s'; d_{yz}, $f_{x(5z^2-3)}$ and $g_{yz(7z^2-1)}$ belong to the representation T_{2z}, just like p_z, etc.

TABLE IV. Integral-n wave functions for methane, at $R=2$.[a,b]

	Ψ_1	Ψ_2	Ψ_3	Ψ_4	Ψ_5
C_1	1.00000	0.89308	0.88097	0.87020	0.86725
C_2		0.44990	0.44072	0.44691	0.44256
C_3			0.17223	0.16875	0.16897
C_4				−0.12064	−0.12320
C_5					0.09105
E (total)	−39.4274	−39.6206	−39.6885	−39.7172	−39.7412

[a] Ψ_k is a k-term wave function of the form Eq. (8), with the linear coefficients given in this table and the nonlinear parameter values given in Table III.
[b] See text, footnote 13.

TABLE V. Nonintegral-n wave functions for methane, at $R=2$.[a,b]

	Ψ_1	Ψ_2	Ψ_3	Ψ_4	Ψ_5
C_1	1.00000	0.89869	0.88620	0.87567	0.87254
C_2		0.43859	0.42948	0.43618	0.43239
C_3			0.17379	0.17042	0.17064
C_4				−0.11793	−0.12049
C_5					0.08983
E (total)	−39.5029	−39.6844	−39.7535	−39.7809	−39.8039

[a] Ψ_k is a k-term wave function of the form Eq. (8), with the linear coefficients given in this table and the nonlinear parameter values given in Table III, last column.
[b] See text, footnote 13.

TABLE VI. Matrix elements for integral-n wave functions for methane, at $R=2$.[a,b]

i \ j	1	2	3	4	5
1	−39.427358	−0.38361370	−0.35426423	+0.17431664	−0.23142626
2		−38.859119	−0.16013209	+0.18796134	−0.08208041
3			−37.466431	+0.00000000	−0.06874010
4				−37.762440	+0.10342790
5					−36.870475

[a] Values of matrix elements of the spin-free Hamiltonian operator for methane, including nuclear-nuclear repulsions, between the component function of Eq. (8), for the parameter values in Table III, second column.
[b] See text, footnote 13.

TABLE VII. Matrix elements for nonintegral-n wave functions for methane, at $R=2$.[a,b]

i \ j	1	2	3	4	5
1	−39.502931	−0.37191616	−0.35845491	+0.17041535	−0.22337523
2		−38.922359	−0.15737498	+0.18655054	−0.08138629
3			−37.536463	+0.00000000	−0.06788628
4				−37.823899	+0.10255276
5					−36.976023

[a] Values of matrix elements of the spin-free Hamiltonian operator for methane, including nuclear-nuclear repulsions, between the component functions of Eq. (8), for the parameter values in Table III, last column.
[b] See text, footnote 13.

Here, for example,

$$d_{yz}=N_d r^{n_d-1}\exp(-\zeta_d r)[(15)^{\frac{1}{2}}(yz)],$$

$$f_{xyz}=N_f r^{n_f-1}\exp(-\zeta_f r)[(105)^{\frac{1}{2}}(xyz)],$$

$$f_{x(5x^2-3)}=N_f r^{n_f-1}\exp(-\zeta_f r)[\tfrac{1}{2}(7)^{\frac{1}{2}}\times(5x^2-3)],$$

$$g_{yz(7z^2-1)}=N_g r^{n_g-1}\exp(-\zeta_g r)[\tfrac{1}{2}(45)^{\frac{1}{2}}yz(7z^2-1)]. \quad (7)$$

These are Slater orbitals, also centered on the carbon, with parameters $n_d, \zeta_d; n_f, \zeta_f; n_{f'}, \zeta_{f'}; n_g, \zeta_g$. An improved wave function for the ground state of methane then is

$$\Psi=C_1\Phi_1+C_2\Phi_2+C_3\Phi_3+C_4\Phi_4+C_5\Phi_5. \quad (8)$$

This function contains four independent linear parameters, seven different principal quantum numbers n, and seven different orbital exponents ζ—18 independent parameters in all.

Determination of the best wave function for methane of the form of Eq. (1) or Eq. (8) requires minimization of the expectation value of the energy as a function

of the parameters, for given R. The energy formulas can be derived in the usual way.[2] Since the component one-electron wave functions have a common center, the only two-center integrals which enter are those representing attractions of electrons for protons. These too can be expressed in terms of one-center integrals, when use is made of expansions of all reciprocal electron-proton distances in spherical harmonics about the carbon nucleus. Indeed, the total potential energy of attraction of one electron for all nuclei can be written as follows:

$$V_{ne}(r,x,y,z)=-(6/r)+\sum_{l=0}^{\infty}A_l(r)\,T_l(x,y,z). \quad (9)$$

Here the quantities T_l are the successive tetrahedral harmonics, normalized to 4π, which belong to the totally symmetric representation A_1 of the tetrahedral group T_d[16]:

$$T_0(x,y,z)=T_s=1,$$

$$T_1(x,y,z)=T_p=0,$$

$$T_2(x,y,z)=T_d=0,$$

$$T_3(x,y,z)=T_f=(105)^{\frac{1}{2}}xyz=(105)^{\frac{1}{2}}\{f\},$$

$$T_4(x,y,z)=T_g=(5/4)(21)^{\frac{1}{2}}[x^4+y^4+z^4-(3/5)]$$
$$=(5/4)(21)^{\frac{1}{2}}\{g\},$$

$$T_5(x,y,z)=T_h=0,$$

$$T_6(x,y,z)=T_i=(231/8)(26)^{\frac{1}{2}}[x^2y^2z^2+(1/22)\{g\}$$
$$-(1/105)]=(231/8)(26)^{\frac{1}{2}}\{i\},$$

$$T_7(x,y,z)=T_j=(11/4)(1365)^{\frac{1}{2}}[\{f\}[x^4+y^4+z^4$$
$$-(5/11)]],$$

$$T_8(x,y,z)=T_k=(65/16)(561)^{\frac{1}{2}}[(x^8+y^8+z^8)$$
$$-(28/5)\{i\}-(210/243)\{g\}-(1/3)]. \quad (10)$$

Also,

$$A_0(r)=A_s=-(4/r_>),$$

$$A_3(r)=A_f=-(4/9)(45/7)^{\frac{1}{2}}(r_<^3/r_>^4),$$

$$A_4(r)=A_g=(4/9)(7/3)^{\frac{1}{2}}(r_<^4/r_>^5),$$

$$A_6(r)=A_i=-(4/9)(32/13)^{\frac{1}{2}}(r_<^6/r_>^7),$$

$$A_7(r)=A_j=(4/9)(91/45)^{\frac{1}{2}}(r_<^7/r_>^8),$$

$$A_8(r)=A_k=-(4/9)(11/51)^{\frac{1}{2}}(r_<^8/r_>^9), \quad (11)$$

where $r_<$ and $r_>$ are the lesser and greater of r and R. For the "spherical model" of Eq. (1), only the $l=0$ term of Eq. (9) contributes, and one has simply

$$V_{ne}(\text{spherical model})=-(6/r)-(4/r_>). \quad (12)$$

For the wave function of Eq. (8), on the other hand, terms up to $l=8$ contribute.

[16] See, for example, D. G. Bell, Revs. Modern Phys. **26**, 311 (1954).

The final energy formulas involve complete and incomplete gamma and beta functions of nonintegral arguments. These can be computed without difficulty on an electronic computer.[2] For the minimizations themselves, parabolic fittings of the energy surfaces in many-parameter space are convenient.[17] The entire calculations are performed on the IBM 650 at the Computation Center of Carnegie Institute of Technology.

III. RESULTS

The results obtained are presented in Tables I–VII.

Spherical Model

Table I gives, for several values of R, the best wave functions for methane of the form Eq. (1), subject to the restriction that the principal quantum numbers are integral: $n_s=1$, $n_{s'}=2$, $n_p=2$. Table II gives corresponding wave functions with the integral-n condition lifted.

Also included in Tables I and II are total energies (including nuclear-nuclear repulsions), and quantities Q which measure the total electronic charge contained within a sphere of radius R. Longuet-Higgins and Brown have shown[18] that in the spherical approximation for methane at the equilibrium R value, $Q=6.92$.

Five-Term Wave Functions

In Tables III–VII are given integral-n and nonintegral-n five-term wave functions for methane of the form Eq. (8), for $R=2$. The nonlinear parameters and total energies are given in Table III. In Tables IV and V are given the linear parameters, and in Tables VI and VII the matrix elements H_{ij}, for the final (best) choice of nonlinear parameters.

Some calculations also were performed for wave functions of this form for $R=2.05$ and $R=2.10$, though these were not done to sufficient precision to yield significant values for equilibrium distance and breathing frequency (see below).[19] Computed energies were, for the integral-n case, -39.736 and -39.726; for the nonintegral-n case, -39.803 and -39.797.

IV. DISCUSSION OF RESULTS

Helpful for an evaluation of the results is a comparison with calculations made by the same method on the neon atom, which methane of course becomes for

[17] The authors are grateful to Dr. Lawrence C. Snyder for furnishing a program for parabolic minimization.

[18] H. C. Longuet-Higgins and D. A. Brown, J. Inorg. & Nuclear Chem. **1**, 60 (1955).

[19] A notable result of these calculations is the considerable extent of "orbital following" observed in the parameters for the d, f, f', and g orbitals (which serve to represent part of the electronic distributions at the protons). As R changes from 2.00 to 2.05 to 2.10, the parameters n_g and n_g/ζ_g for example vary from 9.33 and 2.15 to 9.76 and 2.20 to 10.29 and 2.24.

TABLE VIII. Relationship between the wave function for methane and its united atom counterpart.[a]

Term type	$CH_4(R=2.0a_0)$ Coefficient[c]	$CH_4(R=2.0a_0)$ Energy increment[c]	Ne Coefficient	Ne Energy increment
$(s^2s^{*2}p^6)$	0.873	−39.503	1.00	−128.294[f]
$(s^2s^{*2}p^5d)$	0.432	−0.181	0	0
$(s^2s^*fp^6)$	0.171	−0.069	0	0
$(s^2s^{*2}p^5f')$	−0.120	−0.028	0	0
$(s^2s^{*2}p^5g)$	0.090	−0.025	0	0
Total computed energy		−39.804		−128.294
Experimental energy		−40.522[d,e]		−129.021[g]
Relativistic correction[b]		−0.012		−0.137
Net error		0.706[d]		0.590

[a] All energies in e^2/a_0 units.
[b] A. Fröman, Phys. Rev. **112**, 807 (1958).
[c] Wave function of Table V, last column.
[d] These values assume the heat of sublimation of carbon to be 169.58 kcal/mole (see footnote 20). The net error if the heat of sublimation of carbon is taken to be 125.00 kcal turns out to be 0.636.
[e] Calculated from spectroscopic data found in works cited in footnotes 21–23.
[f] From Saturno and Parr (footnote 3).
[g] Calculated from data found in Moore (see footnote 21).

$R=0$. Such a comparison is given in Table VIII.[20–23] This table shows that the errors in the best wave function obtained here for methane are comparable to those in the best $s^2s^{*2}p^6$ description of neon.[3] That is, the residual energy error of 0.71 a.u. is mainly correlation energy, and this is much the same as the corresponding quantity in neon. Another way to put this would be to say that if one assumed a constant "correlation plus orbital form" correction from neon to methane, one would obtain a computed energy for methane of −40.394 a.u., in error only 0.12 a.u.

TABLE IX. Stretching force constants and equilibrium CH internuclear distances in methane.[a]

Description	k	R_e
Integral-n spherical model[b]	1.71	2.016
Nonintegral-n spherical model[c]	1.84	2.052
Observed	1.30[d]	2.041[e]

[a] See text, footnote 13.
[b] From Table I.
[c] From Table II.
[d] From $k=16\pi^2m_H\omega^2c^2$, with $\omega=2916.5$ cm^{-1} (private communication from B. Stoicheff).
[e] From $R_e=1.093\times10^{-8}$ cm. [D. P. Stevenson and J. A. Ikers, Ann. Rev. Phys. Chem. **9**, 372 (1958)].

[20] L. Brewer and A. W. Searcy, Ann. Rev. Phys. Chem. **7**, 259 (1956).
[21] C. E. Moore, *Atomic Energy Levels* (Natl. Bur. Standards Circ. No. **467**, 1949).
[22] Rossini *et al.*, *Selected Values of Properties of Hydrocarbons and Related Compounds* (American Pet. Inst. Proj. 44, Pittsburgh, 1953), Vol. IV.
[23] Cohen, Crowe, and Dumond, *Fundamental Constants of Physics* (Interscience Publishers, Inc., New York, 1957), p. 265.

The implication about the heat of sublimation of carbon is that the higher value is favored, although certainly not proved, by the calculations. An actual proof could be obtained if a higher order of accuracy could be reached by calculations by this method (see the following).

The energy obtained by Bernal with a spherical model was −39.33 a.u.,[10] compared with the present −39.50 a.u. The calculation by Koide *et al.* included some nonspherically symmetric terms; it gave −39.64 a.u.,[11] compared with the present −39.80 a.u. The final result of Mills, −40.06 a.u., was much better than any

TABLE X. Comparisons among integral-n, nonintegral-n, and Mills' spherically symmetric wave functions for methane, for $R=2$.[a,b]

	Integral-n[c]	Nonintegral-n[d]	Mills'[e]
ϵ_{1s}	−11.14	−11.10	−11.04
ϵ_{2s}*	−0.8945	−0.9070	−0.8935
ϵ_{2p}	−0.4304	−0.4565	−0.4511
$F_0(1s1s)$	3.5421	3.5215	3.4887
$F_0(2s^*2s^*)$	0.5267	0.5275	0.5248
$F_0(2p2p)$	0.4668	0.4598	0.4618
$F_0(1s2s^*)$	0.7377	0.7322	0.7385
$F_0(1s2p)$	0.6406	0.6530	0.6558
$F_0(2s^*2p)$	0.4940	0.4907	0.4903
$G_0(1s2s^*)$	0.0356	0.0343	0.0408
$G_1(1s2p)$	0.0227	0.0344	0.0383
$G_1(2s^*2p)$	0.3286	0.3109	0.3040
E (total)	−39.43	−39.50	−39.38

[a] For definitions of symbols, see Mills.[12] All quantities are in e^2/a_0 units, at $R=2a_0$.
[b] See text, footnote 13.
[c] Wave function of Table I, present paper.
[d] Wave function of Table II, present paper.
[e] From Mills.[12]

of the other values, but for reasons discussed in the appendix it appears to be invalid.

Force constants and equilibrium CH distance predicted by quadratic fitting from the spherical model calculations are given in Table IX. These are satisfactory. Corresponding calculations for five-term wave functions would be expected to have given even better results.

The high n values in Table III require special comment. The ratio n/ζ for an orbital measures the average distance the electron is away from the carbon nucleus.[24] As would be expected, for the orbitals d, f, f', g this is close to 2, just the distance of the protons from the carbon nucleus. The quantity $1/n$ measures the half-width of the electron distribution.[20] For these orbitals this is quite small—these orbitals peak sharply at the protons. Such high n values appear unavoidable in expansions of molecular wave functions about one center.

V. CONCLUSIONS

The wave functions for methane in Table III probably are the best ones presently available for this molecule. They ought to be accurate enough to provide definitive answers to questions about the electronic distribution in the CH bond, although they may not be so good when they are used for calculation of properties such as the proton chemical shift in methane. These and related matters are under consideration and will be reported elsewhere.

This work generates optimism about the systematic application of one-center expansion methods to any molecule containing one heavy atom plus hydrogen atoms. The programming techniques here used for methane were elementary, and the electronic computer employed was of modest size, yet the results were good. Considerable further work is underway involving more advanced programming techniques and a larger computer. It is planned to treat, with an accuracy much surpassing that obtained in the present paper, many different properties of many molecules of the general type AH_n.

[24] Precisely, n/ζ is the most probable value of r, while $1/(2n+1)$ is the average square fractional deviation of r from its average value.

APPENDIX: COMPARISONS WITH THE WORK OF MILLS

In an interesting paper which provided important guides for the present work,[12] Mills has (a) solved numerically the Hartree-Fock equations for the spherical model or atom puff of Sec. II of the foregoing, and (b) estimated the effect of the four protons by a perturbation method. For the spherical model with $R=2$ he obtained a total energy of -39.38 a.u.; for the total energy including the correction for shape he found -40.06 a.u.

These results conflict with the present ones. The $R=2$ energies in Tables I and II are -39.43 and -39.50 a.u., and these only represent *approximations* to the Hartree-Fock solutions! Assuming that there are no mistakes in the present calculations, one concludes that there is a deficiency of the order of magnitude of 0.2 a.u. in Mills' energy. That the latter is not unlikely may be inferred from the detailed comparisons in Table X. It seems probable that the main discrepancy is in the 1s orbital, and that it was the errors inherent to the Hartree-Fock numerical procedures that produced the uncertainty of about 0.2 a.u. in the final total energy. (The presence of the proton sphere at $R=2$ may specially affect the sensitivity of the numerical procedures.)

The final 0.68 a.u. perturbation in the energy obtained by Mills appears to be an overestimate. In the present work the type of orbitals that appear in Mills' final wave function have been included and treated by a rigorous variational scheme, and an improvement of only 0.24 a.u. has been found. More important, Mills' result appears out of line with neon: too good to be true!

On the Reciprocal Relations of Onsager

*Bernard D. Coleman and Clifford Truesdell**

Mellon Institute, Pittsburgh, Pennsylvania

(Received December 18, 1959)

Given any linear relation between forces and fluxes in irreversible thermodynamics, it is shown that redefinition of forces and fluxes by linear combination yields a relation with symmetric matrix. The rate of production of entropy is unchanged by the redefinition. Thus, unless "forces" and "fluxes" are defined by some property more specific than mere occurrence in the expression for production of entropy, there is no content in the statement that the matrix of phenomenological coefficients is or is not symmetric.

CONSIDER a set of n "thermodynamical fluxes" J_i which are linear functions of n "thermodynamical forces" X_i:

$$J_i=\sum_{j=1}^{n}L_{ij}X_j. \tag{1}$$

The "reciprocity theorem of Onsager,"[1] in its most commonly accepted version,[2-4] states the following. *If* each flux J_i is the time derivative of a thermodynamic variable a_i,

$$J_i=\dot{a}_i, \tag{2}$$

if each a_i is an even function[5] of the velocities of the atoms constituting the system and enters into an equation of the form

$$S=\tfrac{1}{2}\sum_{i=1}^{n}\sum_{j=1}^{n}g_{ij}a_ia_j, \tag{3}$$

where S is the entropy of the system (to within a time-independent constant), and *if*, further, the forces X_j have been chosen so that

$$X_j=(\partial S/\partial a_j)=\sum_{i=1}^{n}g_{ij}a_i, \tag{4}$$

then, the matrix $\|L_{ij}\|$ of the phenomenological coefficients L_{ij} in Eq. (1) is symmetric; i.e.,

$$L_{ij}=L_{ji}, \tag{5}$$

for all pairs i, j.

It is assumed throughout this article that the thermodynamical fluxes are independently variable, i.e., free from constraints such as $\sum_i J_i=0$. Modifications necessary when fluxes and forces are redundant are discussed by Meixner[6] and by Hooyman and de Groot.[7]

Equation (3) yields the following expression for the time derivative of the entropy:

$$\dot{S}=\sum_{i=1}^{n}\sum_{j=1}^{n}g_{ij}\dot{a}_ia_j. \tag{6}$$

On comparing this expression with Eqs. (2) and (4), we see that in order for the fluxes J_i and the forces X_i in Eq. (1) to obey Eqs. (2)–(4) of the hypothesis of the reciprocity theorem of Onsager, it is *necessary* that

$$\dot{S}=\sum_{i=1}^{n}X_iJ_i. \tag{7}$$

Now, the fact that Eq. (7) follows from Eqs. (2)–(4) does not mean that the reciprocity theorem of Onsager implies the validity of Eq. (5) for all thermodynamical forces and fluxes which obeys Eqs. (1) and (7). For, even if we ignore the requirement that the fluxes be related to variables which are even functions of atomic velocities, Eqs. (1) and (7) are *not sufficient* for the validity of Eqs. (2)–(4). Merely to exhibit the bilinear form (7) for the production of entropy and to assume its entries J_i and X_i linearly related does not imply that the J_i are time derivatives of thermodynamic variables a_i or that the X_i are determined by Eq. (4). Although this point seems to have been realized by Casimir[2] in 1945, and although his work is mentioned in recent texts,[8,9] the recent literature[10] still abounds with indiscriminate selections of factors J_i and X_i in Eq. (7) on the basis, apparently, of physical intuition, with no reference to the requirements (2)–(4).

It is not the purpose of the present communication either to confirm or to criticize the Onsager reciprocity theorem itself, but rather to remark that the notion that Eqs. (1) and (7) imply Eq. (5) is self-contradictory.

* Visiting Lecturer at Mellon Institute, summer, 1959.

[1] L. Onsager, Phys. Rev. **37**, 405 (1931); **38**, 2265 (1931).

[2] H. B. Casimir, Revs. Modern Phys. **17**, 343 (1945).

[3] S. R. de Groot, *Thermodynamics of Irreversible Processes* (North-Holland Publishing Company, Amsterdam, 1951) Chap. I, Sec. 2, pp. 5–9.

[4] J. O. Hirschfelder, C. F. Curtiss, and R. B. Bird, *Molecular Theory of Gases and Liquids* (John Wiley & Sons, New York, 1954), Chap. 11, Sec. 2a, pp. 705–708.

[5] The modifications required when some of the a_i are odd functions of the velocities are given by Casimir (see footnote 2).

[6] J. Meixner, Ann. Physik (5) **43**, 244 (1943).

[7] G. J. Hooyman and S. R. de Groot, Physica **21**, 73 (1955).

[8] See de Groot (footnote 3), Chap. IV, Sec. 18, p. 41.

[9] See Hirschfelder *et al.* (footnote 4), p. 708, for an indirect reference.

[10] See the discussions in de Groot (footnote 3) of *ordinary diffusion* (Chap. VIII, Sec. 48) and the *Soret effect* (Chap. VIII, Sec. 49). The "Onsager reciprocal relations" derived in the discussion of *momentum transport* on page 710 of Hirschfelder *et al.* (footnote 4) have not been shown to be connected in any way with "microscopic reversibility"; of course, the relations derived there are long familiar consequences of the fact that the response of a fluid is the same for all observers.

Suppose that J_i and X_i are thermodynamical fluxes and forces which obey Eqs. (1), (7), and (5). We shall show that by linear combination of the J_i and X_i we can always construct new fluxes J_i' and forces X_i' which obey Eqs. (1) and (7),

$$J_i'=\sum_{j=1}^{n}L_{ij}'X_j', \tag{1'}$$

$$\sum_{i=1}^{n}X_i'J_i'=\sum_{i=1}^{n}X_iJ_i=\dot{S}, \tag{7'}$$

but yet have a *nonsymmetric* matrix $\| L_{ij}' \|$ of phenomenological coefficients L_{ij}'. Indeed, we can do this in an infinite number of ways. For, let $\| W_{ij} \|$ be *any* nonzero $n\times n$ skew matrix; i.e., let the components of $\| W_{ij} \|$ be such that for all pairs $i, j=1, 2\cdots n$,

$$W_{ij}=-W_{ji} \tag{8}$$

and for at least one such pair with $j\neq i$ let $W_{ij}\neq 0$. Consider the set of fluxes J_i' and forces X_i' defined as follows:

$$J_i'=J_i+\sum_{j=1}^{n}W_{ij}X_j \tag{9}$$

$$X_i'=X_i \tag{10}$$

for all $i, j=1\cdots n$. Then

$$\sum_{i=1}^{n}J_i'X_i'=\sum_{i=1}^{n}J_iX_i+\sum_{i=1}^{n}\sum_{j=1}^{n}W_{ij}X_jX_i. \tag{11}$$

The second term on the right in Eq. (11) is the trace of the product of a skew matrix $\| W_{ij} \|$ with a symmetric matrix $\| X_jX_i \|$, and hence, by a well-known theorem of algebra, is zero. Thus, the J_i' and X_i' obey Eq. (7'). Furthermore, our assumption that the X_i and J_i obey Eq. (1) and the definitions (9) and (10) yield

$$J_i'=\sum_{j=1}^{n}L_{ij}X_j+\sum_{j=1}^{n}W_{ij}X_j=\sum_{j=1}^{n}(L_{ij}+W_{ij})X_j'. \tag{12}$$

On comparing Eq. (12) with Eq. (1') we see that the J_i' and X_i' also obey Eq. (1'), with a matrix $\| L_{ij}' \|$ which is given by

$$\| L_{ij}' \|=\| L_{ij} \|+\| W_{ij} \|. \tag{13}$$

Since $\| L_{ij}' \|$ is the sum of a symmetric matrix $\| L_{ij} \|$ and a nonzero skew matrix $\| W_{ij} \|$, $\| L_{ij}' \|$ is nonsymmetric. Thus, for every choice of forces and fluxes which obey Eqs. (1), (7), and (5), there exist infinitely many choices of forces and fluxes which also obey Eqs. (1) and (7) but which do not obey Eq. (5).

The argument given in the foregoing is reversible in the following sense. Let J_i and X_i be thermodynamical fluxes and forces obeying Eqs. (1) and (7) but not Eq. (5). Then, the nonsymmetric matrix $\| L_{ij} \|$ has a unique decomposition into the sum of a symmetric matrix $\| D_{ij} \|$ and a nonzero skew matrix $\| W_{ij} \|$:

$$\| L_{ij} \|=\| D_{ij} \|+\| W_{ij} \|. \tag{14}$$

Let us define a new set of fluxes J_i^* and forces X_i^* as follows:

$$J_i^*=J_i-\sum_{j=1}^{n}W_{ij}X_j \tag{15}$$

$$X_i^*=X_i. \tag{16}$$

We have

$$\sum_{i=1}^{n}J_i^*X_i^*=\sum_{i=1}^{n}J_iX_i-\sum_{i=1}^{n}\sum_{j=1}^{n}W_{ij}X_jX_i=\sum_{i=1}^{n}J_iX_i;$$

i.e., the J_i^* and X_i^* obey Eq. (7). From the assumption that the J_i and X_i obey Eq. (1), and from Eqs. (15) and (16), we get

$$J_i^*=\sum_{j=1}^{n}L_{ij}X_j-\sum_{j=1}^{n}W_{ij}X_j=\sum_{j=1}^{n}(D_{ij}+W_{ij})X_j$$

$$-\sum_{j=1}^{n}W_{ij}X_j=\sum_{j=1}^{n}D_{ij}X_j^*;$$

i.e., the fluxes J_i^* are related to the forces X_i^* through Eq. (1), but with a symmetric matrix $\| D_{ij} \|$ of phenomenological coefficients. Thus, corresponding to any linear phenomenological relation with a nonsymmetric matrix it is possible, by a mere linear combination of forces and fluxes, to find another yielding the same production of entropy and having a symmetric matrix.

Since any linear phenomenological relation may be replaced by an equivalent one with a symmetric matrix, it might be thought that a phenomenological meaning for Onsager's theorem could be found in some special property of the symmetric case. This is not so. Meixner[11] has shown that if Eqs. (7), (1), and (5) hold for one set of fluxes J_i and forces X_i, then there exist infinitely many other choices of fluxes $J_i^{\$}$ and forces $X_i^{\$}$ also satisfying Eqs. (7), (1), and (5). To find $J_i^{\$}$ and $X_i^{\$}$ with this property one may use the equations

$$X_i^{\$}=\sum_{k=1}^{n}A_{ik}X_k \tag{17}$$

$$J_i^{\$}=\sum_{k=1}^{n}\bar{A}_{ik}^{-1}J_k, \tag{18}$$

where $\| A_{ik} \|$ is an arbitrary invertible (nonsingular)

[11] See Meixner (footnote 6). For a review of this matter, see Sec. 8 of J. Meixner and H. G. Reik, "Thermodynamik der irreversiblen Prozesse," *Handbuch der Physik* (Springer-Verlag, Berlin, 1959), Vol. 3, Part 2.

matrix and $\| \tilde{A}_{ik}^{-1} \| = \| A_{ki} \|^{-1}$. Indeed,

$$X_i^* J_i^* = \sum_{k=1}^{n} \sum_{l=1}^{n} A_{ik} X_k \tilde{A}_{il}^{-1} J_l = \sum_{k=1}^{n} \sum_{l=1}^{n} \delta_{kl} X_k J_l$$

$$= \sum_{k=1}^{n} X_k J_k,$$

and if the J_i, X_i obey Eq. (1), then so do the X_i^*, J_i^*, with a matrix of phenomenological coefficients L_{ij}^* which is the solution of

$$\sum_{l=1}^{n} \sum_{k=1}^{n} \tilde{A}_{ik} L_{kl}^* A_{lj} = L_{ij};$$

i.e.,

$$\| L_{ij}^* \| = \| \tilde{A}_{ik} \|^{-1} \| L_{kl} \| \, \| A_{lj} \|^{-1}. \tag{19}$$

This congruence transformation clearly preserves the symmetry of $\| L_{ik} \|$.

If the matrix $\| L_{ij} \|$ in Eq. (1) is invertible, as is usually assumed, then Eqs. (9) and (10), and also (15) and (16), may be regarded as representing *linear transformations* carried out separately on the fluxes and forces, rather than as defining new forces and fluxes by joint linear combinations of the old. For example, Eqs. (9) and (10) may be written

$$J_i' = \sum_{k=1}^{n} B_{ik} J_k \tag{9'}$$

$$X_i' = \sum_{k=1}^{n} C_{ik} X_k, \tag{10'}$$

where

$$\| B_{ik} \| = \| \delta_{ik} \| + \| W_{ij} \| \, \| L_{jk} \|^{-1} \tag{20}$$

and

$$\| C_{ik} \| = \| \delta_{ik} \|. \tag{21}$$

Of course, Eqs. (20) and (21) make the linear transformations given by Eqs. (9′) and (10′) of a different kind from those given by Eqs. (17) and (18), and this is why Eqs. (9′) and (10′) are able to destroy the symmetry of $\| L_{ij}' \|$. It is easy to show that in order for the linear transformations of the form shown in Eqs. (9′) and (10′) to be compatible with Eqs. (2)–(4), with S being kept invariant, it is necessary and sufficient that the matrices $\| B_{ik} \|$ and $\| C_{ik} \|$ be related as follows:

$$\| B_{ik} \| = \| C_{ki} \|^{-1}. \tag{22}$$

In other words, if we take Eqs. (1)–(4) as the hypothesis of Onsager's theorem, then the choice of the fluxes and forces is greatly limited, and, in fact, if we change the forces and fluxes by linear transformations, the transformations must be of the type discussed by Meixner and exhibited in Eqs. (17) and (18). Such transformations preserve the symmetry of $\| L_{ik} \|$. Hence, a reciprocity theorem based on Eqs. (1)–(4) does not suffer from the logical defects of one based on Eqs. (1) and (7).

In summary, it seems, in phenomenological theories based on Eqs. (7) and (1) alone, there is no content in the statement that $\| L_{ij} \|$ is or is not symmetric. Of the two alternative phenomenological treatments of Onsager's theorem to be found in the current literature, only in that based upon Eqs. (1)–(4) may any physical interpretation be found. In many applications, such as the theory of diffusion, there is no evidence that Eqs. (2) and (4) are satisfied. It is notorious that phenomenological theories of various kinds easily yield a relation of the type (7), while relations of the type (2)–(4) are more difficult to establish. Of course, it is possible that some other choice of fluxes might also lead to Eq. (5). But until the forces and fluxes in any particular case, are *physically identified* by some property more specific than their mere entry into the bilinear form (7), application of Onsager's theorem is precarious.

We close with some remarks on "minimum dissipation principles." Consider a quadratic form Φ characterized by a symmetric matrix $\frac{1}{2}R_{ij}$:

$$\Phi(J_k) = \tfrac{1}{2} \sum_{j=1}^{n} \sum_{i=1}^{n} R_{ij} J_i J_j.$$

Of course, *any* quadratic form can be characterized in such a manner by a *symmetric* matrix. We now note that the statement

$$\dot{S} - \Phi(J_k) = \text{extremum}, \tag{23}$$

i.e.,

$$\delta\{\dot{S} - \Phi(J_k)\} = 0, \tag{24}$$

has no meaning until the manner in which $\dot{S}$ is assumed to depend on the variables J_k is specified. If, in particular, we agree to take $\dot{S}$ as given by Eq. (7) and also to hold the forces X_i constant in computing the variation, then Eq. (24) is equivalent to

$$\sum_{i=1}^{n} \{(\delta J_i)(X_i - \sum_{j=1}^{n} R_{ij} J_j)\} = 0. \tag{25}$$

Equation (25) is equivalent in turn to

$$X_i = \sum_{j=1}^{n} R_{ij} J_j. \tag{26}$$

Now, if we add the usual assumption that R_{ij} is nonsingular, Eq. (26) is equivalent to Eqs. (1) and (5). On the other hand, if we assume that $\dot{S}$ is given by Eq. (6), with $\dot{a}_i = J_i$, and if in Eq. (24) we agree to hold $\sum_i g_{ij} a_i$ constant in computing the variations, then it can easily be shown that Eq. (24) is equivalent to the assertion that Eqs. (1)–(4) imply Eq. (5).

It has just been shown that two different variational principles arising from Eq. (24) lead to a linear phenomenological relation with a symmetric matrix. The

latter principle is precisely equivalent to the formulation in terms of conjugate variables, mentioned at the beginning of the paper. The former, which includes the latter as a special case, is precisely equivalent to the bare assertion of symmetry, shown before to be meaningless unless the variables are identified by some property beyond their mere entry into the bilinear form (7). Thus the principles of minimum dissipation do not in themselves offer any basis for symmetry beyond whatever is present in a direct treatment.

We remark also that the variational principle based on Eqs. (24) and (7) alone is really an infinite family of principles. For each different possible choice of forces and fluxes in Eq. (7), a different set of quantities is held constant in the variations. This fact makes the arbitrariness of the result still more plain and casts further light upon the need for physical identification of forces and fluxes is a self-consistent statement of "Onsager relations" is to be found.[12]

[12] *Note added in proof.* There is earlier literature on the difficulties noted here. In attempt to demonstrate "an error in the calculation of Meixner," J. E. Verschaffelt, Bull. Cl. Sci. Acad. R. Belg. **37**, 853 (1951) gave an example of a linear transformation preserving the production of entropy but destroying the symmetry of linear phenomenological relations. R. O. Davies, Physica **18**, 182 (1952), in an attempt to answer Verschaffelt, exhibited a general class of such transformations, including as a special case our Eqs. (20) and (21), but claimed that those destroying the symmetry "can be of no physical importance." Hooyman, de Groot, and Mazur, Physica **21**, 360 (1955) deny Davies' physical argument but try to straighten the matter out by formulating in more general terms a rule such as Eq. (4) of the present paper for defining the force conjugate to a given flux. Their method is open to the objection raised above. In concrete situations, such as diffusion, to which "irreversible thermodynamics" is said to apply, the variables actually used have never been shown to obey their Eq. (17). Without that equation, their analysis falls back to Meixner's.

THE JOURNAL OF CHEMICAL PHYSICS VOLUME 33, NUMBER 1 JULY, 1960

Quantum Yield for Energy Transfer by Resonance

AADNE ORE

Physics Institute, University of Oslo, Blindern, Norway

(Received January 18, 1960)

The theoretical prediction of quantum yields for electric dipole-dipole energy transfer by resonance is discussed. The common approximation which neglects transfers from each donor to all but the nearest acceptor is extended so as to include transfers to the second-nearest acceptor and, in the limit of very high acceptor concentration, to the third and fourth as well. The total quantum yield and the fractional yields due to transfers to the individual categories of nearest acceptors are evaluated, and the merits of the various approximations are discussed quantitatively.

THE present theoretical discussion concerns the phenomenon of transfer of electronic excitation energy by the mechanism of electrodynamic resonance. The initially excited energy donors (sensitizers) and the potential acceptors (activators) may be atoms or molecules distributed throughout a given medium.

Mathematical discussions in this field are frequently based on the simplifying assumption that one arrives at essentially correct quantitative predictions of observable effects if one considers energy transfer from each donor to its nearest acceptor only. This "first approximation" is, naturally, a satisfactory one when applied to systems in which the acceptor concentration is very low.[1] In the case of concentration depolarization of fluorescence, a slight modification of the approximation in question seems to justify an extension of its applicability to the so-called critical concentration range.[2] In the theory of resonance transfer of energy in crystals, moreover, first-order transfer yields have been considered adequate[3–5] on the ground that the rapid decrease of the transfer probability with increasing interparticle separation would render improbable transfers to all but nearest acceptors.[4] The assumed random distribution of energy acceptors makes this argument not entirely convincing, however. The importance of transfers to other acceptors will be demonstrated in the following.

We shall discuss quantitatively the merits of the first approximation and of the next one in which the possibility of transfer to the second-nearest acceptor is taken into account. In the limit of very high acceptor concentration we shall include transfers to up to four nearest acceptors (A_1, A_2, A_3, and A_4) as counted from each donor. In each case we shall, in addition, evaluate the individual contributions to the average total

[1] Th. Förster, (a) Ann. Physik **2**, 55 (1948); (b) *Fluoreszenz organischer Verbindungen* (Vandenhoeck and Ruprecht, Göttingen, 1951), pp. 172–180.

[2] A. Ore, J. Chem. Phys. **31**, 442 (1959).

[3] D. L. Dexter, J. Chem. Phys. **21**, 836 (1953).

[4] D. L. Dexter and J. H. Schulman, J. Chem. Phys. **22**, 1063 (1954).

[5] S. C. Ganguly and N. K. Chaudhury, Revs. Modern Phys. **31**, 990 (1959).

transfer yield which come from transfers to the respective A_i's.

The mode of transfer of electronic excitation energy to be considered in the following is that of radiationless transfer arising from the overlapping of the "near-zone" electric fields of the two particles involved in each individual transfer process. The particles may be thought of as being, say, molecules in liquid solution or impurities in a crystal. We shall assume, furthermore, that the only interaction of importance is that which stems from the electric dipole term in the standard series expansion[3] of the interaction energy about the interparticle separation R. This assumption implies that the deexcitation of the energy donor and the simultaneous excitation of the acceptor both are allowed (electric dipole) transitions. This type of radiationless energy transfer by resonance is ordinarily the only important one. Detailed quantum mechanical discussions of this mechanism have been presented by Förster[1] and Dexter.[3] The latter has discussed also the importance of higher-order interactions and of exchange effects.

These authors have derived the detailed expression for the probability per second of transfer, which depends on the overlap of the emission and absorption bands of the interacting particles, on the intrinsic or radiative life time of the sensitizer, as well as on the index of refraction of the medium. Again, the dipole-dipole transfer probability is found to be inversely proportional to the interparticle separation R to the sixth power, which reflects the fact that the same interaction energy gives rise also to the familiar van der Waals force.

The dependence of the transfer probability on the interparticle separation is actually all that is needed for carrying out the discussion announced in the foregoing. For our purpose it proves convenient to write the probability of transfer per second (F_i) from a given donor D to a specified acceptor A_i, separated from the former by a distance R_i, in the following manner:

$$F_i = w v_0^2 / v_i^2; \quad v_1 \equiv \tfrac{4}{3}\pi R_i^3; \text{ and } v_0 \equiv \tfrac{4}{3}\pi R_0^3; \qquad (1)$$

and let the parameter w stand for the probability of deexcitation of D per sec by processes other than resonance transfer to A's. The parameter R_0 then must stand for Förster's "critical separation" at which F_i becomes equal to w.[1b,6] (Our way of expressing F_i is a purely formal one. This quantity does not depend on, say, the probability of thermal deexcitation of the sensitizer, which affects the value of both w *and* R_0 in such a way as to leave F_i unchanged.)

We shall follow the usual,[1–5] more or less accurate,[6] procedure of utilizing for the transfer probability its average value for all mutual orientations of the interacting particles. We shall, similarly,[1–5] proceed as if the distribution of particles were truly random and without restrictions put on the possible values of R_i. In his theory of sensitized luminescence in solids, Dexter[3] discusses the correction arising from the impossibility of an A occupying the D site, which in the limit of "infinite" concentration would be an important consideration, as would all details of the discreteness of the lattice. Those numerical results in the following which refer to very high concentration should, therefore, be taken with a grain of salt.

The acceptor concentration, expressed in terms of the average number of A's per unit volume, will be denoted by c. Following Förster[1b,6] we define the "critical concentration" c_0 as that value of c which renders equal to unity the average number of acceptors within a volume of magnitude v_0, e.g., within a sphere of radius R_0. The symbol γ will be used to denote the ratio of the actual concentration to the critical one. Thus, $\gamma = c/c_0 = cv_0$.[7] (It might be mentioned that several other, mutually different, definitions of a "critical concentration" do exist.[1a,3,8])

Discussions on energy transfer by resonance within large assemblages of particles usually concern transfer from photoexcited donors and frequently aim at predicting the quantum yield of transfer under the assumption that energy transfer takes place only from D's to A's. We shall denote by η this yield which is an average taken over all donors or, which amounts to the same, over all conceivable configurations of acceptors relative to a single donor. The symbol $\eta_{(n)}$ will, similarly, be used for the approximate value of this yield which obtains in the nth approximation, in which no attention is paid to the possibility of transfer from each donor to acceptors other than the n nearest to it. The partial yields of which $\eta_{(n)}$ may be considered to consist, and which stem from transfers to the nearest acceptors (A_1's) only, to the second-nearest (A_2's) only, and so on, respectively, will be denoted $\eta_{1(n)}, \eta_{2(n)}, \cdots, \eta_{n(n)}$, respectively:

$$\eta_{(n)} = \sum_i \eta_{i(n)}. \qquad (2)$$

In this equation, as elsewhere in this article, the summation index runs from $i=1$ to $i=n$.

Introducing $x_i \equiv cv_i$ we have, in accordance with Eq. (1),

$$\eta_{(n)} = \langle (\sum_i F_i)/(w + \sum_i F_i) \rangle_{Av}$$
$$= \gamma^2 \langle (\sum_i x_i^{-2})/(1+\gamma^2 \sum_i x_i^{-2}) \rangle_{Av}. \qquad (3)$$

For our random distribution of acceptor particles the probability of the various conceivable configurations of acceptors around a donor is obtainable from Poisson statistics. The probability of finding simultaneously the nearest potential acceptor within a spheri-

[6] Th. Förster, Discussions Faraday Soc., No. **27**, 7 (1959).

[7] The present usage of the symbol γ agrees with the notation of references 1(b) and 2. The corresponding quantity, which Dexter names reduced concentration, is in references 3–5, denoted by y.

[8] Th. Förster, Z. Naturforsch. **4a**, 321 (1949).

TABLE I. Calculated values of the total and fractional quantum yields for energy transfer by resonance at various concentrations of acceptors.

γ	0.1	0.2	0.3	0.4	0.5	0.55	0.6	0.65	1.0	2.0	10.0
$\eta_{(1)}$	0.129	0.227	0.307	0.374	0.430	0.456	0.479	0.501	0.621	0.798	0.982
$\eta_{(2)}$	0.137	0.244	0.332	0.404	0.465	0.493	0.518	0.541	0.666	0.834	0.988
$\eta_{1(2)}$	0.126	0.218	0.290	0.349	0.397	0.418	0.437	0.455	0.549	0.672	0.777
$\eta_{2(2)}$ (%)	7.8	10.7	12.5	13.8	14.8	15.2	15.5	15.9	17.5	19.4	21.4
η	0.143	0.260	0.358	0.439	0.507	0.538	0.565	0.591	0.724	0.886	0.994

cal shell of radius R_1 and of thickness dR_1, the next acceptor within dR_2 at a distance R_2 from the donor, and so on, equals

$$\exp(-x_1)dx_1\cdot\exp[-(x_2-x_1)]dx_2\cdots \times\exp[-(x_n-x_{n-1})]dx_n = \exp(-x_n)dx_1dx_2\cdots dx_n.$$

Equation (3), therefore, amounts to

$$\eta_{(n)}=\gamma^2\int[(\sum_i x_i^{-2})/(1+\gamma^2\sum_i x_i^{-2}) \times\exp(-x_n)dx_1dx_2\cdots dx_n, \quad 0\leq x_1\leq x_2\leq\cdots\leq x_n\leq\infty. \quad (4)$$

The corresponding expression for $\eta_{i(n)}$ is seen to result if one omits the summation symbol in the numerator of the integrand in Eq. (4). (The rapid decrease of the transfer probability F_i with increasing donor acceptor separation R_i justifies the introduction of the infinite upper limit of integration.)

For $n=1$ one obtains from Eq. (4) the well-known first-approximation expression for the total yield[2-5]:

$$\eta_{(1)}=\eta_{1(1)}=\gamma[\mathrm{Ci}(\gamma)\sin\gamma-\mathrm{Si}(\gamma)\cos\gamma+\tfrac{1}{2}\pi\cos\gamma], \quad (5)$$

where Ci and Si are the cosine- and sine-integral functions. Plots of this first-order yield vs the reduced concentration $\gamma=c/c_0$ may be found elsewhere.[3-5] A tabular representation of $\eta_{(1)}$ is more suitable to our purpose, however, and is contained in Table I.

The next approximation $\eta_{(2)}$ to the total yield for transfer is given by Eq. (4) for n equal to two. The respective integrals which yield the numerical values of $\eta_{(2)}$ which are included in the same table can be evaluated by the performing of a simple single integration followed by a numerical integration. Either of the fractional yields $\eta_{1(2)}$ and $\eta_{2(2)}$, which add up to $\eta_{(2)}$, is obtainable in a similar fashion. With the discussion to follow in mind, we present, also in Table I, numerical values of $\eta_{1(2)}$, while $\eta_{2(2)}$ is expressed in percent of the total second-approximation yield $\eta_{(2)}$.

The bottom row of Table I represents the function

$$\eta=\pi^{\frac{1}{2}}q\exp(x^2)[1-\phi(q)], \quad (6)$$

where $q\equiv\frac{1}{2}\pi^{\frac{1}{2}}\gamma$ and $\phi(q)\equiv$ the error integral, which follows[6] from Förster's theory of quenching of fluorescence[8] in which attention is paid to the possibility of energy transfer to any acceptor.[9] The formula was obtained via a derivation of the decay rate of the excited sensitizers.

It is readily found that for very large acceptor concentration, $\gamma=c/c_0\gg1$, simple integrations suffice for the evaluation of each fractional yield for values of n up to $n=3$. For $n=4$ an additional numerical integration is found to be required. In this way one arrives at the values presented in Table II.

It is seen from this table that the asymptotic values obtained in each approximation add up to unity, which is the correct asymptotic value of the total quantum yield for energy transfer in the mathematical limit of infinitely high concentration of acceptors. The first two terms in the series expansion of the right-hand side of Eq. (4) are seen to be

$$\eta_{(n)}\sim1-a_{(n)}/\gamma^2, \qquad \gamma\gg1, \quad (7)$$

which agrees as to form with the asymptotic expression as obtained from Eq. (6). The mathematical expression for the coefficient $a_{(n)}$ in Eq. (7) is readily shown to be equivalent to $n(n+1)$ times the asymptotic value of the fractional yield $\eta_{n(n)}$. Numerical values of $a_{(n)}$ are presented in Table III, again as obtained in the first four approximations.

DISCUSSION

One of the facts borne out by Table I is that at least as much as about 10–20% of all the resonance transfers of energy from donors to acceptors take place, on the average, to acceptors beyond the one which lies closest to each respective donor. This is true at acceptor concentrations covered by the table, i.e., for concentrations from about one-tenth up to about ten times the

TABLE II. Calculated asymptotic values of the fractional quantum yields for energy transfer at very high acceptor concentration.

n	1	2	3	4
$\eta_{1(n)}$	1	0.785	0.726	0.698
$\eta_{2(n)}$		0.215	0.186	0.173
$\eta_{3(n)}$			0.089	0.081
$\eta_{4(n)}$				0.048

[9] For similar theories see M. D. Galanin, J. Exptl. Theoret. Phys. (U. S. S. R.) **28**, 485 (1955), English translation in Soviet Phys. JETP **1**, 2317 (1955); and V. V. Antonov-Romanski and M. D. Galanin, Optika i Spektroskopika **3**, 389 (1957).

TABLE III. Approximate values of the coefficient a occurring in the asymptotic expression for the total quantum yield for transfer.

n	1	2	3	4
$a_{(n)}$	2.0	1.29	1.06	0.95

critical concentration. At very low concentrations almost all transfers will, naturally, take place to nearest acceptors only. At very high concentrations at least about 30% go to other acceptors (cf. Table II).

Table II demonstrates, furthermore, that the approximate values of the fractional yields for transfer to the nearest and to the next-nearest acceptors decrease as one passes from one approximation to the next. The values contained in Table II refer to the extreme case of infinitely large acceptor concentration. They are such as to support the conclusion, however, that for moderate concentrations, at which transfers to relatively more distant acceptors are less probable, the correct percent transfers to nearest and to next nearest acceptors are roughly as obtained in the second approximation (Table I).

In view of the rather large fraction of transfers to second-nearest acceptors implied by the second approximation it might appear surprising that the corresponding approximate values of the total yield exceed by only about 8% or less (cf. Table I) that obtained in the common first approximation. In this context it might be worth pointing out, however, that the first-approximation yield $\eta_{(1)}$ does not represent the true fractional yield for transfer to nearest acceptors (A_1's). The evaluation of $\eta_{(1)}$ as the average of $F_1/(w+F_1)$ implies, to be sure, that one is counting transfers to the A_1's as the only ones which contribute to the transfer yield. This is so because F_1 is the only transfer probability present in the numerator [cf. Eq. (3)]. At the same time one is, however, partly compensating for the effect of this neglect of contributions to the yield from transfers to other A_1's. Thus, the other F_i's have been omitted from the denominator as well, which means that the corresponding modes of deexcitation of the donors have not been included among the *competing* modes of deexcitation for each donor.

Table I shows that $\eta_{(1)} \geq \eta_{1(2)}$. Already the second approximation suffices, therefore, to demonstrate that $\eta_{(1)}$ is a better approximation to the true total yield than would be the true fractional yield for transfer to A_1's only, the correct value of which lies below $\eta_{1(2)}$ (cf. Table II).

Similarly, the value of the total yield $\eta_{(2)}$ obtained in the second approximation exceeds the sum of the true fractional yields for transfer to A_1's and A_2's. It is not surprising, therefore, that the maximum deviation of $\eta_{(2)}$ from η is less than 10%, as shown by Table I.

Dexter[3] defined his "critical concentration" as that concentration for which the transfer yield amounts to one-half. Utilizing the expression (5) he arrived at the corresponding value of $\gamma=0.65$ (cf. Table I). We see from Table I that this value should be reduced to roughly $\gamma=0.56$ or to $\gamma=0.49$, i.e., by about 14% or by 25%, if we go to the next approximation or if we utilize formula (6), respectively.[10]

As we have just seen, the evaluation of that particular concentration at which the yield equals one-half reveals greater relative differences between the merits of the various procedures than did the evaluation of the yield itself at any concentration. Table III shows, furthermore, that the coefficient of the second term in the asymtotic expression (7) is an even more sensitive quantity. The value of $a_{(1)}=2$ is the first-approximation value already given by Dexter and Schulman.[4] Even when going from the third to the fourth approximation we find that the value of this coefficient is lowered by as much as 10%. The value of $a_{(4)}=0.95$, however, is still well above the value of $a=2/\pi=0.64$ which is that predicted by Eq. (6).

ACKNOWLEDGMENT

The work here reported was supported by a grant from A/S Norsk Varekrigsforsikrings Fond.

[10] It should be noted that the value of $\gamma=0.49$ as that for which the yield amounts to one-half may need appreciable corrections depending, in particular, on the extent to which Brownian movements are permitted by the physical state of the medium. The utilization of the orientational average of the transfer probability F_i introduces an inaccuracy, particularly when one deals with resonance transfer in crystals.

THE JOURNAL OF CHEMICAL PHYSICS VOLUME 33, NUMBER 1 JULY, 1960

Thermodynamic Properties of Unipositive Gaseous Elemental Ions

JOHN W. GREEN, DUNCAN E. POLAND, AND JOHN L. MARGRAVE

Department of Chemistry, University of Wisconsin, Madison, Wisconsin

(Received July 9, 1959)

Thermodynamic properties of unipositive gaseous elemental ions were calculated from available energy level data for a range of temperatures from 100° to 50 000°K.

THE currently widespread interest in plasmas, rocket propulsion reactions, and other high-temperature systems in which gaseous ions are of importance, makes desirable a comprehensive tabulation of the thermodynamic functions of ions over an extended range of temperatures. We have compiled such tables for those singly ionized elements whose energy levels have been tabulated by the National Bureau of Standards,[1] considering the ions as ideal monatomic gases. These tables include the free energy function, the heat content function, the heat capacity at constant pressure, and the entropy of these ions for a range of temperatures from 100° to 10 000°K in increments of 100 deg, and in increments of 1000 deg from 10 000° to 50 000°K.[2]

Values for $(F_T^\circ - H_0^\circ)/T$ and $(H_T^\circ - H_0^\circ)/T$ for a few selected temperatures in the range from 298.15° to 10 000°K are presented in Tables I and II, respectively. Additional values for temperatures to 50 000°K are presented in Tables III and IV. These functions were chosen because of their particular utility in high-temperature calculations. Here F_T° is the free energy and H_T° is the heat content at the absolute temperature T. The superscript indicates the functions are referred to the conditions of an ideal gas at 1 atm pressure. S_T° and C_P° may be derived if needed.

The calculations were made using well-known equations which are derived and discussed in texts on statistical thermodynamics.[3] For the purposes of our computation these equations took the form,

$$-(F_T^\circ - H_0^\circ)/T = \tfrac{5}{2}R\ln T + \tfrac{3}{2}R\ln M + R\ln\sum_i Q_i - 7.28353$$

$$(H_T^\circ - H_0^\circ)/T = \tfrac{5}{2}R + (R/T)\sum_i \beta_i Q_i / \sum_i Q_i$$

$$S_T^\circ = -(F_T^\circ - H_0^\circ)/T + (H_T^\circ - H_0^\circ)/T$$

$$C_P^\circ = \tfrac{5}{2}R + (R/T^2)\left[\left(\sum_i \beta_i^2 Q_i / \sum_i Q_i\right) - \left(\sum_i \beta_i Q_i / \sum_i Q_i\right)^2\right],$$

where T = temperature in deg K; M = the chemical scale atomic weight of the ion in grams; $R = 1.98726$ cal mole^{-1} deg^{-1} [4]; $\beta_i = hc\omega_i/k$, ω_i = the energy in cm^{-1} of the ith energy level above the ground level; $hc/k = 1.43880$ cm deg [4]; $Q_i = g_i \exp(-\beta_i/T)$, g_i being the degeneracy $(2J+1)$ of the ith energy level.

The masses used were taken from the last report of the American Chemical Society[5] with the exception of the values for Tc, Rn, and Ra, which were taken as 99, 222, and 226.05, respectively.

The calculations were made on an IBM type 650 MDDPM at the University of Wisconsin's Numerical Analysis Laboratory carrying the equivalent of eight significant figures. However, the energy levels were rounded to five significant figures and were automatically selected by the program so that only those levels which gave an exponent greater than negative 20 at a particular temperature were summed in the calculations. Where values for states were missing in the NBS tabulation, appropriate values were estimated. The number of such values was always a minor fraction of the total number of states summed in the calculation and thus hardly affects the rounded answers presented here.

For this publication the results were taken from the 650 printing and were rounded to five figures.

ACKNOWLEDGMENTS

The authors gratefully acknowledge the aid and patience of Eugene Albright of the Numerical Analysis Laboratory, and the financial assistance of the Wisconsin Alumni Research Foundation, the U.S. Air Force through the Wright Air Development Division, and E. I. du Pont de Nemours, Inc.

[1] C. E. Moore, Natl. Bur. Standards, Circ. No. 467, I (1949); II (1952); III (1957).

[2] A complete tabulation of thermodynamic data for +1, +2, +3, and +4 ions is available as Tech. Note WADC TN 59-420, Wright Air Development Center.

[3] For example, see J. E. Mayer and M. G. Mayer, *Statistical Mechanics* (John Wiley & Sons, Inc., New York, 1940).

[4] E. R. Cohen, J. N. M. Dumond, T. W. Layton, and J. S. Rollett, Revs. Modern Phys. **27**, 363 (1955).

[5] E. Wichers, J. Am. Chem. Soc. **80**, 4121 (1958).

TABLE I. $(F_T^\circ - H_0^\circ)/T$ in cal mole^{-1} deg^{-1}.

Z	Element	298.15°K	1000°K	2000°K	3000°K	4000°K	5000°K	6000°K	7000°K	8000°K	9000°K	10 000°K
2	He	26.535	32.547	35.991	38.005	39.435	40.543	41.449	42.215	42.878	43.463	43.987
3	Li	26.798	32.810	36.254	38.268	39.697	40.806	41.712	42.478	43.141	43.726	44.250
4	Be	28.954	34.967	38.410	40.425	41.854	42.963	43.871	44.643	45.317	45.919	46.466
5	B	28.122	34.134	37.578	39.592	41.021	42.130	43.038	43.810	44.486	45.095	45.655
6	C	31.606	37.886	41.389	43.424	44.863	45.978	46.887	47.657	48.323	48.913	49.442
7	N	32.459	39.020	42.587	44.644	46.099	47.229	48.158	48.949	49.640	50.254	50.807
8	O	32.043	38.055	41.499	43.513	44.943	46.053	46.965	47.743	48.427	49.043	49.605
9	F	33.248	39.770	43.400	45.485	46.951	48.084	49.010	49.795	50.477	51.082	51.627
10	Ne	32.758	39.046	42.689	44.792	46.271	47.411	48.338	49.120	49.795	50.390	50.921
11	Na	30.368	36.381	39.824	41.839	43.268	44.377	45.282	46.048	46.712	47.297	47.820
12	Mg	31.913	37.926	41.369	43.384	44.813	45.922	46.828	47.597	48.266	48.862	49.400
13	Al	30.845	36.858	40.301	42.316	43.745	44.854	45.762	46.533	47.210	47.818	48.378
14	Si	33.148	40.030	43.718	45.818	47.291	48.426	49.350	50.129	50.803	51.399	51.933
15	P	33.345	40.797	44.645	46.817	48.351	49.545	50.526	51.359	52.082	52.722	53.294
16	S	34.115	40.127	43.571	45.589	47.038	48.193	49.172	50.033	50.805	51.505	52.146
17	Cl	34.902	41.342	45.068	47.209	48.719	49.893	50.857	51.678	52.392	53.025	53.592
18	Ar	34.771	40.905	44.552	46.686	48.189	49.346	50.287	51.079	51.762	52.364	52.900
19	K	31.951	37.964	41.407	43.422	44.851	45.959	46.865	47.631	48.295	48.880	49.403
20	Ca	33.403	39.415	42.859	44.887	46.374	47.599	48.670	49.629	50.496	51.283	52.000
21	Sc	36.858	43.493	47.250	49.561	51.253	52.586	53.686	54.621	55.435	56.156	56.804
22	Ti	37.524	45.094	49.206	51.548	53.222	54.543	55.642	56.583	57.409	58.143	58.806
23	V	37.472	44.644	48.669	51.087	52.839	54.238	55.420	56.448	57.360	58.178	58.920
24	Cr	36.362	42.375	45.820	47.862	49.394	50.707	51.912	53.045	54.113	55.114	56.049
25	Mn	36.832	42.844	46.290	48.324	49.816	51.039	52.112	53.091	54.004	54.866	55.680
26	Fe	37.880	44.940	49.104	51.510	53.202	54.516	55.603	56.541	57.373	58.127	58.818
27	Co	37.557	44.026	48.152	50.689	52.507	53.916	55.234	56.185	57.008	57.734	58.384
28	Ni	36.725	42.882	46.594	48.839	50.522	51.902	53.076	54.094	54.990	55.788	56.506
29	Cu	33.399	39.411	42.855	44.870	46.308	47.457	48.458	49.386	50.267	51.107	51.902
30	Zn	34.861	40.873	44.317	46.332	47.761	48.869	49.775	50.541	51.205	51.792	52.319
31	Ga	33.675	39.688	43.131	45.146	46.575	47.684	48.589	49.356	50.022	50.612	51.145
32	Ge	35.174	41.476	45.514	47.874	49.508	50.751	51.751	52.586	53.302	53.930	54.489
33	As	33.925	41.049	45.661	48.268	50.060	51.423	52.521	53.441	54.230	54.922	55.536
34	Se	36.801	42.813	46.257	48.279	49.739	50.912	51.910	52.788	53.573	54.284	54.932
35	Br	37.281	43.307	46.881	49.061	50.641	51.881	52.901	53.768	54.520	55.183	55.776
36	Kr	36.979	42.991	46.455	48.523	50.017	51.188	52.149	52.963	53.668	54.289	54.843
37	Rb	34.283	40.295	43.739	45.753	47.182	48.291	49.197	49.963	50.626	51.211	51.735
38	Sr	35.734	41.747	45.190	47.213	48.684	49.886	50.936	51.879	52.737	53.521	54.242
39	Y	34.573	43.128	47.984	50.627	52.468	53.896	55.069	56.067	56.936	57.707	58.400
40	Zr	37.876	45.476	49.968	52.648	54.568	56.060	57.278	58.306	59.195	59.979	60.680
41	Nb	36.822	45.157	49.790	52.497	54.456	56.012	57.307	58.414	59.378	60.230	60.992
42	Mo	38.188	44.200	47.645	49.692	51.268	52.684	54.031	55.303	56.481	57.557	58.536
43	Tc	38.588	44.625	48.402	50.880	52.692	54.096	55.236	56.196	57.027	57.762	58.422
44	Ru	39.360	45.580	49.506	51.899	53.661	55.084	56.290	57.340	58.271	59.108	59.867
45	Rh	39.202	45.269	48.991	51.288	52.959	54.285	55.395	56.359	57.216	57.990	58.699
46	Pd	38.496	44.516	48.053	50.195	51.736	52.937	53.923	54.765	55.510	56.184	56.806
47	Ag	34.977	40.989	44.432	46.447	47.876	48.985	49.893	50.665	51.343	51.958	52.529
48	Cd	36.477	42.489	45.933	47.947	49.376	50.485	51.391	52.157	52.822	53.409	53.937
49	In	35.162	41.175	44.618	46.633	48.062	49.171	50.077	50.844	51.512	52.106	52.645
50	Sn	36.639	42.660	46.273	48.569	50.254	51.567	52.633	53.525	54.291	54.961	55.557
51	Sb	35.337	41.425	45.489	48.220	50.213	51.750	52.989	54.020	54.900	55.666	56.342
52	Te	35.999	42.011	45.460	47.537	49.145	50.527	51.746	52.824	53.781	54.631	55.392
53	I	38.659	44.672	48.126	50.189	51.700	52.908	53.918	54.787	55.547	56.223	56.830
54	Xe	38.317	44.329	47.774	49.794	51.239	52.373	53.309	54.108	54.804	55.422	55.976
55	Cs	35.598	41.611	45.054	47.069	48.498	49.607	50.513	51.278	51.942	52.527	53.050
56	Ba	37.074	43.092	46.739	49.200	51.072	52.542	53.736	54.733	55.589	56.338	57.006
57	La	38.952	45.926	50.539	53.190	55.035	56.462	57.638	58.649	59.540	60.339	61.064
72	Hf	39.233	45.295	49.227	51.893	53.902	55.502	56.830	57.968	58.964	59.851	60.651
73	Ta	38.724	45.459	50.034	52.934	55.054	56.728	58.111	59.287	60.307	61.205	62.007
74	W	37.946	44.417	48.961	51.897	54.061	55.787	57.232	58.472	59.554	60.510	61.363
75	Re	40.471	46.483	49.927	51.949	53.422	54.649	55.769	56.834	57.851	58.812	59.710
76	Os	41.243	47.268	50.901	53.224	54.976	56.396	57.595	58.634	59.548	60.361	61.092
78	Pt	40.303	46.319	49.868	52.131	53.861	55.270	56.462	57.494	58.404	59.218	59.954
79	Au	36.772	42.784	46.228	48.254	49.750	51.015	52.163	53.224	54.205	55.107	55.935
80	Hg	38.203	44.215	47.659	49.674	51.103	52.212	53.118	53.887	54.557	55.154	55.695
81	Tl	36.881	42.894	46.337	48.352	49.781	50.890	51.795	52.561	53.226	53.812	54.340
82	Pb	38.300	44.312	47.756	49.775	51.224	52.376	53.345	54.188	54.936	55.609	56.220
83	Bi	36.948	42.960	46.404	48.431	49.917	51.150	52.238	53.224	54.121	54.940	55.688
86	Rn	39.883	45.895	49.339	51.353	52.782	53.891	54.797	55.564	56.230	56.818	57.346
88	Ra	38.559	44.571	48.016	50.050	51.552	52.797	53.887	54.860	55.739	56.536	57.264
89	Ac	37.194	43.218	47.099	50.032	52.334	54.157	55.647	56.903	57.991	58.950	59.810

TABLE II. $(H_T°-H_0°)/T$ in cal mole^{-1} deg^{-1}.

Z	Element	298.15°K	1000°K	2000°K	3000°K	4000°K	5000°K	6000°K	7000°K	8000°K	9000°K	10 000°K
2	He	4.9682	4.9682	4.9682	4.9682	4.9682	4.9682	4.9682	4.9682	4.9682	4.9682	4.9682
3	Li	4.9682	4.9682	4.9682	4.9682	4.9682	4.9682	4.9682	4.9682	4.9682	4.9682	4.9682
4	Be	4.9682	4.9682	4.9682	4.9682	4.9689	4.9737	4.9897	5.0231	5.0768	5.1495	5.2371
5	B	4.9682	4.9682	4.9682	4.9682	4.9685	4.9723	4.9888	5.0316	5.1121	5.2352	5.3977
6	C	5.3333	5.0863	5.0282	5.0084	4.9984	4.9926	4.9897	4.9906	4.9969	5.0101	5.0315
7	N	5.7082	5.2135	5.0935	5.0576	5.0566	5.0791	5.1144	5.1544	5.1941	5.2314	5.2653
8	O	4.9682	4.9682	4.9682	4.9683	4.9713	4.9855	5.0212	5.0836	5.1715	5.2794	5.3994
9	F	5.3792	5.3073	5.1719	5.1125	5.0839	5.0754	5.0823	5.1001	5.1244	5.1517	5.1796
10	Ne	5.0533	5.2804	5.2160	5.1588	5.1213	5.0957	5.0774	5.0635	5.0528	5.0442	5.0372
11	Na	4.9682	4.9682	4.9682	4.9682	4.9682	4.9682	4.9682	4.9682	4.9682	4.9682	4.9682
12	Mg	4.9682	4.9682	4.9682	4.9682	4.9684	4.9702	4.9779	4.9965	5.0304	5.0816	5.1503
13	Al	4.9682	4.9682	4.9682	4.9682	4.9685	4.9721	4.9881	5.0300	5.1098	5.2331	5.3983
14	Si	5.8865	5.4362	5.2226	5.1422	5.1003	5.0749	5.0589	5.0506	5.0511	5.0618	5.0845
15	P	6.5335	5.7378	5.4018	5.3291	5.3393	5.3677	5.3933	5.4116	5.4234	5.4308	5.4362
16	S	4.9682	4.9682	4.9694	4.9967	5.0967	5.2698	5.4793	5.6877	5.8712	6.0201	6.1337
17	Cl	5.1192	5.4213	5.3137	5.2537	5.2507	5.2756	5.3077	5.3376	5.3618	5.3800	5.3927
18	Ar	4.9750	5.2134	5.2782	5.2425	5.2036	5.1719	5.1468	5.1269	5.1108	5.0976	5.0866
19	K	4.9682	4.9682	4.9682	4.9682	4.9682	4.9682	4.9682	4.9682	4.9682	4.9682	4.9682
20	Ca	4.9682	4.9682	4.9733	5.0599	5.3173	5.6884	6.0631	6.3730	6.6002	6.7554	6.8591
21	Sc	5.7410	5.3362	5.5758	5.8143	5.9416	6.0086	6.0494	6.0808	6.1097	6.1386	6.1678
22	Ti	6.3321	6.0885	5.8004	5.7792	5.8691	5.9775	6.0716	6.1476	6.2099	6.2633	6.3111
23	V	6.3313	5.7158	5.9127	6.0200	6.1750	6.3795	6.5839	6.7580	6.8950	6.9993	7.0787
24	Cr	4.9682	4.9682	4.9812	5.1411	5.5798	6.2455	6.9967	7.7008	8.2794	8.7108	9.0088
25	Mn	4.9682	4.9682	4.9808	5.0817	5.3216	5.6775	6.1151	6.5998	7.0876	7.5348	7.9129
26	Fe	5.5600	5.9981	5.9762	5.8959	5.8730	5.9170	6.0183	6.1585	6.3177	6.4808	6.6379
27	Co	5.0436	5.7140	6.1768	6.3107	6.3210	6.3026	6.1729	6.1663	6.1641	6.1681	6.1792
28	Ni	4.9748	5.2737	5.4322	5.6849	6.0340	6.3320	6.5381	6.6680	6.7469	6.7951	6.8268
29	Cu	4.9682	4.9682	4.9682	4.9751	5.0475	5.2911	5.7412	6.3162	6.8881	7.3654	7.7186
30	Zn	4.9682	4.9682	4.9682	4.9682	4.9682	4.9682	4.9687	4.9709	4.9771	4.9904	5.0142
31	Ga	4.9682	4.9682	4.9682	4.9682	4.9682	4.9684	4.9701	4.9769	4.9947	5.0303	5.0892
32	Ge	4.9749	5.6550	5.8760	5.7454	5.6179	5.5199	5.4458	5.3892	5.3465	5.3162	5.2979
33	As	5.1479	6.6058	6.5564	6.3065	6.1550	6.0606	5.9926	5.9375	5.8898	5.8472	5.8088
34	Se	4.9682	4.9682	4.9711	5.0176	5.1561	5.3643	5.5913	5.7987	5.9688	6.0980	6.1902
35	Br	4.9682	5.0353	5.2984	5.4473	5.5296	5.5819	5.6135	5.6293	5.6333	5.6291	5.6194
36	Kr	4.9682	4.9715	5.0479	5.1557	5.2275	5.2640	5.2784	5.2801	5.2751	5.2665	5.2562
37	Rb	4.9682	4.9682	4.9682	4.9682	4.9682	4.9682	4.9682	4.9682	4.9682	4.9682	4.9682
38	Sr	4.9682	4.9682	4.9708	5.0288	5.2338	5.5706	5.9479	6.2877	6.5572	6.7583	6.9093
39	Y	5.7306	7.3891	6.6489	6.4237	6.3918	6.4154	6.4527	6.4920	6.5295	6.5640	6.5951
40	Zr	5.9898	6.4167	6.5616	6.6523	6.6857	6.6872	6.6750	6.6619	6.6541	6.6539	6.6605
41	Nb	6.8854	6.7462	6.6502	6.7316	6.8977	7.0498	7.1510	7.2055	7.2291	7.2358	7.2350
42	Mo	4.9682	4.9682	4.9810	5.1929	5.8721	6.8919	7.8757	8.5906	9.0195	9.2371	9.3214
43	Tc	4.9682	5.1014	5.8944	6.2647	6.3095	6.2723	6.2368	6.2223	6.2286	6.2505	6.2833
44	Ru	4.9757	5.4621	5.8184	6.0085	6.2582	6.5080	6.7223	6.8980	7.0413	7.1586	7.2554
45	Rh	4.9683	5.1644	5.5731	5.7477	5.8747	6.0154	6.1725	6.3369	6.4993	6.6533	6.7951
46	Pd	4.9682	5.0094	5.2195	5.3355	5.3715	5.3899	5.4307	5.5136	5.6425	5.8108	6.0067
47	Ag	4.9682	4.9682	4.9682	4.9682	4.9684	4.9716	4.9881	5.0368	5.1388	5.3083	5.5482
48	Cd	4.9682	4.9682	4.9682	4.9682	4.9682	4.9683	4.9693	4.9729	4.9818	4.9989	5.0270
49	In	4.9682	4.9682	4.9682	4.9682	4.9682	4.9688	4.9727	4.9860	5.0170	5.0739	5.1620
50	Sn	4.9682	5.0215	5.4900	5.8051	5.8870	5.8689	5.8180	5.7613	5.7104	5.6711	5.6472
51	Sb	4.9682	5.3020	6.4864	6.9028	6.9241	6.8428	6.7402	6.6379	6.5426	6.4565	6.3807
52	Te	4.9682	4.9682	5.0076	5.3220	5.9061	6.4763	6.8758	7.1025	7.2052	7.2303	7.2104
53	I	4.9682	4.9689	5.0237	5.1710	5.3391	5.4846	5.5950	5.6718	5.7217	5.7515	5.7673
54	Xe	4.9682	4.9682	4.9720	5.0001	5.0523	5.1100	5.1611	5.2015	5.2314	5.2524	5.2666
55	Cs	4.9682	4.9682	4.9682	4.9682	4.9682	4.9682	4.9682	4.9682	4.9682	4.9682	4.9684
56	Ba	4.9682	5.0070	5.7143	6.3824	6.5849	6.5766	6.5090	6.4369	6.3795	6.3456	6.3406
57	La	5.0877	6.5482	6.6206	6.4558	6.3877	6.4142	6.5014	6.6149	6.7305	6.8354	6.9244
72	Hf	4.9682	5.2020	6.2567	6.8462	7.0983	7.2377	7.3374	7.4206	7.4958	7.5653	7.6288
73	Ta	5.0807	6.1827	6.9903	7.2884	7.4471	7.5537	7.6141	7.6369	7.6349	7.6191	7.5967
74	W	4.9873	6.0267	7.0420	7.4125	7.6365	7.8399	7.9960	8.0859	8.1179	8.1109	8.0818
75	Re	4.9682	4.9682	4.9702	5.0243	5.2701	5.7979	6.5332	7.2922	7.9227	8.3699	8.6500
76	Os	4.9682	5.0405	5.5233	5.9377	6.2416	6.4843	6.6702	6.8002	6.8822	6.9277	6.9474
78	Pt	4.9682	4.9915	5.3526	5.8290	6.1887	6.4413	6.6251	6.7637	6.8696	6.9507	7.0133
79	Au	4.9682	4.9682	4.9716	5.0596	5.4033	5.9849	6.6163	7.1449	7.5249	7.7758	7.9348
80	Hg	4.9682	4.9682	4.9682	4.9682	4.9684	4.9704	4.9787	4.9995	5.0386	5.0999	5.1850
81	Tl	4.9682	4.9682	4.9682	4.9682	4.9682	4.9682	4.9686	4.9707	4.9769	4.9909	5.0170
82	Pb	4.9682	4.9682	4.9698	4.9994	5.0937	5.2388	5.3975	5.5424	5.6625	5.7583	5.8364
83	Bi	4.9682	4.9682	4.9727	5.0546	5.3259	5.7503	6.1993	6.5778	6.8554	7.0406	7.1551
86	Rn	4.9682	4.9682	4.9682	4.9682	4.9683	4.9694	4.9726	4.9792	4.9894	5.0032	5.0197
88	Ra	4.9682	4.9682	4.9769	5.0918	5.3918	5.7889	6.1651	6.4643	6.6845	6.8475	6.9791
89	Ac	4.9682	5.0542	6.5514	7.7969	8.1350	8.1788	8.1622	8.1458	8.1424	8.1509	8.1662

TABLE III. $(F_T^\circ - H_0^\circ)/T$ in cal mole^{-1} deg^{-1}.

Z	Element	15 000°K	20 000°K	25 000°K	30 000°K	35 000°K	40 000°K	45 000°K	50 000°K
2	He	46.001	47.431	48.539	49.445	50.211	50.874	51.459	51.983
3	Li	46.264	47.693	48.802	49.708	50.474	51.137	51.722	52.246
4	Be	48.684	50.397	51.834	53.115	54.297	55.395	56.411	57.344
5	B	48.038	50.000	51.647	53.053	54.285	55.389	56.394	57.317
6	C	51.518	53.071	54.350	55.457	56.451	57.370	58.240	59.073
7	N	52.968	54.533	55.769	56.801	57.699	58.510	59.261	59.972
8	O	51.907	53.670	55.082	56.248	57.240	58.112	58.902	59.639
9	F	53.750	55.280	56.476	57.455	58.286	59.013	59.666	60.270
10	Ne	52.959	54.400	55.516	56.427	57.198	57.870	58.471	59.026
11	Na	49.835	51.264	52.372	53.278	54.045	54.712	55.307	55.853
12	Mg	51.587	53.386	55.092	56.743	58.274	59.643	60.848	61.907
13	Al	50.775	52.842	54.798	56.720	58.538	60.177	61.618	62.877
14	Si	54.042	55.666	57.066	58.331	59.487	60.539	61.495	62.360
15	P	55.506	57.109	58.417	59.572	60.631	61.615	62.528	63.371
16	S	54.687	56.518	57.955	59.173	60.262	61.263	62.192	63.054
17	Cl	55.784	57.343	58.573	59.633	60.614	61.557	62.470	63.348
18	Ar	54.955	56.407	57.544	58.513	59.411	60.295	61.186	62.076
19	K	51.418	52.848	53.964	54.906	55.774	56.639	57.534	58.454
20	Ca	54.844	56.993	58.813	60.400	61.780	62.978	64.020	64.934
21	Sc	59.332	61.164	62.605	63.789	64.791	65.654	66.411	67.082
22	Ti	61.404	63.294	64.780	65.999	67.025	67.907	68.678	69.360
23	V	61.837	63.943	65.581	66.910	68.019	68.965	69.786	70.508
24	Cr	59.815	62.492	64.509	66.102	67.404	68.497	69.433	70.249
25	Mn	59.100	61.648	63.624	65.227	66.566	67.711	68.704	69.577
26	Fe	61.635	63.773	65.492	66.917	68.122	69.158	70.060	70.855
27	Co	60.913	62.759	64.228	65.446	66.482	67.378	68.164	68.861
28	Ni	59.296	61.315	62.912	64.232	65.350	66.313	67.155	67.899
29	Cu	55.191	57.643	59.673	61.470	63.081	64.514	65.782	66.901
30	Zn	54.406	56.067	57.616	59.131	60.577	61.906	63.100	64.164
31	Ga	53.317	55.118	56.761	58.298	59.729	61.042	62.231	63.300
32	Ge	56.647	58.266	59.679	61.000	62.244	63.394	64.443	65.390
33	As	57.864	59.505	60.818	61.961	62.997	63.951	64.830	65.638
34	Se	57.480	59.303	60.739	61.963	63.061	64.068	64.996	65.850
35	Br	58.041	59.631	60.875	61.932	62.890	63.788	64.640	65.446
36	Kr	56.965	58.464	59.659	60.731	61.788	62.862	63.932	64.962
37	Rb	53.749	55.185	56.337	57.385	58.441	59.538	60.643	61.712
38	Sr	57.158	59.449	61.408	63.089	64.520	65.741	66.792	67.706
39	Y	61.098	63.040	64.556	65.794	66.834	67.728	68.507	69.196
40	Zr	63.394	65.338	66.850	68.080	69.112	69.997	70.769	71.452
41	Nb	63.922	65.992	67.582	68.861	69.923	70.826	71.608	72.296
42	Mo	62.289	64.858	66.777	68.292	69.531	70.573	71.468	72.248
43	Tc	61.011	62.912	64.420	65.665	66.716	67.621	68.411	69.110
44	Ru	62.874	65.072	66.797	68.206	69.385	70.391	71.264	72.031
45	Rh	61.563	63.714	65.431	66.847	68.039	69.059	69.946	70.726
46	Pd	59.440	61.573	63.358	64.875	66.178	67.308	68.298	69.172
47	Ag	55.097	57.415	59.472	61.267	62.826	64.181	65.364	66.404
48	Cd	56.033	57.724	59.368	61.042	62.650	64.110	65.402	66.537
49	In	54.884	56.826	58.770	60.766	62.672	64.380	65.870	67.164
50	Sn	57.863	59.628	61.200	62.662	64.007	65.219	66.300	67.262
51	Sb	58.883	60.694	62.193	63.527	64.734	65.823	66.799	67.676
52	Te	58.270	60.266	61.850	63.215	64.434	65.532	66.521	67.413
53	I	59.172	60.861	62.266	63.561	64.793	65.953	67.025	68.001
54	Xe	58.119	59.676	61.002	62.281	63.558	64.793	65.948	67.001
55	Cs	55.068	56.546	57.875	59.283	60.778	62.248	63.607	64.829
56	Ba	59.640	61.728	63.534	65.090	66.420	67.558	68.541	69.399
57	La	63.925	65.990	67.587	68.876	69.949	70.862	71.655	72.352
72	Hf	63.788	66.039	67.767	69.149	70.291	71.257	72.090	72.820
73	Ta	65.062	67.190	68.805	70.094	71.159	72.062	72.842	73.528
74	W	64.602	66.847	68.551	69.913	71.039	71.992	72.815	73.537
75	Re	63.292	65.794	67.669	69.150	70.365	71.387	72.265	73.033
76	Os	63.902	65.865	67.360	68.559	69.556	70.406	71.145	71.797
78	Pt	62.838	64.938	66.610	68.007	69.203	70.242	71.155	71.966
79	Au	59.218	61.588	63.438	64.949	66.218	67.305	68.251	69.084
80	Hg	57.924	59.792	61.543	63.214	64.762	66.157	67.396	68.492
81	Tl	56.435	58.126	59.730	61.341	62.915	64.382	65.706	66.885
82	Pb	58.657	60.580	62.359	64.058	65.618	67.005	68.220	69.286
83	Bi	58.628	60.750	62.466	63.949	65.260	66.423	67.455	68.373
86	Rn	59.400	60.883	62.048	63.006	63.820	64.525	65.146	65.702
88	Ra	60.214	62.515	64.424	66.019	67.359	68.496	69.474	70.327
89	Ac	63.132	65.476	67.253	68.661	69.816	70.788	71.623	72.353

TABLE IV. $(H_T^\circ - H_0^\circ)/T$ in cal mole^{-1} deg^{-1}.

Z	Element	15 000°K	20 000°K	25 000°K	30 000°K	35 000°K	40 000°K	45 000°K	50 000°K
2	He	4.9682	4.9682	4.9682	4.9682	4.9682	4.9682	4.9682	4.9682
3	Li	4.9682	4.9682	4.9682	4.9682	4.9682	4.9682	4.9682	4.9689
4	Be	5.7371	6.1965	6.7230	7.3561	7.7965	8.4610	8.7682	8.9190
5	B	6.4339	7.1722	7.5695	7.8541	8.1319	8.4089	8.6568	8.8506
6	C	5.2518	5.5720	5.9046	6.2532	6.6580	7.1338	7.6520	8.1579
7	N	5.3934	5.4899	5.5944	5.7362	5.9398	6.2171	6.5593	6.9391
8	O	5.9626	6.2651	6.3740	6.4134	6.4697	6.6003	6.8360	7.1768
9	F	5.2908	5.3455	5.3664	5.3791	5.4094	5.4843	5.6263	5.8471
10	Ne	5.0154	5.0041	4.9976	4.9972	5.0120	5.0614	5.1714	5.3676
11	Na	4.9682	4.9682	4.9683	4.9700	4.9796	5.0138	5.1018	5.2807
12	Mg	5.7528	6.9102	8.4344	9.6147	10.173	10.281	10.154	9.9249
13	Al	6.5572	7.9331	9.7110	11.320	12.151	12.312	12.114	11.767
14	Si	5.3910	5.9548	6.6267	7.2495	7.7223	8.0236	8.1807	8.2338
15	P	5.4919	5.6914	6.0832	6.6075	7.1419	7.5864	7.9010	8.9018
16	S	6.3464	6.3827	6.5349	6.8602	7.2871	7.7095	8.0535	8.2927
17	Cl	5.4099	5.4428	5.6278	6.0585	6.7056	7.4288	8.0765	8.5644
18	Ar	5.0521	5.0547	5.1677	5.5215	6.1913	7.0973	8.0380	8.8280
19	K	4.9683	4.9769	5.0528	5.3425	6.0004	7.0247	8.1974	9.2385
20	Ca	7.1989	7.8200	8.4892	8.8810	8.9887	8.9203	8.7651	8.5757
21	Sc	6.3104	6.4221	6.4850	6.5018	6.4852	6.4476	6.3986	6.3441
22	Ti	6.5061	6.6308	6.6814	6.6756	6.6349	6.5756	6.5081	6.4382
23	V	7.2850	7.3464	7.3219	7.2440	7.1393	7.0252	6.9114	6.8026
24	Cr	9.3883	9.1797	8.8838	8.5866	8.3098	8.0597	7.8367	7.6387
25	Mn	8.7843	8.8788	8.8284	8.7426	8.6316	8.5007	8.3577	8.2101
26	Fe	7.2467	7.6047	7.7830	7.8309	7.7946	7.7107	7.6032	7.4866
27	Co	6.3246	6.5120	6.6456	6.7094	6.7193	6.6944	6.6492	6.5933
28	Ni	6.9476	7.0983	7.2121	7.2550	7.2378	7.1819	7.1046	7.0175
29	Cu	8.3562	8.7661	9.4887	10.209	10.647	10.783	10.712	10.526
30	Zn	5.3842	6.3050	7.6629	8.9398	9.7499	10.099	10.146	10.032
31	Ga	5.7719	6.8265	7.9342	8.9168	9.6208	10.009	10.146	10.119
32	Ge	5.4137	5.9364	6.7975	7.7064	8.3975	8.8004	8.9707	8.9887
33	As	5.6905	5.7601	6.0567	6.4987	6.9533	7.3260	7.5844	7.7367
34	Se	6.3287	6.3600	6.5505	6.9132	7.3421	7.7277	8.0131	8.1902
35	Br	5.5460	5.5252	5.6577	5.9872	6.4668	6.9922	7.4657	7.8340
36	Kr	5.2084	5.2404	5.5477	6.3177	7.4612	8.6226	9.5002	10.019
37	Rb	4.9713	5.0353	5.3754	6.2375	7.5457	8.8702	9.8433	10.389
38	Sr	7.5489	8.4300	9.0804	9.2985	9.2331	9.0379	8.7986	8.5552
39	Y	6.7118	6.7802	6.7991	6.7750	6.7223	6.6541	6.5794	6.5036
40	Zr	6.7333	6.7762	6.7670	6.7230	6.6603	6.5892	6.5160	6.4440
41	Nb	7.2145	7.1657	7.0715	6.9510	6.8236	6.7001	6.5854	6.4807
42	Mo	9.0978	8.7519	8.4438	8.1656	7.9149	7.6910	7.4925	7.3167
43	Tc	6.5072	6.7025	6.8074	6.8312	6.8021	6.7437	6.6713	6.5940
44	Ru	7.5600	7.7072	7.7424	7.6937	7.5951	7.4730	7.3435	7.2156
45	Rh	7.3199	7.6195	7.7519	7.7608	7.6935	7.5869	7.4637	7.3369
46	Pd	7.0343	7.7711	8.2033	8.4136	8.4736	8.4396	8.3515	8.2350
47	Ag	7.3069	8.7665	9.6136	10.032	10.162	10.111	9.9607	9.7609
48	Cd	5.4228	6.5273	8.3399	9.9566	10.795	11.008	10.891	10.633
49	In	6.0608	7.6459	9.9271	11.863	12.715	12.779	12.480	12.055
50	Sn	5.8294	6.5581	7.5756	8.4420	8.9556	9.1617	9.1715	9.0738
51	Sb	6.2075	6.4613	7.0253	7.6096	8.0268	8.2488	8.3213	8.2979
52	Te	6.9697	6.9673	7.2775	7.7139	8.0923	8.3357	8.4480	8.4628
53	I	5.7897	6.0206	6.6701	7.5749	8.3955	8.9417	9.2147	9.2914
54	Xe	5.3143	5.5911	6.4237	7.6826	8.8506	9.6015	9.9450	10.015
55	Cs	5.0045	5.4013	6.7403	8.8021	10.512	11.383	11.624	11.531
56	Ba	6.8178	7.7444	8.3954	8.6237	8.5908	8.4389	8.2447	8.0438
57	La	7.1558	7.1814	7.1175	7.0148	6.8990	6.7829	6.6725	6.5700
72	Hf	7.8196	7.8010	7.6669	7.4930	7.3154	7.1483	6.9964	6.8602
73	Ta	7.4653	7.3165	7.1511	6.9850	6.8292	6.6882	6.5625	6.4511
74	W	7.8825	7.7169	7.5528	7.3832	7.2168	7.0605	6.9175	6.7884
75	Re	8.8307	8.5441	8.2540	7.9924	7.7585	7.5504	7.3658	7.2022
76	Os	6.8827	6.7582	6.6348	6.5191	6.4127	6.3159	6.2286	6.1501
78	Pt	7.2104	7.4015	7.5912	7.7231	7.7805	7.7751	7.7263	7.6508
79	Au	8.1977	8.2755	8.2977	8.2648	8.1896	8.0875	7.9711	7.8492
80	Hg	5.9441	7.1658	8.5787	9.7027	10.320	10.524	10.481	10.311
81	Tl	5.4399	6.4657	8.0340	9.6355	10.710	11.182	11.249	11.100
82	Pb	6.2604	7.2778	8.7308	9.8359	10.327	10.388	10.232	9.9845
83	Bi	7.3007	7.5008	7.9207	8.3493	8.6342	8.7553	8.7533	8.6746
86	Rn	5.1164	5.1951	5.2434	5.2686	5.2789	5.2802	5.2763	5.2694
88	Ra	7.6463	8.3481	8.7105	8.7481	8.6137	8.4115	8.1935	7.9821
89	Ac	8.1995	8.0655	7.8416	7.6021	7.3780	7.1782	7.0031	6.8503

Thermodynamics, Stationary States, and Steady-Rate Processes. V. A Collection of Corollaries

R. J. TYKODI

Department of Chemistry, Illinois Institute of Technology, Chicago 16, Illinois

(Received November 3, 1959)

A listing is made of a number of direct consequences of the ideas and procedures developed in papers I–IV of the series; the topics considered are *reaction equilibria in concentration and in thermal fields, thermocells, steady bithermal mass flow*, and *compound linkages*. Some general remarks about monothermal fields are relegated to an appended section.

INTRODUCTION

IN Papers I–IV[1] of the series we showed how to analyze situations involving steady heat flow or steady mass flow by dividing up the system of interest into terminal parts (homogeneous regions) and parts on-the-line (gradient-bearing regions) and by subjecting the system to suitable steady-rate operations. In this paper we analyze some additional situations using the methods, notation, and conventions developed in the earlier papers.

REACTION EQUILIBRIA IN CONCENTRATION AND IN THERMAL FIELDS

The Concentration Field

Let us consider the reversible chemical reaction

$$\sum \nu_i A_i = \sum \nu_j B_j \qquad (1)$$

—the reactants A_i being transformed to products B_j with stoichiometric coefficients ν_i and ν_j, respectively—taking place in a reactor of constant volume in a thermostat of temperature T in such a way that the reactants are individually supplied to and the products individually removed from the reaction vessel via semipermeable membranes communicating with terminal parts containing the appropriate species alone. The situation just described is indicated schematically in Fig. 1. If the reactants are supplied to and the products removed from the reaction vessel at suitable steady rates, then the number of equivalents $\dot{n}$ reacting in unit time is given by

$$\dot{n} = -\dot{n}_i/\nu_i = \cdots = \dot{n}_j/\nu_j = \cdots, \qquad (2)$$

where $\dot{n}_k$ (e.g.) is the rate of influx of matter into the kth terminal part containing the product species B_k alone. The condition for no net reaction (equilibrium) in the reactor is, of course, that

$$\Delta G \equiv \sum \nu_j \mu_j - \sum \nu_i \mu_i = 0, \qquad (3)$$

where μ_k (e.g.) is the chemical potential of the B_k species computed for the state of affairs existing in the kth terminal part of the system.

We now wish to investigate the condition for no net reaction in the reaction vessel when the reactor is traversed by the steady flow of a nonreactive or reaction-neutral component C. In Fig. 1 we now include among the terminal parts at i a part C_i containing the nonreactive component C at temperature T and pressure P_{C_i}; similarly at j we have a terminal part C_j containing C at temperature T and pressure P_{C_j}; and we establish a steady flow of component C through the reactor such that $\dot{n}_{C_i} + \dot{n}_{C_j} = 0$.

When there is a steady flow of component C through the reactor but no net reaction ($\dot{n} = 0$) we have[2]

$$\dot{n}_{C_i} \mathfrak{K}_{C_i} + \dot{n}_{C_j} \mathfrak{K}_{C_j} + T\dot{S}^{(r)} = 0, \qquad (4)$$

where

$$\mathfrak{K} \equiv \mathcal{E} + P\bar{V} = \bar{E}(T, P) + P\bar{V}(T, P) + \mathcal{K}(\dot{V}/\text{area}) - \mathcal{K}$$

being the molar kinetic energy of macroscopic motion—and $\dot{S}^{(r)}$ is the rate of accumulation of entropy in the surrounding thermostat. The superior bar is used to denote ordinary molar quantities. Keeping P_{C_i} and P_{C_j} constant we now induce a steady chemical reaction ($\dot{n} \neq 0$) inside the reactor and we have

$$\dot{n}_{C_i}' \mathfrak{K}_{C_i}' + \dot{n}_{C_j}' \mathfrak{K}_{C_j}' + \sum \dot{n}_i \bar{H}_i + \sum \dot{n}_j \bar{H}_j + T\dot{S}^{(r)\prime} = 0, \qquad (5)$$

where we have neglected kinetic energy terms associated with the reactive components and have used primes to indicate values under reaction conditions. It is to be noted that $\dot{n}_{C_i}' + \dot{n}_{C_j}' = 0$ and that $\bar{H} \equiv \bar{E} + P\bar{V}$.

If we subtract Eq. (4) from Eq. (5), let $\Delta Z \equiv Z' - Z$, divide the resulting equation through by $\dot{n}$, pass to the limit of vanishing chemical reaction ($\dot{n} \to 0$) via a sequence of steady-reaction states, and make use of the following limiting expressions

$$\lim_{\dot{n}\to 0} (\Delta \dot{n}_{C_i}/\dot{n}) \equiv \mathfrak{R}_{C_i}, \qquad (6)$$

$$\lim_{\dot{n}\to 0} (\Delta \dot{S}^{(r)}/\dot{n}) = -[\sum \nu_j \bar{S}_j - \sum \nu_i \bar{S}_i + \mathfrak{R}_{C_i}(\bar{S}_{C_i} - \bar{S}_{C_j})], \qquad (7)$$

$$\lim_{\dot{n}\to 0} \{\Delta(\dot{n}_{C_i} \mathfrak{K}_{C_i})/\dot{n}\} = 3\mathfrak{R}_{C_i} \mathfrak{K}_{C_i}, \qquad (8)$$

[1] R. J. Tykodi and T. A. Erikson, J. Chem. Phys. **31**, 1506, 1510, 1517, 1521 (1959).

[2] See Papers I and IV of the series for intermediate details.

we arrive at

$$\Re_C(\mathcal{G}_C{}^{\dagger}-\mathcal{G}_C{}^{\dagger})+\sum\nu_j\mu_j-\sum\nu_i\mu_i=0, \quad (9)$$

or

$$\Delta G=-\Re_C\Delta\mathcal{G}_C{}^{\dagger}, \quad (10)$$

where

$$\mathcal{G}^{\dagger}\equiv\bar{E}+P\bar{V}-T\bar{S}+3\mathcal{K}=3\mathcal{C}-T\bar{S}+2\mathcal{K}.$$

Since the chemical potentials in Eq. (9) are computed *in the terminal parts of the system*—the terminal parts containing reactant species being at the opposite end of the concentration field from those containing product species—it is not surprising that $\Delta G\neq 0$. We saw in Paper I that a flowing component tends to induce a gradient in the chemical potential of a stationary component in a mixture. If we assume that the chemical potentials of the reactive species at the points marked λ_i and λ_j of the concentration field have approximately the same values as in the neighboring terminal parts of the system and that the reactant species i are coupled to the flowing component C via the relations[3]

$$\mu_i{}^{(\lambda i)}-\mu_i{}^{(\lambda j)}=-\Re_i\Delta\mathcal{G}_C{}^{\dagger}, \quad (11)$$

then we can write

$$-\Re_C\Delta\mathcal{G}_C{}^{\dagger}=\sum\nu_j\mu_j{}^{(\lambda j)}-\sum\nu_i\mu_i{}^{(\lambda i)}$$
$$=\sum\nu_j\mu_j{}^{(\lambda j)}-\sum\nu_i\mu_i{}^{(\lambda j)}+\Delta\mathcal{G}_C{}^{\dagger}\sum\nu_i\Re_i, \quad (12)$$

or

$$\Delta G^{(\lambda j)}=-(\Re_C+\sum\nu_i\Re_i)\Delta\mathcal{G}_C{}^{\dagger}. \quad (13)$$

If we assume local equilibrium with respect to the chemical reaction in the concentration field, i.e., if at each point λ of the concentration field $\Delta G^{(\lambda)}=0$, then we see that the gross coupling effect $\Re_C$ can be resolved into individual species effects:

$$\Re_C=-\sum\nu_i\Re_i. \quad (14)$$

In terms of the quantities introduced in Paper I the condition $\Delta G^{(\lambda)}=0$ also requires that

$$\sum\nu_j\mathfrak{r}_j{}^{(j)}-\sum\nu_i\mathfrak{r}_i{}^{(i)}=0, \quad (15)$$

where

$$-\mathfrak{r}_\lambda{}^{(i)}\equiv(\mathrm{grad}\mu_\lambda{}^{(i)})/\Delta\mathcal{G}_C{}^{\dagger}.$$

The Thermal Field

In Fig. 1 if we place a thermostat at temperature T_i so as to encompass the point λ_i and the neighboring terminal parts of the system and similarly arrange a thermostat at temperature T_j around the point λ_j and neighboring terminal parts and, finally, if we let the intervening part of the reaction vessel function as a full-flux linkage, then we shall be in a position to consider the no-reaction condition for a chemical reaction in a thermal field. When there is no net chemical reaction in the system we have the relation

$$\dot{E}(\text{system})=-T_i\dot{S}_i{}^{(r)}-T_j\dot{S}_j{}^{(r)}=0, \quad (16)$$

[3] See Paper I.

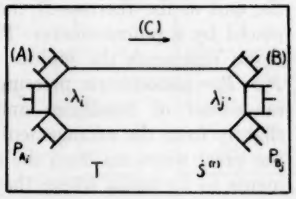

FIG. 1. Chemical reaction in a monothermal concentration field.

and in the case of steady chemical reaction we have (neglecting kinetic energy terms)

$$\sum\dot{n}_i\bar{H}_i+\sum\dot{n}_j\bar{H}_j+T_i\dot{S}_i{}^{(r)\prime}+T_j\dot{S}_j{}^{(r)\prime}=0. \quad (17)$$

Combining Eqs. (16) and (17), dividing the resultant equation through by $\dot{n}$, passing to the limit of no reaction via a sequence of steady-reaction states, and making use of the limiting expression

$$\lim_{\dot{n}\to 0}(\Delta\dot{S}_i{}^{(r)}/\dot{n})\equiv-\sum(\dot{n}_i/\dot{n})(\bar{S}_i-\mathfrak{S}_i)$$
$$=\sum\nu_i(\bar{S}_i-\mathfrak{S}_i), \quad (18)$$

we get

$$\sum\nu_j\mathfrak{H}_j-\sum\nu_i\mathfrak{H}_i=0, \quad (19)$$

or

$$\Delta G\equiv\sum\nu_j\mu_j-\sum\nu_i\mu_i=T_i[\mathfrak{S}]_i-T_j[\mathfrak{S}]_j, \quad (20)$$

where

$$\mathfrak{H}_i\equiv\mu_i+T_i\mathfrak{S}_i \quad \text{and} \quad [\mathfrak{S}]_i\equiv\sum\nu_i\mathfrak{S}_i.$$

Again, the terminal parts of the system being at opposite ends of the thermal field, we are not surprised that $\Delta G\neq 0$. If we were in a position to compute chemical potentials at some point λ in the thermal field, then we should expect that $\Delta G^{(\lambda)}=0$.

If one were desirous of multiplying complications, he could go on to consider the case of a chemical reaction in a simultaneous concentration and thermal field; however, we shall not pursue the subject further.

THERMOCELLS

Thermocouples and thermocells have been treated according to the formalism of irreversible thermodynamics by Holtan *et al.*[4] We considered the thermocouple in Paper III of the series; now we desire to consider the very similar problem of the thermocell. We shall consider by way of example the case recently investigated by Sundheim and Rosenstreich[5]—silver wire electrodes immersed in a molten silver nitrate electrolyte.

The assembly that we shall use in analyzing the $Ag/AgNO_3$ thermocell is indicated schematically in Fig. 2. The circuit includes a cell at ω, which we think of as having a variable emf, used to oppose the emf of the thermocell and to allow us to induce small, steady currents in the circuit; for actually measuring

[4] H. Holtan, P. Mazur, and S. de Groot, Physica **19**, 1109 (1953).

[5] B. R. Sundheim and J. Rosenstreich, J. Phys. Chem. **63**, 419 (1959).

the emf of the thermocell, the cell at ω would be replaced by a potentiometer. The shaded region in the figure represents the molten $AgNO_3$ electrolyte, and $P_\alpha = P_\beta$ = atmospheric pressure. The experimental arrangement of Sundheim and Rosenstreich differed slightly from the arrangement given in Fig. 2 in that the silver wires ran from the molten $AgNO_3$ compartments to ice baths where they were joined to copper wires which in turn ran to the binding posts of the measuring potentiometer; this difference in arrangement, however, is immaterial. The analysis will be conducted in terms of full-flux linkages.[6]

When the cell at ω just counterbalances the emf of the thermocell so that no electrical current flows in the circuit, we have

$$\dot{E}(\text{system}) = -\sum T_i \dot{S}_i^{(r)} = 0, \tag{21}$$

where the summation is over the six reservoirs with Roman indices in Fig. 2. If we now adjust the emf of the cell at ω so as to induce a small, steady electron current $\dot{n}$ in the silver wires and if we let ΔZ_ζ represent the change in the Z property of the cell at ζ associated with the passage of one Faraday $\mathbf{F}$ of electricity through the cell, we get

$$\dot{n}(\Delta H_\alpha + \Delta H_\beta + \Delta H_\omega) + T_\alpha \dot{S}_\alpha^{(r)} + T_\beta \dot{S}_\beta^{(r)} + T \dot{S}_\omega^{(r)} + \sum T_i \dot{S}_i^{(r)\prime} = 0. \tag{22}$$

We arrive at the sought-for relation by combining Eqs. (21) and (22), dividing the resultant equation through by $\dot{n}$, passing to the limit of vanishing electrical current via a sequence of steady electrical flow states, and using the following limiting expressions

$$\lim_{\dot{n}\to 0} (\dot{S}_\omega^{(r)}/\dot{n}) = -[\Delta S_\omega + \bar{S}_e^{(\omega+)} - \bar{S}_e^{(\omega-)} + \bar{S}_e^{(10)} - \bar{S}_e^{(\omega+)} + \bar{S}_e^{(\omega-)} - \bar{S}_e^{(60)}], \tag{23}$$

$$\lim_{\dot{n}\to 0} (\dot{S}_\alpha^{(r)}/\dot{n}) = -[\bar{S}_{Ag}^{(\alpha)} - \bar{S}_+^{(\alpha)} - \bar{S}_e^{(\alpha)}], \tag{24}$$

$$\lim_{\dot{n}\to 0} (\dot{S}_\beta^{(r)}/\dot{n}) = -[\bar{S}_+^{(\beta)} + \bar{S}_e^{(\beta)} - \bar{S}_{Ag}^{(\beta)}], \tag{25}$$

$$\lim_{\dot{n}\to 0} (\Delta \dot{S}_i^{(r)}/\dot{n}) \equiv (-1)^i [\mathfrak{S}_e^{(i)} - \bar{S}_e^{(i)}], \quad i = 1, 2, 5, 6, \tag{26}$$

$$\lim_{\dot{n}\to 0} (\Delta \dot{S}_j^{(r)}/\dot{n}) \equiv (-1)^j [t_+^{(j)} (\bar{S}_+^{(j)} - \mathfrak{S}_+^{(j)}) + t_-^{(j)} (\mathfrak{S}_-^{(j)} - \bar{S}_-^{(j)})], \quad j = 3, 4. \tag{27}$$

The subscripts e, $+$, and $-$ refer to electrons, silver ions, and nitrate ions, respectively; $t_-^{(j)}$ (e.g.) represents the transference number of the nitrate ion in the molten $AgNO_3$ electrolyte computed at temperature T_j; the superior bar indicates quantity per mole (molar or partial molar as the case may be) associated with the relevant species; and superscripts are used to locate places in the circuit and to indicate temperatures. Only the electrode reactions contribute to Eqs. (24) and (25); the transference part of the phenomenon behaves just like the electrical current in a wire, i.e., the ratio of joule heat developed in unit time to the electrical current approaches zero as the current goes to zero.

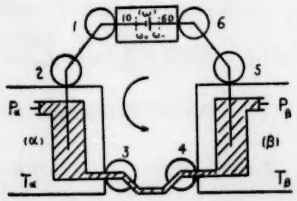

FIG. 2. Schematic assembly used to study the $Ag/AgNO_3$ thermocell. 1, ω, 6—entropy (heat) reservoirs at temperature T; 2, α, 3—entropy reservoirs at temperature T_α; 4, β, 5—entropy reservoirs at temperature T_β; wire segments 10-1-2-α and β-5-6-60—uniform, homogeneous silver wires; 10—point of junction of anode material ($\omega+$) for the cell at ω with silver wire; similar definition for the point 60.

Carrying out the above program we get

$$\Delta G_\alpha + \Delta G_\beta + \Delta G_\omega + \sum (-1)^i T_i \mathfrak{S}_e^{(i)} + T_\alpha [t_+^{(\alpha)} \mathfrak{S}_+^{(\alpha)} - t_-^{(\alpha)} \mathfrak{S}_-^{(\alpha)}] - T_\beta [t_+^{(\beta)} \mathfrak{S}_+^{(\beta)} - t_-^{(\beta)} \mathfrak{S}_-^{(\beta)}] = 0, \tag{28}$$

where

$$\Delta G \equiv \Delta H - T\Delta S,$$

$$\Delta G_\alpha(\text{e.g.}) = \bar{G}_{Ag}^{(\alpha)} - t_-^{(\alpha)} \bar{G}_{AgNO_3}^{(\alpha)} = \mu_{Ag}^{(\alpha)} - t_-^{(\alpha)} [\mu_+^{(\alpha)} + \mu_-^{(\alpha)}]$$

and simplifications have been made possible by the fact that $\bar{Z}_e^{(1)} = \bar{Z}_e^{(10)}$, $\bar{Z}_e^{(2)} = \bar{Z}_e^{(\alpha)}$, etc.

If the emf of the opposing cell at ω is $\mathbf{E}$ under conditions of no electrical current flow and if we introduce the electrochemical potential $\bar{\mu}_e$ of the electron and make use of the relations $-\Delta G_\omega = \mathbf{FE} = \bar{\mu}_e^{(1)} - \bar{\mu}_e^{(6)}$, $\bar{\mu}_e^{(1)} - \bar{\mu}_e^{(2)} = T_2 \mathfrak{S}_e^{(2)} - T_1 \mathfrak{S}_e^{(1)}$, etc.,[7] we can rearrange Eq. (28) to give

$$\mathbf{FE} = \Delta G_\alpha + \Delta G_\beta + \bar{\mu}_e^{(1)} - \bar{\mu}_e^{(2)} + \bar{\mu}_e^{(5)} - \bar{\mu}_e^{(6)} + T_\alpha \mathfrak{S}_\pm^{(\alpha)} - T_\beta \mathfrak{S}_\pm^{(\beta)}, \tag{29}$$

where $\mathfrak{S}_\pm \equiv t_+ \mathfrak{S}_+ - t_- \mathfrak{S}_-$.

For the temperature dependence of the emf of the thermocell we get[7]

$$\mathbf{F}(\partial \mathbf{E}/\partial T_\alpha)_{T,T_\beta} = -\Delta S_\alpha + [\mathfrak{S}_e^{(\alpha)}]^\flat + [\mathfrak{S}_\pm^{(\alpha)}]^\flat = -\bar{S}_{Ag}^{(\alpha)} + t_-^{(\alpha)} \bar{S}_{AgNO_3}^{(\alpha)} + [\mathfrak{S}_e^{(\alpha)}]^\flat + [\mathfrak{S}_\pm^{(\alpha)}]^\flat, \tag{30}$$

$$\mathbf{F}(\partial \mathbf{E}/\partial T_\beta)_{T,T_\alpha} = \bar{S}_{Ag}^{(\beta)} - t_-^{(\beta)} \bar{S}_{AgNO_3}^{(\beta)} - [\mathfrak{S}_e^{(\beta)}]^\flat - [\mathfrak{S}_\pm^{(\beta)}]^\flat, \tag{31}$$

$$\mathbf{F}(\partial \mathbf{E}/\partial T)_{T_\alpha,T_\beta} = [\mathfrak{S}_e^{(6)}]^\flat - [\mathfrak{S}_e^{(1)}]^\flat = 0, \tag{32}$$

[6] See Paper II.

[7] See Paper III.

where

$$-[\mathbb{S}_e^{(\omega)}]^{\vartheta} \equiv (\partial \bar{\mu}_e^{(\omega)}/\partial T_\alpha)_1$$

and

$$[\mathbb{S}_{\pm}^{(\omega)}]^{\vartheta} \equiv \{\partial(T_\alpha \mathbb{S}_{\pm}^{(\omega)} - T_\beta \mathbb{S}_{\pm}^{(\beta)})/\partial T_\alpha\}_\beta.$$

Whereas Sundheim and Rosenstreich[5] have set the term $\mathbb{S}_e^{\vartheta}$ in Eq. (31) equal to a fraction (~ 0.5) of the molar entropy $\bar{S}_e$ associated with the electron, we have shown in Paper III of the series that there are strong reasons for believing that for electrons in wires $\mathbb{S}_e^{\vartheta} = \bar{S}_e$. With Eqs. (29) to (32) we complete our treatment of the thermocell.

STEADY BITHERMAL MASS FLOW

In Paper II we established the conditions for migrational equilibrium in a thermal field. Now we wish to consider one of the situations outlined in Paper II, the thermomolecular pressure case, under circumstances such that there are both heat and mass flows between the terminal parts of the system via a full-flux linkage. The situation to be analyzed is indicated schematically in Fig. 3.

Since we are considering states of steady mass flow, it is evident that the point $(T_\alpha, P_\alpha, T_\beta, P_\beta)$ does not lie on the bitherm for migrational equilibrium[6]; however, we do wish to use states of migrational equilibrium as reference states. Let us pick the $\dot{n}_\omega$ which is positive, $\dot{n}_\alpha$, say; and let our reference state be the state of migrational equilibrium described by $(T_\alpha, P_\alpha', T_\beta, P_\beta)$, where $P_\alpha' = P_\alpha'(T_\alpha, T_\beta, P_\beta)$ is obtained from the equation of correlation or from the experimental bitherm.[6] Thus we blame the mass flow on the fact that $P_\alpha \neq P_\alpha'$. Let us use asterisks (*) to indicate quantities

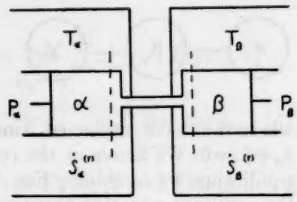

FIG. 3. Steady bithermal flow of a gas through a capillary, full-flux linkage.

computed for the reference state, $\mathbb{S}_\omega(*) = \mathbb{S}_\omega(T_\alpha, P_\alpha', T_\beta, P_\beta)$, for example.

For the state of steady mass flow, then, we have

$$\dot{n}_\alpha \mathcal{K}_\alpha + \dot{n}_\beta \mathcal{K}_\beta + T_\alpha \dot{S}_\alpha^{(r)} + T_\beta \dot{S}_\beta^{(r)} = 0. \tag{33}$$

If we let

$$\dot{S}_\omega^{(r)} \equiv -\dot{n}_\omega\{\bar{S}_\omega(T_\omega, P_\omega) - \mathbb{S}_\omega(*) - \dot{n}_\omega R\mathfrak{N}_\omega\} + \dot{S}_\omega^{(r)}(*), \tag{34}$$

remembering that $\dot{n}_\alpha + \dot{n}_\beta = 0$ and that $T_\alpha \dot{S}_\alpha^{(r)}(*) + T_\beta \dot{S}_\beta^{(r)}(*) = 0$, we get

$$(\mathfrak{H}_\beta + \mathcal{K}_\beta) - (\mathfrak{H}_\alpha + \mathcal{K}_\alpha) = \dot{n}_\alpha(RT_\alpha\mathfrak{N}_\alpha + RT_\beta\mathfrak{N}_\beta); \tag{35}$$

or, equivalently,

$$\mathfrak{H}_\beta - \mathfrak{H}_\alpha = \dot{n}_\alpha \mathfrak{L}_{\alpha\beta} + \mathcal{K}_\alpha - \mathcal{K}_\beta, \tag{36}$$

where $\mathfrak{H}_\omega \equiv \mu_\omega(T_\omega, P_\omega) + T_\omega \mathbb{S}_\omega(*)$, R is the gas constant, and we have introduced the notational convention $\mathfrak{L}_{\alpha\beta} \equiv RT_\alpha\mathfrak{N}_\alpha + RT_\beta\mathfrak{N}_\beta$.[8]

Finally, we wish to examine the influence of a change in T_α at constant T_β, P_β, P_α, on the rate of mass flow, i.e., we wish to compute $(\partial \dot{n}_\alpha/\partial T_\alpha)_{\beta,P\alpha}$. From Eq. (36) we see that

$$(\partial \dot{n}_\alpha/\partial T_\alpha)_{\beta,P\alpha} = \frac{\bar{S}_\alpha - \mathbb{S}_\alpha^{\vartheta}(*) - \dot{n}_\alpha(\partial \mathfrak{L}_{\alpha\beta}/\partial T_\alpha)_{\beta,P\alpha} - \dot{n}_\alpha^2(M\bar{V}_\alpha/A_\alpha^2)(\partial \bar{V}_\alpha/\partial T_\alpha)_{P\alpha}}{\mathfrak{L}_{\alpha\beta} + \dot{n}_\alpha M\Delta(\bar{V}^2/A^2)}, \tag{37}$$

where M is the molecular weight of the gas, A_ω is the cross-sectional area of the ω terminal part, $\Delta Z \equiv Z_\alpha - Z_\beta$, and $-\mathbb{S}_\alpha^{\vartheta}(*) \equiv \{\partial \mu_\alpha(*)/\partial T_\alpha\}_\beta$. We see from Eq. (37) that if we start from a state of migrational equilibrium $\{T_\alpha, T_\beta, P_\alpha(*), P_\beta(*)\}$ and then move to a nearby state $\{T_\alpha + \Delta T_\alpha, T_\beta, P_\alpha(*), P_\beta(*)\}$ the new state will also be one of migrational equilibrium if $\bar{S}_\alpha(*) = \mathbb{S}_\alpha^{\vartheta}(*)$; if $\bar{S}_\alpha(*) \neq \mathbb{S}_\alpha^{\vartheta}(*)$ then the new state will be one of steady bithermal mass flow with $\dot{n}_\alpha = [\bar{S}_\alpha(*) - \mathbb{S}_\alpha^{\vartheta}(*)](\Delta T_\alpha/\mathfrak{L}_{\alpha\beta})$.

COMPOUND LINKAGES

Thus far we have been considering a single linkage connecting two terminal parts of the system. We shall now take up some simple cases involving more than one link and, consequently, more than two terminal parts to the system. We shall investigate by way of example the thermomolecular pressure situation using full-flux, capillary linkages.

Series Linkages

We shall use circles connected by wavy lines to indicate terminal parts plus surrounding thermostats plus connecting full-flux linkage; thus (e.g.) in Fig. 4 the α–β part of the diagram is to be considered equivalent to the detailed version diagrammed in Fig. 3. We shall concern ourselves only with the problem of migrational equilibrium under the given circumstances.

In Fig. 4 for the state of no mass flow we have

$$\dot{E}(\text{system}) = -T_\alpha \dot{S}_\alpha^{(r)} - T_\beta \dot{S}_\beta^{(r)} - T_\gamma \dot{S}_\gamma^{(r)} = 0; \tag{38}$$

and for the state of steady mass flow between α and γ via β,

$$\dot{n}_\alpha \bar{H}_\alpha + \dot{n}_\gamma \bar{H}_\gamma + T_\alpha \dot{S}_\alpha^{(r)\prime} + T_\beta \dot{S}_\beta^{(r)\prime} + T_\gamma \dot{S}_\gamma^{(r)\prime} = 0, \tag{39}$$

[8] We wish to record in this footnote a few relations in terms of the quantities $\mathfrak{H}_\omega(*) \equiv \mu_\omega(*) + T_\omega \mathbb{S}_\omega(*)$; see Paper II for the verification of the first relation: $\mathfrak{H}_\beta(*) = \mathfrak{H}_\alpha(*)$; $\mathfrak{H}_\beta = \mathfrak{H}_\beta(*)$; $\mathfrak{H}_\alpha = \mathfrak{H}_\alpha(*) + \mu_\alpha - \mu_\alpha(*) \cong \mathfrak{H}_\alpha(*) + RT_\alpha \ln(P_\alpha/P_\alpha')$.

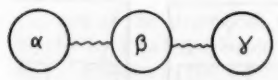

FIG. 4. Two capillary, full-flux linkages arranged in series.

where we have neglected kinetic energy terms and $\dot{n}_\alpha+\dot{n}_\gamma=0$. We arrive at the condition for migrational equilibrium by combining Eqs. (38) and (39), dividing the resultant equation through by $\dot{n}_\alpha$, and passing to the limit of vanishing mass flow via a sequence of steady-flow states; the appropriate limiting expressions are

$$\lim_{\dot{n}_\alpha\to 0}(\Delta\dot{S}_\alpha^{(r)}/\dot{n}_\alpha)\equiv-(\bar{S}_\alpha-\mathfrak{S}_\alpha), \tag{40}$$

$$\lim_{\dot{n}_\alpha\to 0}(\Delta\dot{S}_\beta^{(r)}/\dot{n}_\alpha)\equiv-[\mathfrak{S}_{\beta(\alpha)}-\bar{S}_\beta+\bar{S}_\beta-\mathfrak{S}_{\beta(\gamma)}], \tag{41}$$

$$\lim_{\dot{n}_\alpha\to 0}(\Delta\dot{S}_\gamma^{(r)}/\dot{n}_\alpha)\equiv-(\mathfrak{S}_\gamma-\bar{S}_\gamma). \tag{42}$$

The net result, then, is that

$$\mathfrak{H}_\alpha-\mathfrak{H}_\gamma=T_\beta[\mathfrak{S}_{\beta(\alpha)}-\mathfrak{S}_{\beta(\gamma)}]. \tag{43}$$

Introducing the notation $\mathfrak{H}_{\beta(\omega)}\equiv\mu_\beta+T_\beta\mathfrak{S}_{\beta(\omega)}$, we can also express Eq. (43) as

$$\mathfrak{H}_\alpha-\mathfrak{H}_{\beta(\alpha)}+\mathfrak{H}_{\beta(\gamma)}-\mathfrak{H}_\gamma=0. \tag{44}$$

In Paper II we showed that for a single full-flux linkage $(i-j)$ the migrational equilibrium condition was that $\mathfrak{H}_i-\mathfrak{H}_j=0$; Eq. (44) seems to say that for a number of series-connected full-flux linkages the net effect is merely the sum of the separate effects for each linkage and that $\mathfrak{H}_\omega-\mathfrak{H}_{\beta(\omega)}=0$. Equation (43) also shows us that a difference in the $\mathfrak{H}$ function computed for the terminal parts that serve as (mass) flow source and flow sink, respectively, is a measure of the coupling between the mass flow and the flows of heat to or from the surroundings at points intermediate between the flow source and flow sink.

Branched Linkages

Our final considerations will deal with a branched, capillary, full-flux linkage as indicated schematically in Fig. 5. The steady-flow condition for such a configuration is that $\dot{n}_\alpha+\dot{n}_\beta+\dot{n}_\gamma=0$. For the state of no mass flow we have

$$\dot{E}(\text{system})=-T_\alpha\dot{S}_\alpha^{(r)}-T_\beta\dot{S}_\beta^{(r)}-T_\gamma\dot{S}_\gamma^{(r)}=0; \tag{45}$$

and for the state of steady mass flow (neglecting kinetic energy terms)

$$\dot{n}_\alpha\bar{H}_\alpha+\dot{n}_\beta\bar{H}_\beta+\dot{n}_\gamma\bar{H}_\gamma+T_\alpha\dot{S}_\alpha^{(r)\prime}+T_\beta\dot{S}_\beta^{(r)\prime}+T_\gamma\dot{S}_\gamma^{(r)\prime}=0. \tag{46}$$

Making use of the limiting expressions

$$\lim_{\dot{n}_\omega\to 0}(\Delta\dot{S}_\omega^{(r)}/\dot{n}_\omega)\equiv-(\bar{S}_\omega-\mathfrak{S}_\omega), \tag{47}$$

$$\lim_{\dot{n}_\chi\to 0}(\dot{n}_\omega/\dot{n}_\chi)\equiv\mathfrak{R}_{\omega\chi}, \tag{48}$$

and performing the usual limiting operations on Eqs. (45) and (46), we obtain for the condition of migrational equilibrium the relation

$$\mathfrak{R}_{\alpha\chi}\mathfrak{H}_\alpha+\mathfrak{R}_{\beta\chi}\mathfrak{H}_\beta+\mathfrak{R}_{\gamma\chi}\mathfrak{H}_\gamma=0, \tag{49}$$

where $\mathfrak{R}_{\alpha\chi}+\mathfrak{R}_{\beta\chi}+\mathfrak{R}_{\gamma\chi}=0$ and we have chosen one of the mass flows $\dot{n}_\alpha$, $\dot{n}_\beta$, or $\dot{n}_\gamma$ as a reference parameter and have called it $\dot{n}_\chi$.

CONCLUSION

We could go on examining situations that get more and more complicated, but by now the general methods of procedure should be fairly evident; therefore we bring our catalog of corollaries to a close.

Finally, we should like to list some additional important references[9–11] to the work of devotees of the Belgian school of thermodynamics—De Donder, Prigogine, Defay, etc.—so that the interested reader may have an opportunity to compare the methods developed by these writers for treating open systems and irreversible processes with the procedures outlined in this series of papers.

APPENDED REMARKS ON MONOTHERMAL FIELDS

In Paper I[1] of the series we introduced the idea of a monothermal field—a spatial region in heat communication with a single, external heat reservoir of temperature T and capable of being divided up into terminal parts and parts on-the-line; for processes involving steady mass flow, mass is exchanged between terminal parts, which are homogeneous in intensive variables, via parts on-the-line, which contain the necessary gradients in the intensive properties of the system.

If we have a case involving the steady exchange of mass (of one or of several different chemical types) between terminal parts of a monothermal field, we can apply the first law of thermodynamics to the process and obtain

$$\dot{E}(\text{system})=\dot{Q}-\dot{W}=-T\dot{S}^{(r)}-\dot{W} \tag{50}$$

and

$$\dot{E}(\text{system})=\sum\mathcal{E}_i\dot{n}_i=-T\dot{S}^{(r)}-\dot{W}, \tag{51}$$

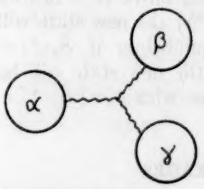

FIG. 5. A branched, capillary, full-flux linkage.

[9] Th. De Donder and P. Van Rysselberghe, *Affinity* (Stanford University Press, Stanford, California, 1936).

[10] I. Prigogine and R. Defay, *Chemical Thermodynamics* (translated by D. H. Everett) (Longmans, Green, and Company, London, 1954).

[11] I. Prigogine, *Etude Thermodynamique des Phenomenes Irreversibles* (Desoer, Liege, 1947). An English translation of this work is in preparation; see the introduction and preface to reference cited in footnote 10.

where the symbols are those defined in Paper I of the series. The sum is taken over the terminal parts of the system only. Let us subtract the product of temperature T and the rate of change of the entropy of the system $\sum \bar{S}_i \dot{n}_i$ from both sides of Eq. (51), and let us introduce σ the rate of entropy production[6] for the steady-flow process, i.e., $\sigma \equiv \dot{S}^{(r)} + \sum \bar{S}_i \dot{n}_i$; we then have

$$-\dot{F}(\text{system}) \equiv -\sum \mathfrak{F}_i \dot{n}_i = T\sigma + \dot{W}, \qquad (52)$$

where $\mathfrak{F}_i \equiv \mathcal{E}_i - T\bar{S}_i$. If there are steady volume changes in the terminal parts, we can do a similar trick with the quantity $\sum P_i \dot{V}_i = \sum P_i \bar{V}_i \dot{n}_i$:

$$-\dot{G}(\text{system}) \equiv -\sum \mathcal{G}_i \dot{n}_i = T\sigma + \dot{W} - \sum P_i \dot{V}_i, \qquad (53)$$

where $\mathcal{G}_i \equiv \mathfrak{F}_i + P_i \bar{V}_i$ and P_i is the pressure inside the terminal part at i. In the frequently occurring case where $\dot{W} - \sum P_i \dot{V}_i = 0$, Eq. (53) takes the well-known form

$$-\dot{G}(\text{system}) = T\sigma. \qquad (54)$$

Now if we apply Eq. (54) [or, more generally, Eq. (53)] to the state of no mass flow (with respect to a given chemical substance) and again to the (primed) state of steady mass flow (with respect to the same substance), we can write

$$-\Delta\dot{G}(\text{system}) = T\Delta\sigma, \qquad (55)$$

where $\Delta Z \equiv Z' - Z$. The condition for migrational equilibrium in the monothermal field is found by dividing Eq. (55) through by the appropriate rate of mass flow into one of the appropriate terminal parts, the kth, say, and then passing to the limit of vanishing mass flow via a sequence of steady-flow states:

$$-\lim_{\dot{n}_k \to 0} \Delta\dot{G}(\text{system})/\dot{n}_k = T \lim_{\dot{n}_k \to 0} \Delta\sigma/\dot{n}_k \qquad (56)$$

or, equivalently,

$$-\lim_{\dot{n}_k \to 0} \sum \Delta(\mu_i \dot{n}_i)/\dot{n}_k - \lim_{\dot{n}_k \to 0} \sum \Delta[(\mathcal{E}_i - \bar{E}_i)\dot{n}_i]/\dot{n}_k = T \lim_{\dot{n}_k \to 0} \Delta\sigma/\dot{n}_k, \qquad (57)$$

since $\mathcal{G}_i - \mu_i = \mathcal{E}_i - \bar{E}_i$ ($\mu_i \equiv \bar{E}_i + P_i\bar{V}_i - T\bar{S}_i$ and $\mathcal{E}_i - \bar{E}_i$ is just the additional energy per mole—kinetic, potential, etc.—needed to describe the system).

In the last section of Paper II[1] we considered the possibility that the condition

$$\lim_{\dot{n}_k \to 0} \Delta\sigma/\dot{n}_k = 0 \qquad (58)$$

was always satisfied in a sequence of steady-flow states.[12] In retrospect we see that in each of the three cases considered in Paper I—phase field, potential field, and monothermal concentration field—and also in the case of reaction equilibrium in a concentration field we implicitly made use of the condition given in Eq. (58).

Errata for Part II [J. Chem. Phys. 31, 1510–1516 (1959)]

Page 1511: Eq. (20) should be a definition and Eq. (14) should be a theorem, with attendant changes in the rest of the paper.

Page 1512, Eq. (31): For $-[T_\chi/R(T_\chi - T_\omega)][\cdots]$ read $-[T_\chi \bar{C}_P/R(T_\chi - T_\omega)][\cdots]$.

Page 1513, two lines below Fig. 2: For *In Fig. 5* read *In Fig. 2.*

Page 1514, three lines below Eq. (44): For *sub-* read *subject.*

[12] See assumptions (A.1) and (A.2) of Paper II; although assumption (A.2) is a little more general than (A.1), in actual practice they are entirely equivalent.

Thermodynamics, Stationary States, and Steady-Rate Processes. VI. Forced Vaporization of Selected Liquids

TED A. ERIKSON,

Chemistry Research Division, Armour Research Foundation of Illinois Institute of Technology, Technology Center, Chicago 16, Illinois

AND

R. J. TYKODI,

Department of Chemistry, Illinois Institute of Technology, Technology Center, Chicago 16, Illinois

(Received January 21, 1960)

The results of forced vaporization experiments are reported for water, carbon tetrachloride, benzene, methanol, and *n*-butyl alcohol. The data, which were obtained at a monothermal temperature of 25°C and with a tapered tube having available areas from 0.2 to 3.4 sq cm, indicate a linear relationship between the logarithm of the steady pressure maintained above the liquid and the steady mass flow per unit area. A number of complicating features in the experimental arrangement are discussed briefly.

INTRODUCTION

IN Paper IV[1] of this series, the forced vaporization data of Alty[2,3] were discussed in terms of the equation

$$\ln P = \ln P_0 - \dot{n}\mathfrak{R} \qquad (1)$$

where P is the steady pressure maintained above the liquid, $\dot{n}$ is the steady mass flow rate, P_0 is the equilibrium vapor pressure at the fixed thermostat temperature (T_1), and $\mathfrak{R}$ is a coefficient defined in terms of the rate of entropy production for the steady vaporization process.

The linear nature of the plot of $\log P$ as a function of $\dot{n}$ was shown for Alty's experiments with water at 18°, 30°, 40°, and 60°C, and for one experiment with carbon tetrachloride at 1.6°C. A specific coefficient was introduced to account for experiments conducted in tubes having different diameters, that is $\mathfrak{R}_A \equiv A\mathfrak{R}$, where A is the area of the liquid-vapor interface.

The measurements reported in this paper were undertaken in order to obtain further data on the process of forced vaporization in an effort to extend the application of Eq. (1). The experiments were performed in a manner similar to that employed by Alty.[2,3] A tapered thin-walled tube was used, however, to permit a broader evaluation of the effect of the tube area. When the specific coefficient is introduced, Eq. (1) becomes

$$\log P = \log P_0 - (\dot{n}_A \mathfrak{R}_A / 2.3) \qquad (2)$$

where $\dot{n}_A$ is the total mass flow divided by the area at the liquid-vapor interface.

EXPERIMENTAL

A diagram of the equipment is shown in Fig. 1. The thin-walled tube was conical, and the initial liquid level could be set by varying the length of the mercury column. The pressure above the liquid was maintained either by controlling the temperature (T) of a thin-walled condensing trap or by throttling the system to vacuum with the throttling valve. The connecting line could be heated (when necessary) to maintain its temperature above the dew point, and thus prevent undue condensation. A trap prevented liquid carryover during degassing operations. In order that the changing mass flow could be monitored with greater sensitivity, the vapor was passed through a Tri-Flat rotameter (02F−1/8−20/5). A 5-gal water bath, equipped with a high speed stirrer and thermostatically controlled to better than ±0.1°C(T_1), surrounded the tapered tube and the rotameter. A similar 3 gal bath surrounded the condensing trap. All levels were read with a Gartner cathetometer having a resolution of ±0.05 mm. The barometer could be evacuated separately so that the atmospheric pressure could be checked during a run.

The selected liquid was added with a hypodermic syringe through the 12/3 B and S joint, which was then capped for the run. The liquid was degassed by full pumping before a run was started. The section of the apparatus containing the tapered tube was about 10 in. long. All connecting tubing was 10 mm in o.d. The area of the tube at any height from a fixed reference point was determined from the derivative of a least-squares relation for a volume-height calibration.

The variables for the forced vaporization process were determined as follows:

The steady pressure above the liquid was evaluated from the sum of the height of the mercury column (corrected for discontinuities between the bath temperature and room temperature) and the height of the liquid resting on the mercury column (corrected for density). The steady mass flow rate was derived from the measured changes in liquid with respect to time. That is, the rate of liquid volume change with respect to time could be evaluated from a plot of typical raw data as shown in Fig. 2 for a water experiment. The volume flow rate was then converted to a mass flow rate at an average tube area varying about 5% or less. During

[1] R. J. Tykodi and T. A. Erikson, J. Chem. Phys. **31**, 1521 (1959).
[2] T. Alty, Proc. Roy. Soc. (London) **A131**, 554 (1931).
[3] T. Alty and F. H. Nicoll, Can. J. Research **4**, 547 (1931).

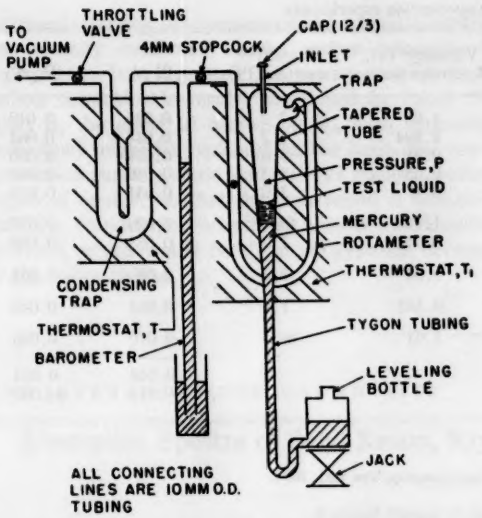

FIG. 1. Diagram of equipment for forced vaporization process.

the course of the continuous run shown in Fig. 2, the tube area decreased from about 0.7 to 0.62 sq cm.

The area of the liquid-vapor interface was evaluated by means of the approximate expression

$$A_s \cong A_t[1+(d/r)] \qquad (3)$$

where A_s is the approximate area of the liquid-vapor interface, A_t is the average tube area at the point where the liquid meniscus touches the wall of the tube, d is the measured liquid meniscus depth, and r is the radius that corresponds to the circular area A_t.

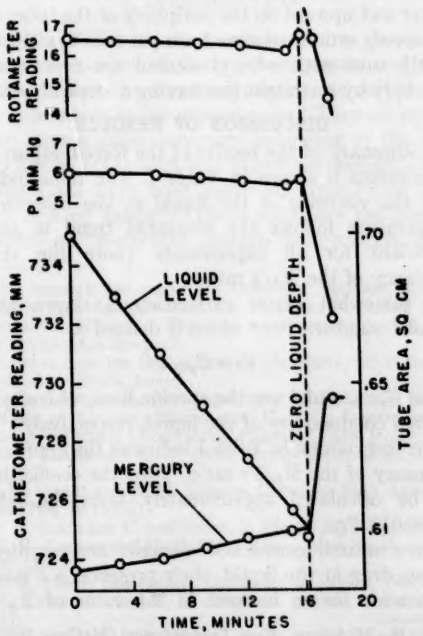

FIG. 2. Raw data from forced vaporization of water at 25°C.

EXPERIMENTAL RESULTS

The data obtained at different tube areas were correlated by means of the specific coefficient and the specific mass flow as in Eq. (2). The forced vaporization data for water are shown in Fig. 3 where $\log P$ is plotted as a function of $\dot{n}_A$. A straight line having a slope of -0.0172 represents the data in a reasonable fashion considering that tube areas and steady pressures were varied from 0.6 to 3.2 sq cm and from 5 to 23 mm Hg, respectively.

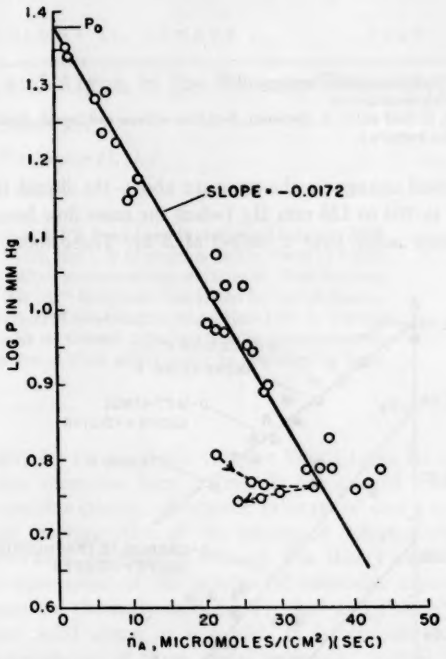

FIG. 3. Logarithm of the steady pressure as a function of the mass flow per unit area of liquid for the forced vaporization of water at 25°C.

With other variables approximately constant (note the series of points for one continuous run connected by the dashed line in Fig. 3), it was found that the liquid depth (above the mercury) affected the mass flow, causing variations of as much as 30%. As the liquid depth decreased, the mass flow reached a maximum at a depth near 20 mm, a minimum at a depth near 2 mm, and finally it increased asymptotically as the depth approached zero (not shown in Fig. 3, see Fig. 2). These effects probably contributed to the uncomfortable scatter of the data.

The experimental technique was altered for the forced vaporization experiments with methanol. The bath temperature (T) was slowly changed to effect a

TABLE I. Summary of forced vaporization experiments.

Compound	Monothermal temp, °C	$\mathfrak{N}_A$, (sec) (cm²)/μM	Viscosity[c] (η), centipoise	Prandtl[c,d] number (Pr)	$\mathfrak{N}_A/\eta$	$\mathfrak{N}_A$/Pr
Water	18[a]	0.0366	1.05	7.4	0.035	0.049
	25[b]	0.0396	0.894	6.2	0.044	0.064
	30[a]	0.0315	0.81	5.6	0.039	0.056
	40[a]	0.0196	0.65	4.3	0.030	0.046
	60[a]	0.0144	0.47	3.0	0.031	0.048
Carbon tetrachloride	1.6[a]	0.0372	1.29	10.0	0.029	0.037
	25[b]	0.0547	0.942	7.9	0.058	0.069
Benzene	25[b]	0.0513	0.64	7.5	0.080	0.068
Methanol	25[b]	0.0340	0.562	7.1	0.061	0.048
n-Butyl alcohol	25[b]	0.213	3.03	46.3	0.070	0.046
					0.048	0.053
					Av ±.016	±.009

[a] Alty's experiments (see Paper IV[1]).
[b] This investigation.
[c] R. C. Reid and T. K. Sherwood, *Properties of Gases and Liquids* (McGraw-Hill Book Company, New York, 1959).
[d] See footnote 4.

gradual change in the pressure above the liquid from 126 to 103 to 125 mm Hg (when the mass flow became exactly zero) over a period of 3 hr. These data, together with one steady run, are represented in Fig. 4(a) by a straight line having a slope of −0.0148.

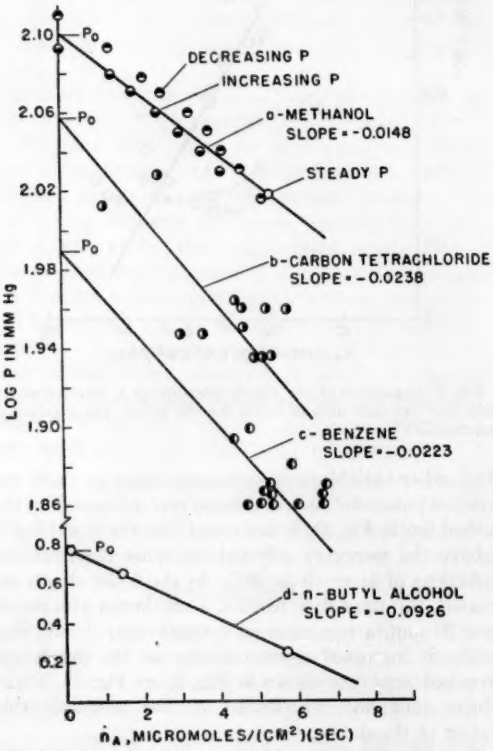

FIG. 4. Logarithm of the steady pressure as a function of the mass flow per unit area for the forced vaporization of selected liquids at 25°C.

Complications were incurred in performing forced vaporization experiments at 25°C with carbon tetrachloride and benzene because of the tendency for the bulk liquid to bump sporadically. The data are represented by straight lines having slopes of −0.0238 and −0.0223, respectively [Figs. 4(b) and 4(c)]. Cathetometer observation of minute particles of foreign matter in a carbon tetrachloride run (P=85 mm Hg) indicated a convective flow which was downward in the center and upward on the periphery of the tube, reaching speeds estimated near 1 cm per sec. The data from steady runs with *n*-butyl alcohol are represented in Fig. 4(d) by a straight line having a slope of −0.0926.

DISCUSSION OF RESULTS

A summary of the results of the forced vaporization experiments is shown in Table I. The table indicates that the viscosity of the liquid at the monothermal temperature follows the measured trend in the $\mathfrak{N}_A$ coefficient for all experiments (note the relative constancy of the $\mathfrak{N}_A/\eta$ ratio).

A somewhat better correlation is shown by the Prandtl number (Pr),[4] which is defined as

$$\mathrm{Pr}=C_p\eta/k \qquad (4)$$

where C_p, η, and k are the specific heat, viscosity, and thermal conductivity of the liquid, respectively.

The last column in Table I indicates the approximate constancy of the $\mathfrak{N}_A$/Pr ratio. Thus the coefficient $\mathfrak{N}_A$ can be calculated approximately from the relation $\mathfrak{N}_A \cong 0.053$ Pr.

Since natural convection currents are retarded by viscous drag in the liquid, their presence is a possible explanation for an increase in the value of $\mathfrak{N}_A$ with

[4] W. H. McAdams, *Heat Transmission* (McGraw-Hill Book Company, New York, 1953), 3rd ed., p. 470.

increased viscosity. The presence of a convection current was visually confirmed in the carbon tetrachloride experiments. It is suggested that the anomaly in Alty's carbon tetrachloride results mentioned in Paper IV[1] (that is, the effect of decreasing $\mathfrak{N}_A$ with increasing mass flow) might be explained on the basis that acute convection currents could lead into the nucleate boiling region of liquids,[4] so that the bulk liquid is disrupted and the liquid-vapor interfacial area is considerably enlarged, which would result in an *apparent* decrease in the value of $\mathfrak{N}_A$.

The improved correlation of $\mathfrak{N}_A$ with the Prandtl number indicates some coupling between convection and conduction. Thus, it would seem that the $\mathfrak{N}_A$ coefficient for the forced vaporization process must depend on the rate of heat transfer to the liquid-vapor interface both by pure conduction *and* by natural convection.

ACKNOWLEDGMENT

The experimental studies reported in this paper were supported by Armour Research Foundation.

THE JOURNAL OF CHEMICAL PHYSICS VOLUME 33, NUMBER 1 JULY, 1960

Absorption Spectra of Solid Xenon, Krypton, and Argon in the Vacuum Ultraviolet*

O. SCHNEPP† AND K. DRESSLER‡

National Bureau of Standards, Washington 25, D. C.

(Received December 3, 1959)

The absorption spectra of solid xenon, krypton and argon at 4.2°K have been investigated between 3500 and 1200 A. In the region between 1510 and 1200 A solid xenon has four absorption bands, three of which lie within less than 800 cm^{-1} of atomic transitions, all being shifted to lower energy in the solid. Solid krypton has two bands between 1250 and 1200 A which lie within 900 cm^{-1} of atomic transitions but are shifted to higher energy in the solid. No absorption was found in solid argon at wavelengths longer than 1200 A. The experimental results are interpreted and discussed on the basis of valence type interatomic interactions in the excited states. It is predicted that the fluorescence spectra of these solids would be displaced to lower energy by about 1 ev.

I. INTRODUCTION

PROPERTIES of the condensed rare gases have been the subject of many investigations and much is known about the thermodynamics and structure of these substances in the ground state.[1] They all crystallize to form a cubic structure belonging to the space group Fm3m (O_h^5) with four atoms per unit cell. X-ray investigations have been made on argon,[2,3] on krypton,[4–7] and on xenon.[6,7] These solids are the simplest examples of "molecular crystals" or crystals bound solely by forces of the van der Waals type. In recent years there has been interest in the excited states of molecular crystals of organic substances[8] and a consistent interpretation of the spectra of these substances have been successfully evolved. The theory used in the interpretation of the spectra of molecular crystals is based on the early work by Frenkel[9] and Peierls[10] who used solid argon as a model. It is obvious that an investigation of these model molecular crystals is desirable. Recently Knox[11] has discussed the excited states of solid argon and has made predictions concerning the absorption spectrum of this substance. It was this theoretical work which largely stimulated the present work.

The absorption spectra of xenon in the gas phase at high pressures, and in the liquid phase have been investigated by McLennan and Turnbull.[12] Their attempts at obtaining the spectrum of the solid were limited to thick films which were opaque to wavelengths shorter than 1800 A presumably owing to high scattering.

* This research was performed under the National Bureau of Standards Free Radicals Research Program, supported by the Department of the Army. This work was supported in part by the Office of Ordnance Research.

† On leave from the Department of Chemistry, Israel Institute of Technology, Haifa, Israel.

‡ Guest Scientist from the Department of Chemistry, Catholic University of America, Washington 17, D.C. Present address: Princeton University Observatory, Princeton, New Jersey.

[1] E. R. Dobbs and G. O. Jones, Repts. Progr. in Phys. **XX**, 516 (1957).

[2] J. De Smedt and W. H. Keesom, Commun. Phys. Lab. Univ. Leiden **178b**, 19 (1925).

[3] F. E. Simon and C. von Simon, Z. Physik **25**, 160 (1924).

[4] W. H. Keesom and H. H. Mooy, Proc. Acad. Sci. Amsterdam **33**, 447 (1930).

[5] H. H. Mooy, dissertation, University of Leiden, 1931.

[6] M. Ruhemann and F. E. Simon, Z. physik. Chem. **15**, 389 (1931).

[7] G. Nasini and A. G. Natta, Rend. Accad. Lincei **11**, 1009 (1930).

[8] D. S. McClure, *Solid State Physics* (Academic Press, Inc., New York, 1959), Vol. VIII, p. 1.

[9] J. Frenkel, Phys. Rev. **37**, 17, 1276 (1931).

[10] R. E. Peierls, Ann. Phys. **13**, 905 (1932).

[11] R. S. Knox, J. Phys. Chem. Solids **9**, 238, 265 (1959).

[12] J. C. McLennan and R. Turnbull, Proc. Roy. Soc. **A129**, 266 (1930); **A139**, 683 (1933).

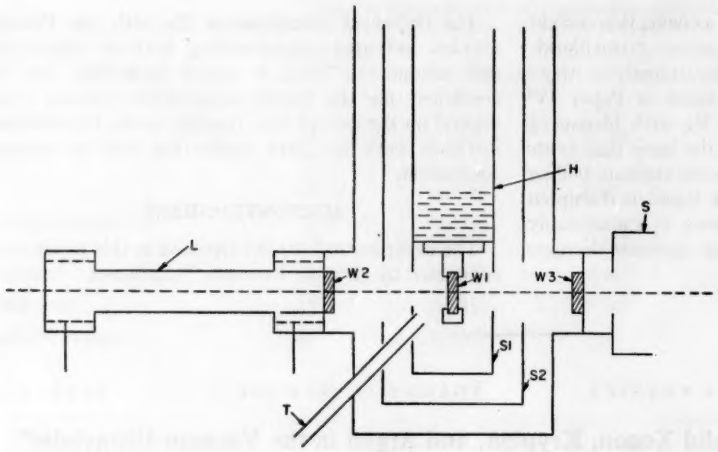

Fig. 1. Schematic representation of the experimental assembly: *H*, helium chamber of double stainless steel Dewar; *W*1, *W*2, *W*3, lithium fluoride windows, 1 mm thick; *S*1, liquid helium cooled radiation shield; *S*2, liquid nitrogen cooled radiation shield; *T*, gas inlet tube for deposition; *L*, light source; *S*, slit of vacuum spectrograph.

Among the very few successful investigations of the absorption spectra of condensed gases in the vacuum ultraviolet are those of Granier-Mayence, Romand, and Vodar.[13] Working with very thin solid films condensed onto a lithium fluoride window at 20°K, these authors obtained the absorption spectra of solid N_2O, NO, O_2, and benzene at wavelengths longer than 1500 A. A similar experimental approach was followed in the present work on the absorption spectra of condensed xenon, krypton, and argon. The investigations were carried out at liquid helium temperature and in a wavelength range limited on the short-wavelength side at 1200 A.

The same apparatus was used to obtain vacuum ultraviolet absorption spectra of other inorganic gases in condensed phases. The results will be published shortly in this Journal.

II. EXPERIMENTAL

The vacuum spectrograph used was a 2-m grating instrument[14] with photographic detection. It employed a Bausch and Lomb replica grating blazed at 3000 A in first order and giving a dispersion of 8.4 A/mm in first order. The grating had been coated with zinc sulfide to improve the reflectivity in the vacuum ultraviolet.[15] Ilford Q2 and Q3 plates were used. The continuous light for the absorption spectra was provided by sources using condensed discharges through krypton and argon as described by Tanaka.[16] The slit width used throughout was 50 μ. The exposure times necessary with the krypton source did not exceed 30 min in first order, but in order to get satisfactory plate blackening down to 1200 A with the argon source in first order, exposures of up to 4½ hr were necessary. Second-order exposures of 10 min with the argon source were found to produce sufficient plate blackening, owing to the blaze of the grating, although there was overlapping first-order radiation of H_2 which was present as an impurity in the light source.

The experimental assembly is illustrated in Fig. 1. A lithium fluoride window *W*1 was mounted in a copper block which was attached by means of a screw to the bottom of the helium container *H*. The window was in good thermal contact with the helium cooled copper by virtue of indium gaskets. Surrounding the lithium fluoride window and also attached to the helium can *H* was a copper shield *S*1 with two holes in the light path and one to admit the gas to be deposited on the cold window. A liquid nitrogen-cooled copper shield *S*2 had similar openings. The outer wall of the double Dewar made of stainless steel was at room temperature and contained two additional lithium fluoride windows *W*2 and *W*3. They separated the Dewar vacuum, in which the cold window was situated, from the source and from the vacuum space of the spectrograph, respectively.

The rare gases to be studied, xenon, krypton, and argon were of high purity. The gas was admitted into the Dewar through a copper tube *T* and condensed on the cold window to form a smooth layer of solid. Before entering the Dewar the gases were passed through a liquid nitrogen trap in the case of argon and krypton and through a dry ice-acetone trap in the case of xenon. The gas flow was controlled by a needle valve and reproducible flow conditions were achieved by measuring the pressure on the high-pressure side of the deposition tube *T* by means of a thermocouple gauge.

The thickness of the film of condensed rare gas on the cold window could only be estimated to an order of

[13] J. Granier-Mayence and J. Romand, Compt. rend. **235**, 1023 (1952); **236**, 1148 (1953); J. Romand and J. Granier-Mayence, J. Phys. Radium **15**, 62 (1954); J. Granier-Mayence and J. Romand, J. Phys. Radium **14**, 428 (1953); J. Romand and B. Vodar, Compt. rend. **233**, 930 (1951).

[14] We are indebted to the Spectroscopy Section of the National Bureau of Standards for the use of the spectrograph.

[15] We are indebted to Dr. G. Hass and Dr. J. T. Cox, U.S. Army Engineer Research and Development Laboratory, Fort Belvoir, Virginia, for the application of this coating.

[16] Y. Tanaka, J. Opt. Soc. Am. **45**, 710 (1955).

magnitude. This was done by measuring the decrease of pressure in the gas storage flask after a known deposition time and controlled flow conditions, and assuming a reasonable deposition geometry. It was also assumed that the thickness of the deposited layer varied linearly with time and with the indicated pressure as described. According to our experience these assumptions are justified within wide limits. The film thicknesses used in obtaining the absorption spectra ranged from the order of 10 A to several thousand A for all three substances investigated. The rate of deposition was always the maximum possible, such that the total thickness was deposited within a few seconds. According to x-ray studies[17] a fast deposition rate is desirable since it may lead to a more ordered structure of the deposit.

The tube T was 9 cm long and had an internal diameter of 3 mm and the pressure readings were adjusted to values between 10^{-3} and 10^{-1} mm Hg, corresponding to flow rates between 10^{-2} and 10^{-4} cm^3/sec of gas at NTP.

Previous investigators[18] reported that they were unable to investigate the absorption spectra of condensed gases at low temperatures below 1500 A because of "general absorption." The same difficulty was encountered in earlier stages of this work and it was found that traces of water vapor, accidentally deposited on the cold window, caused strong absorption below 1600 A.[18] This difficulty existed only as long as the cold window was openly exposed to the vacuum space of the spectrograph. However, after the window $W3$ was inserted, it was found that the cold window remained transparent for hours. As a further precaution, the outer radiation shield $S2$ was cooled to liquid nitrogen temperature at least 30 min prior to cooling the deposition window $W1$. During this period the window was kept at room temperature by blowing warm air through the helium container H. This procedure is believed to be essential for successful low-temperature absorption spectroscopy below 1600 A.

III. EXPERIMENTAL RESULTS

Very strong absorption features were observed for condensed xenon and krypton at liquid helium temperature between 1510 and 1200 A. These results are shown in Figs. 2 to 4 where representative plates of the absorption spectra obtained with a wide range of film thicknesses are reproduced. The levels of the free atoms are indicated for comparison and are labeled by the J values of the upper states. Tables I and II list the wavelengths and frequencies of the absorption features together with their widths. The frequencies of atomic transitions are listed for comparison and shifts from the gas to the solid are indicated where a correspondence between free atom and solid levels is assumed. The wavelengths listed in Tables I and II represent the centers of the bands except for the 1360-A xenon absorption for which the short wavelength edge is given. Half-intensity widths of the bands were determined by visual estimation directly from the plates.

The absorption spectrum of solid xenon in the spectral range investigated consists of four features. In the thinnest films two extremely intense bands were observed, centered at 1485 and 1305 A, respectively, and having half-widths of approximately 500 and 300 cm^{-1}, respectively. These bands broaden symmetrically about their centers when thicker layers are examined. A third band with a sharp short-wavelength edge at 1360 A appears with an intensity about one-third of that of the strong bands and a half-width of 500 cm^{-1}. The fourth absorption is about one-tenth as intense as the strongest features and is centered at 1508 A with a half-width of 200 cm^{-1}. This last band has a very sharp edge on its long-wavelength side which shifts only to 1516 A for layers 1000 times as thick as those needed for observation. At these thicknesses this band is continuous with the intense absorption at 1485 A.

For solid krypton two bands were observed which were very similar in absolute as well as relative intensity to the two long-wavelength bands of solid xenon. The intense band at 1222 A, 300 cm^{-1} in width is preceded by a weaker band at 1244 A, of the same width. The weaker band at longer wavelength has a very sharp long-wavelength edge as is illustrated in Fig. 4 where it can be seen in solid layers varying in thickness by a factor of 100. The edge lies at 1255 A in a layer 200 times thicker than that needed for observation.

No absorption of solid argon was observed above 1200 A although layer thicknesses up to 10 μ, i.e., 1000 times those necessary to see absorption in xenon or krypton were investigated.

IV. DISCUSSION OF RESULTS

The atomic energy levels of xenon, krypton, and argon are described in detail in Moore's *Atomic Energy Levels*.[19] Energy level diagrams are given in Figs. 5 and 6 for the low-lying atomic states and the observed levels of the crystals of xenon and krypton, respectively. The ground states of the atoms are ^1S states with filled p shells. The lowest excited configuration is $5p^56s$ for xenon($4p^55s$ for krypton) and four states result from it, two with $J=1$ to which dipole transitions from the ground state are allowed (full lines in the figures) and one of each $J=2$ and $J=0$ to which transitions are forbidden (broken lines in the figures). Pair coupling or jl coupling is appropriate and this accounts for the characteristic grouping of the states. Recently Tanaka[20] has observed the transitions to the $J=2$ levels in xenon and krypton gases in absorption. They appear at pres-

[17] H. S. Peiser and F. A. Mauer (private communication).
[18] E. J. Cassel, Proc. Roy. Soc. (London) **A153**, 534 (1936); K. Dressler and O. Schnepp (to be published).
[19] C. E. Moore, *Atomic Energy Levels* Natl. Bur. Standards Circ. No. **467**, (1952).
[20] Y. Tanaka (private communication).

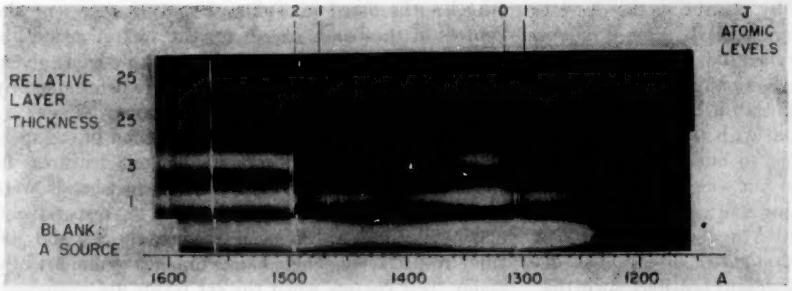

FIG. 2. The absorption spectrum of solid xenon. The light source was an argon source.

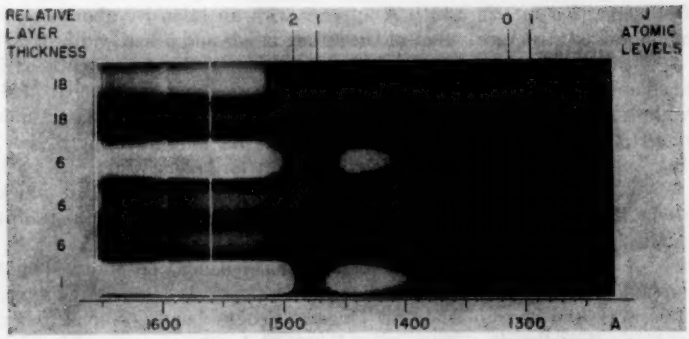

FIG. 3. The absorption spectrum of solid xenon. The light source was a krypton source.

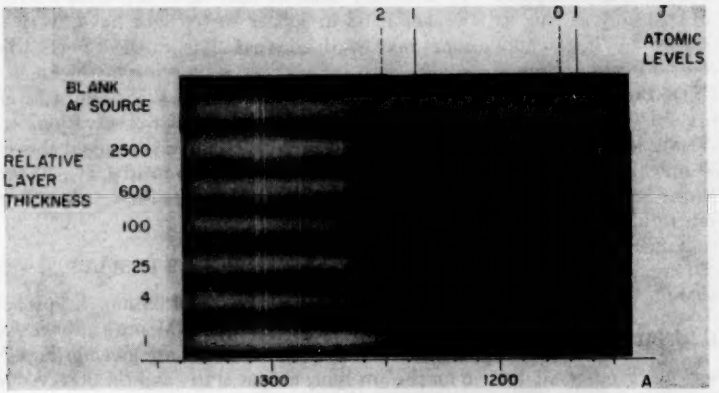

FIG. 4. The absorption spectrum of solid krypton. The light source was an argon source. The spectra were photographed in the second order of the grating.

TABLE I. Absorption bands of solid xenon.

Crystal absorption				Atomic level			Shift: crystal-atom
Wavelength A	Frequency cm^{-1}	Width cm^{-1}	I[a]	Frequency cm^{-1}	J[b]	Character	cm^{-1}
1508	66 310	200	1	67 069	2	*f*	−760
1485	67 340	500	10	68 046	1	*a*	−710
1360	73 530	500	3				
				76 198	0	*f*	
1305	76 630	300	10	77 186	1	*a*	−560

[a] The intensity *I* of the crystal absorptions are given on a comparative scale from 1 to 10.

[b] The *J* value of the upper state of the atom is indicated together with its character to transition to this state from the ground state: "*a*" designates a dipole-allowed transition, "*f*" a dipole-forbidden transition.

TABLE II. Absorption bands of solid krypton.

Crystal absorption				Atomic level			Shift: crystal-atom
Wavelength A	Frequency cm^{-1}	Width cm^{-1}	I	Frequency cm^{-1}	J	Character	cm^{-1}
1244	80 390	300	1	79 973	2	*f*	+420
1222	81 830	300	10	80 918	1	*a*	+910

sures about 10 000 times greater than those needed for observation of the allowed transitions. He did not observe the transitions to the $J=0$ levels. In krypton and argon the states derived from the next higher configuration ($4p^5 5p$ for krypton) lie more than 5000 cm^{-1} above the states discussed. In xenon, however, the analogous states (configuration $5p^5 6p$) lie very close, the lowest of them being only 85 cm^{-1} above the highest level of the configuration $5p^5 6s$. These two close-lying levels both have $J=1$ but they differ in their odd-even character.

Comparison between the crystal absorption spectrum of xenon and its gas spectrum shows that three of the excited states observed in the solid lie very close to atomic states. The two intense absorptions at 1485 and at 1305 A therefore appear to be derived from the atomic transitions to the $J=1$ states of the lowest excited configuration. The weak absorption at 1508 A is similarly interpreted to be derived from the forbidden transition to the atomic $J=2$ state. The shifts between the gas phase and solid state are the same for all three transitions within the widths of the absorption, as indicated in Table I. The two observed absorption features of solid krypton are similarly interpreted as related to the two lowest energy atomic transitions, although it should be noted that the shifts from gas to solid are here different for the two states and are both to higher energy whereas the shifts were all to lower energy in xenon. We shall defer the discussion of the interpretation of the solid xenon absorption at 1360 A to a later paragraph.

Recently Mulliken[21] has investigated the potential curves of diatomic xenon. Although his results are still

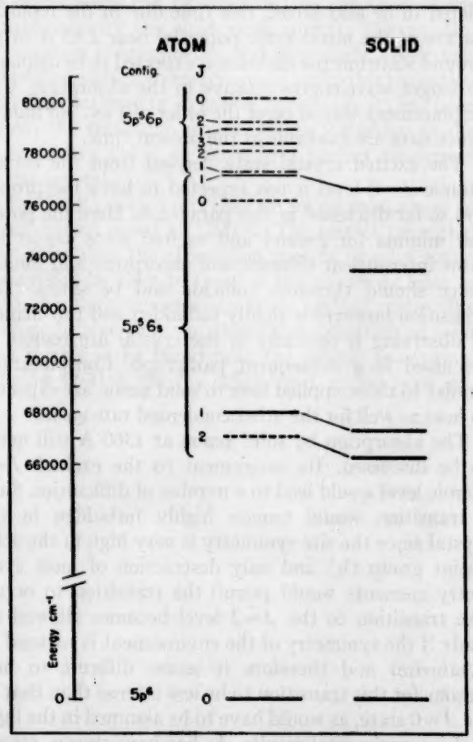

FIG. 5. Energy level diagram of atomic and solid xenon.

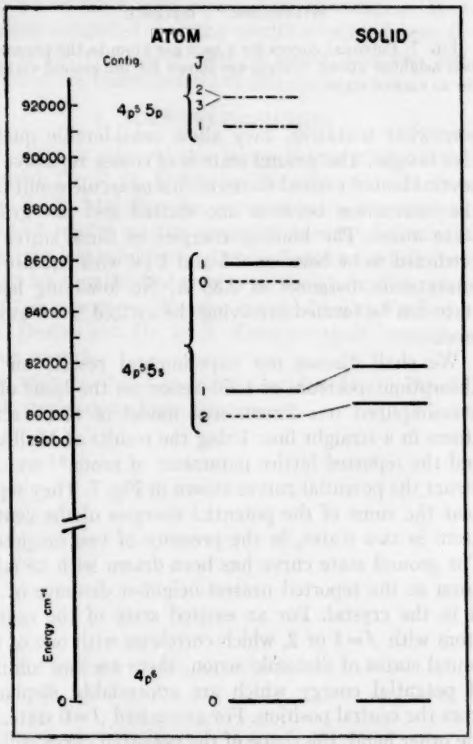

FIG. 6. Energy level diagram of atomic and solid krypton.

[21] R. S. Mulliken (unpublished).

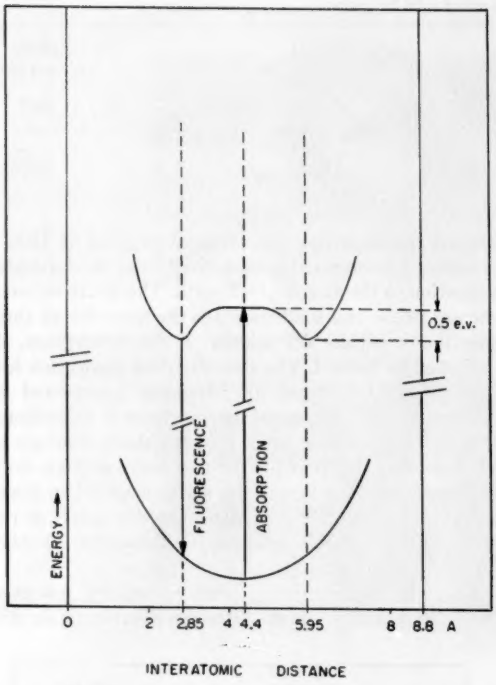

FIG. 7. Potential curves for a rare gas atom in the presence of two neighbor atoms. Curves are shown for the ground state and for an excited state.

somewhat tentative, they allow considerable qualitative insight. The ground state is of course repulsive but several bound excited states of this molecule result from the interaction between one excited and one ground state atom. The binding energies of these states are predicted to be between 0.5 and 1 ev with equilibrium interatomic distances of 2.85 A. No low-lying bound state can be formed involving the excited $J=0$ atomic level.

We shall discuss our experimental results on the absorption spectrum of solid xenon on the basis of an oversimplified one-dimensional model of three xenon atoms in a straight line. Using the results of Mulliken, and the reported lattice parameter of xenon[6,7] we construct the potential curves shown in Fig. 7. They represent the sums of the potential energies of the central atom in two states, in the presence of two neighbors. The ground state curve has been drawn with its minimum at the reported nearest-neighbor distance of 4.4 A in the crystal. For an excited state of the central atom with $J=1$ or 2, which correlates with one of the bound states of diatomic xenon, there are two minima of potential energy which are appreciably displaced from the central position. For an excited $J=0$ state, on the other hand, the shape of the potential curve will be closely similar to that of the ground state. We are thus considering a restricted one-dimensional problem as far as nuclear motions are concerned whereas the real problem is three-dimensional. In addition we are assuming that the electronic excitation is localized on one particular atom in the crystal. This is in contrast to existing theories[9–11] which describe the states of a *rigid* crystal in terms of delocalized "exciton" states. Assumption of rigidity of the lattice involves a serious limitation in view of the basically different types of interactions of an atom with its neighbors in the ground and excited states, i.e., van der Waals and valence-type interactions, respectively. It is hoped that future theoretical work will take account of this difficulty.

During electronic excitation the nuclear coordinates will not change. In a "bound" excited state, the resulting configuration will then be far removed from equilibrium (cf. Fig. 7). Vibrations will therefore be strongly excited and a crude estimate indicates that the vibrational levels of the system will be very closely spaced in this region. Although we have concerned ourselves here with the one-dimensional problem only, we believe that the gross features of the model apply to the real physical situation in the crystal. We therefore conclude that the considerable widths of the observed absorptions are due to the excitation of vibrations which accompanies the electronic excitation. An experiment decisive for the validity of the proposed model suggests itself: the fluorescence spectrum of solid xenon is predicted to be also broad, this time due to the repulsive nature of the interatomic potential near 2.85 A in the ground state but the emission is expected to be displaced to longer wavelengths relative to the absorption. This displacement should be of the order of 1 ev. No fluorescence data are available at the present time.

The excited crystal state derived from the excited atomic $J=0$ level is not expected to have the properties so far discussed in this paragraph. Here the potential minima for ground and excited state are at the same internuclear distance and absorption and fluorescence should therefore coincide and be sharp. This transition however is rigidly forbidden and the chances of observing it optically in the crystal are remote as discussed in a subsequent paragraph. Considerations similar to those applied here to solid xenon are expected to hold as well for the other condensed rare gases.

The absorption by solid xenon at 1360 A still needs to be discussed. Its assignment to the excited $J=0$ atomic level would lead to a number of difficulties. Such a transition would remain highly forbidden in the crystal since the site symmetry is very high in the solid (point group O_h) and only destruction of most symmetry elements would permit the transition to occur. The transition to the $J=2$ level becomes allowed already if the symmetry of the environment is reduced to tetrahedral and therefore it seems difficult to find reasons for this transition to be less intense than that to the $J=0$ state, as would have to be assumed in the light of the experimental results. As has been shown, strong coupling with the lattice vibrations is not expected

to accompany excitation to the $J=0$ state so that no asymmetric distortion would occur which could account for the considerable intensity observed. Finally the shift in energy going from vapor to solid, which would have to be assumed, is much greater than in the case of the other three transitions in xenon. It is here proposed that the absorption represents a transition to a state derived from an atomic $J=1$ state of the configuration $5p^5 6p$. In the diatomic molecule, Mulliken predicts such a state at considerably lower energy than the molecular states derived from the higher of the two $J=1$ levels of the atomic configuration $5p^5 6s$. Due to the noncrossing rule, however, Mulliken indicates that the more stable diatomic state may have to be correlated with the atomic configuration $6s$ rather than $6p$.

We can now interpret all four of the absorption bands observed in solid xenon at 1508, 1485, 1360, and 1305 A, as transitions to excited states of the crystal which are the analogs of four bound excited states of the diatomic molecule. The band at 1508 A arises from a state derived from an atomic state with $J=2$, the 1485 A band from the lower $J=1$ state of the configuration $5p^5 6s$, and both the 1360 and 1306 A bands from the higher $J=1$ state of this configuration.

The transitions in the solid which have been correlated with the electric dipole forbidden atomic transitions to states of $J=2$ have relatively high intensity. This discrepancy can be explained on the basis of the perturbations by the solid environment. The equilibrium position is asymmetric and only slight distortions from perfect cubic symmetry would make this transition allowed, as outlined in an earlier paragraph. As has been implied, the transition would remain forbidden in the site symmetry O_h of an atom in a perfect condensed rare gas crystal.

It has been pointed out that we found solid argon to be transparent down to 1200 A. The results presented above show that the absorption spectra of solid xenon and krypton lie close to those of the atoms, at least as long as we limit ourselves to lower excited states. We therefore believe that the absorption spectrum of solid argon is also to be found near the atomic absorption, i.e. below 1100 A. On the other hand, as has been discussed, the fluorescence spectra are expected to be displaced to longer wavelength by about 1 ev.

No good reason can be given for the opposite sign of the gas to solid spectral shifts for xenon as compared with krypton. In both cases, however, the shifts are small, being less than 0.1 ev.

The microscopic structure of the investigated samples of solid xenon, krypton, and argon needs to be discussed. The question arises what the relationship is between our results and those which would be obtained with perfect crystals. As has been pointed out, the thinnest layers investigated here were only of the order of 10 A thick. This is hardly a good crystal and most of the atoms in such a film will not be at sites of high symmetry. However, it was found that the spectra obtained with samples a thousand times thicker were still fully consistent with the results obtained with the thinnest films. It is thus concluded that the most intense features of the absorption spectra are not affected. The short-range order is also expected to be rather high in the case of krypton and xenon deposited from the gas on a cold surface at 4.2°K according to the work of Peiser and Mauer.[17] In the case of argon there is some doubt concerning long-range order but the short-range environment is not expected to differ greatly from the structure of good crystals although disclocations have been reported to be common. It is therefore concluded that the results presented here do apply to the crystalline state of xenon, krypton, and argon and are characteristic of this state.

V. ACKNOWLEDGMENTS

We wish to acknowledge many illuminating discussions with Dr. P. H. E. Meijer. We wish to thank Professor R. S. Mulliken for permission to use his unpublished results on the potential curves of diatomic xenon. We are indebted to Dr. Y. Tanaka for information on his unpublished results on the absorption spectra of the rare gases. We also are indebted to Professor D. L. Dexter and Dr. R. S. Knox for their comments on our results.

We wish to thank in particular Dr. H. P. Broida for his guidance and encouragement.

Infrared Studies of Crystal Benzene. II. Relative Intensities

CHARLES A. SWENSON* AND WILLIS B. PERSON

Department of Chemistry, State University of Iowa, Iowa City, Iowa

(Received November 12, 1959)

Intensities of the absorption bands observed with a thin sample of polycrystalline benzene have been measured relative to the absorption of ν_{20} at 1036 cm^{-1}. The gas-phase-allowed fundamentals are much the strongest bands in the spectrum. The relative intensities of these fundamentals are considerably different from the relative intensities in the gas or liquid phase. The experimental errors are discussed in detail with the conclusion that the observed difference in relative intensities are well outside any conceivable experimental errors. As a result, it is concluded that existing theories of spectra in condensed phases must be modified to predict different behaviour for each fundamental vibration. Finally, attention is drawn towards some of the anomalies still existing in the assignment of vibrational frequencies in the benzene molecule.

INTRODUCTION

ALTHOUGH there have been several studies in recent years of the infrared intensities of small molecules in the gas phase, only a very few studies of intensities in condensed phases have been made.[1] This situation exists in spite of the need for quantitative studies of this type. Statements have been often made[2] to the effect that there may be drastic changes of intensities in condensed phases, in comparison with the gas-phase studies, with relatively minor changes in frequency. However, all attempts at interpreting the spectra of molecules in condensed phases are based on the idea that the molecule in a condensed phase is not too different from the gas phase. For example, the "oriented gas" model[3] is used almost universally to interpret solid spectra (although always with reservations). The attempts to predict changes in spectra due to the change in dielectric constant[4–6] predict the same change for all the bands, although Buckingham points out that this need not be the case. Needless to say, it would be an extremely desirable situation if the bands had the same relative intensities in condensed phases as they have in the gas phase.

Thus, we have on the one hand dire predictions of marked changes in spectra as the phase changes and on the other hand the naive hope that these changes are really not so bad. It therefore seemed that it was time to make some quantitative measurements. In view of the marked difference between the two viewpoints, even relative intensity measurements would be informative. The experimental difficulties associated with absolute intensity measurements are formidable, and so we decided to determine first the relative intensities of bands appearing in the spectrum of solid benzene.

This molecule was chosen for study because it has the very desirable physical properties that permit ready observation in all three phases. Also, there is considerable information about this molecule: crystal structure,[7] studies of its solid-state spectrum,[8–10] studies of gas-phase intensities,[11] and—coincident with our study—a study of liquid-phase intensities.[12,1(c)] The structure of the benzene crystal seems to indicate that some difficulty due to specific interactions between molecules may be encountered, but this is probably no worse than for most solids.

Our first studies showed that, in spite of all this study, the improved resolution of a double-pass prism spectrometer could give us additional information about the splittings of the benzene fundamentals due to solid-state interactions.[13] These studies showed that each degenerate fundamental possessed a rather complex structure which would cause trouble in intensity studies, due to the fact that even the double-pass prism spectrometer does not have perfect resolving power.

This extra complication was balanced by the discovery that the complexity of the solid-state spectrum due to gas-phase-inactive bands becoming active in the condensed phase had been overemphasized. Earlier studies[8–10] had been designed to study just these changes and had been made on relatively thick crystals of

* Present address: Department of Chemistry, Wartburg College, Waverly, Iowa.

[1] (a) D. F. Eggers, Jr., and C. B. Arend, J. Chem. Phys. **27**, 1405 (1957); (b) C. C. Ferriso and D. F. Hornig, Symposium on Molecular Structure and Spectroscopy, Columbus, Ohio, 1955. (c) I. C. Hisatsune and E. S. Jayadevappa, J. Chem. Phys. **30**, 848 (1959).

[2] See, for example, D. F. Hornig, Discussions Faraday Soc. **9**, 115 (1950).

[3] G. C. Pimentel, A. L. McClellan, W. B. Person, and O. Schnepp, J. Chem. Phys. **23**, 234 (1955).

[4] S. R. Polo and M. K. Wilson, J. Chem. Phys. **23**, 2376 (1955).

[5] W. B. Person, J. Chem. Phys. **28**, 319 (1958).

[6] A. D. Buckingham, Proc. Roy. Soc. (London) **A248**, 169 (1958).

[7] E. G. Cox, Revs. Modern Phys. **30**, 159 (1958).

[8] R. S. Halford and O. A. Schaeffer, J. Chem. Phys. **14**, 141 (1946).

[9] R. D. Mair and D. F. Hornig, J. Chem. Phys. **17**, 1236 (1949).

[10] S. Zwerdling and R. S. Halford, J. Chem. Phys. **23**, 2221 (1955).

[11] (a) H. Spedding and D. H. Whiffen, Proc. Roy. Soc. (London) **A238**, 245 (1956). (b) J. Overend and B. Crawford, Jr. (private communication).

[12] E. S. Jayadevappa, Ph.D. thesis, Kansas State University, 1959.

[13] C. A. Swenson, W. B. Person, D. A. Dows, and R. M. Hexter, J. Chem. Phys. **31**, 1324 (1959).

benzene. When samples of solid benzene were used which were thin enough for studies of the intensities of gas-phase-allowed fundamentals, the spectrum is remarkably simple (see Fig. 1). While it is true that some absorption bands appear which are not present in the gas phase, their intensities are an order of magnitude less than the intensities of the gas-phase-allowed fundamentals.

We thus decided to measure relative intensities of these bands as a first step in a study of the intensities of the bands in solid benzene.

EXPERIMENTAL PART

A. Procedure

The experimental procedure was basically extremely simple. Benzene vapor was condensed onto a window which was cooled to the temperature of liquid nitrogen. The absorption spectrum of the polycrystalline film thus formed was studied, and the intensity of a given band was measured relative to the intensity of the 1036 cm^{-1} fundamental for this same film.

The benzene used was reagent grade and had been dried over sodium wire. This was distilled and the second fraction collected (BP, 80.0±0.3°C). The observed spectrum compared exactly with the literature,[14] indicating that the sample was quite pure. In particular, no absorption was observed from the strong thiophene bands[15] at 713, 835, 1084, 1253, and 1408 cm^{-1}.

The cold cell used in this study was of standard design.[16] A brass cooling block was soldered to a copper-to-glass "housekeeper" seal at the bottom of the reservoir. A 25- x 16- x 5-mm. KBr or CsBr window was mounted in the center of the cooling block. It was clamped tightly against the surface by a brass plate and four screws which screwed into the cooling block. Apiezon "Q" wax was packed around the window to insure good thermal contact. A copper-constantan thermocouple was imbedded in the window so that temperature measurements could be made. The sample was sprayed onto the window through a nozzle which was then turned out of the beam. Further details of this cell are given elsewhere.[17] The cell was connected to a vacuum line. For sampling, an open-end mercury manometer was used for pressures of benzene down to 1 cm of mercury. Below that, a differential dibutylphthalate manometer was used to measure pressures to 1 mm of mercury. Some control of the sampling could be achieved by filling a known volume of the vacuum line to a given pressure measured on the differential manometer, and then condensing all this benzene vapor onto the cooled window. The vapor was deposited rapidly on the window; the time allowed for deposition was approximately 30 sec.

[14] Am. Pet. Inst. Research Project 44, Infrared Absorption Spectrograms, Table 498.
[15] Work cited footnote 14, Table 364.
[16] E. L. Wagner, Ph.D. thesis, Brown University, 1948.
[17] C. A. Swenson, Ph.D. thesis, State University of Iowa, 1959.

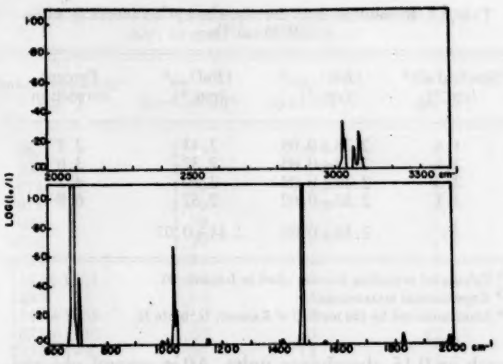

FIG. 1. Survey spectrum of a thin polycrystalline film of benzene. (The thickness is about 10 μ.) Pressure in the filling line: 3.6 cm dibutylphthalate.

The spectra were obtained on a Perkin-Elmer Model 12c spectrometer, which had been converted to double-pass operation. The amplifier was a Perkin-Elmer Model 13 amplifier that contained the proper conversions to permit it to be used for single beam operation. The signal from the amplifier was fed to a Brown recorder, where it was recorded on log paper.

Auxiliary source optics were constructed[17] in order to provide an external focus of the light beam at a position where the cold cell could be accomodated. These external optics as well as the internal optics could be flushed with air that had been passed through alumina columns, and thus reduce the absorption due to atmospheric water and carbon dioxide.

Prisms were selected in order to achieve the best possible resolution in the region of each absorption band. For the four bands at 687, 1036, 1478, and 3063 cm^{-1}, the prisms used were KBr, NaCl, CaF_2, and LiF, respectively. The spectral slit width was between one and three cm^{-1} in all cases. Calibration of the prisms was by the method of Downie, *et al.*[18]

Relative intensities of the four benzene fundamentals were obtained from the spectra of two different bands measured with the same sample film. The amount of sample was chosen so that the absorption intensity for each band was such that it could be measured with the highest degree of accuracy. For every experiment each absorption band was traced in triplicate. A large number of determinations were made of the intensity ratios in order to observe scatter.

Background spectra were run after the cell had been allowed to warm up and the sample film had been distilled off of the window. The background did not always coincide with the wings. In these cases the backgrounds were adjusted on the replots of the absorption bands, as this shift was quite uniform across regions of absorption. At times this amounted to as

[18] A. R. Downie, M. C. Magoon, T. Purcell, and B. Crawford, Jr., J. Opt. Soc. Am., 43, 941 (1953).

TABLE I. Resolution error for the absorption intensity of ν_{20} (1036 cm^{-1}).

Spectral slit[a] (cm^{-1})	$(Bnl)_{expt}$[b] (cm^{-1})	$(Bnl)_{cor}$[c] (cm^{-1})	Percent correction
1.6	2.38±0.08	2.43	2.2
2.1	2.23±0.05	2.32	3.6
2.3	2.40±0.03	2.50	4.2
3.1	2.35±0.02	2.52	6.8
Av	2.34±0.06	2.44±0.07	

[a] Calculated according to work cited in footnote 20.
[b] Experimental measurement.
[c] Areas corrected by the method of Ramsay, footnote 22.

much as 0.15 absorbance units. After several observations of a particular region, the appearance of the background became well known, and was then drawn in on the spectra. This made more observations possible in a shorter amount of time and probably introduced little error.

The spectra were replotted in the usual manner: i.e., $\log(I_0/I)$ vs frequency. The data for the replots were obtained from the strip chart by taking readings of I_0 and I at intervals of 1 cm^{-1} or less. Log (I_0/I) was determined for each interval, and plotted vs frequency. The area under the curve was measured with a Keuffel and Esser compensating polar planimeter. The values of the areas obtained from the three traces of an absorption band were averaged. The area was then multiplied by 2.303 to give the values of the integrated absorbance, *Bnl*.[19] The areas were measured for the band being studied, and for the 1036 cm^{-1} reference band. It was then a simple matter to determine the ratios of the areas and therefore the intensity of this band relative to the intensity of the 1036 cm^{-1} band. The total absorption of the 1036 cm^{-1} doublet integrated from 1017 to 1060 cm^{-1} was used for the standard reference intensity.

B. Error Analysis

In these attempts at measuring even relative intensities of solids, it is possible that sizable errors can occur. For this reason it is necessary to discuss these possibilities and try to estimate the order of magnitude of each error.

1. Resolution

First of all, we should consider the error due to the finite resolving power of our instrument. The half-intensity widths of absorption bands in solids are quite small, and compare with the spectral slit width of a prism spectrometer. We considered in detail the 1036 cm^{-1} fundamental, ν_{20}. As the first paper[13] in this series shows, this band is quite complex, consisting of three components. The half-intensity width of the total band as observed under prism resolution is about 10 cm^{-1}, which is to be compared with a calculated[20] spectral slit width of 1.8 cm^{-1}. However, under grating resolution, we see[13] that this band consists of a still only partially resolved doublet at 1032.6 and 1034.7 cm^{-1}, which has an apparent half-intensity width of 3.4 cm^{-1}, and a singlet at 1039 cm^{-1} with an apparent half-intensity width of 2.3 cm^{-1}! If we apply the criterion of Russell and Thompson,[21] that the ratio of half-intensity width to slit width, $\Delta\nu_{\frac{1}{2}}/s$, be greater than 5 for accurate intensity measurements, then we see that we can expect trouble. In order to determine experimentally the size of the error to be expected, the intensity of the 1036 cm^{-1} band was measured at different spectral slit widths ranging from 1.6 to 3.1 cm^{-1}. The values of *Bnl* are reported in the second column of Table I. These values are all the same within experimental error. This shows either that our slit is already so wide at the narrowest setting that there is little effect as a result of opening it further, or else that the errors due to the finite resolving power of the instrument are not very large.

These effects can be investigated further with the aid of the paper by Ramsey.[22] (Some extrapolation of these tables was necessary for the very narrow bands.) Using the grating spectrum (Fig. 2 of work cited in footnote 13) of this band to give its true band shape, the corrections to the intensity can be calculated. The calculated[22] true half-intensity width of 3.1 cm^{-1} for the doublet at 1033 cm^{-1} indicates that a correction of 2% should be added to the intensity of this doublet, for the spectral slit of 1.6 cm^{-1}. From the calculated true half-intensity width of 1.70 cm^{-1} for 1039.4 cm^{-1} band, we calculate that a correction of 2.8% should be added to its intensity. Thus, since the ratio of the intensity of the 1039 cm^{-1} band to the 1033 cm^{-1} doublet is about 1 to 3, the total correction to be added to the entire band is about 2.3% for this particular spectral slit width. In this way we calculated the corrected values of *Bnl* recorded in the third column of Table I. We see that even for the largest slit the calculated correction to *Bnl* is less than 7%. Furthermore, the scatter of the corrected values is just as bad as the scatter of the uncorrected values, indicating that there is probably little basis for preferring the corrected values. Thus, we conclude that, although this error due to finite resolving power can be fairly large (perhaps as much as 10%), and is one of the limiting errors, still it is not excessive. We have used the uncorrected values for the intensities in all cases, since our spectral slit width for most of the measurements in this region was 1.8 cm^{-1}.

[19] $Bnl = \int_{\text{band}} \ln(T_0/T)_\nu d\nu$. $\text{Ln}(T_0/T)_\nu$ is the apparent absorbance at a given frequency ν, n is the concentration in moles per liter, l is the cell length in cm, and B is the apparent integrated molar absorption coefficient in cm^{-1} cm^3 mM^{-1} (darks).

[20] Calculated from the graphs in the Perkin-Elmer Instruction Manual, Vol. I.

[21] R. A. Russell and H. W. Thompson, Spectrochim. Acta **9**, 133 (1957).

[22] D. A. Ramsey, J. Am. Chem. Soc. **74**, 72 (1952).

For the other bands we do not have sufficient resolution with our small gratings to show the detailed structure such as for ν_{20}. It seems reasonable to expect that the resolution error is no greater for each of these bands than the error for ν_{20}. Table II shows the ratio of half-intensity width for the total band to the spectral slit width for each of the bands we have measured.

We see that for the gas-phase-allowed fundamentals this ratio is high enough so that this expectation is probably correct. The ratio for the band at 1480 cm^{-1} may possibly have more error due to resolution error than the others. However, we note that the weaker gas-phase-inactive fundamentals (e.g., see those around 970–1010 cm^{-1}) are much sharper, and the relative intensity measurements will consequently show greater errors. However, even for these, the calculated corrections are not too large. For the 1010 cm^{-1} band, for example, with a spectral slit width of 1.6 cm^{-1}, we calculate[22] that the correction to be added to the measured intensity is only 22%.

This does mean that the intensity ratios reported for the gas-phase-inactive fundamentals will be associated with errors of this magnitude. They were all measured relative to the intensity of this band at 1010 cm^{-1}, and its ratio to the 1036 cm^{-1} band was used to convert the ratios to the values reported in Table III. Thus, even the relatively wide E_{1u} combination bands will probably be in error. This error is such that the numbers reported for the intensity ratio of wide bands will be too high, possibly by about 25%.

Finally we should point out that we have been considering the error in *absolute* intensities in this discussion. The error depends on the maximum absorbance of the measured band, and this it will be different for each band and hence affect the relative intensity measurement. However, some cancellation of error can be expected. Thus, we conclude that the probable error in the intensity ratios of the gas-phase-allowed fundamentals due to finite resolving power is of the order of 5 to 10%.

2. *Scattering, Reflection, and Nonuniformity*

Jones and Sandorfy[23] have indicated other errors which may be important in studying absorption intensities in solids. These are: nonuniformity of the sample, scattering, and reflection. They also vary with absorbance, so are different for each band, and hence will affect the ratios somewhat. Scattering and reflection generally were negligible in our experiments. The thin polycrystalline films obtained in our studies were usually quite transparent both to visible light and to infrared light. Occasionally the absorbance of the wings of an absorption band did not coincide with the background, indicating some scattering or reflection, but we believe the correction procedure outlined above was sufficient so that the resulting error in *Bnl* is negligible (less than 5%). It is, of course, possible that the change in index of refraction through an absorption band will result in a change in reflectance in this region of the spectrum, which would be undetected. However, preliminary experiments convinced us that, under the experimental conditions suitable for absorption measurements, no observable change in reflectance occurs in the region of absorption of even the strongest bands of solid benzene.

TABLE II. Ratio of the apparent half-intensity width, $\Delta\nu_j^a$, to spectral slit width, s.

Band frequency (cm^{-1})	Spectral slit[a]	$\Delta\nu_j^a$ (cm^{-1})	$\Delta\nu_j^a/s$
687	2	10	5
705	2	3.5	1.7
974	1.79	3.0	1.7
978	1.79	3.0	1.7
987	1.79	3.0	1.7
1010	1.79	2.5	1.4
1036	1.79	10	5.6
1145+1151	1.38	6.5	4.7
1480	1.90	5.5	2.9
1547+1555	1.40	19	13.5
1828+1836	1.65	20	12.1
1973+1980	1.97	14	7.1
3029+3036	1.93	10	5.2
3086+3091	1.93	9	4.7
3067	1.93	5.5	2.8

[a] Calculated as described in work cited in footnote 20.

Nonuniformity of the sample film is a more difficult error to deal with. The spray technique used to prepare the benzene film will possibly result in a film which is thick in the center and which decreases in thickness radially. Jones and Sandorfy show that considerable error can result in the measurement of an intense band in the extreme case when part of the sample area is vacant and part covered.[23] However, for a film of gradually varying thickness this error should be smaller. Also, we should expect that the degree of nonuniformity might vary with each film, depending on the orientation of the nozzle, the speed of deposit, etc. Finally, the error due to nonuniformity will increase as the measured intensity increases, so we should expect differences to show up depending on the film thickness. No systematic trends of this sort appeared; hence, we conclude this possible error also is not excessive. It is very likely one of the limiting errors, and probably accounts for much of the scatter of our data, but since the average scatter in the relative intensities is about 10%, we conclude that this is the upper limit of error due to nonuniformity.

3. *Temperature*

After this phase of our studies of crystal benzene was concluded, we discovered that the intensities of the benzene fundamentals are remarkably temperature

[23] R. N. Jones and F. Sandorfy, in *Techniques of Organic Chemistry* Vol. IX, *Chemical Applications of Spectroscopy* edited by W. West (Interscience Publishers, Inc., New York, 1956), Chap. IV.

TABLE III. Relative intensities.

Gas[a] frequency (cm^{-1}) Ingold *et al.*	Solid[b] frequency M & H	Solid frequency this work	Assignment [c]	$[(\nu_g-\nu_s)/\nu_g]$ $\times 10^3$	Intensity ratio	Limit of integration
671	688	687	$\nu_{11}(A_{2u})$	−22.4	4.92±0.3	640–700
	705	705	ν_{11}+Lattice(?)	...	0.34	700–715
	975	974, 978	$\nu_{17}(E_{2u})$	...	0.10	960–983
	984	987	?	...	0.06	983–995
	1010	1010	$\nu_{12}(B_{2u})$	...	0.07	1000–1015
1037	1036	1033, 1039	$\nu_{20}(e_{1u})$	3.87, −1.93	1.00	1017–1060
	1147	1145, 1151	$\nu_{13}(B_{2u})$	...	0.14	1138–1162
	1255	1255				
	1265	1266	$\nu_{16}+\nu_{10}(E_{1u})$	...	...	...*
	1275	1274				
	1311	1311	$\nu_{14}(B_{2u})$	...	...	...*
	1412	1404, 1415	$\nu_{16}+\nu_5(E_{1u})$	...	...	...*
1485	1478	1476, 1480	$\nu_{19}(e_{1u})$	6.06, 3.36	1.74±0.2	1465–1495
	1547	1547.5, 1560	$\nu_{11}+\nu_{10}(E_{1u})$	...	0.22	1530–1582
	1828	1828, 1833.5	$\nu_{17}+\nu_{10}(E_{1u})$	...	0.66	1812–1870
	1973	1974, 1980	$\nu_{17}+\nu_5(E_{1u})$	...	0.41	1950–2060
	2210	2210	$\nu_{20}+\nu_{19}(E_{1u})$	...	...	...*
3045	3030	3029	ν_{18} in resonance with $\nu_{19}+\nu_9(e_{1u})$	5.25	0.896	2965–3050
		3036		2.95		
					1.42±0.1	
		3086		4.20		
3099	3080	3091		2.59	0.52	3072–3125
3073		3067	$\nu_{18}(B_{1u})$	1.95	0.29	3050–3072

[a] Bailey, Hale, Ingold, and Thompson, J. Chem. Soc. **1936**, 931.
[b] See work cited in footnote 9.
[c] Assignment is that of Mair and Hornig[9] with the numbering system of Zwerdling and Halford.[10]
[d] $(\nu_g-\nu_s)/\nu_g$ is the relative shift, where ν_g is the gas phase frequency and ν_s is the frequency in the solid.
* Not of measurable intensity.

dependent.[17,24] Since we did not take any particular pains to control temperature, this also will contribute to the scatter in our data.

4. *Nature of the Film*

Finally, we must consider the nature of the benzene films we obtain in our procedure. We have maintained that these are polycrystalline films. We mean by this that they are composed of randomly oriented microcrystals. From the nature of the spectrum, we are sure that the samples are crystalline, because we would not observe splitting otherwise. In order to prove that the film was not oriented, we observed the spectrum using polarized infrared radiation. A polarizer was constructed from a pile of AgCl plates inclined at the Brewsterian angle in a cardboard tube.[25] This was introduced into the light beam between the cold cell and the entrance slit of the spectrometer. The spectra were obtained with the polarizer oriented at an angle of +45° and again at −45° with respect to the slits. These two spectra were identical, thus proving that the sample was randomly oriented in the plane of the film. Our evidence showing that there was no orientation perpendicular to the plane of the film is based on the observation of the

[24] D. A. Olsen, Ph.D. thesis, State University of Iowa, 1960.

[25] N. Wright, J. Opt. Soc. Am. 38, 69 (1949).

three components of ν_{20} under grating resolution in roughly the expected intensity ratios. Of course a completely oriented film would show only two of these components. Under prism resolution the appearance of the degenerate fundamentals was the same for the very large number of different samples studied, indicating either a random film or else that the orientation was always the same. Different supporting windows were used (CsBr, KBr, and AgCl) and no change in appearance was noted. When the temperature was raised, the appearance of the band changed, but this change is reversible[24] indicating again that no orientation occurs.

5. Conclusion

In conclusion, we may argue that the errors considered here appear to account for a total error of about 10 to 20% in the values of the relative intensities.

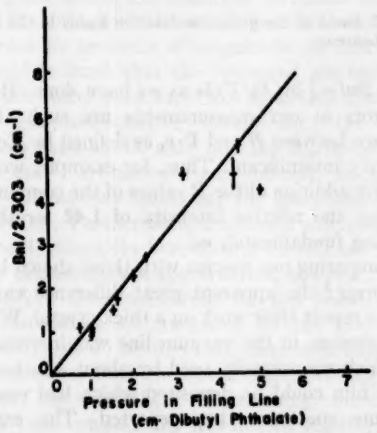

FIG. 2. A Beer's law plot for the integrated intensity, *Bnl*, in solid benzene vs the pressure of benzene vapor in a definite volume of the filling line.

The scatter in results is of this order of magnitude, and the error analysis seems to indicate that this is actually the magnitude of our error.

As a final check on the validity of these measurements, Fig. 2 shows a Beer's Law plot of the measured integrated absorbance, *Bnl*, for the 1036 cm^{-1} band as a function of the pressure in the filling line when a constant volume of the line is filled to the pressure indicated, and the sample distilled to the cold window. This is a rather severe test of the experimental data, and we see that it is met quite well, on the whole. Unfortunately, we do not know how to convert from the pressure units to determine the value of *nl* for the solid film and thus the absolute intensity, *B*, but the plot does provide a good test of the errors in the data.

RESULTS

The appearance of the different gas-phase-allowed fundamentals under our resolution is shown in Figs. 3–6. The gas-phase-inactive fundamentals and the combination bands which were observed in this study are shown in Fig. 7. The characteristic splitting of the degenerate bands is notable. The A_{1u} fundamental at 687 cm^{-1} shows a rather pronounced asymmetry (Fig. 6), but shows no further splitting at this temperature. These figures illustrate the remarkable sharpness of the induced bands (such as those at 974, 978, 986, and 1010 cm^{-1}, for example) which was discussed in connection with Table II. This is to be contrasted with the relatively large half-intensity widths for the gas-phase-allowed fundamentals, and for the even larger values for the combination bands.

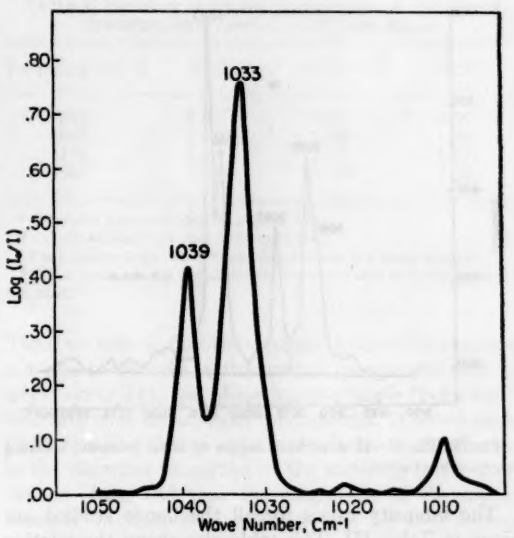

FIG. 3. The E_{1u} fundamental, ν_{20}, at 1036 cm^{-1} in solid benzene.

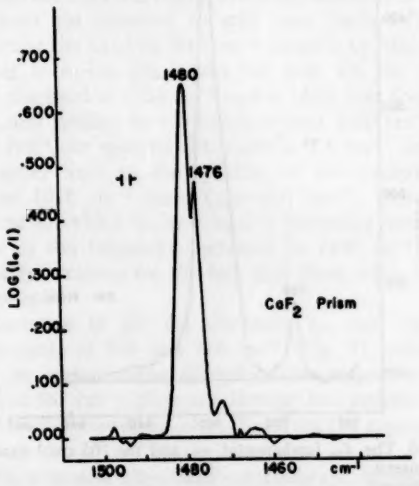

FIG. 4. The E_{1u} fundamental, ν_{19}, at 1480 cm^{-1} in solid benzene.

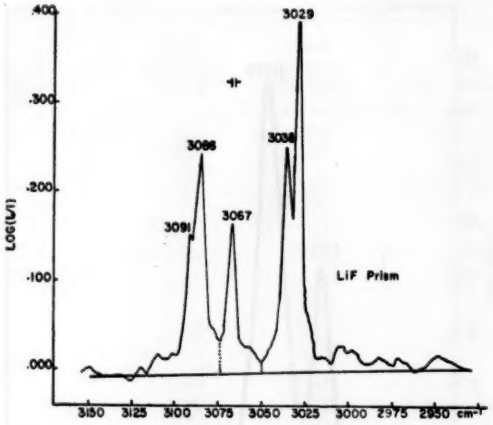

FIG. 5. The C—H stretching region of solid benzene, showing ν_{18}, ν_{13}, and $(\nu_{19}+\nu_8)$.

The intensity ratios for all the bands studied are given in Table III. This table also shows the relative shift in frequency $(\nu_g-\nu_s)/\nu_g$ for each band, and the limits of integration which were used in evaluating the intensities in each region. In addition to the intensity ratios, the average deviations of the measured values from the mean value reported in the table are given. For the ratios of the gas-phase-active fundamentals, about ten measurements were made for each relative intensity value. The scatter reported is, in each case, less than 10%. For the other bands whose relative intensities are reported here, fewer measurements were made and they are thus more likely to be in error.

We realize that there is some objection [26] to integration of $Bnl=\int \ln(T_0/T)d\nu$ as we have done. However, the errors in our measurements are such that the difference between B and $\Gamma\cdot\nu$, as defined by Crawford, is entirely insignificant. Thus, for example, we justify the direct addition of the B values of the components in obtaining the relative intensity of 1.42 for the C–H stretching fundamental, ν_{18}.

In comparing our spectra with those shown by Mair and Hornig,[9] the apparent great difference caused us to try to repeat their work on a thick crystal. When the filling pressure in the vacuum line was increased over that which we normally used by about a factor of 20, a thick film could be deposited which had essentially the same spectrum they reported. The extremely narrow bands which are induced in the solid do not obey Beer's law very well. Thus, their appearance does

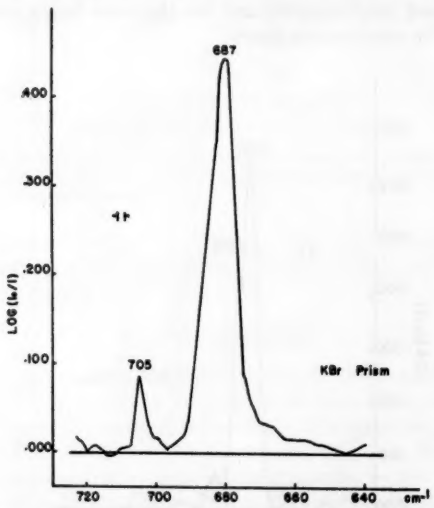

FIG. 6. The A_{2u} fundamental, ν_{11}, and the 705 cm^{-1} band in solid benzene.

[26] B. Crawford, Jr., J. Chem. Phys. **29**, 1042 (1958).

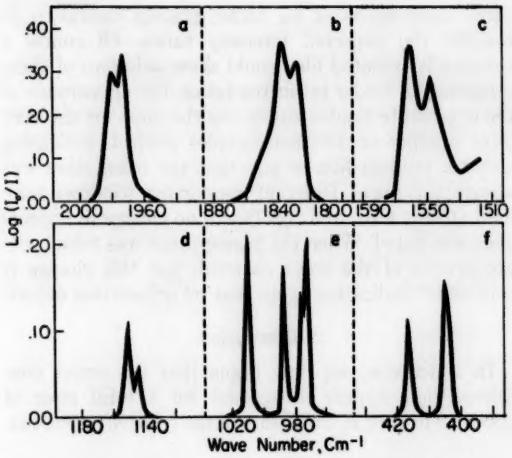

FIG. 7. Some of the gas-phase-inactive bands in the spectrum of solid benzene.

TABLE IV. Classification of bands in crystal benzene.

Very strong (2.5 cm DBT)[a]	Weak (20 cm DBT)[a]	Very weak (45 cm DBT)[a]
687	706	405[b,e]
1036[b]	975[b]	1109[b,d]
1478[b]	987	1177[d]
3030[b]	1010	1250[d]
3090[b]	1145[b]	1311
3067	1550[b]	1405[b]
	1830[b]	1616.5[e]
	1980[b]	1678
		1753[e]
		2011[d]
		2208.5[e]
		2326[e]
		2382[d,e]

[a] Pressure in cm of dibutyl phthalate in filling line.
[b] Bands show a doublet structure.
[c] This band was observed at 62 cm DBT filling pressure.
[d] Band was detected but not of measurable intensity at this pressure.
[e] E_{1u} bands that do not show doublet structure.

not change too much when the amount of benzene changes. If their appearance is used to judge thickness, the result is very misleading. We have classified the absorption bands in solid benzene into three classes in Table IV. The "strong" bands are those of the gas-phase-allowed fundamentals which dominate the spectrum of a thin film (Fig. 1). All the "weak" bands in the second column can be observed in the spectrum of this film, but, in order to measure the intensities of these "weak" bands, the amount of benzene in the film must be increased by a factor of about 10. Then most of the "very weak" bands may be observed, but in order to bring them out so that they may be studied with any certainty, the amount of benzene must be increased again by a factor of two or more.

DISCUSSION

As we stated in the introduction, it is apparent that the gas-phase-active fundamentals dominate the spectrum of the solid, with almost all the other bands being less intense by an order of magnitude. At first glance this would indicate that the "oriented gas model" is very much better than expected. It is true that some of the gas-phase-inactive bands—e.g., the rather mysterious band at 705 cm^{-1} and the B_{1u} fundamental at 3070 cm^{-1}—are unexpectedly intense. In general, though, the intense bands are the gas-phase-allowed fundamentals. Furthermore, frequency shifts are generally small, except the blue shift of the 687 cm^{-1} band.

Closer examination of the situation, however, reveals some marked differences from the gas phase. If the relative intensities are compared for the gas, liquid, and solid (Table V) we find that there have been some striking changes. Both the out-of-plane bending vibration at 687 cm^{-1} and the C–H stretching vibrations at 3000 cm^{-1} are considerably less intense relative to the 1036 cm^{-1} band in the solid phase than in either of the other two phases. The trend in these values is indicated in the liquid phase and extended in the solid. These results show very clearly that any theory of spectra in condensed phases such as the naive index-of-refraction theory[4,5] which predicts the same behavior for all the absorption bands in a molecule, at least as a first approximation, must be incorrect. It will be necessary to provide in the theory an explanation for different behavior of different fundamental vibrations. Furthermore, the changes in intensity are very large, and are associated with minor changes in frequency. These results will therefore make it necessary to discard the idea of the "oriented gas" in any attempts to understand intensities. However, we may hope that the magnitude of these intensity changes will provide a useful tool for studying the intermolecular interactions responsible for them, once these are understood.

It should be noted that the minor changes in frequency which occur suggest that the normal coordinates for the benzene molecule in the crystal are probably not too much different from those in the gas phase.

TABLE V. Summary of the relative intensities of the allowed fundamentals of benzene in the three phases.

Frequency (cm^{-1})	Solid	Liquid[a]	Gas[b]
687	5.26[c]	8.21	9.99
1037	1.00	1.00	1.00
1478	1.74	2.05	1.57
3080	1.71[d]	4.58[d]	7.26

[a] Calculated from work cited in footnote 1(c).
[b] Calculated from work cited in footnote 11(a).
[c] The intensity of the 705 cm^{-1} band is included in this intensity ratio.
[d] The intensity of ν_{14} is included in the liquid and solid intensity values for this band.

Thus, we believe that the changes in intensity ratio are not due to changes in the normal coordinates such as might occur if the gas-phase-inactive bands "borrowed" intensity from an adjacent fundamental. It seems more likely that the change in intensity is due to the change in the electrical properties of the molecule in the condensed phase and that the magnitude of the dipole moment derivative is affected by the neighboring molecules.

During these studies, several new details were observed in the spectrum of solid benzene. For one thing, the splitting of all the degenerate fundamentals was observed for the first time. Every band which we observed and which has been assigned to a degenerate fundamental showed the characteristic splitting shown in Fig. 3 to 5. The very weak E_{2u} fundamental, ν_{16},[27] with components at 405.5 and 417.5 cm^{-1}, has been observed for the first time (see Fig. 7). The only band assigned to a nondegenerate fundamental which splits is the band at 1147 cm^{-1} which is assigned to ν_{15} (B_{2u}). However, all degenerate fundamentals are accounted for, and we have been unable to deduce any combination with E_{1u} symmetry which we can propose as an alternative assignment for this band.

Some combination bands which are assigned to class E_{1u} were not observed to split (see Table IV). In particular the band at 1618 cm^{-1} assigned by Mair and Hornig to $\nu_{12}+\nu_6$ (E_{1u}) does not split. On the other hand the band at 1753 cm^{-1} $\nu_{15}+\nu_6$ (E_{1u}) also does not split, and neither do the bands around 2100 cm^{-1}. At 1600 cm^{-1} our spectral slit width is 1.8 cm^{-1}, setting the upper limit to the splitting of this exceedingly narrow 1618 cm^{-1} band ($\Delta\nu_{\frac{1}{2}} \simeq 2.0$ cm^{-1}). Since the spectral slit width we have used is increasing from this value as the frequency increased to 2100 cm^{-1}, this probably accounts for the fact that these other bands do not split.

Resolution of the E_{2u} vibration, ν_{17}, into its two components at 974 and 978 cm^{-1} (Fig. 7) leaves us with an embarrassing difficulty with respect to the band at 987 cm^{-1}. Mair and Hornig[9] had assigned this band as one component of ν_{17}, but from the appearance

[27] The assignment is from Mair and Hornig[9] and the numbering system is from Zwerdling and Halford.[10]

of our spectra this assignment does not seem likely. Furthermore, the polarization work of Zwerdling and Halford[10] seems more consistent with our assignment of the components of ν_{17}. However, there does not seem to be any logical explanation for this 987 cm^{-1} band. We do not believe it is due to an impurity, for it is always present in all the different benzene samples investigated. It could possibly be due to the A_{1g} fundamental, ν_1, observed at 992 cm^{-1} in the Raman spectrum of the liquid,[28] appearing in violation of the selection rules. If so, it is the only such band to appear with so much intensity, and this explanation, while fascinating, seems unlikely.

The relatively large intensity of the band at 705 cm^{-1} is unexpected. This band has been assigned[29] to a combination between ν_{11} and a librational mode at 17 cm^{-1}. Its high intensity may be due to the fact that it involves the very intense vibration ν_{11}. The recent study of the spectrum of a mixed crystal of benzene in a benzene-d_6 lattice by Olsen[24] indicates that this assignment may be in error. We have included its intensity in the total intensity of the A_{2u} fundamental ν_{11}, when comparing the intensity ratios of this band in various phases.

[28] W. H. Angus, C. K. Ingold, and A. H. Leckie, J. Chem. Soc. **1936**, 925.
[29] R. M. Hexter and D. A. Dows, J. Chem. Phys. **25**, 504 (1956).

CONCLUSION

In conclusion, we have been able to measure relative intensities of infrared vibrations in solid benzene films which we think are accurate to about 10 to 20%. These show definitely that the intensities of all the vibrations do not change uniformly, but each vibration must be treated separately. Thus, although qualitatively the spectrum of the solid is similar to the gas, the pessimistic point of view with respect to the interpretation of spectra of solids seems to be justified. However, the intensity changes from the gas phase are very large, and should thus provide a more sensitive experimental measure of intermolecular interactions than provided by frequency shifts.

ACKNOWLEDGMENTS

It is a pleasure to acknowledge financial support from the Office of Ordnance Research, U.S. Army. One of us (CAS) would like to acknowledge the support of a National Science Foundation Summer Postdoctoral Fellowship.

Theory of Hyperfine Interactions in Aromatic Radicals*

A. D. McLachlan,† H. H. Dearman,‡ and R. Lefebvre§

Gates and Crellin Laboratories of Chemistry, California Institute of Technology, Pasadena, California¶

(Received December 15, 1959)

The relation $a_H = Q\rho$ between the ring proton isotropic hyperfine splitting a_H and the unpaired spin density ρ on the carbon atom in an aromatic hydrocarbon radical is derived under even more general conditions than McConnell and Chesnut's.[1] There are only three essential assumptions in the new theory: (a) that σ-π exchange interaction is small; (b) that an antisymmetrised product $U(\pi)V(\sigma)$, which allows π-π and σ-σ, but not σ-π correlations, is a good first approximation to the ground-state electronic wave function; and (c) that $U(\pi)$ is formed exclusively of π-orbital configurations, and $V(\sigma)$ exclusively of σ ones. In the framework of our theory the unpaired spin density in the molecular plane arises entirely from σ-electron excitations. The general relation $a_N = \mathrm{tr}(\mathbf{Q}^N\boldsymbol{\rho})$ holds for any nucleus N, including C^{13} and N^{14}, which lies in the molecular plane. Here $\boldsymbol{\rho}$ is the π-electron spin-density matrix, and $\mathbf{Q}^N$ a hyperfine coupling matrix, whose elements depend on σ-π exchange integrals and excited σ triplet states. The diagonal elements of $\mathbf{Q}^N$ for C^{13} are estimated in a simple way to be $+41$ gauss for the same carbon atom and -14 gauss for each next neighbor, while experimental data fit the values $+41$ and -6.9 gauss.

INTRODUCTION

ONE of the most interesting recent applications of electron spin resonance has been to study the electronic structure of large planar aromatic hydrocarbon radicals like triphenylmethyl[2–4] and perinaphthenyl,[5,6] and the positive or negative ions of aromatic hydrocarbons.[7–11] The unpaired electrons in these radicals can move over a large conjugated network of carbon atoms, and the magnetic hydrogen nuclei around the edges of the rings serve as probes to measure the unpaired spin distribution. In fact, the Fermi contact hyperfine interaction a_H between the nuclear and electron spins of the radical in solution has been assumed to be directly proportional to the "unpaired spin density" ρ at the carbon atom of the C—H bond. In many radicals the spin density has been calculated theoretically by molecular-orbital[10] or valence-bond[3,6] methods and agrees remarkably well with the measured one, so that this important assumption seems to be well founded, but its theoretical basis has not yet been made quite clear. That is the object of this paper.

Dirac's relativistic theory shows that the spinning electron is magnetically equivalent to an electric current[12]

$$\mathbf{j} = (e\hbar/2mc)\ \mathrm{curl}\langle\psi^*\boldsymbol{\sigma}\psi\rangle, \tag{1}$$

so that besides the dipole-dipole coupling of nuclear and electron spins, which averages out to zero in a rapidly rotating molecule, there is the Fermi contact interaction[13]

$$3\mathcal{C}_2 = (8\pi/3)g(e\hbar/2mc)(\mu_I/I)\sum_k \delta(\mathbf{r}_k - \mathbf{r}_N)\mathbf{S}_k\cdot\mathbf{I}_N, \tag{2}$$

which is proportional to the unpaired spin density

$$\rho(r_N) = \langle\psi \mid \sum_k \delta(\mathbf{r}_k - \mathbf{r}_N)\sigma_k \mid \psi\rangle \tag{3}$$

at the nucleus itself.

The discovery of hyperfine structure from aromatic ring protons[14] was unexpected because the odd electron is in a π molecular orbital with a node in the plane of the C—H bonds. Experiments with deuterated compounds showed[15] that the splitting was not caused by bending vibrations of the C—H bond out of this plane, and Bersohn and McConnell[16,17] showed that $\sigma-\pi$ exchange interaction is responsible.

Figure 1 represents a side view of one C—H bond and the corresponding π orbital in an aromatic hydrocarbon. McConnell and Bersohn both used valence-bond theory to explain how unpaired spin arises on the hydrogen atom. The exchange integral $J(c\pi)$ mixes the normal structure I with the excited one II, and polarizes the

* Sponsored by Office of Ordnance Research, U. S. Army, by the National Science Foundation, and by the U. S. Public Health Service.

† Harkness Fellow of the Commonwealth Fund 1959–1961.

‡ Dow Chemical Fellow 1959–1960.

§ On leave from the Centre de Mécanique Ondulatoire Appliquée, Paris.

¶ Contribution No. 2533.

[1] H. M. McConnell and D. B. Chesnut, J. Chem. Phys. **28**, 107 (1958).

[2] H. S. Jarrett and G. J. Sloan, J. Chem. Phys. **22**, 1783 (1954).

[3] P. Brovetto and S. Ferroni, Nuovo Cimento **5**, 142 (1957).

[4] F. C. Adam and S. I. Weissman, J. Am. Chem. Soc. **80**, 2057 (1958).

[5] P. B. Sogo, M. Nakazaki, and M. Calvin, J. Chem. Phys. **26**, 1343 (1957).

[6] H. M. McConnell and H. H. Dearman, J. Chem. Phys. **28**, 51 (1958).

[7] S. I. Weissman, T. R. Tuttle, and E. de Boer, J. Phys. Chem. **61**, 28 (1957).

[8] E. de Boer, J. Chem. Phys. **25**, 190 (1957).

[9] S. I. Weiss man and E. de Boer, J. Chem. Phys. **26**, 963 (1957).

[10] E. de Bo er and S. I. Weissman, J. Am. Chem. Soc. **80**, 4549 (1958).

[11] A. Carringt on, F. Dravnieks, and M. C. R. Symons, J. Chem. Soc. **1959**, 947.

[12] L. D. Landau and E. M. Lifshitz, *Quantum Mechanics* (Pergamon Press, London, 1958), p. 486.

[13] E. Fermi, Z. Physik **60**, 320 (1930).

[14] Lipkin *et al.*, Science **117**, 534 (1953).

[15] G. Fraenkel and B. Venkataraman, J. Chem. Phys. **24**, 737 (1956).

[16] R. Bersohn, J. Chem. Phys. **24**, 1066 (1956).

[17] H. M. McConnell, J. Chem. Phys. **24**, 764 (1956).

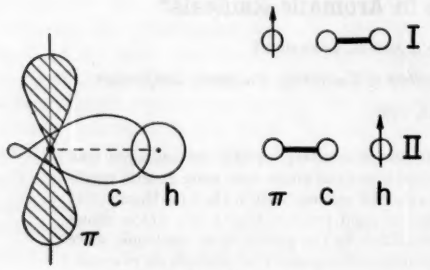

FIG. 1.

C—H bond, giving spin densities of

$$\pm\rho' = [J(\pi h) - J(c\pi)]/2J(ch) \quad (4)$$

in h and c, respectively. Reasonable values of the exchange integrals lead to

$$\rho' = -0.05 \quad (5)$$

in agreement with experiment. Weissman[18] treated the same problem by the molecular-orbital theory. In this theory the two electrons in the C—H bond occupy the orbital $\Sigma = \sqrt{2}^{-1}(c+h)$, while the antibonding orbital $\Sigma^* = \sqrt{2}^{-1}(c-h)$ is empty. The $\sigma-\pi$ exchange integral then mixes the normal state,

$$\Psi_0 = \| \Sigma\Sigma\pi \| \alpha\alpha\beta$$

$$\Psi_1 = \| \Sigma\Sigma^*\pi \| \sqrt{6}^{-1}(2\alpha\alpha\beta - \alpha\beta\alpha - \beta\alpha\alpha), \quad (6)$$

Ψ_0, with the excited doublet configuration Ψ_1, again polarizing the spins of the C—H bond. Here

$$\rho' = [J(\pi h) - J(c\pi)]/2(E_0 - E_1), \quad (7)$$

a result very similar to (4). Jarrett[19] later improved McConnell's calculations and found $\rho' = -0.055$. McConnell[17] also showed by a simple MO treatment of the π electrons that a_H was proportional to the spin density on the carbon atom

$$a_H = Q\rho. \quad (8)$$

Since an electron in the hydrogen 1s orbital has $a_H = 502$ gauss, we may also write

$$a_H = 502\rho': \qquad \rho' = G\rho. \quad (9)$$

Clearly (8) and (9) must hold independently of any particular approximate theoretical treatment of the π electrons, and McConnell, Chesnut, and Robertson[1,20,21] studied this question using the Dirac vector model. They treated the $\sigma-\pi$ exchange interaction as a small perturbation and proved (8) without any restrictive assumptions about the π-electron wave function, but used an average excitation energy ΔE for all excited states to put their perturbation expansion in closed form. This treatment has two weaknesses. It is not clear whether the hyperfine interaction involves excited states of the π electrons as well as the σ ones, nor what properties of the σ electrons will affect the value of Q in different C—H bonds.

In this paper we make a few small changes in McConnell and Chesnut's theory which remove these objections. In particular we show that (i) proportionality holds without any strong assumptions about the σ and π-electron wave functions, (ii) the hyperfine interaction only involves excited states of the σ electrons, and (iii) the value of Q depends on the excited triplet states of the σ bonds and on certain $\sigma-\pi$ exchange integrals.

GENERAL THEORY OF $\delta-\pi$ EXCHANGE INTERACTION

Since we wish to treat the $\sigma-\pi$ exchange interaction as a small perturbation, the first step is to find an approximate wave function for the electrons in the absence of exchange. The terms "σ electron," "π electron," and "exchange" only have precise meanings when the electronic wave function of a molecule is treated by a particular quantum-mechanical approximation. Here we suppose that M-valence electrons of the planar aromatic radical move over m σ orbitals $s_1 \cdots s_m$ which are symmetric across the plane, and the other N move independently of the σ ones over n π orbitals $p_1 \cdots p_n$ which are antisymmetric. The σ orbitals give $2m$ spin orbitals $\sigma_1 \cdots \sigma_{2m}$ from which are formed normalized Slater determinants of the type $\Sigma = \| \sigma_1 \cdots \sigma_M \|$. These Slater determinants are a basic set for constructing wave functions V_j which allow completely for correlation of the M σ electrons among the m different σ orbitals. Similarly the $2n$ π spin orbitals $\pi_1 \cdots \pi_{2n}$ give Slater determinants $\Pi = \| \pi_1 \cdots \pi_N \|$ which may be combined to form correlated π-electron wave functions U_i. The completely antisymmetrical wave functions

$$W_{ij}(1 \cdots N+M)$$

$$= [(N+M)!]^{-\frac{1}{2}} \mathcal{A} U_i(1 \cdots N) V_j(N+1 \cdots N+M) \quad (10)$$

then describe a molecule with N π electrons and M σ electrons, in which full allowance is made for $\pi-\pi$ and $\sigma-\sigma$ electron correlation, but the two groups are correlated only by the exclusion principle. Here $\mathcal{A}$ is the operator

$$\mathcal{A} = \sum_P (-)^P P, \quad (11)$$

and P is any permutation of the electron coordinates $1 \cdots N+M$.

We now consider how the function (10) gives rise to "exchange energy." We use the letters λ, μ, $\nu \cdots$ and α, β, $\gamma \cdots$ for the coordinates of π and σ electrons,

[18] S. I. Weissman, J. Chem. Phys. **25**, 890 (1956).
[19] H. S. Jarrett, J. Chem. Phys. **25**, 1289 (1956).
[20] H. M. McConnell, Proc. Nat. Acad. Sci. U. S. **43**, 721 (1957).
[21] H. M. McConnell and R. E. Robertson, J. Chem. Phys. **28**, 991 (1958).

respectively, and write the complete Hamiltonian in the form

$$\mathfrak{H}=\{\sum_{\mu}v(\mu)+\sum_{\mu<\nu}(e^2/r_{\mu\nu})\}+\{\sum_{\alpha}v(\alpha)+\sum_{\alpha<\beta}(e^2/r_{\alpha\beta})\}+\sum_{\alpha,\mu}(e^2/r_{\alpha\mu})$$
$$=\mathfrak{H}_\pi+\mathfrak{H}_\sigma+\mathfrak{H}_{\sigma\pi}. \tag{12}$$

This Hamiltonian contains no exchange terms; however, let us consider its matrix elements between W_{ij} and W_{kl}:

$$\langle W_{ij}\mid\mathfrak{H}\mid W_{kl}\rangle=[(N+M)!]^{-1}\langle U_iV_j\mid\mathfrak{A}\mathfrak{H}\mathfrak{A}\mid U_kV_l\rangle$$
$$=\langle U_iV_j\mid\mathfrak{H}\sum_P(-)^PP\mid U_kV_l\rangle$$
$$=\langle U_iV_j\mid H'\mid U_kV_l\rangle \tag{13}$$

by a simple contraction. In place of $\mathfrak{H}$ operating on the completely antisymmetric function W_{kl}, one has the *effective Hamiltonian*

$$H'=\mathfrak{H}\sum_P(-)^PP \tag{14}$$

acting on the product $U_k(1\cdots N)\,V_l(N+1\cdots N+M)$. To find H' we have to simplify (14). Now any permutation P of the $N+M$ electrons may be resolved uniquely into the product of $P^\pi(1\cdots N)$ for the π electrons, $P^\sigma(N+1\cdots N+M)$ for the σ electrons, and a transposition $T(\alpha,\beta\cdots\gamma\to\lambda,\mu\cdots\nu)$ of σ and π electrons, with $\alpha<\beta<\cdots\gamma$ and $\lambda<\mu<\cdots\nu$;

$$P=P^\pi P^\sigma T,$$

and

$$\mathfrak{A}=(1+\sum_T(-)^TT)\,\mathfrak{A}^\sigma\mathfrak{A}^\pi. \tag{15}$$

The functions U and V are already antisymmetrized so that

$$H'UV=\mathfrak{H}\sum_P(-)^PP(UV)=\mathfrak{H}(1+\sum_T(-)^TT)UV, \tag{16}$$

and finally since Coulomb forces only act between pairs of electrons, we need only consider transpositions $T(\alpha\to\mu)=P_{\alpha\mu}$ involving a single pair of electrons. Therefore, *in the system of functions* U_i, V_j the Hamiltonian may be written

$$H'=\mathfrak{H}_\sigma+\mathfrak{H}_\pi+\sum_{\alpha,\mu}(e^2/r_{\alpha\mu})\,(1-P_{\alpha\mu})$$
$$=\mathfrak{H}-\sum_{\alpha,\mu}(e^2/r_{\alpha\mu})\,P_{\alpha\mu} \tag{17}$$

in which there is an additional $\sigma-\pi$ exchange term.

At this point we might follow McConnell and Chesnut,[1] ignoring the exchange terms of H', and finding the "unperturbed" electronic wave functions for the ground state and excited states. Instead, it is convenient to define the excited states in terms of a self-consistent field approximation which completely separates σ- and π-electron excitations. As a first approximation to the ground-state wave function we take

$$W_0=\mathfrak{A}U_0V_0, \tag{18}$$

choosing U_0, V_0 to minimize $\mathfrak{H}$ instead of $\mathfrak{H}\mathfrak{A}$:

$$\delta\langle U_0V_0\mid\mathfrak{H}\mid U_0V_0\rangle=0 \tag{19}$$

but

$$\delta\langle W_0\mid\mathfrak{H}\mid W_0\rangle\neq0. \tag{20}$$

Here the π electrons move in the self-consistent field (without exchange) of the σ electrons, and vice versa. In fact, Eq. (19) may also be written

$$\delta\langle U_0\mid\mathfrak{H}_\pi'\mid U_0\rangle=0,$$
$$\delta\langle V_0\mid H_\sigma'\mid V_0\rangle=0; \tag{21}$$

where

$$H_\pi'=\sum_\mu v(\mu)+v_\sigma(\mu)+\sum_{\mu<\nu}(e^2/r_{\mu\nu}),$$
$$H_\sigma'=\sum_\alpha v(\alpha)+v_\pi(\alpha)+\sum_{\alpha<\beta}(e^2/r_{\alpha\beta}), \tag{22}$$

and $v_\sigma(\mu)$, $v_\pi(\alpha)$ are the electrostatic potentials produced by the σ electrons in V_0 or the π electrons in U_0. This "unperturbed" Hamiltonian

$$H_0'=H_\pi'+H_\sigma' \tag{23}$$

defined by the wave function W_0 generates a complete set of separated σ- and π-electron excited states $W_{ij}=U_iV_j$ in which H_0' has eigenvalues $(\eta_i+\epsilon_j)$, which are also eigenfunctions of S_π^2 and S_σ^2. They are also orthonormal since every π orbital is orthogonal to every σ one. These excited states are fictitious ones, in which the excited π electrons move as if the σ electrons were unexcited, and vice versa, so that $v_\sigma(\mu)$ and $v_\pi(\alpha)$ are unchanged. Each excited level U_iV_j is degenerate in $S_{z\pi}$ and $S_{z\sigma}$, and its components can be regrouped to form eigenfunctions of S^2 for the whole radical. The energy E_{ij} of the function W_{ij} is not $\eta_i+\epsilon_j$, since this contains the $\sigma-\pi$ interaction energies twice, but $E_{ij}=(\eta_i+\epsilon_j+F_{ij}-F_{i0}-F_{0j})$, in which F_{kl} is the Coulomb interaction between the π electrons in U_k and the σ electrons in V_l.

Introducing the exchange term as a small perturbation we find that the ground-state wave function becomes

$$\Psi_0=W_0-\sum_{i,j\neq0,0}\frac{\langle U_iV_j\mid H'\mid U_0V_0\rangle}{\Delta E_{ij}}W_{ij};$$
$$\Delta E_{ij}=(\eta_i-\eta_0)+(\epsilon_j-\epsilon_0)+F_{ij}-F_{i0}+F_{00}-F_{0j}. \tag{24}$$

The σ-electron spin density $\rho^\sigma(\mathbf{r})$ for a radical whose spin is along the z axis is defined by the operator

$$\rho^\sigma(\mathbf{r})=\sum_\alpha\sigma_{z\alpha}\delta(\mathbf{r}-\mathbf{r}_\alpha). \tag{25}$$

It vanishes in W_0 and has matrix elements

$$\langle W_{ij}\mid\rho^\sigma(\mathbf{r})\mid W_0\rangle=\delta_{i0}\langle V_j\mid\sum_\alpha\sigma_{z\alpha}\delta(\mathbf{r}-\mathbf{r}_\alpha)\mid V_0\rangle \tag{26}$$

between W_0 and the excited states, so that unpaired

σ-electron spin only arises from σ-electron excited states, for which $\Delta E_{0j}=\epsilon_j-\epsilon_0$, and

$$\rho^\sigma(\mathbf{r}) = -2\sum_j{}' \frac{\langle U_0V_0 \mid H' \mid U_0V_j\rangle\langle V_j \mid \sum_\alpha \sigma_{z\alpha}\delta(\mathbf{r}-\mathbf{r}_\alpha) \mid V_0\rangle}{\epsilon_j-\epsilon_0}. \tag{27}$$

(It does not matter that U_iV_j are not eigenfunctions of $(S_\sigma+S_\pi)^2$, because a unitary transformation of the degenerate level E_{ij} to make S^2 diagonal does not alter the sum of the perturbation expansion.) To simplify (27) we note that the definitions (19) and (21) of W_0 imply that

$$\langle U_0V_0 \mid \mathfrak{IC} \mid U_0V_j\rangle = 0, \tag{28}$$

and then (17) reduces (27) to

$$\rho^\sigma(\mathbf{r}) = 2\sum_j{}' \frac{\langle U_0V_0 \mid \sum_{\alpha\mu}(e^2/r_{\alpha\mu})P_{\alpha\mu} \mid U_0V_j\rangle\langle V_j \mid \sum_\beta \sigma_{z\beta}\delta(\mathbf{r}-\mathbf{r}_\beta) \mid V_0\rangle}{\epsilon_j-\epsilon_0}. \tag{29}$$

The operator $P_{\alpha\mu}$ can be written

$$P_{\alpha\mu} = \bar{P}_{\alpha\mu}\tfrac{1}{2}(1+\mathfrak{o}_\alpha\cdot\mathfrak{o}_\mu) \tag{30}$$

where $\bar{P}_{\alpha\mu}$ exchanges the space coordinates of electrons α and μ. The spatial part $\frac{1}{2}\bar{P}_{\alpha\mu}$ of (30) produces no effect on the electron spins, and the term $\frac{1}{2}\bar{P}_{\alpha\mu}\mathfrak{o}_\alpha\cdot\mathfrak{o}_\mu$ can be replaced by $\frac{1}{2}\bar{P}_{\alpha\mu}\sigma_{z\alpha}\sigma_{z\mu}$ when U_0 is an eigenfunction of S_{zT}, so that

$$\rho^\sigma(\mathbf{r}) = \sum_j \frac{\langle U_0V_0 \mid \sum_{\alpha\mu}\bar{P}_{\alpha\mu}(e^2/r_{\alpha\mu})\sigma_{z\alpha}\sigma_{z\mu} \mid U_0V_j\rangle\langle V_j \mid \sum_{\beta\sigma}\sigma_{z\beta}\delta(r-r_\beta) \mid V_0\rangle}{\epsilon_j-\epsilon_0}. \tag{31}$$

Equation (31) already contains the result we wanted to prove. To see this we define some auxiliary electron density matrices. Let

$$x(\mathbf{r}, \mathbf{s}: \mathbf{r}', \mathbf{s}') \equiv \mathbf{N}\int U_0^*(\mathbf{r}, \mathbf{s})_1 U_0(\mathbf{r}', \mathbf{s}')_1 d\tau_2\cdots d\tau_N \tag{32}$$

be integrated over all values of $\mathbf{r}_2\mathbf{s}_2\cdots\mathbf{r}_N\mathbf{s}_N$, and

$$y_{0j}(\mathbf{r}, \mathbf{s}: \mathbf{r}', \mathbf{s}') \equiv \mathbf{M}\int V_0^*(\mathbf{r}, \mathbf{s})_1 V_j(\mathbf{r}', \mathbf{s}')_1 d\tau_2\cdots d\tau_M, \tag{33}$$

where $\mathbf{r}_\mu$, $\mathbf{s}_\mu$ are the space and spin coordinates of electron μ. From these we derive electron spin-density matrices

$$X(\mathbf{r}\mathbf{r}') \equiv \int x(\mathbf{r}, \mathbf{s}_1: \mathbf{r}', \mathbf{s}_1)\sigma_{z1}d\mathbf{s}_1,$$

$$Y_{0j}(\mathbf{r}'\mathbf{r}) \equiv \int y_{0j}(\mathbf{r}', \mathbf{s}_1: \mathbf{r}, \mathbf{s}_1)\sigma_{z1}d\mathbf{s}_1, \tag{34}$$

which are equivalent to the ordinary spin densities when $\mathbf{r}=\mathbf{r}'$:

$$X(\mathbf{r}\mathbf{r}) \equiv \langle U_0 \mid \rho^\pi(\mathbf{r}) \mid U_0\rangle$$
$$Y_{0j}(\mathbf{r}\mathbf{r}) \equiv \langle V_0 \mid \rho^\sigma(\mathbf{r}) \mid V_j\rangle. \tag{35}$$

Substitution of (34) into the energy matrix element of (31) gives

$$\langle U_0V_0 \mid \sum_{\alpha\mu}\bar{P}_{\alpha\mu}(e^2/r_{\alpha\mu})\sigma_{z\alpha}\sigma_{z\mu} \mid U_0V_j\rangle = \iint X(\mathbf{r}\mathbf{r}')(e^2/\mid \mathbf{r}-\mathbf{r}' \mid)Y_{0j}(\mathbf{r}'\mathbf{r})d\mathbf{r}d\mathbf{r}', \tag{36}$$

while the spin-density term becomes

$$\langle V_j \mid \sum_\beta \sigma_{z\beta}\delta(\mathbf{r}-\mathbf{r}_\beta) \mid V_0\rangle = Y_{j0}(\mathbf{r}\mathbf{r}). \tag{37}$$

These equations are now expressed in terms of the atomic-orbital spin distribution matrices defined by McConnell[22] by resolving X and Y_{0j} into atomic-orbital form. Let

$$X(\mathbf{r}\mathbf{r}') = \sum_{l,m}\rho_{lm}{}^\pi p_m^*(\mathbf{r})p_l(\mathbf{r}')$$
$$Y_{0j}(\mathbf{r}'\mathbf{r}) = \sum_{a,b}\rho^\sigma(0\to j)_{ab}s_b^*(\mathbf{r}')s_a(\mathbf{r}). \tag{38}$$

Comparison with (35) shows that $\rho_{lm}{}^\pi$ is the atomic-orbital spin-density matrix for the π electron ground state and that $\rho^\sigma(0\to j)_{ab}$ is the matrix element of σ-electron spin density between V_0 and V_j. Writing $\langle mb \mid al\rangle$ for the exchange integral

$$\langle mb \mid al\rangle = \iint p_m^*s_a(1)(e^2/r_{12})s_b^*p_l(2)d\tau_1d\tau_2, \tag{39}$$

and substituting the atomic-orbital forms of (36)

$$\langle U_0V_0 \mid \sum_{a\mu}\bar{P}_{a\mu}(e^2/r_{a\mu})\sigma_{za}\sigma_{z\mu} \mid U_0V_j\rangle = \sum_{l,m}\rho_{lm}{}^\pi\langle mc \mid ld\rangle\sum_{c,d}\rho^\sigma(j\to 0)_{cd}, \tag{40}$$

and (37) into (31), we finally obtain the radical's σ-electron spin-density matrix in atomic-orbital form.

$$\rho_{ab}{}^\sigma = \sum_{l,m}\rho_{lm}{}^\pi G_{ml}{}^{ab} \equiv \mathrm{tr}(\varrho^\pi \mathbf{G}^{ab}), \tag{41}$$

[22] H. M. McConnell, J. Chem. Phys. **28**, 1188 (1958).

with

$$G_{ml}^{ab}=\sum_j{}'\frac{\langle mc\mid ld\rangle\sum_{c,d}\rho^\sigma(0\to j)_{cd}\rho^\sigma(j\to 0)_{ab}}{\epsilon_j-\epsilon_0}. \quad (42)$$

Equations (41) and (42) are the general form of the linear relationship between π and σ-electron spin densities. Each element of the ϱ^σ matrix is related to the whole ϱ^π matrix by a different **G** matrix. The excited states are those of the σ electrons only, and as the ground state V_0 of the σ electrons is a singlet, V_j must always be a triplet to give any contribution to $\rho^\sigma(0\to j)$. In practical applications a simpler form of the formidable equation (42) is often useful. We only consider diagonal elements of the matrices ϱ^π, ϱ^σ and neglect many exchange integrals, retaining only

$$\langle mc\mid cm\rangle=J(mc). \quad (43)$$

Then

$$\rho_a{}^\sigma=\sum_m\rho_m{}^\pi G_m{}^a;$$

$$G_m{}^a=\sum_j{}'\frac{J(mc)\sum_c\rho^\sigma(0\to j)_c\rho^\sigma(j\to 0)_a}{\epsilon_j-\epsilon_0}. \quad (44)$$

APPLICATIONS

First we apply the theory of (42) to calculate the spin density on the hydrogen atom of an aromatic C—H bond with one π electron on the carbon atom in orbital π. We treat the C—H bond by molecular-orbital theory, using the notation of Eqs. (6) and (7). Neglect the off-diagonal elements of (42) and write ρ_h for ρ_{kk} to obtain

$$\rho_h=G_\pi{}^h=\frac{J(c\pi)\rho^\sigma(0\to 1)_c\rho^\sigma(1\to 0)_h}{E_1-E_0} \quad (45)$$

where V_0 and V_1 are the ground singlet and excited triplet states of the C—H bond.

$$V_0=\|\,\Sigma(1)\Sigma(2)\,\|\,\alpha\beta$$

$$V_1=\|\,\Sigma(1)\Sigma^*(2)\,\|\,\sqrt{2}^{-1}(\alpha\beta+\beta\alpha). \quad (46)$$

We find

$$\rho^\sigma(0\to 1)_c=-\sqrt{2}^{-1},\qquad \rho^\sigma(0\to 1)_h=+\sqrt{2}^{-1}, \quad (47)$$

and the result is

$$\rho_h=J(c\pi)/2(E_1-E_0)=-\rho_c. \quad (48)$$

This is identical with (7). [We have neglected the small integral $J(\pi h)$.] According to (8) and (9) the experimental value $Q=-23$ gauss for C—H bonds implies that

$$\rho_h=-\rho_c=-0.0458. \quad (49)$$

We can now calculate C^{13} splittings in a similar way, provided we know a_C for an electron in the carbon $2s$ orbital. (Excited states involving the $1s$ electrons are too high in energy to matter.) Torrance's Hartree wave function[23] substituted in (2) gives

$$|\,C{:}\,2s(0)\,|^2/|\,H{:}\,1s(0)\,|^2=9.30,\qquad a_C=1170\text{ gauss}. \quad (50)$$

Treating the methyl radical according to (48), there is an unpaired spin density of $+.046\,\rho_\pi$ in the carbon sp^2 hybrid orbital of each C—H bond, so that the three bonds give $+.046\rho_\pi$ in $C{:}\,2s$, making

$$a_C=Q'\rho:\qquad Q'=+54\text{ gauss}. \quad (51)$$

This agrees reasonably well with the experimental value of 41 ± 3 gauss.[24]

To make similar calculations for other hydrocarbon radicals, we must consider the excited triplet states of C—C as well as C—H bonds. Let $\Sigma_1\cdots\Sigma_k$ be the bonding molecular orbitals of the bonds $1\cdots k$, then according to the method of "equivalent orbitals," the ground state of the σ electrons may be written as a Slater determinant

$${}^1V_0=\|\,(\Sigma_1)^2(\Sigma_2)^2\cdots(\Sigma_k)^2\,\| \quad (52)$$

with two electrons in each bond. If we neglect the interactions between different bonds, the lowest triplet states are those in which only one bond (g) has been excited:

$${}^3V_g=\|\,(\Sigma_1)^2\cdots\Sigma_g\Sigma_g{}^*\cdots(\Sigma_k)^2\,\|\,\sqrt{2}^{-1}(\alpha\beta+\beta\alpha). \quad (53)$$

An obvious extension of (45) then shows that in the bond C_0—C_1 the sp^2 orbitals have unpaired spin-densities

$$\rho_0{}^\sigma=-\rho_1{}^\sigma=-[J(c\pi)/2\Delta E](\rho_0{}^\pi-\rho_1{}^\pi), \quad (54)$$

where ΔE is the singlet-triplet separation of a C—C bond. According to (54), the C^{13} splitting at a carbon atom C_0 joined to three others, C_1, C_2, C_3, should be given by the equations

$$a_C=Q_1\rho_0{}^\pi+Q_2(\rho_1{}^\pi+\rho_2{}^\pi+\rho_3{}^\pi)$$

$$Q_1=-3J(c\pi)/2\Delta E,\qquad Q_2=+J(c\pi)/2\Delta E. \quad (55)$$

This means that the π-electron spin density on each neighboring carbon atom may be almost as important as that on the same atom. The exchange integrals and excitation energies in (54) and (48) are probably quite similar, so that we can use the experimental results on the methyl radical to estimate

$$Q_1=41\text{ gauss},\qquad Q_2=-14\text{ gauss}, \quad (56)$$

for the C—C bonds. Interactions between the different bonds would probably reduce Q_2.

Experimental estimates of Q_1 and Q_2 depend on accurate knowledge of the π-electron spin densities, and so far the only data are from the α position of

[23] C. C. Torrance, Phys. Rev. **46**, 388 (1934).
[24] T. Cole, H. O. Pritchard, N. R. Davidson, and H. M. McConnell, Mol. Phys. **1**, 406 (1958).

naphthalene negative ion[25] ($a_C=7.1$ gauss) and the methyl position of triphenylmethyl[4] ($a_C=26$ gauss). In naphthalene the spin densities derived from experiment[11] ($Q=-24.2$ gauss) are $\rho_\alpha=0.203$, $\rho_\beta=0.076$, $\rho_\gamma=-0.058$, and (56) fits the value of a_C if $Q_1=41$ and $Q_2=6.9$. In triphenylmethyl the spin densities are much less certain, and theoretical calculations vary considerably. Adam and Weissman deduced a spin density of 0.68 at the methyl carbon from the C^{13} splitting in solution, assuming no effect from the first neighbors. This same value also fitted the anisotropic part of the coupling in polycrystalline samples. The present work shows that negative spin densities at the neighbors could appreciably increase the isotropic splitting constant. Also recent studies[26,27] show that next neighbors can make an important contribution to anisotropic couplings in π-electron radicals. Thus, a spin density considerably smaller than 0.68 is compatible with these experiments. The best available interpretation of the EPR spectrum[2,3] suggests that $\rho_0=\rho_p\approx 0.124$ and $\rho_m\approx -0.062$ ($Q=-24.2$ gauss). If $Q_1=41$ and $Q_2=-6.9$ we can now infer that the spin densities at the center and its neighbors are close to 0.580 and -0.108.

Having made a rather incomplete empirical estimate of Q_1 and Q_2, we now make a few predictions of C^{13} coupling constants in other radicals for which experimental data may be forthcoming:

Napthalene$^-$ ion, β position	1.2 gauss
Naphthalene$^-$ ion, γ position	-4.7 gauss
Benzene$^-$ ion	4.5 gauss
p-Benzosemiquinone ion (C═O)	2.4 gauss[28]
p-Benzosemiquinone ion (C—H)	1.8 gauss

CONCLUSIONS

The general theory of Sec. 2 establishes, with the least possible theoretical assumptions, that isotropic hyperfine interactions from nuclei in the plane of a π-electron radical are strictly proportional to the π-electron spin densities. For ring protons the $\sigma-\pi$ exchange interaction is fairly simple, and hyperfine splittings are a good measure of the spin density on the ring, but C^{13} and N^{14} interact with the π electrons on neighboring atoms, so that the interpretation of their splittings is far less certain. A proper theoretical treatment of this effect would have to allow for the interactions between the different C—C bonds, perhaps following Karplus'[29] work on the nuclear spin-spin couplings in hydrocarbons.

We thank Professor Harden M. McConnell for suggesting this investigation, and for many stimulating discussions.

[25] T. R. Tuttle and S. I. Weissman, J. Chem. Phys. **25**, 189 (1956).
[26] H. M. McConnell and J. Strathdee, Mol. Phys. **2**, 129 (1959).
[27] H. M. McConnell, C. Heller, T. Cole, and R. W. Fessenden, J. Am. Chem. Soc. **82**, 766 (1960).
[28] MO spin densities calculated by Bersohn (see footnote 16).
[29] M. Karplus, J. Chem. Phys. **30**, 15 (1959).

Radiolysis of Cyclohexane. I. Pure Liquid Cyclohexane and Cyclohexane-Benzene Solutions

G. R. FREEMAN

Department of Chemistry, University of Alberta, Edmonton, Alberta, Canada

(Received January 4, 1960)

The radiation chemistry of pure liquid cyclohexane and of cyclohexane-benzene solutions has been investigated. The cyclohexane radiolysis system appears to contain at least two distinct activated species, one of which (c-C_6H_{12}'') is subject to "protection" by benzene while the other (c-C_6H_{12}') is not. The approximate yields of these two species, determined by kinetic analysis, are $G(c\text{-}C_6H_{12}'')=3.0\pm0.4$ and $G(c\text{-}C_6H_{12}')=2.4\mp0.4$. In addition to the usual products, cyclohexylcyclohexadiene and dicyclohexadiene have been measured in the cyclohexane-benzene system. A mechanism has been proposed to explain the formation of the major products and the variation of their yields with benzene concentration.

A limiting case calculation for the upper limit of the rate constant for energy transfer between molecules in the present system (10^{13}–10^{14} liters mole/sec) agrees well with a similar calculation, recorded in the literature, for energy transfer in organic solution scintillators. Another limiting case calculation shows that the rate constant for energy transfer might also be considerably smaller than the above value.

INTRODUCTION

THE irradiation of liquid cyclohexane has been widely studied[1–21] but there have been few attempts to examine the system kinetically. In particular, the "protective" effect of benzene on irradiated cyclohexane requires a more complete investigation.

From the original study of the cyclohexane-benzene system[2] it was concluded that the protective effect of benzene was due to energy transfer processes ("sponge-type" protection[22]). Recently it has been noted that hydrogen atom scavenging also occurs,[15] but the final products of the scavenging reaction were not measured. Hydrogen atoms produced by irradiated cyclohexane can also be scavenged by cyclohexene and by idoine.[15,18]

There is little doubt that a sponge-type protection mechanism occurs in the cyclohexane-benze system.[4,7,9] The purpose of the present investigation was to attempt to determine the relative contributions of the various mechanisms.

EXPERIMENTAL

Preparation of the Samples

Eastman spectro-grade cyclohexane and benzene were used. The cyclohexane was purified for some experiments, but no difference in the results was observed.

Samples of 1 and 2 ml were irradiated in sealed Pyrex cells of approximately 2- and 4-ml capacity, respectively. The cells were filled by conventional vacuum techniques.

Irradiation of Samples

The samples were irradiated with Co^{60} γ rays. The dose rates were determined with the Fricke dosimeter using $G(Fe^{+++})=15.6$ and $\epsilon(Fe^{+++}$ in 0.8 N H_2SO_4, 25°C, 304 mμ)$=2225$. The dose rates varied from 5.9×10^{17} to 10.4×10^{17} ev/ml hr for 0.8 N H_2SO_4 at 25°C. The amount of energy absorbed per ml hr in the organic liquids was determined by multiplying the energy absorbed per ml hr in the Fricke dosimeter by the ratio of the electron densities of the two systems. The electron densities, in electron moles/ml, at 25°C are: water, 0.553; Fricke dosimeter, 0.566; cyclohexane, 0.441; benzene, 0.470.

Analysis

The samples were analyzed by low-temperature distillations at −195° and −112°C. Each gas fraction and

* This research was supported by the National Research Council of Canada and the Trans-Mountain Oil Pipeline Company.

[1] C. S. Schoepfle and C. H. Fellows, Ind. Eng. Chem. **23**, 1396 (1931).
[2] J. P. Manion and M. Burton, J. Phys. Chem. **56**, 560 (1952).
[3] C. C. Schubert and R. H. Schuler, J. Chem. Phys. **20**, 518 (1952).
[4] M. Burton and W. N. Patrick, J. Phys. Chem. **58**, 421 (1954).
[5] P. J. Berry and M. Burton, J. Chem. Phys. **23**, 1969 (1955).
[6] M. Burton, P. J. Berry, and S. Lipsky, J. chim. phys. **52**, 657 (1955).
[7] R. H. Schuler and A. O. Allen, J. Am. Chem. Soc. **77**, 507 (1955).
[8] E. N. Weber, P. F. Forsyth, and R. H. Schuler, Radiation Research **3**, 68 (1955).
[9] H. A. Dewhurst, J. Chem. Phys. **24**, 1254 (1956).
[10] M. Burton, J. Chang, S. Lipsky, and M. P. Reddy, J. Chem. Phys. **26**, 1337 (1957).
[11] R. W. Fessenden and R. H. Schuler, J. Am. Chem. Soc. **79**, 273 (1957).
[12] R. H. Schuler, J. Phys. Chem. **61**, 1472 (1957).
[13] A. C. Nixon and R. E. Thorpe, J. Chem. Phys. **28**, 1004 (1958).
[14] M. Hamashima, M. P. Reddy, and M. Burton, J. Phys. Chem. **62**, 246 (1958).
[15] H. A. Dewhurst, J. Phys. Chem. **63**, 813 (1959).
[16] H. A. Dewhurst and R. H. Schuler, J. Am. Chem. Soc. **81**, 3210 (1959).
[17] N. S. Guentner, T. J. Hardwick, and R. P. Nejak, J. Chem. Phys. **30**, 601 (1959).
[18] (a) M. Burton and G. Meshitsuka, Radiation Research **9**, 152 (1958); (b) G. Meshitsuka and M. Burton, Radiation Research **10**, 499 (1959).
[19] R. H. Schuler, J. Phys. Chem. **63**, 925 (1959).
[20] G. A. Muccini and R. H. Schuler, Radiation Research **11**, 456 (1959).
[21] G. E. Adams, J. H. Baxendale, and R. D. Sedgwick, J. Phys. Chem. **63**, 854 (1959).
[22] M. Burton, and S. Lipsky, J. Phys. Chem. **61**, 1461 (1957).

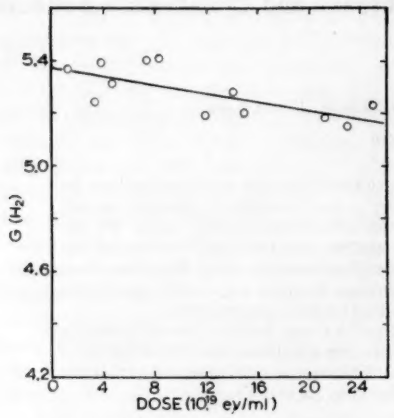

FIG. 1. Hydrogen yield as a function of dose.

the remaining liquid fraction was analyzed by gas chromatography. Gas chromatographic calibration constants were obtained using standard samples.

RESULTS

Pure Cyclohexane

The initial yields of the products were determined by plotting the respective G values (molecules formed per 100 ev absorbed by the system) as a function of the dose and extrapolating to zero dose. The value thus obtained for any product P is represented by $G(P)_i$. The plotted doses refer to the energy absorbed in 1.00 ml of sample at 24°C.

Products Volatile at −195°C

This fraction was 99.6% hydrogen and 0.4% methane. The amount of methane produced was so small that it could not be determined whether the yield varied with the dose. Thus, $G(CH_4)=0.02$ and $G(H_2)_i=5.37$ (see Fig. 1). The least-mean-squares line through the points in Fig. 1 has the equation

$$G(H_2)=5.37-8.2\times10^{-3}\times\text{dose } (10^{19}\text{ ev/ml cyclohexane, 24°C}). \quad \text{(i)}$$

The mean deviation of the points from the line is ±0.05 G units.

Products Volatile at −112°C

The total yield of this fraction appeared to decrease markedly with increasing dose. The results are not definite enough to be reported here, but are sufficiently interesting that the effect will be investigated more fully. At a dose of 8.4×10^{19} ev/ml, $G(-112°C)=0.18$. The fraction was approximately 50 percent ethylene with smaller amounts of ethane, acetylene, propane, and propylene and a trace of butene.

Liquid Products

The liquid products included cyclohexene, a C_9 hydrocarbon, dicyclohexyl, a C_{12} hydrocarbon which, from its retention times on Apiezon L and on silica gel chromatographic columns, was tentatively identified as cyclohexylhexene, and possibly some cyclohexylcyclohexene. The yields are plotted as a function of the dose in Fig. 2. The initial yields are:

Product	G_i
Cyclohexene	2.28
C_9	≈0.1
Dicyclohexyl	1.24
Cyclohexylhexene	0.23
Cyclohexylcyclohexene?	0.1–0.2
Total C_{12}	1.7.

The line through the cyclohexene points was determined by the method of least squares. The mean deviation of the points from the line is ±0.14 G units.

Cyclohexane-Benzene Solutions

The dose received by the cyclohexane-benzene solutions was $2.5\pm0.5\times10^{20}$ ev/ml, 24°C. Since the decrease in product yields with increasing dose in the pure cyclohexane system is probably due to the accumulation of an inhibitor, G_i values will be used in this section for solutions with zero benzene concentration (i.e., pure cyclohexane).

Products Volatile at −195°C

The amounts of methane were too small to measure accurately and became unmeasurable ($G(CH_4)<0.01$) as the benzene concentration was increased.

The hydrogen yield, $G(H_2)$, is plotted in Fig. 3A as a function of the electron fraction of benzene, ϵ_b, in the solution (2).[2]

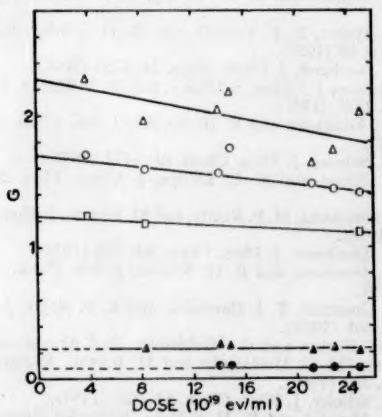

FIG. 2. Liquid product yields as a function of dose. ○ total C_{12}, △ cyclohexene, □ bicyclohexyl, ▲ cyclohexylhexene, ● C_9 hydrocarbon.

The dashed line in Fig. 3A indicates the hydrogen yield that might have been expected if there had been no interaction between the components, and if the energy absorption by a component were proportional to the electron fraction of the component. Thus,

$$G(H_2)_{exp} = G(H_2)_c{}^0\epsilon_c + G(H_2)_b{}^0\epsilon_b \qquad \text{(ii)}$$

where $G(H_2)_c{}^0$ and $G(H_2)_b{}^0$ are the hydrogen yields for pure cyclohexane and for pure benzene, respectively, ϵ_c and ϵ_b are the electron fractions of the respective components and exp stands for "expected".

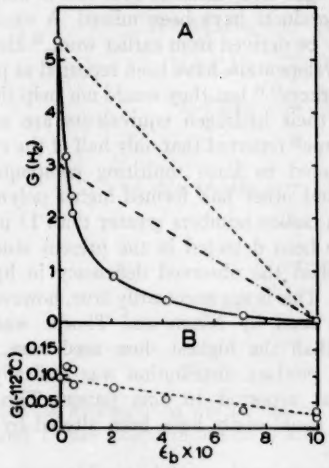

FIG. 3. A: Variation of hydrogen yield with composition of solution; B: Variation of yield of gas volatile at −112°C (excluding hydrogen and methane) with composition of solution; ϵ_b = electron fraction of benzene in solution.

Products Volatile at −112°C

The total yield of this fraction for the mixtures was only slightly lower than the "expected" value if the value of $G(-112°C)_c{}^0$ obtained at the same dose as that received by the cyclohexane-benzene mixtures (2.5×10^{20} ev/ml) is used instead of the value that would be obtained by extrapolation to zero dose. The dashed line in Fig. 3B indicates "$G(-112°C)_{exp.}$"

These results will not be discussed until they have been investigated more fully. The products in this fraction are minor, so the over-all treatment of the reaction will not be much affected.

Liquid Products

Two new liquid products appeared in the cyclohexane-benzene solutions. By comparing their retention times with those of bicyclohexyl, cyclohexylcyclohexene, and biphenyl on Apiezon L and on silica gel columns, they were tentatively identified as cyclohexylcyclohexadiene and dicyclohexadiene. The two peaks were not completely resolved so they were measured as a total. At the lower benzene concentrations (ϵ_b=0.027 and 0.053) the new C_{12} fraction appeared to be about ⅔ cyclohexylcyclohexadiene and ⅓ dicyclohexadiene. The total yield of the two new C_{12} products is plotted in Fig. 4A against the electron fraction of benzene.

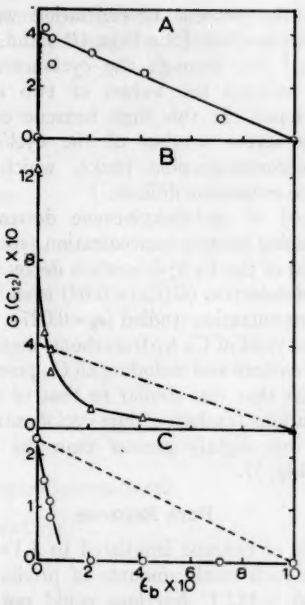

FIG. 4. Variation of yields of C_{12} hydrocarbons with composition of solution. A: cyclohexylcyclohexadiene plus dicyclohexadiene; B: dicyclohexyl; the dot-dash line represents the "interpolated" yield; C: cyclohexylhexene; the dash line represents the "expected" yield.

The yields of dicyclohexyl and cyclohexene decreased rapidly with increasing benzene concentration at low benzene concentrations, and then decreased more

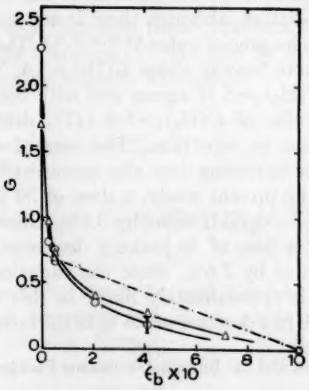

FIG. 5. Variation of cyclohexene and total C_{12} hydrocarbon yields with composition of solution. Δ total C_{12} hydrocarbons, O cyclohexene. The ends of the vertical line through the cyclohexene point at ϵ_b=0.415 indicate the values of two estimates of G(cyclohexene).

slowly as the benzene concentration was increased above about $\epsilon_b = 0.05$. [See Figs. 4B and 5. The ends of the vertical line through the cyclohexene point at $\epsilon_b = 0.415$ indicate the values of two estimates of G(cyclohexene). At this high benzene concentration there was severe overlap of the cyclohexene and benzene chromatographic peaks, which made the cyclohexene estimation difficult.]

The yield of cyclohexylhexene decreased rapidly with increasing benzene concentration (see Fig. 4C).

The yield of the C_9 hydrocarbon decreased to below the limit of detection ($G(C_9) < 0.02$) even in the lowest benzene concentration studied ($\epsilon_b = 0.027$).

The total yield of C_{12} hydrocarbons, measured on the Apiezon L column and including all C_{12} products, varied in a fashion that was similar to that of cyclohexene. For all solutions (excluding pure cyclohexane) the total C_{12} yield was slightly greater than the cyclohexene yield (see Fig. 5).

Pure Benzene

A sample of benzene irradiated to 3.3×10^{20} ev/ml, 24°C gave such small amounts of products that the −195° and −112°C fractions could not be further analyzed. The total yield of each of these fractions was $G(-195°C) = 0.038$ and $G(-112°C) = 0.033$. Gordon and Burton found that hydrogen and acetylene were the only gaseous products formed and that their yields were $G(H_2) = 0.036$ and $G(C_2H_2) = 0.020$.[23] The analytical system was not sensitive enough to detect the liquid products. Various workers have found $G(C_6H_6 \rightarrow \text{polymer}) = 0.75$–$0.93$ and that most of the polymer is of high molecular weight.[2,24,25]

DISCUSSION

Pure Cyclohexane

The hydrogen yield from the radiolysis of cyclohexane appears to be independent of the nature of the ionizing radiation, although there is not general agreement upon its precise value.[2,7,10,12,15,17,21] The values are grouped quite heavily about $G(H_2) = 5.4$. The present value of $G(H_2)_i = 5.37$ agrees well with the only other reported value of $G(H_2)_i = 5.4$ (17), determined by extrapolation to zero dose. The rate of decrease of $G(H_2)$ with increasing dose also agrees well in the two cases. In the present study, a dose of 50 joules/g decreased the integral G value by 3.6%. Guentner *et al.*[17] found that a dose of 50 joules/g decreased the differential G value by 7.6%. Since the variation of $G(H_2)$ with dose is approximately linear in this region, this corresponds to a decrease of 3.8 % in the integral $G(H_2)$.

The decrease in $G(H_2)$ with increasing dose is probably due to the accumulation of olefinic products, which can scavenge hydrogen atoms and perhaps also "protect" cyclohexane by "sponge-type" energy transfer.

Considering the radiolysis of cyclohexane as

$$c\text{-}C_6H_{12} \rightarrow H_2 + X \quad .$$

the total hydrogen deficiency in the initial yields of the products X should be equal to $G(H_2)_i = 5.37$. However, a mass balance of the measured products indicates that the hydrogen equivalent of over one G unit of hydrocarbon products have been missed. A similar conclusion may be derived from earlier work.[15] Hexene-1 and methylcyclopentane have been reported as products by other workers[13,15] but they would not help the situation because their hydrogen equivalents are zero. Nixon and Thorpe[13] reported that only half of the cyclohexane that reacted to form multiring compounds formed dimers and other half formed higher polymers. Products with carbon numbers greater than 13 or 14 would not have been detected in the present study, so this may explain the observed deficiency in hydrocarbon products. This is not necessarily true, however, because the dose used by Nixon and Thorpe was 20 times greater than the highest dose used here, and their observed product distribution was radically different from that reported in this paper. Their primary products could easily have been altered by secondary reactions.

The present results may be used in conjunction with those of Guentner *et al.*[17] and of Dewhurst[15,26] to confirm the difference in liquid product yields obtained at large doses with Co^{60} γ rays and with high-energy charged particles.[16] The difference in yields was ascribed to the difference in dose rate (charged particle dose rate $= 10^{20}$ ev/g sec, γ-ray dose rate $= 4 \times 10^{15}$ ev/g sec). Since the yields are independent of L.E.T., the dose-rate effect cannot be due to the overlapping of tracks. The explanation may lie in thermal reactions.

Cyclohexane-Benzene Solutions

As stated by Manion and Burton,[2] it might be expected that, if there were no interaction between the different components of the solution, the cyclohexane product yields would be directly proportional to the fraction of the absorbed energy that is absorbed directly by the cyclohexane. It has been assumed, for lack of a better function, that the amount of energy absorbed in primary processes in a given component is directly proportional to the electron fraction, ϵ, of that component in the system.[2]

[23] S. Gordon and M. Burton, Discussions Faraday Soc. **12**, 88 (1952).

[24] W. N. Patrick and M. Burton, J. Am. Chem. Soc. **76**, 2626 (1954).

[25] S. Gordon, A. R. Van Dyken, and T. F. Doumani, J. Phys. Chem. **62**, 20 (1958).

[26] The present results suggest that Dewhurst's "dicyclohexyl" might not have been pure dicyclohexyl. Under many conditions of gas-chromatographic analysis the various C_{12} components are not separated.

The experimental results have been tested against several different mechanisms. The following reactions appeared to provide an adequate explanation of the yields of the major products. Other possible reactions will be discussed separately.

$$c\text{-}C_6H_{12} \xrightarrow{I} c\text{-}C_6H_{12}^* \quad (1)$$

$$C_6H_6 \xrightarrow{I^*} C_6H_6^* \rightarrow \text{benzene products} \quad (2)$$

$$c\text{-}C_6H_{12}^* + C_6H_6 \rightarrow c\text{-}C_6H_{12} + C_6H_6 \quad (3)$$

$$c\text{-}C_6H_{12}^* \rightarrow c\text{-}C_6H_{11} + H \quad (4)$$

$$H + c\text{-}C_6H_{12} \rightarrow H_2 + c\text{-}C_6H_{11} \quad (5)$$

$$H + C_6H_6 \rightarrow C_6H_7 \quad (6)$$

$$2c\text{-}C_6H_{11} \rightarrow (c\text{-}C_6H_{11})_2 \quad (7a)$$

$$\rightarrow c\text{-}C_6H_{10} + c\text{-}C_6H_{12} \quad (7b)$$

$$c\text{-}C_6H_{11} + C_6H_7 \rightarrow c\text{-}C_6H_{11}\text{—}C_6H_7 \text{ (cyclohexylcyclohexadiene)} \quad (8a)$$

$$\rightarrow c\text{-}C_6H_{10} + C_6H_8 \text{ (cyclohexadiene)} \quad (8b)$$

$$\rightarrow c\text{-}C_6H_{12} + C_6H_6 \quad (8c)$$

$$2C_6H_7 \rightarrow (C_6H_7)_2 \text{ (dicyclohexadiene)} \quad (9a)$$

$$\rightarrow C_6H_6 + C_6H_8. \quad (9b)$$

The following assumptions will be made:

(1) I and I^* are proportional to ϵ_c and ϵ_b, respectively.

(2) the energy absorbed in the benzene does not affect the cyclohexane reactions ($C_6H_6^* + c\text{-}C_6H_{12} \rightarrow C_6H_6 + c\text{-}C_6H_{12}^*$ will probably not occur to an appreciable extent because the excitation potentials in cyclohexane are greater than those in benzene).

(3) the energy transferred to benzene from $c\text{-}C_6H_{12}^*$ produces negligible amounts of the measured products.

These assumptions were also made or implied by Manion and Burton.[2]

The yields of the individual products will be treated separately.

Hydrogen

The mechanism of Manion and Burton[2] comprised reactions (1)–(5) plus the reaction

$$H + C_6H_6 = H_2 + C_6H_5. \quad (10)$$

They assumed that the hydrogen atoms were "hot" and that "H atoms yielded H_2 by purely random reaction with either of the components of a mixture." However, reaction (10) can be shown to have a negligible influence on the product distribution predicted by the over-all mechanism. Since the major effects of benzene on cyclohexane radiolysis occur at relatively low benzene concentrations, only small amounts of C_6H_5 radicals would be produced. The reaction (exothermic by about 8 kcal/mole)

$$C_6H_5 + c\text{-}C_6H_{12} \rightarrow C_6H_6 + c\text{-}C_6H_{11} \quad (11)$$

might also occur, further reducing the effect of (10). Comparable reactions have been found in the cyclohexane-cyclopentane[20] and cyclohexane-cyclohexene systems.[27]

$$c\text{-}C_6H_{11} + c\text{-}C_6H_{10} \rightarrow c\text{-}C_6H_{12} + c\text{-}C_5H_9$$

$$c\text{-}C_6H_{11} + c\text{-}C_6H_{10} \rightarrow c\text{-}C_6H_{12} + c\text{-}C_6H_9.$$

The yield of hydrogen from cyclohexane, $d[H_2]_c/dt$, predicted by reactions (1)–(9) may be determined by the steady-state method. This gives

$$d[H_2]_c/dt = I\left\{1 + (A + B[c\text{-}C_6H_{12}] + C[C_6H_6])\frac{[C_6H_6]}{[c\text{-}C_6H_{12}]}\right\}^{-1} \quad \text{(iii)}$$

where $A = k_6/k_5$, $B = k_3/k_4$, and $C = k_3k_6/k_4k_5$. In the absence of benzene, one H_2 is produced for each $c\text{-}C_6H_{12}^*$ initially formed; i.e., $I = G(H_2)_c{}^0$. In the presence of benzene $I = G(H_2)_c{}^0\epsilon_c$. Therefore, from Eq. (ii) it may be seen that

$$I = G(H_2)_{exp} - G(H_2)_b{}^0\epsilon_b. \quad \text{(iv)}$$

[27] G. R. Freeman, Can. J. Chem. (to be published).

Similarly, we may put

$$d[H_2]_c/dt = G(H_2)_{obs} - G(H_2)_b{}^0\epsilon_b \qquad (v)$$

Then

$$\frac{I}{dH_{2c}/dt} = \frac{G(H_2)_{exp} - G(H_2)_b{}^0\epsilon_b}{G(H_2)_{obs} - G(H_2)_b{}^0\epsilon_b} = \rho \qquad (vi)$$

and

$$\rho = 1 + (A + B[c\text{-}C_6H_{12}] + C[C_6H_6])\{[C_6H_6]/[c\text{-}C_6H_{12}]\}. \qquad (vii)$$

The experimental results were plotted according to Eq. (vii), assuming relative values for A, B, and C, to determine which set of relative values provided the best fit. A value of B that was large compared to A and C would signify that energy transfer protection is the most important effect of benzene on the cyclohexane system. A value of A that was large compared to B and C would mean that hydrogen atom scavenging is the major function of benzene. If C were large compared to A and B, or if A, B, and C were similar in magnitude, energy transfer and hydrogen atom scavenging would be of comparable importance. The results indicated that the effects were split into two quite distinct benzene concentration regions. At low benzene concentrations ($\epsilon_b < 0.05$) rapid scavenging and/or energy transfer occurred with a certain fraction of the hydrogen atoms and/or excited cyclohexane species. At higher benzene concentrations energy transfer protection seemed to be the major effect of benzene. The variation of the cyclohexadiene polymer yield with benzene concentration indicates that the low concentration effect could be subtracted from the over-all benzene effect to obtain the high concentration effect.

The yield of cyclohexadiene polymers (Fig. 4A) indicates that their precursors are not deactivated even at the higher benzene concentrations—their total yield is directly proportional to ϵ_c. Thus the reactions

$$c\text{-}C_6H_{12}' \rightarrow c\text{-}C_6H_{11} + H \qquad (4')$$

and

$$H + C_6H_6 \rightarrow C_6H_7 \qquad (6)$$

occur rapidly by comparison with

$$c\text{-}C_6H_{12}' + C_6H_6 \rightarrow c\text{-}C_6H_{12} + C_6H_6 \qquad (3')$$

and

$$H + c\text{-}C_6H_{12} \rightarrow H_2 + c\text{-}C_6H_{11} \qquad (5)$$

where c-C_6H_{12}' represents a particular excited species of cyclohexane.

For another excited species, c-C_6H_{12}'', the reaction

$$c\text{-}C_6H_{12}'' + C_6H_6 \rightarrow c\text{-}C_6H_{12} + C_6H_6 \qquad (3'')$$

is sufficiently rapid that it may compete with

$$c\text{-}C_6H_{12}'' \rightarrow c\text{-}C_6H_{11} + H. \qquad (4'')$$

Let the rates of production of c-C_6H_{12}' and c-$C_6H_{12}'' = I'$ and I'', respectively, where

$$I = I' + I'' \qquad (viii)$$

and I, I', and I'' are each directly proportional to ϵ_c. Then we may define an interpolated hydrogen yield, $G(H_2)_{int}$, as

$$G(H_2)_{int} = I'' + G(H_2)_b{}^0\epsilon_b. \qquad (ix)$$

Similarly, we may define

$$\rho'' = \frac{G(H_2)_{int} - G(H_2)_b{}^0\epsilon_b}{G(H_2)_{obs} - G(H_2)_b{}^0\epsilon_b}. \qquad (x)$$

By analogy with Eq. (vii) we see that

$$\rho'' = 1 + (A + B''[c\text{-}C_6H_{12}] + C''[C_6H_6])\frac{[C_6H_6]}{[c\text{-}C_6H_{12}]} \qquad (xi)$$

where $A = k_6/k_5$, $B'' = k_3''/k_4''$, and $C'' = k_3''k_6/k_4''k_5$. Many different plots of the experimental results were made according to Eq. (xi), assuming different sets of values I'' (hence of ρ'') and different relative values of A, B'', and C''. The results could only be fit by a value of B'' that was much larger than A or C'', so Eq. (xi) reduces to

$$\rho'' = 1 + k_3''[C_6H_6]/k_4'' \qquad (xii)$$

The values of I'' that gave the best fit to Eq. (xii) were given by[28]

$$I'' = 3.0\epsilon_c \ (G \text{ units}). \qquad (xiii)$$

The corresponding values of $G(H_2)_{int}$ are shown as a dot-dash line in Fig. 3A. The plot of ρ'' vs $[C_6H_6]$ is shown in Fig. 6. ρ'' may be thought of as the inverse of the fraction of the c-C_6H_{12}'' initially produced that decomposes to produce H, and hence H_2. The slope of the line in Fig. 6 gives $k_3''/k_4'' = 0.78$ liter/mole.

Thus, in pure cyclohexane, $I'' = 3.0$ G units and $I' = 5.4 - 3.0 = 2.4$ G units. These values are only approximate and only correspond to the best fit of the results to Eq. (xii). Actually, the results fit not too badly over a range of $I'' = 3.0 \pm 0.4$ G units, the fit becoming less good as the difference from $I'' = 3.0$ increases. The corresponding range of I' is 2.4 ∓ 0.4 G units.

The fact that the hydrogen atoms from c-C_6H_{12}' can be scavenged by benzene whereas those from c-C_6H_{12}'' cannot, seems to indicate either that the latter hydrogen atoms are hot or that the reaction

$$c\text{-}C_6H_{12}'' \rightarrow c\text{-}C_6H_{10} + H_2 \qquad (12)$$

[28] The cyclohexane-cyclohexene system[27] indicated that the cold hydrogen atoms generated by c—C_6H_{12}' (see later) were not completely scavenged when the electron fraction of cyclohexene was below about 0.1. For the present system, a value of $k_6/k_5 = 200$ (see footnote reference 27) was used to correct for small amounts of unscavenged hydrogen atoms. Eg. at $\epsilon_b = 0.053$ about 93% of the hydrogen atoms would be scavenged. The value of k_6/k_5 used is a crude approximation but the value obtained for the constant in Eq. (xiii) is not very sensitive to the value of k_6/k_5, within reasonable limits.

occurs instead of reaction (4″). This will be discussed again later.

Dicyclohexyl and Cyclohexene

When ϵ_b increases from 0.000 to 0.027 (the lowest benzene concentration studied), $\Delta G(H_2) = -2.21$, $\Delta G(\text{dicyclohexyl}) = -0.79$, and $\Delta G(\text{cyclohexene}) = -1.47$. Thus, the sum of the decreases in dicyclohexyl and cyclohexene yields ($\Delta G = -2.26$) is equal to the decrease in hydrogen yield. This good agreement indicates that the undetected hydrocarbon products from pure cyclohexane radiolysis (equivalent to over one G unit of hydrogen—see Pure Cyclohexane Discussion) are not generated by the excited state(s) represented by $c\text{-}C_6H_{12}'$. Furthermore, the value of the ratio $\Delta G(\text{cyclohexene})/\Delta G(\text{dicyclohexyl}) = 1.86$ is equal to the value of the ratio $G(\text{cyclohexene})_i/G(\text{dicyclohexyl})_i = 1.84$ for pure cyclohexane. If the similarity of these two values is not a coincidence, it is unlikely that reaction (12), or its equivalent involving $c\text{-}C_6H_{12}'$, contribute appreciably to the over-all reaction. This could only be true if the ratios of the rates of the reactions

$$c\text{-}C_6H_{12} \rightarrow c\text{-}C_6H_{11} + H$$

and

$$c\text{-}C_6H_{12} \rightarrow c\text{-}C_6H_{10} + H_2$$

were the same for several different excited species (e.g., $c\text{-}C_6H_{12}'$ and $c\text{-}C_6H_{12}''$).

The interpolated values $G(\text{dicyclohexyl})_{int}$ and $G(\text{cyclohexene})_{int}$ were chosen such that, for pure cyclohexane,

$$(G_i - G_{int})_{\text{dicyclohexyl}} + (G_i - G_{int})_{\text{cyclohexene}} = (G_i - G_{int})_{H_2} = 2.4 \qquad \text{(xiv)}$$

and $(G_i - G_{int})_{\text{cyclohexene}}/(G_i - G_{int})_{\text{dicyclohexyl}} = 1.86$ (xv). The values of $(G_i - G_{int})$ were 1.56 and 0.84 for cyclohexene and dicyclohexyl, respectively. Thus, for pure cyclohexane, $G(\text{cyclohexene})_{int} = 0.72$ and $G(\text{dicyclohexyl})_{int} = 0.40$. For the cyclohexane-benzene solutions it will be assumed that the interpolated yields are directly proportional to ϵ_c (see dot-dash lines in Figs. 4 and 5).

Define $X'' = G(\text{cyclohexene})_{int}/G(\text{cyclohexene})_{obs}$ (xvi)

and

$$Y'' = G(\text{dicyclohexyl})_{int}/G(\text{dicyclohexyl})_{obs}. \qquad \text{(xvii)}$$

If dicyclohexyl and cyclohexene were formed only by combination and disproportionation of cyclohexyl radicals, and if there were no interferences[29] by other species in the system, plots of X'' and Y'' against

[29] Reactions (4′) and (6) would not interfere if they were followed exclusively by reactions (8a) and (8c). Reaction (8b) would increase the cyclohexene yield and decrease the value of X''. The small amount of reactions (9a) and (9b) which occur leave a small excess of $c\text{-}C_6H_{11}$ radicals to react according to (7a) and (7b), which will decrease the values of both X'' and Y''.

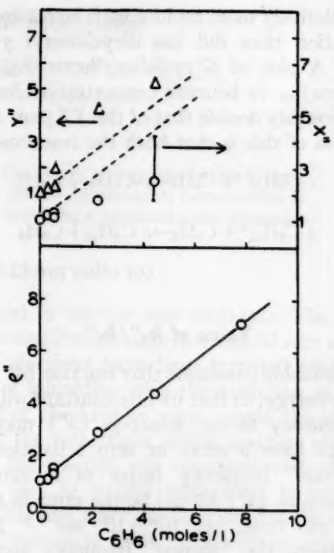

FIG. 6. Variation of ρ'', X'', and Y'' with benzene concentration.

$$\rho'' = [G(H_2)_{int} - G(H_2)_b{}^{\circ}\epsilon_b]/[G(H_2)_{obs} - G(H_2)_b{}^{\circ}\epsilon_b];$$

X'' (circles) $= G(\text{cyclohexene})_{int}/G(\text{cyclohexene})_{obs}$; Y'' (triangles) $= G(\text{dicyclohexyl})_{int}/G(\text{dicyclohexyl})_{obs}$. The dash lines have the same slope as the ρ'' curve. The vertical line through the point for the highest value of X'' indicates the limits of error of that particular sample, due to a poor analysis.

benzene concentrations (e.g moles/liter), should have the slope k_3''/k_4''. It is evident from Fig. 6 that, especially at the higher benzene concentrations, the X'' and Y'' points do not fit on lines with slopes equal to $k_3''/k_4'' = 0.78$ liter/mole. The cyclohexene points fall below the line (i.e., $G(\text{cyclohexene})_{obs}$ is too large) and the dicyclohexyl points fall above the line (i.e., $G(\text{dicyclohexyl})_{obs}$ is too small). This seems to indicate that cyclohexyl radicals also react with something else in the system.

Cyclohexylhexene

The cyclohexylhexene was probably generated by the reactions

$$c\text{-}C_6H_{12}'^{v} \rightarrow c\text{-}C_6H_{11}{}^{*} + H \qquad (13)$$

$$c\text{-}C_6H_{11}{}^{*} \rightarrow CH_2{=}CHCH_2CH_2CH_2CH_2\cdot \qquad (14)$$

$$CH_2{=}CH(CH_2)_4\cdot + c\text{-}C_6H_{11} \rightarrow c\text{-}C_6H_{11}(CH_2)_4CH{=}CH_2 \qquad (15)$$

where $c\text{-}C_6H_{12}'^{v}$ represents a highly excited cyclohexane species and $c\text{-}C_6H_{11}{}^{*}$ represents an excited cyclohexyl radical. The absence of a sudden large decrease in G(cyclohexylhexene) between $\epsilon_b = 0$ and $\epsilon_b = 0.027$ indicates that $c\text{-}C_6H_{12}'^{v}$ is to be classed with the states represented by $c\text{-}C_6H_{12}''$ rather than with those represented by $c\text{-}C_6H_{12}'$. The cyclohexylhexene yield de-

creased relatively more rapidly with increasing benzene concentration than did the dicyclohexyl yield from c-C_6H_{12}''. A plot of $G(\text{cyclohexylhexene})_{exp}/G(\text{cyclohexylhexene})_{obs}$ vs benzene concentration had a slope that was roughly double that of the Y'' plot. A possible explanation of this is that both the reactions

$$c\text{-}C_6H_{12}'^{v}+C_6H_6\rightarrow c\text{-}C_6H_{12}+C_6H_6 \qquad (3'^{v})$$

and

$$c\text{-}C_6H_{11}^{*}+C_6H_6\rightarrow c\text{-}C_6H_{11}+C_6H_6 \quad \text{(or other products)} \qquad (16)$$

occur.

Value of k_3''/k_4''

It is reasonable to assume that reaction (4'') has zero activation energy, so that its rate constant will be equal to its frequency factor. Reaction (3'') may also be assumed to have a small or zero activation energy. The "normal" frequency factor of a unimolecular reaction such as (4'') should be the same in the liquid as in the gas state, i.e., $10^{13}-10^{14}$ sec^{-1}.[30] To a first approximation, the "normal" frequency factor for a bimolecular reaction such as (3'') is the same in the liquid as in the gas state, i.e., 10^{11}–10^{12} liters/mole sec.[30] An activation energy or quantum restrictions would reduce the value of k_3'' to considerably less than 10^{11}–10^{12} liters/mole sec. Thus, if reactions (3'') and (4'') were normal we would have, to a first approximation, $k_3''/k_4''\leq 10^{-2}$ liter/mole.

It is well established that collisions between individual particles, A and B, occur in sets[31–33] because of the cage effect. The total number of collisions per second between A and B, Z_{AB}, will be given by

$$Z_{AB}=(\text{No. of encounters/sec})\times(\text{No. of } A-B \text{ collisions/encounter}).$$

An encounter begins when an A enters a cage with a B in the wall, or vice versa, and ends when either the A or the B diffuses away. In the absence of reaction between A and B, Z_{AB} will be given by the same formula as that used for gases. A correction applied to take into consideration the volume occupied by the molecules themselves should make Z_{AB} in the liquid 10 to 100 times greater than Z_{AB} in the gas.[31] Using the terminology of Williamson and LaMer,[33] the bimolecular reaction rate constant is: $k=pk_D$, where $p=$ probability of reaction per encounter, and $k_D=$ encounter frequency. If $p=1$, k has its maximum value and the reaction is diffusion controlled. Under these circumstances the normal liquid phase frequency factor would be an order of magnitude smaller than the one in the gas phase, for substances such as cyclohexane and benzene.[30] Therefore, "normally" $k_3''/k_4''\leq 10^{-3}$ liter/mole.

The experimental value of $k_3''/k_4''=0.78$ liter/mole is thus greater than the normal value by a factor $\geq 10^3$. This indicates that reaction (4'') is slower than normal, or that reaction (3'') is faster than normal, or both. The two limiting cases will be considered.

The first case requires that $k_4''\lesssim 10^{10}$ sec^{-1}. This means that the excited states of cyclohexane represented by c-C_6H_{12}'' have a lifetime in a given excited species, $\tau\gtrsim 10^{-10}$ sec. This would seem to imply that transfer of excitation energy from a c-C_6H_{12}'' to a benzene molecule would have a greater efficiency than transfer to a cyclohexane molecule.

The second case requires that $k_3''\geq 10^3 k_D\gtrsim 10^{13}$ liters/mole sec. The rate of diffusion of the excitation energy would be much greater than the rate of diffusion of the molecules. The processes would be analogous to those that occur during scintillation in liquid scintillators.[34–37] Assuming the "collision yield" for energy transfer from an excited cyclohexane species to either a cyclohexane or a benzene molecule to be unity,[38] a lower limit can be calculated for the time required to transfer the energy from one molecule to another. Under these conditions, $k_3''\approx 10^{13}$–10^{14} liters/mole sec. The concentrations of cyclohexane and benzene in the pure liquids are 9.2 and 11.2 moles/liter, respectively. Therefore, the time required to transfer energy from one molecule to another would be 10^{-14}–10^{-15} sec. This is the same value as that derived by Kallmann and Furst ("of the order of 10^{-14} sec or less" [footnote reference 34(a), pp. 867–8] for the analogous limiting case mechanism in fluorescent solutions. They felt that this value was too small to be true and discussed other effects that would cause the energy transfer time to be greater than 10^{-14} sec. It is also possible that the true mechanism of energy transfer in the cyclohexane-benzene system lies between the limiting cases 1 and 2. This would allow energy transfer times $>10^{-14}$ sec.

ACKNOWLEDGMENTS

The author would like to express his gratitude to Dr. S. Usiskin for aid with the irradiations and to the Government of Alberta Cancer Clinic for permission to use the Co^{60} therapy unit.

[30] A. A. Frost and R. G. Pearson, *Kinetics and Mechanism* (John Wiley & Sons, Inc., New York, 1956).
[31] E. Rabinowitch, Trans. Faraday Soc. **33**, 1225 (1937).
[32] R. H. Fowler and N. B. Slater, Trans. Faraday Soc. **34**, 81 (1938).
[33] B. Williamson and V. K. LaMer, J. Am. Chem. Soc. **70**, 717 (1948).
[34] (a) H. Kallmann and M. Furst, Phys. Rev. **79**, 857 (1950); (b) **81**, 853 (1951); (c) H. Kallmann and G. J. Brucker, *ibid.* **108**, 1122 (1957).
[35] J. B. Birks, *Scintillation Counters* (McGraw-Hill Book Company, Inc., New York, 1953).
[36] S. C. Curran, *Luminescence and the Scintillation Counter* (Butterworths Scientific Publications, London, 1953).
[37] C. Kittel, *Introduction to Solid State Physics* (John Wiley & Sons, New York, 1956), 2nd ed.
[38] Since a physical, kinetic molecular collision is not necessarily required for this type of excitation transfer, the rate of excitation transfer might be much greater than the kinetic molecular collision rate.[34(c)] The "collision yield" equal to unity would imply that there were no activation energy or steric factor restrictions on the reaction.

Entropy Production in Chemical Reactions

R. P. RASTOGI AND R. C. SRIVASTAVA

Department of Chemistry, Panjab University, Hoshiarpur, India

(Received January 5, 1960)

The generalization of Prigogine and Glansdroff which states that the rate of entropy production is negative in the nonstationary state and zero in the stationary state is verified for reversible isomerization of ammonium thiocyanate and the isomerization of Δ^{α}-pentenoic acid involving a monomolecular triangular reaction.

1. INTRODUCTION

THE second law of thermodynamics merely states that entropy production is positive definite in irreversible processes. However, during recent years developments in the theory of thermodynamics of irreversible processes have yielded valuable information regarding the characteristics of entropy production in the nonequilibrium state.[1] Within the domain of validity of Gibb's equation, entropy production σ can be expressed as $\Sigma J_i X_i$ where J_i is the flow and X_i is the force. In the linear region where the flows are linearly related to forces, σ has a minimum value in the stationary state. According to Prigogine and Glansdroff,[2] for both linear and nonlinear region, the function $m=-\Sigma J_i \dot{X}_i \geq 0$, the equality holding for the stationary state. $\dot{X}_i$ is the time derivative of the force X_i. The purpose of the present note is to examine the validity of last generalization for chemical reactions.

2. REVERSIBLE ISOMERIZATION OF AMMONIUM THIOCYANATE

The kinetics of reversible isomerization of ammonium thiocyanate into thiourea was studied in a thermostat containing glycerine. The temperature was maintained at 170°C with the help of an aniline thermoregulator. The reaction was followed in a big boiling tube which initially contained ammonium thiocyanate. As soon as the whole of ammonium thiocyanate melted, a few cc of the molten mass were withdrawn at regular intervals of time and rapidly chilled. The amount of thiourea in the sample was estimated by the method of Reynold and Warner.[3] The kinetics of this reaction had been the subject of earlier studies but earlier emphasis was more on equilibrium constant. For the present purpose, a knowledge of reaction rates and affinities at different times was needed and hence a detailed study was made.

The reaction proceeds according to the scheme:

$$NH_4SCN \underset{k_b}{\overset{k_f}{\rightleftharpoons}} SC\begin{matrix}NH_2\\ \diagdown\\ \\ \diagup\\ NH_2\end{matrix},$$

where k_f and k_b are the rate constants. The reaction reaches the equilibrium state in about 50 min at 170°C. Some side reactions have been reported such as the formation of guanidine with the evolution of gaseous products. For checking to what extent the side reactions occur the total mass of the reaction mixture at the end of the reaction was compared with the initial mass. The loss in weight amounting to only 0.5% suggested that side reactions do occur but the reactions are not fast enough at 170°C to contribute appreciably. For our purpose this is not a serious defect, as we are mainly concerned with the mere trend of the reaction kinetics necessary for proving this theorem.

If a is the initial concentration of ammonium thiocyanate and x is the amount of thiourea formed in time t, then it follows that

$$k_f+k_b=(2.303/t)\log[x_e/(x_e-x)],$$

where x_e is the equilibrium value. The value of (k_f+k_b) was determined graphically. Since the equilibrium constant is known from the data, the values of k_f and k_b could easily be calculated.

For a single chemical reaction, the generalization implies that

$$V\cdot dA/dt \leq 0,$$

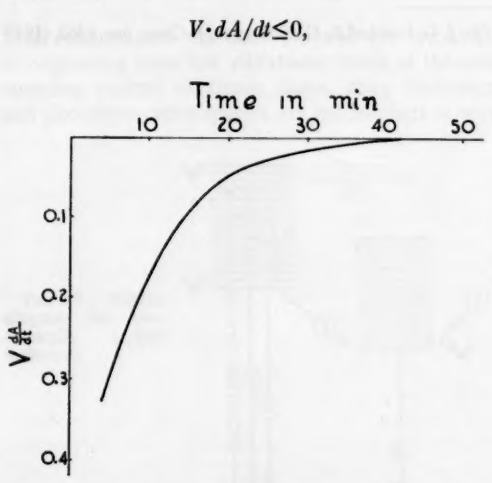

FIG. 1. Test of the generalization for monomolecular reversible isomerization of ammonium thiocyanate.

[1] S. R. de Groot, *Thermodynamics of Irreversible Processes* (North-Holland Publishing Company, Amsterdam, 1952).
[2] P. Glansdroff and I. Prigogine, Physica **20**, 773 (1954).
[3] J. E. Reynold and E. A. Warner, J. Chem. Soc. 1, (1903).

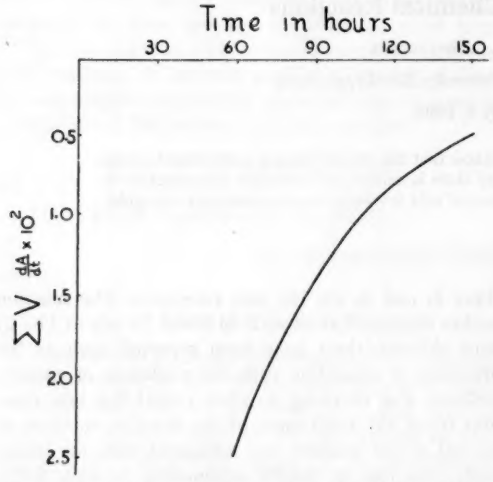

FIG. 2. Test of the generalization for triangular reversible reaction.

where V is the rate of the reaction and A is the affinity. V was calculated from the relation

$$V = k_f(a-x) - k_b x$$

at various intervals of time. The corresponding value of affinity was calculated with the help of vant Hoff's isotherm. When V is plotted against (A/RT) it is found that linear relation between reaction rate and affinity exists for a broader region than could be imagined. dA/dt was determined from the slopes of the curve obtained by plotting A against t. In Fig. 1 $(V \cdot dA/dt)$ is plotted against t to demonstrate that $(V \cdot dA/dt)$ is always less than zero. The curve approaches the time axis asymptotically proving thereby that $V \cdot dA/dt \leq 0$.

3. MONOMOLECULAR TRIANGULAR REACTION

Another interesting case is the isomerization of Δ^{α}-pentenoic acid which has been studied by Ives and Kerlongue.[4] The essential reaction is as follows

$$\begin{array}{ccc} & \overset{(1)}{\rightleftharpoons} & \\ CH_3 \cdot CH_2 \cdot CH{=}CH \cdot COOH & & CH_3CH{=}CH \cdot CH_2 \cdot COOH \\ (3)\uparrow\downarrow & & \uparrow\downarrow(2) \\ & CH_3 \cdot CH_2 \cdot CH(OH) \cdot CH_2COOH. & \end{array}$$

The rate constants for individual reactions have been determined by these workers. From the data at various intervals, the reaction velocities and affinities were calculated in the previous manner. According to Prigogine's theorem we must have

$$V_1 dA_1/dt + V_2 dA_2/dt + V_3 dA_3/dt \leq 0,$$

where the subscripts 1, 2, 3 refer to the reactions involved in the present case. In Fig. 2 $(V_1 \cdot dA_1/dt + V_2 \cdot dA_2/dt + V_3 \cdot dA_3/dt)$ is plotted against time which justifies the theorem.

4. ACKNOWLEDGMENT

One of us (RCS) is grateful to Indian Council of Scientific and Industrial Research for the award of a fellowship.

[4] D. J. G. Ives and R. G. Kerlongue, J. Chem. Soc. 1362, (1940).

Kinetics of Excited Molecules. II. Dissociation Processes

GERALD B. PORTER AND B. T. CONNELLY*

Department of Chemistry, University of British Columbia, Vancouver, Canada

(Received February 5, 1960)

A detailed calculation of the rate of dissociation of an electronically and vibrationally excited molecule (photochemical dissociation) is compared with the experimental data for ketene. The results are consistent with unimolecular reaction rate theory. However, the data are not accurate enough to provide unambiguous values for the parameters in the theory.

A CONSIDERABLE amount of experimental data has been accumulated on the variation of primary quantum yields in ketones,[1] ketene[2] and azoalkanes[3] with pressure, temperature, and exciting wavelength. Since the primary yield is often less than unity, particularly at long wavelengths and at low temperatures, it is important to examine the detailed features of the processes by which electronically excited molecules dissociate. For systems of this type, the detailed reactions of excited molecules are most conveniently represented by a modified Jablonski diagram. Figure 1 depicts the relative energies of the ground electronic state (M), the first excited singlet state ($^1M^n$), and the first triplet state ($^3M^n$). The superscript index n is a measure of the vibrational energy level.

REACTIONS OF THE EXCITED MOLECULES

The reactions of the excited molecules are also shown in Fig. 1. Reaction (1) refers to the dissociation of the vibronic state reached by absorption of radiation:

$$^1M^n = \text{radical fragments}; \quad \text{rate} = k_{1n}(^1M^n). \qquad (1)$$

If other vibronic states at lower energies are appreciably populated, dissociation of these molecules must be taken into account. Collisional degradation of this same vibronic state is represented by reaction (2):

$$^1M^n + M = {}^1M^0 + M; \quad \text{rate} = k_{2n}(^1M^n)(M). \qquad (2)$$

Although this degradation is shown here as a single step (as is frequently assumed for simplicity), it must be a cascade process in which an excited molecule loses only a part of its vibrational energy in each encounter with other molecules in the system. Eventually, unless the molecule dissociates or undergoes internal conversion, it reaches the state $^1M^0$ in vibrational, but not electronic equilibrium, with the surrounding gas.

For some of these systems, reaction (3) may be required by the kinetic data:

$$^1M^n = M; \quad \text{rate} = k_{3n}(^1M^n). \qquad (3)$$

The reason for inclusion of this reaction is that some primary quantum yields, when extrapolated to zero concentration, are less than unity. Reaction (4) is a transition to the ground state from $^1M^0$:

$$^1M^0 = M; \quad \text{rate} = k_4(^1M^0), \qquad (4)$$

which is an internal conversion process analogous to reaction (3), or a radiative process, i.e., fluorescence. Intersystem crossing must be included to account for the observation of phosphorescence. Although intersystem crossing is represented by:

$$^1M^0 = {}^3M^0, \quad \text{rate} = k_5(^1M^0); \qquad (5)$$

in fact, it must occur by the following sequence:

$$^1M^0 = {}^3M^m$$

$$^3M^m + M = {}^3M^0 + M,$$

in which the second reaction is much faster than the first at all experimentally accessible concentrations.

Reaction (6) accounts for phosphorescence, but also includes internal conversion.

$$^3M^0 = M; \quad \text{rate} = k_6(^3M^0). \qquad (6)$$

Both luminescence reactions (4) and (6) are written as originating from low vibrational levels of the corresponding excited electronic states, since fluorescence and phosphorescence spectra are independent of wave-

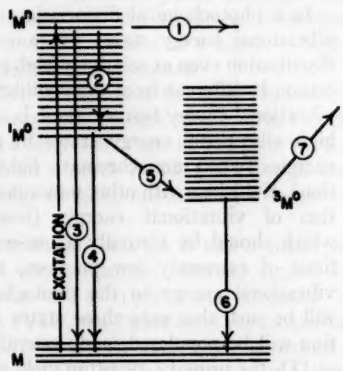

FIG. 1. Energy diagram for electronically excited molecules.

* Present address: DuPont of Canada Ltd., Sarnia, Ontario, Canada.

[1] See W. A. Noyes, Jr., J. E. Jolley, and G. B. Porter, Chem. Revs. 56, 49 (1956).

[2] B. T. Connelly and G. B. Porter, Can. J. Chem. 36, 1640 (1958), Part I of this series.

[3] H. Cerfontain and K. O. Kutschke, Can. J. Chem. 36, 344 (1958).

length in the vapor phase, except perhaps at very low pressure.

The second dissociation reaction has been postulated to explain the increase in primary quantum yield with increasing temperature:

$$^3M^0 = \text{radical fragments}; \qquad \text{rate} = k_7(^3M^0). \quad (7)$$

Since the singlet state usually has a short natural lifetime, ca 1 μsec, and a still shorter actual lifetime, ca 0.01 μsec, judged by fluorescence quantum yields, it would not be possible for the $^1M^0$ state to gain sufficient energy by collision processes to dissociate. On the other hand, since phosphorescence is a forbidden transition, the triplet state $^3M^0$ has a lifetime long enough to achieve vibrational equilibrium and hence to dissociate thermally.

PRIMARY DISSOCIATION OF THE EXCITED SINGLET STATE

Dissociation from those vibronic levels reached by absorption of radiation, except at short wavelengths, is slow enough for collisional degradation to compete, even at total pressures of the order of a few mm. At these pressures, the average time between collisions is of the order of 0.1 μsec. The dissociation process is slow because it involves a rearrangement of vibrational energy. In this respect, dissociation of electronically excited molecules is analogous to unimolecular dissociation of molecules in thermal reactions. As there is a difference in electronic state, less vibrational energy is required in the photochemical case compared to the thermal reaction.

The most important difference between photochemical and thermal dissociation is the distribution of vibrational energy states among molecules. In a thermal reaction, particularly at high pressure, there is essentially a Maxwell-Boltzmann equilibrium distribution, which is only appreciably distorted at high energies, i.e., where the molecules are capable of dissociation. As the pressure is decreased, high-energy molecules are "siphoned" off by reaction and, in the limit of low pressure, second-order kinetics are obeyed, and the rate of reaction is limited by the rate of activation.

In a photochemical dissociation, the distribution of vibrational energy states will not be an equilibrium distribution even at relatively high pressure. The distribution is different from the equilibrium distribution of vibrational energy because there is a constant source of high vibrational energy states in a narrow range of energies (when monochromatic light is used for excitation). Collisions with other molecules lead to a degradation of vibrational energy (toward equilibrium), which should be virtually a one-way process. In the limit of extremely low pressure, the distribution of vibrational energy in the photochemical dissociation will be such that only those states reached by absorption will be populated, and, excepting a reaction such as (3), the primary quantum yield should be unity.

With the assumption of a collisional degradation reaction in which all of the effective vibrational energy is removed in one collision, i.e., only those vibronic states reached by absorption of radiation dissociate, the following general formula can be derived by appropriate steady-state approximation:

$$\phi = [k_{1n} + abk_{2n}(M)]/[k_{1n} + k_{2n}(M) + k_{3n}], \quad (I)$$

where $a = k_5/(k_4+k_5)$, the fraction of $^1M^0$ molecules which cross to the triplet state, and $b = k_7/(k_6+k_7)$, the fraction of $^3M^0$ molecules which dissociate.

In one simplifying approach,[4] it is assumed that k_{3n} is zero, hence Eq. (I) reduces to:

$$\phi/(1-\phi) = [ab/(1-ab)] + [k_{1n}/(1-ab)k_{2n}(M)]. \quad (II)$$

According to this scheme, a plot of $\phi/(1-\phi)$ vs the reciprocal of total pressure (or concentration) should give a straight line from which ab and k_{1n}/k_{2n} can be evaluated. Another simplifying approximation is to neglect Reaction (7), dissociation of the triplet state, in which case, Eq. (I) reduces to[5]:

$$1/\phi = 1 + (k_{3n}/k_{1n}) + [k_{2n}(M)/k_{1n}]. \quad (III)$$

From the linear relation obtained from a graph of $1/\phi$ vs (M), the quantities k_{3n}/k_{1n} and k_{2n}/k_{1n} are determined. The first method works well for hexafluoroacetone,[4] the second for biacetyl,[6] ketene,[5] and the azoalkanes.[3]

CASCADE COLLISIONAL DEACTIVATION

To investigate the possible requirement of more than one collisional encounter of an excited molecule, the following detailed mechanism is assumed:

$$M + h\nu = {}^1M^n; \qquad \text{rate} = I_a$$
$$^1M^n = \text{products}; \qquad \text{rate} = k_n(^1M^n)$$
$$^1M^n + M = {}^1M^{n-1} + M; \qquad \text{rate} = Z(M)(^1M^n)$$
$$^1M^{n-1} = \text{products}; \qquad \text{rate} = {}^kn-1(^1M^{n-1})$$
$$\cdots$$
$$^1M^{m+1} + M = {}^1M^m + M; \qquad \text{rate} = Z(M)(^1M^{m+1})$$
$$^1M^m = \text{deactivation}.$$

The indexes m and n are measures of the vibrational energy of the singlet excited molecule measured from the zero-point vibrational level. Molecules $^1M^m$ and those with lower energy do not dissociate. It is not specified yet how the quantities m and n are related to energy, nor how the rates of dissociation vary with energy. For simplicity, reaction (3) is omitted.

By application of the steady-state approximation, the concentrations of the various excited states can be

[4] P. B. Ayscough and E. W. R. Steacie, Proc. Roy. Soc. (London) **A234**, 476 (1956).
[5] A. N. Strachan and W. A. Noyes, Jr., J. Am. Chem. Soc. **76**, 3258 (1954).
[6] J. Heicklen, J. Am. Chem. Soc. **81**, 3863 (1959).

derived:

$$k_j({}^1M^j)_{ss}=I_a a_j/(M)\prod_j^n[1+a_i/(M)], \quad \text{(IV)}$$

where $a_i=k_i/Z$. For the purpose of calculating the primary quantum yield, only those states which can dissociate are of interest, i.e., $n-j>m$. The sum of the contributions from each vibronic state gives the primary quantum yield of dissociation (with only the singlet states dissociating)

$$\phi=\sum_{m+1}^{n}a_j/(M)\prod_j^n[1+a_i/(M)], \quad \text{(V)}$$

which is identical to

$$\phi=1-\prod_{m+1}^{n}[1/(1+a_i/(M))]. \quad \text{(VI)}$$

At this point, thermal dissociation of the triplet state can be included. Using the quantities a and b as defined for Eq. (I), the total quantum yield for dissociation is:

$$\phi=1-(1-ab)\prod_{m+1}^{n}\{1/[1+a_i/(M)]\}. \quad \text{(VII)}$$

To evaluate Eqs. (VI) and (VII), an assumption must be made about the nature of the quantity a_i. Since the experimental data indicate that the rate of dissociation of excited vibronic states is a function of their energy content, and since three theories of unimolecular dissociation[7–9] lead to similar expressions for the rate constant for dissociation, k_i is assumed to have the form:

$$k_i=\nu(1-\epsilon_m/\epsilon_i)^{s-1}. \quad \text{(VIII)}$$

ν, according to Slater's theory, is an appropriately weighted root-mean-square of the normal mode frequencies of vibration and, according to Eyring's theory, has the value kT/h. In either case, its numerical value should be *approximately* 10^{13} sec^{-1}. ϵ_m and ϵ_i are the *vibrational* energies which correspond to the states of index m and i, respectively, and s is the number of non-degenerate modes of vibration in the molecule. The specific rate constant k_i applies to a state of vibrational energy ϵ_i.

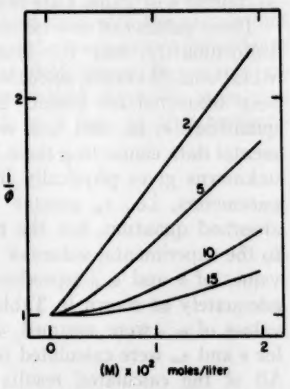

FIG. 2. Calculated quantum yield, $s=9$, $n/m=1.5$, $m=2$, 5, 10, and 15.

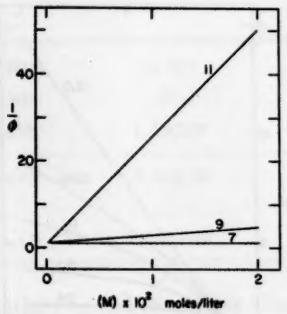

FIG. 3. Calculated quantum yield, $n=41$, $m=30$, $s=7$, 9, and 11.

It simplifies the calculations to make the assumption that each collision results in the loss of a constant amount of vibrational energy, hence, that the vibrational energy is proportional to integral indexes, n, m, etc. Since the calculated results will be compared with the experimental data on ketene principally, s is chosen to be 9, and ν/Z to be 100 mole liter^{-1}, consistent with $\nu=10^{13}$ sec^{-1} and $Z=10^{11}$ mole^{-1} liter sec^{-1}.

When the excitation energy is only slightly greater than the minimum energy required for dissociation, the reciprocal of the primary yield is linear with pressure. At higher energies, e.g., $n>41$, with $m=30$, the same curves are linear only at very high pressure and are concave upwards at low pressure. The slope is zero at zero pressure.

The effect of variation of m (which represents the relative numbers of collisions required for deactivation of vibrational energy) is shown in Fig. 2.

An increase in the number of collisions required for degradation, i.e., decrease of the vibrational energy removed in each collision, aside from the gross effect of increasing the primary quantum yield, increases the departure from linearity of the reciprocal quantum yield with pressure. It also results in a higher extrapolated quantum yield at zero pressure.

When the number of degrees of freedom s is varied, the primary quantum yield changes as shown in Fig. 3. A change in s has a large effect on the behavior of the quantum yield. From $s=6$ to $s=10$, the value of the slope, i.e., an average of k_2/k_1, increases by a factor of almost 50.

All of the curves shown in Figs. 2 and 3 relate to dissociation from nonequilibrium vibronic states. If thermal dissociation of a triplet-state molecule is included, as in Eq. (VII), the variation of the reciprocal of the dissociation yield with concentration changes radically as shown in Fig. 4. The curves have a pro-

[7] L. J. Kassel, *Kinetics of Homogeneous Gas Reactions* (Chemical Catalog Company, Inc., New York, 1932).
[8] S. Glasstone, K. J. Laidler, and H. Eyring, *The Theory of Rate Processes* (McGraw-Hill Book Company, Inc., New York, 1941).
[9] N. B. Slater, Proc. Roy. Soc. (London) **A194**, 112 (1948).

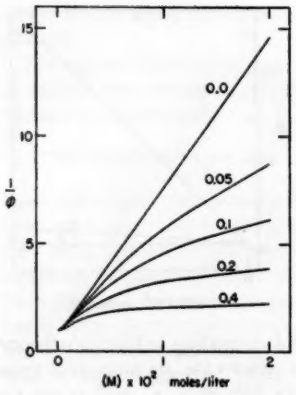

FIG. 4. Calculated quantum yield, including thermal dissociation of triplet molecules, $n=39$, $m=30$, $s=9$, $ab=0$, 0.05, 0.1, 0.2, 0.4.

nounced "S" shape, which is more apparent the larger the value of *ab*. This reverse curvature appears even at relatively low pressure.

COMPARISON WITH EXPERIMENTAL DATA

There are only two reasonably complete sets of photolysis data, ketene[2,5] and hexafluoroacetone,[4,10] suitable for treatment, i.e., in which the variation of primary quantum yield with pressure, temperature, and wavelength has been determined. In other cases, the relevant information is incomplete or is difficult to extract because of complex secondary radical reactions. The chemistry of these two photolyses is particularly simple. For ketene, the products are carbon monoxide and ethylene, and, if the percent conversion is kept small, the primary quantum yield is one-half the carbon monoxide yield. In the case of hexafluoroacetone, the products are carbon monoxide and hexafluoroacetone formed in equal amounts. Either quantum yield is equal to the primary quantum yield. The behavior of these systems is similar in that the primary quantum yield decreases as the wavelength and pressure increase. In the following, theory and experiment are compared for the case of ketene.

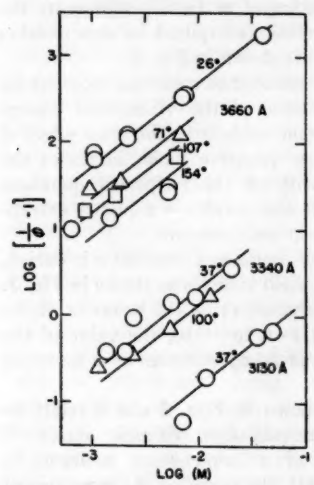

FIG. 5. Experimental quantum yield data for ketene.

The data for ketene are shown in Fig. 5, plotted in log-log form for convenience of representation. The lines are drawn with unit slope, hence the data are assumed to fit the equation:

$$1/\phi = 1 + (k_{2n}/k_{1n})M. \qquad \text{(IX)}$$

In fact, the data are better represented, particularly at the long wavelengths by Eq. (III).

These data are now compared with the theories developed in previous sections. First, we consider the case that a single collision between an excited and a normal molecule deactivates the excited molecule to the extent that it can no longer dissociate, and we apply Eqs. (IX) and (VIII) to the data. In Table I the values of k_{1n}/k_{2n} for ketene obtained from Fig. 5 are summarized. If we now choose 4 A for the collision diameter of ketene and $k_{2n}=Z$, the values of k_{1n} shown in column 4 of Table I are found.

TABLE I. Rate Constants for ketene.

λ (A)	t°C	k_{1n}/k_{2n} (moles/liter)	k_{1n} (sec^{-1})
3660	26	2.2×10^{-6}	1.17×10^{8}
	37[a]	...	1.6×10^{8}
	71	4.5×10^{-6}	2.55×10^{8}
	107	6.8×10^{-6}	4.05×10^{8}
	154	13.8×10^{-6}	8.73×10^{8}
3340	37	4.7×10^{-3}	2.53×10^{8}
	100	7.4×10^{-3}	4.38×10^{8}
3130	37	6.5×10^{-2}	3.50×10^{9}

[a] This value is interpolated.

These values can now be compared with Eq. (VIII). Unfortunately, only the total energy, electronic and vibrational, is known, since the zero-zero energy has not been measured for ketene. There are three unknown quantities, ν, ϵ_m, and ϵ_{0-0}, with three sets of experimental data connecting them. Direct calculation of the unknowns gives physically impossible values for the parameters, i.e., ϵ_m greater than the energy of the absorbed quantum, but the results are very sensitive to the experimental values of k_{1n}. However, reasonable values of ν and ϵ_{0-0} reproduce the experimental data adequately as shown in Table II. In this calculation, values of ϵ_{0-0} were assumed, and then the best values for ν and ϵ_m were calculated to fit the data at 3340 A. All of the calculated results agree with experiment within the probable limits of error. Hence, unless the experimental error can be considerably reduced, or unless an independent measurement of ϵ_{0-0} can be made, it can only be said that the theory qualitatively agrees with the experimental data. But it is reasonable to

[10] G. Giacometti, H. Okabe, and E. W. R. Steacie, Proc. Roy. Soc. (London) **A250**, 287 (1959).

TABLE II.

ϵ_{0-0} (cm^{-1})	0	10 000	15 000	20 000	24 000
ϵ_m (cm^{-1})	25 000	15 200	10 400	5800	2360
ν (sec^{-1})	4.6×10^{14}	2.6×10^{13}	3.8×10^{12}	2.9×10^{11}	1.5×10^{10}
k_{1n} (3660)	1.4×10^{9}	1.4×10^{9}	1.2×10^{9}	1.0×10^{9}	0.85×10^{9}
k_{1n} (3340)	(2.5×10^{9})	...	...	...	...
k_{1n} (3130)	2.3×10^{9}	2.1×10^{9}	1.9×10^{9}	1.4×10^{9}	0.86×10^{9}

assume that ϵ_{0-0} is about 5000 A in order of magnitude, hence the last column in Table II is most nearly correct. The total energy, electronic and vibrational ($\epsilon_{0-0}+\epsilon_m$), is virtually independent of parameters in the theory, ca 25 000 cm^{-1}, which corresponds to 71.5 kcal/mole. The dissociation energy of the carbon-carbon bond in ketene is approximately 55 kcal/mole, hence the photodissociation must lead to excited primary products.

If the more complex case of cascade deactivation is chosen, there is even more difficulty in comparing theory and experiment, because of the additional parameter related to the number of collisions required in deactivation. For the case in which $m=30$ (Figs. 3–5), the experimental data for ketene coincide approximately (and fortuitously) with those curves for values of n of 35, 40, and 44 for 3650, 3340, and 3130 A, respectively. These correspond best to $\epsilon_{0-0}=28$ kcal/mole (9800 cm^{-1}) and $\epsilon_m=43$ kcal/mole (15 000 cm^{-1}). Again, the minimum total electronic and vibrational energy required for dissociation is 71 kcal/mole. However, in this analysis, the magnitude of ϵ_{0-0} is unreasonably small.

When the ketene data are plotted according to Eq. (II), it can be seen that, even at the highest temperature studied, 154°, the quantity ab is less than ca 0.1. Further comparison of these data with the calculations shown in Fig. 4 shows that the temperature dependence of the primary quantum yield cannot be entirely explained by thermal dissociation of triplet molecules. The behavior is, instead, such that at high temperature the molecule is initially excited to a higher vibrational level than it is at low temperatures. This could arise from the higher vibrational energy in the ground state at high temperatures.

Since the vibrational frequencies of ketene are known, the heat capacity can be calculated, and, hence, the additional vibrational energy can also be estimated. This additional energy amounts to 210 cm^{-1}, between 154° and 27°C. If this quantity is applied to the calculations shown in Table II, column 5, the calculated ratio of k_{1n} at 154°C to that of 27°C is 2.2, which can be compared with the experimental ratio of 7.5.

CONCLUSIONS

To decide whether or not unimolecular theory can be used to interpret photodissociation requires very precise experimental data, more precise than is available at present. There is some evidence in the case of hexafluoroacetone that the primary quantum yield at 3130 A extrapolates to a value greater than unity at zero pressure. If this effect is real, it provides a verification of a multistage deactivation of excited molecules. However, the discrepancy is small, and it would be necessary to demonstrate experimentally that a plot of $1/\phi$ vs (M) is convex to the abscissa before an estimate could be made of the number of collisions required for deactivation.

ACKNOWLEDGMENT

This research was made possible through a grant from the National Research Council of Canada.

Nuclear Spin-Lattice Relaxation in Solutions*

RICHARD W. MITCHELL AND MELVIN EISNER

A & M College of Texas, College Station, Texas

(Received February 10, 1960)

T_1 for protons in C_6H_5Cl, C_6H_6, and C_6H_{12} has been measured as a function of concentration in solution with CS_2 and CCl_4. T_1 does not have the dependence on the solution viscosity suggested by the theory of Debye. The rotational relaxation times at infinite dilution are obtained by extrapolation, and the correlation times calculated from these results are compared with the values predicted by the rotating sphere model as well as an inner viscosity and microviscosity model. The inner viscosity model provides the best agreement with the experimental results. The correlation times are found not to be proportional to the volumes of the molecules but seem to be simply related to the moments of inertia as well as the masses of the molecules of interest and the masses of the solvent molecules. An approximate formula which provides good results for the systems above is suggested as $\tau=2I\eta a/\mu kT$, where I is the moment of inertia of the molecule of interest, η is the solvent viscosity, a is the average radius of the molecule, and μ is the reduced mass of the solvent-solute system.

INTRODUCTION

THE nuclear spin-lattice relaxation time T_1 in liquids may be written:

$$1/T_1=1/T_{1\,\mathrm{rot}}+1/T_{1\,\mathrm{trans}}, \quad (1)$$

where $T_{1\,\mathrm{rot}}$ and $T_{1\,\mathrm{trans}}$ are the contributions arising from the random rotational and translational motions, respectively, of the molecules. This relation suggests the possibility of using nuclear spin-lattice relaxation to study those physical properties of liquids which can be related to the molecular motion. Such an investigation has been reported by Giulotto, Lanzi, and Tosca,[1] in which T_1 measurements are used to demonstrate the presence of molecular association in solutions. The generality of the results of Giulotto *et al.* is questionable, however, because of the crudeness of the model used to relate T_1 to the physical properties of liquids. In view of this, T_1 measurements have been extended here to solutions which are free of molecular association, and the T_1 values, particularly, in dilute solutions will be compared to theoretical predictions based on several different models of molecular behavior.

SPIN-LATTICE RELAXATION BY DIPOLE-DIPOLE INTERACTION

The relative motions of a system of nuclear spins arising from the thermal motions of the molecules cause a fluctuating electromagnetic field at the nuclear sites. Bloembergen, Purcell, and Pound[2] have expressed the spectral intensity distribution of these random fields in terms of a correlation time τ. They find that T_1 is inversely proportional to τ for a molecule containing spin $\frac{1}{2}$ nuclei, provided that $\omega\tau\ll1$, where ω is the Larmor frequency of the nuclei. The results of Bloembergen, Purcell, and Pound[2] as corrected by Kubo and Tomita,[3] have been generalized to systems with many nuclei by Gutowski and Woessner.[4] The relaxation time for the ith nucleus may be written:

$$(1/T_{1i})_{\mathrm{rot}}=\hbar^2\gamma_i^2(3\gamma_i^2 2\cdot\sum_j r_{ij}^{-6} +4\gamma_f^2(I_f+1)I_f/3\cdot\sum_f{}^* r_{ij}^{-6})\tau_{\mathrm{rot}} \quad (2a)$$

$$(1/T_{1i})_{\mathrm{trans}}=\pi\hbar^2\gamma_i^2N/a^2(6\gamma_i^2\sum_j 1/r_{ij}^\circ +16\gamma_f^2(I_f+1)I_f/3\cdot\sum_f{}^* 1/r_{ij}^\circ)\tau_{\mathrm{trans}}, \quad (2b)$$

where γ is the gyromagnetic ratio of the nucleus, r is the internuclear distance, I is the nuclear spin, and N is the number of molecules per unit volume. In these formulas, $\sum$ are summations over nuclei of the same type as the ith and $\sum^*$ are over all others. In Eq. (2a) the summations are over nuclei in the same molecule while in Eq. (2b) they are over nuclei of a neighboring molecule, $1/r_{ij}^\circ$ being the mean value of $1/r_{ij}$ for two molecules in contact. In obtaining these results, Gutowski and Woessner have assumed that identical nuclei within a molecule are distinguishable; that is, they have neglected interference effects.

Hubbard,[5] employing a more rigorous treatment which includes interference terms, has calculated the time dependence of the z component of magnetization for systems of 3 and 4 equidistant identical spin $\frac{1}{2}$ particles approaching equilibrium in a field H_0. His results, given below, take into account only the rotational mechanism for relaxation:

$$M_z=M_0+M[0.00689\exp(-1.259t/T_0) +0.743\exp(-3.016t/T_0)], \quad (3a)$$

$$M_z=M_0+M[0.02087\exp(-6.49t/T_0) +0.9791\exp(-4.458t/T_0)]. \quad (3b)$$

* This research was supported by the U.S. Air Force through the Air Force Office of Scientific Research of the Air Research and Development Command under a contract.

[1] L. Giulotti, G. Lanzi and L. Tosca, J. Chem. Phys. **24**, 632 (1956).

[2] N. Bloembergen, E. Purcell and R. V. Pound, Phys. Rev. **73**, 679 (1948).

[3] R. Kubo and K. Tomita, J. Phys. Soc. Japan **9**, 988 (1954).

[4] H. S. Gutowski and D. E. Woessner, Phys. Rev. **104**, 843 (1956).

[5] P. S. Hubbard, Phys. Rev. **109**, 1153 (1958).

M_0 is the equilibrium value of M_z,

$$M=\tfrac{1}{3}\gamma^2\hbar^2H_0(T-T_s)/kTT_s,$$

where T_s is the initial spin temperature and $T_0=r^6/\gamma^4\hbar^2\tau_{\rm rot}$. In Eqs. (3), the coefficient of the first exponential is quite small compared with that of the second. Neglecting this small term in each expression, one obtains $T_{1\,\rm rot}=T_0/3.016$ and $T_{1\,\rm rot}=T_0/4.458$, for the three- and four-spin systems, respectively. The formula of Gutowski and Woessner applied to these two systems gives $T_{1\,\rm rot}=T_0/3$ and $T_{1\,\rm rot}=T_0/4.5$, respectively. Since interference effects should be less for the molecules considered in this experiment than for those considered above, Eq. (2) should give reliable results for the relaxation time.

CORRELATION TIME

I. Rotational

The determination of the correlation time required in Eq. (2a) is closely related to the problem occurring in Debye's theory of dielectric dispersion in polar liquids, wherein the motion of the molecule is assumed to be the same as that of a sphere of radius a imbedded in a viscous fluid. From this model, the dielectric correlation time τ is found to be

$$\tau=(4\pi\eta a^3/kT), \tag{4}$$

where η is the viscosity of the fluid. Although qualitative agreement is found in pure liquids, the results in solutions are less satisfactory. Spernol and Wirtz[6] and Gierrer and Wirtz[7] suggested that in solutions the viscosity η be replaced by a microviscosity $\eta_\mu=\eta f\cdot(r_{\rm solvent})/(r_{\rm solute})$, where f is a constant, and the r's are the cube roots of the volumes per molecule, calculated for the pure liquid.

An alternate point of view was proposed by Hill,[8] who showed that good agreement with dielectric relaxation time could be obtained through the use of the mutual viscosity between the solvent and solute. The mutual viscosity η_{AB} is deduced from the solution viscosity, which is supposed to be given by

$$\eta_m=(f_A^2\eta_A\sigma_A/\sigma_m)+(f_B^2\eta_B\sigma_B/\sigma_m)+(2f_Af_B\sigma_{AB}/\sigma_m) \tag{5}$$

for a binary mixture. Here f_A and f_B are the mole fractions of A and B, respectively, σ_A and σ_B are the average distances between molecules in the liquids A and B, σ_{AB} is the average distance between A and B type molecules, and σ_m is the average distance between molecules in the mixture. Using a model for the mutual viscosity, Hill obtains, for the rotational correlation time of molecules of type B in solution with molecules of type A,

$$\tau=(\tfrac{1}{3}kT)\{6f_A\eta_{AB}\sigma_{AB}K_A^2+3f_B(3-\sqrt{2})\eta_B\sigma_BK_B^2\}, \tag{6}$$

where

$$K_A^2=[(I_{AB}I_B)/(I_{AB}+I_B)][(m_A+m_B)/m_Am_B)],$$

and where I_A and I_B are moments of inertia of A and B about their centers, I_{AB} is the moment of inertia of A about the center of B during collision, and K_B is the radius of gyration of a B-type molecule.

The correlation time for nuclear relaxation involves the correlation of functions belonging to the second-order spherical harmonics, while the function which occurs in dielectric relaxation is $\cos\theta$; a factor of $\frac{1}{3}$ (see p. 701 of footnote reference 2) is therefore required in the above formulas for τ. The appropriate results for nuclear relaxation in dilute solutions are then:

$$\tau\ \text{Debye}=4\pi\eta a^3/3kT \tag{7a}$$

$$\tau\ \text{Microviscosity}=f(r_{\rm solvent}/r_{\rm solute})\tau\ \text{Debye} \tag{7b}$$

$$\tau\ \text{Hill}=K_A^2\sigma_{AB}\eta_{AB}/kT. \tag{7c}$$

II. Translational

The translational relaxation time required in Eq. (2b) is

$$\tau_{\rm trans}=a^2/12D, \tag{8}$$

where a is the "radius" and D is the diffusion coefficient of the molecule. An expression which is commonly used for D is the Stokes-Einstein relation

$$D=kT/6\pi\eta a. \tag{9}$$

In the equation obtained, when Eq. (9) is substituted in Eq. (8), $\tau_{\rm trans}$ has a linear dependence on the fluid viscosity, just as does $\tau_{\rm rot}$ in the Debye expression for the rotational correlation time. Equation (9) would not be expected to give good results for solutions, however, unless the size of the diffusing particle were large compared with that of the solvent molecules. Hill[9] has obtained an expression for the diffusion constant which takes into account the interactions between the molecules. The diffusion coefficient for an A molecule diffusing through a solution of A and B molecules is

$$D=kT/6(\eta_{AB}\sigma_{AB}f_B+\eta_A\sigma_Af_A). \tag{10}$$

Equation (10) appears to give close agreement with experimental results.

From the above expressions for the correlation times, along with Eq. (2), the dependence of T_1 on the physical properties of solutions is obtained.

EXPERIMENTAL PROCEDURE AND RESULTS

The T_1 values displayed in Fig. 1 were measured in a 40-gauss magnetic field H_0, which was provided by a large solenoid described elsewhere.[10] These values were obtained from "rapid passage" data and from the growth or decay of the magnetic moment with time.

[6] Spernol and Wirtz, Z. Naturforsch. **8a**, 522 (1953).
[7] Gierrer and Wirtz, Z. Naturforsch. **8a**, 532 (1953).
[8] N. E. Hill, Proc. Phys. Soc. (London) **67B**, 149 (1954).
[9] N. E. Hill, Proc. Phys. Soc. (London) **68B**, 209 (1955).
[10] R. W. Mitchell and M. Eisner, Rev. Sci. Instr. **28**, 624 (1957).

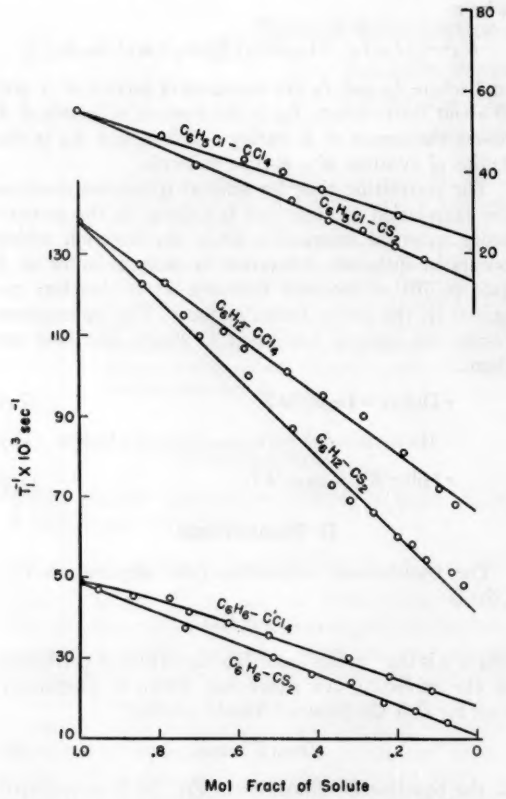

FIG. 1. Spin-lattice relaxation time of protons as a function of mole fraction solute.

For the second method, an auxiliary solenoid, aligned coaxially inside the large solenoid, was used to provide a resultant "polarizing" field which could be adjusted from 0 to $4H_0$. The current in the small solenoid was adjusted to give the desired resultant field and left on long enough for the magnetic moment of the sample to reach its equilibrium value; then the small solenoid was quickly turned off ($t=0$), and the amplitude of the signal was measured in the field H_0. After each amplitude measurement, the polarizing field was turned on again and the measurement was repeated for a different time interval. By making only one amplitude measurement following each polarization, it was possible to obtain good signal-to-noise figures for even the dilute samples and, at the same time, avoid the saturation effects which would occur with repeated observations. The T_1 values obtained from the growth or decay of the magnetic moment agreed with the rapid passage measurements in all cases. In addition, there was no evidence that the magnetic moment was governed by the sum of two or more exponentials as suggested by Hubbard.

The samples used were sealed in Pyrex ampoules after the oxygen had been removed. The oxygen was removed either by vacuum distillation or by a series of freeze, pump, thaw cycles. Both methods were equally effective, but the latter method was used for most of the samples because of the simplicity of the required vacuum system.

The viscosity measurements shown in Table I were obtained with an Ostwald viscosimeter contained in a constant-temperature bath. The viscosimeter was calibrated with water and checked against the known viscosities of the pure components which were used in the solutions.

Equation (5) was employed to calculate the values of $\eta_{AB}\sigma_{AB}$ from the viscosity data and from the known physical constants of the compounds.

DISCUSSION OF RESULTS

The "molecular sphere" model for the rotational [Eq. (7a)] and translational [Eqs. (8) with (9)] correlation times leads to a rather simple dependence of T_1 on the solution viscosity. With these correlation

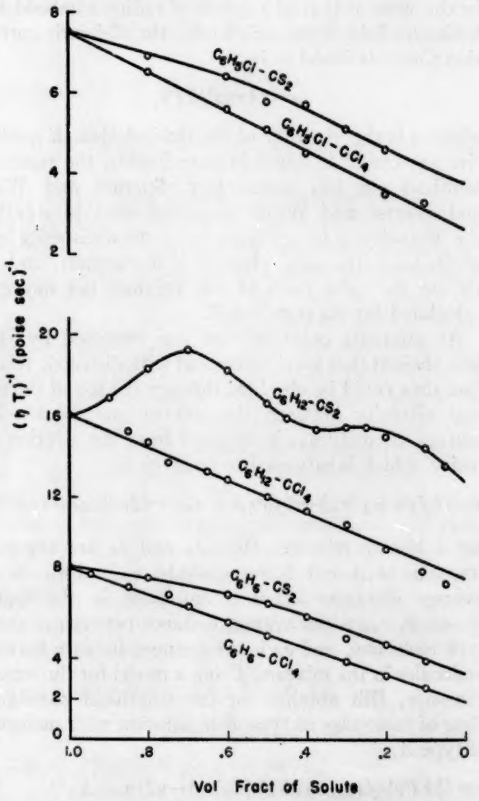

FIG. 2. Viscosity-compensated relaxation times as a function of volume fraction solute.

TABLE I. Measured viscosities and calculated inner viscosities. V = volume fraction of hydrocarbon.

Volume V	1.0	0.8	0.6	0.4	0.2	0	
System	Viscosity in centipoise at 27°C						Av. $\eta_{AB}\sigma_{AB}$ $\times 10^8$ (C.P.-cm)
C_6H_6–CS_2	0.58	0.48	0.41	0.39	0.37	0.35	1.8
C_6H_6–CCl_4	0.58	0.63	0.68	0.74	0.81	0.88	3.8
C_6H_{12}–CS_2	0.87	0.61	0.48	0.43	0.38	0.35	2.0
C_6H_{12}–CCl_4	0.87	0.84	0.84	0.84	0.86	0.88	4.4
C_6H_5Cl–CS_2	0.74	0.61	0.52	0.45	0.39	0.35	2.6
C_6H_5Cl–CCl_4	0.74	0.76	0.78	0.81	0.84	0.88	4λ3

times inserted in Eqs. (2), one can see that $1/\eta T_{1\,\mathrm{rot}}$ for the solute nuclei should not vary with concentration while $1/\eta T_{1\,\mathrm{trans}}$ should decrease as the concentration of the solute molecules decreases. From these considerations, it follows that the relaxation time for the hydrogen nuclei in the solute molecules is related to the volume fraction of the solute by

$$1/\eta T_1 = C_1 + C_2 V + C_3(1-V), \qquad (11)$$

where $C_1 = 1/\eta T_{1\,\mathrm{rot}}$, $C_2 = 1/\eta T_{1\,\mathrm{trans}}$ for the pure solute, V is the fractional volume of the solute and $C_3 = 1/\eta T_{1\,\mathrm{trans}}'$ for the pure solvent (i.e., $T_{1\,\mathrm{trans}}'$ is the contribution to the relaxation of the solute considering the solute molecule to be completely surrounded by solvent molecules). The values for $1/\eta T_1$, Fig. 2, do not exhibit the linear variation with concentration predicted by Eq. (11) except in the cases of C_6H_6–CCl_4 and C_6H_5Cl–CCl_4. It should be noted that the nonlinear behavior is accentuated for the CS_2 solutions which also have the largest viscosity variation. If one contrasts the rather regular behavior of $1/T_1$ for C_6H_{12}–CS_2, Fig. 1, with the $1/\eta T_1$ behavior for this same solution, it would appear that the molecular motion is not very sensitive to the solution viscosity.

It is clear that the rotational, and perhaps the translational, contribution to the relaxation time predicted by the "molecular sphere" model does not agree with the experimental results. It is not possible to examine the translational contribution to T_1 since $T_{1\,\mathrm{rot}}$ and $T_{1\,\mathrm{trans}}$ cannot be separated; however, we can obtain $T_{1\,\mathrm{rot}}$ from an extrapolation of either $1/T_1$ or $1/\eta T_1$ to $V=0$.

Since the nuclei of CS_2 have no magnetic moment, the extrapolated value of T_1, $T_{1\infty}$, for the CS_2 solutions is $T_{1\,\mathrm{rot}}$. The chlorine nucleus however has a magnetic moment, but it is small compared to that of hydrogen; then $T_{1\infty}$ for the CCl_4 solutions should be slightly smaller than $T_{1\,\mathrm{rot}}$ because of the small translational contribution, $T_{1\,\mathrm{trans}}'$ of the CCl_4. At this point one should observe that Eq. (11) predicts that the limit approached by $1/\eta T_1$ in the CCl_4 solution should be slightly larger than the limit approached in the CS_2 solution, while the results, Fig. 2, are just the opposite. This demonstrates that the actual viscosity dependence of the rotational correlation time is less than that predicted by Eq. (8a).

The values for $T_{1\infty}$, Table II, were extrapolated from the curves of Fig. 1 or 2 depending upon which was more regular in the low concentration region. The $T_{1\,\mathrm{rot}}$ values for the CCl_4 solutions were obtained from $T_{1\infty}$ by employing Eq. (11) with $T_{1\,\mathrm{trans}}'$ given by Eq. (2b). Both the Stokes-Einstein and Hill diffusion constant were used to evaluate $T_{1\,\mathrm{trans}}$ in Eq. (2b). A third calculation of $T_{1\,\mathrm{rot}}$ for the CCl_4 solutions was based on an empirical relation suggested by the data in Fig. 1. The experimental values for the CCl_4 solutions were fitted to:

$$1/T_1 = 1/T_{1\,\mathrm{rot}} + f/T_{1\,\mathrm{trans}} + (1-f)/T_{1\,\mathrm{trans}}', \qquad (12)$$

where f is the mole fraction of solute. Three values of T_1 at low concentration were substituted into Eq. (12) to obtain $T_{1\,\mathrm{rot}}$. Also the ratio $T_{1\,\mathrm{trans}}'/T_{1\,\mathrm{trans}}$ calculated from Eq. (2b) was used to eliminate $T_{1\,\mathrm{trans}}'$ from Eq. (12), and then $T_{1\,\mathrm{rot}}$ was calculated from two values of T_1 for the dilute solutions. The values of $T_{1\,\mathrm{rot}}$ calculated by these different methods agreed within about 2%. This good agreement is primarily due to the fact that the translational contribution of the chlorine nuclei is quite small.

CORRELATION TIME CALCULATIONS

The experimental results for $T_{1\,\mathrm{rot}}$ were used in Eq. (2a) to calculate the rotational correlation time for the solute molecules. The values obtained are listed in

TABLE II. Relaxation times at infinite dilution. $T_{1\infty}$ is T_1 extrapolated from Figs. 1 or 2.

	C_6H_6	C_6H_{12}	C_6H_5Cl
$T_{1\infty}$[a] (sec)	56	15.9	44
$T_{1\mathrm{rot}}$[a] (sec)	60	16.2	47
$T_{1\infty} = T_{1\mathrm{rot}}$[b] (sec)	91	22	80

[a] In CCl_4 solvent.
[b] In CS_2 solvent.

TABLE III. Comparison of experimental correlation times with theoretical values calculated from different models.

Substance and solvent		Exp $\tau\times10^{12}$ (sec)	Theoretical $\tau\times10^{12}$ (sec) Hill	Debye	Micro-viscosity	Hill approx.	Ratio of τ's in two solvents Exptl	Hill	Debye	Micro-viscosity	Hill approx.
C_6H_{12}	CS_2	1.1	1.3	6.8	2.8	1.5	0.73	0.54	0.40	0.97	0.52
	CCl_4	1.5	2.4	17	2.9	2.9					
C_6H_6	CS_2	1.5	1.1	4.1	1.4	1.2	0.65	0.58	0.40	1.7	0.52
	CCl_4	2.3	1.9	10	.82	2.3					
C_6H_5Cl	CS_2	2.2	2.6	5.0	2.1	2.5	0.58	0.79	0.40	1.0	0.56
	CCl_4	3.8	3.3	13	2.1	4.5					

Table III along with the theoretical values obtained from Eq. (8). The symmetry of C_6H_{12} and C_6H_5Cl is such that the relation between $T_{1\,\mathrm{rot}}$ and τ, as given by Eq. (2a), depends on the choice of the ith nucleus. The correlation time for these molecules was calculated by considering the experimental $T_{1\,\mathrm{rot}}$ to be the weighted average of the values computed for the different nuclei.

The product of the molecular semiaxes, which were obtained from the paper of Gierrer and Wirtz,[7] was used in place of a^3 in the calculation of the Debye correlation time. The moments of inertia required for the Hill correlation time were calculated using the internuclear distances based on electron-diffraction data. The quantity K_A^2 in Eq. (8c) was evaluated for each of the principal axes of the molecule, and the average of these values was used in the determination of the Hill correlation time.

CONCLUSIONS

It is evident that the Hill theory provides the best agreement with the experimental correlation times. Although the microviscosity correction improves the Debye times considerably, the over-all agreement of these results with the experimental values is not as good as the Hill results. It is interesting to note that the ratios of the correlation times for the molecule in the two different solvents also agree more closely with the Hill theory. This demonstrates that the particular choice made for the molecular radius in calculating the Debye correlation time cannot account for the poor agreement of the Debye times with the experimental data.

The success of the Hill theory does not stem from the use of inner viscosity. Since the values η_{AB} σ_{AB} are found to be approximately twice the values of ηa and, since the average distance between solvent and solute molecules is roughly twice the radius of the solute molecule, the value of η_{AB} is approximately that of η. The important factor of the Hill theory is the K_A^2 term which was introduced in accounting for the momentum transfer from solvent to solute molecules.

The term K_A^2 is of the form of a "reduced moment of inertia" divided by the reduced mass of the solvent-solute system. Since the term I_{AB} is usually large compared with I_B, little error is introduced by replacing the reduced moment of inertia by I_B, the moment of inertia of the solute molecule. Making use of the relations observed above, one can write an approximate expression for the Hill correlation time as

$$\tau=2I\eta a/\mu kT, \tag{13}$$

where I is the average of the principal moments of inertia of the molecule of interest, a is the average of the semiaxes of the molecule, η is the solvent viscosity, and μ is the reduced mass of the solvent-solute system. The rotational correlation times calculated from Eq. (13) are included in Table III. The agreement of these results with the experimental values indicates that the above approximation is quite good.

It is interesting to note that the Hill formula gives considerably better results for C_6H_{12} than for C_6H_6 or C_6H_5Cl and that C_6H_{12} also possesses more symmetry with respect to the moments of inertia about the principal axes. This fact suggests that there may be some significant way of choosing an "average" for the term K_A^2. For instance, if only the moments of inertia perpendicular to the plane of the ring are used in the calculations of for C_6H_6 and C_6H_5Cl, the agreement with the experimental results is much improved. This improvement is most spectacular for the CS_2 solutions, where the difference between experiment and theory becomes about 5%. This result suggests that the probability for rotation of both C_6H_6 and C_6H_5Cl about an axis perpendicular to the plane of the ring is greater than the probability for rotation about the other axes.

It is apparent that the translational mechanism for relaxation is dominant for C_6H_6 and C_6H_5Cl, while the rotational and translational mechanism are about equally important for C_6H_{12}. The rotational contribution to T_1 for C_6H_6 and C_6H_5Cl would then be masked by the translational contribution, except in dilute solutions. The behavior of $1/\eta T_1$ for C_6H_{12}–CS_2 is similar to that observed by Guilotti *et al.*[1] for C_6H_5OH–CCl_4. They interpreted the behavior as a variation of the rotational relaxation time, with the size of the molecular clusters formed by weak interactions between

the C_6H_5OH molecules. This interpretation was based on the Debye model which predicts that the correlation time of a molecule is proportional to its volume. In Table III, one sees that C_6H_{12}, which has the largest molecular volume, has the shortest correlation time. Thus the "molecular sphere" model does not properly account for the variation of the rotational correlation time with either the size of the molecule or the solution viscosity and deviations of $1/\eta T_1$ from linearity are not necessarily related to molecular association.

Vibrational Transitions and the Intermolecular Potential*

ROBERT C. AMME, *University of Denver Research Institute, Denver, Colorado*
AND
SAM LEGVOLD, *Department of Physics, Iowa State University, Ames, Iowa*

(Received January 18, 1960)

Temperature-dependence studies of vibrational collision lifetimes by the authors have indicated that the application of the Schwartz, Slawsky, and Herzfeld theory to substituted methane molecules with heavy surface atoms results in repulsive ranges which are shorter than those expected from a Lennard-Jones 6:12-type interaction. We have shown that the 28:7 potential suggested by Hamann and Lambert for quasi-spherical molecules gives ranges which are in better agreement with experiment. Also, experimental relaxation times of $CHClF_2$-argon and $CHClF_2$-helium mixtures have been used to obtain the collision lifetimes for the $CHClF_2$ molecule undergoing either argon or helium collisions. The results can be explained using the SSH theory, if the 6:12 ranges for helium and argon are averaged with the shorter experimental range for $CHClF_2$.

I. INTRODUCTION

IT has been known for some time that the ease with which vibrational energy transitions occur during molecular collisions depends very sensitively on the "hardness" of the molecules in question. This hardness is expressed in terms of the repulsive portion of the intermolecular potential function. The quantum-mechanical solution to the inelastic collision process was worked out many years ago[1] for a potential of the form: $V=V_0\exp(-\alpha r)$. Since the attractive forces between molecules are relatively slowly varying and therefore not instrumental in the transition process, it is a valid approximation to estimate the repulsive range $1/\alpha=s$ by fitting a more realistic potential function such as the Lennard-Jones 6:12 function to the repulsive exponential forms, making some reasonable assumptions.

This technique was used in the theoretical approach of Schwartz, Slawsky, and Herzfeld,[2] (SSH), and Schwartz and Herzfeld,[3] (SH), for calculating relaxation times, and also by Tanczos[4] using an additional dipole attraction term.

Essential to the validity of the SSH treatment is the condition that $\mu v_0^{*2}/2kT\gg 1$, where μ is the reduced mass of the colliding pair and v_0^* is the most probable relative velocity to result in a transition. Although the halomethanes are heavy molecules, this inequality is not always ideally fulfilled. Tanczos applied the three-dimensional development of Schwartz and Herzfeld to the chloromethanes, for which the ratio appears to be about 4 to 6. For the CH_3Cl molecule, he obtained good agreement with experiment, but for CH_2Cl_2, $CHCl_3$, and CCl_4, the range s resulting from fitting the 6:12 or 6:12:3 potential appeared too large.

In an earlier paper,[5] the authors applied the (SH) treatment to the observed temperature dependence of vibrational relaxation times for several halogen-substituted methanes. The values obtained for s fell in the range 0.12 ± 0.03 angstrom.[6] It was suggested that a repulsion steeper than $(1/r)^{12}$ would be necessary to calculate values this small.

Hamann and Lambert[7] have proposed the use of a Lennard-Jones type 7:28 potential for quasispherical molecules. They used CF_4 as an example and showed that the 7:28 was in much better agreement theoretically than the 6:12.

We have fitted the 7:28 potential to an exponential repulsion in order to determine if this function results in reasonable values for s. We have not included a dipole term, because it increases the complexity and is not expected to change the results noticeably except for cases of very large dipole moments. This is supported by the results of Tanczos in the comparison of the s obtained from the 6:12 and the 6:12:3 potentials. (cf. Tables I and II of footnote reference 4.) Our pur-

* This research was supported in part by the Office of Scientific Research of the Air Research and Development Command, USAF, under contract.

[1] J. M. Jackson and N. F. Mott, Proc. Roy. Soc. (London) **A137**, 703 (1932).

[2] R. N. Schwartz, Z. I. Slawsky, and K. F. Herzfeld, J. Chem. Phys. **20**, 159 (1952).

[3] R. N. Schwartz, and K. F. Herzfeld, J. Chem. Phys. **22**, 767 (1954).

[4] F. I. Tanczos, J. Chem. Phys. **25**, 439 (1956).

[5] R. C. Amme and S. Legvold, J. Chem. Phys. **30**, 163 (1959).

[6] Due to the omission of a factor $\sqrt{2}$, the ranges in Table III of reference 5 should be increased to values stated here.

[7] S. D. Hamann and J. A. Lambert, Australian J. Chem. **7**, 1 (1954).

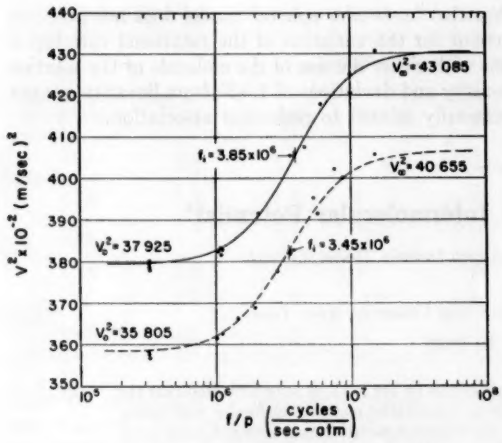

FIG. 1. Ultrasonic dispersion in 95% $CHClF_2$, 5% He (------) and 90% $CHClF_2$, 10% He (——) at 300°K.

pose is to determine if the 7:28 potential predicts the correct experimental range when fitted to the exponential form. We also report here the results of some measurements made on the sound dispersion of gas mixtures containing a halogen-substituted methane $CHClF_2$, monochlorodifluoromethane, plus 5 or 10% either argon or helium.[8] The results are interpreted in terms of the SSH theory.

II. EXPERIMENT

The dispersion of ultrasound due to the relaxation of vibrational specific heat, C_{vib}, in the halomethanes has been found to lie at frequencies in the neighborhood of 1 to 10 Mc. This is due partly to the low vibrational frequencies encountered in these molecules. The intermodal coupling is generally of sufficient magnitude to cause the entire vibrational heat capacity to become deactivated with a single relaxation time τ characteristic of the lowest vibrational mode in the molecule ν_m. Evidently, the collision process is quite efficient in these gases, the collision lifetimes Z_{10} of the lowest vibrational states, often falling considerably below 1000. The average probability that a collision will produce deactivation of a molecule vibrating in its first excited state is given by

$$P_{10}=1/Z_{10}=\{\Re\tau_m[1-\exp(-h\nu_m/kT)]\}^{-1}, \quad (1)$$

where $\Re$ is the gas collision rate per molecule, expressed by

$$\Re=\sqrt{2}n\pi r_0^2\bar{v}(1+S/T) \quad (2)$$

for the Sutherland molecular model. $\bar{v}$ is the mean thermal speed, S the Sutherland constant, and n the number of molecules per cubic centimeter. r_0 is the Sutherland collision diameter, and T is the absolute temperature in degrees Kelvin. τ_m is the relaxation time associated with ν_m and is related to the observed τ by

$$\tau_m=(C_m/C_{vib})\tau, \quad (3)$$

in which C_m is that part of C_{vib} resulting from ν_m.[9]

An acoustic interferometer described by Rossing and Legvold[8,10] was used to determine the dispersion of ultrasonic velocity at 300°K. in both 5% and 10% mixtures of argon and helium in $CHClF_2$. The raw data have been corrected for the effects of absorption[11] and for real gas behavior, using Beattie-Bridgman constants for mixtures[12] and Eq. (19) of footnote 10. The corrected data have been fitted to the ideal gas dispersion equation:

$$V^2(\omega)=\frac{RT}{M}\left[1+R\frac{C_0+\omega^2\tau^2C_\infty}{C_0^2+\omega^2\tau^2C_\infty^2}\right], \quad (4)$$

in which C_0 is the specific heat at constant volume at low frequency and $C_\infty=C_0-C_{vib}$. R is the gas constant in appropriate units, and M is the molecular weight. ω is the angular acoustic frequency: $\omega=2\pi f$.

Figures 1 and 2 show the dependence of ultrasonic velocity on the effective acoustic frequency, i.e., the frequency divided by the pressure in atmospheres, for the helium and argon mixtures, respectively. The ideal gas curves were calculated using a value of C_0= 11.35 cal/mole °C for $CHClF_2$, an average taken from all measured values of V_0, the velocity of ultrasound at low frequency. The data for pure $CHClF_2$ reported in footnote 10 were corrected to this value but are not shown here, since the observed inflection frequency was essentially unchanged.

In Table I are listed the inflection frequencies f_i, the heat capacities C_∞ and C_0, the observed τ, the calculated τ_m and R.

The collision rates $\Re_{AB}$ listed are those of a single $CHClF_2$ or B molecule in otherwise pure argon or

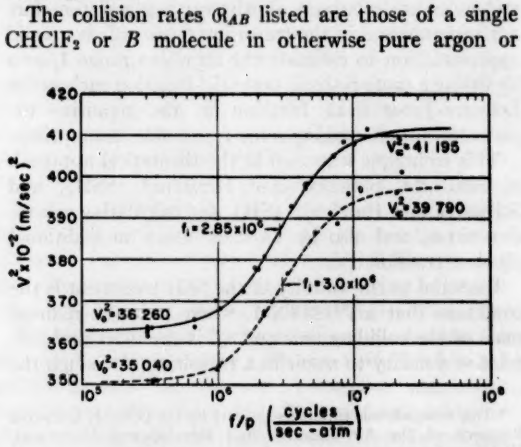

FIG. 2. Ultrasonic dispersion in 95% $CHClF_2$, 5% Ar (------) and 90% $CHClF_2$, 10% Ar (——) at 300°K.

[8] T. D. Rossing and S. Legvold, N.A.C.A. Final Report, (1953), Iowa State University, Ames, Iowa.

[9] ν_m=369 cm^{-1} for $CHClF_2$.

[10] T. D. Rossing and S. Legvold, J. Chem. Phys. 23, 1118 (1955).

[11] W. T. Richards, Revs. Modern Phys. 11, 36 (1939).

[12] J. A. Beattie, J. Am. Chem. Soc. 51, 19 (1929).

TABLE I. Collision constants, specific heats, and relaxation times.

Gas or gas mixture	C_0 (cal/mole °C)	C_∞ (cal/mole °C)	C_m/C_{vib}	r_0 (or r_{AB})A	S or S_{AB}	$\mathfrak{R}$ or $\mathfrak{R}_{AB}$ $\times 10^{-9}$ (sec^{-1})	$f_i\times 10^{-6}$ (sec^{-1})	$\tau\times 10^{8}$ (sec)	$\tau_m\times 10^{8}$ (sec)
$CHClF_2$	11.35	5.96	0.257	4.08	284	9.57	3.17±0.15	9.56±0.42	2.46±0.10
Helium	2.98	2.98	...	1.94	38	5.75	...	...	...
Argon	2.98	2.98	...	3.00	141	6.51	...	...	...
5% He	10.93	5.81	0.257	3.13	104	12.10	3.45±0.15	8.68±0.39	2.23±0.10
10% He	10.51	5.66	0.257	3.13	104	12.10	3.85±0.20	7.67±0.42	1.97±0.11
5% Ar	10.93	5.81	0.257	3.86	200	7.74	3.00±0.10	9.98±0.32	2.56±0.08
10% Ar	10.51	5.66	0.257	3.86	200	7.74	2.85±0.10	10.36±0.35	2.66±0.09

helium, A. $\mathfrak{R}_{AB}$ is given by[13]

$$\mathfrak{R}_{AB}=n_A\pi(r_{AB})^2(\bar{v}_A^2+\bar{v}_B^2)^{\frac{1}{2}}(1+S_{AB}/T), \quad (5)$$

in which $r_{AB}=\frac{1}{2}(r_{0A}+r_{0B})$, from Eq. (2), and S_{AB} is estimated by the relation $S_{AB}\simeq(S_AS_B)^{\frac{1}{2}}$. The Sutherland constants and cross sections are also given in Table I. S_B, the constant for $CHClF_2$, was estimated to be 0.8 times the critical temperature,[14] or 284°K.

It is seen that the inflection frequency f_i, which occurs at $V_i^2=\frac{1}{2}(V_0^2+V_\infty^2)$, does not change greatly with the addition of helium or argon. The collision lifetime for pure $CHClF_2$ is found from Eq. (1) to be already quite small: 196±12. The relaxation time, $\tau=(1/2\pi f_i)(C_0/C_\infty)$, appears to increase slightly with the addition of argon, but decreases with the addition of helium.

III. THE THEORY FOR MIXTURES

A. The Collision Lifetimes

In studying mixtures of gases A and B, the quantity of interest is the relaxation time τ^{AB}. In this study, this corresponds to the relaxation time of a single $CHClF_2$ molecule B in otherwise pure argon or helium A. The expression usually applied is

$$1/\tau=[(1-X)/\tau^B]+(X/\tau^{AB}), \quad (6)$$

where X is the mole fraction of the foreign gas A and the τ^B is the relaxation time observed for pure B. We have used this equation to calculate $\tau_m{}^{AB}$. These values appear in Table II, and the averages have been used along with the calculated collision rates $\mathfrak{R}_{AB}$ to obtain the collision lifetimes using Eq. (1):

$$Z_{10}{}^{AB}=\mathfrak{R}_{AB}\tau_m{}^{AB}[1-\exp(-h\nu_m/kT)].$$

B. Theoretical Transition Probability

If it is assumed that single quantum jumps are the governing process for vibration transitions, the average probability P_{10} per collision that a deactivation will occur is given for a diatomic molecule $b-c$ by[15]

$$P_{10}{}^{-1}=Z_{10}$$
$$=1.017(r_0/r_c)^2Y(2,2)Z_0Z_{vib}Z_{trans}\,e^{-\epsilon/kT}(1-e^{-\theta/T})^{-1}, \quad (7)$$

in which

$$Y(2,2)\simeq 0.76[(1+1.1(\epsilon/kT)], \qquad \theta=h\nu_m/k,$$

$$Z_{vib}=\frac{1}{2\pi^2}\frac{\theta'}{\theta}\frac{M_bM_c(M_A+M_b+M_c)}{(M_b^2+M_c^2)M_A}, \qquad \theta'=0.815\theta^2\mu s^2,$$

and

$$Z_{trans}=\pi^2(3/2\pi)^{\frac{1}{2}}(\theta/\theta')^2(T/\theta')^{1/6}$$
$$\times\exp[3/2(\theta'/T)^{1/3}-\theta/2T].$$

M represents the molecular or atomic weight. M_A is that of the impinging atom or molecule, and $\mu=M_A(M_b+M_c)/(M_A+M_b+M_c)$. s is in angstrom units, and Z_0 is a steric factor which expresses the probability that molecule $b-c$ is properly oriented in space upon collision. ϵ is the Lennard-Jones potential parameter. For complex polyatomic molecules, additional coefficients are required which are obtained through a normal coordinate treatment. The procedure is described by Tanczos. Equation (7) is expected to be applicable to collisions for which the interaction po-

TABLE II. Average collision lifetimes from relaxation times $\tau_m{}^{AB}$

Gas mixture	$\tau_m{}^{AB}\times 10^8$ (sec)	$Z_{10}{}^{AB}$
$CHClF_2$+5% Ar	11	675±50 (av)
+10% Ar	10	
+5% He	0.81	75±8 (av)
+10% He	0.70	

[13] A. Eucken and Rudolf Becker, Z. physik. Chem. **B27**, 235 (1934).
[14] W. Licht and D. G. Stechert, J. Chem. Phys. **48**, 23 (1944).
[15] K. Herzfeld and T. Litovitz, *Absorption and Dispersion of Ultrasonic Waves* (Academic Press, Inc., New York, 1959), Chap. VII.

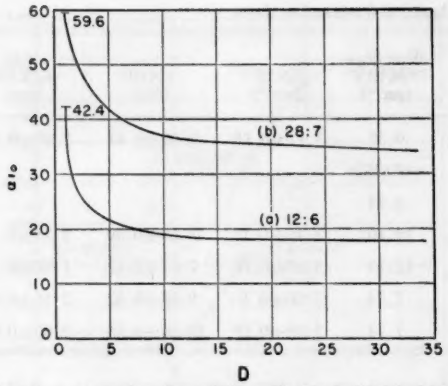

FIG. 3. αr_0 as a function of the ratio $D=\mu v_0^2/2\epsilon$ for (a) the 12:6 potential (cf. Schwartz, Slawsky, and Herzfeld), and (b) the 28:7 potential.

tential possesses no deep minimum as does the case of CO_2 and H_2O.

The addition of a light, monatomic gas is generally believed to influence the adjustment rate of the vibrational energy of the base gas by causing a decrease in μ and thus a decrease in Z_{10}. This effect is well known. However, the collision lifetime is even more sensitive to any change in the repulsive range s. If both the base gas B and the added gas A are known to separately obey the 6:12 potential,

$$V_A=4\epsilon_A[(r_{0A}/r)^{12}-(r_{0A}/r)^6],$$
$$V_B=4\epsilon_B[(r_{0B}/r)^{12}-(r_{0B}/r)^6], \quad (8)$$

then the potential function V_{AB} may be approximated by

$$V_{AB}=4(\epsilon_A\epsilon_B)^{\frac{1}{2}}[(r_{AB}/r)^{12}-(r_{AB}/r)^6],$$

where

$$r_{AB}=\tfrac{1}{2}(r_{0A}+r_{0B}).$$

If V_A and V_B do not differ greatly, the potential V_{AB} and hence its representation by an exponential repulsion will not be vastly different from that of V_B. Suppose, however, that V_B is of a different form, such as

$$V_B=4\epsilon_B[(r_{0B}/r)^{28}-(r_{0B}/r)^7], \quad (9)$$

while V_A remains of the 6:12 form. Then the function V_{AB} will differ significantly from V_B and yield a repulsive range that may be considerably longer than that for V_B. It is the product μs^2 which must be considered in order to determine the gross effect on Z_{10}, and not μ alone.

In order to obtain s from the 7:28 potential, we follow the technique of SSH, selecting a repulsive potential

$$V=V_0\exp[-\alpha(r-r_c)]-\epsilon,$$

where ϵ is now the Lennard-Jones 7:28 parameter, and r_c is the classical turning point, or the separation at which $V(r)=+\frac{1}{2}\mu v_0^2$. v_0 is the relative velocity at $r=\infty$. We then equate this function to the 7:28 potential at $r=r_c$. We also equate the derivatives of these functions at this point. We obtain first

$$r_c=r_0[\tfrac{1}{2}+\tfrac{1}{2}(1+\gamma^2 D)^{\frac{1}{2}}]^{-1/21}, \quad (10)$$

expressing the classical turning point as a function of the 7:28 parameter r_0 and the relative kinetic energy at $r=r_0$. γ is the ratio $(r_0/r_c)^7$, and $D=\frac{1}{2}\mu v_0^2/\epsilon+1$.

The final result is

$$\alpha=(7/r_0)[\tfrac{1}{2}+\tfrac{1}{2}(1+\gamma^2 D)^{\frac{1}{2}}]^{1/21}[(4\gamma^4-\gamma)/(\gamma^4-\gamma+\tfrac{1}{4})]. \quad (11)$$

The function αr_0 is plotted in Fig. 3, along with that obtained by SSH using the 6:12 potential. It is seen that, where SSH obtained the approximation $s\simeq r_0/17.5$ for large D, the 7:28 result is $s\simeq r_0/34$. For the halomethanes, $r_0\simeq 4$ to 5.5 A, giving an $s\simeq 0.10$ to 0.16 A, depending on D, which is in close agreement with experimental results. 0.16 A would bring Tanczos' calculations on CCl_4 into much better agreement. The value he obtained from the 6:12 potential was 0.24 A, which resulted in a Z_{10} of about nine times the experimental value.

III. DISCUSSION

To interpret the results from the $CHClF_2$-He and -Ar mixtures, we may approximate the range for unlike molecular collisions thus:

$$s_{AB}=\tfrac{1}{2}(s_A+s_B)\simeq\tfrac{1}{2}(r_{0A}/17.5+0.11), \quad (12)$$

using the value $s_B=0.11$ for $CHClF_2$ from the temperature-dependence studies.[5] Table III indicates the values for s and μs^2.

One sees that for helium, the drastic reduction in μ more than overcomes the increase in s, so that helium is expected to be a good catalyst for the reduction of Z_{10}. For argon plus $CHClF_2$, however, the quantity μs^2 is seen to be larger than for $CHClF_2$ alone, and the reverse effect is expected.

Using the estimated values of s, we apply Eq. (7) with $M_b+M_c=86.48$, $M_A=39.94$ and 4.00, respectively, to determine the changes expected in the collision lifetime.

Assuming $(r_0/r_c)_{AB}^2\cdot(r_c/r_0)^2\simeq 1$:

$$Z_{10}^{AB}=Z_{10}\frac{86.48}{M_A}\frac{M_A+86.48}{2(86.48)}\left(\frac{\theta'}{\theta'_{AB}}\right)^{7/6}\frac{Y(2,2)^{AB}}{Y(2,2)}$$
$$\times\exp\{\tfrac{3}{2}[(\theta'_{AB}/T)^{1/3}-(\theta'/T)^{1/3}]+[(\epsilon-\epsilon_{AB}/kT]\},$$

TABLE III. Calculated Z_{10}^{AB} using estimated repulsive ranges.

Gas	μ	$r_0(A)$	$s(A)$	s^2	μs^2	Z_{10}^{AB} (calc)
$CHClF_2$	43.24	5.0	0.11	0.012	0.52	...
He	...	2.6	0.149	...	...	...
Ar	...	3.42	0.195	...	...	...
$CHClF_2$-Ar	27.4	...	0.153	0.024	0.64	613
$CHClF_2$-He	3.82	...	0.130	0.017	0.065	125

where ϵ_{AB} is approximated: $\epsilon_{AB}=(\epsilon_A\epsilon_B)^{\frac{1}{2}}$, and Z_{10} is the experimental value of 196±12 for $CHClF_2$. ϵ_B is taken from the relation: $1.28\,\epsilon/k\simeq T_c$, the critical temperature.

The resulting $Z_{10}{}^{AB}$ given in Table III for the argon case is in good agreement with that observed (Table II). That for helium is 1.67 times the observed value, which is fair agreement considering the approximations made.

IV. CONCLUSIONS

Both the temperature dependence of collision lifetimes in the halomethanes observed earlier and the results presented here on the study of catalytic effects of helium and argon on $CHClF_2$ at room temperature indicate the need for a potential function with a repulsion much steeper than the 6:12 or 6:12:3 function. The 7:28 function appears to fulfill this need and, for these molecules, brings the SSH theory into better agreement with experiment.

V. ACKNOWLEDGMENT

The authors wish to acknowledge the assistance and criticisms of Leonard Valley of the Iowa State University.

THE JOURNAL OF CHEMICAL PHYSICS VOLUME 33, NUMBER 1 JULY, 1960

Theorem on Separability of Electron Pairs*

TADASHI ARAI

Department of Chemistry, Carnegie Institute of Technology, Pittsburgh, Pennsylvania
and
Quantum Chemistry Group, University of Uppsala, Uppsala, Sweden

(Received February 29, 1960)

The theorem that two functions $\Lambda_A(12)$ and $\Lambda_B(12)$ span subspaces which are mutually perpendicular if the functions are orthogonal to each other in the strong sense;

$$\int\Lambda_A^*(12)\Lambda_B(13)d\tau_1=0,$$

is proved here. The theorem is important for the study of chemical bonds.

TO describe chemical binding, it is very important to provide a theoretical definition of the chemical bond correctly.[1] We shall prove in the following a theorem which could provide such a definition since each of the pair functions $\Lambda(12)$ introduced here is general enough to accept additional conditions required for describing the characteristics of an individual chemical bond and deformation of it due to chemical substitution and so on. Still they are separated into perpendicular subspaces so that each of them can have reality in the quantum mechanical language.

First, we shall define the pair functions as follows: (1) Each of the pair functions $\Lambda_A(12)$ and $\Lambda_B(12)$ is an antisymmetric and normalized function of two electrons:

$$\Lambda_A(21)=-\Lambda_A(12),\qquad \Lambda_B(21)=-\Lambda_B(12). \quad (1)$$

(2) Each can be expanded in terms of an arbitrary complete set of orthonormal spin orbitals:

$$\Lambda_A(12)=\sum_{k,l}a_{kl}\psi_k(1)\psi_l(2),$$
$$\Lambda_B(12)=\sum_{m,n}b_{mn}\psi_m(1)\psi_n(2). \quad (2)$$

Then we obtain the following theorem:

Theorem: If $\Lambda_A(12)$ and $\Lambda_B(12)$ are mutually orthogonal in the strong sense:

$$\int\Lambda_A^*(12)\Lambda_B(13)d\tau_1\equiv 0,\qquad \text{for } A\neq B, \quad (3)$$

then it is possible to decompose the space $\mathfrak{R}$ into mutually perpendicular subspaces $\mathfrak{R}_A$ and $\mathfrak{R}_B$ in such a way that $\Lambda_A(12)$ belongs to $\mathfrak{R}_A$ only and not to $\mathfrak{R}_B$ and $\Lambda_B(12)$ belongs to $\mathfrak{R}_B$ but not to $\mathfrak{R}_A$, that is, there exists a complete set of orthonormal functions ϕ_k which can be partitioned into subsets

$$\phi_1,\ \phi_2,\cdots\phi_\varrho \quad\text{and}\quad \phi_{\varrho+1},\ \phi_{\varrho+2},\cdots$$

such that $\Lambda_A(12)$ can be expanded in terms of $\phi_1,\cdots\phi_\varrho$ only:

$$\Lambda_A(12)=\sum_{k,l\leq\varrho}p_{kl}\phi_k(1)\phi_l(2), \quad (4)$$

* This work was supported in part by the Office of Ordnance Research, U.S. Army under contract with Carnegie Institute of Technology and also by the Wright Air Development Center of the Air Research and Development Command, U.S. Air Force, through its European Office under contract with University of Uppsala.

[1] A. C. Hurley, J. Lennard-Jones, and J. A. Pople, Proc. Roy. Soc. (London) **A220**, 446 (1953); J. M. Parks and R. G. Parr, J. Chem. Phys. **28**, 335 (1958).

whereas, in the expansion of $\Lambda_B(12)$, $\phi_1, \cdots \phi_g$ do not appear:

$$\Lambda_B(12)=\sum_{m,n>g} q_{mn}\phi_m(1)\phi_n(2). \tag{5}$$

We shall prove the theorem in the following. By expanding $\Lambda_A(12)$ and $\Lambda_B(13)$ in terms of ψ functions, the strong orthogonality condition (3) now gives

$$0=\sum_{l,n}\Big(\sum_k a_{kl}^* b_{kn}\Big)\psi_l^*(2)\psi_n(3).$$

All the products $\psi_l^*(2)\psi_n(3)$ which appear in this equation are linearly independent. This means that

$$\sum_k a_{kl}^* b_{kn}=0.$$

We shall write the matrices (a_{kl}) and (b_{mn}) as A and B, respectively. Then this equation is written as

$$A^\dagger B=0, \tag{6}$$

where $A^\dagger$ means the Hermitian conjugate of A.

Since $\Lambda_A(12)$ is antisymmetric and all the products $\psi_k(1)\psi_l(2)$ in Eq. (2) are linearly independent, we find that

$$a_{kl}=-a_{lk}.$$

Similarly

$$b_{kl}=-b_{lk}.$$

Therefore both A and B are antisymmetric matrices:

$$\tilde{A}=-A,$$

$$\tilde{B}=-B,$$

where $\tilde{A}$ and $\tilde{B}$ are transposes of A and B, respectively.

Now we consider a product $C=AA^\dagger$ of matrix A. The matrix is Hermitian since

$$C^\dagger=(AA^\dagger)^\dagger=AA^\dagger=C.$$

This means that there exists a unitary matrix U, with which the Hermitian matrix C can be brought into diagonal form by a similarity transformation such that

$$U^{-1}CU=D, \tag{8}$$

where D is a diagonal matrix.[2] For convenience, we shall assume that the first g diagonal elements d_1, d_2, $\cdots d_g$ of D are nonzero but others are all zero, so that D can be illustrated as

$$D=\begin{pmatrix} d_1 & 0 & \cdots & 0 & 0 & \cdots \\ 0 & d_2 & \cdots & \cdots & \cdots & \cdots \\ \vdots & & & \vdots & & \\ 0 & \cdots & \cdots & d_g & \cdots & \cdots \\ 0 & & & 0 & & \\ \vdots & & & \vdots & \vdots & \\ \vdots & & & \vdots & & \ddots \end{pmatrix}$$

or we can write this as a supermatrix:

$$D=\begin{pmatrix} D(g\times g) & 0(g\times\bar{g}) \\ 0(\bar{g}\times g) & 0(\bar{g}\times\bar{g}) \end{pmatrix} \tag{9}$$

where $D(g\times g)$ is a $g\times g$ diagonal matrix with nonvanishing elements d_1, d_2, $\cdots d_g$ and $0(g\times\bar{g})$ is a $g\times(N-g)$ zero matrix. N is the total number of basic functions ψ_k, whereas $\bar{g}\equiv N-g$. Both N and g can be infinite.

By multiplying Eq. (6) by A, we obtain that

$$0=AA^\dagger B; \qquad 0=U^{-1}AA^\dagger UU^{-1}B=DF, \tag{10}$$

where $F=U^{-1}B$ and $D=U^{-1}AA^\dagger U=U^{-1}CU$. By rewriting Eq. (10), we find that

$$\sum_l d_{kl}f_{ln}=d_{kk}f_{kn}=0,$$

since D is diagonal. Of course d_{kl} and f_{ln} here represent elements of matrices D and F, respectively. Therefore

$$f_{kn}=0, \qquad \text{for } k\leq g,$$

where $d_{kk}\neq 0$. This means that at least the first g rows of matrix F vanish so that we can write F as

$$F=\begin{pmatrix} 0(g\times\bar{g}) & 0(g\times\bar{g}) \\ F(\bar{g}\times g) & F(\bar{g}\times\bar{g}) \end{pmatrix}. \tag{11}$$

We shall define a matrix E as $E=U^{-1}A$, then we find that

$$E^\dagger=A^\dagger U,$$

and

$$EE^\dagger=D.$$

This equation is written as

$$\sum_l e_{kl}e_{nl}^*=d_{kn}=d_k\delta_{kn}, \qquad \text{for } k\leq g,$$

$$=0, \qquad \text{for } k>g,$$

where e_{kl} is kl element of matrix E. By considering the

[2] For instance, E. P. Wigner, *Group Theory* (Academic Press, Inc., New York, 1959), p. 26.

diagonal elements d_{kk}, we obtain

$$\sum_i c_{ki}c_{ki}^* = \sum_i |c_{ki}|^2 = d_k, \quad \text{for } k \leq g,$$
$$= 0, \quad \text{for } k > g.$$

Therefore we find that

$$c_{ki} = 0, \quad \text{for } k > g,$$

or

$$E = \begin{pmatrix} E(g\times g) & E(g\times\bar{g}) \\ 0(\bar{g}\times g) & 0(\bar{g}\times\bar{g}) \end{pmatrix}. \tag{12}$$

By introducing a row matrix $\Psi(1) = (\psi_1(1), \psi_2(1), \cdots)$ consisting of a complete set of spin orbitals used in Eq. (2), the pair functions (2) are written as

$$\Lambda_A(12) = \Psi(1) A \tilde{\Psi}(2),$$
$$\Lambda_B(12) = \Psi(1) B \Psi(2), \tag{13}$$

where $\tilde{\Psi}(2)$ is the transpose of $\Psi(2)$, namely,

$$\tilde{\Psi}(2) = \begin{pmatrix} \psi_1(2) \\ \psi_2(2) \\ \vdots \end{pmatrix}.$$

By the use of the unitary matrix U obtained in Eq. (8) we shall transform our basis from Ψ and $\tilde{\Psi}$ to $\Phi = \Psi U$ and $\tilde{\Phi} = \tilde{U}\tilde{\Psi}$. Then

$$\Lambda_A(12) = \Psi(1) U U^{-1} A \tilde{U}^{-1} \tilde{U} \tilde{\Psi}(2) = \Phi(1) P \tilde{\Phi}(2),$$
$$\Lambda_B(12) = \Psi(1) U U^{-1} B \tilde{U}^{-1} \tilde{U} \tilde{\Psi}(2) = \Phi(1) Q \tilde{\Phi}(2);$$

where

$$P = U^{-1} A \tilde{U}^{-1} = E \tilde{U}^{-1},$$
$$Q = U^{-1} B \tilde{U}^{-1} = F \tilde{U}^{-1}. \tag{14}$$

Since A and B are antisymmetric as is shown in Eq. (7)' we find that

$$\tilde{P} = U^{-1} \tilde{A} \tilde{U}^{-1} = -U^{-1} A \tilde{U}^{-1} = -P.$$

Similarly $\tilde{Q} = -Q$, that is, P and Q are also antisymmetric. On the other hand, Eqs. (14) and (12) or (11) indicate that P and Q should have the following structures:

$$P = E\tilde{U}^{-1} = \begin{pmatrix} E(g\times g) & E(g\times\bar{g}) \\ 0(\bar{g}\times g) & 0(\bar{g}\times\bar{g}) \end{pmatrix} \begin{pmatrix} V(g\times g) & V(g\times\bar{g}) \\ V(\bar{g}\times g) & V(\bar{g}\times\bar{g}) \end{pmatrix}$$
$$= \begin{pmatrix} X(g\times g) & X(g\times\bar{g}) \\ 0(\bar{g}\times g) & 0(\bar{g}\times\bar{g}) \end{pmatrix},$$

$$Q = F\tilde{U}^{-1} = \begin{pmatrix} 0(g\times g) & 0(g\times\bar{g}) \\ F(\bar{g}\times g) & F(\bar{g}\times\bar{g}) \end{pmatrix} \begin{pmatrix} V(g\times g) & V(g\times\bar{g}) \\ V(\bar{g}\times g) & V(\bar{g}\times\bar{g}) \end{pmatrix}$$
$$= \begin{pmatrix} 0(g\times g) & 0(g\times\bar{g}) \\ Y(\bar{g}\times g) & Y(\bar{g}\times\bar{g}) \end{pmatrix},$$

where off-diagonal elements $X(g\times\bar{g})$ and $Y(\bar{g}\times g)$ should vanish because P and Q are antisymmetric matrices. This means that P has its nonvanishing elements within the first g rows and g columns, and Q does not have nonvanishing elements in the first g rows nor in the first g columns. This proves our theorem and $\Lambda_A(12)$ and $\Lambda_B(12)$ can be written as Eqs. (4) and (5).

It is also possible to prove the theorem without using Eq. (8). Here we regard Eq. (6) as N sets of N linear equations of vectors $\mathbf{a}_{\cdot i}^* = (a_{1i}^*, a_{2i}^*, \cdots)$ such that

$$\sum_k b_{kn} a_{ki}^* = 0, \qquad n = 1, 2, \cdots N, \tag{15}$$

where n indicates differences in sets. Then we find that

$$\mathbf{a}_{\cdot n}^* = 0, \quad \text{for every } n,$$

or

$$|b_{kn}| = 0.$$

Since the first assumption should be excluded because of $\Lambda_A(12) \neq 0$, we find that N equations (15) and vectors $\mathbf{a}_{\cdot i}^*$ are not linearly independent. By a suitable transformation, we can rearrange the matrix B in such a way that all elements in the k_1th row and k_1th column are zero and also $a_{k_1 l} = 0$ for every l. Excluding the k_1th elements therefore, we obtain $n-1$ linear equations similar to Eq. (15). By repeating the process, we finally obtain a nonvanishing determinant $|b_{kn}| \neq 0$. The corresponding elements a_{kn} in the matrix A should therefore be zero together with off-diagonal parts which correspond to $X(\bar{g}\times g)$ and $X(g\times\bar{g})$ in the former proof.

In both cases, we have proved that $\Lambda_A(12)$ should occupy the whole space $\mathfrak{R}_A$ described by g orthogonal functions $\phi_1, \phi_2, \cdots \phi_g$ but $\Lambda_B(12)$ will not necessarily occupy the rest of the space. It is easily proved that there could exist a third subspace $\mathfrak{R}_C$ if there is a function $\Lambda_C(12)$ orthogonal to both $\Lambda_A(12)$ and $\Lambda_B(12)$ in the same manner as Eq. (3). Then we can easily generalize the theorem as follows.

Theorem: If there exist strong orthogonality relations (3) between every possible pair I and J of H pair functions $\Lambda_A(12), \Lambda_B(12), \cdots \Lambda_H(12)$, then we are able to decompose the space $\mathfrak{R}$ into mutually perpendicular H subspaces $\mathfrak{R}_A, \mathfrak{R}_B, \cdots \mathfrak{R}_H$ in such a way that each of functions $\Lambda_I(12)$ is localized to the corresponding subspace $\mathfrak{R}_I$ and is independent of others.

We shall recall the fact that pair functions are described by g independent basic functions ϕ in the subspace $\mathfrak{R}_A$. It is possible to construct $h-1$ independent pair functions $\Lambda_{A1}(12), \cdots \Lambda_{Ah-1}(12)$ such that (1) Every two of h functions $\Lambda_A(12), \Lambda_{A1}(12), \cdots \Lambda_{Ah-1}(12)$ are orthogonal to each other in the ordinary sense:

$$\int \Lambda_{Ai}^*(12) \Lambda_{Aj}(12) d\tau_1 d\tau_2 = \delta_{ij}, \quad i, j = 0, 1, \cdots h-1, \tag{16}$$

where $h=\frac{1}{2}g(g-1)$. (2) Every one of them is orthogonal to pair function $\Lambda_I(12)$ which belongs to the other subspace $\mathfrak{R}_I$ in the strong manner:

$$\int \Lambda_{Ai}^*(12)\Lambda_I(13)d\tau_1 \equiv 0.$$

In order to discuss the electronic structure of molecules with more than two bonds, we can associate a group of functions $\Lambda_{Ai}(12)$ to bond A, $\Lambda_{Bj}(12)$ to bond B and so on. By imposing the strong orthogonality condition (3) only, we can divide the space into perpendicular subspaces $\mathfrak{R}_A$, $\mathfrak{R}_B$, $\cdots$ such that each of the bonds is described within the corresponding subspace. A group of functions $\Lambda_{Ai}(12)$ can be associated with deformation of bond A due to chemical substitution or excitation of molecules. Of course the mutual orthogonality (16) between functions $\Lambda_{Ai}(12)$ in a group may not always be necessary as long as we do remember the fact that only h of them could be independent. Mutual correlation between bonds can be treated as interaction between perpendicular subspaces. For example, we shall consider a group of molecules A_iB_i, where each of them consists of two bonds A_i and B_i. Differences in bonds A_i are due to chemical substitution. Then the other bond B_i may be deformed by the effect of the substitution in bond A. Such phenomena are described by a series of pair functions $\Lambda_{Ai}(12)$ $\Lambda_{Bi}(34)$. Since $\Lambda_{Ai}(12)$ and $\Lambda_{Bi}(12)$ belong to independent subspaces, the concept of the chemist's chemical bond is clearly preserved in the quantum mechanical description. Still we can take mutual interaction between bonds into account.

ACKNOWLEDGMENTS

Finally, the author would like to thank Professor R. G. Parr for his continuous encouragement and never ending support. In fact, without his stimulation the article might not have been written. The author would also like to thank Dr. P. O. Löwdin for the valuable discussion on this subject and Dr. H. Shull and Dr. T. L. Allen for their interest.

Isoelectronic Extrapolation of Electron Affinities

B. Edlén

Physics Department, University of Lund, Lund, Sweden

(Received March 1, 1960)

An expression based on theoretical considerations and containing three adjustable constants has been derived for the purpose of extrapolating ionization potentials along isoelectronic sequences. When used to extrapolate electron affinities of the elements of the first and second short period, the formula is found to yield results that are correct within the error limits of the experimental data at present available.

INTRODUCTION

A KNOWLEDGE of the electron affinities of neutral atoms is of importance in several connections, but the experimental determination as well as a theoretical calculation of these quantities meets with great difficulties. Therefore, various attempts have been made to derive their values by extrapolation from the ionization potentials of related atoms and positive ions. The results have on the whole been disappointing, as the error usually turned out to be of the same order of magnitude as the quantity itself, unless quite arbitrary corrections were applied.[1] The failure can be attributed partly to the use of inadequate extrapolation methods and partly to the relatively large errors in many of the ionization potentials given in the literature. The purpose of the present note is to show that with due attention to both these sources of error one can obtain useful results by a simple and straightforward procedure.

[1] For a review of this work see L. M. Branscomb, *Advances in Electronics and Electron Physics* (Academic Press, Inc., New York, 1957), Vol. IX, p. 43. See also work cited in footnote 4.

EXTRAPOLATION FORMULA

The most obvious method, and probably the only practicable one, is the extrapolation of ionization energies along the isoelectronic sequence of which the negative ion is the zeroth member. Regarding the choice of the form of the extrapolation formula we first note that the adjustable constants should be as few as possible, because in general only a small number of input data are available for their determination. It should be remembered that in most isoelectronic sequences the ionization potentials are accurately and independently determined only for the first few spectra of the sequence. The rest of the values given in the literature are based on extrapolations of various kinds.

Using the theoretically correct expansion of the atomic energy in terms of an effective charge $Z-S$, and accepting the hydrogenic coefficient for the quad-

TABLE I. Isoelectronic extrapolation of electron affinities.

Ground term designation			Adopted term values (kilokaysers) T_3		T_2		T_1		T_0 extrapolated kilokaysers	ev	Observed[a] ev
	$2s$	$^2S_{\frac{1}{2}}$	B^{++}	305.93	Be^+	146.882	Li	43.487	He^-	1.51	0.19	
	$2s^2$	$^1S_0$	C^{++}	386.22	B^+	202.81	Be	75.192	Li^-	6.59	0.82	
$2s^2$	$2p$	$^2P_{\frac{1}{2}}$	N^{++}	382.75	C^+	196.66	B	66.93	Be^-	−1.56	−0.19	
$2s^2$	$2p^2$	$^3P_0$	O^{++}	443.00	N^+	238.751	C	90.814	B^-	2.65	0.33	
$2s^2$	$2p^3$	$^4S_{\frac{3}{2}}$	F^{++}	505.5	O^+	283.24	N	117.22	C^-	10.04	1.24	1.12±0.06
$2s^2$	$2p^4$	$^3P_2$	Ne^{++}	511.8	F^+	281.94	O	109.837	N^-	0.41	0.05	
$2s^2$	$2p^5$	$^2P_{\frac{1}{2}}$	Na^{++}	577.8	Ne^+	330.4	F	140.524	O^-	11.83	1.47	1.465±0.005
$2s^2$	$2p^6$	$^1S_0$	Mg^{++}	646.32	Na^+	381.2	Ne	173.932	F^-	28.21	3.50	3.48±0.05
	$3s$	$^2S_{\frac{1}{2}}$	Al^{++}	229.44	Mg^+	121.268	Na	41.449	Ne^-	−4.60	−0.57	
	$3s^2$	$^1S_0$	Si^{++}	270.14	Al^+	151.860	Mg	61.669	Na^-	3.80	0.47	
$3s^2$	$3p$	$^2P_{\frac{1}{2}}$	P^{++}	243.40	Si^+	131.836	Al	48.279	Mg^-	−2.59	−0.32	
$3s^2$	$3p^2$	$^3P_0$	S^{++}	280.9	P^+	159.3	Si	65.743	Al^-	4.19	0.52	
$3s^2$	$3p^3$	$^4S_{\frac{3}{2}}$	Cl^{++}	319.5	S^+	188.2	P	84.58	Si^-	11.77	1.46	
$3s^2$	$3p^4$	$^3P_2$	Ar^{++}	328.6	Cl^+	192.07	S	83.559	P^-	6.25	0.77	
$3s^2$	$3p^5$	$^2P_{\frac{1}{2}}$	K^{++}	369.2	Ar^+	222.848	Cl	104.60	S^-	17.34	2.15	2.07±0.07
$3s^2$	$3p^6$	$^1S_0$	Ca^{++}	410.7	K^+	254.9	Ar	127.110	Cl^-	29.87	3.70	3.69±0.05

[a] Observed electron affinities from the following sources: F^- and Cl^- from D. Cubicciotti, J. Chem. Phys. **31**, 1646 (1959); O^- and C^- from L. M. Branscomb, D. S. Burch, S. J. Smith, and S. Geltman, Phys. Rev. **111**, 504 (1958); S^- from L. M. Branscomb and S. J. Smith, J. Chem. Phys. **25**, 598 (1956).

ratic term in Z, we obtain the following expression for the binding energy T of an electron with principal quantum number n belonging to an atomic system of nuclear charge Z and containing N electrons:

$$T/(R/n^2)=\zeta^2+2a\zeta-b+c(\zeta+a)^{-1}, \qquad (1)$$

where $\zeta=Z-(N-1)$ and a is the asymptotic value for a penetration parameter p defined by $\zeta+p=Z-S$. This expression contains three constants to be determined empirically. It has been used for some time by the author and found to be the best three-parameter form for extrapolating ionization potentials.[2]

When using formula (1) for the extrapolation of electron affinities it is convenient to transform it into the explicit expression that gives the electron affinity T_0 directly in terms of the ionization energies T_1, T_2, and T_3 of the first three members of the same isoelectronic sequence (the indices corresponding to $\zeta=0$, 1, 2, 3):

$$T_0=3T_1-3T_2+T_3+Q,$$

$$Q=\frac{3(T_1-2T_2+T_3-2R/n^2)(-T_1+2T_2-T_3+6R/n^2)}{T_1-4T_2+3T_3-12R/n^2}. \qquad (2)$$

For the constants R/n^2 we adopt the values $R/2^2=27.434$ kK and $R/3^2=12.193$ kK (kK=kilokayser=10^3 cm^{-1}).

RESULTS AND DISCUSSION

The results obtained by applying formula (2) to the first and second short periods are shown in Table I. The adopted values of T_1, T_2, and T_3 are included. As an essential part of the investigation these input values were carefully checked and revised by reevaluation of series limits and by using relations[3] that connect the energies of ns^2np^k as a function of k. The values given in Table I, some of which differ significantly from those in the literature, are believed to be the best that can be derived from the spectroscopic data available at present. These data, however, are in several cases so incomplete that one must still assign rather wide error limits to many of the ionization energies. The estimated accuracy is roughly indicated by the number of decimals retained.

It is obvious that any attempt to work with more than three adjustable constants would meet with great difficulties because of the lack of accurate data for higher ζ values. This makes it questionable whether the more elaborate formula proposed by Johnson and Rohrlich[4] can be used with advantage until the spectroscopic data have been substantially improved. Their formula is equivalent to (1) with an additional term in $(\zeta+a)^{-2}$ and with the coefficient of ζ^2 adjustable. This gives five constants to be determined. Recognizing the difficulties, Johnson and Rohrlich derived the constants by relying on the asymptotic trend of the ionization potentials for large ζ values. However, the physical significance of this procedure is doubtful because the values for large ζ originate for the most part from previous empirical extrapolations, and therefore little more can be achieved than a retracing of the trend that was arbitrarily chosen in this previous work.

The last column of Table I contains all the observed values of electron affinities that appear to be sufficiently accurate to serve as a check on the extrapolation. Although the significance of the agreement is reduced somewhat by the fact that in each one of the

[2] See a forthcoming article in the *Encyclopedia of Physics* (Springer-Verlag, Heidelberg), Vol. 27.

[3] Compare M. A. Catalán and F. R. Rico, Anales Real Soc. Espan. fis. quim. (Madrid) **54A**, 5, 289 (1958).

[4] H. R. Johnson and F. Rohrlich, J. Chem. Phys. **30**, 1608 (1959).

sequences concerned there are some uncertain values for T_2 or T_3, the comparison seems to indicate that the formula would predict the electron affinities to at least 0.1 ev. An improvement of the input values of these sequences is needed before the accuracy of the method can be more precisely ascertained. On the other hand, the spectroscopic data of the first four sequences in the first period and the first three sequences of the second period are sufficiently reliable to preclude any significant changes in the result of the extrapolation. The positive value obtained for He^- is, therefore, unavoidable and may possibly indicate that the formula gives too high values in the beginning of the first period.

The value obtained for N^- is so close to zero that the sign cannot be definitely settled by the present method. However, as suggested by Branscomb,[5] the existence of negative atomic ions of nitrogen does not need to depend on this question, because the ^1D state, built on the metastable state ^2D of the neutral atom, will have a considerable lifetime. Extrapolating the electron affinity of the ^2D state by means of formula (2) and using the values $T_1=120.777$, $T_2=295.15$, and $T_3=527.1$[6] for the difference $^2D-^1D$ we obtain $T_0=8.5$ kK $=1.05$ ev.

[5] See G. Boldt, Z. Physik **154**, 330 (1959).

[6] In order to connect doublets and quartets in Ne IV an estimated value of 41.18 kK was used for the difference $^2D_{5/2}-^4S_{\frac{1}{2}}$.

THE JOURNAL OF CHEMICAL PHYSICS VOLUME 33, NUMBER 1 JULY, 1960

Ionization of Cu, Ag, and Au by Electron Impact*

NORMAND C. BLAIS AND JOSEPH B. MANN

Los Alamos Scientific Laboratory, University of California, Los Alamos, New Mexico

(Received February 8, 1960)

The relative ionization probabilities of copper, silver, and gold by electron impact have been studied near threshold. Nearly monoenergetic electrons, obtained by means of the retarding potential difference method, were employed. Narrow peaks were found superimposed on the ion yield that arises from transition to the ion ground state. It was possible to correlate these peaks with groups of energy levels, many of which are known to autoionize. The ionization probability curve for formation of doubly ionized gold was also obtained and found to be a sum of linear functions of the electron excess energy. The onset of each linear section indicated the presence of an excited state of Au III. Three energy levels were located at 2.2_8, 3.9_2, and 7.8_1 ev above the ground state.

INTRODUCTION

WITH the development of the "retarding potential difference" (RPD) method[1] for obtaining monoenergetic electron beams, details of the electron impact ionization phenomenon near threshold energies can be studied. Heretofore, beams suitable for this purpose were difficult to obtain, and the energy spread associated with the usual methods of producing an electron beam obscured any details that might be present. Often, the ionization potentials measured were doubtful, since no threshold was directly visible.

Applying the RPD method, Hickam[2] reported the appearance of peaks in otherwise linearly rising ionization probability curves for zinc, cadmium, and mercury. Similar peaks had previously been observed for mercury,[3] and structure that could be ascribed to peaks also appeared in the ionization curve of krypton.[4] All of this structure was interpreted as arising from autoionization from discrete levels lying above the lowest ionization potential of the elements[5]; i.e., a radiationless transition takes place from the discrete state to a continuum state at the same energy. In none of these cases was it possible to establish the identity of the levels responsible for the phenomena.

In connection with another experiment using the RPD method, the relative ionization probability curve for Ag was examined and found to exhibit several peaks. Some correlation with the known levels of Ag was made, and the work was extended to Cu and Au in the hope of making a more definite identification of those levels that contributed to the additional ionization.

APPARATUS AND PROCEDURE

Atoms were produced by heating the metal to the desired rate of evaporation in an electron-bombarded tantalum crucible. Regulation of both the electron current and potential was sufficient for a short-term crucible temperature stability of better than $\pm\frac{1}{2}$°C. The long-term drift in temperature was about 10–15°C

* This work was sponsored by the U. S. Atomic Energy Commission.

[1] R. E. Fox, W. M. Hickam, D. J. Grove, and T. Kjeldaas, Jr., Rev. Sci. Instr. **26**, 1101 (1955).

[2] W. M. Hickam, Phys. Rev. **95**, 703 (1954).

[3] W. B. Nottingham, Phys. Rev. **55**, 203 (1939).

[4] R. E. Fox, W. M. Hickam, and T. Kjeldaas, Jr., Phys. Rev. **89**, 555 (1953).

[5] E. U. Condon and G. H. Shortley, *The Theory of Atomic Spectra* (Cambridge University Press, New York, 1951), p. 369.

in 6 hr. Fifty milligrams of metal was more than sufficient for 70 hr of operation.

The RPD source of ionizing electrons has been described previously.[1] Although several modifications were made for the needs of this experiment, the characteristics of the sources used were essentially the same as those described in the reference. The total electron beam was about 1μa, and the difference current was 0.2 μa with a standard RPD of 0.1 v.

The resulting ion beam was analyzed in a first-order, single-focus mass spectrometer, utilizing a 60-deg, 12-in. radius magnetic analyzer. Only the magnetic field was changed to focus on different e/m ratios.

Detection of the ion signal was by means of a 12-stage electron multiplier-vibrating reed electrometer combination. The multiplier was of the Allen type[6] with the conversion dynode modified for end-on operation. With an ion current of 2×10^{-14} amp, a typical output was 90 mv with a signal-to-noise ratio of 100.

Typically, a run required 6 hr with each point recorded for 5–7 minutes. This allowed reading the difference ion current to an accuracy of 2% or better. A standardizing point, usually the largest reading during the run, was taken every 3 or 4 points to correct for ion beam intensity drift. Effects attributable to space charges in the ionizing region appeared if the electron beam exceeded about 2 μa. This restriction on the ionizing beam current meant that the largest ion currents used were of the order of 10^{-14} amp.

For each metal, six to 10 runs were made covering the desired electron energy range. Differences in optimizing the adjustments of the source parameters were invariably apparent, so that conditions were never identical. Some of the runs were made by increasing the electron energy and others by decreasing the energy to the disappearance point. For Ag and Au, two sources each were used to get the data.

EXPERIMENTAL RESULTS AND DISCUSSION

Cu, Ag, and Au have similar ground-state configurations ($d^{10}s^2S_{1/2}$), and as Figs. 2, 4, and 6 indicate, they also have many equivalent levels arising from inner electron excitation that lie above the ionization potentials. Resonance can occur between some of these levels and levels that lie at the same energy but in the continuum. If such a radiationless transition takes place, an electron leaves the atom; i.e., the atom has autoionized. The phenomenon is sometimes observed in the optical spectrum, because the perturbation of the discrete level by the resonance causes a broadening of the level.

Both Cu and Ag are known to exhibit many lines broadened by autoionization.[7] The widths of several Cu lines of special interest have been measured,[8] but unfortunately, except for Cu, specific information on autoionizing levels is meager. Some corresponding groups of levels in both Cu and Ag are known to have similar autoionizing properties, and, therefore, the similarities between the three elements have been assumed to hold wherever information is lacking for particular levels.

Curves of the individual runs for each metal were shifted along the energy axis to make the threshold values coincide with the spectroscopic value of the ionization potential[9] and normalized at a convenient point. An average curve was then obtained from these and is shown here for each singly ionized metal. This eliminated any small features in the ionization probability curves that might have appeared spuriously in a single run. Those features retained in the average curves, which will be discussed here, were those that appeared consistently in the individual runs.

To begin the analysis for each metal, a smooth, monotonically increasing curve was drawn, connecting the threshold point with that region on the ionization curve above which energy no structure was seen to occur. This new curve was taken to represent the ionization probability to the ground state of the ion and was close to a straight line for the first few volts.[4] An additional requirement was that this curve should not cross the ionization curve at any point. The difference between the ionization curve and the new curve was then the additional ionization due to excitation to autoionizing levels, and some limits as to where the resulting peaks started and ended were deduced. Admittedly, this procedure is inexact, but, guided by the fact that the peaks were not large compared to ionization to the ion ground state and by knowledge of the ionizing electron energy spread, a group of peaks which were consistent with each other was obtained. Although one did not hope to locate individual levels, groups of levels, at least, were found.

1. Ag

Figure 1 shows the relative ionization probability curve for silver, and Fig. 2 gives the essential features of the energy-level structure.[9] Alongside the level scheme are the peaks obtained by applying the procedure outlined above. The arrows correspond to the beginning of each peak. The peaks have been numbered, beginning from the ionization threshold. We assign levels or groups of levels to the peaks as follows:

Peak 1: The level $^4D_{5/2}$ in the configuration $4d^95s(^3D)5p$. Although the levels $^4D_{7/2}$ and $^4F_{3/2}$ are also concordantly located, they are known to be sharp. The $^4D_{5/2}$ level is quite broad in comparison,[7] which we attribute to autoionization. This assignment would place the threshold for the peak some 0.1 ev below the level, but this is not unreasonable in view of the uncertainty in the exact shape of the ion-current curve so close to the ionization potential.

[6] James S. Allen, Rev. Sci. Instr. **18**, 739 (1947).
[7] A. G. Shenstone, Phys. Rev. **57**, 895 (1940); Phil. Trans. Roy. Soc. (London) **A241**, 297 (1948).
[8] C. W. Allen, Phys. Rev. **39**, 42, 55 (1932).
[9] Natl. Bur. Standards Circ. No. 467, Vols. 2 and 3.

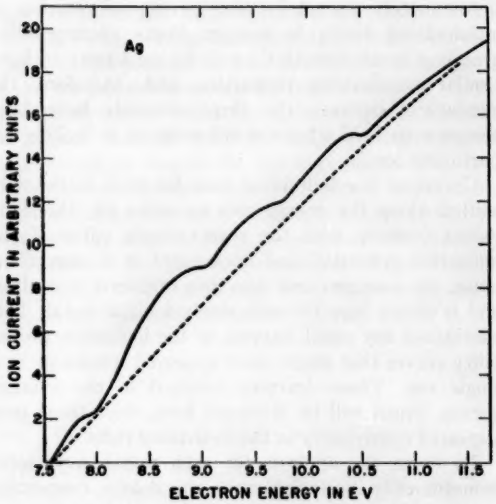

FIG. 1. Ionization probability curve for the formation of Ag^+.

Peak 2: Probably all four levels $^2P_{3/2,1/2}$, $^2D_{3/2}$, $^4D_{1/2}$ in the same configuration as for peak 1. These levels are extremely broad (~0.06 ev wide), indicating a very strong coupling to the continuum.

Peak 3: Possibly all four of the levels ^2P, ^2F, in the configuration $4d^9 5s(^1D)5p$. One of each pair of these levels has been observed to be very broad.[7] Transitions from the remaining two have not been seen, possibly because they too are broadened by autoionization. There are identical states in the continuum with which all four levels can couple.

Peak 4: The levels $^4D_{3/2}$ and $^4D_{5/2}$ in the configuration $4d^9 5s(^3D)6s$. These levels are known to autoionize, while the level $^4D_{7/2}$, although more closely located to the threshold of the peak, gives sharp lines in the optical spectrum.[7]

Peak 5: The level $^2D_{3/2}$ in the same configuration as peak 4 and a group of levels in the group $4d^9 5s(^3D)6p$, with some contribution from the group $4d^9 5s5d$. The group in Cu corresponding to the latter group is known to contain many autoionizing levels.[7] This last peak is very small—barely larger than the uncertainty in the ion current.

A distinctive feature to be noticed is that, although the transition probability to the continuum from a level should decrease rapidly with energy the higher the level is above the ionization limit, the heights of the peaks do not vary greatly with energy. Shenstone observed this same phenomenon of levels broadened by autoionization high above the ionization potential of Ag.[7]

2. Cu

In Cu and Au, the locations of the energy levels equivalent to those discussed for Ag will be different in relation to the ionization potentials. The justification for all of our assignments will be more firm if the peaks shift accordingly with Cu and Au. Figure 4 shows that we should see peaks arising only from those levels in Cu that are equivalent to the ones assigned to peaks 4 and 5 in Ag. In Cu, all the other levels—i.e., those that are equivalent to the levels giving rise to peaks 1, 2, and 3 in Ag—lie below the ionization potential. Figures 3 and 4 show this to be the case. The $3d^9 4s(^3D)5s$ and $3d^9 4s(^1D)5s$ groups are a little more separated for Cu than for Ag, and so two small peaks (1 and 2) can be partially resolved. We attribute the peaks to the ^2D groups in each configuration. All four levels show broadened lines in the optical spectrum,[7,8] but the broadest of these are the $(^3D)\ ^2D_{3/2}$ and the $(^1D)\ ^2D_{5/2}$. The third peak is apparently a sum of many small peaks, and its onset is in good agreement with the start of the levels $3d^9 4s(^3D)5p$. The remaining contributions, at higher energies, are due to $3d^9 4snp$ $(n>5)$ and $3d^9 4snd$ $(n\geq 4)$. Here again, transitions from many of the levels give pronounced broad lines.[7] Unfortunately, the level spacing is small—beyond the limits of resolution of our experiment.

It is apparent at once that compared to the ionization to the ion ground state, the peaks for Cu are much smaller than for Ag, indicating a lower probability for autoionization. As a matter of fact, two of the levels $(^4D_{3/2,5/2})$ in the $3d^9 4s(^3D)5s$ group do not seem to give a measurable amount of autoionization to the Cu curve, while in Ag they do.

The highest-energy peak for Cu is seen to be more pronounced, relative to the lower-energy peaks, than

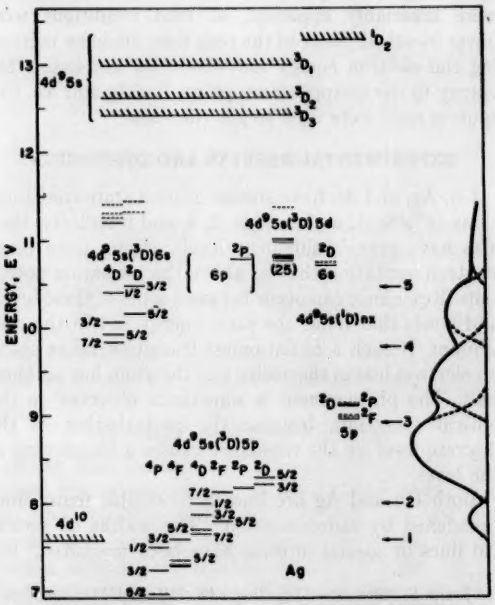

FIG. 2. Partial term level diagram for silver, with peaks attributed to auto-ionization. Only those levels arising from the excitation of a 4*d* electron are shown.

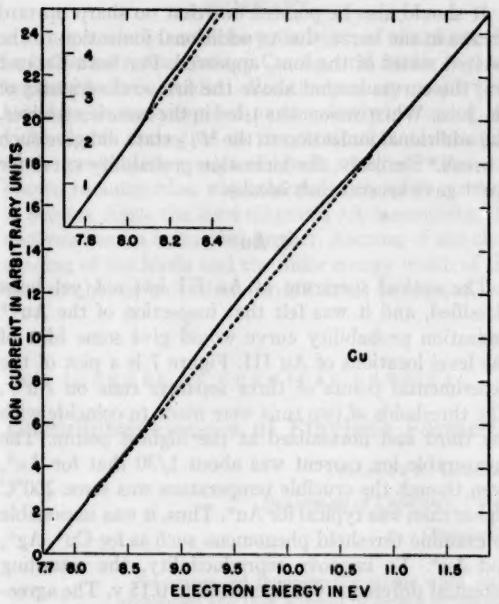

FIG. 3. Ionization probability curve for the formation of Cu^+.

that for Ag. This is probably because the levels responsible do not lie so high in energy above the ionization potential.

3. Au

For gold, only 13 levels have been located above the ionization potential. These are of the configuration $5d^9 6s6d$. All 34 possible levels of this configuration should lie above the ionization potential.[10] Of the groups

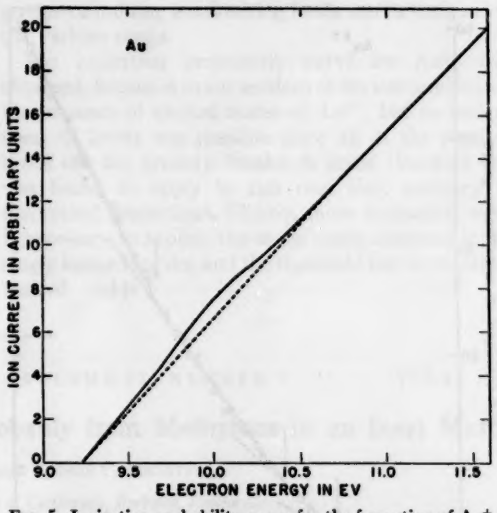

FIG. 5. Ionization probability curve for the formation of Au^+.

equivalent to those discussed in Au and Ag, there should also be four levels of the configuration $5d^9 6s7s$ lying above the ionization potential, as well as most of the 23 levels of $5d^9 6s7p$. The dotted line in Fig. 6 indicates the probable location of the $6s7s$ group.[10] By analogy with other parts of the spectrum, the $6s7p$ group should be only slightly below the $6s6d$ group, placing some of these levels very close to the ionization potential. The ionization probability curve for Au is shown in Fig. 5. One peak is easily visible, but a more careful analysis indicates that this peak is superimposed on an extended peak of small magnitude that starts near the ionization potential. If the portion of the curve immedi-

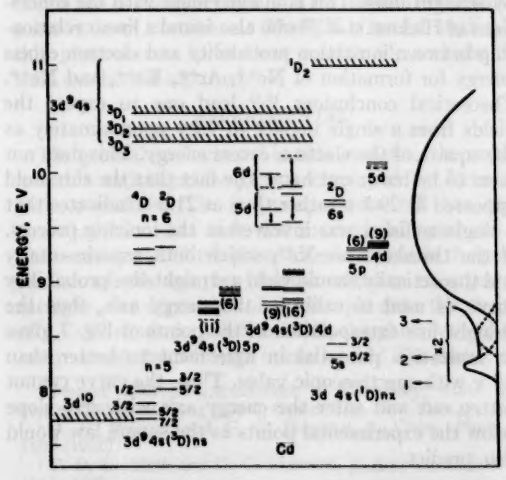

FIG. 4. Partial term level diagram for copper, with peaks attributed to autoionization. The levels shown are for the excitation of a $3d$ electron.

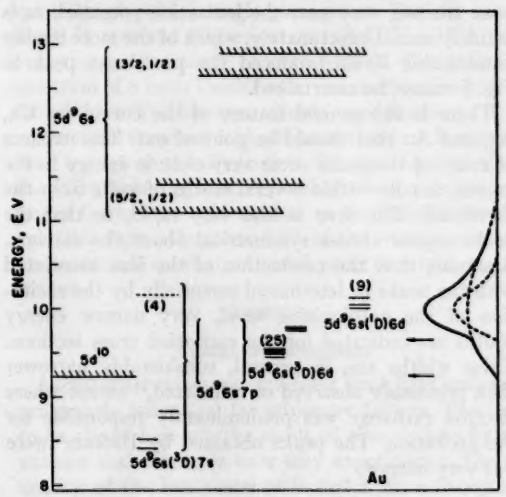

FIG. 6. Partial term level diagram for gold. The levels shown arise from the excitation of a $5d$ electron. The peaks are attributed to autoionization.

[10] J. R. Platt and R. A. Sawyer, Phys. Rev. 60, 866 (1941).

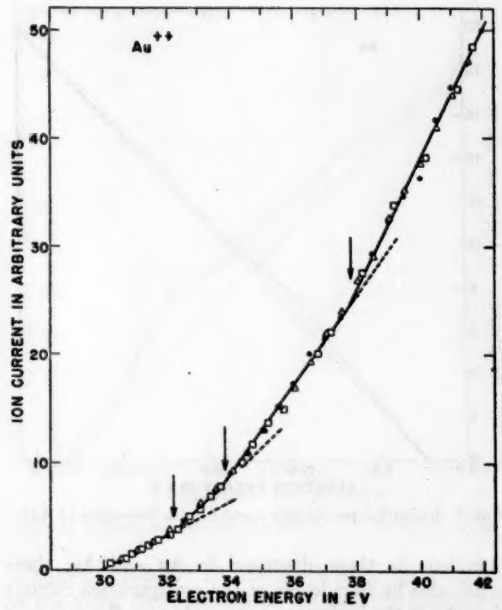

FIG. 7. Ionization probability curve for the formation of Au^{++}. Each arrow indicates the onset of additional ionization arising from the presence of an energy level of the ion.

ately above threshold, which appears to be a straight line, is extrapolated to higher energy, it lies above the observed yield curve. This is similar to previous observations for Hg[2] but less pronounced.

As in Cu and Ag, many of the levels in the groups mentioned above probably autoionize to some extent. Since the level spacing becomes small compared to the electron energy spread, we would expect a long smeared peak starting very near the ionization potential, as is actually seen. Unfortunately, which of the more readily autoionizing levels produced the prominent peak in Fig. 5 cannot be ascertained.

There is one general feature of the curves for Cu, Ag, and Au that should be pointed out. The maxima of many of the peaks occur very close in energy to the onsets, usually within several tenths of volts from the thresholds. The drop is also very rapid, so that the peaks appear almost symmetrical about the maxima. Assuming that the production of the ions associated with the peaks is determined essentially by the excitation of the autoionizing level, very narrow energy widths are indicated for the excitation cross sections. These widths are, in general, considerably narrower than previously observed or calculated,[11] except where electron exchange was predominantly responsible for the excitation. The peaks obtained by Hickam[2] were also very narrow.

[11] H. S. W. Massey and E. H. S. Burhop, *Electronic and Ionic Impact Phenomena* (Oxford University Press, New York, 1952), Chap. 3.

It should also be pointed out that no sharp upward breaks in the curve, due to additional ionization to the excited states of the ions, appeared. For both Cu and Au, the curves extend above the first excited states of the ions. When xenon was tried in the same ion sources, the additional ionization to the $^2P_{1/2}$ state did give such a break.[4] Similarly, the ionization probability curve for Au^{++} gave several such breaks.

4. Au^{++}

The optical spectrum of Au III has not yet been classified, and it was felt that inspection of the Au^{++} ionization probability curve would give some idea of the level locations of Au III. Figure 7 is a plot of the experimental points of three separate runs on Au^{++}. The thresholds of two runs were made to coincide with the third and normalized at the highest points. The measurable ion current was about 1/30 that for Au^+, even though the crucible temperature was some 200°C higher than was typical for Au^+. Thus, it was impossible to examine threshold phenomena such as for Cu^+, Ag^+, and Au^+. To improve reproducibility, the retarding potential difference was increased to 0.15 v. The agreement between the points does indicate the accuracy it is possible to attain in this type of work.

Several features of this curve are worth noting. Definite breaks occur at 2.2_6, 3.9_2, and 7.8_1 v above threshold. This indicates the presence of energy levels of the ion which can be excited by the electron impact to give additional ionization. It is not possible to assign any specific levels, since the other members of the isoelectronic series, Pt II and Hg IV, indicate a multitude of levels below the first break.

The regions between the breaks are best represented by straight lines. This is in agreement with the conclusions of Hickam *et al.*,[12] who also found a linear relationship between ionization probability and electron excess energy for formation of Ne^{++}, Ar^{++}, Kr^{++}, and Xe^{++}. Theoretical conclusions [13,14] lead one to expect the yields from a single impact to vary approximately as the square of the electron excess energy. This does not seem to be borne out here. The fact that the threshold appeared at 29.7 v rather than at 21.2 v indicates that a single collision was involved in the ionizing process. If the threshold for Xe^+, which both experimentally and theoretically should yield a straight-line probability curve, is used to calibrate the energy axis, then the straight line extrapolation of the points of Fig. 7 gives an ionization potential in agreement to better than 0.2 v with spectroscopic value. Thus, the curve cannot flatten out and enter the energy axis with zero slope below the experimental points as the square law would also predict.

[12] W. M. Hickam, R. E. Fox, and T. Kjeldaas, Jr., Phys. Rev. **96**, 63 (1954).
[13] Gregory H. Wannier, Phys. Rev. **100**, 1180 (1955).
[14] Sidney Geltman, Phys. Rev. **102**, 171 (1956).

SUMMARY

Using a nearly monoenergetic beam of electrons, the ionization near threshold of Cu, Ag, and Au by electron impact has been studied. Relatively sharp peaks were found to be superimposed on the slowly increasing ion yield due to ionization to the continuum. Correlation of the peaks with groups of levels, many of which are known to autoionize, was achieved with a fair measure of success. Since the level diagrams are incomplete, the analysis cannot be carried further. Because of the close spacing of the levels and the finite energy width of the electron beam, individual levels cannot be located, but groups containing autoionizing levels can be assigned to the various peaks.

The ionization probability curve for Au^{++} was obtained. Breaks in linear sections of the curve indicated the presence of excited states of Au^{++}, but no assignment of levels was possible since all of the possible levels did not produce breaks. A linear threshold law was found to apply in this case also, contrary to theoretical predictions. Clearly, more theoretical work is necessary to explain the sharp peaks observed in the singly ionized curves, and the threshold law for multiply ionized yields.

THE JOURNAL OF CHEMICAL PHYSICS VOLUME 33, NUMBER 1 JULY, 1960

Chemiluminescence of Ethylene Formed Probably from Methylene in an Inert Matrix

THEODORE D. GOLDFARB* AND GEORGE C. PIMENTEL

Department of Chemistry, University of California, Berkeley, California

(Received January 28, 1960)

An orange-red luminescence occurs when diazomethane suspended in solid nitrogen or solid argon is photolyzed and then warmed to permit diffusion. Spectrographic and visual studies of this thermoluminescence are reported here. Conditions favorable for the production of the luminescence also result in relatively high yields of ethylene as a final product. Furthermore, a deuteration effect is observed. For CH_2N_2 the recorded spectrum consists of a distinct feature at 6030 A and an extremely weak feature near 6530 A. Deuterated diazomethane produces a spectrum with two distinct features at 6055 and 6405 A, and one or more weaker absorptions between 6700 and 6800 A. The emission is assigned to chemiluminescence of ethylene and a tentative interpretation is given in terms of two excited states of ethylene ($Z \rightarrow V$).

IN recent publications from these Laboratories,[1,2] mention has been made of an orange-red chemiluminescence observed during the diffusion of reactive fragments of diazomethane and its deuterated counterparts in inert matrices at 20–40°K. Careful studies of this phenomenon have been conducted, and the results are herein reported.

EXPERIMENTAL

The general method used in this work was the matrix isolation technique frequently employed by Pimentel and co-workers. The low-temperature cell has been described,[3] as have been the methods of synthesis of diazomethane[2] and the procedures involved in the preparation of the samples of diazomethane in argon or nitrogen, the deposition of the sample onto the surface of a CsBr window cooled to 20°K, the photolysis of the sample, and the diffusion operation.[1,2,4] The mole ratio of the matrix gas (M) and diazomethane (R) are indicated by the mole ratio M/R.

Emission spectra were photographed on preexposed Eastman Kodak 103aF plates using a Steinheil $f/3$ spectrograph with a single glass prism. The slit width was 0.25 mm and dispersion averaged 275±25 A/mm over the spectral range 5850 to 6400 A. The emission spectrum of a neon Geisler tube was used for frequency calibration. To increase speed, modifications were made in the standard cold cell base[2] to bring the sample close enough to the slit so that the glowing area filled the $f/3$ collimating lens. A polished-silver reflector was placed behind the cold window to increase further the available light. About one-fifth of the window was left unobstructed so that infrared spectra could be recorded.

RESULTS

Visual Observations

Visual observations of extremely weak light emissions are greatly influenced by subjective factors. The facts to be stated here are the result of observations by the authors and others in over fifty experiments. The intensity of the luminescence varied from a barely detectable grayish-looking glow visible only to a dark-adapted eye to a distinct orange-red emission easily

* Present address: Department of Chemistry, State University College on Long Island, Oyster Bay, New York.

[1] D. E. Milligan and G. C. Pimentel, J. Chem. Phys. **29**, 1405 (1958).

[2] T. D. Goldfarb and G. C. Pimentel, J. Am. Chem. Soc. **82**, 1865 (1960).

[3] E. D. Becker and G. C. Pimentel, J. Chem. Phys. **25**, 224 (1956).

[4] T. D. Goldfarb, Doctoral dissertation, University of California, Berkeley, California, 1959.

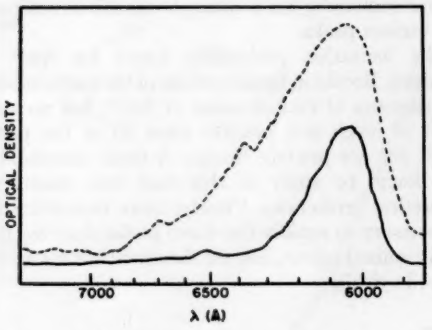

FIG. 1. Microphotometer tracings of luminescence spectra: —— Normal diazomethane; ---- 60% deuterated diazomethane.

seen against a light level bright enough to read by. The duration of the luminescence varied from a few seconds to more than seven minutes.

Several parameters were varied during the many experiments: the value of M/R (from <100 to >2000), the rate at which the sample was warmed from 20° to 40°K, the percentage of sample photolyzed, and the wavelength of the light used for photolysis.The general pattern of behavior was similar in all of these experiments. The glow became apparent before the thermocouple in the cold window registered a rise of more than one or two degrees. The glow increased gradually in intensity as the temperature rose to about 27°K. The glow then intensified rapidly, and the temperature rise accelerated. The temperature continued to rise rapidly, but the glow became dimmer after the temperature reached about 32°K. If the sample was cooled again to 20°K, the glow was abruptly extinguished. If, instead, the sample was allowed to continue to warm up, the glow became gradually dimmer and then died out rapidly at a temperature of 42° to 45°K. The temperatures quoted above are for a nitrogen matrix. Slightly higher temperatures were found when argon was used, but these are based on fewer experiments and are less certain.

The intensity of the glow seems to be influenced by many factors. For a given number of micromoles of diazomethane photolyzed, the glow appears brighter at higher values of M/R. At M/R below 100, it is barely visible. At $M/R=500$, the intensity of the glow definitely increases when the number of micromoles photolyzed is doubled. Deuteration has no obvious effect on the intensity. The rate at which the sample is warmed has a definite effect. If the same total number of photons are emitted, the intensity should increase if the period during which they are emitted is shortened. The maximum intensity (determined both visually and in the spectrographic experiments) is achieved when the sample is allowed to warm very slowly. When the light used for photolysis is passed through filters that absorb all of the light of wavelength less than 3400 A (Corning 7830) or 2800 A (Corning 7740), no luminescence occurs at all during diffusion. Luminescence is also absent when oxygen or water is present at high concentration in the matrix.

One of the most significant facts in this rather complex picture is that a comparison with the infrared absorption spectra[1,2,4] indicates that the intensity of the glow can be correlated with the amount of ethylene produced during diffusion. In particular, experimental factors which eliminate the luminescence but do not prevent photolysis (the use of filtered light for photolysis or the addition of water or oxygen) also eliminate the formation of ethylene. Conversely, in all experiments which resulted in a bright glow, relatively large amounts of ethylene were formed.

Spectrographic Results

At best, the intensity of the luminescence is low, and its duration short for spectroscopic study. Experimentation eventually revealed the best compromise between speed and dispersion within the range of the available spectrographic equipment, as described earlier. Microphotometer tracings of the spectra obtained using normal and $60\pm5\%$ deuterated diazomethane are shown in Fig. 1. The spectrum from the deuterated sample (broken line, Fig. 1) shows two distinct maxima at 6055 ± 25 and 6405 ± 25 A (i.e., 16 520 and 15 610 cm^{-1}) with one or more additional features in the region 6700 to 6800 A. The spacing between the distinct maxima is 910 cm^{-1} with an estimated uncertainty of ±65 cm^{-1}. The tracing of the spectrum from the nondeuterated sample shows an intense maximum at $6030\pm$ 25 A (16 580 cm^{-1}) and a hint of a second maximum at 6530 ± 30 A (15 310 cm^{-1}). Repeated microphotometer tracings and visual examination of the plate verify the reality of the second maximum. The spacing between these features is 1270 ± 70 cm^{-1}.

Since the widths of the intense bands are greater than the spectral resolution, they are intrinsically determined by the emitting system. The definite effect of deuterium substitution on the spacing of the bands proves that they are emitted by a hydrogen-containing molecule.

A rough measurement was made to determine the number of photons involved in the luminescence. A silicon carbide Globar (Perkin-Elmer) was placed sufficiently close to the slit of the spectrograph to fill the collimator lens. The temperature of the bar was measured with an optical pyrometer. Spectra were recorded under the same optical conditions used in the luminescence measurements and with exposure time adjusted to provide the same plate darkening in this spectral region. By graphical integration of the blackbody radiation law,[5] the number of quanta emitted per second over this wavelength region was estimated. Multiply-

[5] R. A. Smith, F. E. Jones, and R. P. Chasmar, *The Detection and Measurement of Infrared Radiation* (Oxford University Press, New York, 1957), p. 35.

ing this by the approximate emissivity of the globar[6] (~0.6) and by the required exposure time leads to a value of the order of 10^{-9} Einsteins for the number of photons emitted in the luminescence experiments.

DISCUSSION

The observed correlation between the intensity of the luminescence and the formation of ethylene during diffusion leads naturally to the proposal that the process responsible for the light emission is

$$A+B\rightarrow C_2H_4^*$$

$$C_2H_4^*\rightarrow C_2H_4^{\pm}+h\nu.$$

$C_2H_4^*$ is ethylene in an excited state and $C_2H_4^{\pm}$ is either the ground state or a lower excited state. A and B are most likely a CH_2 radical and diazomethane molecule or two CH_2 radicals. Thus, the over-all reaction could be either

$$CH_2+CH_2N_2=C_2H_4+N_2$$

$$\Delta H=-101 \text{ kcal}(35\,300 \text{ cm}^{-1})$$

or

$$2CH_2=C_2H_4$$

$$\Delta H=-122 \text{ kcal}(43\,700 \text{ cm}^{-1}).$$

These values of ΔH permit consideration of only the few lowest-lying energy levels of ethylene.

A simple argument shows that there are two singlet and one triplet excited states of ethylene within the prescribed energy limit. The C=C and C—C bond energy difference is known to be about 80 kcal/mole and excitation of a bonding π electron to an antibonding state implies about this much excitation. However, this energy estimate is based on retention of a planar configuration in the excited state. With the rupture of the π bond, however, there is no longer a constraint to planarity. In fact, the eclipsed positions of the protons in the planar arrangement guarantee that the energies of the first two excited states, both singlet and triplet, will be lowered as the molecule becomes nonplanar. A third state would involve excitation of both π bonding electrons. This would be a singlet state as a result of the Pauli exclusion principle.

Detailed treatments of the excited states of ethylene have been made by Mulliken[7] and Walsh.[8] These treatments agree on the general geometrical configurations of the molecule in its various states. The four lowest states correspond to those described above. Mulliken's symbols for these states are N for the ground state, T and V for the first excited triplet and singlet states, and Z for the second excited singlet state. We have adopted this notation in this paper.

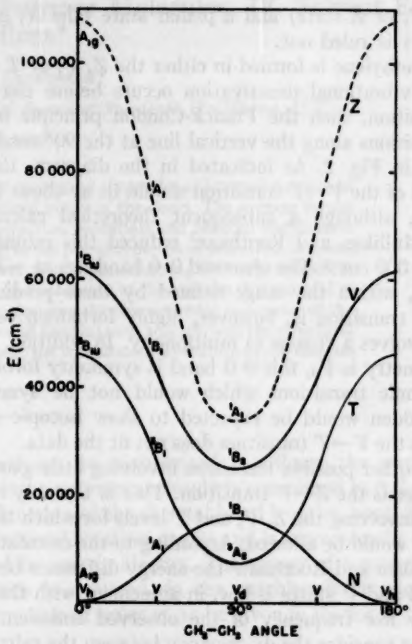

FIG. 2. Electronic states of ethylene as a function of CH_2—CH_2 angle.

Mulliken and Roothaan have estimated the energies of these states as a function of the angle between the planes defined by the CH_2 groups,[9] as reproduced in Fig. 2. The energy relationships for the planar configurations (symmetry V_h) were estimated from spectral data. The diagram in the vicinity of the perpendicular configuration (symmetry V_d) is less certain since it is based on theoretical considerations and extrapolations of the spectral data. We have added in Fig. 2 the probable energy dependence of the Z state (the dotted line) together with appropriate symmetry designations. Mulliken and Roothaan[9] predicted that this state is higher than the V state by 0.6 ev in the 90° configuration (V_d). The state should have an energy dependence on the angle between CH_2 groups similar to that of the V and T states and, in the planar form, should be approximately twice as high above the N state as the average of the V and T states.

Figure 2 aids in evaluation of the red-glow spectrum as a possible ethylene transition. The observed emission appears to be caused by a highly favored zero-zero transition as indicated by the smallness of the isotopic shift of the strongest band and the asymmetric appearance of the emission spectrum. The Franck-Condon principle dictates a transition involving little geometry change between the states producing such a spectrum. Hence, a transition between a nonplanar state (the

[6] See p. 313 of footnote reference 5.
[7] R. S. Mulliken, Phys. Rev. **41**, 751 (1932); J. Chem. Phys. **3**, 517 (1935).
[8] A. D. Walsh, J. Chem. Soc. **1953**, 2325.
[9] R. S. Mulliken and C. C. J. Roothaan, Chem. Rev. **41**, 219 (1947).

T, V, or Z state) and a planar state (the N, ground state) is ruled out.

If ethylene is formed in either the Z, V, or T states and vibrational deactivation occurs before electronic transition, then the Franck-Condon principle implies transitions along the vertical line at the 90° configuration in Fig. 2. As indicated in the diagram, the 0–0 band of the $V \rightarrow T$ transition should lie at about 17 500 cm^{-1}, although a subsequent theoretical calculation by Mulliken and Roothaan[9] reduced this estimate to $\sim$12 000 cm^{-1}. The observed 0–0 band lies at $\sim$16 520 cm^{-1}, within the range defined by these predictions. This transition is, however, highly forbidden because it involves a change in multiplicity. In addition, if the symmetry is V_d, this 0–0 band is symmetry forbidden. Vibronic transitions which would not be symmetry forbidden would be expected to show isotopic shifts. Thus the $V \rightarrow T$ transition does not fit the data.

Another possible transition involving little geometry change is the $Z \rightarrow V$ transition. This is the only transition involving the Z, V, and T levels for which the 0–0 band would be allowed. According to the calculation of Mulliken and Roothaan[9] the energy difference between the Z and V states is low, in agreement with the relatively low frequency of the observed emission. (We do not consider the discrepancy between the calculated frequency, 0.6 ev=4830 cm^{-1}, and the observed frequency, 16 520 cm^{-1}, to be excessive in view of the uncertainties in such theoretical estimates.) The allowed vibronic transitions would involve only completely symmetric vibrational degrees of freedom. In view of the large isotopic effect on the spacing of the observed features, the completely symmetric CH_2 bending mode ν_3 may be involved. This vibration has a frequency of 1342 cm^{-1} for the ground state of C_2H_4, and it is calculated to shift to 1047 cm^{-1} for C_2HD_3.[10] We expect the corresponding vibrational frequencies of the V state to be similar, and it is reassuring that the measured vibrational spacings, $\sim$1270 and 910 cm^{-1}, are reasonably close to the values of ν_3 in the N state.

Thus the predicted $Z \rightarrow V$ transition of ethylene is compatible with the experimentally observed luminescence spectrum. If the emission is indeed due to chemiluminescence of ethylene, then only about one out of each 10^4 molecules undergoes the observed transition. This low quantum yield does not, however, provide a basis for rejecting the $Z \rightarrow V$ assignment. It is possible that only a small fraction of the molecules are formed in the Z state, and it is also likely that competing deactivation processes would be efficient in the solid state.

Of course, it is possible that the luminescence involves other reactions than those listed and producing some other chemiluminescent, hydrogen-containing molecule. This proposal must be considered since the formation of other products during diffusion has been reported[1] (methane, propylene, and polyethylene) and the ethylene accounts for only 5–10% of the decomcomposed diazomethane.[1] It is even possible that a minor product is the cause. Such a product might be produced in very small amounts (so that infrared detection is not possible), yet it might display chemiluminescence with a high quantum yield. Though these alternatives cannot be eliminated, we believe that chemiluminescence accompanying ethylene formation is the most likely explanation of the red-glow phenomenon.

CONCLUSIONS

The foregoing evidence shows that during the diffusion of the photolysis products of diazomethane in a solid matrix an emission occurs as a result of an electronic transition between states of a hydrogen-containing molecule. The Franck-Condon principle predicts similar geometries for the emitting molecule in the states involved. Experimental evidence indicates a correlation between the intensity of the luminescence and the formation of ethylene during the diffusion process. The $Z \rightarrow V$ transition of ethylene is offered as the most likely explanation of the observed facts.

ACKNOWLEDGMENTS

The authors would like to express their sincere gratitude for fellowship aid (to TDG) from Texaco Inc. and for research support by the American Petroleum Institute Research Project 54 and the United States Air Force through AFOSR of the Air Research and Development Command under contract.

[10] B. Crawford, Jr., J. E. Lancaster, and R. G. Inskeep, J. Chem. Phys. **21**, 678–686 (1953).

Neighbor Interactions and Internal Rotations in Polymer Molecules. IV. Solvent Effect on Internal Rotations*

SHNEIOR LIFSON† AND IRWIN OPPENHEIM†

Weizmann Institute of Science, Rehovoth, Israel, and National Bureau of Standards, Washington, D. C.

(Received February 15, 1960)

Solvent chain-element interactions affect the probability distribution of the angles of internal rotation of a polymer chain and give rise to an average torque on the skeletal bonds of the chain. The average torque and its potential are derived in terms of polymer-solvent interaction potentials and reduced distribution functions. The energy of the polymer molecule, as it was applied in the previous papers of this series, is shown to be the potential of the average torque in the neighbor interaction approximation. This approximation, though insufficient by itself, provides a theoretical basis for the application of the random flight model of polymer molecules and, at the same time, improves upon it by deriving the characteristic parameter of the model (the length of the statistical chain element) as a function of temperature, solvent, and the structural parameters of the polymer chain. Following these considerations, the complementary nature of the theories of neighbor interaction and excluded volume is discussed.

I. INTRODUCTION

RECENT work on neighbor interactions and internal rotations in polymers has been concerned mainly with the effect of higher orders of neighbor interaction on the calculation of the mean-square end-to-end distance $\langle h^2 \rangle$, since it was evident from previous results,[1] in which only first-neighbor interactions were included, that higher orders are by no means negligible. The mathematical problem of accounting for higher-neighbor interaction is that of averaging over interdependent internal rotation angles. Ptitsyn and Sharonov[2,3] and Lifson[4] provided a partial solution of the problem by studying the effect of interactions between neighboring bulky groups of vinylic-type polymers. In this case, a pair of adjacent internal rotation angles enclosed between these groups is interdependent, but the different pairs are independent of each other if the interactions between the hydrogen atoms of the $-CH_2-$ groups as well as those between farther bulky groups are neglected. More recently, the calculation of $\langle h^2 \rangle$ for molecules with interdependent internal rotations due to second- and higher-order neighbor interactions has been performed by Lifson[5] and by Nagai[6] and has been modified and utilized in the interpretation of experimental results by Hoeve.[7]

The essential features of the theory of neighbor interactions and internal rotations as hitherto developed can be summarized as follows: the geometry of a linear polymer molecule is considered in full detail as a function of the skeletal bond lengths, bond angles, and internal rotation angles and is conveniently represented by matrix algebra. The energy of a molecule of n bonds is assumed, in the neighbor-interaction approximation of order m, to be given in the form

$$E=\sum_{i=1}^{n-m+1} E_i^{(m)}(\phi_i, \cdots, \phi_{i+m-1}), \tag{1}$$

namely, as a sum of functions $E_i^{(m)}$, each dependent on m consecutive internal rotation angles. The distribution function of the polymer molecule, $\exp(-E/kT)$, is then applied to obtain the partition function of the system by matrix methods related to those used in the Ising-model and Markoff-chain theories. By a proper coupling of the matrix representations of the structure of the polymer molecule and its energy distribution, square averages of vectorial properties like the end-to-end distance or electric moments are obtained.

In the present paper, we consider the nature of the energy function $E_i^{(m)}$ for a system composed of a single polymer molecule dissolved in a solvent of low molecular weight, and obtain an expression for $E_i^{(m)}$ in terms of interaction potentials and distribution functions of nonpolymeric solutions. These functions are usually considered to be dependent on the scalar distances between the interacting particles. In polymer solutions, however, they may be considered to be functions of the internal rotation angles of the polymer chain because of the restrictions imposed by the bonding of the chain elements.

We shall show that

$$\sum_{i=1}^{n-m+1} E_i^{(m)}$$

represents, in the mth-order neighbor interaction approximation, the potential of the average torque on the skeletal bonds of the polymer chain, averaged over the

* Presented at the 139th meeting of the American Chemical Society, Cleveland, April, 1960.

† Present address: Physics Section, Convair-San Diego, San Diego, California.

[1] See, for example, T. M. Birshtein and O. B. Ptitsyn, Zhur. Fiz. Khim. **28**, 213 (1954), and other references quoted there. See also: K. Nagai, J. Chem. Phys. **30**, 660 (1959); A. Borsellino, J. Chem. Phys. **30**, 857 (1959).

[2] O. B. Ptitsyn and J. A. Sharonov, J. Tech. Phys. U.S.S.R. **27**, 2744, 2762 (1957).

[3] M. V. Volkenshtein, J. Polymer Sci. **29**, 441 (1958).

[4] S. Lifson, J. Chem. Phys. **29**, 80, 89 (1958).

[5] S. Lifson, J. Chem. Phys. **30**, 964 (1959).

[6] K. Nagai, Busseiron Kenkyu **2-5**, 364 (1959); J. Chem. Phys. **31**, 1169 (1959).

[7] C. A. J. Hoeve, J. Chem. Phys. **32**, 888 (1960).

solvent configuration space, as a function of the internal rotation angles of the chain. The torque on a skeletal bond is affected by both intra-polymer and solvent-polymer interactions. The contribution of the solvent-polymer interaction to the average torque can be related qualitatively to the effect of the rotation around a skeletal bond on the solvation of the polymer molecule in the vicinity of this bond. Quantitatively, it is determined by the average moments of the solvent forces on the two branches of the chain connected by a bond with this bond as an axis of rotation. Each of these average moments would have been zero if it were not for the effect of one branch on the distribution of the solvent molecules in the vicinity of the other branch. This effect, expressed in terms of solvent chain-element distribution functions, determines the statistical weight in calculating the average torque.

In the last section, some general aspects of the theory of neighbor interactions and internal rotations in polymers are discussed. It is indicated that the neighbor-interaction approximation, though insufficient by itself, provides a theoretical basis for the application of the random flight model of polymer molecules and, at the same time, improves upon it by deriving the characteristic parameter of the model, the so-called length of the statistical chain element, as a function of temperature, solvent, and the structural parameters of the polymer chain. Following these considerations, the excluded volume theory of interactions between distant elements should be interpreted as calculating the derivation of the real behavior of polymer chains from their calculated behavior due to interactions between neighbor elements.

II. THE POTENTIAL ENERGY OF NEIGHBOR INTERACTIONS

We consider a system consisting of a single polymer molecule and a large number N of solvent molecules. The polymer molecule is made up of $n+1$ groups, or chain elements, connected by n bonds which form a linear chain. For our present purpose, it is sufficient to consider a polymer molecule of the type $(-CRR'-)_n$. Generalization to more complicated periodic structures does not involve new principles and might be undertaken later, together with numerical computations.

The relative position of the chain elements is determined by the C–C bond lengths b and supplementary bond angles θ, which will be assumed to be fixed, and by the internal rotation angles $\phi_1, \phi_2, \cdots, \phi_n$. ϕ_i is the internal rotation angle of the ith bond connecting the skeletal carbons C_{i-1} and C_i. The bond lengths and bond angles within each element are also assumed to be fixed so that the element can be considered to be a rigid body. In order to complete the specification of the spatial configuration of the polymer molecule, it is necessary to determine the position vector of one of the skeletal carbons, say the vector $\mathbf{R}_k$ of the carbon C_k, and the three Eulerian angles, α, β, and γ, which determine the spatial orientation of the kth chain element with respect to a fixed reference coordinate system chosen arbitrarily. Thus, the configuration of the polymer molecule is completely specified by the $(n+6)$th dimensional vector $R^{n+6}=(\mathbf{R}_k, \alpha, \beta, \gamma, \phi^n)$ with differential volume element $d\mathbf{R}_k \sin\alpha d\alpha d\beta d\gamma d\phi^n$, where ϕ^n and $d\phi^n$ are, respectively, abbreviations for $\phi_1, \phi_2, \cdots, \phi_n$ and $d\phi_1, d\phi_2, \cdots d\phi_n$. It will be noticed that the assumption of fixed bond lengths and bond angles is equivalent to the specification of $5n$ coordinates since the specification of the $n+1$ chain elements as independent, oriented rigid bodies would require $6(n+1)$ coordinates. In fact, each angle of internal rotation ϕ_i may be interpreted as being the Eulerian angle γ_i of the ith chain element, if the coordinate system of this chain element is properly chosen relative to the $(i-1)$th chain element.

Since we are considering a uniform homogeneous system of large dimensions, the position and orientation of the polymer molecule are not of physical interest. Thus, we may fix the coordinate system in one of the chain elements, say the kth one, and consider the configuration of the polymer to be completely specified by ϕ^n. The configurations of the solvent molecules will be represented in the coordinate system fixed in the kth element by three-dimensional position vectors $\mathbf{R}_{ks}$, representing the vector distance of the solvent molecule s from the skeletal carbon C_k, with corresponding volume elements $d\mathbf{R}_{ks}$. We assume that the solvent molecules behave as if they are spherically symmetric, so that their angular orientation can be disregarded. The $3N$-dimensional vector of the solvent configuration space will be denoted by $\mathbf{R}_{ks}{}^N$ and the corresponding volume element by $d\mathbf{R}_{ks}{}^N$.

The potential energy $V^{(n,N)}$ of the system will be represented as a sum of pair interactions

$$V^{(n,N)}(\phi^n, \mathbf{R}_{ks}{}^N) = \sum_{\substack{i<j \\ 0}}^{n} V_{ij} + \sum_{i=0}^{n}\sum_{s=1}^{N} V_{is} + \sum_{\substack{s<t \\ 1}}^{N} V_{st}. \qquad (2)$$

V_{ij} is the intramolecular interaction potential between the ith and the jth polymer chain elements. For near-neighbor elements, i.e., when $j-i$ is small, it is necessary to consider V_{ij} as a function of the relative positions of all the atoms comprising the two chain elements. In this case, $V_{ij}=V_{ij}(\phi_{i+1}, \cdots, \phi_j)$. For elements that are farther apart, the detailed structure of the elements becomes less important, and it is sufficient to approximate V_{ij} by a function of the scalar distance between the skeletal carbons, C_i and C_j. In this case, $V_{ij}=V'_{ij}(\phi_{i+2}, \cdots, \phi_{j-1})$. Limiting our attention to neighbor interactions, it will be assumed that V_{ij} vanishes if it depends on more than m consecutive internal rotation angles. In this approximation, the first double sum in Eq. (2) may be written as a single sum,

$$\sum_{i=1}^{n-m+1} V_i{}^{(m)}(\phi_i, \cdots, \phi_{i+m-1}),$$

with

$$V_i^{(m)} = \sum_{j=1}^{i+m-1} V_{i-1\ j}(\phi_i, \cdots, \phi_j) + V'_{i-2\ i+m-1} + V'_{i-2\ i+m}. \tag{3}$$

In this way, the mth order approximation takes into account interactions between up to $m+3$ consecutive chain elements. It should be noted that the choice of m is not limited formally, but the computational difficulties increase so rapidly with m, that $m=2$, or at most $m=3$, seems to be the practical limit at present.

V_{is} is the interaction potential between a solvent molecule and a chain element. We shall assume here that V_{is} is a function of the scalar distance, R_{is} between the two. Now R_{is} and, therefore, V_{is} are functions of the vector distance $\mathbf{R}_{ks}$ and the internal rotation angles which determine the position of the ith chain element relative to the origin. Thus, we have

$$V_{is}(R_{is}) = V_{is}(\phi_{i+2}, \cdots, \phi_k; \mathbf{R}_{ks}) \quad i<k \tag{4a}$$

$$V_{is}(R_{is}) = V_{is}(\phi_{k+1}, \cdots, \phi_{i-1}; \mathbf{R}_{ks}) \quad i>k. \tag{4b}$$

As in the case of intramolecular interactions, one may consider a more detailed interaction dependent on the orientation of the ith chain element with respect to the solvent molecule. In this case, V_{is} will also depend on ϕ_{i+1} for $i<k$ and on ϕ_i for $i>k$.

The interaction potential V_{st} between solvent molecules s and t is assumed to be a function of their scalar distance $R_{st}=|\mathbf{R}_{ks}-\mathbf{R}_{kt}|$. It is independent of the internal rotation angles and will be shown not to contribute to the potential of the average torque.

III. DISTRIBUTION FUNCTIONS AND POTENTIALS OF AVERAGE TORQUE

In order to describe the effect of solvent chain-element interactions on the average properties of the polymer, it is useful to introduce the concepts of reduced distribution functions.[8] We consider our system of N solvent molecules and one polymer molecule, with $n+1$ chain elements, confined in a large volume V, to be described by a classical canonical ensemble. The normalized distribution function in the configuration space of N solvent molecules and one polymer molecule is

$$P^{(n,N)} = Z^{-1} \exp[-\beta V^{(n,N)}], \tag{5}$$

where $\beta=1/kT$, and Z, the configurational partition function of the system, is given by

$$Z = \int \cdots \int \exp[-\beta V^{(n,N)}] d\phi^n d\mathbf{R}_{ks}{}^N d\mathbf{R}_k \sin\alpha d\alpha d\beta d\gamma. \tag{6}$$

Reduced generic distribution functions depending on the coordinates of a set of n_s solvent molecules $\mathbf{R}_{ks}{}^{n_s}$ and on the internal rotation angles of the polymer chain ϕ^n are defined by the relation

$$P^{(n,n_s)} = [N!/(N-n_s)!] \int \cdots \int P^{(n,N)} d\mathbf{R}_{ks}{}^{N-n_s}. \tag{7}$$

In particular, $P^{(n,0)} = P^{(n)}(\phi^n)$ describes the probability distribution of the configurations of the polymer in the system, in which the configurations of all of the solvent molecules have been averaged over. Similarly, $P^{(n,1)}(\phi^n; \mathbf{R}_{ks})$ describes the probability distribution of the polymer molecule in a configuration ϕ^n and a solvent molecule at $\mathbf{R}_{ks}$, averaged over the configuration space of all other solvent molecules. The correlation function $g^{(n,1)}(\phi^n; \mathbf{R}_{ks})$ is defined by

$$g^{(n,1)} = P^{(n,1)}/\rho P^{(n)}, \tag{8}$$

where $\rho=N/V$ is the number density of the solvent molecules in the system.

It will be shown presently that the function $W^{(n)}$, defined by

$$-\beta W^{(n)} = \ln P^{(n)}, \tag{9}$$

and the average torque $\tau_k{}^{(n)}$ on the kth bond of the chain, averaged over the solvent configuration space at constant ϕ^n, are related by

$$\tau_k{}^{(n)} = -\partial W^{(n)}/\partial\phi_k, \tag{10}$$

i.e., that $W^{(n)}$ is the potential of the average torque.

Consider the moments of the forces on the two branches of the polymer chain connected by the kth bond, taking the kth bond as an axis. The moment of the lower branch is given by

$$M_1 = -(\partial/\partial\phi_k) V^{(n,N)}(\phi^n; \mathbf{R}_{ks}{}^N), \tag{11}$$

where ϕ_i, $i=1, \cdots, n, \neq k$, and $\mathbf{R}_{ks}{}^N$ are held fixed. Similarly, the moment of the upper branch around the same axis is given by

$$M_2 = (\partial/\partial\phi_k) V^{(n,N)}(\phi^n; \mathbf{R}_{k-1,s}{}^N), \tag{12}$$

where here the coordinate system is fixed in the $(k-1)$th chain element, ϕ_i, $i=1, \cdots, n, \neq k-1$, and $\mathbf{R}_{k-1,s}{}^N$ are held fixed, and the sense of positive rotation is the same as for M_1.

When the angles ϕ^n are held fixed, the effect of the moments is to produce an angular acceleration of the whole chain, given by $(M_1+M_2)/(I_1+I_2)$, where I_1 and I_2 are, respectively, the moments of inertia of the two branches, with the kth bond as an axis. In addition, there is a torque τ_k on the kth bond if ϕ_k is to be held fixed, since otherwise the two branches would experience different angular accelerations. The torque is given by

$$2\tau_k = M_1 - M_2 - [(I_1-I_2)/(I_1+I_2)](M_1+M_2). \tag{13}$$

The angular acceleration of the molecule as a whole, averaged over the solvent configuration space at constant ϕ^n, is evidently zero. Averaging the terms in

[8] See T. L. Hill, *Statistical Mechanics* (McGraw-Hill Book Company, Inc., New York, 1956), Chap. 6.

solvent configuration space, as a function of the internal rotation angles of the chain. The torque on a skeletal bond is affected by both intra-polymer and solvent-polymer interactions. The contribution of the solvent-polymer interaction to the average torque can be related qualitatively to the effect of the rotation around a skeletal bond on the solvation of the polymer molecule in the vicinity of this bond. Quantitatively, it is determined by the average moments of the solvent forces on the two branches of the chain connected by a bond with this bond as an axis of rotation. Each of these average moments would have been zero if it were not for the effect of one branch on the distribution of the solvent molecules in the vicinity of the other branch. This effect, expressed in terms of solvent chain-element distribution functions, determines the statistical weight in calculating the average torque.

In the last section, some general aspects of the theory of neighbor interactions and internal rotations in polymers are discussed. It is indicated that the neighbor-interaction approximation, though insufficient by itself, provides a theoretical basis for the application of the random flight model of polymer molecules and, at the same time, improves upon it by deriving the characteristic parameter of the model, the so-called length of the statistical chain element, as a function of temperature, solvent, and the structural parameters of the polymer chain. Following these considerations, the excluded volume theory of interactions between distant elements should be interpreted as calculating the derivation of the real behavior of polymer chains from their calculated behavior due to interactions between neighbor elements.

II. THE POTENTIAL ENERGY OF NEIGHBOR INTERACTIONS

We consider a system consisting of a single polymer molecule and a large number N of solvent molecules. The polymer molecule is made up of $n+1$ groups, or chain elements, connected by n bonds which form a linear chain. For our present purpose, it is sufficient to consider a polymer molecule of the type $(-CRR'-)_n$. Generalization to more complicated periodic structures does not involve new principles and might be undertaken later, together with numerical computations.

The relative position of the chain elements is determined by the C–C bond lengths b and supplementary bond angles θ, which will be assumed to be fixed, and by the internal rotation angles $\phi_1, \phi_2, \cdots, \phi_n$. ϕ_i is the internal rotation angle of the ith bond connecting the skeletal carbons C_{i-1} and C_i. The bond lengths and bond angles within each element are also assumed to be fixed so that the element can be considered to be a rigid body. In order to complete the specification of the spatial configuration of the polymer molecule, it is necessary to determine the position vector of one of the skeletal carbons, say the vector $\mathbf{R}_k$ of the carbon C_k, and the three Eulerian angles, α, β, and γ, which determine the spatial orientation of the kth chain element with respect to a fixed reference coordinate system chosen arbitrarily. Thus, the configuration of the polymer molecule is completely specified by the $(n+6)$th dimensional vector $R^{n+6}=(\mathbf{R}_k, \alpha, \beta, \gamma, \phi^n)$ with differential volume element $d\mathbf{R}_k \sin\alpha d\alpha d\beta d\gamma d\phi^n$, where ϕ^n and $d\phi^n$ are, respectively, abbreviations for $\phi_1, \phi_2, \cdots, \phi_n$ and $d\phi_1, d\phi_2, \cdots d\phi_n$. It will be noticed that the assumption of fixed bond lengths and bond angles is equivalent to the specification of $5n$ coordinates since the specification of the $n+1$ chain elements as independent, oriented rigid bodies would require $6(n+1)$ coordinates. In fact, each angle of internal rotation ϕ_i may be interpreted as being the Eulerian angle γ_i of the ith chain element, if the coordinate system of this chain element is properly chosen relative to the $(i-1)$th chain element.

Since we are considering a uniform homogeneous system of large dimensions, the position and orientation of the polymer molecule are not of physical interest. Thus, we may fix the coordinate system in one of the chain elements, say the kth one, and consider the configuration of the polymer to be completely specified by ϕ^n. The configurations of the solvent molecules will be represented in the coordinate system fixed in the kth element by three-dimensional position vectors $\mathbf{R}_{ks}$, representing the vector distance of the solvent molecule s from the skeletal carbon C_k, with corresponding volume elements $d\mathbf{R}_{ks}$. We assume that the solvent molecules behave as if they are spherically symmetric, so that their angular orientation can be disregarded. The $3N$-dimensional vector of the solvent configuration space will be denoted by $\mathbf{R}_{ks}^N$ and the corresponding volume element by $d\mathbf{R}_{ks}^N$.

The potential energy $V^{(n,N)}$ of the system will be represented as a sum of pair interactions

$$V^{(n,N)}(\phi^n, \mathbf{R}_{ks}^N) = \sum_{\substack{i<j \\ 0}}^{n} V_{ij} + \sum_{i=0}^{n}\sum_{s=1}^{N} V_{is} + \sum_{\substack{s<t \\ 1}}^{N} V_{st}. \qquad (2)$$

V_{ij} is the intramolecular interaction potential between the ith and the jth polymer chain elements. For near-neighbor elements, i.e., when $j-i$ is small, it is necessary to consider V_{ij} as a function of the relative positions of all the atoms comprising the two chain elements. In this case, $V_{ij}=V_{ij}(\phi_{i+1}, \cdots, \phi_j)$. For elements that are farther apart, the detailed structure of the elements becomes less important, and it is sufficient to approximate V_{ij} by a function of the scalar distance between the skeletal carbons, C_i and C_j. In this case, $V_{ij}=V'_{ij}(\phi_{i+2}, \cdots, \phi_{j-1})$. Limiting our attention to neighbor interactions, it will be assumed that V_{ij} vanishes if it depends on more than m consecutive internal rotation angles. In this approximation, the first double sum in Eq. (2) may be written as a single sum,

$$\sum_{i=1}^{n-m+1} V_i^{(m)}(\phi_i, \cdots, \phi_{i+m-1}),$$

with

$$V_i^{(m)} = \sum_{j=1}^{i+m-1} V_{i-1\ j}(\phi_i, \cdots, \phi_j) + V'_{i-2\ i+m-1} + V'_{i-2\ i+m}. \tag{3}$$

In this way, the mth order approximation takes into account interactions between up to $m+3$ consecutive chain elements. It should be noted that the choice of m is not limited formally, but the computational difficulties increase so rapidly with m, that $m=2$, or at most $m=3$, seems to be the practical limit at present.

V_{is} is the interaction potential between a solvent molecule and a chain element. We shall assume here that V_{is} is a function of the scalar distance, R_{is} between the two. Now R_{is} and, therefore, V_{is} are functions of the vector distance $\mathbf{R}_{ks}$ and the internal rotation angles which determine the position of the ith chain element relative to the origin. Thus, we have

$$V_{is}(R_{is}) = V_{is}(\phi_{i+2}, \cdots, \phi_k; \mathbf{R}_{ks}) \quad i<k \tag{4a}$$

$$V_{is}(R_{is}) = V_{is}(\phi_{k+1}, \cdots, \phi_{i-1}; \mathbf{R}_{ks}) \quad i>k. \tag{4b}$$

As in the case of intramolecular interactions, one may consider a more detailed interaction dependent on the orientation of the ith chain element with respect to the solvent molecule. In this case, V_{is} will also depend on ϕ_{i+1} for $i<k$ and on ϕ_i for $i>k$.

The interaction potential V_{st} between solvent molecules s and t is assumed to be a function of their scalar distance $R_{st}=|\mathbf{R}_{ks}-\mathbf{R}_{kt}|$. It is independent of the internal rotation angles and will be shown not to contribute to the potential of the average torque.

III. DISTRIBUTION FUNCTIONS AND POTENTIALS OF AVERAGE TORQUE

In order to describe the effect of solvent chain-element interactions on the average properties of the polymer, it is useful to introduce the concepts of reduced distribution functions.[8] We consider our system of N solvent molecules and one polymer molecule, with $n+1$ chain elements, confined in a large volume V, to be described by a classical canonical ensemble. The normalized distribution function in the configuration space of N solvent molecules and one polymer molecule is

$$P^{(n,N)} = Z^{-1} \exp[-\beta V^{(n,N)}], \tag{5}$$

where $\beta=1/kT$, and Z, the configurational partition function of the system, is given by

$$Z = \int \cdots \int \exp[-\beta V^{(n,N)}] d\phi^n d\mathbf{R}_{ks}{}^N d\mathbf{R}_k \sin\alpha d\alpha d\beta d\gamma. \tag{6}$$

Reduced generic distribution functions depending on the coordinates of a set of n_s solvent molecules $\mathbf{R}_{ks}{}^{n_s}$ and on the internal rotation angles of the polymer chain ϕ^n are defined by the relation

$$P^{(n,n_s)} = [N!/(N-n_s)!] \int \cdots \int P^{(n,N)} d\mathbf{R}_{ks}{}^{N-n_s}. \tag{7}$$

In particular, $P^{(n,0)} = P^{(n)}(\phi^n)$ describes the probability distribution of the configurations of the polymer in the system, in which the configurations of all of the solvent molecules have been averaged over. Similarly, $P^{(n,1)}(\phi^n; \mathbf{R}_{ks})$ describes the probability distribution of the polymer molecule in a configuration ϕ^n and a solvent molecule at $\mathbf{R}_{ks}$, averaged over the configuration space of all other solvent molecules. The correlation function $g^{(n,1)}(\phi^n; \mathbf{R}_{ks})$ is defined by

$$g^{(n,1)} = P^{(n,1)}/\rho P^{(n)}, \tag{8}$$

where $\rho=N/V$ is the number density of the solvent molecules in the system.

It will be shown presently that the function $W^{(n)}$, defined by

$$-\beta W^{(n)} = \ln P^{(n)}, \tag{9}$$

and the average torque $\tau_k{}^{(n)}$ on the kth bond of the chain, averaged over the solvent configuration space at constant ϕ^n, are related by

$$\tau_k{}^{(n)} = -\partial W^{(n)}/\partial\phi_k, \tag{10}$$

i.e., that $W^{(n)}$ is the potential of the average torque.

Consider the moments of the forces on the two branches of the polymer chain connected by the kth bond, taking the kth bond as an axis. The moment of the lower branch is given by

$$M_1 = -(\partial/\partial\phi_k) V^{(n,N)}(\phi^n; \mathbf{R}_{ks}{}^N), \tag{11}$$

where ϕ_i, $i=1, \cdots, n, \neq k$, and $\mathbf{R}_{ks}{}^N$ are held fixed. Similarly, the moment of the upper branch around the same axis is given by

$$M_2 = (\partial/\partial\phi_k) V^{(n,N)}(\phi^n; \mathbf{R}_{k-1,s}{}^N), \tag{12}$$

where here the coordinate system is fixed in the $(k-1)$th chain element, ϕ_i, $i=1, \cdots, n, \neq k-1$, and $\mathbf{R}_{k-1,s}{}^N$ are held fixed, and the sense of positive rotation is the same as for M_1.

When the angles ϕ^n are held fixed, the effect of the moments is to produce an angular acceleration of the whole chain, given by $(M_1+M_2)/(I_1+I_2)$, where I_1 and I_2 are, respectively, the moments of inertia of the two branches, with the kth bond as an axis. In addition, there is a torque τ_k on the kth bond if ϕ_k is to be held fixed, since otherwise the two branches would experience different angular accelerations. The torque is given by

$$2\tau_k = M_1 - M_2 - [(I_1-I_2)/(I_1+I_2)](M_1+M_2). \tag{13}$$

The angular acceleration of the molecule as a whole, averaged over the solvent configuration space at constant ϕ^n, is evidently zero. Averaging the terms in

[8] T. L. Hill, *Statistical Mechanics* (McGraw-Hill Book Company, Inc., New York, 1956), Chap. 6.

Eq. (13), the corresponding average moments and average torque are seen to be related by

$$\tau_k^{(n)} = M_1^{(n)} = -M_2^{(n)}, \tag{14}$$

where the averages are defined by

$$\tau_k^{(n)} = (1/P^{(n)}) \int \cdots \int P^{(n,N)} \tau_k d\mathbf{R}_{ks}{}^N. \tag{15}$$

Now, making use of Eqs. (5), (9), (11), and (14), we obtain

$$-\frac{\partial W^{(n)}}{\partial \phi_k} = \frac{1}{P^{(n)}} \int \cdots \int P^{(n,N)} \left(-\frac{\partial V^{(n,N)}}{\partial \phi_k} \right) d\mathbf{R}_{ks}{}^N$$

$$= \frac{1}{P^{(n)}} \int \cdots \int P^{(n,N)} M_1 d R_{ks}{}^N$$

$$= \tau_k^{(n)}. \tag{16}$$

Thus, $W^{(n)}$ is, in fact, the potential of the average torque [Eq. (10)].

Introducing $V^{(n,N)}$ of Eq. (2) into Eq. (16), we may write $\tau_k^{(n)}$ as a sum of two contributions, one due to intrapolymer interactions, the other due to solvent polymer interactions. The solvent-solvent interactions do not contribute to the average torque $\tau_k^{(n)}$, since V_{ss} is independent of ϕ_k. Applying Eqs. (7) and (8), $\tau_k^{(n)}$ can be written as

$$\tau_k^{(n)} = -\sum_{i=1}^{k-1} \sum_{j=k}^{n} (\partial V_{ij}/\partial \phi_k) - \rho \sum_{i=1}^{k-2} \int g^{(n,1)} (\partial V_{is}/\partial \phi_k) d\mathbf{R}_{ks}. \tag{17}$$

The second sum contains only $k-2$ terms, since V_{is} is independent of ϕ_k for $i > k-2$, according to Eqs. (4). Each of the integrals in Eq. (17) represents the average moment on the ith chain element due to the solvent, with $\rho g^{(n,1)} dR_{ks}$ being the conditional probability of finding a solvent molecule within a differential volume element $d\mathbf{R}_{ks}$ at $\mathbf{R}_{ks}$, when the polymer is in a configuration ϕ^n.

The integral in Eq. (17) is formally exact for any value of k, $1 \leq k \leq n$. However, it can be simplified considerably. This simplification emphasizes the nature of the solvent polymer interaction contribution to the average torque. We consider the average moment on the lower branch assuming that the chain elements $k+1, \cdots, n$ of the upper branch have been removed. Denoting the polymer-solvent correlation function of this system by $g^{(k,1)}$, we obtain for the average moment, with the kth bond as an axis.

$$M_1^{(k)} = -\rho \sum_{i=1}^{k-2} \int g^{(k,1)} (\partial V_{is}/\partial \phi_k) d\mathbf{R}_{ks} = 0. \tag{18}$$

$M_1^{(k)}$ is zero because it is identical with the total moment on the chain of k bonds. By subtracting Eq. (18) from Eq. (17), we obtain

$$\tau_k^{(n)} = -\sum_{i=1}^{k-1} \sum_{j=k}^{n} (\partial V_{ij}/\partial \phi_k) - \rho \sum_{i=1}^{k-2} \int [g^{(n,1)} - g^{(k,1)}] (\partial V_{is}/\partial \phi_k) d\mathbf{R}_{ks}. \tag{19}$$

The function $g^{(n,1)} - g^{(k,1)}$ vanishes at all points $\mathbf{R}_{ks}$ where the upper branch does not affect the distribution of the solvent molecules. Thus, it is seen clearly that the contribution of the solvent to the average torque is determined by the perturbation of the solvent distribution around one of the branches, caused by the interference of the other branch.

When $\tau_k^{(n)}$ is known as a function of the internal rotation angles, the potential of the average torque can be obtained by computing the work performed against the average torques in twisting all the bonds of the chain, one after the other, from an initial arbitrary state given by $\phi_1^0, \phi_2^0, \cdots, \phi_n^0$ (abbreviated as ϕ^{0n}) to the final state ϕ^n. This work is

$$W^{(n)}(\phi^n) - W^{(n)}(\phi^{0n}) = -\sum_{k=1}^{n} \int_{\phi_k^0}^{\phi_k} \tau_k^{(n)} (\phi_1 \cdots, \phi_{k-1}, \phi_k', \phi_{k+1}^0, \cdots, \phi_n^0) d\phi_k'. \tag{20}$$

In the next section, we shall consider some simplifications necessary for the evaluation of Eq. (19) and Eq. (20), in the neighbor-interaction approximation.

IV. NEIGHBOR-INTERACTION APPROXIMATION

According to Eq. (19), the average torque $\tau_k^{(n)}$ is the sum of two terms. One represents the direct interaction between the two branches of the polymer chain, connected by the kth bond; the other represents the indirect interaction between the two branches through their effect on the solvent distribution. Since both interaction potentials V_{ij} and V_{is} are short ranged, only those chain elements of the two branches which are located near each other in a given configuration ϕ^n contribute significantly to the average torque. In the neighbor-interaction approximation, it is assumed that the main contribution to $\tau_k^{(n)}$ comes from the chain elements in the neighborhood of the kth skeletal bond. Configurations in which chain elements widely separated along the chain happen to be located near each other are assumed to be rare and therefore negligible. The average torque $\tau_k^{(n)}$ is accordingly determined in this approximation as a function of the internal-rotation angle ϕ_k and a limited number of neighboring angles. A neighbor-interaction approximation is considered to be of order m if the *potential* of the average torque can be expressed as a sum of functions, each depending on m consecutive internal-rotation angles. Consequently, the average torque is expressed as a sum of m functions, each dependent on not more than m consecutive internal-rotation angles among the angles

$\phi_{k-m+1}, \cdots, \phi_{k+m-1}$. In order to obtain this form from Eq. (19), terms involving V_{ij} and V_{is} which depend on more than m angles must be neglected. In addition, approximations must be made for $g^{(n,1)}$ and $g^{(k,1)}$. We shall denote the approximate quantities by inserting (m) as a left superscript, e.g., ${}^{(m)}\tau_k^{(n)}$ is the mth order neighbor-interaction approximation of the average torque $\tau_k^{(n)}$.

The intramolecular contribution to ${}^{(m)}\tau_k^{(n)}$ can be written, by Eq. (3), as a sum of m terms, each dependent on m consecutive angles among the $2m-1$ angles $\phi_{k-m+1}, \cdots, \phi_{k+m-1}$

$$ {}^{(m)}\tau_{k,\text{intra}}{}^{(n)} = -\sum_{i=k-m+1}^{k} (\partial/\partial\phi_k) V_i{}^{(m)}(\phi_i, \cdots, \phi_{i+m-1}). \tag{21} $$

Similarly, the solvent contribution reduces to

$$ {}^{(m)}\tau_{k,\text{solv}}{}^{(n)} = \sum_{i=k-m+1}^{k} {}^{(m)}\tau_{ki}{}^{(n)}(\phi_i, \cdots, \phi_{i+m-1}), \tag{22} $$

with

$$ {}^{(m)}\tau_{ki}{}^{(n)} = -\rho \int {}^{(m)}\Delta g^{(n,1)} (\partial V_{i-2,s}/\partial\phi_k) d\mathbf{R}_{ks}, \tag{23} $$

in which ${}^{(m)}\Delta g^{(n,1)}$ is the mth order approximation for $g^{(n,1)} - g^{(k,1)}$ and is assumed to be different from zero only if $\mathbf{R}_{ks}$ is in the vicinity of the kth bond. This vicinity includes, in this approximation, the $2m+2$ chain elements $k-m-1, \cdots, k+m$ whose positions depend on the $2m-1$ angles $\phi_{k-m+1}, \cdots, \phi_{k+m-1}$ according to Eqs. (4). Therefore, we choose ${}^{(m)}\Delta g^{(n,1)}$ as a function of these angles and $\mathbf{R}_{ks}$ at most,

$$ \begin{aligned} {}^{(m)}\Delta g^{(n,1)} &= {}^{(m)}\Delta g^{(n,1)}(R_{k-m-1,s}, \cdots, R_{k+m,s}) \\ &= {}^{(m)}\Delta g^{(n,1)}(\phi_{k-m+1}, \cdots, \phi_{k+m-1}; \mathbf{R}_{ks}) \end{aligned} \tag{24} $$

Another limitation is imposed on ${}^{(m)}\Delta g^{(n,1)}$ by the requirement that ${}^{(m)}\tau_{k,\text{solv}}{}^{(n)}$, like ${}^{(m)}\tau_{k,\text{intra}}{}^{(n)}$, should be a sum of m functions, each dependent on not more than m consecutive angles. This requirement is essential since we wish to obtain the potential of the average torque from ${}^{(m)}\tau_k{}^{(n)}$ through Eq. (20) in the form

$$ \sum_{i=1}^{n-m+1} E^{(m)}(\phi_i, \cdots, \phi_{i+m-1}). $$

To meet these requirements, we introduce for each ${}^{(m)}\tau_{ki}{}^{(n)}$ [Eq. (23)] a function ${}^{(m)}\Delta g_i{}^{(n,1)}(\phi_i, \cdots, \phi_{i+m-1}; \mathbf{R}_{ks})$ defined by

$$ \begin{aligned} {}^{(m)}\Delta g_i{}^{(n,1)} &= {}^{(m)}g_i{}^{(n,1)}(R_{i-2,s}, \cdots, R_{i+m,s}) \\ &\quad - {}^{(k-i+1)}g^{(k,1)}(R_{i-2,s}, \cdots, R_{k,s}) \\ &= {}^{(m)}g_i{}^{(n,1)}(\phi_i, \cdots, \phi_{i+m-1}; \mathbf{R}_{ks}) \\ &\quad - {}^{(k-i+1)}g^{(k,1)}(\phi_i, \cdots, \phi_k; \mathbf{R}_{ks}). \end{aligned} \tag{25} $$

This yields

$$ \begin{aligned} &{}^{(m)}\tau_{ki}{}^{(n)}(\phi_i, \cdots, \phi_{i+m-1}) \\ &= -\rho \int {}^{(m)}\Delta g_i{}^{(n,1)}(\phi_i, \cdots, \phi_{i+m-1}; \mathbf{R}_{ks}) \\ &\quad \times (\partial/\partial\phi_k) V_{i-2,s}(\phi_i, \cdots, \phi_k; \mathbf{R}_{ks}) d\mathbf{R}_{ks}, \end{aligned} \tag{26} $$

as required.

The effects of more chain elements of the set $k-m-1, \cdots, k+m$ on ${}^{(m)}\Delta g^{(n,1)}$ can be retained provided we introduce the superposition approximation.[9] This approximation, though not essential in the formal development of the theory, has the great advantage of making it possible to represent the potential of the average torque in terms of the pair correlation function $g_{js}(R_{js})$ of a solvent molecule s and a chain element j. Let the function $\delta_{js}(R_{js})$ be defined by

$$ \delta_{js}(R_{js}) = g_{js}(R_{js}) - 1. \tag{27} $$

The correlation of a solvent molecule and the chain elements $k+1, \cdots, i+m$ of the upper branch can be expressed in this approximation as

$$ \begin{aligned} g(R_{k+1}, \cdots, R_{i+m}) &= \prod_{j=k+1}^{i+m} (1+\delta_{js}) \\ &= 1 + \sum_j \delta_{js} + \sum_{j'<j} \delta_{j's}\delta_{js} + \cdots + \delta_{k+1,s}\cdots\delta_{i+m,s}, \end{aligned} \tag{28} $$

and the function ${}^{(m)}\Delta g_i{}^{(n,1)}$ takes the form

$$ {}^{(m)}\Delta g_i{}^{(n,1)} = \sum_{j=k+1}^{i+m} \delta_{js}\Big(1 + \sum_{j'<j} \delta_{j's} + \cdots\Big) \prod_{l=j-m-2}^{k} g_{ls}. \tag{29} $$

The product of functions g_{ls} represents the correlation of the chain elements of the lower branch with a solvent molecule. By making the lowest value of l dependent on j, ${}^{(m)}\Delta g_i{}^{(n,1)}$ is expressed as a sum of terms, each dependent on the m consecutive internal rotation angles $\phi_{j-m}, \cdots, \phi_{j-1}$ and can be written as

$$ {}^{(m)}\Delta g_i{}^{(n,1)} = \sum_{j=k-m+1}^{i} {}^{(m)}\Delta g_{ij}{}^{(n,1)}(\phi_j, \cdots \phi_{j+m-1}; \mathbf{R}_{ks}). \tag{30} $$

Introducing Eq. (30) into Eqs. (23) and (22) and changing the order of summation, we obtain

$$ {}^{(m)}\tau_{k,\text{solv}}{}^{(n)} = \sum_{j=k-m+1}^{k} {}^{(m)}\tau_{kj}{}^{(n)}(\phi_j, \cdots, \phi_{j+m-1}), \tag{31} $$

with

$$ \begin{aligned} {}^{(m)}\tau_{kj}{}^{(n)} &= -\rho \sum_{i=j}^{k} \int {}^{(m)}\Delta g_{ij}{}^{(n,1)}(\phi_j, \cdots, \phi_{j+m-1}; \mathbf{R}_{ks}) \\ &\quad \times (\partial/\partial\phi_k) V_{i-2,s}(\phi_i, \cdots, \phi_k; \mathbf{R}_{ks}) d\mathbf{R}_{ks}. \end{aligned} \tag{32} $$

Equation (32) meets the requirements of the mth order approximation and, at the same time, contains a sig-

[9] J. G. Kirkwood, J. Chem. Phys. 3, 300 (1935).

nificantly higher correlation than that represented in Eq. (26).

We consider now the neighbor-interaction approximation of the potential of the average torque. Introducing Eq. (22) with either Eq. (26) or Eq. (32) into Eq. (20) and using Eq. (3) for the intramolecular potential, we have

$$W^{(n)}(\phi^n)=\sum_{i=1}^{n-m+1}V_i^{(m)}+\sum_{k=m}^{n}\sum_{i=k-m+1}^{k}\int {}^{(m)}\tau_{ki}^{(n)}\times(\phi_i,\cdots,\phi_k';\phi_{k+1}^0,\cdots,\phi_{i+m-1}^0)\,d\phi_k'+\text{constant}$$

$$=\sum_{i=1}^{n-m+1}V_i^{(m)}+\sum_{i=1}^{n-m+1}\sum_{k=1}^{i+m-1}\int {}^{(m)}\tau_{ki}^{(n)}\times(\phi_i,\cdots,\phi_k';\phi_{k+1}^0,\cdots,\phi_{i+m-1}^0)\,d\phi_k'+\text{constant}, \quad (33)$$

where a few terms pertaining to the ends of the chain have been neglected. Thus the potential of average torque is obtained in this approximation as a sum of functions of m consecutive angles

$$W^{(n)}(\phi^n)=\sum_{i=1}^{n-m+1}E_i^{(m)}(\phi_i,\cdots,\phi_{i+m-1})+\text{constant}, \quad (34)$$

with

$$E_i^{(m)}(\phi_i,\cdots,\phi_{i+m-1})=V_i^{(m)}+\sum_{k=1}^{i+m-1}\int {}^{(m)}\tau_{ki}^{(n)}\times(\phi_i,\cdots,\phi_k';\phi_{k+1}^0,\cdots,\phi_{i+m-1}^0)\,d\phi_k'. \quad (35)$$

By deriving the potential of the average torque in the form of Eq. (34), we arrive, in fact, at the starting point of the theory of neighbor interactions as hitherto developed in the previous papers of this series[4,5] and by other authors.[2,3,6] The energy E was introduced in the introduction [Eq. (1)], in correspondence with previous work, as the energy of the polymer chain. However, considering the polymer chain and the solvent as one system, a comparison of Eqs. (1) and (34) shows that E actually is the potential of the average torque $W^{(n)}$ in the mth order approximation. Introducing $W^{(n)}$ from Eq. (34) into Eqs. (9) and (6), the partition function of the system, as well as the mean square end-to-end distance are derived, to this approximation, by the matrix methods described previously.[5,6]

V. RELATION TO OTHER THEORIES

In conclusion we should like to make a few general comments on the theory of neighbor interactions and its place with respect to other theories of polymers, particularly those dealing specifically with nonneighbor interactions such as the theories of excluded volume and the second virial coefficient of polymer solutions.

Most theories of polymer solutions introduce the statistical segment as an adaptable parameter in the *random chain* model in which the actual chain, composed of $n+1$ groups of chain elements connected by n bonds of length b with fixed bond angles and restricted rotation, is replaced by a model of n statistical segments of length a connected by joints of completely free rotation.[10] The statistical segment length a is so chosen that the mean square end-to-end distance $\langle h^2\rangle$ is given by

$$\langle h^2\rangle=na^2. \quad (36)$$

The parameter a characterizes the Gaussian distribution of the configurations of the chain.

The Gaussian distribution is not limited, however, to completely random chains, but also applies to systems in which there are interactions between a limited number of neighboring elements. Thus, real polymer molecules, in the approximation in which interactions between distant chain elements are neglected, exhibit a Gaussian distribution in the limit of large n[11,12]. Therefore, $\langle h^2\rangle$ of the real molecule may be written, in this approximation, as

$$\langle h^2\rangle=snb^2. \quad (37)$$

The proportionality factor s might be termed the *stiffness* parameter of the polymer molecule and is related to the statistical segment length of the random flight model by

$$a^2=sb^2. \quad (38)$$

The main result of the theory of neighbor interactions and internal rotations in polymer molecules is the determination of the value of s by statistical-mechanical considerations, as a function of bond lengths, bond angles, constants of intramolecular neighbor-interaction potentials, solvent-polymer interactions, and temperature. The theory of neighbor interactions cannot provide by itself a satisfactory solution to the problem of polymer dimensions, since, by its very nature, it must neglect interactions between widely separated chain elements. These long-range interactions are now well known to be nonnegligible, giving rise to the so-called excluded volume effect[11,13,14] which demonstrates a non-Gaussian behavior of the polymer chain. However, the theory of neighbor interaction might advantageously replace the random flight model as the starting point from which practically all theories of interaction between widely separated chain elements proceed. Such a coupling of the theories of "short-range" and "long-range" interactions is not only interesting from the statistical-mechanical point of view, but is of direct consequence in the application of the theories of excluded volume and the second virial

[10] The number of segments is sometimes taken as n' proportional to n, in which case a is replaced by a' to fit Eq. (36). In this way, it is possible to make the model conform with an additional requirement, say, that $n'a'=nb$, as suggested by W. Kuhn.

[11] B. H. Zimm, W. H. Stockmayer and M. Fixman, J. Chem. Phys. **21**, 1716 (1953).

[12] C. M. Tchen, J. Chem. Phys. **20**, 214 (1952).

[13] P. J. Flory, *Principles of Polymer Chemistry* (Cornell University Press, 1953).

[14] For a critical review and references to recent work on the excluded volume effect and the second virial coefficient, see W. H. Stockmayer, International Symposium on Macromolecules, Wiesbaden, October, 1959; and Makromol. Chem. **35**, 54 (1960).

coefficient. It indicates that the "unperturbed dimensions" or the length of the statistical segment, related to the stiffness parameter by Eqs. (37) and (38), must be considered as functions of temperature and dependent on solvent.

ACKNOWLEDGMENT

One of the authors (S. L.) wishes to thank Professor P. Doty for his kind hospitality at the Department of Chemistry, Harvard University, during a period in which a portion of this work was performed.

THE JOURNAL OF CHEMICAL PHYSICS VOLUME 33, NUMBER 1 JULY, 1960

Theory of Singlet-Triplet Splittings in Large Biradicals*

HARDEN M. MCCONNELL†

Gates and Crellin Laboratories of Chemistry,‡ California Institute of Technology, Pasadena 4, California

(Received January 25, 1960)

A perturbation calculation is used to estimate small ground-state singlet-triplet splittings in large biradicals in which two triphenylmethyl groups are bridged at para positions by polyene, polyphenylene, polymethylene, or ether groups. The calculated splittings are orders of magnitude larger than the rates of spin exchange reported by Reitz and Weissman for some of these biradicals.

INTRODUCTION

JARRETT, Sloan, and Vaughan[1] have observed paramagnetic resonance in a number of biradicals with the general formula shown in Fig. 1, where the bridging group X is polymethylene $(-CH_2-)_n$, polyphenylene, and ether $(-O-)$. The sharpness of the observed paramagnetic resonance spectra in liquid solution at room temperature indicates that there is comparatively little dipolar interaction between "the two" unpaired electrons. This result suggests the qualitative notion that these biradicals may be regarded as two weakly interacting triphenylmethyl (TPM) monoradicals. In fact, the observability of paramagnetic resonance in these molecules supports this idea of weakly interacting TPM groups; otherwise, one would expect at least some of these molecules to be diamagnetic. The observed paramagnetism shows that if the lowest electronic state is indeed a singlet in some of the molecules, the singlet and first-excited triplet state cannot be separated by an energy that is very much larger than kT at room temperature.

More recently, Reitz and Weissman[2] have reported the observation of paramagnetic resonance of 4,4′-oxybistriphenylmethyl (corresponding to $X=-O-$ in the above formula) with C^{13} substitution at the central atoms of the TPM groups. The observed C^{13}-hyperfine structure appears to be that of two isolated monoradicals (spin $S=\frac{1}{2}$ for each) rather than a single molecule with strongly coupled spins ($S=1$). These results imply that the rate of spin exchange between the two halves of this molecule is slow compared to the observed C^{13}-hyperfine splittings, $\Delta\nu$, which are of the order of 100 Mc. Similar results have been found[3] when the bridging group X is dimethylene $(-CH_2-)_2$. One possible interpretation of this slow rate of spin exchange is that the paramagnetic triplet state is nearly degenerate with an electronic singlet state. That is, if the singlet-triplet separation $\Delta U/h$ is less than the C^{13}-hyperfine splitting $\Delta\nu$, then the calculated paramagnetic resonance spectrum is that of two "noninteracting" monoradicals. The purpose of the present paper is to make theoretical order-of-magnitude estimates of ΔU for TPM biradicals so as to ascertain whether or not $\Delta U/h$ could possibly be less than the hyperfine interaction $\Delta\nu$. Theoretical estimates of singlet-triplet splittings in large molecules have been made previously by Diatkina and Syrkin[4] and by Jarrett, Sloan, and Vaughan[1] using Hückel molecular-orbital theory without configuration interaction for the π electrons. Since,

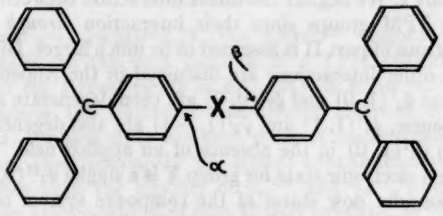

FIG. 1. General formula for biradical.

* Sponsored by the National Science Foundation, the Office of Ordnance Research, U. S. Army, and by the U. S. Public Health Service.

† Alfred P. Sloan Fellow.

‡ Contribution No. 2552.

[1] H. S. Jarrett, G. J. Sloan, and W. R. Vaughan, J. Chem. Phys. **25**, 697 (1956).

[2] D. C. Reitz and S. I. Weissman, J. Chem. Phys. **27**, 968 (1957).

[3] S. I. Weissman (private communication).

[4] M. Diatkina and J. Syrkin, Acta Physicochim. U.R.S.S. **25**, 23 (1946).

however, one is here concerned with the estimation of an exceedingly small molecular-electronic energy separation, an *a priori* calculation with elementary valence-bond theory, or molecular-orbital theory, could hardly be expected to be reliable. Such calculations typically involve errors in the energy of an electronic state of the order of an electron volt, and the error in the calculated ΔU could easily be of the same order. We must estimate singlet-triplet splittings that cannot be much more than kT at room temperature (10^{-2} ev) but which may be as small as 10^{-7} ev. Therefore, we use a perturbation procedure designed to estimate ΔU directly and to avoid any direct calculation of the individual energies of the singlet and triplet states.

PERTURBATION CALCULATION

In this calculation, we assume a fixed nuclear framework. We assume further that the two TPM groups *do interact only weakly* so that the spin distribution in each is at least qualitatively similar to the known[5,6] spin distribution in the TPM radical itself. We estimate the singlet-triplet splitting that *must* then be present if no other strong interactions (e.g., charge-transfer resonance) are assumed. These other "strong interactions," if they do contribute at all to ΔU, must almost certainly tend to increase $|\Delta U|$ for those biradicals with singlet ground states.

Let the biradical be divided into two parts. Part I consists of the two TPM groups, and part II is the bridging group X. We need consider explicitly only the π electrons in part I and let N_{I} represent the number of these electrons. $N_{\mathrm{I}}=38$. In the calculation, N_{II} electrons in part II are considered. These electrons may be entirely π electrons, as in the case of our calculation for the ethylene and phenylene bridges; but, for the ether and methylene bridges, it is absolutely necessary to include σ electrons among the N_{II} electrons in part II. Approximate eigenfunctions for the N_{I} electrons in group I and the N_{II} electrons in group II are designated $\psi_i^{\mathrm{I}}(S^{\mathrm{I}}, S_s^{\mathrm{I}})$ and $\psi_j^{\mathrm{II}}(S^{\mathrm{II}}, S_s^{\mathrm{II}})$. These functions are individually normalized and antisymmetric. The corresponding zero-order energies are E_i^{I} and E_j^{II}. There is no degeneracy of the *ground* electronic states of parts I and II except for the singlet-triplet degeneracy of part I. We neglect the direct interaction between the two TPM groups since their interaction *through* the electrons of part II is assumed to be much larger. Direct first-order interactions are discussed in the Appendix. States $\psi_1^{\mathrm{I}}(1, 0)$ and $\psi_1^{\mathrm{I}}(0, 0)$ are then degenerate and, of course, $\psi_1^{\mathrm{I}}(1, 1)$ and $\psi_1^{\mathrm{I}}(1, -1)$ are also degenerate with $\psi_1^{\mathrm{I}}(1, 0)$ in the absence of an applied field. The lowest electronic state for group X is a singlet $\psi_1^{\mathrm{II}}(0, 0)$.

Consider now states of the composite system of N electrons that are antisymmetric in all of the electrons and that are eigenfunctions of $\mathbf{S}^2$ and S_z where

$$\mathbf{S}=\mathbf{S}^{\mathrm{I}}+\mathbf{S}^{\mathrm{II}}. \tag{1}$$

Without loss of generality, the discussion is limited to states for which $S_z=0$. Normalized, antisymmetric, approximate ground triplet- and singlet-state wave functions for the entire system then are:

$$\Psi_{11}^0(1, 0)=\mathbf{A}\psi_1^{\mathrm{I}}(1, 0)\psi_1^{\mathrm{II}}(0, 0), \tag{2}$$

$$\Psi_{11}^0(0, 0)=\mathbf{A}\psi_1^{\mathrm{I}}(0, 0)\psi_1^{\mathrm{II}}(0, 0). \tag{3}$$

Here $\mathbf{A}$ is the antisymmetrizer, and, if we assume for simplicity that ψ_i^{I} and ψ_j^{II} are orthogonal with respect to the permutation of an electron in I with an electron in II, then $\mathbf{A}$ is simply

$$\mathbf{A}=[(N!N_{\mathrm{I}}!N_{\mathrm{II}}!)^{\frac{1}{2}}]^{-1}\sum_{r=1}^{N!}\delta_r P_r, \tag{4}$$

where P_r is one of the $N!$ permutation operators for N objects, $\delta_r=1$ for an even permutation, and $\delta_r=-1$ for an odd permutation. Later, however, we must consider problems where ψ_i^{I} and ψ_j^{II} are definitely not orthogonal with respect to this twofold permutation. The zero-order functions for the entire system $\Psi_{ij}^0(S, S_z)$ have energy $E_i^{\mathrm{I}}+E_j^{\mathrm{II}}$. The two lowest states $\Psi_{11}^0(1, 0)$ and $\Psi_{11}^0(0, 0)$ are then degenerate in this approximation. The degeneracy of these states is removed by interaction with the higher-energy states $\Psi_{ij}^0(S, S_z)$. We do not consider excited charge-transfer states in which charge is transferred between X and a TPM group, or between TPM groups. Such interactions could hardly do anything but increase $|\Delta U|$ for biradicals with singlet ground states, since the lowest electronic states of the positive and negative ions of TPM are known to be singlets. Our calculations are further simplified by the fact that the excited states we consider are four or more electron volts above the ground state of the composite system, and the excited state contributions can be treated by elementary perturbation theory. Excitation of the electrons in group X gives rise to a set of excited states of the total system of the form $\Psi_{1i}^0(1, 0)$ and $\Psi_{1i}^0(0, 0)$, and the interaction (or "mixing") of these states with the ground states removes the singlet-triplet degeneracy. The zero-order excited states $\Psi_{1i}^0(1, 0)$ are of two types, designated $\bar{\Psi}_{1j}^0(1, 0)$ and $\tilde{\Psi}_{1k}^0(1, 0)$. The $\bar{\Psi}_{1j}^0(1, 0)$ states are

$$\bar{\Psi}_{1j}^0(1, 0)=\mathbf{A}\psi_1^{\mathrm{I}}(1, 0)\psi_j^{\mathrm{II}}(0, 0) \tag{5}$$

and correspond to the simple excitation of part II: $\psi_1^{\mathrm{II}}(0, 0)\rightarrow\psi_j^{\mathrm{II}}(0, 0)$. States designated $\tilde{\Psi}_{1k}^0(1, 0)$ are called "mixed" since, for these states, the electrons of part II make a finite contribution to the total spin S of the biradical:

$$\tilde{\Psi}_{1k}^0(1, 0)=\mathbf{A}\psi_1^{\mathrm{I}}(0, 0)\psi_k^{\mathrm{II}}(1, 0) \tag{6a}$$

$$\tilde{\Psi}_{1k}^{0\prime}(1, 0)=\mathbf{A}(1/\sqrt{2})[\psi_1^{\mathrm{I}}(1, -1)\psi_k^{\mathrm{II}}(1, 1)-\psi_1^{\mathrm{I}}(1, 1)\psi_k^{\mathrm{II}}(1, -1)]. \tag{6b}$$

[5] P. Brovetto and S. Ferroni, Nuovo cimento **5**, 142 (1957).
[6] F. C. Adam and S. I. Weissman, J. Am. Chem. Soc. **80**, 2057 (1958).

The excited states $\Psi_{1i}{}^0(0, 0)$ are also of two types. States designated $\bar{\Psi}_{1i}{}^0(0, 0)$ are simply

$$\bar{\Psi}_{1i}{}^0(0, 0) = A\psi_1{}^{\mathrm{I}}(0, 0)\psi_i{}^{\mathrm{II}}(0, 0). \quad (7)$$

The "mixed" excited states $\tilde{\Psi}_{1m}{}^0(0, 0)$ are linear combinations of product functions

$$\tilde{\Psi}_{1m}{}^0(0, 0) = (1/\sqrt{3})[\psi_1{}^{\mathrm{I}}(1, 1)\psi_m{}^{\mathrm{II}}(1, -1) + \psi_1{}^{\mathrm{I}}(1, -1)\psi_m{}^{\mathrm{II}}(1, 1) - \psi_1{}^{\mathrm{I}}(1, 0)\psi_m{}^{\mathrm{II}}(1, 0)]. \quad (8)$$

This state is mixed in the sense that the electrons of part II are excited and make a finite contribution to the total spin of the state (zero, in this case). Quartet electronic states of part II can combine with the triplet state of part I to form a composite triplet state. However, in second order, this triplet state does not mix with the ground triplet state $\Psi_{11}{}^0(1, 0)$ and so is not considered further. The energies of the lowest electronic states with $S_z=0$ are then, to second order,

$$E_{11}(1, 0) = [\Psi_{11}{}^0(1, 0) \mid \mathcal{H} \mid \Psi_{11}{}^0(1, 0)] - \sum_i |[(\Psi_{1i}{}^0(1, 0) \mid \mathcal{H} \mid \Psi_{11}{}^0(1, 0)]|^2 \Delta E_{1i}{}^{-1} \quad (9)$$

$$E_{11}(0, 0) = [\Psi_{11}{}^0(0, 0) \mid \mathcal{H} \mid \Psi_{11}{}^0(0, 0)] - \sum_j |[\Psi_{1j}{}^0(0, 0) \mid \mathcal{H} \mid \Psi_{11}{}^0(0, 0)]|^2 \Delta E_{1j}{}^{-1}, \quad (10)$$

where

$$\Delta E_{1i} = E_i{}^{\mathrm{II}} - E_1{}^{\mathrm{II}}.$$

The triplet-singlet energy splitting is then

$$\Delta U = E_{11}(1, 0) - E_{11}(0, 0). \quad (11)$$

In calculating this energy difference from the two perturbation formulas in Eqs. (9) and (10), it is found that the two first-order energy terms

$$[\Psi_{11}{}^0(1, 0) \mid \mathcal{H} \mid \Psi_{11}{}^0(1, 0)]$$

and

$$[\Psi_{11}{}^0(0, 0) \mid \mathcal{H} \mid \Psi_{11}{}^0(0, 0)]$$

cancel one another as long as one neglects the direct interaction of the two TPM groups. One also finds that, although the excited states $\Psi_{1j}{}^0$ can make large contributions to the second-order terms in Eqs. (9) and (10), these states make no contribution to ΔU. Only the "mixed" states contribute to ΔU. It is convenient to express this energy difference in terms of atomic orbital spin-density matrices[7] $\rho_{\lambda\mu}{}^A$ and $\rho_{\omega\nu}{}^B$ of the two separate TPM groups (A and B) that constitute part I and also in terms of an atomic orbital transition spin-density matrix of part II, $\gamma_{rs}{}^{lk}$, defined below:

$$N_{\mathrm{I}}[\psi_1{}^{\mathrm{I}}(1, 1) \mid S_{ms}{}^{\mathrm{I}} \mid \psi_1{}^{\mathrm{I}}(1, 1)]' = \tfrac{1}{2}\sum_{\lambda\mu}\rho_{\lambda\mu}{}^A\phi_\mu{}^{A*}(r')\phi_\lambda{}^A(r) + \tfrac{1}{2}\sum_{\omega\nu}\rho_{\omega\nu}{}^B\phi_\nu{}^{B*}(r')\phi_\omega{}^B(r) \quad (12)$$

$$N_{\mathrm{II}}[\psi_1{}^{\mathrm{II}}(0, 0) \mid S_{ms}{}^{\mathrm{II}} \mid \psi_k{}^{\mathrm{II}}(1, 0)]' = \sum_{rs}\gamma_{rs}{}^{lk}\phi_s{}^*(r')\phi_r(r). \quad (13)$$

The prime on the matrix element on the left-hand side of Eq. (12) indicates that (a) the integration is to be carried out over the variables of all electrons, except for the space variables of electron n and that (b), before the integration is carried out, the space variables of electron n are primed ($r_n \rightarrow r'$) in $[\psi_1{}^{\mathrm{I}}(1, 1)|$. The atomic orbitals $\phi_\mu{}^A$, $\phi_\omega{}^B$, ϕ_r are centered on TPM group A, TPM group B, and on part II, respectively. The matrix element in Eq. (13) is developed in the same way. In terms of these quantities, it is a straightforward but not trivial calculation to show that the triplet-singlet splitting is

$$\Delta U = -4\sum_{k\lambda\mu rs\omega\nu tu}\Delta E_k{}^{-1}\rho_{\lambda\mu}{}^{A*}\gamma_{rs}{}^{k1*}J_{\mu sr\lambda}{}^*\rho_{\omega\nu}{}^B\gamma_{tu}{}^{k1}J_{ru\,t\omega} + \text{complex conjugate.} \quad (14)$$

Here

$$J_{\mu sr\lambda} = [\phi_\mu{}^{A*}(r_m)\phi_s{}^*(r_n) \mid e^2/r_{mn} \mid \phi_r(r_m)\phi_\lambda{}^A(r_n)]. \quad (15)$$

Usually, there is little difficulty in finding the largest terms in Eq. (14). Without any doubt, the π orbitals of the TPM groups that contribute most significantly to Eq. (14) are $\phi_\alpha{}^A$ and $\phi_\beta{}^B$, the atomic π orbitals of the TPM groups A and B that are centered on para carbon atoms α and β (see Fig. 1) which are directly bonded to the bridging group X. The largest contribution to ΔU for any of the groups X under considertaion is then

$$\Delta U = -4\rho^2\sum_{krstu}\Delta E_k{}^{-1}\gamma_{rs}{}^{k1*}J_{\alpha sr\alpha}\gamma_{tu}{}^{k1}J_{\beta u t\beta} + \text{complex conjugate.} \quad (16)$$

Here $\rho=\rho_{\alpha\alpha}=\rho_{\beta\beta}=0.18$, the known[5,6] diagonal spin density on the para position of a TPM radical. To find the largest terms in Eq. (16), it is necessary to examine the transition spin-density matrices of Eq. (13) for each state k of each group X under consideration. Most commonly the largest contribution to ΔU arises from the product of $\gamma_{aa}{}^{k1*}$ and $\gamma_{bb}{}^{k1}$, where ϕ_a is an atomic orbital of part II that overlaps, or "interacts" most strongly with $\phi_\alpha{}^A$, and ϕ_b is the corresponding atomic orbital of part II that overlaps or interacts most strongly with $\phi_\beta{}^B$. If X is a symmetrical group, so that $|\gamma_{aa}{}^{k1}| = |\gamma_{bb}{}^{k1}|$ and $J=J_{\alpha a a\alpha}=J_{\beta b b\beta}$,

[7] H. M. McConnell, J. Chem. Phys. 28, 1188 (1958).

then this important contribution to ΔU can be written

$$\Delta U = -4\rho^2 J^2 \sum_k \Gamma_k \Delta E_k^{-1} \tag{17a}$$

$$\Gamma_k = \gamma_{aa}^{k1*}\gamma_{bb}^{k1} + \gamma_{aa}^{k1}\gamma_{bb}^{k1*} \tag{17b}$$

However, for certain problems, Eq. (17) may not be applicable in that the largest contribution can arise from a pair of orbitals of II, say p and p', each of which interacts equally strongly with ϕ_a^A and ϕ_β^B. This case, in which the principal contribution is proportional to the factor $|\gamma_{pp'}^{k1}|^2$, is illustrated in the subsequent discussion of the ether bridge. However, the problems covered by Eq. (17) are the more common, and we shall discuss this mechanism for the triplet-singlet splitting in some detail.

The quantity Γ_k defined in Eq. (17b) can be either positive or negative, depending upon the nature of the electronic state k of the bridging group. In applying Eq. (17) to the estimation of triplet-singlet splittings in the biradicals, we shall use elementary electronic-structure theories to estimate the order-of-magnitude of the Γ_k's and shall use experimental data for the excitation energies ΔE_k. This is the goal we have sought—nowhere do we require a highly accurate electronic wave function to make the necessary calculations.

APPLICATIONS

In general, one is interested in bridging groups X that are composed of a number of subgroups. Practical examples are polymethylene groups $-(CH_2)_n-$, poly-paraphenylene groups

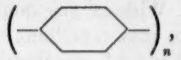

and polymetaphenylene groups

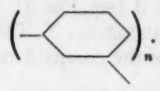

First, however, it will be convenient to treat the bridging effects of the individual subgroups.

σ-Electron Bond

Suppose two TPM groups are directly coupled by a single σ-electron bond between TPM carbon atoms α of A and β of B. Of course, the direct π-electron interaction completely dominates the triplet-singlet splitting ΔU in this case, but we nonetheless shall consider the σ-electron contribution to ΔU, designated ΔU^σ. (This direct π-electron interaction is discussed in the Appendix.) Here group X, or part II, is the two-σ-electron bond system, described approximately by orbitals built up from ϕ_a centered on carbon atom α and ϕ_b centered on β. The two σ orbitals are, say, sp^2 hybrids and are directed toward one another. The simple valence-bond approximation for the bonding singlet and antibonding triplet is

$$\psi_1^{II}(0,0) = \tfrac{1}{2}[1/(1+S^2)^{\frac{1}{2}}][\phi_a(1)\phi_b(2)+\phi_b(1)\phi_a(2)] \times [\alpha(1)\beta(2)-\beta(1)\alpha(2)] \tag{18}$$

$$\psi_1^{II}(1,0) = \tfrac{1}{2}[1/(1-S^2)^{\frac{1}{2}}][\phi_a(1)\phi_b(2)-\phi_b(1)\phi_a(2)] \times [\alpha(1)\beta(2)+\beta(1)\alpha(2)]. \tag{19}$$

Thus, $\gamma_{aa}^{1k} = -\gamma_{bb}^{1k} = 0.5(1-S^4)^{-\frac{1}{2}}$, and the σ-electron contribution to the triplet-singlet splitting tends to place the singlet state of the biradical lowest, as follows:

$$\Delta U^\sigma = [2\rho^2 J^2/(1-S^4)\Delta E_\sigma]. \tag{20}$$

S is the overlap integral, and ΔE_σ is the singlet-triplet excitation energy. Of course, other triplet states could contribute but, in general, the other states will tend to be of less importance because of the higher excitation energies and lower Γ_k values. For this problem, J is of the order of 1 ev,[8] and ΔE_σ is of the order of 10 ev.[9] Thus, ΔU^σ is of the order of 10^{-2} ev, or 100 cm^{-1}. This splitting does not depend upon the angle of twist of one TPM group relative to the other.

Ethylene π-Electron Bridge

The bridging of two TPM groups by an ethylene group $-C=C-$ cannot be discussed without making some modifications in the basic Eqs. (14) to (17). This is because for the π-electron bridge—in contrast to a σ-electron bridge—the interacting atomic π orbitals of part II (ϕ_a and ϕ_b) are not orthogonal to the neighboring π orbitals of TPM groups A and B, i.e., ϕ_α^A and ϕ_β^B. This means that ψ_i^I and ψ_j^{II} are not orthogonal with respect to twofold (and higher) permutations, as was assumed earlier. Thus, the normalization factor in Eq. (4) is no longer correct, and various terms in $\mathcal{H}$ in addition to the e^2/r_{ij} terms now contribute to the triplet-singlet splitting. For an order-of-magnitude calculation, we adopt the program of the semiempirical valence-bond theory as far as the interaction of parts I and II are concerned. All terms contributing to the nondiagonal matrix elements of $\mathcal{H}$ that arise from multiple permutations of electrons in part I with electrons in part II are neglected, and overlap is omitted in the normalization of Eq. (4). With this approximation Eq. (17a) becomes

$$\Delta U = -4\rho^2\alpha^2 \sum_k \Gamma_k \Delta E_k^{-1}, \tag{21}$$

where α is the valence bond "resonance integral"

$$\alpha = [\phi_\alpha^{A*}(r_m)\phi_a^*(r_n) \,|\, \mathcal{H} \,|\, \phi_a(r_m)\phi_\alpha^A(r_n)], \tag{22}$$

which has the semiempirical value -1.6 ev.

[8] H. M. McConnell and D. B. Chesnut, J. Chem. Phys. **28**, 10 (1958).
[9] S. Aono, Prog. Theoret. Phys. (Kyoto) **21**, 779 (1959).

The first excited π-electron triplet state of ethylene with energy ΔE_π doubtless makes the largest contribution to the triplet-singlet splitting.

$$\Delta U^\pi=[2\rho^2\alpha^2/(1-S^4)\Delta E]. \quad (23)$$

The result in Eq. (23) is obtained by using a valence-bond theory for the two π electrons of ethylene to estimate Γ_k [cf. Eqs. (18)–(20)]. The simple molecular-orbital approximation for the two π electrons yields a similar result. Although the lowest π-electron triplet state of ethylene has not yet been observed experimentally, its energy is certainly within a few thousand wave numbers of the known ^1B excited state. Therefore, $\Delta E_\pi=5$–6 ev and $\Delta U\sim 0.04$ ev or ~ 300 cm^{-1}, and the singlet state is lowest.

Phenylene π-Electron Bridge

Here again the lowest-energy π-electron triplet states doubtless make the largest contribution to ΔU, and, therefore, we consider only the electronic states of benzene that arise from the lowest-energy, singly excited, molecular-orbital configuration. These states are $^3B_{1u}$, $^3B_{2u}$, and $^3E_{1u}$. The molecular-orbital functions of Goeppert-Meyer and Sklar[10] lead to the Γ_k values given in Table I.

In Table I, the plus and minus signs following $^3E_{1u}$ refer to the two degenerate components of this doubly degenerate state. Also listed in Table I are the corresponding values of ΔU calculated from Eq. (21), taking $\alpha=-1.6$ ev, $\rho=0.18$, the values of Γ_k listed in Table I, together with the best available information[11] on the energies of these states: $\Delta E(^3B_{1u})=3.59$ ev, $\Delta E(^3E_{1u})=4.14$ ev. Note that the meta bridging places the triplet state lowest, whereas the ortho and para bridging place the singlet state lowest.

Ether Bridge

This group presents a special problem in that one can distinguish at least three interactions that can contribute to ΔU. The pure σ-electron contribution is considered later. The charge-transfer triplet state might also make a contribution. However, we consider for the present only a pure π-electron triplet state which makes a significant contribution to ΔU. Let the ground state π-electron configurational function for the two π-electrons of the oxygen atom be

$$\psi_1^{II}(0,0)=(1/\sqrt{2})p(1)p(2)(\alpha\beta-\beta\alpha). \quad (24)$$

Let p' be an excited $3p$ atomic orbital of oxygen, and consider the triplet state,

$$\psi_1^{II}(1,0)=\tfrac{1}{2}[p(1)p'(2)-p'(1)p(2)](\alpha\beta+\beta\alpha). \quad (25)$$

[10] M. Goeppert-Meyer and A. L. Sklar, J. Chem. Phys. **6**, 645 (1938).

[11] R. Pariser, J. Chem. Phys. **24**, 250 (1956).

TABLE I. Values of Γ_k for phenylene bridging.

State	Ortho	Meta	Para
$^3B_{1u}$	$-1/18$	$1/18$	$-1/18$
$^3B_{2u}$	0	0	0
$^3E_{1u}(+)$	$1/72$	$-1/72$	$-1/36$
$^3E_{1u}(-)$	$1/72$	$-1/72$	$-1/36$
ΔU	$+0.0029$ ev	-0.0029 ev	$+0.0074$ ev

For these functions, we have a transition spin-density matrix $\gamma_{pp'}{}^{11}$ which is

$$\gamma_{pp'}{}^{11}=-1/\sqrt{2}. \quad (26)$$

From Eq. (14), we readily see that *this state* makes the following contribution to ΔU:

$$\Delta U^\pi=-4\rho^2K_{app'a}{}^2/\Delta E. \quad (27)$$

Here

$$K_{app'a}=[\phi_a{}^{A*}(i)p^*(j)\,|\,\mathcal{H}\,|\,p'(i)\phi_a{}^A(j)]. \quad (28)$$

Note that this interaction puts the triplet state lowest. It is probable that this splitting is of the same order as that estimated above for ethylene. Note also that the CH bonding electrons in a CH_2 bridging group can be treated in just this same fashion. If one were to approximate the transition spin-density matrix for the CH bond with molecular-orbital theory, then p in Eq. (24) could be taken to be the bonding orbital and p' in Eq. (25) the antibonding orbital. Equation (26) would then be applicable, except for the overlap correaction.

The Chain Bridge

Let us now consider a bridging group X that is built up from a number of subgroups so as to form a chain. Examples are the polymethylene and polyphenylene systems. Let the subgroups be designated x_1, x_2, $\cdots$, x_r, $\cdots x_N$. For example, in the case of polymethylene $-(CH_2)_n-$, we shall consider $N=n+1$ carbon-carbon single bonds. In the case of the polyphenylene system, we consider N benzene rings joined all meta, or all para to one another. The problem is then to evaluate the summation in Eq. (16), bearing in mind that each triplet state of the subgroup becomes N triplet states of the chain. Let $\omega_r{}^k$ be a wave function for the chain in which subgroup r is excited to its triplet state k. The function $\omega_r{}^k$ then describes a situation in which group r is in its triplet state k and all other subgroups are in their ground singlet states. The N-fold degeneracy of this problem is removed by exchange interactions between the subgroups, and we limit the discussion to next-neighbor interactions represented by

the spin transfer integral β_k:

$$(\omega_r^k \mid \mathcal{H} \mid \omega_{r+1}^k) = \beta_k. \tag{29}$$

The triplet state of the bridging system is designated $\psi_{kj}^{II}(1, 0)$, where j refers to some particular linear combination of the ω_r^k:

$$\psi_{kj}^{II}(1, 0) = \sum_r c_r^j \omega_r^k. \tag{30}$$

Note that the coefficients c_r^j do not depend on the k index. The energy is

$$\Delta E_{kj} = \Delta E_k + \epsilon_j^k. \tag{31}$$

For subgroups x_r, to which Eq. (17) is individually applicable, the corresponding generalization to a chain of N subgroups is

$$\Delta U = -4\rho^2 J^2 \sum_{k,j} \Gamma_{kj} (\Delta E_k + \epsilon_j^k)^{-1}. \tag{32}$$

If the ω_r^k are all chosen to have the same phase, then

$$\Gamma_{kj} = \Gamma_k c_1^j c_N^j, \tag{33}$$

where Γ_k is referred to any one individual subgroup. Since β_k may reasonably be assumed to be considerably smaller than ΔE_k (the triplet excitation energy for any individual subgroup), and since ϵ_j^k is of the order of β_k, the energy denominator in Eq. (32) can be expanded to yield the general formula

$$\Delta U = -4\rho^2 J^2 \sum_k \sum_{j=1}^{j=N} \sum_{\lambda=0}^{\infty} (\Gamma_k c_1^j c_N^j / \Delta E_k) (-\epsilon_j^k / \Delta E_k)^\lambda. \tag{34}$$

The coefficients c_r^j and the energies ϵ_j^k can be deduced *by analogy* with the molecular-orbital theory[12] of the linear polyenes. The results are:

$$c_r^j = [2/(N+1)]^{\frac{1}{2}} \sin[rj\pi/(N+1)] \tag{35}$$

$$\epsilon_j^k = 2\beta_k \cos[j\pi/(N+1)]. \tag{36}$$

When Eqs. (35) and (36) are substituted in Eq. (34), it is found that the summation on j can be carried out. This summation for arbitrary λ usually gives zero; by retaining only the lowest value of λ in Eq. (34) that *does not give zero* when the j summation is made, one obtains the following result, which holds for both even and odd N:

$$\Delta U = -4\rho^2 J^2 \sum_k (\Gamma_k / \Delta E_k) (-\beta_k / \Delta E_k)^{N-1}. \tag{37}$$

Perhaps the most interesting application of Eq. (37) is to the problem of the polymethylene chain, $-(CH_2)_n-$. If we consider the $N = n+1$ carbon-carbon single bonds, we see from Eq. (20) and Eq. (37) that the pure σ-electron contribution for the chain is simply

$$\Delta U^\sigma = [2\rho^2 J^2/(1-S^4)\Delta E_\sigma](-\beta/\Delta E_\sigma)^{N-1}. \tag{38}$$

[12] See C. A. Coulson and R. Daudel, *Dictionary of Values of Molecular Constants* (Mathematical Institute, Oxford, 1955), Vol. III.

The first term in parentheses on the right-hand side of Eq. (38) has already been estimated to be $\sim 10^{-2}$ ev. The transfer integral β is probably *positive* and of the order of 1 ev, and we may take ΔE_σ to be of the order of 10 ev. Thus,

$$\Delta U^\sigma \sim (-1)^{N+1} 10^{-(N+1)} \text{ ev}. \tag{39}$$

Note that the odd-membered chain puts the singlet lowest, and the even-membered chain puts the triplet lowest. A chain of $N \sim 5$ CH_2 groups is estimated to give a splitting of $\sim 10^{-6}$ ev, or ~ 100 Mc. Of course, for the polymethylene bridge, one should properly also include the CH bonding electrons. One can easily develop an equation similar to Eq. (38) for this problem, but it is very unlikely that these electrons can change the above estimates by more than an order of magnitude.

In treating a chain bridge X that is built up from a number of π-conjugated subgroups x_r, $r = 1, 2, \cdots, N$, it is, of course, necessary to be sure that the interaction between the subgroups is not so large that our degenerate system perturbation theory is not adequate. That is, in Eq. (30) must we include states ω_r^k with different k values? And are the singlet state components of ω_r^k strongly modified relative to the singlet state functions of the isolated subgroups? The rapid convergence with increasing N of the optical absorption spectra of the para polyphenyls, and meta polyphenyls, certainly suggests that the present treatment is at least qualitatively adequate for these bridging groups, and the moderate convergence of the spectra of the polyenes indicates that our method is perhaps not too bad, even for this bridging group. Detailed calculations on the polyphenyls will not be attempted here. For this system, the *rate* of decrease of triplet-singlet splitting with increasing chain length is estimated to be *of the order of three* for each additional phenyl group.

CONCLUSIONS

The foregoing calculations are clearly consistent with the room-temperature paramagnetism of TPM-type biradicals that are bridged with polymethylene, ether, or phenylene groups. On the other hand, our estimates are in direct contradiction with the interpretation of the C^{13}-hyperfine structure that requires the triplet-singlet splitting ΔU to be less than 100 Mc, or 3×10^{-3} cm^{-1}. For example, we require a polymethylene bridge of ca 5 CH_2 groups to obtain a triplet-singlet splitting of the order of 100 Mc, whereas Reitz and Weissman observe slow spin exchange with a bridge of 2 CH_2 groups.[2,3] For this bridge, we estimate the three carbon-carbon single bonds alone would contribute a splitting which is 100–1000 times larger than the hyperfine splitting. The discrepancy is even more marked for the σ-electron contribution in the case of the ether bridge. We cite these cases for particular consideration since the perturbation method used in the present paper can hardly be criticized on the

grounds that the TPM interactions are here "too strong" to be handled by a perturbation method. Other biradicals, such as

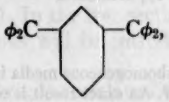

could be treated using Eq. (14) or Eq. (16), but it would not be certain in such cases that a simple perturbation method was rapidly convergent. See also the following Appendix for a brief discussion of the problem of direct first-order coupling.

On the basis of this work we draw the conclusion that the observed slow rate of spin exchange in these biradicals must have some other explanation. It is possible that one must consider coupling between electronic and nuclear motions,[13] or spin-orbit interactions, or, most probably, sources of experimental errors.

ACKNOWLEDGMENTS

The author wishes to thank Dr. T. R. Waite and Dr. A. D. McLachlan for a number of stimulating and helpful discussions. He is also indebted to Professor S. I. Weissman and Dr. H. S. Jarrett for helpful correspondence concerning experimental aspects of these problems.

APPENDIX

DIRECT INTERACTIONS

For some biradicals that show paramagnetic resonance in solution at room temperature, such as the Chichibabin hydrocarbon (see Fig. 2),[14] it is clear that one must consider the first-order terms in Eqs. (9) and (10) if ΔU in this type of molecule is to be estimated by a perturbation procedure in which the zero-order states correspond to spin distributions of unperturbed TPM groups. If we make the crude but classic approximation of valence-bond theory—neglect of π-electron atomic orbital overlaps *except* in the evaluation of matrix elements of $\mathcal{H}$—then the first-order contribution to the triplet-singlet splitting ΔU^0 arising from the π-electron interactions alone is

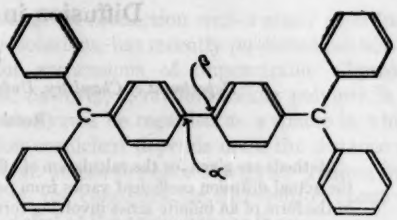

FIG. 2. The Chichibabin hydrocarbon.

$$\Delta U^0 = -\rho^2\alpha,$$

where ρ is again the para carbon atom spin density ($=0.18$) and α is the usual valence-bond "resonance integral" for orbitals centered on atoms α and β, which here has the semiempirical value -1.6 ev if it is assumed that the two TPM groups are coplanar. This triplet-singlet splitting is 0.06 ev, or 500 cm^{-1}, with the singlet state lowest. As the rings are twisted relative to one another, this contribution to the splitting will decrease, but the second-order $\sigma-\pi$ exchange mechanism will still ensure a finite splitting ($\sim 10^{-2}$, ev, or ~ 100 cm^{-1}). Of course, our estimate of the direct $\pi-\pi$ contribution to the splitting is on rather shaky grounds in that one cannot be sure that the interaction between these directly coupled systems is so weak that a first-order theory is adequate. On the other hand, a more elaborate calculation of this splitting would probably only yield a somewhat larger result.

[13] H. M. McConnell, Bull. Am. Phys. Soc. Ser II **4**, 415 (1959).
[14] C. A. Hutchison, A. Kowalsky, R. C. Pastor, and G. W. Wheland, J. Chem. Phys. **20**, 1485 (1952).

Diffusion in Inhomogeneous Media

STEPHEN PRAGER

Department of Chemistry, University of Minnesota, Minneapolis 14, Minnesota

(Received December 31, 1959)

Methods are given for the calculation of effective diffusion coefficients for inhomogeneous media in which the actual diffusion coefficient varies from point to point in a random manner. An exact result is obtained in the form of an infinite series involving correlations between diffusion coefficients at n different points. A procedure for deriving approximate expressions involving only two-point correlations is also developed, and applied, in particular, to the important special case of diffusion through a porous material.

INTRODUCTION

THE problem of diffusion in inhomogeneous media such as mixed solids, emulsions, etc., has received relatively little attention, although the mathematically analogous problem of the dielectric behavior of such materials has been extensively discussed.[1] With the exception of some work by Brown,[2] all treatments presented so far require some idealization that replaces the actual material with one of a more or less regular geometry, where conventional methods can be applied to the solution of the partial differential equations involved. While such approaches are undoubtedly useful, it must be realized that the properties of the actual material, unlike those of the idealized model, are not explicitly known as functions of position—they can only be characterized statistically, for example, through suitable n-point averages. It seems desirable, therefore, to attempt the calculation of effective diffusion coefficients (or dielectric constants, or thermal conductivities, or electrical conductivities) directly in terms of such statistical information, and several methods, both exact and approximate, for accomplishing this are presented in this paper.

MATHEMATICAL FORMULATION

In a homogeneous medium the diffusion coefficient may be measured by cutting a slab of the material in question and maintaining the concentration of diffusing substance on the two faces at different values $c_1<c_2$ until a steady state is reached; the flux P of diffusing substance through the slab is then simply related to the diffusion coefficient D.

$$D=l\,|\,P\,|/(c_2-c_1), \tag{1}$$

where l is the thickness of the slab. The same experiment may also be carried out with an inhomogeneous material, and, provided that l is large compared with the scale of the inhomogeneities, Eq. (1) will give an effective diffusion coefficient $D^{(e)}$ characteristic of the material and the diffusing substance.

If the actual diffusion coefficient D were known in detail as a function of position $\mathbf{r}=(x_1, x_2, x_3)$, one could, in principle at least, calculate $D^{(e)}$ by solving the steady-state diffusion equation[3,4]

$$(Dc_{,i})_{,i}=0, \tag{2}$$

with boundary conditions

$$c(0, x_2, x_3)=c_1 \qquad c(l, x_2, x_3)=c_2, \tag{3}$$

to obtain the concentration distribution $c(\mathbf{r})$ within the slab. Knowledge of $c(\mathbf{r})$ would permit evaluation of the flux vector

$$P_i(\mathbf{r})=-D(\mathbf{r})c_{,i}, \tag{4}$$

and particularly of its average,

$$\langle P_i\rangle=V^{-1}\int_V P_i(\mathbf{r})\,d\mathbf{r} \tag{5}$$

taken over some sufficiently large volume V within the slab; substitution of $\langle P_i\rangle$ for P in Eq. (1) would then give $D^{(e)}$.

As has already been said, however, $D(\mathbf{r})$ is known only in a statistical sense. There is, of course, a great variety of such statistical descriptions and the selection of the one to be used is to some extent governed, as we shall see, by the nature of the material for which $D^{(e)}$ is to be calculated. For the greater part of this paper we shall find it mathematically convenient to use the set of correlations $F_{\nu_1\cdots\nu_n}{}^{(n)}$ between the diffusion coefficient at $\mathbf{r}$ and the gradient of its logarithm at the points $\mathbf{r}+\boldsymbol{\varrho}^{(1)}$, $\mathbf{r}+\boldsymbol{\varrho}^{(2)}$, $\cdots$, $\mathbf{r}+\boldsymbol{\varrho}^{(n)}$:

$$F_{\nu_1\cdots\nu_n}{}^{(n)}(\boldsymbol{\varrho}^{(1)}, \cdots, \boldsymbol{\varrho}^{(n)})=\langle D(\mathbf{r})\prod_{j=1}^{n}\phi_{,\nu_j}(\mathbf{r}+\sum_{k=1}^{j}\boldsymbol{\varrho}^{(k)})\rangle, \tag{6}$$

[1] C. J. F. Böttcher, *Theory of Electric Polarization* (Elsevier Publishing Company, New York, 1952), p. 415.

[2] W. F. Brown, J. Chem. Phys. **23**, 1514 (1955).

[3] The summation convention is used throughout this paper. Indices appearing after the comma indicate differentiation with respect to the corresponding position coordinate (for example the components of ∇c are $c_{,1}$, $c_{,2}$, and $c_{,3}$).

[4] Equation (2) assumes that the distribution coefficient κ of the penetrant is constant throughout the medium. If, as is to be expected, κ is also a function of position, then, at equilibrium, c/κ, and not c, will be the position independent quantity. In this case Eq. (2) must be replaced by

$$(D\kappa(c/\kappa)_{,i})_{,i}=0,$$

which is formally identical with (2), and can be treated by the same methods. To correct for variable κ, D should be replaced by $D\kappa$ in all calculations of $D^{(e)}$ described in this paper, and the $D^{(e)}$ so obtained should be divided by the average value of κ.

where

$$\phi = \ln D - \langle \ln D \rangle \tag{7}$$

and angular brackets denote the averaging process defined by Eq. (5). In the last section, however, other types of correlations will be introduced to deal with porous materials.

The problem, then, is to relate $D^{(e)}$ to the $F_{x_1 \cdots x_n}^{(n)}$. Before turning to this, however, we shall first discuss a number of special situations where $D^{(e)}$ can be obtained exactly in closed form.

SOME SIMPLE CASES

Two trivial and well-known examples for which exact solutions are possible are those where $D = D(x_2, x_3)$ and $D = D(x_1)$, the diffusion proceeding in the x_1 direction. In the former case

$$D^{(e)} = \langle D \rangle, \tag{8}$$

while in the latter

$$D^{(e)} = \langle D^{-1} \rangle^{-1}; \tag{9}$$

neither example is suitable for the representation of a three-dimensional isotropic medium. A somewhat better choice for that purpose is the assumption

$$D = L(x_1)\, L(x_2)\, L(x_3), \tag{10}$$

which permits an exact solution of (2) in the form

$$c = X_1(x_1) + X_2(x_2) + X_3(x_3), \tag{11}$$

provided that

$$X_{1,1} = [A_1 / L(x_1)], \qquad X_{2,2} = [A_2 / L(x_2)],$$
$$X_{3,3} = [A_3 / L(x_3)], \tag{12}$$

where the A_i are constants. The flux vector that corresponds to this concentration distribution is

$$P_1 = -L(x_2)\, L(x_3)\, A_1, \qquad P_2 = -L(x_1)\, L(x_3)\, A_2,$$
$$P_3 = -L(x_1)\, L(x_2)\, A_3, \tag{13}$$

so that the effective diffusion coefficient becomes

$$D^{(e)} = |\langle \mathbf{P} \rangle| / |\langle \nabla c \rangle| = \langle L \rangle^2 / \langle L^{-1} \rangle = \langle D \rangle^{2/3} \langle D^{-1} \rangle^{-1/3}. \tag{14}$$

Equation (14) is probably the best expression for $D^{(e)}$ involving only single point averages of D and functions of D. If the relative fluctuations in D are everywhere of small amplitude, (14) will closely predict the difference between $\langle D \rangle$ and $D^{(e)}$; on the other hand, if D vanishes over a finite fraction of the total volume, as in the case of a porous material, (14) gives $D^{(e)} = 0$, which is certainly not correct in general.

The type of material represented by a dilute suspension of a high polymer is another example where $D^{(e)}$ may be computed in a relatively straightforward manner. Here each polymer molecule may be regarded as surrounded by an infinite body of suspending medium. The case of polymer coils that are completely impenetrable to the diffusing substance is well known, and Wang,[5] in connection with a study of diffusion in protein solutions, has recently published calculations of $D^{(e)}$ for suspensions of impenetrable ellipsoids. In general, however, a random-coiling polymer in dilute suspension must be regarded as a sphere in which the diffusion coefficient depends upon the distance r from the center. In the presence of a mean gradient in the x_1 direction, the concentration distribution about such a coil centered at the origin has the form

$$C(x_1, x_2, x_3) = x_1 f(r) + c(0, 0, 0) \tag{15}$$

and substitution of this into Eq. (2) gives

$$(d^2 f / dr^2) + [(d\phi/dr) + (4/r)](df/dr) + (1/r)(d\phi/dr) f = 0, \tag{16}$$

with f being required to be finite both at $r = 0$ and $r = \infty$ [ϕ is defined by Eq. (7)]. If $D(r)$ is known, $f(r)$ can be found by solving (16), although numerical procedures will in general be necessary. In terms of f, the effective diffusion coefficient in a solution containing n polymer molecules per unit volume can then be shown to be, to first order in n,

$$D^{(e)} = D_0 \{1 - 4\pi n \lim_{r \to \infty} [r^3 ([f(r)/f(\infty)] - 1)]\}, \tag{17}$$

where $D_0 [= D(\infty)]$ is the diffusion coefficient in the pure solvent. To extend (17) to terms of higher order in n, account must be taken of the interaction between the concentration distributions surrounding different polymer molecules.

SERIES SOLUTION OF THE GENERAL PROBLEM[6]

Returning now to the problem of expressing $D^{(e)}$ in terms of the correlations $F^{(n)}$, we first rewrite Eq. (2) in the form

$$c_{,ii} + \phi_{,i} c_{,i} = 0. \tag{18}$$

If the term $\phi_{,i} c_{,i}$ is formally treated as a distribution of sources, (18) can be transformed into an integral equation for the concentration gradient,

$$c_{,i}(\mathbf{r}) = \langle c_{,i} \rangle + (4\pi)^{-1} \int \frac{\phi_{,l}(\mathbf{r}+\boldsymbol{\rho})\, c_{,l}(\mathbf{r}+\boldsymbol{\rho})}{\rho^3} \rho_{,i}\, d\boldsymbol{\rho}, \tag{19}$$

which can be solved by iteration:

$$c_{,i} = c_{,i}^{(0)} + c_{,i}^{(1)} + c_{,i}^{(2)} + \cdots, \tag{20}$$

where

$$c_{,i}^{(n)}(\mathbf{r}) = (4\pi)^{-1} \int \frac{\phi_{,l}(\mathbf{r}+\boldsymbol{\rho})\, c_{,l}^{(n-1)}(\mathbf{r}+\boldsymbol{\rho})}{\rho^3} \rho_{,i}\, d\boldsymbol{\rho}$$
$$c_{,i}^{(0)} = \langle c_{,i} \rangle. \tag{21}$$

[5] J. H. Wang, J. Am. Chem. Soc. **76**, 4755 (1954).

[6] The approach of this section bears some similarity to Brown's calculation[3] of dielectric constants in inhomogeneous media. The two treatments are not directly comparable, however, because of a difference in the choice of the source term in Eq. (18). This strongly affects the nature of the series obtained, and it is only in the limit of very small fluctuations (Eq. 28) that our results are equivalent to Brown's.

Equations (20) and (21) are a solution only in a very formal sense, since the function $\phi(\mathbf{r})$ appearing in the recursion formula for $c_{,i}^{(n)}$ is not explicitly known. However, this manner of expressing $c_{,i}$ lends itself especially well to the calculation of the mean flux, which can now be obtained simply by multiplying Eq. (20) by $D(\mathbf{r})$, and averaging over-all values of $\mathbf{r}$:

$$\langle P_i\rangle=-[\langle D\rangle\langle c_{,i}\rangle+\langle Dc_{,i}^{(1)}\rangle+\langle Dc_{,i}^{(2)}\rangle+\cdots]. \quad (22)$$

By repeated use of (21), $c_{,i}^{(n)}$ can be expressed in terms of the mean concentration gradient $\langle c_{,i}\rangle$; substituting the result into (22) and interchanging the operations of averaging over $\mathbf{r}$ and integrating over the $\boldsymbol{\varrho}^{(k)}$, we finally obtain

$$\langle P_i\rangle=-D_{il}^{(e)}\langle c_{,l}\rangle$$

$$D_{ij}^{(e)}=\langle D\rangle\delta_{ij}+(4\pi)^{-1}\sum_{n=1}^{\infty}\int\frac{F_{\nu_1\cdots\nu_n-ij}^{(n)}(\boldsymbol{\varrho}^{(1)},\cdots,\boldsymbol{\varrho}^{(n)})}{(\rho^{(1)}\cdots\rho^{(n)})^3}$$

$$\times\rho_{\nu_1}^{(1)}\rho_{\nu_1}^{(2)}\cdots\rho_{\nu_n-1}^{(n)}d\boldsymbol{\varrho}^{(1)}\cdots d\boldsymbol{\varrho}^{(n)}. \quad (23)$$

In the case of a medium that is isotropic on the average, the diffusion tensor $D_{ij}^{(e)}$ turns into a scalar diffusion coefficient, and Eq. (23) becomes

$$D^{(e)}=\langle D\rangle+(12\pi)^{-1}\sum_{n=1}^{\infty}\int\frac{F_{\nu_1\cdots\nu_n}^{(n)}(\boldsymbol{\varrho}^{(1)},\cdots\boldsymbol{\varrho}^{(n)})}{(\rho^{(1)}\cdots\rho^{(n)})^3}$$

$$\times\rho_{\nu_n}^{(1)}\rho_{\nu_1}^{(2)}\cdots\rho_{\nu_n-1}^{(n)}d\boldsymbol{\varrho}^{(1)}\cdots d\boldsymbol{\varrho}^{(n)}. \quad (24)$$

The first correction to $\langle D\rangle$ in Eq. (23) may be transformed, through use of Gauss' theorem, to give

$$D_{ij}^{(e)}=\langle D\rangle\left[\delta_{ij}-(4\pi)^{-1}\int\frac{G(\boldsymbol{\varrho})}{\rho^3}\left(\delta_{ij}-3\frac{\rho_i\rho_j}{\rho^2}\right)d\boldsymbol{\varrho}+\cdots\right]$$

$$=\langle D\rangle\left[\delta_{ij}-\tfrac{1}{3}\tilde{G}(0)\,\delta_{ij}\right.$$

$$\left.-(4\pi)^{-1}\int\frac{G(\boldsymbol{\varrho})-\tilde{G}(\rho)}{\rho^3}\left(\delta_{ij}-3\frac{\rho_i\rho_j}{\rho^2}\right)d\boldsymbol{\varrho}+\cdots\right], \quad (25)$$

where

$$G(\boldsymbol{\varrho})=\langle D(\mathbf{r})\phi(\mathbf{r}+\boldsymbol{\varrho})\rangle/\langle D\rangle \quad (26)$$

and $\tilde{G}(\rho)$ is $G(\boldsymbol{\varrho})$ averaged over-all orientations of the vector $\boldsymbol{\varrho}$. For an isotropic material $G(\boldsymbol{\varrho})$ and $\tilde{G}(\rho)$ are equal, so that

$$D^{(e)}=[\langle D\rangle-\tfrac{1}{3}\langle D\phi\rangle+\cdots], \quad (27)$$

i.e., the first correction to $\langle D\rangle$ in this case involves only the one-point average $\langle D\phi\rangle$, and correlations between values of the diffusion coefficient at different points appear only in terms of order ϕ^2 or higher. If this first correction is to be sufficient, then the fluctuation in the diffusion coefficient must be very small, and ϕ can be replaced by $(D-\langle D\rangle)/\langle D\rangle$, so that (27) becomes

$$D^{(e)}\cong\langle D\rangle\{1-\tfrac{1}{3}[(\langle D^2\rangle-\langle D\rangle^2)/\langle D\rangle^2]\}. \quad (28)$$

It can readily be shown that both Eqs. (14) and (17) are equivalent to (28) for small fluctuations of D.

For a porous material, where the probability of D vanishing is finite, the individual terms in the series (24) become infinite, because of the logarithmic dependence of ϕ on D, so that the effective diffusion coefficient becomes an indeterminate quantity. Actually, the series approach to the calculation of $D^{(e)}$ becomes impractical long before this point is reached, since one does not in general expect to have the $(n+1)$-point correlation $F_{\nu_1\cdots\nu_n}^{(n)}$ available for $n>1$ (indeed, even obtaining the two-point correlation $F_{\nu_1}^{(1)}$ is by no means a trivial problem). An expression for $D^{(e)}$ involving only $F_{\nu_1}^{(1)}$, even though it would necessarily be approximate, would be very much more useful than Eq. (24), and in the next section we shall develop methods for obtaining results of this nature.

EXPRESSIONS FOR $D^{(e)}$ INVOLVING ONLY TWO-POINT CORRELATIONS

To express $D^{(e)}$ in terms of two-point correlations, we may use an approach closely analogous to one often made in the statistical theory of turbulence.[7] We start by multiplying Eq. (18), written at a point $\mathbf{r}+\mathbf{s}$, by $\exp[\phi(\mathbf{r})]$, and then average with respect to $\mathbf{r}$. Since the operations of averaging over $\mathbf{r}$ and differentiating with respect to $\mathbf{s}$ commute, the result can be put into the form

$$\langle\exp[\phi(\mathbf{r})]c_{,i}(\mathbf{r}+\mathbf{s})\rangle_{,i}$$

$$+\langle\exp[\phi(\mathbf{r})]\phi_{,i}(\mathbf{r}+\mathbf{s})c_{,i}(\mathbf{r}+\mathbf{s})\rangle=0. \quad (29)$$

Equation (29) may be regarded as an equation for the function

$$h_{,i}(\mathbf{s})\equiv\langle\exp[\phi(\mathbf{r})]c_{,i}(\mathbf{r}+\mathbf{s})\rangle. \quad (30)$$

Unfortunately, however, it is not a closed equation, since nothing is known about the second term. In order to obtain a useful result, some additional relationship between $h_{,i}$ and $\langle\exp[\phi(\mathbf{r})]\phi_{,i}(\mathbf{r}+\mathbf{s})c_{,i}(\mathbf{r}+\mathbf{s})\rangle$ must be postulated.

With this in mind, we now ask the following general question: suppose that we have three random variables u, v, w, with a joint probability density $p^{(3)}(u, v, w)$; is there any *reasonable* way of expressing $p^{(3)}$ in terms of the two-variable distributions $p_{uv}^{(2)}(u, v)$, $p_{vw}^{(2)}(v, w)$, and $p_{uw}^{(2)}(u, w)$? A general, exact relation between $p^{(3)}$ and the $p^{(2)}$'s certainly does not exist. The answer to our question depends therefore on what, precisely, is meant by reasonable. We shall require a reasonable relationship to satisfy the following two conditions:

(a) If any variable, for example, u, is independent of the other two, then $p^{(3)}$ must reduce to $p_{vw}^{(2)}(v, w)\,p_u^{(1)}(u)$, where $p_u^{(1)}$ is the single-variable distribution for u.

[7] G. K. Batchelor, *The Theory of Homogeneous Turbulence* (Cambridge University Press, New York, 1953), p. 79.

(b) If $p^{(3)}$ is integrated with respect to any one variable, for example, u, the result must be $p_{vw}^{(2)}(v,w)$.

Thus, the superposition approximation

$$p^{(3)}(u,v,w)=\frac{p_{uv}^{(2)}(u,v)\,p_{vw}^{(2)}(v,w)\,p_{uw}^{(2)}(u,w)}{p_u^{(1)}(u)\,p_v^{(1)}(v)\,p_w^{(1)}(w)}, \quad (31)$$

which is frequently used for molecular distribution functions in the statistical mechanics of fluids,[8] is not reasonable by our standards, since, although it satisfies condition (a), it does not satisfy (b).

A satisfactory $p^{(3)}$–$p^{(2)}$ relationship is more easily obtained in terms of the characteristic functions

$$\psi^{(3)}(\alpha,\beta,\gamma)=\int\exp[i(u\alpha+v\beta+w\gamma)]p^{(3)}(u,v,w)\,dudvdw$$

$$\psi_{uv}^{(2)}(\alpha,\beta)=\int\exp[i(u\alpha+v\beta)]p^{(2)}(u,v)\,dudv, \quad \text{etc.}$$

$$\psi_u^{(1)}(\alpha)=\int\exp(iu\alpha)\,p^{(1)}(u)\,du, \quad \text{etc.} \quad (32)$$

than in terms of the distribution functions themselves. In terms of the ψ's, the conditions for reasonableness become

(a) If u is independent of both v and w, then

$$\psi^{(3)}(\alpha,\beta,\gamma)=\psi_{vw}^{(2)}(\beta,\gamma)\psi_u^{(1)}(\alpha)$$

(b) $$\psi^{(3)}(\alpha,\beta,0)=\psi_{uv}^{(2)}(\alpha,\beta), \quad \text{etc.}$$

It is evident that a superposition of $\psi^{(2)}$'s according to the scheme (31) will satisfy both conditions:

$$\psi^{(3)}(\alpha,\beta,\gamma)=\frac{\psi_{uv}^{(2)}(\alpha,\beta)\psi_{vw}^{(2)}(\beta,\gamma)\psi_{uw}^{(2)}(\alpha,\gamma)}{\psi_u^{(1)}(\alpha)\psi_v^{(1)}(\beta)\psi_w^{(1)}(\gamma)}. \quad (33)$$

There certainly exist distributions for which Eq. (33) holds exactly (a multinormal distribution is an example), but even if this is not the case, we may at least expect it to be a reasonably good approximation. If we accept the validity of (33), then the average $\langle e^u vw\rangle$ can be decomposed into products of two-variable averages:

$$\langle e^u vw\rangle=-\partial^2\psi^{(3)}/\partial\beta\partial\gamma\,|_{\alpha=1,\beta=\gamma=0}$$
$$=\langle(v-\langle v\rangle)(w-\langle w\rangle)\rangle\langle e^u\rangle$$
$$+(\langle ve^u\rangle\langle we^u\rangle/\langle e^u\rangle). \quad (34)$$

Returning to Eq. (29), we now make the identifications

$$u=\phi(\mathbf{r}), \quad v=\phi_{,i}(\mathbf{r}+\mathbf{s}), \quad w=c_{,i}(\mathbf{r}+\mathbf{s}), \quad (35)$$

so that the second term on the left in Eq. (29) becomes

$$\langle\exp[\phi(\mathbf{r})]\phi_{,i}(\mathbf{r}+\mathbf{s})c_{,i}(\mathbf{r}+\mathbf{s})\rangle=\langle e^\phi\rangle\langle\phi_{,i}c_{,i}\rangle$$
$$+G_{,i}(\mathbf{s})h_{,i}(\mathbf{s}). \quad (36)$$

[8] H. S. Green, *The Molecular Theory of Fluids* (North-Holland Publishing Company, Amsterdam, 1952), p. 71.

From Eq. (18) it is apparent that $\langle\phi,_i c,_i\rangle$ must vanish, otherwise there would be a net accumulation or depletion of diffusing material in the system. Substitution of (36) into (29) then gives

$$h_{,ii}+G_{,i}h_{,i}=0, \quad (37)$$

which is again a diffusion equation of the type (18), with h and G replacing c and ϕ. The boundary conditions on (37) are

$$h_{,i}(\mathbf{s})\xrightarrow[s\to\infty]{}\langle e^\phi\rangle\langle c_{,i}\rangle \quad (38)$$

$$h_{,i}(0,0,0) \quad \text{finite.}$$

For an isotropic medium h can be written

$$h(\mathbf{s})=\langle e^\phi\rangle g(s)s_i\langle c_{,i}\rangle+h(0,0,0), \quad (39)$$

where $g(s)$ satisfies the ordinary differential equation

$$(d^2g/ds^2)+[(dG/ds)+(4/s)](dg/ds)$$
$$+s^{-1}(dG/ds)g=0 \quad (40)$$

with boundary conditions

$$g(\infty)=1 \qquad g(0) \text{ finite.} \quad (41)$$

In terms of the function $g(s)$, the flux of diffusing material is readily found to be

$$P_i=\langle D\rangle g(0)\langle c_{,i}\rangle, \quad (42)$$

so that the effective diffusion coefficient is simply

$$D^{(e)}=\langle D\rangle g(0). \quad (43)$$

As an application of Eq. (43), we consider the case of an isotropic material consisting of two regions 1 and 2 randomly dispersed in each other, with a diffusion coefficient D_1 prevailing in region 1, and D_2 in region 2. If we define $p_{12}(s)$ as the probability that of two points a distance s apart one will lie in region 1 while the other lies in region 2, it follows that

$$G(s)=[(D_2-D_1)/\langle D\rangle][\sigma_1\sigma_2-\tfrac{1}{2}p_{12}(s)]\ln(D_2/D_1), \quad (44)$$

where σ_1 and σ_2 are the volume fractions occupied by regions 1 and 2, respectively. The function $p_{12}(s)$ goes from a minimum of 0 at $s=0$ to a maximum of $2\sigma_1\sigma_2$ at $s=\infty$; in order to get a solution of (40) without resorting to numerical procedures, we postulate

$$p_{12}(s)=\begin{cases}(2\sigma_1\sigma_2/R)s & (s<R)\\ 2\sigma_1\sigma_2 & (s>R).\end{cases} \quad (45)$$

The $g(s)$ corresponding to (45) is

$$g(s)=\begin{cases}\dfrac{R^3A}{s^3}\left(\dfrac{a^2s^2}{R^2}+\dfrac{2as}{R^2}+2-2\exp(as/R)\right) & (s>R)\\[2ex] \dfrac{R^3B}{s^3}+1 & (s<R),\end{cases} \tag{46}$$

where

$$a=\sigma_1\sigma_2[(D_2-D_1)/\langle D\rangle]\ln(D_2/D_1), \tag{47}$$

and the constants A and B must be chosen so as to make g and its first derivative continuous at $s=R$:

$$A=-(3/2a)/(e^a-1-a),$$
$$B=[(3-a)/a]-[\tfrac{3}{2}a/(e^a-1-a)]. \tag{48}$$

According to Eq. (43), therefore, the effective diffusion coefficient is

$$D^{(e)}=\langle D\rangle[\tfrac{1}{2}a^2/(e^a-1-a)]. \tag{49}$$

The principal interest of Eq. (49) is in the limiting behavior that it predicts when one of the diffusion coefficients, for example, D_2, tends to zero or to infinity; the former case is of particular importance, since it corresponds to diffusion in the void region of a porous material. For $D_2\to 0$

$$D^{(e)}\to\tfrac{1}{2}\sigma_1\sigma_2^2[\ln(D_1/D_2)]^2D_1^{\sigma_1}D_2^{\sigma_2}\to 0, \tag{50}$$

and for $D_2\to\infty$

$$D^{(e)}\to\tfrac{1}{2}\sigma_2\sigma_1^2[\ln(D_2/D_1)]^2D_1^{\sigma_1}D_2^{\sigma_2}\to\infty. \tag{51}$$

Whether or not the effective diffusion coefficient in a porous material is actually zero, as predicted by Eq. (50), depends of course on the pore geometry. If the void region (region 1) is completely enveloped by the solid (region 2), for example if the pores are just bubbles frozen in by the solidification of a melt, then $D^{(e)}$ will indeed vanish. On the other hand, if the pores form a system of interconnected passageways permitting access between any two points in the void region, then $D^{(e)}$ will be finite; Eq. (50) is clearly unsuitable for materials of this sort. In what follows we shall refer to these two geometries as closed and open, respectively. Thus, both for very small and for very large values of D_2, Eq. (49) corresponds to a material in which region 2 is open and region 1 is closed.

Two-point averages such as $G(s)$ are clearly incapable of distinguishing between closed and open geometries. Indeed, the whole concept of describing an inhomogeneous material by a set of n-point averages breaks down at this point, for, in principle at least, a region may be changed from open to closed by the insertion of extremely thin barriers whose presence will not affect any of the averages $F_{r_1\cdots r_n}^{(n)}$. The open or closed nature of the void and solid regions should, therefore, be regarded as a supplementary piece of information that must be available before even approximate calculations of effective diffusion coefficients can be made for porous materials.

To treat a porous material whose void region is open, the approach developed in this section must be modified so as to give a finite value of $D^{(e)}$ in the limit $D_2\to 0$. For this purpose the diffusion Eq. (2) is more useful than the alternate form (18). If (2) is written at a point $\mathbf{r}+\mathbf{s}$, multiplied by $D(\mathbf{r})$ and averaged with respect to $\mathbf{r}$, the result is

$$\langle D(\mathbf{r})D(\mathbf{r}+\mathbf{s})c_{,i}(\mathbf{r}+\mathbf{s})\rangle_{,i}=0. \tag{52}$$

Let us now postulate that $\phi(\mathbf{r})$, $\phi(\mathbf{r}+\mathbf{s})$, and $c_{,i}(\mathbf{r}+\mathbf{s})$ are jointly distributed in the same manner as the variables u, v, and w in Eq. (33). The average appearing in Eq. (52) then corresponds to

$$\langle e^{u+v}w\rangle=-i(\partial\psi^{(3)}/\partial\gamma)|_{\alpha=\beta=1,\gamma=0}$$
$$=\langle e^{u+v}\rangle[(\langle we^u\rangle/\langle e^u\rangle)+(\langle we^v/\langle e^v\rangle)-\langle w\rangle], \tag{53}$$

so that Eq. (52) becomes

$$(H(\mathbf{s})k_{,i}(\mathbf{s}))_{,i}=0, \tag{54}$$

where

$$H(\mathbf{s})=\langle D(\mathbf{r})D(\mathbf{r}+\mathbf{s})\rangle \tag{55}$$

and

$$k_{,i}(\mathbf{s})=\frac{\langle D(\mathbf{r})c_{,i}(\mathbf{r}+\mathbf{s})\rangle}{\langle D\rangle}+\frac{\langle D(\mathbf{r})c_{,i}(\mathbf{r})\rangle}{\langle D\rangle}-\langle c_{,i}\rangle. \tag{56}$$

Equation (54) has once again the form of a diffusion equation with $H(\mathbf{s})$ and $k(\mathbf{s})$ acting, respectively, as the diffusion coefficient and the concentration. If the material is isotropic, H depends on the magnitude of $\mathbf{s}$ alone, and k can be written

$$k(\mathbf{s})=q(s)s_i(\langle Dc_{,1}\rangle/\langle D\rangle)+k(0,0,0), \tag{57}$$

the function $q(s)$ satisfying the differential equation

$$(d^2q/ds^2)+[(d\ln H/ds)+(4/s)](dq/ds)$$
$$+s^{-1}(d\ln H/ds)q=0 \tag{58}$$

with boundary conditions

$$q(\infty)=1, \qquad q(0) \text{ finite}. \tag{59}$$

The effective diffusion coefficient is then obtained from (56) and (57):

$$D^{(e)}=\langle D\rangle/[2-q(0)]. \tag{60}$$

Since $H(0)=\langle D^2\rangle$ is always greater than $H(\infty)=\langle D\rangle^2$, it follows that $q(0)$ must be less than 1, and since $H(s)$ is positive for all values of s, $q(0)$ must also be positive. The effective diffusion coefficient predicted by Eq. (60) will therefore always lie between $\frac{1}{2}\langle D\rangle$ and $\langle D\rangle$, and will remain finite so long as $\langle D\rangle$ remains finite. Thus, in the case of a two-region material, $D^{(e)}$ will be finite for D_2 going to zero, but will become

infinite as D_2 approaches infinity, so that Eq. (60) corresponds to both region 1 and region 2 being open.

For a porous material, where D_2 is zero, $H(s)$ is given by

$$H(s)=D_1^2[\sigma_1-\tfrac{1}{2}p_{12}(s)], \tag{61}$$

and, if we assume $p_{12}(s)$ to have the form

$$p_{12}(s)=\begin{cases}2\sigma_1(1-e^{-bs}) & [s<-(\ln\sigma_1)/b]\\ 2\sigma_1\sigma_2 & [s>-(\ln\sigma_1)/b],\end{cases} \tag{62}$$

Eq. (58) can be solved exactly, just as Eq. (40) could be solved exactly for the $p_{12}(s)$ given by (45). The $D^{(e)}$ calculated according to Eq. (60) is then

$$D^{(e)}=D_1\sigma_1\frac{(\sigma_2+\sigma_1\ln\sigma_1)}{2(\sigma_2+\sigma_1\ln\sigma_1)-\tfrac{1}{2}\sigma_1(\ln\sigma_1)^2}. \tag{63}$$

Finally, to treat a material containing a closed region in which the diffusion coefficient is infinite (diffusion of a gas through a solidified foam would come close to this), we write the diffusion equation in the form

$$P_{i,i}=0$$
$$\epsilon_{ijk}(P_j/D)_{,k}=0, \tag{64}$$

where ϵ_{ijk} is the Levi-Civita symbol. Multiplying (64) at a point $\mathbf{r}+\mathbf{s}$ by $1/D(\mathbf{r})$ and averaging with respect to $\mathbf{r}$ then leads to

$$\langle P_i(\mathbf{r}+\mathbf{s})/D(\mathbf{r})\rangle_{,i}=0$$
$$\epsilon_{ijk}\left\langle\frac{P_j(\mathbf{r}+\mathbf{s})}{D(\mathbf{r})D(\mathbf{r}+\mathbf{s})}\right\rangle_{,k}=0 \tag{65}$$

If $-\phi(\mathbf{r})$, $-\phi(\mathbf{r}+\mathbf{s})$, and P_i are now identified with the random variables u, v, w of Eq. (53), we obtain an equation of the same form as (64), with

$$I(\mathbf{s})\equiv 1/\langle 1/[D(\mathbf{r})D(\mathbf{r}+\mathbf{s})]\rangle \tag{66}$$

acting as a diffusion coefficient, and

$$Q_i(\mathbf{s})\equiv\frac{\langle P_i(\mathbf{r}+\mathbf{s})/D(\mathbf{r})\rangle}{\langle 1/D\rangle}+\frac{\langle P_i(\mathbf{r})/D(\mathbf{r})\rangle}{\langle 1/D\rangle}-\langle P_i\rangle \tag{67}$$

as a flux vector:

$$Q_{i,i}(\mathbf{s})=0$$
$$\epsilon_{ijk}(Q_j(\mathbf{s})/I(\mathbf{s}))_{,k}=0 \tag{68}$$

For an isotropic material, I depends on the magnitude of $\mathbf{s}$ alone, and Q_i may be written

$$Q_i(\mathbf{s})=\langle 1/D\rangle^2 I(s)[m(s)s_l(\langle P_l/D\rangle/\langle 1/D\rangle)]_{,i}, \tag{69}$$

which automatically satisfies the second of Eqs. (68), and reduces the first to the ordinary differential equation

$$(d^2m/ds^2)+[(d\ln I/ds)+(4/s)](dm/ds)$$
$$+s^{-1}(d\ln I/ds)m=0 \tag{70}$$

with boundary conditions

$$m(\infty)=1, \qquad m(0) \text{ finite}. \tag{71}$$

The effective diffusion coefficient then is

$$D^{(e)}=\langle 1/D\rangle^{-1}[2-(\langle 1/D\rangle^2/\langle 1/D^2\rangle)m(0)], \tag{72}$$

as can be seen from Eqs. (67) and (69).

When Eq. (72) is applied to a two-region material, the calculated $D^{(e)}$ goes from zero for $D_2=0$ to a finite limit as D_2 becomes infinite, corresponding to a geometry with both region 1 and region 2 closed. In the limit $D_2\to\infty$,

$$I(s)=D_1^2/[\sigma_1-\tfrac{1}{2}p_{12}(s)], \tag{73}$$

and, if $p_{12}(s)$ is given by (62), the effective diffusion coefficient becomes

$$D^{(e)}=D_1\{(2/\sigma_1)+[\tfrac{1}{2}(\ln\sigma_1)^2/(\sigma_2+\ln\sigma_1)]\}. \tag{74}$$

ACKNOWLEDGMENTS

It is a pleasure to acknowledge here the support of a grant made by the John Simon Guggenheim Memorial Foundation. This work is currently being sponsored by the U. S. Air Force, and part of the results reported here were obtained under a contract monitored by the Air Force Office of Scientific Research of the Air Research and Development Command, Washington, D. C.

Compression and Phase Transitions of Solid NH_3, SiF_4, H_2S, and CF_4*

JOHN W. STEWART

University of Virginia, Charlottesville, Virginia

(Received February 22, 1960)

Isothermal PV curves of solid NH_3, SiF_4, H_2S, and CF_4 have been observed by the direct piston displacement method up to pressures of 20 000 kg/cm² at various temperatures between 100° and 200°K. Relative volume changes and compressibilities are given for each substance except CF_4. Phase transitions have been observed as discontinuities in the piston motion. NH_3 exhibits no phase transitions. Phase diagrams are given for the other three substances. Comparison with previous work in the case of H_2S shows only partial agreement. In some instances the approximate volume changes accompanying the phase transitions have been determined.

I. INTRODUCTION

PV isotherms and phase transition parameters to 20 000 kg/cm² pressure have been observed for solid NH_3, SiF_4, and H_2S at various low temperatures. Some additional data have been obtained for CF_4. The piston displacement technique previously described[1,2] has been employed. The gases are condensed into the high-pressure cylinder and pressure applied directly to the samples after solidification. Plasticity of the samples is relied upon to transmit the uniaxial compressive applied stress throughout the sample as hydrostatic pressure. This method is valid only for nonbrittle substances with low shear strength. Past experience has shown that brittle behavior of a solidified gas sample is accompanied by crunching sounds and irregular piston motion as the pressure is varied. Except at the lowest temperatures, such behavior was not observed for the substances considered here.

The NH_3, SiF_4, and H_2S were obtained from Matheson lecture bottles. The CF_4 was from a sample supplied earlier through the kindness of Dr. R. M. Joyce of the DuPont Experimental Station, Wilmington, Delaware. The SiF_4 and H_2S were dried by passing through silica gel; purification was not found necessary for the NH_3 and CF_4. The purities were of the order of 99.5% or higher.

II. EXPERIMENTAL DETAILS

Unexpected difficulty was encountered in condensing the H_2S into the sample holders. Even when a constant temperature slightly above the triple point was maintained by a dry ice-acetone bath, the filling capillary invariably blocked after a small quantity of H_2S had condensed. This blocking was believed to have been caused by formation of a hydrate ($H_2S \cdot 6H_2O$) of much higher melting point. Successful condensation was achieved only after especially dried H_2S had been supplied by the Matheson Company. The gas was passed through a silica gel drying tube which was reactivated before each run. A larger diameter capillary was used for the filling tube than had been necessary previously. This capillary was heated electrically to prevent blocking at the entrance to the sample chamber.

SiF_4 was also difficult to condense, because of its high triple point pressure (1320 mm Hg). The range of temperature for which condensation can occur without capillary blocking is very small. Even with the larger capillary first used for H_2S, a full cylinder of solid SiF_4 was never obtained.

As in the previous work,[1,2] the position of the piston was observed both for monotonically increasing and decreasing pressure. The hysteresis caused by friction in the sample holder varied considerably from run to run. It was generally less near the melting points of the substances than at lower temperature. The ammonia samples tended to have the largest friction, up to 20% of the maximum pressure. The magnitude of the friction was, as before, reduced by lining the cylinder with two layers of 0.005-in. indium foil.[3] To prevent extrusion of the solid, a brass ring of triangular cross section was placed ahead of the piston. Correction for friction was made by averaging the pressure on the two sides of the hysteresis curve at constant piston displacement. Account was also taken of the stretch of the press (by a blank run with no sample in the sample holder), and of the dilation of the pressure cylinder.

Sample holders of several diameters were used, ranging from $\frac{5}{8}$ in. (maximum pressure 3000 kg/cm²) to $\frac{1}{4}$ in. (maximum pressure 19 000–20 000 kg/cm²). The larger diameter holders gave more accurate PV data at the lowest pressures than could be obtained by extrapolation of the $\frac{1}{4}$ in. holder data below the equivalent frictional pressure. At least one run in a large holder was made near each temperature for which a PV curve was determined. The curves from the large and small cylinders agreed satisfactorily in the region of overlap.

Temperature control was obtained in a variable temperature cryostat of the Swenson type,[4] using liquid nitrogen as the coolant. Regulation to ±0.5 to 1.0°K was readily achieved. Temperature measure-

* Supported by the Office of Ordnance Research, U. S. Army.

[1] J. W. Stewart, J. Phys. Chem. Solids **1**, 146 (1956).

[2] J. W. Stewart and R. I. LaRock, J. Chem. Phys. **28**, 425 (1958).

[3] R. Stevenson, J. Chem. Phys. **27**, 656 (1957).

[4] C. A. Swenson and R. Stahl, Rev. Sci. Instr. **25**, 608 (1954).

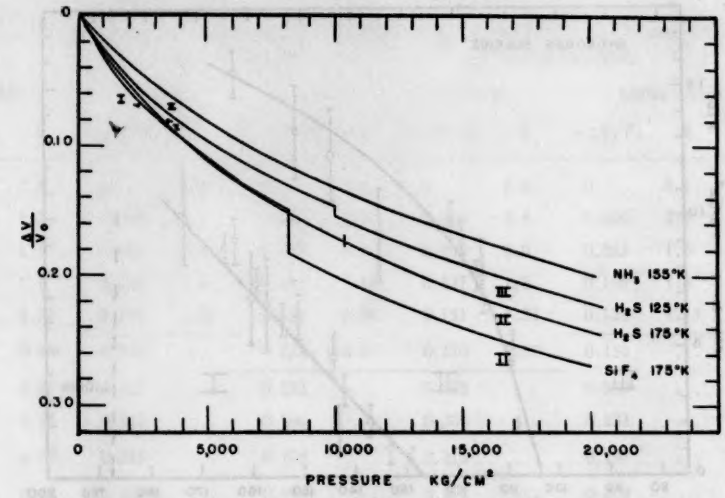

FIG. 1. Typical isotherms for solid NH_3, SiF_4, and H_2S.

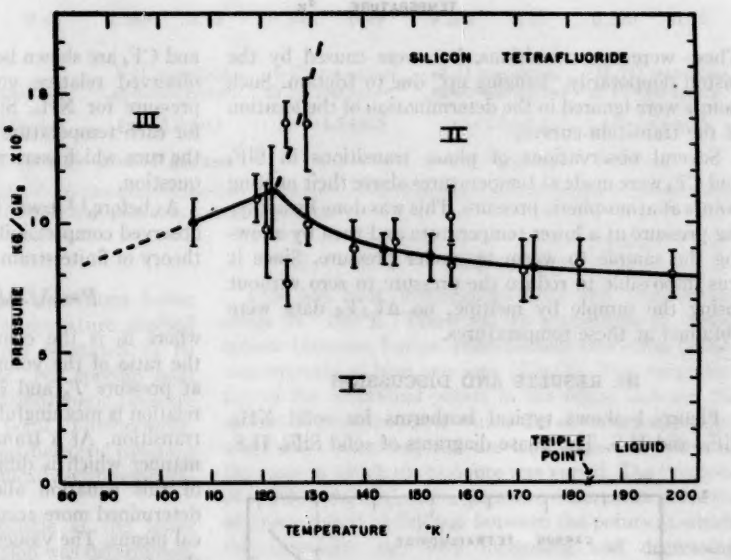

FIG. 2. Phase diagram of solid SiF_4.

ment was by means of an indium resistance thermometer described elsewhere.[5,6]

Phase transitions in the solids were observed as discontinuities in the volume versus pressure curves. First-order transitions with large volume changes are readily identifiable in this apparatus, but the friction prevents distinguishing between a small first-order transition and a second-order transition with merely a break in the slope of the V vs P curve. Transitions of either type could normally be detected while a run was in progress by means of the drifting of the piston after the pressure was changed. Except at the lowest pressures, the piston normally reached equilibrium within a few seconds after the application of each increment of weight on the dead weight gauge pan. The actual transition pressure was always taken as the mean of the apparent transition pressures with increasing and with decreasing pressure.

In order to locate the transitions as accurately as possible, the difference between the actual volume vs pressure curve and a straight line joining the points of lowest and highest pressure was plotted against pressure. This effectively magnified the scale of departures from a smooth curve. In most cases the transition points were easily identifiable. A few irregularities were observed with no apparent temperature correlation.

[5] J. W. Stewart, Rev. Sci. Instr. **30**, 949 (1959).
[6] G. K. White and S. B. Woods, Rev. Sci. Instr. **28**, 638 (1957).

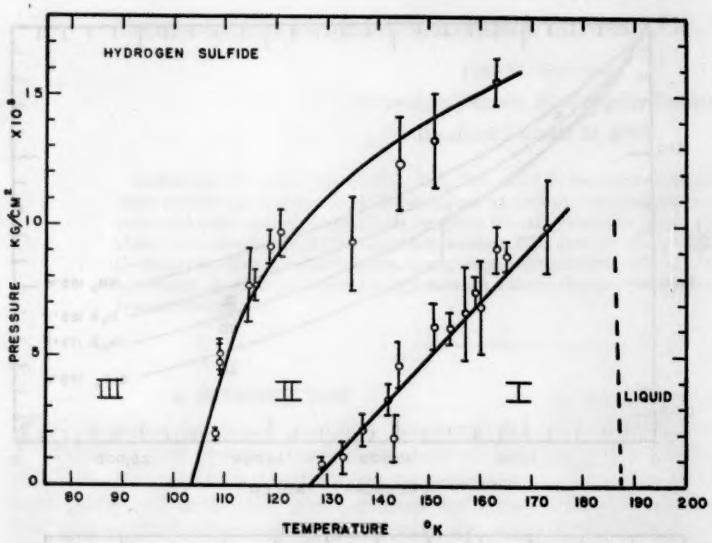

FIG. 3. Phase diagram of solid H_2S.

These were not transitions, but were caused by the piston temporarily "hanging up" due to friction. Such points were ignored in the determination of the location of the transition curves.

Several observations of phase transitions in SiF_4 and CF_4 were made at temperatures above their melting points at atmospheric pressure. This was done by applying pressure at a lower temperature and then by allowing the sample to warm up under pressure. Since it was impossible to reduce the pressure to zero without losing the sample by melting, no $\Delta V/V_0$ data were obtained at these temperatures.

III. RESULTS AND DISCUSSION

Figure 1 shows typical isotherms for solid NH_3, SiF_4, and H_2S. The phase diagrams of solid SiF_4, H_2S, and CF_4 are shown below in Figs. 2–4. Table I lists the observed relative volume decreases as functions of pressure for NH_3, SiF_4, and H_2S. The results shown for each temperature were computed by averaging all the runs which were within 10°K of the temperature in question.

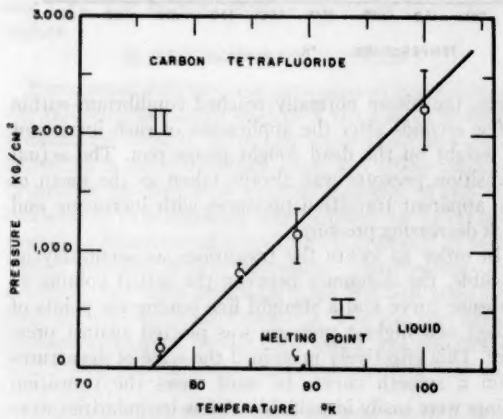

FIG. 4. Phase diagram of solid CF_4.

As before,[1,2] it was found convenient to represent the observed compressibility data in terms of Murnaghan's theory of finite strain.[1,7] This gives

$$P=(3/2\beta_0)[y^7-y^5][1-\xi(y^2-1)],$$

where β_0 is the compressibility at zero pressure, y the ratio of the volume V_0 at $P=0$ to the volume V at pressure P, and ξ is an adjustable constant. This relation is meaningful only for pressure below that of a transition. At a transition both β_0 and ξ change in a manner which is difficult to interpret. Differentiation of this equation allows the compressibilities to be determined more accurately than is possible by graphical means. The values of β in Table I were obtained in this manner for pressures below the transition, and estimated from the slopes of the curves for $P=20\,000$ kg/cm². The indicated values of ξ are those which give the best fit to the data.

The PV data are presented as relative volume decreases rather than as molar volumes because the available values of the densities of these substances do not appear to be sufficiently reliable, especially as to their temperature variation. The method previously used in this laboratory[2] for measurement of densities of solid CF_4, argon, and low melting hydrocarbons at 77°K is not applicable at the higher temperatures of present interest.

[7] F. Birch, J. Geophys. Research **56**, 227 (1952).

TABLE I. Compression of solid NH_3, SiF_4, and H_2S.

	NH_3 $MP=195°K$				SiF_4 $MP=183°K$				H_2S $MP=188°K$			
	155°K		110°K		175°K		105°K		175°K		125°K	
Pressure Kg/cm²	$-\Delta V/V_0$	β[a]	$-\Delta V/V_0$	β	$-\Delta V/V_0$	β	$-\Delta V/V_0$	β	$-\Delta V/V_0$	β	$-\Delta V/V_0$	β
0	0	2.1	0	2.1	0	3.9	0	2.6	0	3.6	0	3.1
2000	0.037	1.7	0.034	1.7	0.060	2.3	0.043	1.7	0.054	2.5	0.050	2.1
4000	0.068	1.4	0.062	1.4	0.096	1.8	0.071	1.4	0.095	1.9	0.083	1.6
6000	0.093	1.2	0.087	1.1	0.124	1.4	0.092	1.16	0.127	1.5	0.108	1.3
8000	0.114	1.1	0.108	0.99	0.148	1.21	0.111	0.98	0.151	1.32	0.128	1.13
10000	0.132	1.0	0.124	0.88	0.200	...	0.128	0.87	0.170	1.17	0.154	...
12000	0.148	0.92	0.137	0.81	0.217	...	0.152	...	0.188	...	0.170	...
14000	0.162	0.85	0.148	0.74	0.232	...	0.166	...	0.204	...	0.184	...
16000	0.174	0.79	0.158	0.69	0.245	...	0.178	...	0.219	...	0.197	...
18000	0.186	0.73	0.167	0.66	0.257	...	0.190	...	0.231	...	0.208	...
20000	0.198	0.69	0.175	0.63	0.269	0.81	0.200	0.69	0.242	0.77	0.220	0.75
	No transition		No transition		I–II transition at 8200 kg/cm²		I–III transition at 10 200 kg/cm²		I–II transition at 10 400 kg/cm²		II–III transition at 10 000 kg/cm	
	$\xi=-1.2\pm0.2$		$\xi=-3.0\pm1.0$		$\xi=-3.7\pm0.3$		$\xi=-4.5\pm0.5$		$\xi=-2.3\pm0.2$		$\xi=-3.5\pm0.5$	
	$\rho=0.824$[8] gm/cm³		$\rho=0.832$[8] gm/cm³		$\rho=2.17$[9] gm/cm³				$\rho=1.17$[10] gm/cm³			

[a] β is the "instantaneous" compressibility, $-(1/V)(\partial V/\partial p)_T$, given in units of $(kg/cm^2)^{-1}$ $(\times 10^{-6})$.

NH_3

Solid ammonia shows no phase transitions below 19 000 kg/cm² in the range of temperature studied (100°–160°K). Its crystal structure is stated to be approximately face-centered cubic. No specific heat anomalies have been reported at atmospheric pressure between 20°K and the melting point. Furthermore, Smyth and Hitchcock[12] find that the dielectric constant of solid ammonia increases monotonically with temperature.

Ammonia evidently becomes brittle at the lower temperatures at which its compression was determined. The observed $\Delta V/V_0$'s at 110°K are too small compared with the values at 155°K, and the much larger value of ξ at the lower temperature also suggests that hydrostatic pressure was not being transmitted. Friction was considerably greater at 110° than at 155°K. It was therefore not feasible to go to lower temperatures.

SiF_4

This has been investigated over the temperature range 97°–200°K. There are no transitions at atmospheric pressure, but an unmistakable first order transition appears at high pressure (Fig. 2). The uncertainties of the individual points in the figure indicate the spread of pressures over which the observed transition could have occurred, and are based upon the sizes of the steps in which the pressure was varied. The "regions of indifference," (i.e., the pressure differences in excess of those caused by friction between the points at which the transition ran with increasing and decreasing pressure) were considerably larger than these uncertainties. The regions of indifference tended to be greater at low temperatures. Several runs below 100°K indicated no transition, although one was observed clearly at 108°K. This is believed to be the result of increasing sluggishness of the transition as the temperature is lowered. Phase I may exist as a metastable state at high pressure, somewhat analogous to the case of α and β mercury at low temperature.[13] No anomalies in the specific heat of solid SiF_4 at atmospheric pressure have been reported.

The I–II–III triple point at $T=123°K$, $P=11\ 200$ kg/cm² is somewhat uncertain. There seems to be little

[8] E. C. McKelvy and C. S. Taylor, Sci. Papers Bur. Standards, No. 465, **18**, 655 (1923).
[9] G. Natta, Gazz. chim. ital. **60**, 911 (1930).
[10] E. Justi and H. Nitka, Physik. Z. **37**, 435 (1936).
[11] L. Vegard and S. Hillesund, Avhandl. Norske Videnskaps Akad. Oslo. I. Mat. Naturv. Kl. (1942).
[12] C. P. Smyth and C. S. Hitchcock, J. Am. Chem. Soc. **56**, 1084 (1934).
[13] C. A. Swenson, Phys. Rev. **111**, 82 (1958).

doubt that the principal first order transition curve slopes down on either side of this point, but the two observations of the hypothetical II–III transition shown in Fig. 2 are based on extremely small discontinuities in the V vs P data. The ΔV data are not accurate enough to check for thermodynamic consistency at the triple point. Owing to the difficulty of condensing SiF_4 without blocking the filling capillary, it was not possible to obtain a large sample which would have increased the sensitivity of the ΔV measurements. It is not feasible in this apparatus to vary the temperature at constant pressure in order to confirm the existence of this transition.

Above 140°K, the observed values of the relative volume change for the I–II transition were fairly consistent. They tended to increase slowly with rising temperature. Between 140° and 200°K, the average of nine separate I–II $\Delta V/V_0$'s was 0.031 ± 0.010, corresponding to a change in molar volume of 1.5 ± 0.5 cm³/mole. The I–II transition curve may intersect the melting curve at a somewhat higher temperature than was reached in the present investigation. There appear to have been no experimental observations of the melting curve of SiF_4 above the triple point (1320 mm Hg, 182.9°K). The observed II–III ΔV was less than 0.2 cm³/mole, and this transition could conceivably be second order.

X-ray diffraction studies at atmospheric pressure show that the silicon atoms in phase I of SiF_4 form a body-centered cubic structure. The over-all lattice is molecular rather than ionic. The higher pressure phases would presumably be close packed.

H_2S

There has been more previous work on solid H_2S than is the case for the other substances under consideration. The two phase transitions at atmospheric pressure were first observed by Giauque and Blue.[14] Their specific heat measurements indicated a first-order transition at 103.6°K, and an anomaly such as is characteristic of second order transitions at 126.2°K. Kruis and Clusius[15] determined the latent heat of the lower transition to be 568.3 cal/mole, and the excess heat at the upper transition (over a range of several degrees) to be 108.7 cal/mole. Dielectric constant,[12] visual,[16] and nuclear magnetic resonance[17] observations of solid H_2S indicate no change in the face-centered cubic structure at 126.2°K, but do suggest a change to a slightly anisotropic state at 103.6°K. The dielectric constant jumps[12] from 3.5 to 21 as the temperature is raised through 103.6°K.

Previous pressure studies have been made to 250 kg/cm² by Clusius[18] for the lower transition, and by Stevenson[19] to 10 000 kg/cm² for the whole phase diagram. Figure 3 shows the result of the present investigation. The agreement for the slopes of the I–II and II–III transitions is fairly good. However, Stevenson's phases δ and κ have not been observed in the present study. For these he reports volume changes of the order of one-quarter to one-half his values for the I–II and II–III transitions. The present measurements seem to preclude the existence of any discontinuities as large as these. The difficulty of distinguishing transitions with small volume changes from frictional irregularities of piston motion in this apparatus has been discussed previously.[20]

The observed $\Delta V/V_0$ for the lower transition near atmospheric pressure (0.006 ± 0.001) corresponds to a molar ΔV of 0.16 ± 0.03 cm³/mole. With the latent heat of Clusius,[15] the Clausius-Clapeyron equation gives $dP/dT=900$ kg/cm²°K at $P=0$, agreeing satisfactorily with the initial slope of the observed transition curve (Fig. 3). This result compares reasonably well with the measured values of 680 kg/cm²°K reported by Clusius and Weigand,[18] and 660 kg/cm²°K obtained from the phase diagram of Stevenson.[19] The latter reports a single value of $\Delta V/V_0$ for this transition to be 0.0021 (at 4000 atm pressure). This corresponds to a change of molar volume of 0.06 cm³/mole, which appears to be too small.

Possibly both the transition curves intersect the melting curve. Stevenson[19] has evidence from one experimental point near 10 000 atm that the melting line is nearly vertical. No other observations of the melting curve seem to exist, nor have there been any direct measurements of the very small volume change upon melting at atmospheric pressure, from which the zero pressure slope of the melting curve might be calculated.

The x-ray diffraction studies of Justi and Nitka[9] indicate that the sulfur atoms in all three phases occupy a face-centered cubic lattice, with a change of less than 1% in the lattice constant (5.77 A) between 20° and 150°K. More recently, Reding and Hornig[21] have examined the infrared absorption spectra of thin films of solid H_2S at 66°, 112° and 140°K. They also conclude that the sulfur atoms occupy fcc sites in all three phases. The transitions apparently arise from variation of the positions of the hydrogen atoms. Phase III is shown to be ordered, while I and II are disordered. The basic cubic structure is quite open so that rearrangements of the hydrogens are possible without appreciable changes in the lattice constant. The nuclear magnetic resonance measurements of Alpert[17] show that neither

[14] W. F. Giauque and R. W. Blue, J. Am. Chem. Soc. **58**, 831 (1936).
[15] A. Kruis and K. Clusius, Z. Physik. Chem. **B38**, 156 (1937).
[16] A. Kruis and K. Clusius, Physik. Z. **38**, 511 (1937).
[17] N. L. Alpert, Phys. Rev. **75**, 398 (1949).
[18] K. Clusius and K. Weigand, Z. Elektrochem. **44**, 678 (1938).
[19] R. Stevenson, J. Chem. Phys. **27**, 147 (1957).
[20] J. W. Stewart, J. Phys. Chem. Solids **12**, 122 (1959).
[21] F. P. Reding and D. F. Hornig, J. Chem. Phys. **27**, 1024 (1957).

transition arises from a change of rotational states of the molecules (as is the case with CH_4). The optical anisotropy of phase III observed by Kruis and Clusius[16] can, it is believed, be accounted for by a small (less than 1%) distortion of the basic cubic lattice.

CF_4

Some additional data have been obtained for solid CF_4. Figure 4 shows the first order transition at higher temperatures than previously.[2] This transition was first observed thermally at atmospheric pressure at 76.2°K by Eucken and Schroeder.[22] We have observed a volume change of 1.8 cm³/mole at 89°K, and, earlier,[2] 2.2 cm³/mole at 77.3°K. The experimental value of dP/dT is 97 kg/cm² °K. This and the latent heat of transition observed by Eucken and Schroeder[22] lead to a calculated ΔV of 2.0 cm³/mole for the transition at atmospheric pressure. The observed transition parameters thus appear to be consistent.

Evidently, the structure of neither phase of solid CF_4 has been determined experimentally. Wyckoff[23] makes no mention of this substance. The silicon atoms in SiF_4 occupy bcc sites, while in CBr_4, another similar compound, the structure is known to be similar to that of SnI_4 above 47°C, and monoclinic below 47°C. One can only speculate on the basis of the moderately large volume change (approximately 4%) that the low temperature modification of CF_4 is close packed, while phase I is not.

The I–II transition line may or may not intersect the melting curve. The variation of melting temperature with pressure for CF_4 has apparently never been determined. There do not appear to exist observations of the densities of liquid and solid at the melting point.

IV. ACKNOWLEDGMENTS

The author wishes to acknowledge the assistance of Major Robert F. Patterson and James N. Boyd in the recording of the data, and also that of Phillip Sommer in the construction of much of the apparatus.

[22] A. Eucken and F. Schroeder, Z. Physik. Chem. **B41**, 307 (1938).

[23] R. W. G. Wyckoff, *Crystal Structures* (Interscience Publishers, Inc., New York, 1951).

THE JOURNAL OF CHEMICAL PHYSICS VOLUME 33, NUMBER 1 JULY, 1960

On the Assumptions Underlying Droplet Vaporization and Combustion Theories*

F. A. WILLIAMS

Division of Engineering and Applied Physics, Harvard University, Cambridge 38, Massachusetts

(Received February 18, 1960)

A study is undertaken to determine the range of validity of the assumptions that (a) the liquid temperature is constant and equal to the boiling temperature for a burning droplet, (b) the instantaneous vaporization rate of a droplet at a given size is the same as that of a constant-diameter sphere of the same size, and (c) the duration of the initial unsteady period is much less than the total vaporization time of a droplet. It is shown that assumption (a) may lead to observable differences between the theoretical and experimental burning rates for low-energy fuels, that for practical purposes assumption (b) is probably always valid, and that approximation (c), which is most accurate for large values of the temperature at infinity, may lead to a 20% error in the computed value of the total vaporization time. The calculated duration of the initial unsteady period compares favorably with experiments on droplet ignition delay times.

I. INTRODUCTION

THEORIES which have been successful in predicting the rate of decrease of the radius of vaporizing[1] or burning[2,3] droplets are based upon a number of plausible assumptions with ranges of validity which apparently have not been well determined theoretically. Although the success of these theories is a strong indication that the hypotheses are valid for the experiments to which the theories have been compared, it is nevertheless of interest to attempt to discover regions in which one or more of the underlying assumptions fail and to estimate the magnitude of the resulting corrections to the vaporization rate. In this paper we shall investigate the three assumptions (a) that the liquid temperature is constant and equal to the boiling temperature for a burning droplet, (b) that the instantaneous vaporization rate of a droplet at a given size is the same as that of a constant-diameter sphere of the same size (i.e., the quasi-steady-state hy-

* This research was supported in part by the U. S. Air Force under a contract monitored by the AF Office of Scientific Research of the Air Research and Development Command.

[1] I. Langmuir, Phys. Rev. **12**, 368–370 (1918).

[2] G. A. E. Godsave, *Fourth International Symposium on Combustion* (Williams and Wilkins Company, Baltimore, Maryland, 1953), pp. 818–830.

[3] M. Goldsmith and S. S. Penner, Jet Propulsion **24**, 245–251 (1954).

pothesis), and (c) that the duration of the unsteady ignition period is much less than the total burning time of a droplet. Our results tend to confirm the approximate validity of the existing theories.

The basic equations are developed and put into a suitable dimensionless form in Sec. II. In Sec. III we compute the actual steady-state surface temperature, first for a vaporizing droplet (without combustion) and then for a burning droplet. The effect upon the vaporization rate of the difference between the surface temperature and the boiling temperature is calculated for typical cases. Approximate solutions for the corrections to the evaporation rates of vaporizing and burning droplets, caused by the finite rate of decrease in droplet size, are presented in Sec. IV. It is shown that these corrections are usually less than 1% for solutions of the kind considered. A discussion of the results of a numerical integration of a simplified unsteady droplet vaporization problem is given in Sec. V. The time required for the droplet temperature and evaporation rate to approach their quasi-steady-state values is estimated and compared with experimental results.

II. BASIC EQUATIONS

A. Equations[4]

We shall consider the spherically symmetric molecular transport process occurring in an infinite gaseous atmosphere surrounding a spherical droplet. The only independent variables are the radial distance from the center of the droplet and time. For our equations of state, continuity, mass conservation of chemical species j, and energy conservation, we choose, respectively,

$$p=\rho RT \tag{1}$$

$$(\partial\rho/\partial t)+(1/r^2)(\partial/\partial r)(r^2\rho v)=0 \tag{2}$$

$$\rho(\partial Y_j/\partial t)+\rho v(\partial Y_j/\partial r)-(1/r^2)(\partial/\partial r)[r^2\rho D(\partial Y_j/\partial r)]=(\nu_j''-\nu_j')w \qquad j=1,\cdots,n \tag{3}$$

$$\rho(\partial T/\partial t)+\rho v(\partial T/\partial r)-(1/r^2)(\partial/\partial r)[r^2(\lambda/c_p)(\partial T/\partial r)]=(q/c_p)w, \tag{4}$$

where all symbols are defined in the list of symbols. In order that R may be treated as a constant in Eq. (1) it is assumed that the system is composed of a mixture of ideal gases, all of which have the same molecular weight. Since we are dealing with a deflagration problem, p is constant by virtue of the momentum equation. Equation (3) is based upon the additional assumptions that thermal diffusion is of negligible importance, the binary diffusion coefficients of all species are the same, and there is a single one-step chemical reaction of the form

$$\sum_{j=1}^{n}\nu_j' S_j \rightarrow \sum_{j=1}^{n}\nu_j'' S_j$$

where S_j represents the symbol for chemical species j. Equation (4) is strictly valid only when the further requirements that the heat capacities of all components are constant and equal are satisfied. Since we are interested in the order of magnitude of corrections to established theories, it is believed that these and our subsequent simplifying assumptions are permissible; useful methods for removing many of these assumptions have been developed (see, for example, footnote 3).

B. Dimensionless Form

In order to put Eqs. (1) through (4) into an appropriate dimensionless form we shall assume that $\lambda/c_p=\rho D=$constant and let the subscript 0 identify conditions at the droplet surface (in the gaseous phase). Introducing the dimensionless radial coordinate $\sigma=r/r_0$, time

$$\tau=\int(\rho D/\rho_0 r_0^2)\,dt,$$

density $\gamma=\rho/\rho_0$, mass flow rate per unit solid angle $\mu=r^2\rho v/r_0\rho D$, reaction rate $\omega=wr_0^2/\rho D$, and rate of decrease of droplet diameter $\epsilon=-(r_0\rho_0/\rho D)\,dr_0/dt$, we then find that the governing equations become

$$\gamma=T_0/T \tag{5}$$

$$\epsilon\sigma(\partial\gamma/\partial\sigma)+(\partial\gamma/\partial\tau)+(1/\sigma^2)(\partial\mu/\partial\sigma)=-\gamma(d\ln\rho_0/d\tau) \tag{6}$$

$$\epsilon\sigma\gamma(\partial Y_j/\partial\sigma)+\gamma(\partial Y_j/\partial\tau)+(\mu/\sigma^2)(\partial Y_j/\partial\sigma)-(1/\sigma^2)(\partial/\partial\sigma)[\sigma^2(\partial Y_j/\partial\sigma)]=(\nu_j''-\nu_j')\omega \qquad j=1,\cdots,n \tag{7}$$

$$\epsilon\sigma\gamma(\partial T/\partial\sigma)+\gamma(\partial T/\partial\tau)+(\mu/\sigma^2)(\partial T/\partial\sigma)-(1/\sigma^2)(\partial/\partial\sigma)[\sigma^2(\partial T/\partial\sigma)]=(q/c_p)\omega. \tag{8}$$

The definitions of σ and τ illustrate that in the present problem the "natural" units of length and time are r_0 and (r_0^2/D_0), respectively.

The nonlinear couplings appearing in Eqs. (5) through (8) indicate that general solutions to unsteady droplet combustion problems would be difficult to obtain. In Secs. III and IV of this paper we shall therefore restrict our attention to cases in which γ, μ, T, and Y_j depend only upon σ; as the droplet diameter decreases the properties of the gas remain constant at a given value of r/r_0. It may be emphasized that the solution resulting from this similarity type of approximation is not restricted to the case $dr_0/dt=0$. However, it must also be pointed out that rigorously our conclusions will not be of general validity. It is a consequence of this similarity assumption that ϵ and ρ_0 are

[4] The equations presented in this section are easily derived from the general fluid dynamical equations given in S. S. Penner [*Chemistry Problems in Jet Propulsion* (Pergamon Press, New York, 1957), Part III], for example.

constants, and Eqs. (6) through (8) reduce to the total differential equations

$$\epsilon\sigma^3(d\gamma/d\sigma)+(d\mu/d\sigma)=0 \tag{9}$$

$$\epsilon\sigma^2\gamma(dY_j/d\sigma)+\mu(dY_j/d\sigma)-(d/d\sigma)[\sigma^2(dY_j/d\sigma)] = (\nu_j''-\nu_j')\sigma^2\omega, \quad j=1,\cdots,n, \tag{10}$$

$$\epsilon\sigma^2\gamma(dT/d\sigma)+\mu(dT/d\sigma)-(d/d\sigma)[\sigma^2(dT/d\sigma)] = (q/c_p)\sigma^2\omega. \tag{11}$$

C. Boundary Conditions

Before going on to the treatment of specific corrections, it is convenient to state some important boundary conditions which are valid for all of the cases that we shall consider. The values of the dependent variables are physically specified at $r=\infty$ (denoted by the subscript ∞). Conservation of mass of the liquid in the droplet requires that

$$4\pi r_0^2\rho_l(dr_0/dt) = -4\pi r_0^2\rho_0[v_0-(dr_0/dt)],$$

where ρ_l is the density of the liquid. If this equation, which states that the rate of change of the mass of the droplet equals the total mass flow rate relative to the droplet surface, is solved for dr_0/dt and the solution is expressed in our dimensionless notation, then we find

$$\epsilon=\mu_0/[(\rho_l/\rho_0)-1]. \tag{12}$$

It is assumed that the gaseous chemical species which are not initially in the liquid drop will not diffuse into the liquid. If these species are denoted by the subscripts $j=n-m,\cdots,n$, then there must be no net mass flow of these species relative to the droplet surface at $r=r_0$, i.e.,

$$4\pi r_0^2\rho_0 Y_{j,0}[v_0-(dr_0/dt)]-4\pi r_0^2\rho_0 D_0(\partial Y_j/\partial r)_0=0, \quad j=n-m,\cdots,n.$$

This statement of the fact that diffusion cancels the convective mass flow of species j may be written in dimensionless notation as

$$(dY_j/d\sigma)_0=(\mu_0+\epsilon)\,Y_{j,0} \quad j=n-m,\cdots,n. \tag{13}$$

A similar boundary condition for the energy equation is a consequence of the requirement that the energy transferred from the gas to the droplet by conduction goes into the latent heat of vaporization of the evaporating liquid and raising the average temperature of the droplet. We shall let L equal the latent heat of vaporization per gram, let $c_{p,l}$ represent the constant heat capacity of the liquid, and assume for simplicity that the temperature of the liquid is T_0. The enthalpy balance at the droplet surface then shows that

$$4\pi r_0^2\lambda_0(\partial T/\partial r)_0=4\pi r_0^2\rho_0[v_0-(dr_0/dt)]L+\tfrac{4}{3}\pi r_0^3\rho_l c_{p,l}(dT_0/dt)$$

which may be expressed in dimensionless form as

$$(dT/d\sigma)_0=\beta(\mu_0+\epsilon)(L/c_p), \tag{14}$$

where

$$\beta=1-\left(\frac{c_{p,l}}{L}\frac{dT_0}{dt}\right)\Big/\left(\frac{3}{r_0}\frac{dr_0}{dt}\right)$$

is the ratio of the total heat transferred to that required for vaporization, and use has been made of Eq. (12). The effect of a variation of temperature within the droplet may be accounted for by slightly modifying the equation for β.

III. DROPLET SURFACE TEMPERATURES

In order to determine the range of validity of the assumption that the surface temperature of a burning droplet is constant and equal to the boiling temperature, we must use the Clausius-Clapeyron equation which determines the droplet surface temperature T_0.[5] To avoid possible physicochemical complications associated with the vaporization of multicomponent liquids, it will be assumed that the droplet is composed of a single chemical species denoted by the subscript 1. If we make the further reasonable assumptions that $\rho_l\gg\rho_0$, $r_0\gtrsim 1\ \mu$ so that surface tension effects are negligible, and Eq. (1) is valid, then the Clapeyron equation may be written in the integrated form

$$Y_{1,0}=\exp\left[-\int_{T_0}^{T_b}(L/RT^2)dT\right], \tag{15}$$

where T_b is the boiling temperature of the liquid. The use of Eq. (15), which is based upon the assumption of phase equilibrium, may be questioned on the grounds that we are dealing with rate processes; however, kinetic theory estimates of the limit of validity of the Clapeyron equation show that typical droplet vaporization and burning rates are too slow by a few orders of magnitude for Eq. (15) to be significantly violated.

In this section we shall neglect the vaporization rate correction arising from the fact that $dr_0/dt\neq 0$; i.e., it will be assumed here that $\epsilon=0$ since the effect of finite ϵ is dealt with in the following section. Equation (9) then shows that $\mu=$constant, and Eqs. (10) and (11) undergo obvious simplifications. We shall first treat the case of vaporization without combustion and then consider the diffusion flame reaction $F+O\rightarrow 2P$ in the flame surface approximation.

A. Vaporization

When there are no chemical reactions in the gas then $\omega=0$ and we may treat the components $j=n-m,\cdots,n$ as a single constituent by using the identity

$$\sum_{j=n-m}^{n} Y_j=1-Y_1.$$

[5] S. Glasstone, *Textbook of Physical Chemistry* (D. Van Nostrand Company, Inc., Princeton, New Jersey, 1946), pp. 443–460.

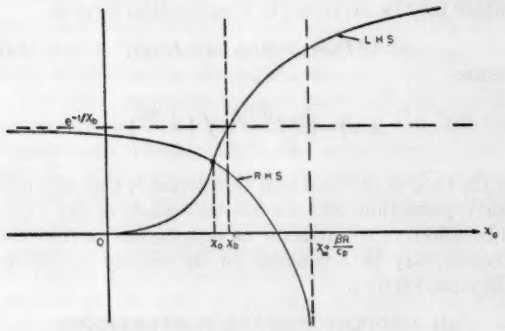

FIG. 1. Determination of the droplet surface temperature from Eq. (23).

Equations (10) and (11) become

$$\mu(dY_1/d\sigma)-(d/d\sigma)[\sigma^2(dY_1/d\sigma)]=0 \qquad (16)$$

and

$$\mu(dT/d\sigma)-(d/d\sigma)[\sigma^2(dT/d\sigma)]=0 \qquad (17)$$

which (since μ=constant) may easily be integrated twice with the result that

$$Y_1=\left(\frac{Y_{1,0}-Y_{1,\infty}e^{-\mu}}{1-e^{-\mu}}\right)+\left(\frac{Y_{1,\infty}-Y_{1,0}}{1-e^{-\mu}}\right)e^{-\mu/\sigma} \qquad (18)$$

and

$$T=\left(\frac{T_0-T_\infty e^{-\mu}}{1-e^{-\mu}}\right)+\left(\frac{T_\infty-T_0}{1-e^{-\mu}}\right)e^{-\mu/\sigma}. \qquad (19)$$

By substituting Eqs. (18) and (19) into the boundary conditions expressed by Eqs. (13) (summed from $j=n-m$ to n) and (14), we determine $Y_{1,0}$ and T_0 in terms of μ and the specified properties at ∞, viz.

$$Y_{1,0}=1-(1-Y_{1,\infty})e^{-\mu}, \qquad (20)$$

$$T_0=T_\infty-\beta(L/c_p)(e^{\mu}-1). \qquad (21)$$

The solution of Eq. (20) for μ provides an interpretation of the evaporation rate in terms of "diffusion-controlled" vaporization, while Eq. (21) may be considered to determine μ for "heat-transfer-controlled" vaporization.

If μ is eliminated from Eqs. (20) and (21), then the equation

$$Y_{1,0}=\left(Y_{1,\infty}+\frac{T_\infty-T_0}{\beta(L/c_p)}\right)\Big/\left(1+\frac{T_\infty-T_0}{\beta(L/c_p)}\right) \qquad (22)$$

is obtained relating $Y_{1,0}$ to T_0. The two independent Eqs. (15) and (22) determine the steady-state values of the droplet surface temperature and vapor pressure.

If it is assumed that L is constant between the temperatures T_0 and T_b, then Eqs. (15) and (22) show that the surface temperature may be found by solving the equation

$$\exp(-1/\chi_0)=\exp(-1/\chi_b)\left(\frac{(\beta R Y_{1,\infty}/c_p)+\chi_\infty-\chi_0}{(\beta R/c_p)+\chi_\infty-\chi_0}\right) \qquad (23)$$

for χ_0 (here $\chi\equiv RT/L$).

A graphical method for solving Eq. (23) is illustrated in Fig. 1, from which it can be seen that there is a unique solution χ_0. The solution to Eq. (23) for χ_0 as a function of χ_∞ with various values of $Y_{1,\infty}$ is plotted in Fig. 2 for the case $\beta R/c_p=1$, $\chi_b=1$. From Eq. (21) it follows that the sections of the curves in Fig. 2 for which $\chi_0>\chi_\infty$ correspond to condensation, while we must have $\chi_0<\chi_\infty$ for droplet vaporization. It may be seen from Fig. 2 or Eq. (23) that χ_0 and $Y_{1,0}$ increase as $Y_{1,\infty}$ and χ_∞ increase; as χ_∞ approaches infinity χ_0 asymptotically approaches χ_b and $Y_{1,0}$ goes to unity. Hence it follows that the assumption $T_0\approx T_b$ will be valid for a vaporizing droplet when T_∞ is sufficiently large. From Fig. 2 it is seen that for $Y_{1,\infty}=0.5$, (T_b-T_0) is less than 10% of T_b when $T_\infty\geq 5L/R$. Since the gas temperature usually reaches a value much larger than this minimum T_∞ in the neighborhood of a burning droplet, we might infer that the approximation $T_0\approx T_b$ will be quite accurate for droplet combustion problems such as those considered in the following paragraphs.

B. Combustion

For the case[4] in which the droplet is composed of fuel $F(j=1)$ which reacts at a flame surface with oxidizer $0(j=2)$ contained in the surrounding atmosphere to form products $P(j=3)$ by the chemical equation $F+0\rightarrow 2P$, the governing differential equations [Eqs. (10) and (11)] become

$$\mu(dY_j/d\sigma)-(d/d\sigma)[\sigma^2(dY_j/d\sigma)]=(\nu_j''-\nu_j')\sigma^2\omega \qquad j=1,2,3 \qquad (24)$$

and

$$\mu d\theta/d\sigma()-(d/d\sigma)[\sigma^2(d\theta/d\sigma)]=\sigma^2\omega. \qquad (25)$$

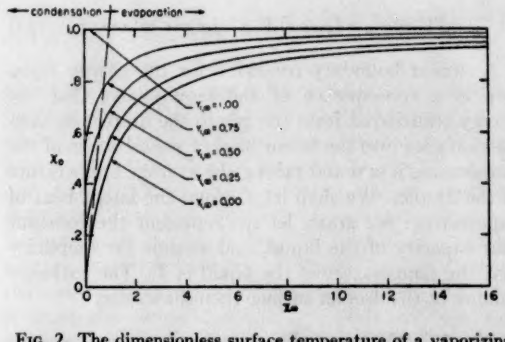

FIG. 2. The dimensionless surface temperature of a vaporizing droplet as a function of the dimensionless temperature at infinity for various values of $Y_{1,\infty}$ with $\beta R/c_p=1$ and $\chi_b=1$.

Here it has been assumed that $n=3$, $m=1$, $\nu_1''-\nu_1'=-1$, $\nu_2''-\nu_2'=-1$, $\nu_3''-\nu_3'=2$, and we have introduced the definition $\theta\equiv c_pT/q$ in Eq. (25). From Eqs. (24) and (25) it is seen that

$$\mu(d/d\sigma)(Y_2+\theta)-(d/d\sigma)[\sigma^2(d/d\sigma)(Y_2+\theta)]=0 \quad (26)$$

and

$$\mu(d/d\sigma)(Y_2-Y_1)-(d/d\sigma)[\sigma^2(d/d\sigma)(Y_2-Y_1)]=0, \quad (27)$$

which, supplemented by known boundary conditions, will be found to be sufficient for determining the burning rate. Zeldovich[6] was apparently one of the earliest investigators to propose using Eqs. (26) and (27) in place of Eqs. (24) and (25).

Since the linear operator appearing in Eqs. (26) and (27) is the same as that appearing in Eqs. (16) and (17), it follows that the solutions to Eqs. (26) and (27) are of the same form as those given in Eqs. (18) and (19). By substituting the solutions to Eqs. (26) and (27) into the boundary conditions given by Eqs. (13) and (14), we find that

$$[(Y_{2,\infty}+\theta_\infty)-(Y_{2,0}+\theta_0)]/(e^\mu-1)=\beta(L/q)+Y_{2,0} \quad (28)$$

and

$$[(Y_{2,\infty}-Y_{1,\infty})-(Y_{2,0}-Y_{1,0})]/(e^\mu-1)=1-Y_{1,0}+Y_{2,0}. \quad (29)$$

For a burning fuel droplet in an oxidizing atmosphere $Y_{1,\infty}=0$ and the values of $Y_{2,\infty}$ and θ_∞ are known. Only in the flame surface approximation is the additional boundary condition $Y_{2,0}=0$ valid.[7] When $Y_{2,0}=0$, Eqs. (15), (28), and (29) constitute three equations for the three unknowns $Y_{1,0}$, θ_0, and μ. By solving Eq. (28) for μ, it is seen that after θ_0 is determined the burning rate is given by

$$\mu=\ln[1+(q/\beta L)(\theta_\infty-\theta_0+Y_{2,\infty})]. \quad (30)$$

If μ is eliminated from Eqs. (28) and (29), and Eq. (15) with L=constant is then used to eliminate $Y_{1,0}$, we find that the equation

$$\exp[-(c_pL/Rq)(1/\theta_0)]=\exp[-(c_pL/Rq)(1/\theta_b)]\times\left[\frac{\theta_\infty-\theta_0+Y_{2,\infty}[1-(\beta L/q)]}{\theta_\infty-\theta_0+Y_{2,\infty}+(\beta L/q)}\right] \quad (31)$$

determines the dimensionless droplet surface temperature θ_0.

[6] Y. B. Zeldovich, Zhur. Tek. Fiz. **19**, No. 10 (1949); English translation NACA TM 1296 (1950).

[7] W. Nachbar (personal communication).

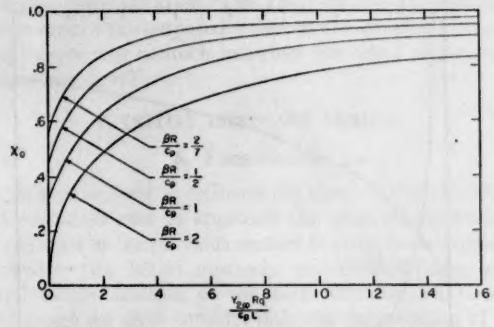

FIG. 3. The dimensionless surface temperature of a burning droplet as a function of the dimensionless heat of reaction for various values of $\beta R/c_p$ with $\chi_b=1$, $\chi_\infty=1$, and $Y_{2,\infty}=\frac{1}{2}$.

The fact that Eq. (31) is of exactly the same form as Eq. (23) may be seen more clearly by writing Eq. (31) in terms of χ, viz.

$$\exp(-1/\chi_0)=\exp(-1/\chi_b)\times\left[\frac{(RqY_{2,\infty}/c_pL)-(\beta RY_{2,\infty}/c_p)+\chi_\infty-\chi_0}{(RqY_{2,\infty}/c_pL)+(\beta R/c_p)+\chi_\infty-\chi_0}\right]. \quad (32)$$

Hence we expect the graphical method of solution illustrated in Fig. 1 to be useful here. In Fig. 3, χ_0 is plotted as a function of the dimensionless heat of reaction $Y_{2,\infty}Rq/c_pL$ for the case $\chi_b=1$, $\chi_\infty=1$, and $Y_{2,\infty}=\frac{1}{2}$ with various values of $\beta R/c_p$. It may be seen from Eq. (32) that $T_0\approx T_b$ when the heat of reaction is sufficiently large; e.g., according to Fig. 3, $(T_b-T_0)<0.1T_b$ for $Y_{2,\infty}Rq/c_pL\geq 4.3$ (which is true for many fuels) in the case $\beta R/c_p=\frac{2}{7}$ (which corresponds to a diatomic gas when $\beta=1$). From Fig. 3 it is also seen that the approximation $T_0\approx T_b$ becomes invalid when a sizeable fraction of the heat transferred to the droplet is used in raising the average droplet temperature ($\beta\gg 1$).

The effect of the approximation $T_0\approx T_b$ upon the droplet burning rate is illustrated in Fig. 4, where we have plotted the dimensionless burning rate μ, computed from Eq. (30), as a function of $Y_{2,\infty}Rq/c_pL$ for $\chi_b=1$, $\chi_\infty=1$, $Y_{2,\infty}=\frac{1}{2}$, and $\beta R/c_p=\frac{2}{7}$. The difference between μ and the approximate burning rate (μ_I), computed from Eq. (30) with the assumption that $\chi_0=\chi_b$, is also shown in Fig. 4. Since μ depends logarithmically upon T_0, a substantial error in T_0 produces only a small change in μ; e.g. $(\mu-\mu_I)/\mu<.03$ when $(T_b-T_0)/T_b<0.15$ according to Fig. 4. The approximation $T_0\approx T_b$ produces an error greater than 10% in the computed value of the burning rate only for very small heats of reaction, namely when $Y_{2,\infty}Rq/c_pL<1$, a condition under which few fuels can be ignited.

IV. EFFECT OF SURFACE REGRESSION RATE

In studying the effect of the rate of decrease of droplet diameter upon the burning rate, we shall assume

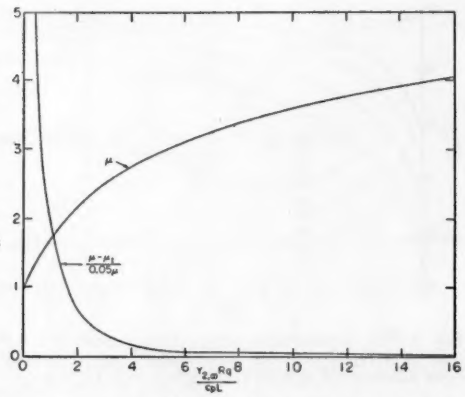

FIG. 4. The dimensionless burning rate and the error in the burning rate caused by the approximation $T_0=T_b$ for the case $\chi_b=1$, $\chi_\infty=1$, $Y_{2,\infty}=\frac{1}{2}$, and $\beta\bar{R}c_p=2/7$.

that T_0 is known and neglect the corrections discussed in the previous section resulting from the boundary condition given by Eq. (15). An explicit solution for the unrealistic case in which density is constant is presented in Part A. We also consider an evaporating droplet for which the vapor behaves as an ideal gas (Part B), and the oxidation of a fuel droplet in the flame surface approximation (Part C).

A. Constant-Density Vaporization

For the case of constant density $\gamma=1$ and Eq. (5) must be discarded. Equation (9) then shows that μ is constant, and Eq. (11) becomes

$$(\mu+\epsilon\sigma^3)(dT/d\sigma)-(d/d\sigma)[\sigma^2(dT/d\sigma)]=0, \quad (33)$$

because $\omega=0$. Since T_0 and T_∞ are known, Eqs. (33) and (14) will be sufficient for determining the burning rate; Eqs. (10) and (13) are needed only in finding the concentration profiles and $Y_{j,0}$. By treating $dT/d\sigma$ as a new dependent variable in Eq. (33), the equation may easily be integrated twice with the result

$$T=T_0+(\beta L/c_p)(\mu+\epsilon)\int_1^\sigma \times\exp\{\mu[1-(1/\sigma)]+(\epsilon/2)(\sigma^2-1)\}(d\sigma/\sigma^2), \quad (34)$$

where use has been made of the boundary condition given in Eq. (14). Since Eq. (12) relates ϵ to μ, Eq. (34) shows that the vaporization rate should be determined in terms of T_∞ and other known properties of the system by solving the equation

$$(\mu+\epsilon)\int_1^\infty \exp\{\mu[1-(1/\sigma)]+(\epsilon/2)(\sigma^2-1)\}(d\sigma/\sigma^2) = c_p(T_\infty-T_0)/\beta L \quad (35)$$

for μ.

Unfortunately, for the case of a vaporizing droplet ($\mu>0$, $\epsilon>0$), the integral in Eq. (35) diverges, implying that in this case there exists no solution of the assumed similarity type consistent with the boundary condition $T_\infty<\infty$. For a condensing droplet ($\mu\leq 0$, $\epsilon\leq 0$) the integral in Eq. (35) is convergent and may be estimated by transforming from σ to $\eta=(\sigma-1)/\sigma$ as the independent variable. Equation (35) then becomes

$$\frac{c_p(T_\infty-T_0)}{\beta L}=(\mu+\epsilon)\int_0^1 \exp\{\mu\eta+\tfrac{1}{2}\epsilon[(1-\eta)^{-2}-1]\}d\eta$$
$$=(\mu+\epsilon)\int_0^1 \exp\{(\mu+\epsilon)\eta+\tfrac{3}{2}\epsilon\eta^2+\cdots\}d\eta, \quad (36)$$

where the exponent has been expanded in powers of η. Since the integrand assumes its maximum value at $\eta=0$, when μ and ϵ are negative, the largest contribution to the integral will come from the region near $\eta=0$. It is therefore reasonable to approximate the integral by neglecting all but the first term in the expansion in Eq. (36), i.e.,

$$\mu+\epsilon\approx\ln\{1+[c_p(T_\infty-T_0)/\beta L]\}. \quad (37)$$

By using Eq. (12) and the definition of ϵ in Eq. (37), we find that the growth rate is approximately

$$dr_0/dt\approx-(\rho_0D_0/\rho_1r_0)\ln\{1+[c_p(T_\infty-T_0)/\beta L]\}. \quad (38)$$

It is important to note that in the derivation of Eq. (38), no assumptions concerning the magnitudes of ϵ are involved. Nevertheless, the resulting approximate value of dr_0/dt is exactly the same as that obtained from the usual treatments which set $\epsilon=0$. Since typically $\rho_1/\rho_0\sim 10^3$, Eq. (12) shows that the term ϵ also contributes only 0.1% to the value of μ computed from Eq. (37). It is concluded that the mass rate of condensation of a droplet is nearly equal to the mass flow rate into a porous sphere under the same ambient conditions.

In the case of a vaporizing droplet ($\epsilon>0$), since ϵ is small the integrand in Eq. (35) begins to grow rapidly only at values of r larger than the size of a conventional apparatus. Hence it may be reasonable to assume that the similarity solution is valid from the droplet surface to a designated large value of σ at which the physical boundary condition $T=T_\infty$ is applied, and to allow for nonsimilar flow at larger values of σ. The vaporization rate would then be determined unambiguously by T_∞. In this case Eq. (37) would be of approximate validity even when $\epsilon>0$, provided the evaporation rate correction is determined by the change in properties near the droplet surface (i.e., provided the expansion in powers of η is valid). The accuracy of these approximations depends upon the experimental configuration; it is obviously possible to design experiments which would violate the similarity assumption.

B. Ideal Gas Vaporization

In this and the following section we obtain approximate burning rate corrections without proving that there exists a similarity solution consistent with the boundary condition $T_\infty < \infty$. The analysis presented in the previous section leads us to suspect that rigorously acceptable similarity solutions may not exist, particularly for vaporizing droplets. In such cases our results will be meaningful only if we resort to the argument presented in the preceding paragraph.

For ideal gas vaporization $\omega=0$ and γ is given by Eq. (5). In Appendix A it is shown that by expanding T in powers of ϵ, ($T=T^{(0)}+\epsilon T^{(1)}+\cdots$ where $T^{(0)}$ is the solution for a porous sphere), Eqs. (9) and (11) may be reduced to a series of linear equations for $T^{(1)}$, $T^{(2)}$, etc. By neglecting terms of order ϵ^2 on the basis that ϵ is small, and by expanding the equation for $T^{(1)}$ in powers of η about $\eta=0$, it is then demonstrated in Appendix A that

$$\mu_0=\mu_0^{[0]}+\epsilon\mu_0^{[1]}, \tag{39}$$

where

$$\mu_0^{[0]}=\ln[\alpha^{-1}(\psi_\infty+\alpha-1)] \tag{40}$$

is the value of μ_0 computed by assuming $\epsilon=0$, and

$$\mu_0^{[1]}=-(1+\mu_0^{[0]})\exp(-\mu_0^{[0]}). \tag{41}$$

In Eq. (40) $\psi_\infty=T_\infty/T_0$ and $\alpha=\beta L/c_pT_0$. From Eqs. (12), (39), and (41) and the definition of ϵ, it follows that

$$dr_0/dt=-(\rho D/\rho_l r_0)\mu_0^{[0]} \times\{1-(\rho_0/\rho_l)[1-(1+\mu_v^{[0]})\exp(-\mu_0^{[0]})]\}^{-1}. \tag{42}$$

From Eq. (42) we find that $dr_0^2/dt=$constant, a result which is a necessary consequence of the similarity approximation. Equations (39) and (42) show that the correction always produces a slight decrease in μ_v and a slight increase in the calculated magnitude of dr_v/dt. The order of magnitude of the corrections to μ_0 and dr_0/dt is 0.1% for typical values of ρ_0/ρ_l. We conclude that the error in the computed value of dr_0/dt for a vaporizing or condensing droplet, introduced by the assumption $\epsilon=0$, will be observable only for unrealistically large value of ρ_0/ρ_l.

C. Combustion

We treat the same system that was considered in Sec. III B. The details of the analysis, which are analogous to those employed in Sec. IV B, are presented in Appendix B. The results are exactly the same as in the preceding section, except that in this case the mass flow rate for $\epsilon=0$ is

$$\mu_0^{[0]}=\ln[1+\delta^{-1}(\theta_\infty-\theta_0+Y_{2,\infty})], \tag{43}$$

where $\delta\equiv\beta L/q$. The remarks of the previous section concerning the nature and magnitude of the correction therefore also apply to burning droplets in the flame surface approximation. The effect of the assumption $\epsilon=0$ upon the computed value of the droplet surface regression rate is much less than the effect of the assumption $T_0=T_b$.

V. INITIAL UNSTEADY PERIOD

A. Formulation

It is of interest to estimate the time required for the vaporization rate to approach the quasi-steady value computed in the previous section in order to determine whether the initial unsteady period constitutes an appreciable fraction of the total vaporization time. Although we shall consider only the vaporization of a system of the type treated in Secs. III A and IV B, the results may be of approximate validity for the thermal ignition of fuel droplets, provided the preignition time composes the major portion of the unsteady period.

The correct way to treat this problem is to solve Eqs. (5) through (8) with $\omega=0$ and specified initial and boundary conditions. While this procedure is quite feasible with the aid of automatic computing machines, even the additional reasonable approximation $\epsilon=0$ will not enable us to solve the equations analytically. However, if initially there exists nearly steady-state conditions and the imposed boundary conditions vary slowly with time, then it may be expected that the temperature and concentration profiles in the gas will differ only slightly from the steady-state profiles. Specifically, if the initial configuration is one of equilibrium or quasi-steady-state vaporization and the fractional change in all coefficients and boundary conditions in the characteristic time (r_0^2/D_0) is much less than unity, then the terms involving derivatives with respect to τ in Eqs. (5) through (8) will be much smaller than those involving $\partial/\partial\sigma$ and the solutions will be almost the same as those obtained in Secs. III and IV. For the sake of simplicity we shall investigate only those slow variations, in which case the appropriate solutions to Eqs. (5) through (8) have already been obtained and our task is to study relations between the constants and boundary conditions of these equations.

In view of the results of the preceding section, we shall let $\epsilon=0$. The solutions for $Y_{1,0}$ and T_0 are therefore given by Eqs. (20) and (21). Equation (15) relates $Y_{1,0}$ to T_0, and Eq. (12) determines dr_0/dt in terms of μ. Thus Eqs. (20) and (21) imply that dr_0/dt is determined by T_∞, $Y_{1,\infty}$, β, and physicochemical properties of the system. In view of the definition of β (see Sec. II C), we therefore shall obtain two simultaneous first-order ordinary differential equations for $T_0(t)$ and $r_0(t)$, the solutions of which depend upon the specified functions $T_\infty(t)$ and $Y_{1,\infty}(t)$.

If $c_{p,l}$ and c_p are constant over the temperature range of interest, then L is a linear function of T_0 and may be expressed as

$$L=(c_{p,l}-c_p)(T_c-T_0), \tag{44}$$

where T_c is a constant which equals the temperature at the critical point only if $c_{p,l}$ and c_p are constant between T_0 and the critical temperature. If Eq. (44) is substituted into Eq. (15) and the integration is performed, then it is found that

$$Y_{1,0}=\phi^{-\epsilon}\exp[-\kappa\phi_c(\phi^{-1}-1)] \tag{45}$$

where $\phi\equiv T_0/T_b$, $\kappa\equiv(c_{p,l}-c_p)/R$, and $\phi_c\equiv T_c/T_b$. By solving Eq. (20) for μ and using Eq. (12) and the definition of ϵ, we obtain

$$-\frac{r_0\rho_l}{\rho D}\frac{dr_0}{dt}=\ln\left[\frac{1-Y_{1,\infty}}{1-\phi^{-\epsilon}\exp[-\kappa\phi_c(\phi^{-1}-1)]}\right], \tag{46}$$

where use has been made of Eq. (45) and the fact that $(\rho_l/\rho_0)-1\approx\rho_l/\rho_0$. By solving Eq. (21) for β, using Eq. (46) to eliminate μ, and employing Eq. (44) to eliminate L in relating β to dT_0/dt, we find

$$\frac{(c_{p,l}/c_p)(d\phi/dt)}{(3/r_0)(dr_0/dt)}=\frac{\phi_\infty-\phi}{\{(1-Y_{1,\infty})/(1-\phi^{-\epsilon}\exp[-\kappa\phi_c(\phi^{-1}-1)])\}-1}-\frac{R}{c_p}\kappa(\phi_c-\phi), \tag{47}$$

where $\phi_\infty\equiv T_\infty/T_b$. Introducing dimensionless time and droplet radius variables defined as $\xi\equiv(3c_p\rho D/c_{p,l}\rho r_{0,i}^2)t$ and $\zeta\equiv(3c_p/c_{p,l})\ln(r_{0,i}/r_0)$ where the subscript i on r_0 identifies the initial value of r_0 (at $t=0$), it is seen that Eqs. (46) and (47) become

$$\frac{d\zeta}{d\xi}=\exp\{\tfrac{3}{2}[1+(R/c_p)\kappa]\zeta\}\ln\left[\frac{1-Y_{1,\infty}}{1-\phi^{-\epsilon}\exp[-\kappa\phi_c(\phi^{-1}-1)]}\right] \tag{48}$$

and

$$\frac{d\phi}{d\zeta}=\frac{\phi_\infty-\phi+Y_{1,\infty}(R/c_p)\kappa(\phi_c-\phi)-[\phi_\infty-\phi+(R/c_p)\kappa(\phi_c-\phi)]\phi^{-\epsilon}\exp[-\kappa\phi_c(\phi^{-1}-1)]}{\phi^{-\epsilon}\exp[-\kappa\phi_c(\phi^{-1}-1)]-Y_{1,\infty}} \tag{49}$$

where the right-hand side of Eq. (47) has been rationalized. Since the definition of ξ indicates that $\xi\sim10^3\tau$, functions which vary rapidly with ξ may still vary sufficiently slowly with τ for our basic approximations to remain valid. Equations (48) and (49) indicate that the integral

$$\zeta=\int_{\phi_i}^{\phi}\frac{[\phi^{-\epsilon}\exp[-\kappa\phi_c(\phi^{-1}-1)]-Y_{1,\infty}]d\phi}{\phi_\infty-\phi+Y_{1,\infty}(R/c_p)\kappa(\phi_c-\phi)-[\phi_\infty-\phi+(R/c_p)\kappa(\phi_c-\phi)]\phi^{-\epsilon}\exp[-\kappa\phi_c(\phi^{-1}-1)]} \tag{50}$$

may be performed first in order to determine ζ as a function of ϕ, after which ξ is given as a function of ζ by the equation

$$\xi=\int_0^{\zeta}\exp\{-\tfrac{3}{2}[1+(R/c_p)\kappa]\zeta\}\left\{\ln\left[\frac{1-Y_{1,\infty}}{1-\phi^{-\epsilon}\exp[-\kappa\phi_c(\phi^{-1}-1)]}\right]\right\}^{-1}d\zeta. \tag{51}$$

B. Discussion of Results

We shall consider a system which, initially in equilibrium at $\phi=\phi_i$ and $r_0=r_{0,i}$ (viz, $\phi_\infty=\phi_i$ and $Y_{1,\infty,i}=Y_{1,0,i}=\phi_i^{-\epsilon}\exp[-\kappa\phi_c(\phi_i^{-1}-1)]$), is subjected to a jump in ϕ_∞ and $Y_{1,\infty}$ at $t=0$, after which ϕ_∞ and $Y_{1,\infty}$ are held constant.[8] The time required for the system to adjust to a new equilibrium condition or to approach quasi-steady vaporization is then computed from Eqs. (50) and (51). The calculations have been carried out with $\kappa=\frac{7}{2}$ and $R/c_p=\frac{2}{7}$, which corresponds to a diatomic gas with $c_{p,l}=2c_p$, and for $\phi_c=\frac{3}{2}$, which is approximately valid for many hydrocarbons at atmospheric pressure. For $\phi_i=0.8$ ($Y_{1,0,i}=0.588$) we present in Figs. 5 and 6 the dependence of ϕ and $(r_0/r_{0,i})^2$, respectively, upon ξ for various values of ϕ_∞ with $Y_{1,\infty}=Y_{1,0,i}$. Similar computations with $\phi_\infty=\phi_i$ and $Y_{1,\infty}<Y_{1,0,i}$ show the same kind of results, except that as ξ increases ϕ decreases approaching an asymptotic value less than ϕ_i. For other choices of ϕ_∞ and $Y_{1,\infty}$, the asymptotic solution is one of condensation, equilibrium, or evaporation depending (respectively) upon whether the value of $Y_{1,\infty}$ is greater than, equal to, or less than the value of $Y_{1,0}$ computed from Eq. (45) by setting $\phi=\phi_\infty$. For droplets which eventually ignite upon heating, solutions of the type illustrated in Figs. 5 and 6 may be referred to as "thermal ignition," since the composition at $r=\infty$ remains fixed ($Y_{1,\infty}=Y_{1,\infty,i}$).

From Fig. 5 it is seen that the time required for the droplet temperature to approach within 0.1% of its asymptotic value decreases significantly as T_∞ increases. This time is the same as that required for

[8] Although such a jump strictly violates our assumption of small time derivatives, nevertheless it is expected that the error will be restricted to small time intervals ($\xi\ll1$). Since ξ is the time used in the computation, we could replace the jump condition by a linear rise for $0<\xi<10^{-3}$, after which ϕ_∞ and $Y_{1,\infty}$ are held constant. This change would restore the validity of our approximation that $\partial/\partial\tau$ is small, and would leave our solutions virtually unchanged in the range of interest $\xi>10^{-3}$.

the development of steady-state vaporization, because when ϕ becomes constant then dr_0^2/dt is also constant according to Eq. (46). From the definition of ξ, it follows that the time required for the droplet temperature to approach its steady-state value is proportional to $\rho_l r_{0,i}^2/\rho D$, i.e., a small droplet radius and a high thermal conductivity of the gas favor a short unsteady period.

In addition to illustrating the dependence of the droplet radius upon time during the unsteady period, Fig. 6 enables us to estimate the fraction of the total vaporization time occupied by unsteady processes. As ϕ_∞ increases, there is a sizeable decrease in the total vaporization time and also a decrease in the ratio of the duration of the unsteady period to the total vaporization time. The unsteady period (defined as the time required for the droplet temperature to reach 99.9% of its asymptotic value) occupies roughly $\frac{1}{2}$ of the total vaporization time for $\phi_\infty=1.5$ and about $\frac{1}{4}$ of the total vaporization time when $\phi_\infty=10$. Thus, although the unsteady period is shorter than the steady-state period, it comprises a nonnegligible fraction of the lifetime of the droplet. If it is assumed that steady-state conditions hold throughout the entire droplet history, then the total vaporization time is underestimated by approximately 20%.

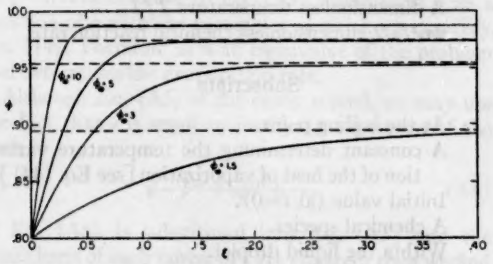

FIG. 5. The dimensionless droplet temperature as a function of the dimensionless time for various values of the dimensionless temperature at infinity, with $\phi_i=0.8$, $\kappa=7/2$, $R/c_p=2/7$, $\phi_c=3/2$, and $Y_{1,\infty}=Y_{1,0,i}$.

C. Comparison with Experiments

Our analysis applies only to the preignition period and accounts only for molecular transport processes (e.g., radiation and nonspherically symmetric convection are neglected). The treatment might therefore be expected to apply to small droplets ($10\,\mu<r<100\,\mu$) in sprays, where the small inertia of a droplet prevents the development of large convective velocities. It is nevertheless of some interest to compare our results with experiments on the ignition of larger single droplets.[9(a)–(c)] In Fig. 7 we reproduce the experimental values of $(r_0/r_{0,i})^2$ vs t given by Nishiwaki[9(c)] for α-methylnaphthalene with $r_{0,i}^2=0.35$ mm^2. Since $T_b=240$°C and $T_\infty=713$°C, the experiment corresponds to $\phi_i=0.58$ and $\phi_\infty=1.92$. For the purpose of a rough comparison we have superimposed the theoretical curve for $\phi_i=0.8$, $\phi_\infty=2$ (t was related to ξ by using $c_{p,l}=2c_p$, $\rho_l=1.025$ g/cm^3, $\rho D=5\times10^{-4}$ g/cm sec, and $r_{0,i}^2=0.35\times10^{-2}$ cm^2). The agreement, which is reasonable (within 10%) in the preignition region, would be improved somewhat by using $\phi_i=0.58$ in the theoretical calculation.

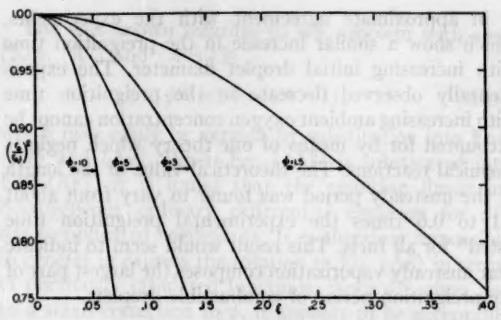

FIG. 6. The square of the ratio of the droplet radius to its initial value as a function of the dimensionless time for various values of the dimensionless temperature at infinity, with $\phi_i=0.8$, $\kappa=7/2$, $R/c_p=2/7$, $\phi_c=3/2$, and $Y_{1,\infty}=Y_{1,0,i}$.

The experimental values of the preignition time obtained in works cited in footnotes 9(a)–(c) have been conveniently collected by Wise and Agoston.[10] If we assume that the preignition time is the same as the unsteady vaporization time computed in the previous section, then this data may be compared with our theoretical results. The theoretical prediction that the duration of the unsteady period is proportional to $r_{0,i}^2$

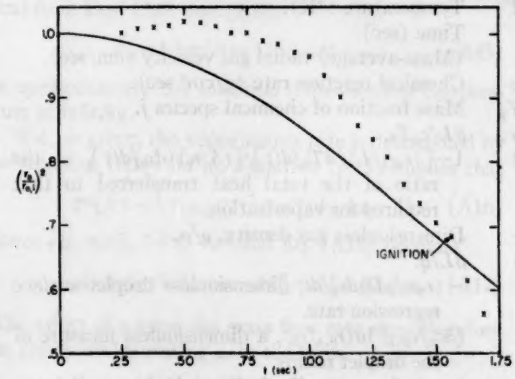

FIG. 7. Comparison between the dependence of $(r_0/r_{0,i})^2$ upon time for an experiment[9(c)] (crosses) with α-methylnaphthalene at $\phi_i=0.58$ and $\phi_\infty=1.92$ and for the theory (solid line) with $\phi_i=0.8$ and $\phi_\infty=2$.

[9] (a) H. C. Hottel, G. C. Williams, and H. C. Simpson, *Fifth International Symposium on Combustion* (Reinhold Publishing Corporation, New York, 1955), pp. 101–129; (b) K. Kobayasi, *ibid.*, pp. 141–148; (c) N. Nishiwaki, *ibid.*, pp. 148–151.

[10] H. Wise and G. A. Agoston, *Burning of a Liquid Droplet*, Advances in Chemistry Series, No. 20 (American Chemical Society, 19 8), pp. 116–135.

is in approximate agreement with the experiments, which show a similar increase in the preignition time with increasing initial droplet diameter. The experimentally observed decrease in the preignition time with increasing ambient oxygen concentration cannot be accounted for by means of our theory which neglects chemical reactions. The theoretical value of the length of the unsteady period was found to vary from about 1.1 to 0.6 times the experimental preignition time listed[10] for all fuels. This result would seem to indicate that unsteady vaporization composes the largest part of the preignition period of combustible droplets.

ACKNOWLEDGMENTS

The author would like to thank Dr. William Nachbar for interesting discussions relating to this work. Thanks are also extended to Mrs. Marion Remillard for typing and proofreading the manuscript.

NOTATION

c_p Specific heat capacity at constant pressure for the gas (cal/g °K).
$c_{p,l}$ Specific heat capacity at constant pressure for the liquid (cal/g °K).
D Binary diffusion coefficient (cm²/sec).
L Latent heat of vaporization (cal/g).
m Number of chemical species initially in the liquid droplet.
n Total number of chemical species.
p Pressure [(d/cm²)×(cal/erg)].
q Heat of (gaseous) reaction (cal/g of products formed).
R Ideal gas constant (cal/g °K).
r Radial distance from the center of the droplet (cm).
S_j Symbol for chemical species j.
T Temperature (°K).
t Time (sec).
v (Mass-average) radial gas velocity (cm/sec).
w Chemical reaction rate (g/cm³ sec).
Y_j Mass fraction of chemical species j.
α $\beta L/c_pT_0$.
β $1-[(c_{p,l}/L)(dT_0/dt)]/[(3/r_0)(dr_0/dt)]$, the ratio of the total heat transferred to that required for vaporization.
γ Dimensionless gas density, ρ/ρ_0.
δ $\beta L/q$.
ϵ $-(r_0\rho_0/\rho D)dr_0/dt$, dimensionless droplet surface regression rate.
ζ $(3c_p/c_{p,l})\ln(r_{0,i}/r_0)$, a dimensionless measure of the droplet radius.
η $(\sigma-1)/\sigma$, normalized dimensionless radial coordinate.
θ A dimensionless temperature c_pT/q.
κ $(c_{p,l}-c_p)/R$.
λ Thermal conductivity of the gas (cal/cm sec °K).
μ $r^2\rho v/r_0\rho D$, dimensionless radial mass flow rate per unit solid angle.
μ_I The value of μ computed from Eq. (30) with the assumption that $T_0=T_b$.
$\mu_0^{[0]}$ The value of μ_0 computed by assuming that $\epsilon=0$.
$\mu_0^{[1]}$ The first-order correction to μ_0 caused by the fact that $\epsilon\neq 0$ [see Eq. (39)].
ν_j' The stoichiometric coefficient for species j appearing as a reactant.
ν_j'' The stoichiometric coefficient for species j appearing as a reaction product.
ξ $(3c_p\rho D/c_{p,l}\rho_l r_{0,i}^2)t$, a dimensionless time variable.
ρ Density of the gas (g/cm³).
ρ_l Density of the liquid (g/cm³).
σ Dimensionless radial coordinate r/r_0.
τ $\int(\rho D/\rho_0 r_0^2)dt$, a dimensionless time variable.
ϕ Dimensionless droplet surface temperature T_0/T_b.
ϕ_∞ T_∞/T_b.
χ A dimensionless temperature RT/L.
ψ A dimensionless temperature T/T_0.
ω $wr_0^2/\rho D$, dimensionless chemical reaction rate.

Subscripts

b At the boiling point.
c A constant determining the temperature variation of the heat of vaporization [see Eq. (44)].
i Initial value (at $t=0$).
j A chemical species.
l Within the liquid droplet.
0 At the droplet surface.
1 The chemical species composing the droplet.
2 The oxidizer contained in the surrounding atmosphere.
3 The inert products of the chemical reaction.
∞ At $r=\infty$.

Superscripts

(0) First term in an expansion in powers of ϵ [e.g., see Eq. (A.6)].
(1) Coefficient of the second term in an expansion in powers of ϵ [e.g., see Eq. (A.6)].

APPENDIX A. SURFACE REGRESSION RATE CORRECTION FOR IDEAL GAS VAPORIZATION

We present here the details of the analysis for Sec. IV B. When $\omega=0$ and the vapor behaves as an ideal gas, we may substitute Eq. (5) into Eqs. (9) and (11) to obtain the governing pair of equations,

$$-(\epsilon\sigma^3/\psi)(d\psi/d\sigma)+\psi(d\mu/d\sigma)=0 \qquad \text{(A1)}$$

and

$$(\epsilon\sigma^3/\psi)(d\psi/d\sigma)+\mu(d\psi/d\sigma)-(d/d\sigma)[\sigma^3(d\psi/d\sigma)]=0, \qquad \text{(A2)}$$

where the dimensionless temperature is defined as $\psi = T/T_0$. By adding Eqs. (A1) and (A2) we find that

$$(d/d\sigma)[\mu\psi - \sigma^2(d\psi/d\sigma)] = 0, \tag{A3}$$

which may be integrated with the aid of the boundary condition given in Eq. (14) to show that

$$\sigma^2(d\psi/d\sigma) - \mu\psi = \mu_0(\alpha-1) + \alpha\epsilon, \tag{A4}$$

where $\alpha \equiv \beta L/c_p T_0$. It appears to be impossible to obtain any additional integrals of Eqs. (A1) and (A2).

It is convenient to use Eq. (A4) to eliminate the variable μ from Eq. (A1). If this is done and the independent variable is changed from σ to $\eta = (\sigma-1)/\sigma$, then Eq. (A1) becomes

$$\psi(d^2\psi/d\eta^2) = \{(d\psi/d\eta) - \mu_0(\alpha-1) - \alpha\epsilon + [\epsilon/(1-\eta)^3]\}(d\psi/d\eta), \tag{A5}$$

with the boundary conditions $\psi = 1$ at $\eta = 0$ and $\psi = \psi_\infty$ at $\eta = 1$. The solution to Eq. (A5) would yield ψ as a function of σ with the parameter μ_0 which must satisfy Eq. (14). Therefore μ_0 is an eigenvalue of the problem and determines the evaporation rate.

Although Eq. (A5) is not easily solved, we may use the fact that ϵ is small to justify an expansion of the form

$$\psi = \psi^{(0)} + \epsilon\psi^{(1)} + \cdots. \tag{A6}$$

If Eq. (A6) is substituted into Eq. (A5) and the coefficients of each power of ϵ are equated, then we find

$$\psi^{(0)}\frac{d^2\psi^{(0)}}{d\eta^2} = \left[\frac{d\psi^{(0)}}{d\eta} - \mu_0(\alpha-1)\right]\frac{d\psi^{(0)}}{d\eta} \tag{A7}$$

and

$$\psi^{(0)}\frac{d^2\psi^{(1)}}{d\eta^2} - \left[2\frac{d\psi^{(0)}}{d\eta} - \mu_0(\alpha-1)\right]\frac{d\psi^{(1)}}{d\eta} + \frac{d^2\psi^{(0)}}{d\eta^2}\psi^{(1)} = \left[\frac{1}{(1-\eta)^3} - \alpha\right]\frac{d\psi^{(0)}}{d\eta}. \tag{A8}$$

By performing the same expansion in Eq. (14), it is found that the boundary conditions become

$$(d\psi^{(0)}/d\eta)_0 = \alpha\mu_0 \tag{A9}$$

and

$$(d\psi^{(1)}/d\eta)_0 = \alpha. \tag{A10}$$

According to the above scheme, $\psi^{(0)}$ is the solution to the problem when $\epsilon = 0$ and $\psi^{(1)}$ is the first approximation to the correction for $\epsilon \neq 0$. Although physically T_∞ is specified and this in turn determines μ_0, for the purpose of solving Eq. (A8) it is more convenient to specify μ_0 and solve for T_∞. Thus, we shall treat μ_0, α, and T_0 as known fixed constants and solve for $T_\infty = T_\infty^{(0)} + \epsilon T_\infty^{(1)}$. We must therefore use $\psi_0^{(0)} = 1$, $\psi_0^{(1)} = 0$, and Eqs. (A7) through (A10) to determine $\psi_\infty = \psi_\infty^{(0)} + \epsilon\psi_\infty^{(1)}$.

The well-known solution to the problem with $\epsilon = 0$ [Eqs. (A7) and (A9)] is

$$\psi^{(0)} = 1 + \alpha(e^{\mu_0\eta} - 1), \tag{A11}$$

which may easily be verified by substitution into Eqs. (A7) and (A9). When Eq. (A11) is substituted into Eq. (A8), it is found that the resulting linear inhomogeneous ordinary differential equation for $\psi^{(1)}$ has complicated coefficients. It is therefore impossible in general to express the solution to Eq. (A8) in terms of previously tabulated functions. Since $\psi^{(1)}$ gives rise to a small correction to ψ, it appears to be acceptable to expand Eq (A8) in powers of η about $\eta = 0$ and keep only the first few terms in order to estimate the magnitude of the correction. It must be recognized, however, that this procedure will not yield the correct functional form for $\psi^{(1)}$.

If we expand Eq. (A8) in powers of η and collect the coefficients of each power, then the constant term shows that

$$\left(\frac{d^2\psi^{(1)}}{d\eta^2}\right)_0\psi_0^{(0)} - \left[2\left(\frac{d\psi^{(0)}}{d\eta}\right)_0 - \mu_0(\alpha-1)\right]\left(\frac{d\psi^{(1)}}{d\eta}\right)_0 + \left(\frac{d^2\psi^{(0)}}{d\eta^2}\right)_0\psi_0^{(1)} = (1-\alpha)\left(\frac{d\psi^{(0)}}{d\eta}\right)_0. \tag{A12}$$

By using Eqs. (A10) and (A11) and the fact that $\psi_0^{(1)} = 0$, we find

$$(d^2\psi^{(1)}/d\eta^2)_0 = 2\alpha\mu_0. \tag{A13}$$

According to Eqs. (A10) and (A13), the Taylor expansion of $\psi^{(1)}$ is

$$\psi^{(1)} = \alpha\eta + \alpha\mu_0\eta^2 + \cdots. \tag{A14}$$

Thus, neglecting higher-order terms, $\psi_\infty^{(1)} = \alpha(1+\mu_0)$, and from Eqs. (A6) and (A11)

$$\psi_\infty = 1 + \alpha(e^{\mu_0} - 1) + \epsilon\alpha(1+\mu_0) \tag{A15}$$

is approximately the modified dimensionless temperature at infinity.

If ψ_∞ is given, the vaporization rate is determined by solving Eq. (A15) for μ_0. Equation (A15) implies that

$$e^{\mu_0}[1 + \epsilon(1+\mu_0)e^{-\mu_0}] = \alpha^{-1}(\psi_\infty + \alpha - 1). \tag{A16}$$

Since ϵ is small, $1 + \epsilon x = e^{\epsilon x}$ and Eq. (A16) becomes

$$\mu_0 = \ln[\alpha^{-1}(\psi_\infty + \alpha - 1)] - \epsilon(1+\mu_0)e^{-\mu_0}. \tag{A17}$$

The effect of ϵ upon the mass flow rate may therefore be expressed by writing μ_0 in the form

$$\mu_0 = \mu_0^{[0]} + \epsilon\mu_0^{[1]}, \tag{39}$$

where

$$\mu_0^{[0]} = \ln[\alpha^{-1}(\psi_\infty + \alpha - 1)] \tag{40}$$

is the value of μ_0 computed by assuming $\epsilon = 0$. By comparing Eqs. (A17) and (39), it is seen that

$$\mu_0^{[1]} = -(1+\mu_0^{[0]})\exp(-\mu_0^{[0]}), \tag{41}$$

where the fact that ϵ is small has justified the use of $\mu_0^{[0]}$ in place of μ_0 in the last term of Eq. (A17). The significance of Eqs. (39) through (41) is discussed in Sec. IV B.

APPENDIX B. SURFACE REGRESSION RATE CORRECTION FOR BURNING DROPLETS

We present here the details of the analysis for Sec. IV C. The procedure is analogous to that employed in Appendix A. Using Eq. (5) and introducing the variables θ and η, we find that Eq. (9) becomes

$$-\epsilon\theta_0[1/(1-\eta)^3](1/\theta^2)(d\theta/d\eta)+(d\mu/d\eta)=0. \quad \text{(B1)}$$

If Eq. (11) is multiplied by c_p/q and added to Eq. (10) with $j=2$, it is seen that

$$\{\epsilon\theta_0[1/(1-\eta)^3](1/\theta)+\mu\}(d/d\eta)(Y_2+\theta) - (d^2/d\eta^2)(Y_2+\theta)=0. \quad \text{(B2)}$$

By substituting $\theta=\theta^{(0)}+\epsilon\theta^{(1)}$, $Y_2=Y_2^{(0)}+\epsilon Y_2^{(1)}$, and $\mu=\mu^{(0)}+\epsilon\mu^{(1)}$ into Eqs. (B1) and (B2) and equating the coefficients of each power of ϵ, we obtain the equations

$$d\mu^{(0)}/d\eta=0, \quad \text{(B3)}$$

$$(d^2/d\eta^2)(Y_2^{(0)}+\theta^{(0)})-\mu^{(0)}(d/d\eta)(Y_2^{(0)}+\theta^{(0)})=0, \quad \text{(B4)}$$

$$(d\mu^{(1)}/d\eta)=\theta_0[1/(1-\eta)^3](1/\theta^{(0)})^2(d\theta^{(0)}/d\eta), \quad \text{(B5)}$$

and

$$(d^2/d\eta^2)(Y_2^{(1)}+\theta^{(1)})-\mu^{(0)}(d/d\eta)(Y_2^{(1)}+\theta^{(1)}) - (d/d\eta)(Y_2^{(0)}+\theta^{(0)})\mu^{(1)} =\theta_0[1/(1-\eta)^3](1/\theta^{(0)})(d/d\eta)(Y_2^{(0)}+\theta^{(0)}). \quad \text{(B6)}$$

By means of a similar expansion, the boundary conditions given in Eqs. (13) and (14) become

$$[(d/d\eta)(Y_2^{(0)}+\theta^{(0)})]_0=\delta\mu_0^{(0)} \quad \text{(B7)}$$

and

$$[(d/d\eta)(Y_2^{(1)}+\theta^{(1)})]_0=\delta(1+\mu_0^{(1)}), \quad \text{(B8)}$$

where $\delta\equiv\beta L/q$. We may impose the additional boundary conditions $\theta_0^{(0)}=\theta_0$, $Y_{2,0}^{(0)}=0$, $\mu_\infty^{(0)}=\mu_0$, $\theta_0^{(1)}=0$, $Y_{2,0}^{(1)}=0$, and $\mu_0^{(1)}=0$, in which case Eqs. (B3), (B4), and (B7) become identical to those for the problem in which $\epsilon=0$ and Eqs. (B5), (B6), and (B8) are to be solved for $Y_{2,\infty}^{(1)}+\theta_\infty^{(1)}$ in order to relate μ_0 to $Y_{2,\infty}+\theta_\infty$.

The well-known solution to Eqs. (B3), (B4), and (B7) is $\mu^{(0)}=\mu_0$ and

$$Y_2^{(0)}+\theta^{(0)}=\theta_0-\delta+\delta e^{\mu_0\eta}. \quad \text{(B9)}$$

The linear equations for $\mu^{(1)}$ and $Y_2^{(1)}+\theta^{(1)}$ [Eqs. (B5) and (B6)] are too complicated to be solved explicitly. By expanding Eq. (B6) about $\eta=0$, we find from the first term

$$[(d^2/d\eta^2)(Y_2^{(1)}+\theta^{(1)})]_0-\mu_0^{(0)}[(d/d\eta)(Y_2^{(1)}+\theta^{(1)})]_0 -[(d/d\eta)(Y_2^{(0)}+\theta^{(0)})]_0\mu_0^{(1)} =(\theta_0/\theta_0^{(0)})[(d/d\eta)(Y_2^{(0)}+\theta^{(0)})]_0. \quad \text{(B10)}$$

Using known boundary conditions [e.g., Eqs. (B7) and (B8)], Eq. (B10) becomes

$$[(d^2/d\eta^2)(Y_2^{(1)}+\theta^{(1)})]_0=2\delta\mu_0, \quad \text{(B11)}$$

which implies that the Taylor expansion for $Y_2^{(1)}+\theta^{(1)}$ is

$$Y_2^{(1)}+\theta^{(1)}=\delta\eta+\delta\mu_0\eta^2+\cdots, \quad \text{(B12)}$$

where use has been made of Eq. (B8) and other boundary conditions. Keeping only the first two terms in Eq. (B12), we find from Eqs. (B9) and (B12) that

$$Y_{2,\infty}+\theta_\infty=\theta_0-\delta+\delta e^{\mu_0}+\epsilon\delta(1+\mu_0). \quad \text{(B13)}$$

In typical droplet burning problems, all quantities appearing in Eq. (B13) except μ_0 and ϵ [which is related to μ_0 by Eq. (12)] will be known. Hence the burning rate may be determined by solving Eq. (B13) for μ_0. Proceeding exactly as in Appendix A, we find

$$\mu_\infty=\mu_0^{[0]}+\epsilon\mu_0^{[1]}, \quad \text{(B14)}$$

$$\mu_0^{[0]}=\ln[1+\delta^{-1}(\theta_\infty-\theta_0+Y_{2,\infty})], \quad \text{(B15)}$$

and

$$\mu_0^{[1]}=-(1+\mu_0^{[0]})\exp(-\mu_0^{[0]}), \quad \text{(B16)}$$

which are of exactly the same form as Eqs. (39) through (41) except for the expression for $\mu_0^{[0]}$. It is therefore obvious that Eq. (42) is valid in the present case. The consequences of Eqs. (B14) through (B16) are discussed in Sec. IV C.

THE JOURNAL OF CHEMICAL PHYSICS VOLUME 33, NUMBER 1 JULY, 1960

Molecular Collision Cross Sections from Infrared Absorption Measurements*

HAROLD BABROV,† GEORGE AMEER, AND WILLIAM BENESCH

Department of Physics, University of Pittsburgh, Pittsburgh, Pennsylvania

(Received January 22, 1960)

Through measurement of the equivalent width (fractional integrated absorption) of collision-broadened lines of the P branch of the HCl fundamental vibration-rotation band at 3.5 μ, the Lorentz half-widths of these lines have been determined and optical collision cross sections deduced therefrom. The cross sections which have been obtained are those for collisions between HCl molecules and Ar, CO_2, CO, D_2, H_2, HBr, He, Ne, N_2, O_2, as well as other molecules of HCl. One of the more interesting aspects of these cross sections is their dependence on the rotational state of the absorbing molecule and the various forms which this J dependence takes for the different foreign gases. The line widths range between the extremes of 0.233 and 0.0111 cm^{-1} $atmos^{-1}$ while the collision cross sections range between 3.04×10^{-14} and 0.091×10^{-14} cm^2. Also reported are recently measured values of the strengths for the first eight lines of the P branch of the HCl fundamental. The strength of this band based on these measurements has been found to be 143 ± 5 cm^{-2} $atmos^{-1}$ at 300°K.

INTRODUCTION

THE widths of molecular vibration-rotation lines have been the subject of a rather large number of investigations spread over a long span of years. The more recent of these have been increasingly concerned with the dependence of the widths on the rotational quantum number, J.[1-4] As a matter of fact, the pattern which has been emerging in this field has been that of strikingly individual behavior of the line widths as they reflect the various parameters in the molecular interactions and the different states of the absorbing molecules. Thus, the reverse process, that of acquiring appreciable insight into the workings of a system involving interacting molecules through observation of the effects of collisions on the absorption lines, although at times regarded as something of a will o' the wisp, continues to manifest symptoms of becoming realizable.

Unhappily, much of the richness and specificity of the information which apparently is latent in this type of data has been obscured by the state of affairs arising from the circumstance that no truly direct measurement of line width is available in the infrared. Faced with measurements giving indication of unreliability in the form of lack of internal consistency and reproducibility, investigators have hesitated to attempt broad presentations of patterns of molecular line widths, but have rather attempted to lay foundations for improving the methods of investigation.

The work of D. F. Smith[1] on HF provides an exception to the trend described above. In this study, the problem of the relative broadening ability of various molecules as a function of rotational quantum number is attacked for its own sake, the matter of putting these widths on an absolute basis being relegated to a brief supplementary paragraph.

In presenting here a description of our investigations it would perhaps be well, then, to preface our remarks with an expression of our feeling that while a major portion of our effort and anxiety was at times associated with the problem of establishing reliable absolute line widths, it is the individual idiosyncrasies of the broadening behavior that constitute the principal area of interest. Indeed, it may be said that while accurate absolute values are certainly a factor in facilitating comparisons with other types of measurements such as the widths or shifts obtained with other bands or other absorbers, it is the scope of the data in each of several experiments which will ultimately determine how meaningful a comparison is possible among them.

PROCEDURE

The line strengths, the self-broadened line widths, and the widths of lines as broadened by ten selected foreign gases have been measured for the first eight lines of the P branch of the fundamental vibration-rotation spectrum of HCl.

The data were obtained by a previously described method which is based on the direct measurement of the equivalent width, W, of these lines.[5] The equivalent width of an absorption line is defined as the area under the apparent absorption curve (the line profile as modified by the instrumental slit function) normalized by the observed intensity in the absence of absorption. For spectral slit functions whose transmission is dependent only on the distance (on the wave-number scale) from the transmission peak, it is possible to show that the equivalent width is independent of the details of the shape and width of the slit function and in fact is

* This research was supported in part by the U. S. Air Force through the Air Force Office of Scientific Research of the Air Research and Development Command under contract and by the Geophysics Research Directorate under contract.

† Present Address: The Warner & Swasey Company, 32-16 Downing Street, Flushing 54, New York.

[1] D. F. Smith, Conference on the Broadening of Spectral Lines, University of Pittsburgh, 1955.

[2] W. S. Benedict, R. Herman, G. E. Moore, and S. Silverman, Can. J. Phys. **34**, 850 (1956).

[3] G. A. Kuipers, J. Mol. Spectroscopy **2**, 75 (1958).

[4] D. R. Eaton and H. W. Thompson, Proc. Roy. Soc. (London) **A251**, 458 (1959).

[5] H. Babrov, G. Ameer, and W. Benesch, J. Mol. Spectroscopy **3**, 185 (1959).

equal to the equivalent width that would be measured with an instrument of infinite resolution. Thus

$$W=\frac{1}{I_0}\int_{-\infty}^{+\infty}[I_0-I(\nu)]d\nu=\int_{-\infty}^{+\infty}[1-\exp k(\nu)L]d\nu$$

where $k(\nu)$ is the absorption coefficient; L, the optical path; I_0, the apparent intensity of the radiation in the absence of absorption; and $I(\nu)$, the wave-number-dependent apparent intensity in the presence of absorption.

Ladenburg and Reiche[6] have shown that, when the Lorentz line shape obtains, the equivalent width is given by

$$W=\int_{-\infty}^{+\infty}[(1-\exp k(\nu)L]d\nu=2\pi\alpha f(x) \qquad (1)$$

where

$$x=SL/2\pi\alpha,$$

and

$$f(x)=xe^{-x}[J_0(ix)-iJ_1(ix)].$$

In the above relation S is the line strength and α is the half-width of $k(\nu)$.

From Eq. (1) it is clear that the widths of Lorentz shaped lines of known strength can be determined from their equivalent widths. Described in the earlier mentioned work[5] is a two part experiment, also based on Eq. (1), which allows the determination of line strength, and reported there are the strengths of the first eight lines of the P branch of the fundamental band of HCl. These strength measurements have been found to contain certain small errors which will be discussed briefly in the next section. Remeasured line strengths corrected for these errors will be presented in the last section.

The line widths are calculated from Eq. (1) by a rapid iteration procedure using the measured equivalent widths of these lines together with the line strengths. All of the widths have been subjected to the corrections described below. (The self-broadened and N_2-broadened line widths have been remeasured and subjected to those corrections since the earlier publication.[5]) It should be pointed out that the errors in the measured line widths can be and have been minimized by choosing the gas pressures judiciously.

The grating spectrometer used in this work is of the Czerny-Turner configuration and has a resolution of about 0.5 cm^{-1} in the region of the HCl fundamental, which is sufficient to leave well resolved the isotopic structure of the HCl spectrum. The optical path of the spectrometer includes a 1-m long absorption cell through which the radiation passes twice and in which the gases under observation are placed. A Kodak filter is used to eliminate interference from higher orders of radiation shorter than the wavelength under observation. The radiation is detected by a PbTe photoconductor which is cooled with liquid nitrogen.

[6] R. Ladenburg and F. Reiche, Ann. Physik **42**, 181 (1911).

TABLE I. Line strengths. (Units: cm^{-2} atm^{-1} at 300°K. Theoretical strengths are based on a band strength of 143.3.)

	Experimental		Theoretical	
Line	HCl^{35}	HCl^{37}	HCl^{35}	HCl^{37}
P_1	4.96	1.61	5.023	1.638
P_2	8.16	2.66	8.389	2.734
P_3	9.32	3.04	9.500	3.098
P_4	8.91	2.90	8.648	2.818
P_5	6.72	2.19	6.674	2.179
P_6	4.54	1.48	4.471	1.461
P_7	2.70	0.883	2.633	0.8615
P_8	1.41	0.463	1.374	0.4499

The equivalent width data is obtained by placing the required pressure of HCl and broadening gas in the absorption cell and scanning the spectral region of the desired line. The area under the resulting absorption curve is measured with a polar planimeter. This area is recorded together with I_0, the spectral dispersion, the gas temperature, and the pressures of the absorber and broadener gas. For purposes of the later corrections, also recorded are the height of the absorption curve and the wave-number interval over which the area of the absorption curve was planimetered.

CORRECTIONS

Before the experiments on line strengths and widths were inaugurated an extensive series of tests and calibrations was completed. However, the appearance of a small but consistently reproducible decrease in the nitrogen broadened equivalent widths of the P_1 and P_2 lines, as remeasured following the lapse of about a year, led to a thorough recheck of the possible sources of error in these experiments. This search resulted in the discovery of an apparent nonlinearity in the response of the lead telluride detector to light intensity and the detection of a small (2.6 mole %) CO_2 impurity in the HCl.

Except for a knee at the very lowest light intensities, the effect of the nonlinearity of the detector is described by an equation of the form $E=AI^{1.05}-C$, where E is the recorder output (mv), I is the intensity of the light incident on the detector, and C ranges from 0.39 to 0.5 mv, depending on the gain setting of the amplifier. The units of $AI^{1.05}$ are mv, so the value of A depends on the units used for I; however, it is not necessary to evaluate A in order to correct for the nonlinearity of the detector. The line strengths reported in the results are for pure HCl; they are the measured strengths divided by 0.974, the mole fraction of HCl in the cylinder of HCl which was obtained commercially. The self-broadened equivalent widths reported here have been corrected for the broadening due to the CO_2 in the HCl cylinder. In line with the policy of making all corrections which can affect the results by more than 1%, wing corrections[2] have been made for all of the equivalent widths used in this work.

TABLE II. Line widths of the HCl P branch. (Units: cm^{-1} atm^{-1} at 300°K.)

Broadening gas	P_1	P_2	P_3	P_4	P_5	P_6	P_7	P_8
Ar	0.0649	0.0381	0.0345	0.0283	0.0241	0.0204	0.0215	0.0141
CO_2	0.167	0.140	0.103	0.0889	0.0727	0.0660	0.0502	0.0471
CO	0.117	0.0999	0.0960	0.0835	0.0677	0.0596	0.0571	0.0346
D_2	0.0723	0.0524	0.0397	0.0330	0.0329	0.0324	0.0337	0.0351
H_2	0.0811	0.0601	0.0456	0.0356	0.0263	0.0252	0.0250	0.0261
HBr	0.144	0.144	0.153	0.150	0.144	0.133	0.105	0.104
HCl	0.207	0.233	0.231	0.227	0.207	0.171	0.145	0.124
He	0.0215	0.0201	0.0192	0.0177	0.0174	0.0171	0.0188	0.0156
Ne	0.0250	0.0216	0.0188	0.0176	0.0160	0.0135	0.0128	0.0111
N_2	0.0926	0.0851	0.0723	0.0642	0.0593	0.0434	0.0363	0.0267
O_2	0.0706	0.0508	0.0384	0.0334	0.0294	0.0271	0.0218	0.0215

The calibrations and corrections sketched above are described elsewhere in considerable detail.[7] The net result of all the corrections is rather small. The corrections for the nonlinearity of the detector results in decreases of from 8 to 11% from the measured equivalent widths. The wing corrections resulted in increases of from 3 to 7% in the measured equivalent widths. The net effect of both these corrections was to reduce the equivalent widths by some 3.5 to 6.5%. The correction for the CO_2 impurity increases all line strengths by 2.6%. As a result of all the corrections, the band strength quoted in the results is 2.5% lower than the uncorrected band strength. Therefore, the theoretical line strengths are 2.5% lower than they would be if no corrections had been made. However, the corrected SL were 5.1% lower than the uncorrected because the measured HCl pressures were 2.6% higher than the true pressures. This decrease in SL partially compensates for the decreased equivalent widths used in the line width calculations, so the corrected line widths are from 2 to 8% lower than the uncorrected ones.

RESULTS AND DISCUSSION

Table I shows the strengths for the lines of the P branch of the HCl fundamental. The theoretical strengths are arrived at from the distribution calculated by Herman and Wallis,[8] into which scheme has been inserted a band strength of 143 cm^{-2} atm^{-1} at 300°K and a value of 0.988 for the adjustable parameter, θ, which appears in the theoretical distribution of line strengths. The band strength is a weighted average of the band strengths calculated from each of the experimental line strengths, the weighting factor being proportional to the line strength. The value of θ was determined by Benedict, Herman, Moore, and Silverman[2] from experimental strengths of lines of the same $|m|$ in the P and R branches. The theoretical and experimental strengths are in excellent agreement, the maximum deviation being about 4%. The discrepancies are probably due to errors in the measurement of the equivalent widths used to determine the experimental strengths. One of these equivalent width measurements could be as much as 5% in error, leading to an estimated error of about 5% for any of the individual experimental strengths. However, because the quoted band strength is an average of many individual strength measurements, it is believed to be more accurate than any of the individual measurements. Thus the estimated error in the band strength is about 4%. A detailed discussion of the sources of error in the equivalent widths and estimates of the amount of error due to each source are given in Babrov *et al.*,[7] Secs. III B1 and IV B.

Table II gives the results for the widths of the individual lines of the HCl P branch as broadened by eleven gases. In all cases except that of self-broadening the listed line widths are those of the HCl^{35} line. The self-broadened widths are a weighted average of the HCl^{35} and HCl^{37} widths, the weighting factor being 3 for the HCl^{35} width and 1 for the HCl^{37} width. Table III gives the data of Table II in terms of HCl-broadening gas cross sections (calculated by the usual formula). Fig. 1(a)–(k) graphically depicts the J variation of the cross sections for each of the broadening gases (J being the rotational quantum number of the initial state of the line). As explained in Babrov *et al.*[7] (Appendix B) the relative error in the measured equivalent width is magnified by a factor of 2 or more in the line width calculated from that equivalent width, so the accuracy in the equivalent width data is the controlling factor in the accuracy of the resulting line width (and cross section). An individual line width may be as much as 13% in error; however, this is a conservative (pessimistic) estimate, and in most cases the error is probably less than this amount.

There are two striking facts about the cross sections displayed in Table III and Fig. 1; the first is the large variation of cross sections when different broadening gases are used, and the second is that for most of the gases the cross section changes greatly from one rotational line to another. The J variation of the cross sections is not readily predictable from a casual consideration of the usual molecular parameters. A large interaction energy between the absorbing molecule and the broadening molecule usually leads to a large colli-

[7] H. Babrov, G. Ameer, and W. Benesch, AFOSR TR-59-207, Final Report under Contract AF18(600)-986, University of Pittsburgh, 1959.

[8] R. Herman and R. F. Wallis, J. Chem. Phys. **23**, 637 (1955).

TABLE III. Optical collision cross sections for the HCl P branch. (Units: $10^{-14} \times cm^2$.)

Broadening gas	P_1	P_2	P_3	P_4	P_5	P_6	P_7	P_8
Ar	0.863	0.506	0.458	0.376	0.321	0.271	0.285	0.188
CO_2	2.27	1.90	1.39	1.21	0.988	0.897	0.682	0.640
CO	1.41	1.21	1.16	1.01	0.820	0.723	0.691	0.419
D_2	0.421	0.305	0.231	0.192	0.191	0.189	0.196	0.204
H_2	0.342	0.254	0.192	0.150	0.111	0.106	0.106	0.110
HBr	2.20	2.20	2.33	2.28	2.19	2.02	1.61	1.59
HCl	2.70	3.04	3.02	2.96	2.69	2.23	1.89	1.61
He	0.124	0.116	0.111	0.103	0.101	0.099	0.109	0.091
Ne	0.275	0.237	0.207	0.194	0.176	0.148	0.141	0.122
N_2	1.12	1.03	0.877	0.778	0.719	0.526	0.440	0.323
O_2	0.887	0.639	0.483	0.419	0.369	0.341	0.274	0.270

sion cross section but does not necessarily guarantee a great J variation; e.g., the HBr cross sections show relatively little J dependence although HBr is the best foreign gas broadener used. Neither is a knowledge of the type of interaction potential between the broadening molecule and the absorber sufficient to permit prediction of the proper J dependence. A comparison of the HCl-He and HCl-Ar cross sections illustrates this point very well. Both of these broadeners are noble gases (so presumably the type of interaction potential between each of these and HCl is the same), yet the Ar cross sections show a very pronounced J dependence while the He cross sections exhibit very little J dependence.

Deuterium was chosen as one of the broadening gases in an attempt to determine the velocity dependence of cross sections. D_2 and H_2 have different velocities but are the same electrically. Therefore it might have been expected that the ratio of the HCl-D_2 cross sections to the HCl-H_2 cross sections would be some function of the mass ratio only. However, the cross-section ratio was found to be J dependent. This means that either the velocity dependence of the cross section is different for each rotational state of HCl, or that the different distributions of the rotational levels of the two perturbers cause the different J variation of the HCl-H_2 and HCl-D_2 cross sections.

In viewing the line-broadening data of the present work in the light of other experimental work which has been done in this field, it should be reiterated that the available data is not profuse. In general the other experimental measurements show the same type of behavior as that reported here; the line widths are usually highly J dependent and the type of J dependence is a function of the broadening gas. The data of Benedict, Herman, Moore, and Silverman[2] on the line widths of the HCl 0–1 vibration-rotation spectrum can be compared directly with the data of this work. The self-broadened line widths are in very good agreement (well within the experimental error of the two experiments). The agreement for the nitrogen broadened widths is not quite so good, but the marked decrease in line width with increasing J is unmistakable in both sets of data. The self-broadened DCl widths published by Eaton and Thompson[4] have the same sort of J dependence as that of HCl; the line spacing of DCl is smaller so the peak is near $J=4$ rather than 2 or 3, but the peak line width of 0.23 cm^{-1} atm^{-1} is nearly identical with that of HCl and the shape of the width-vs-J curve is quite similar. Their self-broadened line widths for CO show a J dependence which is more nearly typical of broadening by a foreign gas such as argon or oxygen than that of any previously reported self-broadened widths. The work of Kuipers[8] and Smith[1] on the line widths of HF show a J dependence of nearly the same shape as those reported here for self-broadening and for each of the six foreign gas broadeners which are the same as those used in the present work.

The J variation of the shifts of the lines of the HCl 0–2 vibration-rotation band obtained by Kimel, Hirschfeld, and Jaffe[9] seems to exhibit a strong correlation with the line-width data reported here. The shifts of the P-branch lines by He are almost independent of J. Those induced by Ar increase to the red as J increases, as also do those induced by CO. Additionally, the shapes of these shift-vs-J curves strongly suggest the corresponding shapes appearing in the present work. It is to be hoped that a combination of line-shift data and line-width data will lead to a better insight into the collision process than either type of data taken alone.

Figure 2 shows the experimental self-broadened cross sections of the present work and theoretical cross sections as calculated from the work of P. W. Anderson.[10] Anderson's curve splits into two sections, showing the upper and lower limits of the calculated cross section for each J. Perhaps more important than any disagreement in absolute value of the cross sections is the fact that the experimental points show the effect of resonance to a smaller degree than does the theoretical curve; i.e., there is not as pronounced a peak for the experimental cross sections associated with the densely populated states ($J=2$, 3, and 4) as predicted by the theory. In this connection it may be noted that the J dependence

[9] M. A. Hirshfeld, J. H. Jaffe, and S. Kimel, J. Chem. Phys. 32, 297 (1960).
[10] P. W. Anderson, dissertation, Harvard University, 1949.

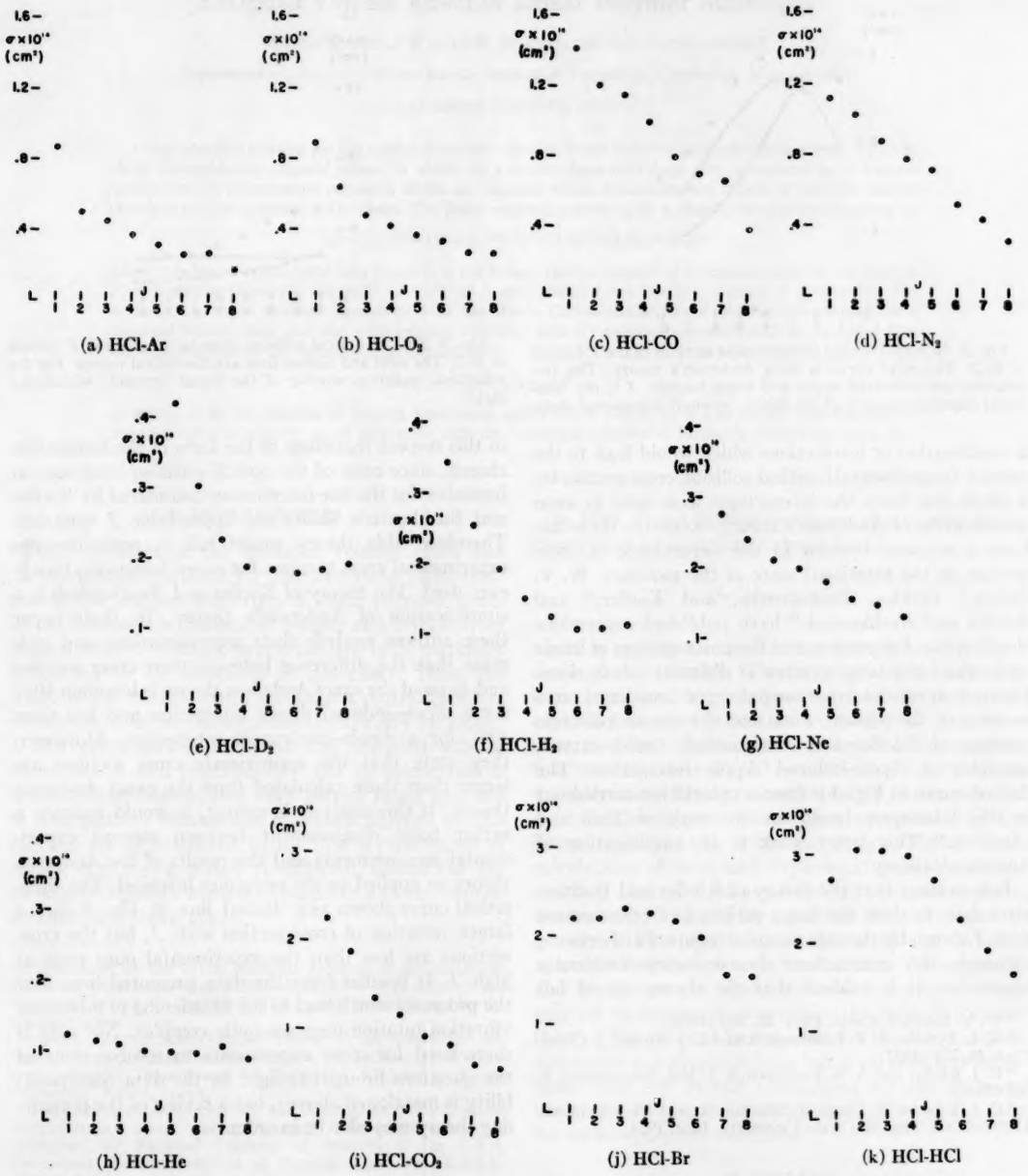

FIG. 1. Optical collision cross sections in the P branch of HCl. J is the rotational quantum number of the initial (ground) vibrational state.

of the HBr-HCl cross sections is quite similar to that of the self-broadened cross sections. An experiment which suggests itself as a check of the resonance contribution to the cross section is a study of HCl when broadened by DCl or vice versa. The energy levels of these two gases are spaced differently, but in other respects their interactions are the same. So a difference between the measured cross section for self-broadening and that for broadening by the isotopic molecule could be ascribed to the resonance effect.

For a number of years after Anderson's reasonably successful application of his theory to self-broadening, theoretical work in the field of collision broadening by foreign gases was confined largely to attempts at finding

FIG. 2. HCl-HCl optical collision cross sections in the P branch of HCl. The solid curve is from Anderson's theory. The two branches are estimated upper and lower bounds. J is the rotational quantum number of the initial (ground) vibrational state.

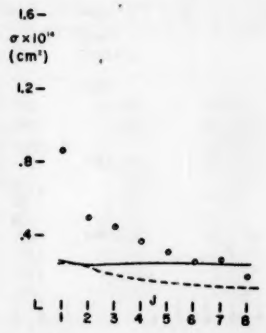

FIG. 3. HCl-Ar optical collision cross sections in the P branch of HCl. The solid and dashed lines are theoretical curves. J is the rotational quantum number of the initial (ground) vibrational state.

a combination of interactions which would lead to the correct (experimental) optical collision cross section for a single line when the interactions were used in some modification of Anderson's theory. Recently there has been a renewed interest in the dependence of cross section on the rotational state of the molecule. W. V. Smith,[11] Perkins, Bushkovitch, and Kieffer,[12] and Kieffer and Bushkovitch[13] have published expressions showing the J dependence of the cross sections of linear molecules for a large number of different interactions. Figure 3 shows the experimental argon broadened cross sections of the present work and the theoretical cross sections of Kieffer and Bushkovitch (solid curve), assuming a dipole-induced dipole interaction. The dashed curve in Fig. 3 is from a calculation carried out in this laboratory based on the work of Tsao and Curnutte.[14] This latter work is an amplification of Anderson's theory.

It is evident that the theory of Kieffer and Bushkovitch fails to show the large variation of cross section with J shown by the experimental points. Furthermore, although the interaction chosen seems eminently reasonable, it is evident that the theory would fail in this respect regardless of the form of the interaction chosen, since none of the optical collision cross section formulas, for the five interactions considered by Kieffer and Bushkovitch, shows any appreciable J variation. Therefore, this theory would fail to reproduce the experimental cross sections for every foreign gas broadener used. The theory of Kieffer and Bushkovitch is a simplification of Anderson's theory. In their paper these authors analyze their approximations and estimate that the difference between their cross sections and those of the exact Anderson theory is less than 10% for a dipole-induced dipole interaction and less than 30% for a dipole-quadrupole interaction. Moreover, they state that the approximate cross sections are larger than those calculated from the exact Anderson theory. If this analysis is correct, it would indicate a rather basic disagreement between current experimental measurements and the results of the Anderson theory as applied to the molecules involved. The theoretical curve shown as a dashed line in Fig. 3 has a larger variation of cross section with J, but the cross sections are less than the experimental ones even at high J. It is clear from the data presented here that the processes which lead to the broadening of molecular vibration-rotation lines are quite complex. Not only is there need for more experiments to resolve some of the questions brought to light by the data (one possibility is mentioned above), but a review of the present-day theory may also be in order.

[11] W. V. Smith, J. Chem. Phys. **25**, 510 (1956).
[12] K. L. Perkins, A. V. Bushkovitch, and L. J. Kieffer, J. Chem. Phys. **26**, 779 (1957).
[13] L. J. Kieffer and A. V. Bushkovitch, J. Mol. Spectroscopy **2**, 558 (1958).
[14] C. J. Tsao and B. Curnutte, Scientific Report 1A-8, Contract AF19(122)65, The Ohio State University, June, 1954.

Excluded Volume Effect of Linear Polymer Molecules*

MICHIO KURATA,† WALTER H. STOCKMAYER, AND ANTONIO ROIG‡

Department of Chemistry, Massachusetts Institute of Technology, Cambridge, Massachusetts

(Received March 14, 1960)

A new closed expression for the excluded volume effect of linear polymer molecules is developed with the aid of an equivalent ellipsoid model, in which the polymer chain with fixed ends is replaced by a uniform distribution of unconnected segments within an ellipsoid whose dimensions are chosen to give the correct principal radii of gyration of the chain. The linear expansion factor α for a chain of N segments is given by

$$(\alpha^3-\alpha)/N^{\frac{1}{2}}=\{(1+\tfrac{1}{2}\alpha^{-2})^{-\frac{1}{2}}\}^{-1}(4/3)^{5/2}(3/2\pi)^{\frac{1}{2}}(\beta/a^3)$$

where a is the effective bond length and β is the binary cluster integral of a segment pair. In contrast to Flory's familiar equation, the ratio $(\alpha^5-\alpha^3)/N^{\frac{1}{2}}$ is an increasing function of α instead of a constant. The new equation is in excellent agreement with the Monte Carlo calculations of Wall and Erpenbeck for a diamond lattice chain and also with existing viscosity data for various polymer solutions, provided that the expansion factor is evaluated from the equation

$$[\eta]/[\eta]_\theta=\alpha^{3.43}$$

in accord with the theories of Kurata-Yamakawa and Ptitsyn-Eisner. It is also shown that the present equation for α is in rather good agreement with the numerical solution of Fixman's differential equation.

I. INTRODUCTION

THE problem of the excluded volume effect has essential importance for the structural interpretation of the solution properties of linear polymer molecules, because the molecular weight and temperature dependences of solution properties are both markedly influenced by the existence of this effect. Thus, the study of the volume effect has been a central problem of polymer solution theory since its discovery by Flory.[1]

The perturbation theory of the excluded volume effect now is well established,[2–6] but its application is unfortunately limited to a very narrow range near the Θ temperature, because the equations derived by this method are all restricted to the first several terms of slowly converging series. A different theoretical approach is therefore needed to establish a closed expression for the volume effect.

In 1949, Flory[1] derived by means of an approximate theory such an equation in closed form,

$$\alpha^5-\alpha^3=\text{const}N^{\frac{1}{2}} \tag{1}$$

where α represents the linear expansion factor for a chain of N segments. This is now widely used as a basic equation for interpreting solution properties, especially in good solvents. Experimental test, however, does not fully support this equation but suggests that the ratio $(\alpha^5-\alpha^3)/N^{\frac{1}{2}}$ evaluated from the intrinsic viscosity data displays a maximum at some value of N.[7,8] Furthermore, a more direct comparison of the Flory equation (1) with the recent Monte Carlo calculations of Wall and Erpenbeck[9] indicates on the contrary that the ratio $(\alpha^5-\alpha^3)/N^{\frac{1}{2}}$ is an increasing function of N, as will be seen later. In this paper we propose a new approximate theory of the excluded volume effect in order to resolve these discrepancies, and we discuss the configurational behavior of linear polymer molecules in solution in the light of the new theory. The proposed expression for the linear expansion factor α is simple in form but gives excellent agreement with the Monte Carlo data for the diamond lattice chain[9] and also with the intrinsic viscosity data for various polymer solutions.

II. THEORY

According to the statistical theory of chain configuration, the mean-square end-to-end distance $\langle L^2\rangle$ of a chain of $N+1$ segments (or of N links) is approxi-

* Presented at the 137th National Meeting of the American Chemical Society, Cleveland, Ohio, April, 1960. This research was supported in part by the Office of Ordnance Research and by the Quartermaster Corps.

† Sloan Foreign Post-Doctoral Fellow of the School for Advanced Study, Massachusetts Institute of Technology. Permanent address: Department of Industrial Chemistry, Kyoto University, Kyoto, Japan.

‡ Appointment supported by the International Cooperation Administration under Visiting Research Scientists Program administered by National Academy of Sciences of the U.S.A. Permanent address: Institute of Physical Chemistry, C.S.I.C. Madrid, Spain.

[1] P. J. Flory, J. Chem. Phys. **17**, 303 (1949).

[2] E. Teramoto, Busseiron Kenkyu (in Japanese) **39**, 1 (1951); **40**, 18 (1951); **41**, 14 (1951). Proc. Intern. Conf. Theoret. Phys., Kyoto and Tokyo, Japan **1953**, 410 (1954).

[3] B. H. Zimm, W. H. Stockmayer, and M. Fixman, J. Chem. Phys. **21**, 1716 (1953).

[4] M. Fixman, J. Chem. Phys. **23**, 1656 (1955).

[5] M. Kurata, H. Yamakawa, and E. Teramoto, J. Chem. Phys. **28**, 785 (1958).

[6] W. H. Stockmayer, International Symposium on Macromolecules, Wiesbaden, West Germany, October, 1959; and Makromol. Chem. **35**, 54 (1960).

[7] W. R. Krigbaum and P. J. Flory, J. Polymer Sci. **11**, 37 (1953). See also, P. J. Flory, *Principles of Polymer Chemistry* (Cornell University Press, Ithaca, New York, 1953), Chap. XIV.

[8] N. T. Notley and P. Debye, J. Polymer Sci. **24**, 275 (1957).

[9] F. T. Wall and J. J. Erpenbeck, J. Chem. Phys. **30**, 634 (1959).

mately written in the form[4,10,11]

$$\langle L^2\rangle = \frac{\int L^2 \exp(-3L^2/2Na^2)\exp\left[-\tfrac{1}{2}\beta\int\rho_L^2(\mathbf{r})d\mathbf{r}\right]4\pi L^2 dL}{\int \exp(-3L^2/2Na^2)\exp\left[-\tfrac{1}{2}\beta\int\rho_L^2(\mathbf{r})d\mathbf{r}\right]4\pi L^2 dL}, \tag{2}$$

where a is the length of a link and $\rho_L(\mathbf{r})$ is the number of segments per unit volume at a point $\mathbf{r}$ from the center of mass of the chain with fixed end-to-end vector $\mathbf{L}$. The symbol β represents the binary cluster integral which is defined as

$$\beta = \int_0^\infty \{1-\exp[-w(R)/kT]\}4\pi R^2 dR \tag{3}$$

where $w(R)$ represents the pair potential of average force as a function of the intersegmental distance R.

To develop the calculation, we assume an equivalent ellipsoid model, in which the polymer chain with fixed ends is replaced by a uniform distribution of unconnected segments within an ellipsoid of revolution whose dimensions are chosen to give the correct principal radii of gyration of the chain. For a specified $\mathbf{L}$, these are[12]

$$\langle S_x^2\rangle = (Na^2/36)[1+(3L^2/Na^2)],$$
$$\langle S_y^2\rangle = \langle S_z^2\rangle = Na^2/36. \tag{4}$$

Here the x axis is chosen in the direction of the end-to-end vector $\mathbf{L}$. As the volume V_L of this ellipsoid is[13]

$$V_L = \text{const}\,Na^2L[1+(Na^2/3L^2)]^{\frac{1}{2}} \tag{5}$$

we can simply put

$$\rho_L(\mathbf{r}) = N/V_L = \frac{\text{const}}{a^2L[1+(Na^2/3L^2)]^{\frac{1}{2}}} \tag{6}$$

or

$$\tfrac{1}{2}\beta\int\rho_L^2(\mathbf{r})d\mathbf{r} = \beta N^2/2V_L = \text{const}\left(\frac{\beta N^{\frac{1}{2}}}{a^3}\right)\left[\frac{Na^2/L^2}{1+(Na^2/3L^2)}\right]^{\frac{1}{2}}. \tag{7}$$

Substituting Eq. (7) into Eq. (2), we obtain

$$\langle\alpha^2\rangle = \frac{\int_0^\infty \alpha^4 \exp\{-\tfrac{3}{2}\alpha^2 - 3Cz/\alpha[1+(1/3\alpha^2)]^{\frac{1}{2}}\}d\alpha}{\int_0^\infty \alpha^2 \exp\{-\tfrac{3}{2}\alpha^2 - 3Cz/\alpha[1+(1/3\alpha^2)]^{\frac{1}{2}}\}d\alpha} \tag{8}$$

with

$$\alpha^2 = L^2/Na^2 \tag{9}$$

and

$$z = (3/2\pi)^{\frac{3}{2}}(\beta N^{\frac{1}{2}}/a^3). \tag{10}$$

Here C is a numerical constant. According to Hermans and Overbeek,[12] an integral of this type can be evaluated by replacing it by the square of α^*, at which the function $\alpha^3\exp\{-\tfrac{3}{2}\alpha^2 - 3Cz/\alpha[1+(1/3\alpha^2)]^{\frac{1}{2}}\}$ attains its maximum value. Thus, using this approximation, we obtain

$$\alpha^3 - \alpha = Cz/[1+(1/3\alpha^2)]^{\frac{1}{2}}. \tag{11}$$

Here the symbol α is used instead of $\alpha^* \simeq \langle\alpha^2\rangle^{\frac{1}{2}}$, for the sake of simplicity.

On the other hand, according to the perturbation theory,[2-5] the same α is rigorously expressed in the series form,[14]

$$\alpha^2 - 1 = \tfrac{4}{3}z - (\tfrac{10}{3} - \tfrac{88}{27}\pi)z^2 + \cdots. \tag{12}$$

Hence, adjusting the numerical constant C in Eq. (11) to the first coefficient of z in Eq. (12), we arrive at our final result:

$$\alpha^3 - \alpha = \{(1+\tfrac{1}{3}\alpha^{-2})^{-\frac{1}{2}}\}^{-1}(\tfrac{4}{3})^{5/2}(3/2\pi)^{\frac{3}{2}}(\beta N^{\frac{1}{2}}/a^3). \tag{13}$$

It is now well known that the Flory equation (1) can be derived[4,10,11] from Eq. (2) if we put

$$\tfrac{1}{2}\beta\int\rho_L^2(\mathbf{r})d\mathbf{r} = \text{const}\left(\frac{\beta N^{\frac{1}{2}}}{a^3}\right)\frac{N^{\frac{1}{2}}a^3}{L^3} \tag{14}$$

instead of Eq. (7). The essential assumption for obtaining this L^{-3} dependence of the interaction energy is the spherical distribution of segments about the center of molecular mass, and no detailed picture of the distribution is needed. Similarly, the L^{-1} dependence of the interaction energy characterizes the present theory. The present equation (13) may be regarded as a natural extension of Flory's, because axial symmetry of the segment distribution would be more consistent than the spherical one with the condition of a specified end-to-end vector.

III. BEHAVIOR OF THE PRESENT EQUATION

In contrast to Flory's equation (1), the new equation (13) indicates that the ratio $(\alpha^5-\alpha^3)/N^{\frac{1}{2}}$ should be an increasing function of α instead of a constant. This prediction is strongly supported by the recent Monte Carlo data of Wall and Erpenbeck for a diamond lattice chain.[9] This is demonstrated in Fig. 1, where the

[10] E. F. Casassa and T. A. Orofino, J. Polymer Sci. **35**, 553 (1959).
[11] T. B. Grimley, Trans. Faraday Soc. **55**, 681 (1959).
[12] J. J. Hermans and J. Th. G. Overbeek, Rec. trav. chim. **67**, 761 (1948).
[13] Elementary geometric calculations yield

$$\text{Constant in Eq. (5)} = (4\pi/3)(5/36)^{\frac{1}{2}}\sqrt{3} = 0.375$$

and

$$C \text{ in Eqs. (8) and (11)} = 0.151,$$

respectively. Thus, as α approaches unity, the equation (11) becomes

$$\alpha^2 - 1 = 0.098\,z - \cdots,$$

which is to be compared with Eq. (12) obtained by the perturbation theory.

[14] The square term of z is due to Fixman (see footnote 4).

two combinations of α and the number of links n, i.e., $(\alpha^5-\alpha^3)/n^{\frac{1}{2}}$ and $(\alpha^2-\alpha)[1+(1/3\alpha^2)]^{\frac{1}{2}}/n^{\frac{1}{2}}$, calculated from the Monte Carlo data are shown by white and black circles, respectively. In accordance with Eq. (13), the former gradually increases with n but the latter does not.

Figure 2 illustrates a more thorough comparison of the theory with the Monte Carlo data. Before proceeding to the explanation of this figure, let us recall the definitions of our model chain, often called the equivalent random chain, and of the real chain. In the former, which is specified by three parameters, say N, a and β, any short-range interference such as fixation of valence angles or hindrance to bond rotation is completely neglected. On the other hand, the real chain is, of course, subjected to various kinds of short-range interference as well as the long-range one. To specify this real chain, therefore, we need a different set of parameters from the above set. These may be the number of valence bonds n in its principal chain, the length of each valence bond a_0, the binary cluster integral of each structural segment β_0 and some additional parameters for specifying the short range interferences. Concerning these parameters, the general theory of the Markoff process yields a familiar relation,

$$\langle L^2\rangle_0 = Na^2 = sna_0^2, \tag{15}$$

where $\langle L^2\rangle_0$ is the mean-square end-to-end distance in absence of the long range interference and s represents a proportionality factor independent of n but generally dependent on temperature. It is also familiar that, in the case of a simple "*atactic*" chain, s is given as

$$s=\frac{1-\cos\theta}{1+\cos\theta}\cdot\frac{1+\langle\cos\phi\rangle}{1-\langle\cos\phi\rangle}, \tag{16}$$

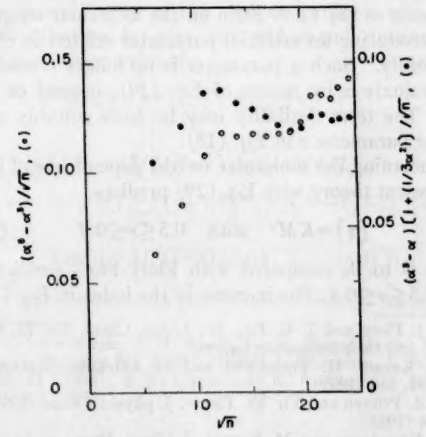

FIG. 1. The test of constancy of two combinations of α and n: white circles represent $(\alpha^5-\alpha^3)/n^{\frac{1}{2}}$ and black circles represent $(\alpha^2-\alpha)[1+(1/3\alpha^2)]^{\frac{1}{2}}/n^{\frac{1}{2}}$.

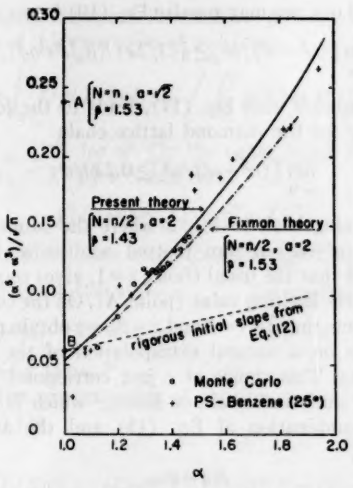

FIG. 2. The Flory ratio $(\alpha^5-\alpha^3)/n^{\frac{1}{2}}$ as function of α.

where θ is the valence angle between the neighboring bonds and ϕ is the rotation angle.[15,16]

Thus, using the latter set of parameters, we can uniquely specify the diamond lattice chain of Wall and Erpenbeck as

$$a_0=1, \qquad s=2,$$
$$\beta_0=(4/3)^{\frac{1}{2}}=1.53, \tag{17}$$

because the binary cluster integral for lattice solutions should be equal to the volume per a lattice point.[6] On the contrary, we can still not give the unique specification of the equivalent random chain, for any arbitrary choice of c in the following relation satisfies Eq. (15):

$$N=n/c \quad \text{and} \quad a=(c\cdot s)^{\frac{1}{2}}a_0. \tag{18}$$

As long as the unperturbed dimension $\langle L^2\rangle_0$ alone is concerned, it is utterly meaningless to worry about the c value. Thus, a rather arbitrary choice that $c=1$ has so far been used by many authors because of its simplicity. However, this is not true in the present problem of the excluded volume effect.

Substituting Eq. (18) into Eq. (13) or Eq. (12), we obtain

$$\lim_{\alpha\to 1}[(\alpha^5-\alpha^3)/n^{\frac{1}{2}}]=\tfrac{4}{3}(3/2\pi)^{\frac{3}{2}}(\beta/c^2s^{\frac{1}{2}}a_0^3). \tag{19}$$

As the effective segment is generally larger than the

[15] Concerning the detailed nature of s, see, for example, S. Lifson, J. Chem. Phys. **29**, 80 (1958); **30**, 964 (1959); K. Nagai, J. Chem. Phys. **30**, 660 (1959); **31**, 1169 (1959) and other references quoted there.

[16] S. Lifson and I. Oppenheim, J. Chem. Phys. (to be published). They indicate that a proper account of the solvent-solvent and the solvent-polymer segment interaction does not disturb the Markoffian character of the problem at least in an approximate sense.

structural one, we may rewrite Eq. (19) into

$$\lim_{\alpha\to 1}[(\alpha^5-\alpha^3)/n^{\frac{1}{2}}]\geq\tfrac{4}{3}(3/2\pi)^{\frac{3}{2}}(\beta_0/c^3s^{\frac{1}{2}}a_0^3), \quad (20)$$

which, together with Eq. (17), leads to the following inequality for the diamond lattice chain

$$\lim_{\alpha\to 1}[(\alpha^5-\alpha^3)/n^{\frac{1}{2}}]\geq 0.239/c^2. \quad (21)$$

Now, turning back to Fig. 2 where the Monte Carlo data of $(\alpha^5-\alpha^3)/n^{\frac{1}{2}}$ are plotted against α, we can easily find that the usual choice $c=1$, gives too large a figure for the limiting value (point A). On the contrary, if we assume that $c=s=2$ and $\beta=\beta_0$, we obtain point B, which lies on a natural extrapolation of the Monte Carlo data. This choice of c just corresponds to the preferred statistical chain of Kuhn,[17] which is defined by the combination of Eq. (15) and the auxiliary condition,

$$Na=na_0. \quad (22)$$

The solid curve in Fig. 2 illustrates a best fit curve of Eq. (13) which is written by using the parameter values,

$$N=n/2, \quad a=2 \quad \text{and} \quad \beta=1.43. \quad (23)$$

The agreement of the theory and the Monte Carlo data is quite satisfactory over whole range of α, and the value of β obtained by the curve fitting is in good agreement with that of β_0 obtained by purely geometric consideration.

In this connection, we remember the previous analysis of the light-scattering data for polystyrene in cyclohexane,[18] in which the value of 7 A for the diameter of one skeleton segment of polystyrene chain was obtained with the aid of the perturbation theory and the concept of the preferred equivalent chain. Because of the empirical coincidence of β with β_0 mentioned above this value now may be given some physical significance as an average diameter of $-CH_2-$ and $-CHC_6H_5-$ units.

Several years ago, Fixman[4] derived an approximate differential equation for α on the basis of quite different statistical considerations. This is

$$z\alpha(d\alpha/dz)=1-\alpha^2+2(z/\alpha), \quad (24)$$

which after numerical integration[19] yields the dashed curve of Fig. 2, in rather good agreement with the present equation. Fixman considered the approximation to be poor because it gives a rather small value for the coefficient of z^2 in series expansion of α^2. That is, the coefficient is -0.67 in Fixman's theory, -0.22 in the present theory, and -2.07 in the rigorous equation (12). However, it now appears that this inadequacy has only a minor effect. For the sake of comparison, there is also shown in Fig. 2 the initial slope corresponding to the rigorous equation (12) by the broken line. It is also to be noted that the present theory and Fixman's both predict

$$\lim_{z\to\infty}\alpha^3/z=\text{const.} \quad (25)$$

This indicates that the asymptotic dependence of the chain dimensions on the molecular weight M would be

$$\langle L^2\rangle^{\frac{1}{2}}\propto\langle S^2\rangle^{\frac{1}{2}}\propto M^{2.0}, \quad (26)$$

instead of

$$\langle L^2\rangle^{\frac{1}{2}}\propto M^{1.8} \quad (27)$$

which is obtained from Eq. (1).

IV. INTERPRETATION OF VISCOSITY DATA

Turning now to the intrinsic viscosity data on linear polymers, we recall that Krigbaum and Flory[7] found the value of the Flory ratio, $(\alpha^5-\alpha^3)/M^{\frac{1}{2}}$ to pass through a maximum for several systems. They evaluated the expansion factors from the Flory-Fox equation[20]

$$[\eta]/[\eta]_\Theta=\alpha^3, \quad (28)$$

which has more recently been shown to be somewhat erroneous. If better account is taken of the non-Gaussian character of chains with excluded volume, the above equation is replaced by[18,21–23]

$$[\eta]/[\eta]_\Theta=\alpha^{2.43}, \quad (29)$$

and if the existing viscosity data for the systems polystyrene-benzene, polyisobutylene-cyclohexane and polyisobutylene-diisobutylene are recalculated on this basis, the experimental Flory ratio no longer displays a maximum but becomes a monotonically increasing function of M, in accord with the present theory. Crosses in Fig. 2 illustrate this statement, the data for the polyisobutylene systems being omitted here for the sake of clarity.

Krigbaum some years ago tried to interpret the dependence of the Flory ratio on the molecular weight,[24] by introducing an artificial parameter related to chain "*flexibility*." Such a parameter is no longer needed, if we evaluate α by means of Eq. (29), instead of Eq. (28). The term flexibility may be more suitably used for the parameter s in Eq. (15).

Concerning the molecular weight dependence of $[\eta]$, the present theory with Eq. (29) predicts

$$[\eta]=KM^\nu \quad \text{with} \quad 0.5\leq\nu\leq 0.9 \quad (30)$$

which is to be compared with Flory-Fox's prediction that $0.5\leq\nu\leq 0.8$. The increase in the index in Eq. (26)

[17] W. Kuhn, Kolloid-Z. **68**, 2 (1934).
[18] M. Kurata and H. Yamakawa, J. Chem. Phys. **29**, 311 (1958), Sec. E4.
[19] M. Fixman, Doctoral thesis, M.I.T., 1953.
[20] P. J. Flory and T. G. Fox, Jr., J. Am. Chem. Soc. **73**, 1904 (1951); and their succeeding papers.
[21] M. Kurata, H. Yamakawa and H. Utiyama, Makromol. Chem. **34**, 139 (1959).
[22] O. B. Ptitsyn and Yu. Ye. Eisner, J. physic. Chem. (USSR) **32**, 2464 (1958).
[23] H. Yamakawa and M. Kurata, J. Chem. Phys. (to be published). The effect of polydispersity is also to lower the exponent of α in $[\eta]/[\eta]_\Theta$.
[24] W. R. Krigbaum, J. Chem. Phys. **23**, 2113 (1955).

is partly offset by the decrease in the index of Eq. (29) making the difference from the Flory-Fox theory in the viscosity-molecular weight relationship rather small. However, it should be noted here that the present theory does not exclude values of ν larger than 0.8, such as have been reported by several authors[25] for flexible polymers in good solvents.

V. MISCELLANEOUS

We here show some additional calculations to reinforce the foregoing results, some of which seem initially to be rather fortuitous.

First, a calculation like the above can be easily developed for a two-dimensional chain, with an "equivalent ellipse" model whose dimensions are chosen to give the correct principal radii of gyration of the chain:

$$\langle S_x^2\rangle=(Na^2/24)[1+(2L^2/Na^2)], \qquad (31)$$

$$\langle S_y^2\rangle=Na^2/24$$

The final result corresponding to Eq. (13) is

$$\alpha^3-\alpha=\{[1+(1/2\alpha^{-2})]^{-\frac{1}{2}}\}^{-1}(\tfrac{3}{2})^{\frac{1}{2}}(2\pi)^{-1}(\beta N/a^2). \qquad (32)$$

The agreement of this equation with Monte Carlo calculations for planar lattice chains[8] (three-choice two-dimensional square lattice chain) is satisfactory, and again the preferred statistical length is the best choice for the value of a. The comparison is not reproduced here.

Thus we may conclude that the choice of the preferred statistical chain as the equivalent random chain is appropriate for the purpose of evaluation of the β value from solution properties, though further progress in the statistical theory is still required to establish rigorously the relation between β and β_0.

Secondly, we show another application of the Hermans and Overbeek method for approximate evaluation of an integral of type (8). According to the perturbation theory of the excluded volume effect,[2-5] the distribution function for end-to-end distance is given in a power series of z,

$$p(L)=p^{(0)}(L)[1+g(L)+\cdots] \qquad (33)$$

with

$$p^{(0)}(L)=(3/2\pi Na^2)^{\frac{1}{2}}\exp(-3L^2/2Na^2),$$

$$g(L)=-(z/\sqrt{N})\sum_{j>i}[(j-i)^{\frac{1}{2}}]^{-1}\{N/[N-(j-i)]\}^{\frac{1}{2}}$$

$$\times\exp\{-3L^2(j-i)/2a^2N[N-(i-i)]\}, \qquad (34)$$

where $g(L)$ represents the "single contact" correction for the ideal Gaussian distribution $p^{(0)}(L)$. The substitution of this expansion of $p(L)$ into

$$\langle L^2\rangle=\int_0^\infty L^2p(L)4\pi L^2dL\Big/\int_0^\infty p(L)4\pi L^2dL \qquad (35)$$

yields Eq. (12) for α^2. On the other hand, if we approximate $p(L)$ by a closed form

$$p(L)=p^{(0)}(L)\cdot\exp[g(L)] \qquad (36)$$

we obtain after some complicated integrations

$$\alpha^2-1=\tfrac{4}{3}z+0.95z^2+\cdots, \qquad \text{for small } z;$$

$$\alpha=\tfrac{4}{3}z, \qquad \text{for } z\to\infty. \qquad (37)$$

as shown by James.[26]

Now the maximization of the function $L^3\cdot p^{(0)}(L)\cdot\exp[g(L)]$ is

$$\left\{L^{-1}-(L/Na^2)+(zL/a^2)\sum_{j>i}\{(j-i)^{\frac{1}{2}}[N-(j-i)]^{5/2}\}^{-1}\right.$$

$$\left.\times\exp\left[-\frac{3L^2}{2Na^2}\cdot\frac{(j-i)}{N-(j-i)}\right]\right\}_{L=L^*}=0 \qquad (38)$$

which after replacing the summation by integration yields

$$\alpha^2-1=1.446z\alpha. \qquad (39)$$

This calculation is very simple in comparison with that of James, but the result (39) yields

$$\alpha^2=1+1.446z+1.045z^2+\cdots, \qquad \text{for small } z;$$

$$\alpha=1.446z, \qquad \text{for large } z; \qquad (40)$$

which are both in excellent accord with Eq. (37). This may be counted as a support of the Hermans and Overbeek approximation used in our theory.

Finally, it must also be noted that the unperturbed dimension $\langle L^2\rangle_0$ does not necessarily coincide with the dimension $\langle L^2\rangle_\Theta$ at the Θ temperature, because the s in Eq. (15) generally depends on both the temperature and solvents. In other words, we can write

$$\langle L^2\rangle_{0,T}/\langle L^2\rangle_\Theta=\langle S^2\rangle_{0,T}/\langle S^2\rangle_\Theta=s(T)/s(T=\Theta), \qquad (41)$$

which is not identically one, and we can never perform the direct observation of $\langle S^2\rangle_{0,T}$ (the unperturbed mean-square radius of gyration at T). However, the excellent constancy of the new combination of α and M, i.e., $(\alpha^3-\alpha)[1+(1/3\alpha^2)]^{\frac{1}{2}}/M^{\frac{1}{2}}$, would make it possible to evaluate the unperturbed dimension from observed $\langle L^2\rangle$ vs M relationship at any given temperature.

[25] See for example, J. H. Baxendale, S. Bywater, and M. G. Evans, J. Polymer Sci. **1**, 237 (1946); J. Bisschops, J. Polymer Sci. **17**, 81 (1955); S. N. Chinai and R. A. Guzzi, J. Polymer Sci. **21**, 417 (1956).

[26] H. M. James, J. Chem. Phys. **21**, 1628 (1953). He derived a closed expression for α, which need not be reproduced here.

"Forbidden" Character in Allowed Electronic Transitions*†

ANDREAS C. ALBRECHT

Department of Chemistry, Cornell University, Ithaca, New York

(Received December 21, 1959)

A theory for calculating the intensity of "forbidden" character in allowed electronic transitions is given based upon the early work of Herzberg and Teller. It is seen how both symmetric and nontotally symmetric vibrations may be active in the perturbation, and the temperature dependence of "forbidden" intensity is explicitly obtained for harmonic oscillator wave functions. As an example the case of certain *p*-disubstituted benzenes is discussed in detail. A model derivative normal coordinate analysis is used to calculate perturbation energies in terms of electronic wave function parameters. It is seen how the magnitude of "forbidden" character is very sensitive to the detailed nature of the mixing electronic wave functions. Several trial functions are introduced to calculate the ratio of "forbidden" to allowed character in the near ultraviolet band. Comparison is made with recent observations of mixed polarization in two benzene derivatives. Finally, the possible significance of "forbidden" character with respect to radiationless transitions is briefly discussed.

1. INTRODUCTION

IN 1933[1] Herzberg and Teller outlined a theory of vibronic transitions in polyatomic molecules. Part of their study deals with the consequences of neglecting the nuclear coordinate dependence of electronic wave functions when calculating intensities of electronic transitions. This dependence was introduced by regarding nuclear displacement as a perturbation with the equilibrium nuclear configuration electronic wave functions as the unperturbed, zeroth-order functions. Vibronic selection rules were derived and it was shown how transitions forbidden in the zeroth order nevertheless appear as a result of the mixing of the zeroth-order functions by suitable nontotally symmetric vibrations.

The Herzberg-Teller theory is qualitative in its formulation and only recently have actual attempts been made to calculate higher-order intensity corrections. Forbidden transitions in benzene have been studied by Craig,[2] Murrell and Pople,[3] and Liehr[4,5] and a forbidden transition in formaldehyde has been investigated by Pople and Sidman.[6] These calculations have each met with some success. While, strictly speaking, only the calculations by Pople and co-workers[3,6] and Liehr[5] employ the Herzberg-Teller formalism, Liehr[7] reports in a critical study of all benzene calculations that the Herzberg-Teller theory is adequate provided one uses the correct zeroth-order functions.

Common to all reported vibronic calculations to date is their sole concern with transitions forbidden in the zeroth order. A general theory of vibronic transitions is in no way confined to forbidden transitions. One can expect that at least for weakly allowed transitions the first-order correction may be significant. For example, early reference[8–10] can be found to the simultaneous presence of "forbidden" (first-order) and allowed (zeroth-order) components in the weak near-ultraviolet band systems of certain benzene derivatives. Moffitt[11] has discussed the importance of the "forbidden" component in certain accidentally weak bands in the cata-condensed hydrocarbons and examples have been found in naphthalene[12] and azulene.[13] Recent polarization studies on two benzene derivatives, *p*-dimethoxybenzene (DMB)[14] and N, N, N′, N′-tetramethyl-paraphenylenediamine (TMPD),[15] suggest that the first-order correction, or "forbidden" component, can play an important role even in cases where the zeroth-order intensity is relatively strong.

The present investigation, which is based on the Herzberg-Teller approach, deals with the problem of calculating the ratio of "forbidden" to allowed intensities in allowed electronic transitions. The general theory is presented including the temperature dependence of the "forbidden" intensity. The theory is then applied to the case of the *p*-disubstituted benzenes using the results of a normal coordinate analysis that has been performed on a model derivative. It is found possible to leave that part of the calculation dependent on the electronic wave functions in terms of parameters—these being fixed by any given choice of electronic functions. General conclusions are reached which

* This work was supported in part by the National Science Foundation.

† Presented in part before the Symposium on Molecular Structure and Spectroscopy, The Ohio State University, Columbus, June, 1959.

[1] G. Herzberg and E. Teller, Z. physik. Chem. **B21**, 410 (1933).
[2] D. P. Craig, J. Chem. Soc. **1950**, 59.
[3] J. N. Murrell and J. A. Pople, Proc. Phys. Soc. (London) **A69**, 245 (1956).
[4] A. D. Liehr, Z. Naturforsch. **13a**, 311, 596 (1958).
[5] A. D. Liehr, thesis, Harvard University, 1955.
[6] J. A. Pople and J. W. Sidman, J. Chem. Phys. **27**, 1270 (1957).
[7] A. D. Liehr, Can. J. Phys. **35**, 1123 (1957); **36**, 1588 (1957).
[8] H. Sponer and S. H. Wollman, Phys. Rev. **57**, 1078A (1940).
[9] H. Sponer and E. Teller, Revs. Modern Phys. **13**, 75 (1941).
[10] A. L. Sklar, J. Chem. Phys. **10**, 135 (1942); also Revs. Modern Phys. **14**, 232 (1942).
[11] W. Moffitt, J. Chem. Phys. **22**, 320 (1954).
[12] D. S. McClure, J. Chem. Phys. **22**, 1668 (1954); **24**, 1 (1956).
[13] J. W. Sidman and D. S. McClure, J. Chem. Phys. **24**, 757 (1956).
[14] A. C. Albrecht and W. T. Simpson, J. Chem. Phys. **23**, 1480 (1955).
[15] A. C. Albrecht, Symposium on Molecular Structure and Spectroscopy, the Ohio State University, Columbus, June, 1958. See paper submitted to J. Am. Chem. Soc.

are then illustrated through the use of several sets of trial wave functions. Empirical energies and allowed intensities are introduced to calculate the "forbidden" to allowed ratio in the near ultraviolet bands of DMB and TMPD. Finally, brief mention is made of possible significance of "forbidden" character from the point of view of radiationless transitions.

2. THEORY

A. General

The Herzberg-Teller theory has been made explicit by various authors.[3,5,6] We shall here outline the theory in a manner most convenient for our purposes.

Under the Born-Oppenheimer approximation, the zeroth-order vibronic wave function of a molecule is expressed as the product of an electronic wave function and a vibrational wave function. Thus for the jth vibrational level of the kth electronic state the vibronic wave function is written

$$\Phi_{kj}=\Theta_k(x, Q)\phi_j^k(Q), \tag{1}$$

where Θ_k is the electronic wave function and ϕ_j^k the vibrational wave function. The coordinate symbols x and Q refer to the complete set of internal coordinates required to locate all the electrons and all the nuclei, respectively. In particular since almost all our information relates to the ground electronic state, Q shall represent the complete set of normal coordinates for that state. Since these coordinates, with appropriate shift of origin, completely span the nuclear space of infinitesimal displacements, wave functions belonging to excited electronic states may in principle also be expressed in terms of the ground state Q. The transition probability between vibronic states[16] g, i and k, j is given by the square of the absolute value of the transition moment:[17]

$$P_{gi,kj}=|\mathbf{M}_{gi,kj}|^2, \tag{2}$$

where

$$\mathbf{M}_{gi,kj}=\int\mathfrak{M}_{g,k}(Q)\phi_i^g(Q)\phi_j^k(Q)dQ \tag{3}$$

and

$$\mathfrak{M}_{g,k}=\int\Theta_g(x, Q)\mathbf{m}_e(x)\Theta_k(x, Q)dx, \tag{4}$$

where $\mathbf{m}_e(x)$ represents the electronic terms of the electric dipole moment operator. The nuclear terms are omitted because of orthogonality of the electronic wave functions.

The integrated transition probability for that part of an electronic transition originating in the ith vibrational state of the ground level shall be written

$$P_{gi,k}=\sum_j P_{gi,kj}=\sum_j|\mathbf{M}_{gi,kj}|^2. \tag{5}$$

The sum contains a $(3N-6)$-fold infinity of terms for a nonlinear N-atomic molecule. It is convenient[3] at this point to invoke the quantum-mechanical sum rule.[18] However, since the $\phi_j^k(Q)$ $(j=1, 2,\cdots)$ constitute a complete orthogonal set in $\bar{Q}$ space (the normal coordinate space of electronic state k), not in Q space, the rule must be applied with caution. With certain qualifications,[19] therefore, one obtains

$$\sum_j|\mathbf{M}_{gi,kj}|^2=\int\phi_i^g(Q)\mathfrak{M}_{g,k}^2(Q)\phi_i^g(Q)dQ \tag{6}$$

and with Eq. (5) and typical notation for averaging,

$$P_{gi,k}=\langle\mathfrak{M}_{g,k}^2\rangle_{ii}. \tag{7}$$

Finally, the total transition probability for the electronic transition is

$$P_{g,k}=\sum_i B_iP_{gi,k}=\sum_i B_i\langle\mathfrak{M}_{g,k}^2\rangle_{ii}, \tag{8}$$

where B_i is the Boltzmann weighting factor for the ith vibrational state and the sum again contains a $(3N-6)$-fold infinity of terms.

In order to calculate the constants $\langle\mathfrak{M}_{g,k}^2\rangle_{ii}$ it is necessary to derive an explicit form for $\mathfrak{M}_{g,k}^2(Q)$. As Eq. (4) shows, this in turn requires an expression revealing the explicit dependence of the electronic wave functions on Q. It is the basis of the Herzberg-Teller theory to treat nuclear motion as a perturbation in the electronic Schrödinger equation and to use as zeroth-order wave functions those valid for the equilibrium nuclear positions of the ground electronic state. Thus we write

$$\Theta_k(x, Q)=\Theta_k^0+\sum_s\lambda_{ks}(Q)\Theta_s^0, \tag{9}$$

where

$$\lambda_{ks}(Q)=\int\Theta_k^0\mathfrak{IC}'(Q)\Theta_s^0dx\Big/(E_s^0-E_k^0)$$
$$=H_{ks}'(Q)/\Delta E_{sk}^0 \tag{10}$$

[16] The subscript g shall always refer to the ground electronic state unless it is found as part of a group-theoretical species label.

[17] Real wave functions are assumed for simplicity in notation.

[18] See, for example, N. F. Mott and I. N. Sneddon, *Wave Mechanics and Its Applications* (Oxford University Press, New York), pp. 94–95.

[19] The correct form for the right-hand side of Eq. (6) is actually found to be

$$\int\phi_i^g(Q)\mathfrak{M}_{g,k}^2(Q)\phi_i^g(Q)\,|\,J^{-1}(\bar{Q}/Q)|\,dQ.$$

If we regard the transformation linking the $\bar{Q}$ with the Q as at most involving a shift of origin and a rotation of axes (orthonormal, affine), then the absolute value of the Jacobian is unity and Eq. (6) follows. This assumption is implicit in most theories of electronic transitions. It is presumed that at least for slight displacement of equilibrium configuration it is a valid assumption. [That the conventional sum rule is formally not applicable in this problem was first pointed out by A. D. Liehr (private communication). It is his helpful and responsive criticism that has led to this footnote.]

with $\mathcal{H}'$ representing the first-order perturbation in the Hamiltonian. A superscript zero refers to equilibrium nuclear position; thus $\Theta_k^0=\Theta_k(x,0)$. Similarly, the energies refer to the electronic energies for the ground state equilibrium configuration. The sum in Eq. (9) extends over all electronic states other than state k.

Introducing Eq. (9) into Eq. (4) we obtain

$$\mathfrak{M}_{g,k}(Q)=\mathfrak{M}_{g,k}{}^0+\sum_s \lambda_{ks}(Q)\mathfrak{M}_{g,s}{}^0, \tag{11}$$

where

$$\mathfrak{M}_{g,l}{}^0=\int \Theta_g{}^0\mathbf{m}_e(x)\Theta_l{}^0 dx. \tag{12}$$

(We shall assume throughout that the ground electronic state does not mix to any important extent under vibrational perturbation.) Upon substituting Eq. (11) into Eq. (6) and anticipating that in this treatment λ_{ks} shall be an odd function of Q (see below), we obtain, with Eq. (7),

$$P_{g,k}=(\mathfrak{M}_{g,k}{}^0)^2+\sum_s\sum_i B_i\langle\lambda_{ks}{}^2\rangle_{ii}(\mathfrak{M}_{g,s}{}^0)^2 \tag{13}$$

for the total intensity.

Equation (13) reveals how the polarizations of the "forbidden" components in a band are determined by the polarizations of the allowed zeroth-order g, s transitions. One can conclude that whenever mixed polarization is found in a single electronic transition the presence of "forbidden" character is indicated. The converse does not hold. As illustrated below it is possible for the "forbidden" component to be polarized in the same direction as the allowed component. Thus the absence of mixed polarization does not necessarily indicate absence of "forbidden" character.

Finally, the ratio of "forbidden" to allowed character may be written as

$$R_k=\sum_s\sum_i B_i\langle\lambda_{ks}{}^2\rangle_{ii}(\mathfrak{M}_{g,s}{}^0/\mathfrak{M}_{g,k}{}^0)^2 \tag{14}$$

and with Eq. (10),

$$R_k=\sum_{s,i} B_i\langle H_{ks}{}'^2\rangle_{ii}\{(\mathfrak{M}_{g,s}{}^0/\mathfrak{M}_{g,k}{}^0)^2(\Delta E_{sk}{}^0)^{-2}\}, \tag{15}$$

where the notation for the double sum has been simplified. The quantities enclosed in brackets are best obtained empirically. The remaining important parameter, $\langle H_{ks}{}'^2\rangle_{ii}$, will be treated in detail after a brief discussion of the vibronic selection rules.

B. Vibronic Selection Rules

The Q dependence of the transition moment (and hence "forbidden" character) appears only when for at least one s neither λ_{ks} nor $\mathfrak{M}_{g,s}{}^0$ vanishes (Eq. 11). The latter condition immediately limits the combining states s to the upper state in an allowed pure electronic transition. The symmetries of such upper states are group-theoretically defined. Now for $\lambda_{ks}(Q)$ not to vanish, the integrand in Eq. (10) must be the basis of a representation containing at least once the totally symmetric irreducible representation of the group of the molecule. Since the symmetry properties of $\Theta_s{}^0$ are defined, given the symmetry species of $\Theta_k{}^0$, the symmetry properties of $\mathcal{H}'$ are then determined. For example, in the group D_{2h},[20] $\Theta_s{}^0$ can belong only to species $B_{1u}(z)$, $B_{2u}(y)$, or $B_{3u}(x)$ (assuming a totally symmetric ground state) and if the state of interest, $\Theta_k{}^0$, belongs say to the species B_{2u} then $\mathcal{H}'$ must belong, respectively, to the species B_{3g}, A_g, or B_{1g}, as far as its behavior in electron space is concerned. As shall be seen presently this is equivalent to specifying the species of vibration that can participate in the perturbation. Thus originate the Herzberg-Teller selection rules for vibronic transitions. Their emphasis, however, is normally on the role of nontotally symmetric vibrations in forbidden transitions. The example shows that when dealing with a correction to an allowed intensity, totally symmetric vibrations may also participate. This point has been recognized previously by several investigators[21(a)] and is of course of singular importance in diatomic spectra.[21(b)]

C. Perturbation Energy

Since we shall employ empirical values for the transition probabilities and energy differences appearing in Eq. (15) it remains only to calculate $\langle H'_{ks}{}^2\rangle_{ii}$ in order to evaluate R_k. The perturbing potential $\mathcal{H}'$ is taken as all terms of order Q in the expansion of the correct electronic Hamiltonian $\mathcal{H}$ in powers of normal coordinates about the equilibrium nuclear configuration. Thus

$$\mathcal{H}'=\sum_a(\partial\mathcal{H}/\partial Q_a)_0 Q_a$$

$$=-\sum_a\{(\partial/\partial Q_a)\sum_{l=1}^{n}\sum_{\sigma=1}^{N}(Z_\sigma e^2/r_{l\sigma})\}Q_a. \tag{16}$$

The second equality follows because the only nuclear-dependent part of the Hamiltonian is the coulomb potential between electron and nucleus. The subscript a goes over all of the normal modes while the indices l and σ run over the n electrons and N nuclei being considered.

Since the Hamiltonian is invariant to the operations of the group of the molecule, $(\partial\mathcal{H}/\partial Q_a)_0$ has the same symmetry properties in electron space that Q_a has in the nuclear space.

It is useful to change variables in the bracketed expression of Eq. (16) from normal coordinates to some local Cartesian set. If for atom σ this set be $\xi_\sigma{}^1$, $\xi_\sigma{}^2$,

---

[20] For the character table and the notation used here see J. Chem. Phys. **23**, 1997 (1955).

[21] (a) Early mention of this can be found in footnote reference 9. A more recent reference, for example, is H. McConnell and D. S. McClure, J. Chem. Phys. **21**, 1296 (1953). (b) For a discussion of the variation of the electronic transition moment with interatomic separation in diatomic molecules, see for example P. A. Fraser, Can. J. Phys. **32**, 515 (1954) and references cited therein.

$\xi_\sigma{}^3$ then, for electron l and nucleus σ,

$$(\partial \mathcal{H}_{l\sigma}/\partial Q_a)_0 = (\partial \mathcal{H}_{l\sigma}/\partial r_{l\sigma})_0 (\partial r_{l\sigma}/\partial Q_a)_0 = (\partial \mathcal{H}_{l\sigma}/\partial r_{l\sigma})_0 \times \{\sum_{f=1}^{3} (\partial r_{l\sigma}/\partial \xi_\sigma{}^f)_0 (\partial \xi_\sigma{}^f/\partial Q_a)_0\}, \quad (17)$$

where $\mathcal{H}_{l\sigma}$ is just $(Z_\sigma e^2)/r_{l\sigma}$.

The first factor in each of the terms of the bracketed expression is the appropriate direction cosine of the vector $\mathbf{r}_{l\sigma}$. The second factor is an element of the matrix which transforms the normal coordinates into the local cartesian system. The matrix must be obtained from a normal coordinate analysis of the molecule under consideration. Recognizing that $\mathcal{H}'$ is a one-electron operator one can carry out the integration in Eq. (10) over all but one electron and then sum over the n indistinguishable one-electron integrals that remain to obtain

$$H_{ks}' = \sum_a Q_a h_{ks}{}^a \quad (18)$$

with

$$h_{ks}{}^a = \sum_{f=1}^{3} \sum_{\sigma=1}^{N} \{(\partial \xi_\sigma{}^f/\partial Q_a)_0 \int \rho_{sk}(p) (\partial \mathcal{H}_{p\sigma}/\partial r_{p\sigma})_0 \times (\partial r_{p\sigma}/\partial \xi_\sigma{}^f)_0 dx_p\}, \quad (19)$$

where

$$\rho_{sk}(p) = n \int \Theta_s{}^0 \Theta_k{}^0 dx' \quad (20)$$

is the one-electron transition density found in the formalism of Murrell and Pople.[3] The integration in Eq. (20) is over all but, say, the pth electron. The symbol $h_{ks}{}^a$ represents the perturbation energy per unit displacement of normal mode a resulting from the coupling of electronic states k and s. It shall be convenient to symbolize the normal coordinate coefficient by $\xi_\sigma{}^f(a)$ and the electronic integral by $I_\sigma{}^f(s, k, a)$ (see Appendix A). Equation (19) now becomes

$$h_{ks}{}^a = \sum_{f,\sigma} \xi_\sigma{}^f(a) I_\sigma{}^f(s, k, a), \quad (19a)$$

where multiple sums are understood.

Now in Appendix A it is shown that when some molecular symmetry is present there exist group-theoretically determined relationships among the $I_\sigma{}^f(s, k, a)$ and that in fact these relationships must be identical to those existing among the $\xi_\sigma{}^f(a)$. Suppose, therefore, we write

$$\eta_{\sigma,f}(a, \sigma^*, f^*) = I_\sigma{}^f(s, k, a)/I_{\sigma^*}{}^{f^*}(s, k, a) = \xi_\sigma{}^f(a)/\xi_{\sigma^*}{}^{f^*}(a),$$

where $\eta_{\sigma,f}$ is determined group-theoretically and σ^* and f^* refer to a chosen reference center and reference cartesian coordinate, respectively. Equation (19a) may now be rewritten to give

$$h_{ks}{}^a = \sum_{f^*,\sigma^*} \xi_{\sigma^*}{}^{f^*}(a) I_{\sigma^*}{}^{f^*}(s, k, a) (\sum_{\sigma,f} \eta_{a,f}{}^2(a, \sigma^*, f^*)). \quad (19b)$$

The sums over σ and f can extend over all $3N$ values ($f=1, 2, 3$; $\sigma=1, 2, \cdots, N$); however, for a given σ^* and f^*, $\eta_{\sigma,f}$ may vanish for many σ and f. The sums over σ^* and f^* go over the minimum number of reference centers and cartesian coordinates required by symmetry. When normal mode a is a member of a degenerate set then additional relationships occur among the electronic integrals (as among the normal coordinate coefficients) for all members of the set. The minimum number of integrals required is given by group theory as outlined in Appendix A. The greater the symmetry the smaller this number.

D. Temperature Dependence of the "Forbidden" Intensity

It appears that no more formal reduction of the integrals is possible. However, since the nuclear coordinate dependence of $\mathfrak{M}_{g,k}{}^2(Q)$ is now explicit through Eqs. (11), (10), and (18) it is possible to carry out the averaging over nuclear coordinates indicated in Eq. (6). The results may be summarized by rewriting Eq. (15) as follows:

$$R_k = \sum_{s,a} (\sum_i B_i \langle Q_a{}^2 \rangle_{ii}) (h_{ks}{}^a)^2 \{(\mathfrak{M}_{g,s}{}^0/\mathfrak{M}_{g,k}{}^0)^2 (\Delta E_{sk}{}^0)^{-2}\} \quad (15a)$$

Furthermore, the sum over i in this last equation can be evaluated for harmonic oscillator wave functions (see Appendix B). Thus, finally,

$$R_k = hN^0(8\pi^2)^{-1} \sum_{s,a} (\nu_a{}^{-1} \coth u_a) (h_{ks}{}^a)^2 \times \{(\mathfrak{M}_{g,s}{}^0/\mathfrak{M}_{g,k}{}^0)^2 (\Delta E_{sk}{}^0)^{-2}\}, \quad (15b)$$

where $u_a = h\nu_a/(2kT)$.

Equation (15b), with $h_{ks}{}^a$ given by Eq. (19b) is the general expression, based on the Herzberg-Teller theory, for the ratio of "forbidden" to allowed character in the transition to the kth electronic state at temperature T. It has been assumed only that the ground state does not mix [because of an unfavorable $(\Delta E_{s0}{}^0)^{-2}$] and that the vibrational wave functions are the harmonic oscillator functions. It is evident that other things being equal, "forbidden" character will manifest itself most strongly in a weak band [small $(\mathfrak{M}_{g,k}{}^0)^2$] having an intense band [large $(\mathfrak{M}_{g,s}{}^0)^2$] in the vicinity [small $(\Delta E_{sk}{}^0)^2$]. However, as we shall presently see, the perturbation energy per unit displacement, $h_{ks}{}^a$, is a very sensitive function of the detailed nature of electronic functions $\Theta_k{}^0$ and $\Theta_s{}^0$. Therefore, favorable energy and intensity factors is a necessary but not a sufficient condition to bring out a strong "forbidden" component.

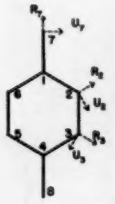

FIG. 1. The local cartesian coordinates and the numbering of the nuclei for a para-disubstituted benzene derivative.

3. AN EXAMPLE: PARA-DISUBSTITUTED BENZENE DERIVATIVES

A. General Considerations

Since polarization data have been obtained[14,15] for two para-disubstituted benzene derivatives and since it is hoped to explain these data in terms of "forbidden" character, the general case of para-disubstituted benzene derivatives (of actual or effective D_{2h} symmetry) shall now be examined.

Only derivatives having influential ortho-para directing substituents are to be considered. Interest shall be confined to the "forbidden" character in the near-ultraviolet band. Moreover, we shall consider mixing with the nearest excited state only at 0°K. It is believed[14,22] that for all such derivatives the first excited state (state k) is a $B_{2u}(D_{2h})$ state and the second (state s) is $B_{1u}(D_{2h})$. The vibrations active in mixing these two states must belong to the species b_{3g} (Sec. 2B).

The task shall be to evaluate the square of the perturbation energy at 0°K for a model derivative in terms of a minimum number of parameters which take on values determined in any given problem by the specific wave functions chosen. That is, $hN^0/(8\pi^2)\sum_a(h_{ks}{}^a)^2\nu_a{}^{-1}$ of Eq. (15b) must be calculated. The remaining factors in Eq. (15b) shall be taken as empirically given. To evaluate $h_{ks}{}^a$ according to Eq. (19b) we must know: (1) the $\xi_\sigma{}^{J*}(a)$ (from a normal coordinate analysis), (2) the $I_\sigma{}^{J*}$ (using parameterized electronic wave functions), and (3) the $\eta_{\sigma,f}{}^2$ (from group theory).

The local cartesian coordinates are chosen as illustrated in Fig. 1. R_σ is the radial displacement (positive outward) of atom σ and U_σ is the tangential displacement of atom σ (positive clockwise). The out-of-plane modes cannot contain a vibration of species b_{3g} and need not be considered.

An in-plane normal coordinate analysis has been completed[23] for a model derivative having para substituents of mass 20 and a C$-X$ distance of 1.40 A. All in-plane $\xi_\sigma{}^J(a)$ have been determined including those for the b_{3g} vibration needed here. Although an unmodified benzene force field was used, the normal frequencies obtained correspond rather markedly to the observed frequencies of p-difluorobenzene. Furthermore, normal coordinates for p-dideuterobenzene and 2, 3, 5, 6-tetradeuterobenzene are available[24] and have also been used in the present calculations. As will be seen it appears that the influence on R_k of the substituent through the $\xi_\sigma{}^J(a)$ is slight and negligible when compared to the influence through the electronic integrals $I_\sigma{}^J$. This fortunately serves to justify the use of one model derivative for the normal coordinate analysis when considering a variety of derivatives.

To calculate the electronic integrals we first take advantage of group theory to reduce the number of integrals to a minimum as described earlier. By applying the operations of the group (D_{2h}) to any given local cartesian coordinate one can generate a set that forms the basis of a reducible representation of the group. We are interested only in those sets giving rise to reducible representations containing, on reduction, the B_{3g} representation. It is found that there are four sets (exclusive of sets based on hydrogen coordinates) which can be generated in the foregoing sense: $\{U_7, U_8\}$, $\{U_1, U_4\}$, $\{R_2, R_3, R_5, R_6\}$, and $\{U_2, U_3, U_5, U_6\}$. Selecting arbitrarily for our σ^* centers, 7, 1, and 2, the electronic integrals requiring evaluation $I_\sigma{}^{J*}$ are simply $I_7{}^U$, $I_1{}^U$, $I_2{}^R$, and $I_2{}^U$. [Similarly one need only take $\xi_7{}^U(a)$, $\xi_1{}^U(a)$, $\xi_2{}^R(a)$, and $\xi_2{}^U(a)$ from the normal coordinate analysis.] We shall assume that a reasonably correct set of wave functions can be obtained, in principle, through an LCAO–ASMO calculation with complete configuration interaction using $2pz$ Slater atomic orbitals (for all centers) with $Z=3.18$. The availability of appropriate integrals[4] has dictated this choice for the basic atomic orbitals and has also imposed the choice of a C$-X$ distance of 1.40 A. As shall be seen it appears that neither the arbitrary choice of a $2pz$ orbital with $Z=3.18$ for the substituent nor a C$-X$ distance of 1.40 A can lead to any serious error in the qualitative conclusions that shall be reached. Now the transition density ρ_{sk} (Eq. 20), where state s belongs to species B_{1u} and state k to B_{2u}, belongs to the species B_{3g}. Whatever the details of the correct wave functions, the one-electron transition density will ultimately reduce to densities defined in terms of the overlap of atomic orbitals located either on one center or on two centers. These overlap densities form the basis of a B_{3g} representation. On considering all possible one- and two-center overlap densities, one finds only five which generate sets, under the operations of the group, which form the basis of the B_{3g} representation. There is the one-center set of overlaps {2–2, 3–3, 5–5, 6–6} which can be generated, say, starting with the 2–2 overlap density. Then there are the two-center sets {1–2, 3–4, 4–5, 6–1} and {7–3, 8–2, 8–6, 7–5} which can be generated by starting with, say, the 1–2 overlap density and the 7–3 overlap density, respectively. We have a set generated by the 7–2 overlap density, namely, {7–2, 8–3, 8–5, 7–6}, and finally a set generated by the 1–3 overlap, namely, {1–3, 2–4, 4–6, 5–1}. Each contribution to the overlap density will be weighted by the product of the coefficients of the combining orbitals. Since it is only necessary to be

[22] A. C. Albrecht and W. T. Simpson, J. Am. Chem. Soc. 77, 4454 (1955).
[23] A. C. Albrecht (submitted to J. Mol. Spectroscopy).
[24] A. C. Albrecht (submitted to J. Mol. Spectroscopy).

concerned with the generating overlap densities 2–2, 1–2, 7–3, 7–2, and 1–3, it is sufficient to introduce just five parameters to represent the correct weighting coefficient for each of these overlap densities. All other coefficients for each set are simply related by group theory, and in fact for the B_{3u} species, they alternate in sign going around the ring. The five parameters are not independent since only four atomic orbitals are involved. However, from the outset we shall drop the contribution from the set {7–3, 8–2, 8–6, 7–5} since all overlap densities are in effect weighted by the appropriate overlap integral and for this set that integral is very small. Thus there remain four independent parameters as illustrated in Fig. 2. It is now possible to carry out all of the necessary integrations giving results depending only on these parameters. The evaluation of one integral is illustrated in Appendix C.

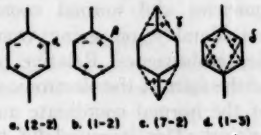

FIG. 2. The electronic transition-density parameters for arbitrary wave functions.

Finally, it is necessary to combine the electronic integrals with the $\xi_{\sigma s}{}^{f*}(a)$ and to introduce $\sum_{\sigma,f}\eta_{\sigma,f}{}^2$ (a, σ^*, f^*) for each set. It happens that the latter sum is just equal numerically to the size of the set whenever the irreducible representation is one dimensional (such as in the present case). The $\eta_{\sigma f}$'s appropriate for $\xi_\sigma{}^U(a)$, $\xi_\sigma{}^R(a)$ (as well as for $I_\sigma{}^U$ and $I_\sigma{}^R$) may be found in footnote reference 23 for several symmetries. After squaring $h_{ks}{}^a$ and multiplying by $hN^0/(8\pi^2\nu_a)$, the sum over a completes the calculation.

Calculations have been made using the integrals published by Liehr[4] which are based on the correct evaluation[25] of the integral appearing in Eq. (19) using Slater $2pz$ atomic orbitals ($Z=3.18$). The $\xi_\sigma{}^{f*}(a)$ and ν_a are obtained from the normal coordinate analyses of *p*-di-*X*-benzene, *p*-dideuterobenzene, or 2,3,5,6-tetradeuterobenzene. In the first case calculations were done with and without the $I_7{}^U$ electronic integral to determine directly what influence the substituent motion has in the perturbation. Calculations were also done within the simple point-charge approximation used by Murrell and Pople,[3] where the perturbation energy results from the interaction of a point-charge transition density with a set of effective dipoles centered on the nuclei. The results are summarized inTable I. Each entry corresponds to the square of the perturbation energy in electron volts originating with a given product of the electron density parameters. All necessary overlap integrals and constants are included. Thus to calculate the entire perturbation energy (squared) one need only specify α, β, γ, and δ as determined by

[25] In this evaluation the Z_σ in $Z_\sigma e^2/r_{i\sigma}$ is properly regarded as a function of r_{ij}.

TABLE I. Coefficients[a] of the electronic density parameters in (ev)[2].

Derivative			α^2	β^2	γ^2	δ^2	$\alpha\beta$	$\alpha\gamma$	$\alpha\delta$	$\beta\gamma$	$\beta\delta$	$\gamma\delta$
1,4 di-*X*	Point[b] charge approx	Without subst[d]	0.66945	0.50756	0.00891	0.00327	0.90663	0.12917	−0.04679	0.11229	0.01267	−0.00177
		With subst	0.71430	0.51176	0.00829	0.00327	0.93867	0.12725	−0.04713	0.11356	0.01270	−0.00186
	Exact[c]	Without subst[d]	0.77853	0.16936	0.00859	0.00315	0.60202	0.13751	−0.04745	0.06534	0.00433	−0.00158
		With subst	0.81591	0.17174	0.00800	0.00315	0.62184	0.13659	−0.04774	0.06587	0.00432	−0.00167
1,4 di-D	Exact[c]	With subst	1.03598	0.18318	0.00969	0.00314	0.72189	0.19063	−0.04523	0.07955	0.00438	−0.00182
2,3,5,6 tetra-D	Exact[c]	With subst	1.14738	0.18849	0.01198	0.00309	0.77108	0.22335	−0.04626	0.08702	0.00465	−0.00174

[a] All necessary overlap integrals have been included in these coefficients.
[b] See footnote reference 3.
[c] See footnote reference 4.
[d] The contribution from the motion of the substituent is neglected.

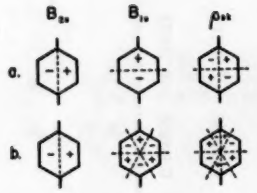

FIG. 3. Diagrams showing how an α and β with the same signs (a) or with opposite signs (b) are obtained depending on the details of the combining wave functions.

the products of atomic orbital coefficients and weigh the appropriate products $\alpha^2, \beta^2, \cdots, \beta\gamma, \cdots$ etc., by the entries of Table I and then sum. This sum is the quantity $hN^0/(8\pi^2)\sum_a (h_{ks}{}^a)^2 \nu_a{}^{-1}$ of Eq. (15b), the square of the perturbation energy (in ev), which we set out to determine in this section.

B. General Conclusions

There are a number of important general observations that may be made on the basis of the results found in Table I. First it is evident that the parameters α and β are relatively dominant in their influence. Furthermore, the magnitude of the vibronic interaction shall be critically sensitive to the relative signs of α and β since the cross term, $\alpha\beta$, also contributes strongly. Thus other things equal (intensities and state energies) one can expect relatively strong "forbidden" character if α and β are similar in sign and magnitude. If they are similar in magnitude, but opposite in sign then the "forbidden" component can be very weak. In Fig. 3 examples of the two possible cases are given. Thus, while the allowed intensities of both B_{1u} states might be very similar (in D_{2h} symmetry) the "forbidden" character induced in the B_{2u} transition can be remarkably different.

A second observation is that the point-charge approximation must be a bad one in this case, unless β is very small. The difference between the exact calculation and that of the point-charge approximation is striking in those terms containing β. The contribution through β is large in general because β represents an effective density very near centers 1 and 2 and the interaction energy squared is roughly inversely proportional to the fourth power of distance between the charge and the moving nuclei. It is just at small distances where the true charge densities cannot be represented by point charges. Whenever β-type density is important then the point-charge approximation must not be used.

A third general observation appears in order. The substituent orbital finds its expression through the parameter γ. The contribution of this type density to the energy is relatively small and therefore there can be little sensitivity to the nature of the participating atomic orbital. While a larger X orbital and smaller C–X distance would no doubt raise the contribution of γ-type density, such a combination is not typical nor is it likely that the contribution would become influential. In the same vein one can anticipate that two electronic wave functions will not mix strongly if one of them is a charge-transfer-type state represented adequately by a configuration in which an electron, say, is promoted from a substituent to the ring. In the one-electron configuration language the transition density ρ_{sk} represents the overlap of that part of the two configurations which differ (which in fact are orthogonal). Thus ρ_{sk} between a charge-transfer state and a state involving only electron promotion within the benzene nucleus can lead only to γ-type density, and therefore to relatively weak "forbidden" character. On the other hand, if γ-type density only is important then there can be no question either of reinforcement or destruction in the sense of Fig. 3. These points are illustrated more carefully in Sec. 3C.

Finally one detects a moderate insensitivity to the normal coordinate analysis. True, only ring modes seem to be important, yet even among these the frequencies and normal coordinates[23,24] have changed considerably on going from *p*-di-*X*-benzene to the deuterobenzenes. Relative to the dominant influence of the form of the electronic wave functions, the details of the normal coordinate analysis are apparently not critical. This is especially true when one is satisfied with only qualitative observations.

We are now in a position to choose trial wave functions first to illustrate some of the generalizations just made and second actually to compute R_k [Eq. (15c)] for different functions and compare these with the experimental findings.

C. Calculation of "Forbidden" Character Using Trial Wave Functions

In order to carry through a calculation for R_k it is necessary to obtain α, β, γ, and δ. Trial wave functions will be chosen in the spirit of the recently developed semiempirical approach[26,27] as applied by Murrell[28] to molecules similar to those considered here.

The correct benzene-derivative B_{2u} and B_{1u} functions are composed of appropriate linear combinations of benzene-type states (or "locally excited" states) $\Psi_V(B_{2u})$, $\Psi_U(B_{1u})$, $\Psi_X(E_{1u_a})$, $\Psi_Y(E_{1u_b})$, and charge-transfer states. That is, in general, for any *p*-disubstituted derivative we shall write

$$\Theta_k{}^0(B_{2u}) = b_1\Psi_V + b_2\Psi_Y + b_3\Psi_B$$
$$\Theta_s{}^0(B_{1u}) = a_1\Psi_U + a_2\Psi_X + a_3\Psi_A, \qquad (21)$$

where Ψ_A and Ψ_B are charge-transfer states of B_{1u} and B_{2u} symmetry, respectively. Since only ortho-para directing substituents are considered the charge-transfer states will consist only of those involving the transfer of an electron from the substituent into the ring. In order to calculate applicable electron-density param-

[26] M. J. S. Dewar and H. C. Longuet-Higgins, Proc. Phys. Soc. (London) **A67**, 795 (1954).
[27] J. A. Pople, Proc. Phys. Soc. (London) **A68**, 81 (1955).
[28] J. N. Murrell, Proc. Phys. Soc. (London) **A68**, 969 (1955).

TABLE II. Electronic parameters for various component state interactions.[a]

B_{2u} Components		B_{1u} Components		
		Ψ_U	Ψ_X	Ψ_A
Ψ_V	α	None	0.31834 [1/(2√3)]	... (...)
	β		−0.15507 (...)	... (...)
	γ		... (...)	−0.22833 [−1/(2√2)]
	δ		0.63667 (1/√3)	... (...)
	ρ_{ak}		$(\psi_4\psi_5+\psi_3\psi_6)$	$[(-1/\sqrt{2})\psi_3\psi_5]$
Ψ_Y	α	0.07754 (...)	None	... (...)
	β	−0.63667 (−1/√3)		... (...)
	γ	... (...)		−0.22833 [−1/(2√2)]
	δ	0.15507 (...)		... (...)
	ρ_{ak}	$(\psi_4\psi_5-\psi_3\psi_6)$		$[(-1/\sqrt{2})\psi_3\psi_5]$
Ψ_B	α	... (...)	... (...)	0.19794 (1/(4√3))
	β	... (...)	... (...)	−0.39587 [−1/(2√3)]
	γ	−0.22833 [−1/(2√2)]	−0.22833 (−1/2√2)	... (...)
	δ	... (...)	... (...)	0.39587 [1/(2√3)]
	ρ_{ak}	$[(-1/\sqrt{2})\psi_3\psi_6]$	$[(-1/\sqrt{2})\psi_3\psi_6]$	$(\psi_4\psi_6)$

[a] Values in parentheses and/or brackets are for MO's normalized without overlap.

eters to be used with Table I it is necessary to specify the $2pz$ atomic orbital basis of the state functions. We begin with the following set of MO's each normalized either to include all overlap[29] or to include no overlap (coefficients in parentheses):

$$\psi_6=0.5485(\omega_1-\omega_2+\omega_3-\omega_4+\omega_5-\omega_6) \quad (\tfrac{1}{6})^{\frac{1}{2}}$$

$$\psi_5=0.3381(2\omega_1-\omega_2-\omega_3+2\omega_4-\omega_5-\omega_6) \quad (\tfrac{1}{12})^{\frac{1}{2}}$$

$$\psi_4=0.5855(-\omega_2+\omega_3-\omega_5+\omega_6) \quad (\tfrac{1}{4})$$

$$\psi_3=0.4567(\omega_2+\omega_3-\omega_5-\omega_6) \quad (\tfrac{1}{4})$$

$$\psi_2=0.2637(2\omega_1+\omega_2-\omega_3-2\omega_4-\omega_5+\omega_6) \quad (\tfrac{1}{12})^{\frac{1}{2}}$$

$$\psi_1=0.3238(\omega_1+\omega_2+\omega_3+\omega_4+\omega_5+\omega_6) \quad (\tfrac{1}{6})^{\frac{1}{2}}$$

$$\psi_+=0.7071(\omega_7+\omega_8) \quad (\tfrac{1}{2})^{\frac{1}{2}}$$

$$\psi_-=0.7071(\omega_7-\omega_8) \quad (\tfrac{1}{2})^{\frac{1}{2}}, \quad (22)$$

where ω_σ is a $2pz$ Slater orbital ($Z=3.18$) for all σ.

In the ground state, ψ_1, ψ_2, ψ_3, ψ_+, and ψ_- are regarded as filled. Singly excited configurations only are considered and the usual intraconfigurational interaction[11] is used to express the benzene state functions correctly. Thus letting χ_i^j represent[30] the properly antisymmetrized product of molecular orbitals where one electron has been promoted from orbital i to orbital j, we may write

$$\Psi_U=1/\sqrt{2}(\chi_3^4+\chi_2^5) \qquad \Psi_V=1/\sqrt{2}(\chi_3^5-\chi_2^4)$$

$$\Psi_X=1/\sqrt{2}(\chi_3^4-\chi_2^5) \qquad \Psi_Y=1/\sqrt{2}(\chi_3^5+\chi_2^4)$$

$$\Psi_A=\chi_-^5 \qquad \Psi_B=\chi_-^4. \quad (23)$$

It is now useful to set up a table of transition-density parameters for the nine possible interaction components connecting the B_{1u} and B_{2u} states [Eqs. (21)] of the derivative. The parameters using MO's normalized with and without (in parentheses) overlap are presented in Table II, together with the functional form for ρ_{ak}. A given choice of a's and b's [Eqs. (21)] can lead to the proper set of parameters. Thus, regarding the entries of Table II as the components of a matrix, $\alpha=\sum_{ij}a_jb_i\alpha_{ij}$, and similarly for β, γ and δ.

It is to be noted that according to Table II, if either Θ_s^0 or Θ_k^0 is entirely a charge-transfer-type state while the other has no charge-transfer character, then one has only γ-type density and therefore relatively weak "forbidden" intensity as recognized at the end of Sec. 3B. If both states are purely charge-transfer states, then there is a clear case of having α and β similar in magnitude, but opposite in sign resulting once more in weak "forbidden" character [see Fig. 3(b)]. On the other hand, there do not appear to be any simple generalizations for cases where Θ_s^0 and Θ_k^0 are mixtures of all three states. It is interesting to point out with regard to the locally excited states that transition density arises only through the mixing of the V with the X state and the U with the Y state. Had we considered totally symmetric perturbations, state V would have also mixed with state Y and state U with state X. The contribution to "forbidden" intensity from the mixing of locally excited states may be large or small

[29] The necessary overlap integrals were obtained from footnote reference 4. Overlap of the two substituent orbitals is neglected.

[30] See footnote reference 3 for the description and use of this notation. The state functions (Eqs. 21 and 23) are labeled X, Y, U, and V instead of β, β, p, and α to avoid confusion with the electron-density parameters.

TABLE III. Coefficients for the trial wave functions [see Eq. (21)].

Coefficient number i	Wave function set I a_i	I b_i	II a_i	II b_i	III a_i	III b_i	IV a_i	IV b_i	V a_i	V b_i
1 (U, V)	0.707	0.707	0.707	0.707	...	$(x)^{\frac{1}{2}}$	0.447	0.760	0.707	0.707
2 (X, Y)	$\pm$0.707	$\pm$0.707	$\pm$0.707	$\mp$0.707	...	$(1-x)^{\frac{1}{2}}$	−0.358	−0.268	...	0.707
3 (A, B)	...	...	...	...	1.000	...	0.820	−0.591	0.707	...

TABLE IV. Calculated perturbation energies and "forbidden" intensity for TMPD and DMB.[a]

Trail wave function sets		I[b]	II[b]	III	IV	V	Obs
Perturbation energies (squared) in (ev)$^2\times10^2$		1.194 (2.140)	7.524(10.098)	0.083 (0.200)	0.643 (0.495)	1.475 (2.203)	(DMB) 13.9 (TMPD) 2.47
The ratio of "forbidden" to allowed intensity in near uv band: R_k	DMB	0.032 (0.057)	0.200 (0.269)	0.002 (0.005)	0.017 (0.013)	0.039 (0.059)	0.37
	TMPD	0.140 (0.250)	0.880 (1.182)	0.010 (0.023)	0.075 (0.058)	0.173 (0.258)	0.29

[a] Values in parenthesis are obtained when MO's are normalized without overlap.
[b] Since these involve locally excited states only, no I_7^U was used.

depending ultimately on the signs and relative magnitudes of α and β.

In Table III several sets of a's and b's are listed to represent functions Θ_s^0 and Θ_k^0 corresponding either to extreme hypothetical cases (sets I, II, and III) or to somewhat more realistic cases (sets IV and V). Sets I and II correspond to the complete breakup of the benzene intraconfigurational interaction. The B_{2u} and B_{1u} states are now single configurations. Thus for set I the B_{2u} state is either χ_3^4 or χ_2^5 while the B_{1u} state is either χ_3^5 or χ_3^4. In either case the transition density, ρ_{sk}, is $\psi_4\psi_5$ which corresponds to a case depicted in Fig. 3(b) where α and β have opposite signs. Set II on the other hand, assigns to the B_{2u} state the configurations χ_3^4 or χ_2^5, while the B_{1u} state now is either χ_2^4 or χ_3^5. In either case, the transition density is $\psi_3\psi_3$ which corresponds to Fig. 3(a) where α and β have the same signs. As shall be seen, set II brings out a very large "forbidden" character, while set I shows only a weak "forbiddenness." Set III corresponds to the case where one function is purely charge transfer, while the other contains no charge-transfer character. The coefficients for set IV were determined by a calculation similar to the one on aniline by Murrell.[28] The predicted electronic energies are not in very good agreement with experiment so that this set of functions must be regarded as only a crude attempt to depict the states of the benzene derivatives here considered. Similarly set V represents an arbitrary choice of constants with the intention of showing how it is possible for some charge-transfer character to be present without greatly inhibiting "forbiddenness." In this connection it appears realistic to assign at least some charge-transfer character to the B_{1u} state (especially for TMPD) and at the same time to regard the B_{2u} state to a considerable extent a mixture of V and Y states.[28,31,32] The transition-density parameters are obtained for each set as described above, appropriate products are taken and weighted by the data of Table I, and then summed to give the perturbation energy (squared) in (ev)^2. The results are found in the first row of Table IV. The remaining empirical parameters of Eq. (15b) are presented in Table V for the two examples DMB and TMPD. Finally, the last two rows of Table IV represent the calculated R_k based on the empirical data and the calculated perturbation energies. The experimental R_k for DMB has been calculated from the polarized single crystal spectrum previously reported[14] and the determination of R_k for TMPD in a rigid glass solution is described in detail elsewhere.[15]

D. Discussion of Results

It is clear from the results obtained how sensitive the perturbation energy is to the nature of the combining wave functions. For example, wave-function sets II and III give effects differing by almost two orders of magnitude. Set II [which corresponds to the case depicted in Fig. 3(a)] appears to represent a maximum effect within the original choice of wave functions. Set

[31] L. Goodman, C. Ross, and H. Shull, J. Chem. Phys. **26**, 474 (1957).
[32] L. Goodman and H. Shull, J. Chem. Phys. **27**, 1388 (1957).

TABLE V. Experimental energies and allowed intensities for DMB and TMPD.[a]

Cmpd	State	Energy (ev)	Allowed intensity (A)^2	$(\mathfrak{M}_{g,k}^{\circ} \mid \mathfrak{M}_{g,s}^{\circ})^2(\Delta E_{sk}^{\circ})^{-2}$ in (ev)$^{-2}$
DMB	B_{2u}	4.23	0.095	2.66
	B_{1u}	5.39	0.34	
TMPD	B_{2u}	3.87	0.095	11.7
	B_{1u}	4.63	0.64	

[a] All data obtained from A. C. Albrecht, thesis, University of Washington, 1954.

III, on the other hand, representing the mixing of a charge-transfer state with a locally excited state simply is not sensitive to the perturbation. Set I, the example corresponding to Fig. 3(b), does have a considerably weaker contribution than does set II.

It appears that the general remarks made earlier are borne out by these calculations. Nor are the qualitative comparisons dependent on whether or not the MO's are normalized with overlap.

How successfully are the experimental results anticipated? While the R_k's obtained span a range which almost encompasses the two observed R_k's, when attempts are made to choose representative wave functions the results invariably are weaker than what is observed. This is particularly striking in the case of DMB. First, it is to be noted that the calculations were done for $T=0°K$; however, changes in R_k upon going to higher temperatures are not expected to be very large. Secondly, mixing with higher excited states has been neglected. When "nearest-neighbor" mixing is weak, the contributions to R_k from mixing with more energetic states may become important and in general is certain to contribute. In fact, if "nearest-neighbor" mixing is weak because of a situation depicted in Fig. 3(b) then it is likely that mixing with a higher state is of the favorable type [Fig. 3(a)] especially within a framework of declining intraconfigurational interaction. All things considered we shall conclude that the calculations do not discourage identifying the observed mixed polarization in TMPD with "forbiddenness." However, this cannot be said for the case of DMB. Here it might be important to emphasize a fact that is normally ignored. The symmetry of DMB is by no means D_{2h} (nor in fact is that of TMPD—although here the deviation is much less serious). Perhaps more importantly the bond distances of DMB in the crystalline state[33] indicate a deviation of the benzene nucleus from D_{2h} symmetry in exactly the sense of a b_{3g} vibration. It is possible that this can explain the large observed R_k although the matter has not yet been completely rationalized in this manner.

Finally, it appears that the results permit one to conclude that in neither TMPD nor DMB do we have examples where there is mixing between states one of which is charge transfer, the other locally excited. It has been proposed that[28,34] in dimethylaniline the B_{1u} state is a charge-transfer state. However, TMPD is apparently not a planar molecule,[35] and therefore the charge-transfer character in the B_{1u} band may not dominate. Conversely, in the case of dimethylaniline one would predict very weak mixed polarization in the near-ultraviolet band if indeed it does represent an example having set III type of functions.

Generally speaking, it will not be possible to make full use of the information provided by an experimental R_k, nor to critically evaluate the Herzberg-Teller theory, until it is possible to choose wave functions much more confidently. Experimental work is now under way on a series of related compounds in which at least a trend in the nature of the wave functions is predictable. In addition, it is hoped that exploration of trial functions for weakly substituted derivatives and comparison with available data will help to guide the choice of correct wave functions.

E. Case of Weak Para-Disubstitution

All considerations so far have dealt with *p*-disubstituted benzenes having "strong" substituents. In the case of purely inductive substitution, the B_{1u} state tends not to acquire allowed character while the B_{2u} state does become allowed through the mixing of Ψ_V with Ψ_Y.[11,32] In such cases there can be no question of borrowing from the neighboring still "forbidden" B_{1u} band. The "forbidden" component in the near-ultraviolet band must derive from the high energy B_{2u} state (from the perturbed E_{1u_b} benzene state) through totally symmetric vibrations or from the high energy B_{1u} state (from the unperturbed E_{1u_a} benzene state) through b_{2g} vibrations.

Preliminary consideration of the problem reveals the possibility of constructive or destructive interferences that do not occur in benzene itself. A comprehensive study of this is under way.

4. SUMMARY AND FURTHER GENERAL COMMENTS

The general outline for the calculation of the "forbidden" part of an allowed transition is given within

[33] T. H. Goodwin, M. Przybylska, and J. M. Robertson, Acta Cryst. 3, 279 (1950).

[34] L. Goodman (private communication); see also E. G. McRae and L. Goodman, J. Mol. Spectroscopy (to be published).

[35] See footnote 19 of footnote reference 22.

the Herzberg-Teller framework. It is seen how both totally symmetric and nontotally symmetric vibrations can lead to "forbidden" character. In both cases, the intensity of the "forbidden" component is sensitive to temperature. Where nontotally symmetric vibrations are active, the "forbidden" component appears polarized in an opposite manner to the polarization of the pure electronic component. Thus the presence of mixed polarization in a band belonging to a single electronic transition is direct evidence for "forbidden" character. The absence of mixed polarization does not preclude "forbiddenness."

A calculation based on a normal coordinate analysis of a model *p*-disubstituted benzene derivative is presented in terms of parameters to be fixed by choice of electronic functions. It is found that the extent of mixing under the vibrational perturbation is very sensitively dependent on the details of the nodal patterns of the combining functions. Two locally excited states with favorable nodal patterns mix the best, while a charge-transfer state and a locally excited state do not mix well. It appears that the analysis does not depend critically on the substituent motion nor on the details of the normal coordinate analysis. Electronic parameters are calculated for trial wave functions and empirical energies and intensities taken for two examples where mixed polarization has been found. The results obtained bear out the general conclusions made solely on the basis of the parameterized calculation. They also do not discourage the interpretation of the observed mixed polarization, in at least one example, as evidence for "forbidden" character. However, much more theoretical and experimental work is needed before one can confidently test the Herzberg-Teller theory and also make full use of the information combined in temperature-dependent intensities and mixed-polarization observations.

It appears that one can safely expect that all electronic bands contain "forbidden" character to some degree. In diatomic molecules states of identical symmetry may mix under totally symmetric vibrations. In highly conjugated systems, the excited electronic states can mix with favorable energy denominators. While the extent of mixing may be small in many cases, it nevertheless may be important from the point of view or radiationless internal conversion processes. It has been suggested[9] how the nontotally symmetric vibrations bring about radiationless transitions between electronic states of different symmetries. It remains to be seen whether a perturbation treatment based on pure electronic zeroth-order functions can adequately predict probabilities for radiationless transitions. Thinking has proceeded more along lines dealing with the intersection of regions of potential energy hypersurfaces. This would not appear to invite the use of pure electronic basis functions. However, it may be that at least qualitative conclusions are valid. The presence of "forbidden" character in bands which is borrowed from their neighboring bands (both at lower and higher energies) is certainly suggestive of an explanation for the success in condensed systems of radiationless transitions between excited states in their competition with radiative processes, and the measure of the amount of "forbiddenness" may relate to the intensity of these transitions. The ground electronic state on the other hand is normally energetically isolated from other states of the same multiplicity. The mixing of it with other states through vibrational perturbation is very unlikely. This of course agrees with the observation that radiative transitions from the first excited state to the ground state are competitive with radiationless processes. Azulene has been found to emit from its second excited singlet.[36] The first excited singlet is of a different symmetry and the "forbiddenness" permitting a radiationless transition should appear in the lower state as mixed polarization in the lowest absorption band. No such mixed polarization has been found.[13] On the basis of our considerations, this can be taken as direct independent evidence that the probability for the radiationless transition from the second singlet to the first is very small and stands in agreement with the observation of anomalous emission. On the other hand, each phenomenon may be simply a relatively independent reflection of the great separation of the two states in this instance.

While more exact theoretical exploration along these lines may prove interesting, a real test of any theory must await the successful solution to the problem of determining rates of radiationless transitions among excited states.

ACKNOWLEDGMENTS

The author is very grateful to Professor C. A. Coulson for several clarifying discussions. He wishes also to thank Professor B. Widom and Professor R. Bersohn for helpful comments and criticism.

He is especially indebted to Professor G. Dresselhaus for his critical comments concerning the group-theoretical treatment in Appendix A, and to Dr. A. D. Liehr for valuable discussions and his criticism of the manuscript.

APPENDIX A

Group-Theoretical Reduction of the Perturbation Energy

If the direct-product representation of an integrand contains the totally symmetric representation M times, then there are M independent ways of writing the integrand such that each function constitutes the basis of the totally symmetric representation. Except for coincidences, there must arise M different values of the

[36] M. Beer and H. C. Longuet-Higgins, J. Chem. Phys. **23**, 1390 (1955).

integral. Thus in the vibronic problem consider vibrations of species b which couple electronic states s and k. If $M_1(s, k, b)$ is the number of times the totally symmetric representation Γ_1 is contained in the direct product representation $\Gamma_s \times \Gamma_k \times \Gamma_b$, then there are $M_1(s, k, b)$ different perturbation energy integrals or $3N \times M_1(s, k, b)$ electronic integrals if the $3N$ components of each are counted. On the other hand, the minimum number of integrals required for all species of vibration may be had by counting the number of Γ_1's in $\Gamma_s \times \Gamma_k \times \Gamma_\xi$, where Γ_ξ is the representation for which the set of $3N$ local cartesian coordinates is a basis. The minimum number of integrals for species b is obtained by counting the Γ_1's in $M_b(s, k)$ $(\Gamma_b \times \Gamma_\xi)$, where $M_b(s, k)$ is the number of times Γ_b appears in $\Gamma_s \times \Gamma_k$. Further, one can subdivide this minimum number by separately counting the Γ_1's in $M_b(s, k)$ $(\Gamma_b \times \Gamma_\xi^f)$ $(f=1, 2, 3)$.[37]

The question of reducing the great number of integrals appearing in the formal theory to the minimum number presents itself. It will be shown how group-theoretical relationships among the $I_\sigma^f(s, k, a)$ may be obtained and how in fact these are identical to the relationships existing among the normal coordinate coefficients.

Suppose that the ath normal mode is a member of a degenerate set of normal modes $1, 2, \cdots, l_b$ belonging to the species b. One can speak of the perturbation energy due to the set of normal modes

$$h_{ks}{}^b = \sum_{a=1}^{l_b} h_{ks}{}^a. \tag{A1}$$

The sum of terms belonging to atom σ in Eq. (A1) reads $\xi_\sigma{}^1(1) I_\sigma{}^1(s, k, 1) + \xi_\sigma{}^2(1) I_\sigma{}^2(s, k, 1) + \cdots + \xi_\sigma{}^2(4) I_\sigma{}^2(s, k, 4) + \cdots + \xi_\sigma{}^3(l_b) I_\sigma{}^3(s, k, l_b)$ [see Eq. (19a)]. Let this sum be written as the matrix product of a row and a column matrix, $\xi_\sigma{}^\dagger \mathbf{I}_\sigma$, to give

$$h_{ks}{}^b = \sum_\sigma \xi_\sigma{}^\dagger \mathbf{I}_\sigma. \tag{A2}$$

Now let $\mathbf{P}_R$ represent an appropriate operator corresponding to the transformation R which is an element of the symmetry group of configuration space for the molecule under consideration.[38] Because of the properties of $\mathbf{P}_R$ and because $h_{ks}{}^b$ and the elements of the row and column vectors are constants, one may write

$$\mathbf{P}_R h_{ks}{}^b = \sum_\sigma \mathbf{P}_R \xi_\sigma{}^\dagger \mathbf{P}_R \mathbf{I}_\sigma = \sum_\sigma \xi_\sigma{}^\dagger \mathbf{P}_R \mathbf{I}_\sigma = \sum_\sigma \xi_\sigma{}^\dagger \mathbf{I}_\sigma = h_{ks}{}^b. \tag{A3}$$

On the other hand,

$$\mathbf{P}_R \mathbf{I}_\sigma = \mathbf{A}_\sigma(R) \mathbf{I}_{\sigma+x} = \mathbf{I}_\sigma \tag{A4}$$

and

$$\mathbf{P}_R \xi_\sigma = \mathbf{B}_\sigma(R) \xi_{\sigma+x} = \xi_\sigma, \tag{A5}$$

where the first equalities arise when considering the original functional form of the vector elements. For example,

$$I_\sigma^f(s, k, a) = \mathbf{P}_R I_\sigma^f(s, k, a) = \int \mathbf{P}_R \rho_{sk}{}^a \mathbf{P}_R \mathcal{H}_\sigma'^f dx_p$$

$$= \sum_{\sigma=1}^{l_b} \sum_{g=1}^{3} A_{\sigma g}(R, \sigma, s, k, a) I_{\sigma+x}{}^g(s, k, a), \tag{A6}$$

where $\rho_{sk}{}^a$ is that component (group-theoretically determined) of the transition density ρ_{sk} [Eq. (20)], which has a nonvanishing interaction with vibrational component a, and where $\mathcal{H}_\sigma'^f$ is just $(\partial \mathcal{H}_{p\sigma}/\partial \xi_\sigma^f)_0$ [see Eq. (19)]. For a similar application of $\mathbf{P}_R$ see Wigner.[39]

Thus, in general, the effect of $\mathbf{P}_R$ is to express the vectors ξ_σ and $\mathbf{I}_\sigma$ in terms of the vectors $\xi_{\sigma+x}$ and $\mathbf{I}_{\sigma+x}$, the orthogonal transformation matrices being $\mathbf{B}_\sigma(R)$ and $\mathbf{A}_\sigma(R)$, respectively. Now

$$\mathbf{P}_R \xi_\sigma{}^\dagger \mathbf{P}_R \mathbf{I}_\sigma = \xi_{\sigma+x}{}^\dagger \mathbf{B}_\sigma{}^\dagger(R) \mathbf{A}_\sigma(R) \mathbf{I}_{\sigma+x} = \xi_{\sigma+x} \mathbf{I}_{\sigma+x}. \tag{A7}$$

The last equality follows because the contribution from center $\sigma+x$ to the total energy is invariant with respect to the operations of the group [Eqs. (A3), (A4), (A5)] and the middle expression in Eq. (A7) represents the total contribution of center $\sigma+x$ in the transformed $h_{ks}{}^b$. Thus it follows that $\mathbf{B}_\sigma(R) = \mathbf{A}_\sigma(R)$ for all R and σ since these have been arbitrarily chosen. This shows that the identical group-theoretically defined relationships hold among the $\xi_\sigma^f(a)$'s as among the $I_\sigma^f(s, k, a)$'s [Eqs. (A4), (A5)]. The relationships among the $\xi_\sigma^f(a)$'s arise automatically from a normal coordinate analysis and may be directly carried over to the electronic integrals. Alternatively, one can carry out the operations indicated in Eq. (A6) for several R and σ to obtain sets of simultaneous equations, whose solution yields the desired relationships. If one relationship reads, for example, $I_\sigma^f = \eta_{\sigma,f}(a, \sigma^*, f^*)\, I_{\sigma^*}^{f^*}$ [and similarly for $\xi_\sigma^f(a)$] then Eq. (19b) follows. If the size l_b of the set b (of which a is a member) is greater than one (degenerate), then not only will relationships among integrals (and cartesian coefficients) for a given a exist but in addition relationships will exist among integrals (and cartesian coefficients) for different a of the degenerate set. Examples of these relationships may be found in Table VII of footnote reference 23 for

[37] For the D_{2h} molecules considered $M_b(B_{1u}, B_{3u}) = 1$ for $b = b_{3g}$ and zero for all other species. The number of Γ_1's in $b_{3g} \times \Gamma_\xi^f$ are two for $f = R$, two for $f = U$ and none for $f = Z$. All electronic integrals may therefore be reduced to four.

[38] See E. P. Wigner, *Group Theory* (Academic Press, Inc., New York, 1959), Chaps. 11 and 12.

[39] See p. 115 of footnote reference 38.

D_{6h}, D_{3h}, and D_{2h} symmetry for both degenerate and nondegenerate species. These relationships are based on a choice of local cartesian coordinates causing $\mathbf{A}_\sigma(R)$ to correspond directly to elements of a *reduced* representation of the given group. Where irreducible representations are one dimensional, such as in this paper, the matrices $\mathbf{A}\sigma(R)$ are diagonal with elements ± 1 which in turn are directly equal to the η's.

Necessary in the foregoing is that $\mathbf{P}_R\mathbf{I}_\sigma$ and $\mathbf{P}_R\xi_\sigma$ are always defined. It is possible that the symmetry in electronic space is higher than that in nuclear space (isotopic substitution). For operations on both matrices to be defined, the group of lower symmetry must be considered. Nevertheless, relationships, not valid for the $\xi_\sigma{}^f(a)$'s, will hold among the $I_\sigma{}^f(s, k, a)$'s because of the higher symmetry in electronic space, and these are the same as among the $\xi_\sigma{}^f(a)$ for the molecule in fullest symmetry (nonisotopic or fully isotopic).

APPENDIX B

Temperature Dependence of "Forbidden" Intensity

In order to obtain the temperature dependence of "forbidden" intensity or of the ratio R_k of "forbidden" to allowed intensity it is necessary to evaluate $\sum_i B_i\langle Q_a{}^2\rangle_{ii}$ [Eq. (15b)]. The parameter i goes over $(3N-6)$-fold infinity of vibrational states. B_i is the Boltzmann weighting factor for state i. It is chosen so that

$$\sum_i B_i = 1. \tag{B1}$$

Suppose the ith vibrational state corresponds to the normal mode 1 excited by $v_1{}^i$ quanta, the normal mode 2 excited by $v_2{}^i$ quanta and, say, the normal mode a excited by $v_a{}^i$ quanta. We then may write

$$B_i = \exp\{-h/(kT)\,(\sum_a \nu_a v_a{}^i)\}$$
$$\{\prod_a (1-\exp[-h\nu_a/(kT)]\}, \tag{B2}$$

which is normalized according to Eq. (B1). Now $(Q_a{}^2)_{ii}$ depends only on the degree of excitation in the ath normal mode so that for normalized harmonic oscillator wave functions we have[40]

$$\langle Q_a{}^2\rangle_{ii} = (v_a{}^i+\tfrac{1}{2})/\gamma_a \tag{B3}$$

with $\gamma_a = 4\pi^2\nu_a/(hN^0)$. The sum of Eq. (B1) may be carried out over all degrees of excitation for each normal mode but the ath to give

$$\sum_i B_i\langle Q_a{}^2\rangle_{ii} = \sum_{v_a=0}^{\infty}[(v_a+\tfrac{1}{2})/\gamma_a](1-u_a')u_a{}'^{v_a}, \tag{B4}$$

where $u_a' = \exp\{-h\nu_a/(kT)\}$. The remaining sum is also readily carried out to give

$$1/2\gamma_a\{(1+u_a')/(1-u_a')\},$$

and with $u_a = h\nu_a/(2kT)$ we finally have

$$\sum_i B_i\langle Q_a{}^2\rangle_{ii} = (2\gamma_a)^{-1}\coth u_a, \tag{B5}$$

the desired relationship.[41]

APPENDIX C

Evaluation of an Electronic Integral

As an example the evaluation of that part of the electronic integral $I_2{}^R$ due to γ-type transition density [see Fig. 2(c)] will be outlined. Formally, the integral $I_2{}^R$ reads [see Eq. (19)]

$$I_2{}^R = \int \rho_{sk}(\partial\mathcal{H}_{p2}/\partial r_{p2})_0(\partial r_{p2}/\partial\xi_2{}^R)_0 dx_p, \tag{C1}$$

where $(\partial r_{p2}/\partial\xi_2{}^R)$ is the direction cosine of the vector connecting electron p and nucleus 2 with respect to the radial local cartesian coordinate R_2 (see Fig. 1). Liehr[4] shows how the problem can be reduced to the determination of the direction cosines for vectors connecting the various transition-density centers and the appropriate electronic integrals for each center. On referring again to Fig. 2(c), we shall distinguish the four γ-type transition-density centers by writing γ, γ', γ'', γ''' for the 7–2, 8–3, 8–5, and 5–7 overlaps. Further, let d, d', d'', d''' represent, respectively, each of the distances separating the four transition density centers and atomic center 2, and let the direction cosines read $\cos(d, R_2)$, $\cos(d', R_2)$, $\cos(d'', R_2)$, and $\cos(d''', R_2)$. The electronic density parameters do not include the appropriate overlap factors so that here s_{02} is included, the overlap of two $2pz$ Slater orbitals ($Z=3.18$) separated by $(\sqrt{3})\,(1.40)$ A—the separation of the atoms concerned. Thus we have

$$I_2{}^R\{\gamma\} = \gamma s_{02}[I_0(d)\cos(d, R_2) - I_0(d')\cos(d', R_2)$$
$$+I_0(d'')\cos(d''', R_2) - I_0(d'')\cos(d''', R_2)], \tag{C2}$$

where use has been made of the fact that $\gamma=-\gamma'=\gamma''=-\gamma'''$ (the transition density belongs to the B_{3g} species) and the electronic integrals remaining have been designated as $I_0(d)$, $I_0(d')$, etc. The direction cosines are, respectively, 0, $5/[2(13)^{\frac{1}{2}}]$, $4/(19)^{\frac{1}{2}}$, and $\frac{1}{2}$; and the distances d, d', d'', d''' in units of 1.40 A are $\sqrt{3}/2$, $(13)^{\frac{1}{2}}/2$, $(19)^{\frac{1}{2}}/2$, and $\frac{3}{2}$, respectively. The neces-

[40] E. B. Wilson, Jr., J. C. Decius, and P. C. Cross, *Molecular Vibrations* (McGraw-Hill Book Company, New York, 1955), p. 290. [The normalization of the normal coordinates used here (see footnote references 23 and 24) introduces Avogadro's number, N^0.]

[41] A similar more specialized version of the temperature dependence, not based on Eq. (6), may be found in a paper by A. D. Liehr and C. V. Ballhausen [Phys. Rev. **106**, 1161 (1957), Eq. (4)].

sary integrals for these distances and the overlap integral, s_{02} [as $I_2(\sqrt{3}x_{01})$], may be found in Appendix IV of footnote reference 4. The result is

$$I_2^R\{\gamma\}=\gamma[0-0.2625+0.2386-0.2746]=-0.2985,$$

where the units are in $(Z^2e^2/a_0^2)\ 10^{-2}$. (5.201 ev/A for $Z=3.18$.)

Similar procedures must be followed to obtain the α, β, and δ components of I_2^R and to evaluate the remaining integrals[42] I_2^U, I_1^U, and I_7^U.

[42] In evaluating I_2^U one integral was estimated by extrapolating appropriate available integrals. Only later was it discovered that the estimated integral had in fact also been reported by Liehr. The value obtained by extrapolation was sufficiently correct to cause negligible error in the entries of Table I.

THE JOURNAL OF CHEMICAL PHYSICS VOLUME 33, NUMBER 1 JULY, 1960

Vibronic Calculations in Benzene*

ANDREAS C. ALBRECHT

Department of Chemistry, Cornell University, Ithaca, New York

(Received December 21, 1959)

A group-theoretical reduction incorporating normal-coordinate parameters is applied to obtain expressions for the oscillator strengths of forbidden B_{2u}, B_{1u}, and E_{2g} transitions in benzene in terms of the minimum number of electronic integrals. The simplification obtained encourages the testing of wave functions within the Herzberg-Teller framework as well as empirical evaluation of the theory. An investigation is made of the possible effect of isotopic substitution on forbidden intensities. The group-theoretical reduction is carried out for 1,4 dideuterobenzene, *sym*-benzene-d_2, 2,3,5,6-tetradeuterobenzene, benzene-d_6, and a hypothetical molecule *p*-di-*X*-benzene (where $(X)=20$ and $C-X=1.40$ A). It is observed that the B_{2u} and B_{1u} transitions are very insensitive to mass effects independent of the nature of the electronic functions. On the other hand, E_{2g} transitions may or may not show a significant sensitivity depending on the details of the wave functions. By way of illustration, oscillator strengths are calculated for all compounds for B_{2u}, B_{1u}, and two E_{2g} transitions using conventional benzene ASMO functions and published integrals. The distribution of oscillator strengths among all active normal modes is given for benzene, benzene-d_6, and *p*-di-*X*-benzene. It is found that especially for the E_{2g} transitions the distribution among normal modes is considerably more sensitive to mass effects than is the total oscillator strength.

A general expression is given for the temperature dependence of "forbidden" transition probabilities.

INTRODUCTION

ATTEMPTS to calculate the intensities of "forbidden" transitions in benzene[1–5] have met with various degrees of success. In a critical study of all benzene vibronic calculations Liehr[6] reports that with exact solutions of the equilibrium nuclear configuration electronic Schrödinger equation a theory that mixes equilibrium configuration electronic wave functions through vibrational perturbation (Herzberg-Teller[7]) should be entirely adequate for predicting forbidden intensities. It is the lack of strictly correct wave functions that has led to at least one important refinement[2,4] and to semiempirical approaches containing a variety of assumptions. In the preceding paper[8] (henceforth referred to as I) the theory for calculating "forbidden" intensity in allowed electronic transitions has been formulated based on the Herzberg-Teller approach. There a group-theoretical reduction of the vibronic problem is presented that incorporates the necessary normal coordinate parameters to express "forbidden" intensities in terms of a minimum number of integrals that alone depend on the choice of electronic wave functions. This simplification not only encourages the testing of wave functions and approximations (within the Herzberg-Teller framework) but it also encourages a search for empirical methods of testing the theory.

The group-theoretical reduction has been carried out for benzene and it is found that only two "one-center" electronic integrals are needed to calculate the intensity of the B_{2u} and the B_{1u} transitions. Four such integrals are required for E_{2g} transitions. By applying the reduction to several isotopic derivatives and a model benzene derivative a partial study of the effect of mass on forbidden intensities has been carried out.

* Supported in part by the National Science Foundation.

[1] D. P. Craig, J. Chem. Soc. **1950**, 59.

[2] A. D. Liehr, thesis, Harvard University, 1955.

[3] J. N. Murrell and J. A. Pople, Proc. Phys. Soc. **A69**, 245 (1956).

[4] A. D. Liehr, Z. Naturforsch. **13a**, 596 (1958).

[5] For an extensive discussion and further calculations see A. D. Liehr, The William E. Moffitt Memorial Session, International Conference on Molecular Quantum Mechanics, University of Colorado, Boulder, Colorado, June 21–27, 1959. [Text to be published in the conference proceedings, Revs. Modern Phys. **32** (April, 1960).]

[6] A. D. Liehr, Can. J. Phys. **35**, 1123 (1957); **36**, 1588 (1958).

[7] G. Herzberg and E. Teller, Z. physik. Chem. (Leipzig) **B21**, 410 (1933).

[8] A. C. Albrecht, J. Chem. Phys. **33**, 156 (1960), this issue.

It appeared that a study of intensities in deuterated benzenes might be especially interesting (if effects exist) since the electronic integrals do not change on isotopic substitution. The published[9] data on the normal coordinates for benzene and benzene-d_6 indicated sufficient mixing among the hydrogen (deuterium) and carbon modes not to discourage such an investigation. Moreover, a larger number of vibrations are vibronically active in the derivatives of lower symmetry. The normal coordinates in terms of local cartesian coordinates have been obtained[10] for benzene,[11] 1,4-dideuterobenzene, *sym*-benzene-d_3, 2, 3, 5, 6-tetradeuterobenzene, benzene-d_6, and a model benzene derivative *p*-di-*X*-benzene[12] where *X* has a mass of twenty and the C–*X* distance is 1.40 A. The reduction of the vibronic calculations is carried out for "B_{2u}," "B_{1u}," and "E_{2g}" transitions for each molecule. It is found that in general the mass effect is essentially insignificant. On the basis of the reduction alone (independent of electronic wave functions), it is predicted that there should be no variation in intensity among the isotopic benzenes. The stability of the B_{2u} and B_{1u} intensities is maintained even in the *p*-di-*X*-benzene (assuming D_{6h} electronic states). In contrast, the E_{2g} intensity can change markedly in the latter compound from its value in benzene, depending on the details of the D_{6h} wave functions. These observations have important bearing on "forbidden" intensities in D_{6h} or D_{3h} substituted benzenes.

In what follows the general theory is given based on the development in I and a temperature-dependent "forbidden" oscillator strength is obtained. Group theory is then applied to the benzene problem. The reduction is presented in detail (according to active normal modes) for benzene, benzene-d_6, and *p*-di-*X*-benzene. The results are summarized for all six molecules. Finally, by way of illustration, conventional ASMO functions are used to calculate oscillator strengths using empirical energies and allowed intensities. This is followed by a discussion.

THEORY

1. General

The Herzberg-Teller formalism for calculating "forbidden" intensities shall be taken directly from I. There an expression has been obtained for the ratio, R_k, of "forbidden" to allowed intensity in the transition from the ground electronic state, g, to the excited electronic state, k. Thus, Eq. (15b) of I reads

$$R_k=hN^0/(8\pi^2)\sum_{s,a}(\nu_a^{-1}\coth u_a)\,(h_{ks}{}^a)^2 \times\{(\mathfrak{M}_{g,s}{}^0/\mathfrak{M}_{g,k}{}^0)^2(\Delta E_{sk}{}^0)^{-2}\} \quad (1)$$

where h is Planck's constant, N^0 is Avogadro's number, $u_a=h\nu_a/(2kT)$, and ν_a is the frequency of the ath normal mode of the ground state. $\mathfrak{M}_{g,s}{}^0$ and $\mathfrak{M}_{g,k}{}^0$ are allowed transition moments based on pure electronic wave functions (for ground state equilibrium configuration). $\Delta E_{sk}{}^0$ is the difference in the pure electronic energy of state s and k. The term $h_{ks}{}^a$ is the perturbation energy per unit displacement of normal mode a resulting from the coupling of states k and s. The sum goes independently over all electronic states (except state k) and in general over all $3N-6$ normal modes, a. Now R_k simply represents the ratio of the second terms to the first in the Herzberg-Teller type expansion of the transition probability, $P_{g,k}$ [see Eqs. (13) and (14) of I]. By definition "forbidden" transitions are those for which the first term $(\mathfrak{M}_{g,k}{}^0)^2$, vanishes. By isolating the second terms in Eq. (1) [multiply by $(\mathfrak{M}_{g,k}{}^0)^2$] we have for the temperature-dependent transition probability of a "forbidden" transition:

$$P_{g,k}=hN^0/(8\pi^2)\sum_{s,a}(\nu_a{}^{-1}\coth u_a)\,(h_{ks}{}^a)^2 \times\{(\mathfrak{M}_{g,s}{}^0)^2(\Delta E_{sk}{}^0)^{-2}\}. \quad (2)$$

In keeping with previous practice we shall choose $T=0°\text{K}$[13] and use oscillator strengths instead of transition probabilities. We finally have

$$f_{g,k}=(hN^0/8\pi^2)\sum_{s,a}(\nu_a{}^{-1})\,(h_{ks}{}^a)^2 \times[(f_{g,s}{}^0)\,(E_k{}^0/E_s{}^0)\,(\Delta E_{sk}{}^0)^{-2}] \quad (3)$$

for the oscillator strength of a "forbidden" transition at 0°K. The quantity in brackets in Eq. (3), involving allowed intensities, $f_{g,s}{}^0$, and pure electronic energies $E_k{}^0$ and $E_s{}^0$, shall normally be regarded as empirically determined. The burden of any calculation then rests on the determination of $h_{ks}{}^a$ for all a and s. Eq. (19) of I reads

$$h_{ks}{}^a=\sum_{j=1}^{3}\sum_{\sigma=1}^{N} \times\{(\partial\xi_\sigma{}^j/\partial Q_a)_0\int\rho_{sk}(p)\,(\partial\mathfrak{IC}_{p\sigma}/\partial r_{p\sigma})_0(\partial r_{p\sigma}/\partial\xi_\sigma{}^j)_0 dx_p\} \quad (4)$$

where $(\partial\xi_\sigma{}^j/\partial Q_a)_0$ is the coefficient for normal coordinate Q_a of the jth local Cartesian coordinate at nucleus σ. The integral is over the space of the pth electron where

$$\rho_{sk}(p)=n\int\Theta_s{}^0\Theta_k{}^0 dx' \quad (5)$$

is a one-electron transition density resulting from the one-electron nature of the perturbation operator.[3] $\Theta_s{}^0$ and $\Theta_k{}^0$ are pure electronic functions, n is the number of electrons, and the integration is over all

[9] D. H. Whiffen, Proc. Roy. Soc. (London) **A248**, 131 (1955).
[10] A. C. Albrecht (submitted to J. Mol. Spectroscopy).
[11] The force field used is a slightly modified Whiffen force field involving negligible changes in the normal coordinates. Thus, all previous benzene vibronic work based on the Whiffen normal coordinates remains entirely unaffected.
[12] A. C. Albrecht (submitted to J. Mol. Spectroscopy)
[13] While this is not necessary in view of Eq. (2), a thorough investigation of the temperature dependence now underway shows that this assumption is not a critical one at room temperatures and below.

space but that of electron p. In Eq. (4) $(\partial r_{p\sigma}/\partial \xi_\sigma^j)_0$ is the direction cosine or the vector, $\mathbf{r}_{p\sigma}$, linking electron p with nucleus σ. $\mathcal{H}_{p\sigma}$ is just the coulomb potential between electron p and nucleus σ, $(Z_\sigma e^2/r_{p\sigma})$. It proves convenient to symbolize the normal coordinate coefficients by $\xi_\sigma^j(a)$ and the electronic integrals by $I_\sigma^j(s, k, a)$ to give

$$h_{ks}^a = \sum_{j,\sigma} \xi_\sigma^j(a) I_\sigma^j(s, k, a). \tag{6}$$

Finally, in Appendix A of I it is shown how Eq. (6) may be greatly simplified through the use of group theory. It is proven that the identical relationships holding among the $\xi_\sigma^j(a)$ hold also among the $I^j(s, k, a)$ permitting one to write

$$h_{ks}^a = \sum_{f^*,\sigma^*} \xi_{\sigma^*}^{j*}(a) I_{\sigma^*}^{j*}(s, k, a) \{ \sum_{\sigma,j} \eta_{\sigma j}^2(a, \sigma^*, f^*) \} \tag{6a}$$

where the sum over f^* and σ^* goes over a minimum number of atomic centers and corresponding cartesian coordinates. The expression in brackets is group-theoretically determined where

$$\eta_{\sigma j}(a, \sigma^*, f^*) = I_\sigma^j(s, k, a)/I_{\sigma^*}^{j*}(s, k, a) = \xi_\sigma^j(a)/\xi_{\sigma^*}^{j*}(a).$$

In any problem where the normal coordinate coefficients, $\xi_{\sigma^*}^{j*}(a)$, are known it is then possible to obtain the total perturbation energy (squared)

$$hN^0/(8\pi^2)(\nu_a^{-1})(h_{ks}^a)^2,$$

in terms of the minimum number of electronic integrals $I_{\sigma^*}^{j*}(s, k, a)$. Any set of integrals with the necessary empirical (or calculated) intensities and energies can then lead directly to a calculated oscillator strength [Eq. (3)].

2. GROUP THEORETICAL REDUCTION OF THE VIBRONIC CALCULATIONS IN BENZENE

Speaking generally, "forbidden" transitions to upper states B_{2u}, B_{1u}, and E_{2g} in benzene can acquire intensity when these states mix with E_{1u} and A_{2u} states—the only possible upper states in allowed transitions of D_{6h} molecules (assuming a totally symmetric ground state). For the perturbation energy,

$$\int \Theta_k^0 \mathcal{H}' \Theta_s^0 dx (k = B_{2u}, B_{1u}, E_{2g}; s = E_{1u}, A_{2u}),$$

not to vanish, the direct product representation of the integrand must contain at least once the totally symmetric representation. Since[14] $B_{1u} \times E_{1u}$ and $B_{2u} \times E_{1u} = E_{2g}$ while $E_{2g} \times E_{1u} = E_{1u} + B_{1u} + B_{2u}$, the representation based on $\mathcal{H}'$ must contain E_{2g} species to permit the mixing of B_{1u} and B_{2u} states with E_{1u} states and it must contain E_{1u}, B_{1u}, or B_{2u} species to permit the mixing of E_{2g} and E_{1u} states. Similarly it is found that B_{1g}, B_{2g}, and E_{2u} perturbations are required to mix respectively the B_{2u}, B_{1u}, and E_{2g} states with A_{2u} states. Now $\mathcal{H}'$ must have the same symmetry properties in electron space that the perturbing normal mode has in the configuration space of the nuclei (see I). Thus, the normal modes active in the perturbation are prescribed in each instance. Furthermore, group theory can prescribe the correct form of integrand functions that are the basis of the reduced form of the direct product $(\Gamma_s \times \Gamma_k)$ representation. That is, the exact form is given for the electronic functions that interact with each of the normal mode species. For example, consider the case of the mixing of electronic states E_{2g} and E_{1u}. If the pair of degenerate orthogonal components for each state be labeled a[15] and b (E_{2g_a}, E_{2g_b}, E_{1u_a}, E_{1u_b}) then one must consider the four possible mixings: aa, ab, ba, and bb, corresponding to $E_{2g_a}E_{1u_a}$, $E_{2g_a}E_{1u_b}$, $E_{2g_b}E_{1u_a}$, and $E_{2g_b}E_{1u_b}$. This set of four functions constitutes the basis of a four-by-four reducible representation which upon reduction contains in block form the irreducible representations of the E_{1u}, B_{1u}, and B_{2u} species. The similarity transformation that accomplishes the reduction also provides the matrix that transforms the original set into four appropriate linear combinations which interact with vibrations e_{1u_a}, e_{1u_b}, b_{1u}, and b_{2u}. It is interesting to note that this problem is group-theoretically identical to the one of constructing proper excited electronic state functions in benzene from the four configurations which arise upon the promotion of one electron from the filled degenerate e_{1u} MO's to the empty e_{2g} MO's. In any case, the exact form of the basis functions thus derived depends on the chosen form (and sign) of the degenerate components. If a common form found in footnote references 9 and 10 is used, then one finds e_{1u_a} perturbing $2^{-\frac{1}{2}}(bb+aa)$, e_{1u_b} perturbing $2^{-\frac{1}{2}}(ba-ab)$, b_{1u} perturbing $2^{-\frac{1}{2}}(bb-aa)$ and b_{2u} perturbing $2^{-\frac{1}{2}}(ba+ab)$. The case of B_{2u} or B_{1u} mixing with E_{1u} is much more straightforward. The e_{2g_a} modes mix the $B_{2u} - E_{1u_b}$ and $B_{1u} - E_{1u_a}$ states, while the e_{2g_b} modes mix the $B_{2u} - E_{1u_a}$ and $B_{1u} - E_{1u_b}$ states.

In the present investigation we shall consider mixing only with an E_{1u} state since in fact it is the E_{1u} state at 1800 A that is most available for mixing with states of lower energy. (Since no b_{1g} vibration exists there is no other possibility for the B_{2u} state and with the AO basis used below there generally can be no interaction with the A_{2u} state.)

Once it is clear how a given normal mode is active in a vibration there remain in general $3N$ electronic integrals $I_\sigma^j(s, k, a)$ $(\sigma = 1, 2, 3, \cdots, N; j = 1, 2, 3)$ to evaluate for each normal mode. This number is greatly reduced

[14] The group-theoretic notation used here is that recommended by "Report on notation for the spectra of polyatomic molecules," J. Chem. Phys. **23**, 1997 (1955).

[15] The symbol a has three different meanings in this paper. It is used in conjunction with b to label degenerate components. In the expressions h_{ks}^a, $\xi_\sigma^j(a)$ and elsewhere it normally refers to the ath normal mode, one of $3N-6$ modes. It is also used to imply the symmetry species label of the ath normal mode. In this sense it is used in $I_\sigma^j(s, k, a)$, Γ_a and $\eta_{\sigma j}(a, \sigma^*, f^*)$. It is hoped that in context confusion will not arise.

TABLE I. The relative magnitudes of the local cartesian coefficients $\zeta_\sigma^R(a)$ and $\zeta_\sigma^U(a)$ and the relative magnitudes of the electronic integrals $I_\sigma^R(s,k,a)$ and $I_\sigma^U(s,k,a)$.

A. D_{6h} symmetry

Species of the ath normal mode and type (R or U)

Center number	B_{1u}		B_{2u}		E_{2g}				E_{1u}			
					E_{2ga}		E_{2gb}		E_{1ua}		E_{1ub}	
	R	U	R	U	R	U	R	U	R	U	R	U
1	x	0	0	x	x	0	0	$(-2/3^{\frac{1}{2}})y$	x	0	0	$(2/3^{\frac{1}{2}})y$
2	$-x$	0	0	$-x$	$-\frac{1}{2}x$	y	$(3^{\frac{1}{2}}/2)x$	$(1/3^{\frac{1}{2}})y$	$\frac{1}{2}x$	y	$(-3^{\frac{1}{2}}/2)x$	$(1/3^{\frac{1}{2}})y$
3	x	0	0	x	$-\frac{1}{2}x$	$-y$	$(-3^{\frac{1}{2}}/2)x$	$(1/3^{\frac{1}{2}})y$	$-\frac{1}{2}x$	y	$(-3^{\frac{1}{2}}/2)x$	$(-1/3^{\frac{1}{2}})y$
4	$-x$	0	0	$-x$	x	0	0	$(-2/3^{\frac{1}{2}})y$	$-x$	0	0	$(-2/3^{\frac{1}{2}})y$
5	x	0	0	x	$-\frac{1}{2}x$	y	$(3^{\frac{1}{2}}/2)x$	$(1/3^{\frac{1}{2}})y$	$-\frac{1}{2}x$	$-y$	$(3^{\frac{1}{2}}/2)x$	$(-1/3^{\frac{1}{2}})y$
6	$-x$	0	0	$-x$	$-\frac{1}{2}x$	$-y$	$(-3^{\frac{1}{2}}/2)x$	$(1/3^{\frac{1}{2}})y$	$\frac{1}{2}x$	$-y$	$(3^{\frac{1}{2}}/2)x$	$(1/3^{\frac{1}{2}})y$

B. The D_{3h} group.

The species of the ath normal mode and type (R or U)

Center number	E'			
	E_a'		E_b'	
	R	U	R	U
1	x	0	0	$(2/3^{\frac{1}{2}})z$
2	$-\frac{1}{2}y$	w	$(3^{\frac{1}{2}}/2)y$	$(1/3^{\frac{1}{2}})w$
3	$-\frac{1}{2}x$	z	$(-3^{\frac{1}{2}}/2)x$	$(-1/3^{\frac{1}{2}})z$
4	y	0	0	$(-2/3^{\frac{1}{2}})w$
5	$-\frac{1}{2}x$	$-z$	$(3^{\frac{1}{2}}/2)x$	$(-1/3^{\frac{1}{2}})z$
6	$-\frac{1}{2}y$	$-w$	$(-3^{\frac{1}{2}}/2)y$	$(1/3^{\frac{1}{2}})w$

C. The D_{2h} group.

The species of the ath normal mode and type (R or U)

Center Number	A_g		B_{3g}		B_{1u}		B_{2u}	
	R	U	R	U	R	U	R	U
1	x	0	0	w	x	0	0	w
2	y	w	x	z	y	w	x	z
3	y	$-w$	$-x$	z	$-y$	w	x	$-z$
4	x	0	0	w	$-x$	0	0	$-w$
5	y	w	x	z	$-y$	$-w$	$-x$	$-z$
6	y	$-w$	$-x$	z	y	$-w$	$-x$	z

by group-theoretical considerations. In Appendix A of I, it is shown how the minimum number of integrals required may be found and further how all remaining integrals may be simply expressed in terms of this minimum number. Recognizing that the perturbation operator, $\mathcal{H}'$, in its most general form is the basis of the same representation that the $3N$ dimensional vector, ξ, of cartesian displacements is, then the integrand of the perturbation energy may be analyzed for the number of times Γ_1 (totally symmetric representation) appears in $\Gamma_\sigma \times \Gamma_k \times \Gamma_\xi$. This is the minimum number of integrals required. Furthermore, once a suitable local cartesian system has been chosen the minimum number of I_σ^f for each f may be found by separately analyzing $\Gamma_\sigma \times \Gamma_k \times \Gamma_{\xi^f}$ ($f=1, 2, 3$) for the number of Γ_1's. Here ξ^f is an N-dimensional vector of the displacement coordinates of type f.

More to the point, however, once the proper basis functions have been chosen, is the analysis[15] of $\Gamma_a \times \Gamma_{\xi^f}$ for the number of Γ_θ's. This gives the minimum number of electronic integrals required for perturbation through normal mode a. For benzene a most convenient choice of local cartesian displacement coordinates consists of (for atom σ) the radial displacement vector R^σ (positive outward), the tangential displacement vector U_σ (positive clockwise) and the out-of-plane displacement vector Z_σ. (We shall consider only carbon motion in the perturbation.) In place of $\Gamma_{\xi^f}(f=R, U, Z)$ let us write simply Γ_R, Γ_U, and Γ_Z. The characters for these three representations are readily constructed and the number of Γ_1's in $\Gamma_a \times \Gamma_R$, $\Gamma_a \times \Gamma_U$ and $\Gamma_a \times \Gamma_Z$ for all relevant a are easily counted. Thus, it is found in the $E_{2g}-E_{1u}$ mixing the e_{1u} perturbation requires only two electronic integrals, one of type I_σ^U and one of type I_σ^R. The b_{1u} perturbation requires one integral of type R which we shall call J_σ^R and the b_{2u} perturbation requires one integral of type U which we shall call J_σ^U. Thus, altogether only four "one-center" integrals, I_σ^R, I_σ^U, J_σ^R, and J_σ^U, are required to calculate the oscillator strength of an E_{2g} transition. These integrals are the $I_{\sigma^*}^{f*}$ found in Eq. (6a) where σ^* may be somewhat arbitrarily chosen (integrals may vanish on some centers). For the forbidden B_{2u} and B_{1u} transitions, where the e_{2g} modes are active, it is found that each case requires two integrals, an I_σ^R and an I_σ^U integral, all others being related to these by the group-theoretically determined $\eta_{\sigma f}$'s [Eq. (6a)].

With the minimum number of required integrals established, it is now necessary to specify the η's that relate all other integrals to these few. In Tables IA, B,

and C appear entries that represent the relative magnitudes of the local cartesian coefficients for relevant types and species of groups D_{6h}, D_{3h} and D_{2h}, respectively. These relationships are group-theoretically determined and were verified in the normal coordinate analysis.[10] As a consequence of Appendix A in I these entries also represent the relationships among the electronic integrals for each type and species. This is true provided the same form (and sign) for the degenerate components has been used for the electronic functions as for the symmetry coordinates in the normal coordinate analysis. In the vibronic problem the sign is unimportant since it is the square of the energy that enters [Eq. (2)]. The symbols x, y, z, and w therefore represent either $\xi_\sigma{}^{j*}(a)$ or $I_\sigma{}^{j*}(s, k, a)$. For example, the entry in the third row of Table IA under column R of E_{2g_b} means both $I_3{}^R(s, k, e_{2g_b}) = (-3^{\frac{1}{2}}/2) I_1{}^R(s, k, e_{2g_a})$ and $\xi_3{}^R(e_{2g_b}) = (-3^{\frac{1}{2}}/2)\xi_1{}^R(e_{2g_a})$. The η's themselves are simply the ratio of a given pair of entries in any one column, the reference (or starred) entry appearing in the denominator. For example (Table IA), $\eta_{3R}(e_{2g_b}, 2, R) = -1$. Tables IB and C apply to vibronic problems for D_{3h} and D_{2h} molecules. In the present study, these tables are needed only for the normal coordinate coefficients. Under isotopic substitution the pure electronic wave functions see only a D_{6h} potential and the η's derived from Table IA still apply.[16]

It now requires but a short step to obtain $h_{ks}{}^a$ [Eq. (6a)] by incorporating the $\xi_\sigma{}^{j*}(a)$ but leaving the $I_\sigma{}^{j*}$ as parameters. This in turn can be squared and multiplied by $hN^0/(8\pi^2\nu_a)$ to give, in reduced form, the complete nonempirical part of the oscillator strength [Eq. (3)]. This has been done for benzene, 1,4-dideuterobenzene, *sym*-benzene-d_3, 2,3,5,6-tetradeuterobenzene, benzene-d_6, and the hypothetical molecule *p*-di-*X*-benzene already described (see also I). The results of the group-theoretical reduction are presented in detail only for benzene and the last two mentioned compounds. Tables IIA, B, and C deal with the B_{1u} and B_{2u} transitions while Tables IIIA, B, and C are concerned with E_{2g} transitions. A summary for all molecules is given in Tables IVA and B. To illustrate, consider the entries for normal mode 7*a* in Table IIA. For the e_{2g_a} species we have, using Table IA and Eq. (6a), $h_{ks}{}^{7a} = 3[\xi_1{}^R(7a) I_1{}^R(s, k, e_{2g_a})] + 4[\xi_2{}^U(7a) I_2{}^U(s, k, e_{2g_a})]$. From Table IIIe of footnote reference 10, $\xi_1{}^R(7a)$ is found to be -0.05215 (g)$^{-\frac{1}{2}}$ and $\xi_2{}^U(7a)$ is -0.00572 (there labeled R_{1a}' and U_{2a}', respectively). Incorporating these values into $h_{ks}{}^{7a}$, squaring, and multiplying by $hN^0/(8\pi^2 c\omega_a)$ ($\times 10^{16}$ to convert to A^2) gives $(\times 10^2)\, 0.0136 (I_1{}^R)^2 + 0.0003 (I_2{}^U)^2 + 0.0040\, I_1{}^R I_2{}^U$, the entries for normal mode 7*a*. Here $\omega_a = 3043$ cm^{-1}. All calculations were in fact done with an IBM 650 computer immediately following the normal coordinate program.

[16] This does not contradict the requirement that the same relationships hold among the $I_\sigma{}^j$'s as among the $\xi_\sigma{}^j(a)$'s since all relationships in Tables IB and C are contained in Table IA.

TABLE II. The "e_{2g}" normal mode coefficients for the B_{2u} and B_{1u} electronic integrals and the calculated oscillator strengths.

A. Benzene: e_{2g_a} modes.

Frequencies in cm^{-1}		Coefficients for integrals (A)$^2\times 10^2$ $(I_1{}^R)^2$	$(I_2{}^U)^2$	$(I_1{}^R I_2{}^U)$	Oscillator strengths $\times 10^2$ B_{2u}	B_{1u}
	e_{2g_a}					
7*a*	3043	0.0136	0.0003	0.0040	0.001	0.020
8*a*	1600	0.0452	0.2513	0.2131	0.056	2.025
9*a*	1174	0.0359	0.0092	0.0363	0.000	0.160
6*a*	610.8	0.4344	0.2418	−0.6482	0.252	0.421
Total e_{2g_a}		0.5291	0.5026	−0.3946	0.309	2.626

B. Benzene-d_6: e_{2g_a} modes

	e_{2g_a}					
7*a*	2274	0.0415	0.0047	0.0278	0.001	0.118
8*a*	1546	0.0327	0.2736	0.1892	0.067	2.102
9*a*	863.3	0.0678	0.0032	−0.0294	0.013	0.007
6*a*	575.7	0.3781	0.2176	−0.5736	0.224	0.390
Total e_{2g_a}		0.5201	0.4991	−0.3860	0.305	2.617

C. 1,4-Di-*X*-benzene: a_g and b_{3g} modes

	a_g					
1	3063	0.0043	0.0001	0.0012	0.000	0.006
2	1676	0.0791	0.1706	0.2324	0.028	1.739
3	1286	0.0530	0.0492	−0.1022	0.037	0.108
4	1126	0.0035	0.0519	0.0271	0.012	0.307
5	805.9	0.1542	0.1456	−0.2996	0.121	0.358
6	399.2	0.1987	0.0810	−0.2538	0.096	0.102
Total a_g		0.4928	0.4984	−0.3949	0.294	2.620
	b_{3g}					
11	3043	0.0138	0.0003	0.0041	0.001	0.021
12	1587	0.0440	0.2223	0.1979	0.056	2.111
13	1304	0.0056	0.0043	0.0098	0.000	0.084
14	650.0	0.4110	0.1862	−0.5532	0.214	0.269
15	424.0	0.0385	0.0433	−0.0816	0.035	0.120
Total b_{3g}		0.5129	0.4564	−0.4230	0.306	2.605

It can be seen from Tables IA and B how perturbation energies due to "*a*" and "*b*" degenerate components are equal. Calculate $h_{ks}{}^a$ for the e_{2g_b} component for example. It is seen that with Table IA and Eq. (6a) an expression is obtained identical to the one for the e_{2g_a} species.

Finally, Tables II–IV also contain calculated oscillator strengths where the necessary electronic integrals have been evaluated using ASMO functions and the tabulations of Liehr.[4] These calculations shall now be discussed.

CALCULATION OF OSCILLATOR STRENGTHS FOR ASMO FUNCTIONS

To evaluate the electronic integrals to be used in conjunction with the data of Tables II–IV, it is necessary first to obtain ρ_{sk}, which depends on $\Theta_s{}^0$ and $\Theta_k{}^0$ [Eq. (5)], and then to perform the integration indicated in Eq. (4). Whenever $\Theta_s{}^0$ and $\Theta_k{}^0$ are ultimately based on LCAO type functions (even when they are ASMO with CI), the transition densities will be decomposable into simple component densities such as

TABLE III. The "e_{1u}", "b_{1u}" and "b_{2u}" normal mode coefficients for the E_{2g} electronic integrals and the calculated oscillator strengths.

A. Benzene: e_{1ua}, b_{1u}, and b_{2u} modes

Frequencies in cm^{-1}		Coefficients for integrals (A)$^2\times10^2$ $(I_1^R)^2$	$(I_2^U)^2$	$(I_1^R I_2^U)$	Oscillator strengths $\times10^2$ E_{2g7}	E_{2g8}
	e_{1ua}					
20a	3078	0.0126	0.0002	0.0029	0.026	0.002
19a	1480	0.0416	0.1455	0.1557	0.402	1.080
18a	1035	0.1220	0.0835	0.2019	0.544	0.610
Total e_{1ua}		0.1762	0.2292	0.3605	0.972	1.692
	b_{1u}	$(J_1^R)^2$	$(J_1^U)^2$			
13	3067	0.0268	...		...	...
12	1012	0.7512	...		...	...
Total b_{1u}		0.7780	...		...	...
	b_{2u}					
14	1307	...	0.7112		...	...
15	1148	...	0.1689		...	...
Total b_{2u}		...	0.8801		...	...

B. Benzene-d_6: e_{1ua}, b_{1u} and b_{2u} modes

	e_{1ua}					
20a	2287	0.0368	0.0020	0.0173	0.088	0.014
19a	1324	0.0665	0.2329	0.2489	0.642	1.728
18a	808.8	0.0848	0.0101	0.0585	0.232	0.070
Total e_{1ua}		0.1881	0.2450	0.3247	0.962	1.812
	b_{1u}	$(J_1^R)^2$	$(J_1^U)^2$			
13	2283	0.0790	...		...	...
12	961.1	0.6888	...		...	...
Total b_{1u}		0.7678	...		...	...
	b_{2u}					
14	1285	...	0.8637		...	...
15	825.1	...	0.0159		...	...
Total b_{2u}		...	0.8796		...	...

C. p-Di-X-benzene: b_{1u} and b_{2u} modes.

Frequencies in cm^{-1}		Coefficients for integrals (A)$^2\times10^2$ $(I_1^R)^2$	$(I_2^U)^2$	$(I_1^R I_2^U)$	$(J_1^R)^2$	$(J_1^U)^2$	Oscillator strengths $\times10^2$ E_{2g7}	E_{2g8}
	b_{1u}							
18	3071	0.0043	0.0000	0.0010	0.0178	...	0.008	0.000
19	1563	0.0664	0.0764	0.1425	0.0393	...	0.528	0.812
20	1276	0.0267	0.0118	−0.0355	0.2462	...	0.016	0.118
21	1026	0.0637	0.0510	0.1140	0.3140	...	0.322	0.398
22	637.6	0.0226	0.2186	−0.1405	0.1410	...	0.060	1.658
Total b_{1u}		0.1837	0.3578	0.0815	0.7583	...	0.934	2.986
	b_{2u}							
23	3078	0.0130	0.0002	0.0031	...	0.0000	0.026	0.002
24	1407	0.0591	0.1539	0.1907	...	0.0281	0.512	1.204
25	1285	0.0099	0.0190	0.0274	...	0.7992	0.070	0.142
26	1092	0.0851	0.0802	0.1653	...	0.0527	0.302	0.414
27	331.6	0.2698	0.1938	−0.4574	...	0.0008	0.072	1.496
Total b_{2u}		0.4369	0.4471	−0.0709	...	0.8808	0.982	3.258

TABLE IV. The summed normal mode coefficients for the electronic integrals and calculated oscillator strengths for benzene and five derivatives.

A. B_{1u} and B_{2u} transitions

Molecule	Total coefficients for electronic integrals $(A)^2\times10^2$ $(I_1^R)^2$	$(I_2^U)^2$	$(I_1^R I_2^U)$	Oscillator strengths $\times10^2$ B_{2u}(obs 0.14)[a]	B_{1u}(obs 9.4)[b]
Benzene	1.0582	1.0052	−0.7892	0.618	5.252
1,4-Dideuterobenzene	1.0523	1.0028	−0.7836	0.614	5.248
Sym-benzene-d_3	1.0492	1.0015	−0.7806	0.613	5.244
2,3,5,6-Tetradeuterobenzene	1.0461	1.0005	−0.7778	0.612	5.242
Benzene-d_6	1.0402	0.9982	−0.7720	0.610	5.234
1,4-Di-*X*-benzene[c]	1.0057	0.9548	−0.8179	0.600	5.225

B. E_{2g} transitions

Molecule	Total coefficients for electronic integrals $(A)^2\times10^2$ $(I_1^R)^2$	$(I_2^U)^2$	$(I_1^R I_2^U)$	$(J_1^R)^2$	$(J_1^U)^2$	Oscillator strengths $\times10^2$ $E_{2g\gamma}$ (obs 9.4)[b]	$E_{2g\delta}$ (obs 9.4)[b]
Benzene	0.3524	0.4584	0.7210	0.7780	0.8801	1.944	3.384
1,4-Dideuterobenzene	0.3621	0.4710	0.6966	0.7707	0.8800	1.940	3.480
Sym-benzene-d_3	0.3656	0.4756	0.6833	0.7723	0.8799	1.934	3.516
2,3,5,6-Tetradeuterobenzene	0.3694	0.4807	0.6713	0.7712	0.8798	1.930	3.554
Benzene-d_6	0.3762	0.4900	0.6494	0.7678	0.8796	1.924	3.624
1,4-Di-*X*-benzene[c]	0.6206	0.8049	0.0106	0.7583	0.8808	1.916	6.244

[a] H. B. Klevens and J. R. Platt, Technical Reports of the Laboratory of Molecular Structure and Spectra, University of Chicago, (1954–1954).
[b] V. J. Hammond and W. C. Price, Trans. Faraday Soc. **51**, 605 (1955). (Neither the E_{2g} state nor the B_{1u} state has been absolutely identified.)
[c] Benzene electronic wave functions assumed for this molecule.

those depicted in Fig. 1 for E_{2g_a} and E_{1u_a} species. Here the heavy dot marks the midpoint between a pair of atomic orbitals whose product constitutes a contribution to the transition density of a given type.

It is useful to apply group theory once more, this time to count the number of component transition densities that exist for each species when the electronic wave functions are ultimately based on six equivalent atomic orbitals. It is only necessary to count the number of times the species of interest is contained in the direct product representation $\Gamma_{\text{hexagon}}{}^2$. Γ_{hexagon} is the reducible representation based on a hexagon of six equivalent centers. Counting only one set of signs for each component density, one finds that there are in effect three each of the E_{2g} and E_{1u} type, there are two of the B_{1u} type and only one of the B_{2u} type. In addition it is found that there are no B_{1g}, B_{2g}, or E_{2u} types so that in this rather general case there can be no question of mixing with an A_{2u} state (see also footnote reference 4).

If Slater $2p_z$ ($Z=3.18$) atomic orbitals are chosen as a basis then one can use the integrals tabulated by Liehr[4] to obtain energies (per A) for each of the nine basic component transition densities. Then any choice of electronic functions will specify the coefficients for each of these densities to give directly the total electronic integral.

To illustrate, we choose the conventional ASMO benzene functions, which have been succinctly presented by Murrell and Pople,[3] and are given here in Table V together with empirical energies and intensities. The notation is a mixture of that used in I and

TABLE V. B_{2u}, B_{1u}, E_{2g}, and E_{1u} state functions in benzene, observed energies, and intensities.

State function	Symmetry	Energies in ev (obs)	Oscillator strengths $\times10^2$ (obs)
$\Theta_V=2^{-\frac{1}{2}}(\chi_3{}^5-\chi_2{}^4)$	B_{2u}	4.9	0.14[a]
$\Theta_U=2^{-\frac{1}{2}}(\chi_3{}^4+\chi_2{}^5)$	B_{1u}	6.2	9.4[b]
$\Theta_{\gamma a}=2^{-\frac{1}{2}}(\chi_1{}^5-\chi_2{}^6)$	$E_{2g_a}(\gamma)$		
$\Theta_{\gamma b}=2^{-\frac{1}{2}}(\chi_1{}^4-\chi_3{}^6)$	$E_{2g_b}(\gamma)$		
$\Theta_{\delta a}=2^{-\frac{1}{2}}(\chi_1{}^5+\chi_2{}^6)$	$E_{2g_a}(\delta)$	6.2[c]	9.4[c]
$\Theta_{\delta b}=2^{-\frac{1}{2}}(\chi_1{}^4+\chi_3{}^6)$	$E_{2g_b}(\delta)$		
$\Theta_X=2^{-\frac{1}{2}}(\chi_3{}^5+\chi_2{}^4)$	E_{1u_a}	7.0	44[b]
$\Theta_Y=2^{-\frac{1}{2}}(\chi_3{}^4-\chi_2{}^5)$	E_{1u_b}	7.0	44[b]

[a] H. B. Klevens and J. R. Platt, Technical Report of the Laboratory of Molecular Structure and Spectra, University of Chicago (1953–1954).
[b] V. J. Hammond and W. C. Price, Trans. Faraday Soc. **51**, 605 (1955).
[c] Assumed.

TABLE VI. E_{2g_a} and E_{1u_a} transition densities and electronic integrals for ASMO functions.

A. Transition densities and integrals I_1^R, I_2^U

Transition	Integrand of ρ_{sk} (Eq. 5) (for component a perturbation only)	Symmetry of ρ_{sk}	Transition density in terms of component densities (see Fig. 1)	The electronic integrals (ev/A) I_1^R	I_2^U
B_{2u}	$\Theta_Y\Theta_Y$	E_{2g_a}	$-1.1027(T_1+T_3)+0.2686T_2$	1.1784	−2.2837
B_{1u}	$\Theta_U\Theta_X$	E_{2g_a}	$-0.2686(T_1+T_3)+1.1027T_2$	1.1030	3.1700
E_{2g_γ}	$2^{-\frac{1}{2}}(\Theta_{\gamma a}\Theta_X-\Theta_{\gamma b}\Theta_Y)=2^{\frac{1}{2}}\Theta_{\gamma a}\Theta_X$	E_{1u_a}	$-0.4245(S_1+S_3)+1.1489S_2$	1.6967	1.2212
E_{2g_δ}	$2^{-\frac{1}{2}}(\Theta_{\delta a}\Theta_X-\Theta_{\delta b}\Theta_Y)=2^{\frac{1}{2}}\Theta_{\delta a}\Theta_X$	E_{1u_a}	$-1.1489(S_1+S_3)+0.4245S_2$	0.1274	3.5128

B. I_1^R and I_2^U integrals for each component transition density (see Fig. 1) (ev/A)

	T_1	T_2	T_3	S_1	S_2	S_3
I_1^R	−1.3681	0.7867	0.4912	0.1396	1.6629	0.3640
I_2^U	2.8290	3.5924	0.1171	3.8926	2.5394	0.1033

that of footnote reference 3 but should be sufficiently clear. These functions have been chosen without any illusions concerning their suitability.[6] The basis MO's are given in I [Eq. (22)] normalized to include all overlap. In Table VIA the necessary transition densities are indicated including the coefficients of the component transition densities depicted in Fig. 1. Interaction with the ath degenerate component only is considered since the contribution from the b component is identical. In Table VIB the integrals (in ev/A) are given for each of the component densities. The evaluation of a typical integral has been described in Appendix C of I and will not be discussed here. The component integrals in Table VIB are combined as indicated in Table VIA and there tabulated. These total integrals are used directly with the reduced data in Tables II–IV and the empirical factor [bracketed expression in Eq. (3)] is constructed from the data in Table V to give the reported oscillator strengths.

The present choice of E_{2g} and E_{1u} wave functions has led to the following interesting simplification. The proper transition-density combinations which mix with each of the possible vibrations are, listing the E_{2g} component first, $2^{-\frac{1}{2}}(aa-bb)$ (e_{2g_a}), $2^{-\frac{1}{2}}(ab+ba)$ (e_{2g_b}), $2^{-\frac{1}{2}}(aa+bb)$ (b_{1u}), and $2^{-\frac{1}{2}}(ab-ba)$ (b_{2u}). Upon working out the functional form (independent of AO's) for each of these product functions (and for either E_{2g_γ} or E_{2g_δ}) it is discovered that $aa=-bb$ and $ab=ba$. Thus, accidentally, the b_{2u} and b_{1u} vibrations cannot be active in the present treatment. However, any breakdown of the configurational interaction as represented in the E_{2g_γ} and E_{2g_δ} functions will activate the b_{1u} and b_{2u} perturbations.

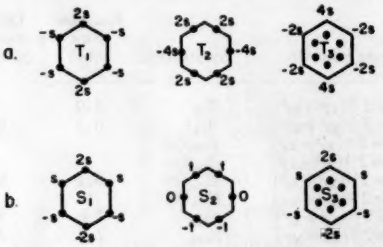

FIG 1. Six of the nine component transition densities arising when the electronic functions have an atomic orbital basis: (a) the E_{2g_a} densities; (b) the E_{1u_a} densities. Each dot is located midway between a pair of atomic orbitals whose overlap constitutes a contribution to the transition density. ($s=1/6$ and $t=\frac{1}{2}$.)

DISCUSSION

Consider the summed coefficients for integrals summarized in Table IV for all six molecules. It is quite apparent that whatever the nature of the electronic functions (and hence electronic integrals) the present theory predicts that there can be no significant variation of intensity for B_{2u} and B_{1u} transitions upon isotopic substitution. From the start it must be emphasized that perturbation due to carbon motion only has been considered throughout. Even when para substituents of mass 20 are introduced there still can be very little change. If a trend is to be discerned, it is seen that all three coefficients become smaller as the total mass of all substituents increases. There is no obvious dependence on symmetry. While *sym*-benzene-d_3 has 14 active vibrations and the D_{6h} derivatives have eight, the influence on carbon motion, if any, apparently has more to do with total substituent mass than the formal symmetry.

Analogous trends in coefficients, somewhat stronger and in the reverse direction, are evident in the e_{1u} perturbation of the E_{2g} transition. Here the jump to *p*-di-*X*-benzene shows the greatest change of all. Table IIIC shows how these changes originate largely through the "e_{1u_δ}"-type modes. On the other hand, the coefficients for b_{1u} and b_{2u} perturbations, potentially strong, show very little sensitivity to substituent mass and, if anything decrease very slightly upon substitution. These results are understandable in light of the

extent of "carbon mode" and "substituent mode" mixing in each of the active modes, the e_{1u} frequencies showing the greatest extent of mixing.[10,12]

The above observations suggest that if electronic wave functions are such as to emphasize appropriate e_{1u} perturbation then there may be a chance of distinguishing the controversial E_{2g} and B_{1u} transitions by mass effects alone in D_{6h} or D_{3h} benzene derivatives. This assumes that one can smoothly extrapolate the experience with *p*-di-*X*-benzene to D_{3h} and D_{6h} derivatives as appears to be the case among the isotopic benzenes. On the other hand, relatively significant changes in electronic functions on going from benzene to D_{3h} or D_{6h} derivatives may so alter the transition density that any mass effect becomes obscured. It happens that the E_{2g_b} function used here to calculate oscillator strengths gives a mass sensitive intensity that almost doubles on going from benzene to *p*-di-*X*-benzene. Such a change contrasts strikingly with the predicted steadiness of the B_{1u} intensity. It is by no means clear that the E_{2g} functions chosen here are at all realistic. For example Murrell and McEwen[17] show that doubly excited configurations are very important and Craig[18] reports that a valence-bond calculation by Lyons reveals b_{1u} first and e_{1u} next in ability to perturb the E_{2g} state. The latter observation would at best indicate a much weaker mass effect.

Sklar[19] has attempted to isolate the forbidden intensity in the "B_{2u}" bands of a whole series of benzene derivatives by interpolating from "forbidden" intensities in benzene, *sym*-tri-*X*-benzene, and hexa-*X*-benzene where usually cases with methyl or chloro substituents were considered. A steady increase in intensity with increase in total substituent mass was observed within a given series. This lead to the assumption that formal symmetry is unimportant as far as vibrational perturbation is concerned just as has been suggested here. The change in intensity with increasing total substituent mass, however, is quite large. Our calculations would indicate that this change is entirely due to a change in electronic functions and not to a mass effect. This interpretation for the more than two-fold enhancement of intensity upon going from benzene to hexamethylbenzene must be applied with some caution. It may be that the calculated insensitivity to mass breaks down significantly when the effective substituent mass approaches that of carbon. It is hoped that these matters will be better understood after completing a study of vibronic problems in weakly substituted benzenes now in progress.

A second interesting result of the group-theoretical reduction concerns the relative activity of various vibrations. Again certain general conclusions may be drawn without specifying details of the electronic state functions. The effect of mass is now more apparent although still it is not strong for the B_{2u} and B_{1u} transitions (Tables IIA–C). The four "carbon mode" frequencies, originally 6*a* (and 6*b*) and 8*a* (and 8*b*), maintain their dominance throughout although this is somewhat obscured in *p*-di-*X*-benzene. In benzene and benzene-d_6 the e_{2g} "substituent modes" are sufficiently isolated not to contain much carbon motion and therefore are not influential in the perturbation. In *p*-di-*X*-benzene the separation is no longer so pure[12] and several frequencies are active. On the other hand, the e_{1u} modes (Tables IIIA–C), which are not so clearly separated into substituent motion and carbon motion, show a distribution that is considerably more mass sensitive. It is seen that the so-called "substituent modes" 18*a* (and 18*b*) can contribute very significantly to the perturbation. The b_{1u} and b_{2u} frequencies involve relatively distinct separation of motion so that each species has one major contributing vibration with little mass effect.

Apart from the observed intensity itself the most widely used criterion for testing theory is the reported[20] exclusive activity of the 6*a* (and 6*b*) modes in the B_{2u} transition in benzene and the isotopic derivatives. Table IIA reveals how I_1^R and I_2^U having opposite signs would tend to favor the 6*a* frequency while with equal signs mode 8*a* is likely to be more active. Table VIB shows that to obtain integrals with opposite signs the transition density must contain a lot of type T_1 density. This is an "even" type density in the language of Moffitt[21] which is to be associated with $B_{2u}-E_{1u}$ interaction. Although T_3 density is also in this category its contribution is not influential. Thus, it is seen that the predominance of the 6*a* mode in the B_{2u} perturbation lies in the "even" nature of the perturbation and is correctly predicted by the present theory. [Even after the MO's are normalized including all overlap the "even" transition density still dominates (Table VIA).] The B_{1u} state is sensitive to "odd" perturbations[21] (see also Table VIA) so that the 8*a* mode is likely to dominate. The true relative activity of the two frequencies in the B_{2u} transition is obscured by the fact that we ask for the relative activity of ground state frequencies via the sum rule that has been employed in the theory (see I). It is hoped both to test the theory and to directly ascertain the relative activity of the frequencies by trying to match the observed[22] temperature dependence of the B_{2u} intensity using an expression based on Eq. (2).

Finally, some comment is necessary concerning the calculated oscillator strengths. The results (Tables II–IV) do serve to illustrate some of the conclusions just reached. However, agreement with experiment is

[17] J. N. Murrell and K. Lenore McEwen, J. Chem. Phys. **25**, 1143 (1956).
[18] D. P. Craig, Revs. Pure and Appl. Chem. (Australia) **3**, 207 (1953).
[19] A. L. Sklar, J. Chem. Phys. **10**, 135 (1942).
[20] F. M. Garforth, C. K. Ingold, and H. G. Poole, J. Chem. Soc. **1**, 409, 413, 414 (1948).
[21] W. Moffitt, J. Chem. Phys. **22**, 320 (1954).
[22] F. Almasy and H. Laemmel, Helv. Chim. Acta **34**, 462 (1951).

very poor. It is appropriate to compare these calculations with those by Murrell and Pople[3] based on the same wave functions (except for normalization of the MO's). Murrell and Pople used a point-charge approximation to evaluate the electronic integrals and did not include transition densities of types T_3 and S_3. Further, they considered only "carbon modes." It has been seen that the latter assumption is a serious one for the e_{1u} perturbation. Otherwise any gross difference in results is probably due to the different methods used for evaluating integrals. Their reported oscillator strengths ($\times 10^2$) for B_{2u}, B_{1u}, E_{2g_x}, and E_{2g_y} transitions are, respectively, 1.19, 39.8, 5.81, and 18.5. The results obtained here are consistently lower giving better agreement for the B_{2u} transition but worse for the 2000-A intensity. It must be concluded that either the theory is at fault or that the ASMO functions employed are very poor solutions of the pure electronic Schrödinger equation. That the latter is no doubt the case is the tenor of the critical analysis given by Liehr.[6]

SUMMARY

A group-theoretical reduction which incorporates normal coordinate parameters (based on carbon motion only), is presented for Herzberg-Teller type calculations in benzene. The simplification achieved can be useful for the testing of trial electronic functions and the making of assumptions in evaluating integrals. The same reduction has been carried out for five benzene derivatives, four of them isotopic and one a model *p*-disubstituted derivative with a substituent having a mass of 20. It is found that B_{2u} and B_{1u} transitions are very insensitive to mass changes while E_{2g} transitions may or may not be somewhat more sensitive depending on the nature of the correct electronic wave functions. For nonisotopic derivatives of D_{6h} or D_{3h} symmetry there may be a chance of distinguishing E_{2g} and B_{1u} states by mass effects alone. Furthermore, the results suggest that any marked variation in "B_{2u}" or "B_{1u}" intensity in such derivatives should be attributed to changes in electronic functions and not mass effects.

It is found how certain vibrations dominate in their influence in a manner relatively independent of substituent mass. In particular, it is seen how the 6*a* (and 6*b*) modes perturb B_{2u} states and the 8*a* (and 8*b*) modes perturb the B_{1u} states because of the respective "even" and "odd" character of the transition densities.

Oscillator strengths have been calculated using the conventional benzene ASMO functions. Certain basic integrals are tabulated and the calculation is outlined in a manner permitting the easy testing of any kind of ASMO functions. The results, which agree very poorly with experiment, nevertheless serve to illustrate many of the general conclusions made on the basis of the reduction alone.

No attempt has been made to improve agreement with observation by exploring trial functions. Instead it is hoped that it will be possible to test the basic theory by attempting to fit an observed B_{2u} oscillator strength vs temperature curve using the theoretical expression which after the group-theoretical reduction contains only two electronic integrals as parameters.

ACKNOWLEDGMENTS

The author is very grateful to Professor G. F. Dresselhaus for his criticism and several clarifying remarks concerning group-theoretical problems. He also wishes to thank Dr. A. D. Liehr for a number of helpful discussions concerning his vibronic studies and for his criticism of the manuscript.

Radiative Lifetime of the $B\ ^2\Sigma^+$ State in N_2O^+

I. E. DAYTON,* F. W. DALBY, AND R. G. BENNETT

Radiation Physics Laboratory, Engineering Dept., E. I. du Pont de Nemours & Company, Inc., Wilmington, Delaware

(Received February 29, 1960)

The radiative mean lifetime of the upper electronic state ($B\ ^2\Sigma^+$) giving rise to the 3541 A band of N_2O^+ has been measured to be $\tau = (2.6 \pm 0.2) \times 10^{-7}$ sec, which corresponds to an oscillator strength $f = (3.65 \pm 0.28) \times 10^{-3}$. Information about the emission spectrum of N_2O^+ is also presented.

I. INTRODUCTION

RECENT papers from this Laboratory[1-3] have reported measurements of the radiative lifetime of electronic transitions in N_2^+, CO^+, CH, and NH. If the degeneracy of the levels is known, the oscillator strength and optical extinction coefficient can be calculated using the theory developed by Einstein.[4] This approach enables one to obtain oscillator strengths and extinction coefficients for free radicals and ions which are too reactive to be handled by conventional techniques. The results have particular application to problems in chemical kinetics and astrophysics.

The present paper reports the application of these techniques to a polyatomic molecule. The radiative lifetime of the $B\ ^2\Sigma^+$ state of the nitrous oxide ion has been measured and the oscillator strength has been calculated. Information about the emission spectrum of N_2O^+ is also presented.

The experimental method has been reported in detail in an earlier paper.[1] The gas sample at a pressure of a few microns is bombarded by a pulsed low-energy electron beam. The light emitted from the excited gas is measured as a function of time after the beam has been turned off.

II. RESULTS

Emission Spectrum of N_2O^+

The emission spectrum observed when nitrous oxide at a pressure of 5 μ was bombarded with 250-v electrons is shown in Fig. 1. The photograph was made using a Hilger medium quartz spectrograph. The spectrum agrees rather well with that recently reported by Brocklehurst[5] and ascribed by him to N_2O^+. The N_2O^+ spectrum resulting from electron bombardment is remarkably clean, showing N_2^+, N_2, and NO bands in only weak to moderate intensity. In an effort to improve band identification and wavelength measurements, the emission spectrum of nitrous oxide in a hollow cathode discharge was recorded in the second and third orders of a 3.4 m spectrograph equipped with a 5-in., 30 000-line/in. grating. Table I gives the wavelengths and intensities of the bands.

Samples of NO and NO_2 were bombarded with electrons under the same conditions as in the N_2O experiments. The resulting spectra were very different and showed none of the bands listed in Table I. The structure of the bands resulting from the electron bombardment of N_2O is sufficiently complex in both vibrational and rotational structure that it cannot be due to a diatomic molecule. The structure of the bands appears similar to the bands of CO_2^+[6,7] and NCO,[8] which are isoelectronic with N_2O^+. All these facts make it highly probable that the observed bands are due to

TABLE I. Wavelengths and intensities of the emission spectrum of N_2O^+. Wavelengths given to five significant figures are based on the preliminary analysis of plates taken on a 3.4-m grating spectrograph by D. E. Paul. Other wavelengths are obtained from measurements on Fig. 1.

λ(A)	I[a]	λ(A)	I[a]	λ(A)	I[a]
3380.4	S	3613.4	M	3823.5	M
3382.3		3615.5		3825.3	
3395.8	S	3656.1	MS	3841.8	MS
3398.0		3658.3		3843.5	
3428.9	W	3661	M	3845.3	S
3429.5				3847.4	
3457.4	MS	3673.2	MS	3864.2	S
3459.2		3675.0		3866.1	
3470.0	MS	3688.8	VS	3928.9	W
3472.2		3690.7		3930.9	
3516	MS	3707.0	VS	3943	W
3520.7	M	3709.1			
3541.7	VS	3719.6	W	3965.5	W
3543.6		3722.0		3966.8	
3558.6	VS	3746.5	M	4007.3	MW
3560.8		3747.1		4009.0	
3596.1	MS	3764.0	MW	4030.1	MW
3597.9		3765.9		4032.5	
3608.9	M	3774.0	MW	4140.7	W
		3775.2		4142.7	

[a] Intensities: VS: very strong; M: medium; W: weak.

* Permanent address: Physics Department, Swarthmore College, Swarthmore, Pennsylvania.

[1] R. G. Bennett and F. W. Dalby, J. Chem. Phys. **31**, 434 (1959).

[2] R. G. Bennett and F. W. Dalby, J. Chem. Phys. **32**, 1716 (1960).

[3] R. G. Bennett and F. W. Dalby, J. Chem. Phys. **32**, 1111 (1960).

[4] A. Einstein, Physik. Z. **8**, 121 (1917).

[5] B. Brocklehurst, Nature **182**, 1366 (1958).

[6] F. Buesco-Sanllehi, Phys. Rev. **60**, 556 (1951).

[7] S. Mrozowski, Phys. Rev. **72**, 691 (1947).

[8] Holland, Style, Dixon, and Ramsey, Nature **182**, 336 (1958).

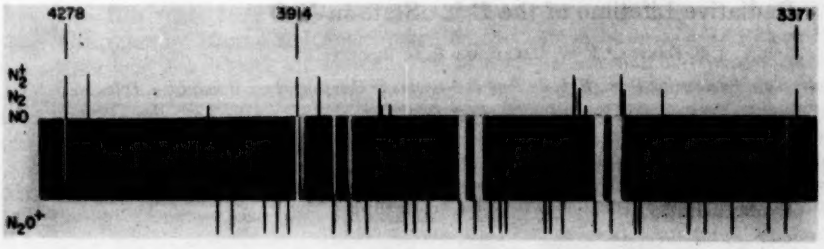

FIG. 1. Emission spectrum resulting from the bombardment of nitrous oxide at 5-μ pressure with 250-v electrons. Photographed with a Hilger medium quartz spectrograph.

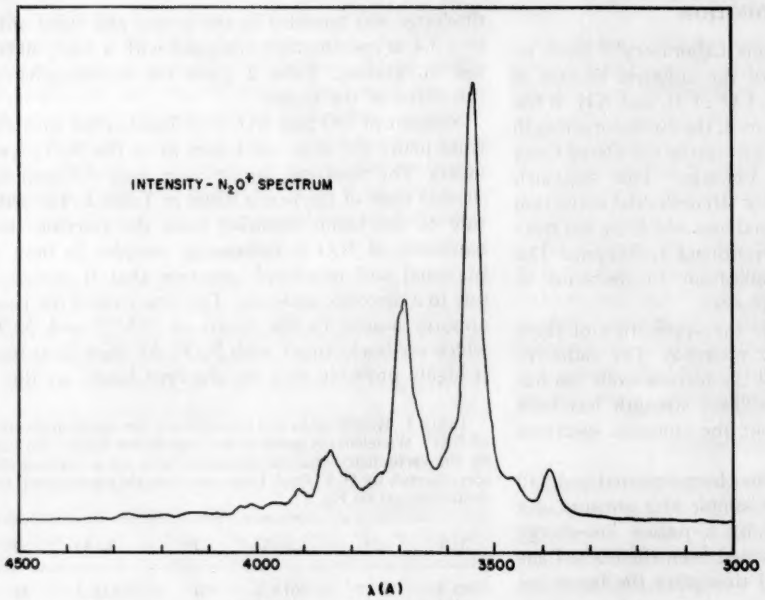

FIG. 2. Emission spectrum resulting from the bombardment of nitrous oxide at 5-μ pressure with 250-v electrons. The spectrum was recorded using a 0.5-m Bausch and Lomb grating monochromator and photomultiplier detector. The vertical scale (intensity) is linear. No other structure was observed in the range from 2000 to 6000 A.

N_2O^+. Callomon[9] has recently completed a rotational analysis of the O–O band at 3541 A which shows unambiguously that the transition is the type $^2\Sigma-{}^2\Pi(i)$ of a linear molecule.

The preliminary analysis of the high-resolution plates indicates that the strong bands near 3850 A, 3700 A, and 3550 A all start from the same level, whereas the strong band near 3390 A starts from a different level.

Radiative Lifetime

Figure 2 shows the N_2O^+ emission spectrum as recorded by a 0.5-m Bausch and Lomb grating monochromator and DuMont K1306 (uv-sensitive) photomultiplier detector. The lower resolution serves better to exhibit the gross intensity variations over the spectrum and is more nearly compatible with the resolution of the interference filters discussed below.

An interference filter was used to isolate the strong peak at 3541 A. The maximum transmission of the filter is at 3570 A, and the full width at half maximum is 180 A. The electron bombarding energy was 250 v, the electron pulse duration was 2.4×10^{-7} sec, and the photomultiplier pulse duration was 1.3×10^{-7} sec. The mean lifetime of the level, based on a series of 30 measurements, is $(2.6\pm0.2)\times10^{-7}$ sec. The standard error quoted is based both upon the observed reproducibility of the data and estimated uncertainties in the calibration of the time base. No change in lifetime was observed over the pressure range from 0.5 to 5.0 μ. A series of four measurements on the peak at 3700 A gave the same lifetime as that quoted above for the stronger peak.

III. DISCUSSION

The filter passband was wide enough so that contributions from the 3700-A and 3390-A peaks were included in the measurement of the 3550 A peak. As noted above, there is experimental and theoretical evidence that the 3700-A peak originates from the same level as the 3550-A peak and hence its inclusion should not perturb the measurement. The 3390-A

[9] J. H. Callomon, Proc. Chem. Soc. 313 (October 1959).

peak is very much smaller and could contribute no more than 10% to the light transmitted by the filter.

Since the radiative lifetime was found to be independent of pressure, one can conclude that collision quenching and trapping of resonance radiation do not occur in the pressure range used in this experiment. It is more difficult to rule out the possibility that the measured lifetime is due to cascading from higher states. The most convincing demonstration would be to measure the lifetime with an electron energy only slightly above threshold, but this was not possible with the present apparatus. It is known that the excitation probability under electron bombardment decreases markedly for the higher excited states of atoms,[10] and it seems reasonable that the same result should hold for molecules. This result taken with the fact that no other bands were observed in the range from 2000 A to 6000 A makes it plausible that the upper state is being excited directly and not by cascading from higher levels.

The lifetime, τ, is related to the oscillator strength, f, of the electronic transition by the expression[11]

$$f=(mc\lambda^2/8\pi^2e^2)\,(d_m/d_n)\,\tau^{-1},$$

where d_m and d_n are the degeneracy of the upper and lower electronic states, respectively, and λ is the wavelength of the transition. Substituting numerical values gives

$$f=(3.65\pm0.28)\times10^{-3}.$$

The degeneracies d_m and d_n are determined from Callomon's analysis of the spectrum[9] to be equal to 1 and 2, respectively.

ACKNOWLEDGMENTS

It is a pleasure to thank V. F. Hanson and R. L. McCarthy for their continued support and encouragement during this work, and D. E. Paul for making his preliminary high-dispersion plates available to us. We are grateful to Professor J. H. Callomon for private communication of his rotational analysis.

[10] H. S. W. Massey and E. H. S. Burhop, *Electronic and Ionic Impact Phenomena* (Oxford University Press, New York, 1956).

[11] G. Herzberg, *Molecular Spectra and Molecular Structure—Diatomic Molecules* (D. Van Nostrand and Company, Inc., Princeton, New Jersey, 1950).

Molecular Structure of Iodine Heptafluoride

ROBERT E. LAVILLA AND S. H. BAUER

Department of Chemistry, Cornell University, Ithaca, New York

(Received February 29, 1960)

Electron diffraction photographs taken in 1951 are here reanalyzed. All measurements and intensity estimates had been made visually; in the computations, allowance is made for the relative phase change of the scattering amplitudes between the iodine and fluorine atoms. Within a spread of 0.06 A, the I—F distances are approximately equal; the average value is 1.825±0.015 A. The molecular symmetry is almost D_{5h}, in agreement with spectroscopic and crystal structure results. However, the electron diffraction patterns clearly indicate that the five fluorine atoms in the girdle are not coplanar and possibly are not equally spaced from the central iodine. The disorder reported in the crystalline state and the unusually broad NMR spectra of the liquid are readily accounted for by a sequential puckering about the polar axis and the possible out-of-phase extension from the axis of the girdle atoms. Revised values for the thermodynamic functions of the ideal gas are included.

A. INTRODUCTION

IODINE heptafluoride is unique in being the only known example of a seven coordinated binary molecular compound. The first investigation of its structure by physical means was reported by Lord *et al.*[1] They recorded the Raman and infrared spectra of the heptafluoride in the liquid and gaseous states, respectively. With the sample at room temperature, they concluded that the molecule had a point group symmetry of D_{5h}, a pentagonal bipyramid. A nuclear magnetic resonance absorption study of the liquid at room temperature by Gutowsky and Hoffman[2] showed multiple F^{19} absorption lines which were unexpectedly broad for a liquid. The simplest interpretation of these multiple absorption lines is that the F^{19} nuclei are in nonequivalent structural positions. This eliminates the planar D_{7h} configuration and is consistent with the D_{5h} structure. Overlap of the individual lines did not permit a more detailed analysis.

A preliminary analysis[3] of electron diffraction data on IF_7 vapor, at −65°C, led to pentagonal bipyramidal structure. The five I–F distances in the girdle were found to be roughly 1.83 A, and the two apical I–F distances were roughly 1.94 A. Recently, Burbank and Bensey[4] reported on the basis of an x-ray crystal structure analysis that the solid existed in a cubic phase from 0° to −120°C. but transformed to an orthorhombic phase below −120°C. For the cubic modification at −110°C, their data "suggests that the structure is so disordered that the statistical symmetry *Im3m* is attained by a free rotation or random orientation of the molecule around a molecular axis which is distributed with equal probability along each of the three axes." No diagrams or positional parameters were given for the cubic phase. In the case of the orthorhombic phase at −145°C, the crystal was found to belong to the space group *Aba*2 and possesses large thermal motions which were not adequately accounted for. Donohue's[5] interpretation of the positional parameters of the orthorhombic phase reported by Burbank and Bensey is in agreement with the D_{5h} molecular symmetry. Seven nearly equal I–F distances were reported (1.80 A) with a standard deviation of ±0.05 A.

The reported I–F distances agree reasonably well with the sum of the ionic crystal radii[6] for I^{7+} and F^- (1.86 A); the sum of covalent radii[7] is 1.94 A. This model leads to a separation of 2.12 A for the neighboring F–F distance in the girdle. However, the sum of van der Waals radii[8] for F–F is 2.70 A; clearly strong repulsions must be present between adjacent fluorine atoms in the girdle, possibly leading to a staggered configuration and a departure from strict D_{5h} symmetry.

We have reexamined the old electron diffraction photographs. These data were analyzed by improved procedures with the objective of testing the planarity of the F_5 girdle and ascertaining the cause of the disorder reported present in the crystal at the low temperature.

B. EXPERIMENTAL

A sample of iodine heptafluoride was generously furnished by Professor Schumb and Dr. Lynch. Figure 1 illustrates the all-metal vacuum distillation line, in which the sample was purified and distilled into the sample holder which fitted the electron diffraction apparatus. The noncondensible material (at liquid-N_2 temperature) present in the original cylinder (*A*) was pumped off; the temperature of (*A*) was then raised to distill its contents into (*B*) and (*D*) which were kept at dry-ice and liquid-N_2 temperatures, respectively. The valve isolating (*D*) was closed, (*B*) raised to room temperature, and the system pumped to

[1] R. C. Lord *et al.*, J. Am. Chem. Soc. **72**, 522 (1950).
[2] H. S. Gutowsky and C. J. Hoffman, J. Chem. Phys. **19**, 1259 (1951).
[3] S. H. Bauer, J. Phys. Chem. **56**, 343 (1952).
[4] R. A. Burbank and F. N. Bensey, Jr., J. Chem. Phys. **27**, 981 (1957).
[5] J. Donohue, J. Chem. Phys. **30**, 1618 (1959).
[6] L. Pauling, *Nature of the Chemical Bond* (Cornell University Press, Ithaca, New York, 1948), 2nd ed., p. 346.
[7] L. Pauling, work cited in footnote 6, p. 189.
[8] V. Schomaker and D. P. Stevenson, J. Am. Chem. Soc. **63**, 37 (1941).

a good vacuum. The most volatile fraction of IF_7 was then distilled from (D) (by warming the latter to dry-ice temperatures) into the sample holder (E), which was maintained at liquid-N_2 temperatures. After closing(V_4), the sample holder was uncoupled from the line, fitted with a 'comparison' type nozzle,[9] and inserted into the electron diffraction apparatus. The sample was maintained at −65°C (vapor pressure: 10 mm Hg) during the electron diffraction experiments.

The electron diffraction photographs were taken in 1951 with the apparatus described by Hastings and Bauer,[10] using a sector originally cut for uranium hexafluoride; the corrected intensity extended to an angular opening given by $q=76.5$. Gold foil was used for calibration; the sample-plate distance was $L\approx 20$ cm, and the wavelength, $\lambda\approx 0.053$ A. Diffraction patterns showing seven halos were recorded on Kodak microfilm, which was processed in Kodak D-11 developer for five minutes. We estimate that at $q\approx 80$ an apparent distortion of the intensity pattern was produced by a rapid change in the sector aperture, and this coincided with the outer seventh (broad) maximum. This feature was not used in the radial distribution summation. The dashed inner portion of the seventh halo, Fig. 2, is what we believe to be its correct shape and approximate position. Note also that the envelope of the intensity curve gradually decreases and then begins to increase again. The minimum is termed the 'cutoff' point[11] and is where the amplitude due to the dominating scattering pair of atoms reaches zero and thereafter changes sign.

C. PROCEDURE

The experimental intensity curve was drawn from the measured positions of the maxima and minima and their visually estimated relative intensities. In the low-angle range, $q\leq 27$, a theoretical intensity curve was calculated using constant coefficients, Eq. (1), and matched to the experimental curve. For the theoretical

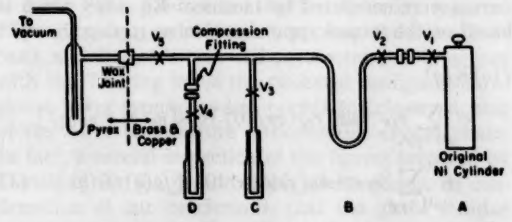

FIG. 1. All-metal distillation unit used in preparing the sample for electron diffraction. D and C are thin-walled for better temperature control.

[9] R. B. Harvey, F. A. Keidel, and S. H. Bauer, J. Appl. Phys. **21**, 860 (1950).
[10] J. M. Hastings and S. H. Bauer, J. Chem. Phys. **18**, 13 (1950).
[11] R. Glauber and V. Schomaker, Phys. Rev. **89**, 667 (1953); J. A. Ibers and J. A. Hoerni, Acta Cryst. **7**, 405 (1954).

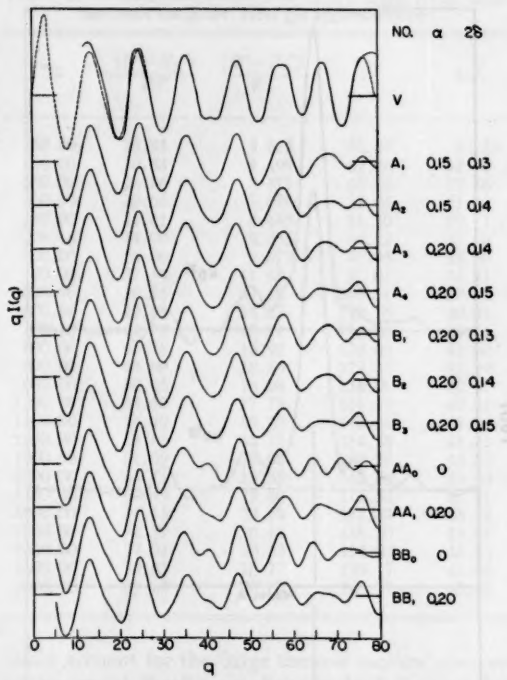

FIG. 2. Electron diffraction intensity curves for IF_7. Curves A_n and B_n were computed by the conventional approximation, Eq. (1), and curves AA_n and BB_n were computed with complex scattering amplitudes, Eq. (3).

intensity curve,

$$(q\pi/10)I(q)=\sum_{i,j}{}'(Z_iZ_j/r_{ij})\sin[r_{ij}(q\pi/10)];$$

$$q=(40/\lambda)\sin\tfrac{1}{2}\theta \quad (1)$$

a pentagonal bipyramid model was assumed, with seven equal I–F distances of 1.82 A. To allow for the phase shift in the electron scattering atomic form factors for iodine ($Z=53$) and fluorine ($Z=9$), an estimated 'apparent splitting'[11] ($2\delta=0.15$) of the I–F interatomic distances was introduced. The composite intensity curve was then inverted by

$$rD(r)=\sum_{q=1}^{q_{max}}(q\pi/10)I(q)\exp(-\gamma q^2)\sin[r(q\pi/10)]. \quad (2)$$

The parameter γ was chosen so that $\exp(-\gamma q^2)=0.1$ at $q_{max}=70$, to give the first radial distribution curve (RD′). This curve shows a very high peak at 1.83 A and two considerably lesser peaks centered at 2.52 and 3.58 A. The peak at 1.83 A is rather broad; extraneous high and low frequency ripples are superposed on the distribution curve, with an unaccountable maximum at $r<1$ A. These extraneous features were smoothed out by successive adjustments of the visually estimated intensity based on well-known probable psychovisual misinterpretations of the diffraction

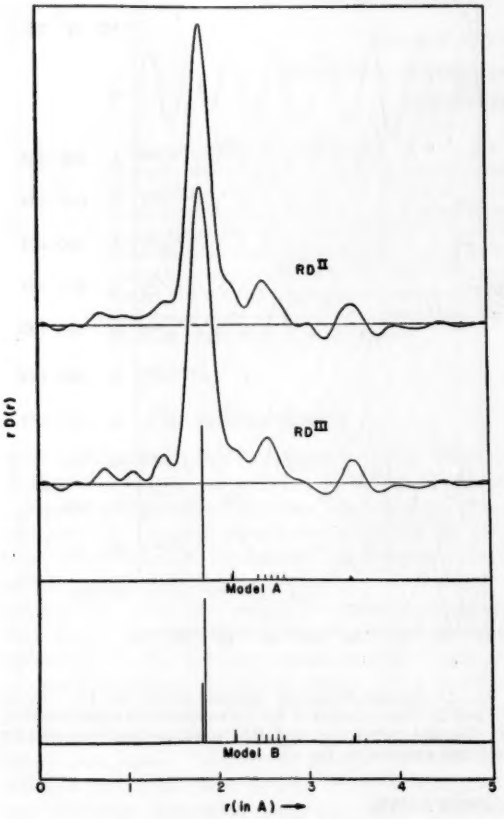

FIG. 3. Radial distribution curves of IF_7.

intensity. Figure 2 (V) shows the last corrected composite intensity curve used in the inversion to give RD″ (Fig. 3) which we consider to be reliable.

To test the sensitivity of the RD curve with respect to the terminal q value, Eq. (2) was summed for $q_{max}=61$; i.e., for the first five halos of the final composite intensity curve, to give RD‴. The major change was a shift of the 2.52-A peak to 2.58 A and a small change in the periodicity of the ripple.

D. MODELS AND CORRELATION

The highly symmetric 1.83-A peak indicates that the I–F distances are either all 1.83-A or split only by a few hundreds of an angstrom around the 1.83 value. On this basis, the interatomic distances in models with assigned D_{5h} symmetry were computed on the assumption either of seven equal I–F distances or of two groups (two and five) which differ slightly. The positions and relative weights of the RD peaks for the models with seven equal I–F distances (1.83 A) showed fair agreement with RD″, but the combination of five at 1.84 A and two at 1.81 A was somewhat better. However, neither model predicted the observed breadth of the two lesser peaks of RD″. Nevertheless, theoretical intensity curves were calculated, Eq. (1), for these two models with a range of 'apparent splittings,' $0.10<2\delta<0.20$, in increments of $\Delta(2\delta)=0.01$ A. The correlation of these curves with the experimental curve (V) was not acceptable in any case; the region of disagreement extended from $q>50$. We were forced to conclude that the molecule had a somewhat distorted configuration. To account for the breadth as well as the positions of the RD″ peaks, one must assume that the molecular structure does not possess strict D_{5h} symmetry.

The heavy lines underneath RD″ indicate the interatomic distances and the weights nZ_iZ_j/r_{ij} for models A and B which showed the best correspondence. Model A is a pentagonal bipyramid with seven equal I–F distances at 1.83 A. Four fluorine atoms in the girdle are staggered above and below the plane; starting with a fluorine atom in the plane, in a clockwise direction, the average assumed positions of the remaining atoms are α above, $\alpha/2$ below, $\alpha/2$ above, and α below, where α is a parameter to be determined. It is presumed that these girdle atoms oscillate normal to the girdle plane in phase, to give a sequential puckering to the F_5 ring. Model B consists of five girdle I–F distances at 1.84 A, with the fluorine atoms staggered similar to model A and two apical I–F distances of 1.81 A. In both models, the apical F atoms were assumed to be on the polar axis. A more realistic model would provide for precession of the apical F atoms about the polar axis, in phase with the rotational puckering of the girdle atoms.

Theoretical intensity curves were calculated, Eq. (1), for models A and B for various 'apparent splittings' and values of α. Those which showed the best correlation with the experimental curve V (A_n and B_n) are plotted in Fig. 2. One should note that, although the comparison is good for the sensitive region at the cutoff at $q\approx63$, the agreement at the 4th minimum ($q\approx40.5$) is poor.

To find the best model, one which shows the observed features at the 4th minimum, theoretical intensity curves were computed by means of Eq. (3)[12] which is based on the second approximation scattering theory[11]:

$$I(q)K(q) = \sum_{\text{all } r_{IF}} r_{IF}^{-1}\sin[r_{IF}(q\pi/10)]\cos[\eta_I(q)-\eta_F(q)] + \sum_{\text{all } r_{FF}} r_{FF}^{-1}\sin[r_{FF}(q\pi/10)][f_F(q)/f_I(q)]. \quad (3)$$

The values of the phase angle, $\eta_i(q)$, and the complex scattering amplitudes, $f_i(q)$, were obtained from Ibers and Hoerni's[11] tables using the transformation they suggested for operation at a different wavelength. Curves AA and BB in Fig. 2 show the best over-all agreement with the observed intensity. For comparison,

[12] J. A. Hoerni and J. A. Ibers, Phys. Rev. 91, 1182 (1953).

AA_0 and BB_0 are included to demonstrate the lack of agreement for these models when α is set to zero(coplanar girdle).

It is not possible to determine from the available diffraction data which of the two models (A or B) is correct. The introduction of a temperature factor would undoubtedly introduce a closer correspondence between the computed and estimated curves, but more accurate intensity data are essential. From the data at hand, one may conclude that in the gaseous state iodine heptafluoride is a pentagonal bipyramid, with the girdle atoms slightly displaced from a plane, possibly as described in the preceding section, with $\alpha=0.20$ A and average $\langle IF\rangle_{Av}=1.825\pm0.015$ A. On the basis of the available data, it was not possible to determine whether the I–F distances are equal; a maximum spread of about 0.06 A could be accommodated. To us, model B appears to be the most probable configuration.

It is worth noting that the observed 'cutoff' at $q\approx63$ is in fair agreement with the value expected for I–F, $q=65$. Also, that over-all agreement of AA and BB with V compared to that shown by A_n and B_n clearly indicates the inadequacy of the conventional approximation, Eq. (1).

E. DISCUSSION

The maximum distance between adjacent fluorines in the girdle is 2.20 A, which is 0.08 A larger than that present in the model with a planar girdle and equal I–F. Since the sum of the van der Waals radii is 0.50 A greater, the strong nonbonding repulsion has been only slightly alleviated by the puckering. It is presumed that further distortion is countered by reduction in the magnitude of total overlap of the bonding obitals. These observations account for the ease with which IF_7 loses two fluorines, as measured by a comparison of the *average* bond dissociation energy for IF_5, 62.2 kcal, and IF_7, 53.9 kcal.[13]

The 'free rotation' or random orientation of the molecule around a molecular axis[4] found in the cubic crystal phase is now readily interpreted as being associated with the nonplanarity of the girdle atoms. The change of point group ($Im3m$ to $Aba2$) and density ($\rho_{cubic}=1.596$ g/cc, $\rho_{ortho}=1.661$ g/cc, as computed from Burbank and Bensey's unit cell parameters) is in accord with the 'freezing in' of the puckered configuration to give a lower symmetry and permit the closer packing of the lower temperature orthorhombic crystal phase. In fact, a careful inspection of the figures prepared by Donohue[5] for the orthorhombic phase shows, as confirmation of our conclusions, that the girdle fluorine atoms are staggered about the girdle plane, except for the F_1 atom which is in the plane. Although this puckered rotation is not a true rotation since it does not possess an angular momentum, the movement of the girdle atoms a few tenths of an angstrom could easily account for the 'large thermal motion' observed in the crystal. Small inequalities in the I–F separations and deviation from coplanarity account also for the unusually large width of the NMR lines in the study of the liquid phase.

TABLE I. Thermodynamic functions for IF_7 (rigid rotor, simple harmonic oscillator, ideal gas approximation).

T°K	$-\frac{(F°-H_0°)}{RT}$	$\frac{(H°-H_0°)}{RT}$	$S°$	$C_p°$
50.00	23.95	4.015	55.57	8.183
100.00	26.83	4.499	62.26	12.50
150.00	28.86	5.671	68.62	19.36
200.00	30.68	7.079	75.05	25.32
250.00	32.41	8.448	81.20	29.77
298.16	34.00	9.635	86.72	32.86
300.00	34.06	9.677	86.93	32.96
400.00	37.14	11.68	97.01	36.93
500.00	39.91	13.18	105.51	39.11
600.00	42.42	14.32	112.76	40.41
700.00	44.70	15.21	119.06	41.24
800.00	46.78	15.92	124.60	41.80
900.00	48.69	16.50	129.55	42.19
1000.00	50.45	16.98	134.01	42.47
1200.00	53.62	17.73	141.79	42.84
1400.00	56.40	18.29	148.41	43.07
1600.00	58.87	18.72	154.18	43.22
1800.00	61.09	19.06	159.27	43.33
2000.00	63.11	19.33	163.84	43.40
2500.00	67.49	19.84	173.54	43.51
3000.00	71.14	20.19	181.48	43.58
3500.00	74.27	20.44	188.20	43.61
4000.00	77.01	20.63	194.03	43.64
4500.00	79.45	20.77	199.17	43.66
5000.00	81.64	20.89	203.77	43.67

The puckered rotation is a motion superimposed upon the normal vibrational modes and, as in the case of cyclopentane,[14] does not necessitate that within the limited resolution of the infrared and Raman spectra there be noticeable departure from the selection rules for D_{5h} symmetry. If IF_7 had a puckered girdle, the symmetry numbers would be either one or two (instead of 10), depending on the precise distortion. It will prove interesting to compare measured with calculated entropies. As yet, no heat capacity data have been reported for iodine heptafluoride. Thermodynamic functions have been calculated by Evans, Munson, and Wagman[15] on the assumption of strict D_{5h} symmetry with five girdle I–F bonds at 1.83 A and two apical I–F bonds equal to 1.93 A. These have been revised. The thermodynamic functions given in Table I are based on a molecular configuration with all I–F distances equal to 1.825 A, $\alpha=0.20$ A, and the apical atoms are displaced by 0.10 A from the polar axis. The projections of the polar I–F bonds onto the girdle plane fall 30° to each side of the I–F ($\alpha=0$) bond. The rotational con-

[13] L. Slutsky and S. H. Bauer, J. Am. Chem. Soc. **76**, 270 (1954).

[14] J. E. Kilpatrick, K. S. Pitzer, and R. Spitzer, J. Am. Chem. Soc. **69**, 2483 (1947). For more recent discussions, refer to J. P. McCullough *et al.*, J. Am. Chem. Soc. **81**, 5880 (1959) and K. S. Pitzer and W. E. Donath, J. Am. Chem. Soc. **81**, 3213 (1959).

[15] W. H. Evans, T. R. Munson, and D. D. Wagman, J. Research Nat. Bur. Standards **55**, 147 (1955).

stants are:

$$A=5.303\times10^{-2}\ \text{cm}^{-1}$$

$$B=6.034\times10^{-2}$$

$$C=5.901\times10^{-2}$$

$$\sigma=2.$$

The vibrational frequencies were taken from the published Raman and infrared spectra.[1] The free energy, enthalpy, and entropy were computed on an IBM 704 with a code set up by Sitney.[16]

[16] L. R. Sitney, Report (LA-2278) issued by LASL, May 8, 1959, PUBCO-I.

ACKNOWLEDGMENTS

We thank Professor Schumb and Dr. Lynch for providing the sample of iodine heptafluoride used in this investigation and Dr. Ross Harvey for assistance in taking the electron diffraction photographs. We also acknowledge the help of Miss Dorothy J. Shea in the programing of the computation for the IBM 650 and the kindness of Richard Lesser of the Computing Center at Cornell University for making their facilities available to us. We sincerely thank Dr. Russell E. Duff for computing the thermodynamic functions.

This work was supported in part by the Office of Naval Research.

THE JOURNAL OF CHEMICAL PHYSICS VOLUME 33, NUMBER 1 JULY, 1960

Application of Symmetry Principles to the Rotation-Internal Torsion Levels of Molecules with Two Equivalent Methyl Groups

ROLLIE J. MYERS,* *Department of Chemistry, University of California, Berkeley 4, California*

AND

E. BRIGHT WILSON, JR.,† *Mallinckrodt Chemical Laboratory, Harvard University, Cambridge 38, Massachusetts*

(Received February 12, 1960)

The set of coordinate transformations, corresponding to symmetry operations, which leave invariant the Hamiltonian operator for a molecule with two equivalent methyl groups, is obtained. These constitute a group which is a direct product of two simple groups, i.e., $C_{3v}\times C_{3v}$. The possible species for the energy levels, their degeneracies, their statistical weights, and the selection rules are worked out by group theory techniques which use only the properties of the smaller groups. The higher symmetry and higher degeneracies given by approximate Hamiltonians are briefly discussed.

THE recent applications of microwave spectroscopy to molecules containing two or more symmetrically equivalent internal rotors[1–3] (usually CH_3 groups) provide interesting and somewhat more complicated applications of well-known symmetry principles. With the aid of group theory, it is possible to obtain, in advance of the solution of the wave equation, the symmetry species possible for the various energy levels, their degeneracies (apart from approximate or accidental degeneracies), the symmetry selection rules, the symmetry factoring of any secular equations, the nuclear spin statistical weights, etc. The present paper will illustrate these methods on acetone. The results apply equally to dimethyl ether, and to any other molecule which consists of two methyl groups attached to a framework in such a manner that, when the methyl groups are rigidly fixed in their equilibrium conformations, the whole molecule has C_{2v} or C_2 symmetry. If rotation about the twofold axis interchanges equivalent atoms other than those in the methyl groups, appropriate modifications of the spin weights are needed, as for example in $(CH_3)_2SiH_2$.

* This research was supported in part by a grant from the Petroleum Research Fund administered by the American Chemical Society. Grateful acknowledgement is hereby made to the donors of said fund.

† This research was made possible in part by support extended Harvard University by the Office of Naval Research under contract.

[1] P. Kasai and R. J. Myers, J. Chem. Phys. **30**, 1096 (1959).
[2] L. Pierce, J. Chem. Phys. **31**, 547 (1959).
[3] J. D. Swalen and C. C. Costain, J. Chem. Phys. **31**, 1562 (1959); and private communication. Their paper contains a brief discussion of the present symmetry problem and the statistical weights.

ROTATIONAL HAMILTONIAN AND ITS SYMMETRY GROUP

Swalen and Costain[3] have written the Hamiltonian function for over-all and internal rotation in the form

$$H=B_xP_x^2+CP_y^2+A_zP_z^2+F(p_1^2+p_2^2)$$
$$+F'(p_1p_2+p_2p_1)-2Q_xP_x(p_1+p_2)-2Q_zP_z(p_1-p_2)$$
$$+\tfrac{1}{2}V_1(2-\cos3\alpha_1-\cos3\alpha_2)+V_{12}\cos3\alpha_1\cos3\alpha_2$$
$$+V'_{12}\sin3\alpha_1\sin3\alpha_2, \quad (1)$$

in which P_x, P_y, P_z are the components of total angular momentum along the principal axes, p_1, p_2 are momenta

associated with the internal rotation angles α_1 and α_2, and the other symbols are various molecular constants. The axes are labeled so that x lies along the C—O bond and y is perpendicular to the C-C-C plane (see Fig. 1). The angles α_1 and α_2 both increase on rotating the methyl groups clockwise viewed outward.

Inspection of this Hamiltonian shows that it is not invariant to the ordinary twofold rotations about the principal inertial axes, as would be the case for a rigid asymmetric rotor. The coupling of internal and external rotation requires that changes in α_1 and α_2, the internal rotation angles, accompany the transformations on θ, ϕ, and γ (the Eulerian angles[4]). Thus the following are valid symmetry transformations:

$$C_{2x}\colon \theta\to\pi-\theta,\ \phi\to\phi+\pi,\ \gamma\to-\gamma,\ \alpha_1\to\alpha_2,\ \alpha_2\to\alpha_1$$
$$(\therefore P_x\to P_x,\ P_y\to-P_y,\ P_z\to-P_z,\ p_1\to p_2,\ p_2\to p_1)$$
$$C_{2y}\colon \theta\to\pi-\theta,\ \phi\to\phi+\pi,\ \gamma\to\pi-\gamma,\ \alpha_1\to-\alpha_1,\ \alpha_2\to-\alpha_2$$
$$(\therefore P_x\to-P_x,\ P_y\to P_y,\ P_z\to-P_z,\ p_1\to-p_1,\ p_2\to-p_2)$$
$$C_{2z}\colon \theta\to\theta,\ \phi\to\phi,\ \gamma\to\gamma+\pi,\ \alpha_1\to-\alpha_2,\ \alpha_2\to-\alpha_1$$
$$(\therefore P_x\to-P_x,\ P_y\to-P_y,\ P_z\to P_z,\ p_1\to-p_2,\ p_2\to-p_1)$$
$$C_{31}^n\colon \theta\to\theta,\ \phi\to\phi,\ \gamma\to\gamma,\ \alpha_1\to\alpha_1+2\pi n/3,\ \alpha_2\to\alpha_2,\ (n=1,2)$$
$$(\therefore P_x\to P_x,\ P_y\to P_y,\ P_z\to P_z,\ p_1\to p_1,\ p_2\to p_2)$$
$$C_{32}^m\colon \theta\to\theta,\ \phi\to\phi,\ \gamma\to\gamma,\ \alpha_1\to\alpha_1,\ \alpha_2\to\alpha_2+2\pi m/3,\ (m=1,2).$$

The above operations, plus the identity operation, plus all possible distinct products, constitute a group (hereafter called group I) of 36 transformations of the coordinates which leave the Hamiltonian invariant. The effect of these on the momenta, indicated in the parentheses above, is fairly obvious but could be determined if necessary from the known relations[5] between the P_x, P_y, P_z, p_1, p_2 and the kinetic energy in terms of $\dot\theta$, $\dot\phi$, $\dot\gamma$, $\dot\alpha_1$, and $\dot\alpha_2$. The invariance also requires that the equilibrium conformations of the two methyl groups be symmetrically placed (under C_{2z}).

SYMMETRY SPECIES AND SELECTION RULES

In most past applications of group theory to rigid molecules,[6a] the symmetry groups required were standard crystallographic point groups for which the division of the elements into conjugate classes, the irreducible representations (symmetry species), and the characters have long been available. Molecules with internal rotors can require groups for which these items must be worked out.

However, it will be shown that the group required is of the form of a *direct product*[6b] of two simple groups, actually $C_{3v}\times C_{3v}$. The elements, classes, species, and characters for a direct product are simply the corresponding products from the two smaller groups and can therefore be written down at once. The character table[6c] for C_{3v} is given in Table I.

To see that group I is $C_{3v}\times C_{3v}$, it is convenient to transform the Hamiltonian by introducing[7]

$$\alpha_+=\tfrac{1}{2}(\alpha_1+\alpha_2),\qquad \alpha_-=\tfrac{1}{2}(\alpha_1-\alpha_2)$$
$$p_+=(p_1+p_2),\qquad p_-=(p_1-p_2) \tag{2}$$

whence

$$H=B_xP_x^2+CP_y^2+A_zP_z^2+\tfrac{1}{2}F_xp_+^2+\tfrac{1}{2}F_zp_-^2+V_1$$
$$\times(1-\cos3\alpha_+\cos3\alpha_-)+[(V_{12}-V_{12}')/2]\cos6\alpha_+$$
$$+[(V_{12}+V_{12}')/2]\cos6\alpha_-$$
$$-2Q_xP_zp_+-2Q_yP_zp_- \tag{3}$$

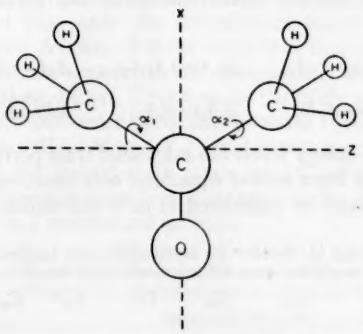

FIG. 1. Model for acetone showing orientation of Cartesian axes and signs of internal rotation angles.

[4] The symbol γ is used instead of the customary χ so that the latter can be used for the character.
[5] E. Bright Wilson, Jr., and J. B. Howard, J. Chem. Phys. 3, 818 (1935).
[6] (a) See, for example, E. B. Wilson, Jr., J. C. Decius, and P. C. Cross, *Molecular Vibrations* (McGraw-Hill Book Company, New York, 1955); (b) *ibid.*, p. 320; (c) *ibid.*, p. 325.
[7] The form is similar to Eq. (4) of Swalen and Costain (see footnote 3) except that we define the coupled angles and momenta differently and we have corrected a factor of $(2)^{\frac{1}{2}}$ error in their Eq. (4).

TABLE I. Characters for species of C_{3v}.

$C_{3v}(6)$	E	$2C_3$	$3\sigma_v$
A_1	1	1	1
A_2	1	1	−1
E	2	−1	0
χ^{vib}	3	0	±1

in which $F_x=F+F'$ and $F_z=F-F'$. Examination shows that the operations E, $(C_{31}C_{32}^2,\ C_{31}^2C_{32})$, $(C_{2x},\ C_{2x}C_{31}C_{32}^2,\ C_{2x}C_{31}^2C_{32})$ leave α_+ unchanged. These operations form the group C_{3v} on the angle α_- and are a subgroup of I which we shall designate C_{3v}^-. Also the operations E, $(C_{31}C_{32},\ C_{31}^2C_{32}^2)$, $(C_{2z},\ C_{2z}C_{31}C_{32},\ C_{2z}C_{31}^2C_{32}^2)$ leave α_- unchanged and form the group C_{3v} for the angle α_+. These latter operations form a different subgroup C_{3v}^+ of I. The elements of C_{3v}^- are distinct (except E) from those of C_{3v}^+ and commute with them. Since there are 36 product elements, these must include all the elements of group I, which is therefore $C_{3v}^-\times C_{3v}^+$.

Although the character table for group I could now be written down immediately, this is not necessary since all the desired results can be obtained from Table I, as will be shown. The species for group I are nine products, A_1A_1, A_1A_2, A_1E, A_2A_1, A_2A_2, A_2E, EA_1, EA_2, and EE of those of C_{3v}^- and C_{3v}^+. It is now seen that nondegenerate levels (species A_1A_1, A_1A_2, A_2A_1, and A_2A_2 corresponding to the ordinary four group species for the rigid asymmetric rotor), doubly degenerate levels (species A_1E, A_2E, EA_1, and EA_2) and quadruply degenerate levels (species EE) are possible, even in the completely accurate solution of the given Hamiltonian.

Since the dipole moment μ must lie along x, which is in A_1 of C_{3v}^- and in A_2 of C_{3v}^+, μ is in A_1A_2. Consequently, electric dipole transitions are permitted as follows:

$$A_1A_1\leftrightarrow A_1A_2;\quad A_2A_1\leftrightarrow A_2A_2;\quad A_1E\leftrightarrow A_1E;$$
$$A_2E\leftrightarrow A_2E;\quad EA_1\leftrightarrow EA_2;\quad EE\leftrightarrow EE. \quad (4)$$

If the energy levels are calculated from perturbation theory or from secular equations, only functions of one species need be considered in each calculation. In the next section we show the correspondence between the species of $C_{3v}^-\times C_{3v}^+$ and appropriate sets of basis functions.

TABLE II. Species[a] for asymmetric rotor functions.

	C_{2z}	C_{2x}	C_{3v}^-	C_{3v}^+	$C_{3v}^-\times C_{3v}^+$
A	+1	+1	A_1	A_1	A_1A_1
B_x	+1	−1	A_1	A_2	A_1A_2
B_z	−1	+1	A_2	A_1	A_2A_1
B_y	−1	−1	A_2	A_2	A_2A_2

[a] In acetone and dimethyl ether I_z is the smallest moment of inertia and I_y is the largest. In these cases the King, Hainer, and Cross notation is as follows: $A=ee$, $B_x=oo$, $B_z=eo$, $B_y=oe$. In other molecules a different correlation is possible.

TABLE III. Species of product wave functions.

	Asymmetric rotor functions			
	A	B_x	B_z	B_y
Internal torsion functions	A_1A_1	A_1A_1	A_1A_2	A_2A_1	A_2A_2
	A_1A_2	A_1A_2	A_1A_1	A_2A_2	A_2A_1
	A_1E	A_1E	A_1E	A_2E	A_2E
	A_2A_1	A_2A_1	A_2A_2	A_1A_1	A_1A_2
	A_2A_2	A_2A_2	A_2A_1	A_1A_2	A_1A_1
	A_2E	A_2E	A_2E	A_1E	A_1E
	EA_1	EA_1	EA_2	EA_1	EA_2
	EA_2	EA_2	EA_1	EA_2	EA_1
	EE	EE	EE	EE	EE

SYMMETRY OF APPROXIMATE WAVE FUNCTIONS

If the coupling between internal and over-all rotation is ignored, the Hamiltonian of Eqs. (1) or (3) is separable and approximate solutions can therefore be written in the form of the product of an asymmetric rigid rotor function and an internal torsional function. In limiting situations, these functions will show extra degeneracies, which may be partially split in the general case.

The symmetry species for the rigid rotor functions and the internal torsion functions will be obtained separately and then combined to give the species for the over-all product functions.

The rigid-rotor functions divide into the four species A, B_x, B_y, B_z of the well-known Four group. This is a subgroup of I with the correlations shown in Table II.

The species under group I for the internal torsion functions will be obtained below for several cases. To combine these with those of the external rotational factor requires the multiplication properties of group I. These follow directly from the multiplication properties of C_{3v}, which are

$$A_1\times A_1=A_1;\quad A_2\times A_2=A_1;\quad A_1\times A_2=A_2\times A_1=A_2,$$
$$A_1\times E=A_2\times E=E\times A_1=E\times A_2=E,$$
$$E\times E=A_1+A_2+E. \quad (5)$$

These rules lead to Table III which shows the over-all symmetry species in terms of the species for the possible external rotational functions (labeling

TABLE IV. Species for internal torsional functions, high-barrier case.

n_-	n_+	Species
Even	Even	$A_1A_1+A_1E+EA_1+EE$
Even	Odd	$A_1A_2+A_1E+EA_2+EE$
Odd	Even	$A_2A_1+A_2E+EA_1+EE$
Odd	Odd	$A_2A_2+A_2E+EA_2+EE$

columns) and those for the internal torsion functions (labeling rows).

High Barrier Case

Here the wave functions for internal torsion can be approximated by the products of harmonic oscillator functions, either in α_1 and α_2, or in α_+ and α_-. It is easier to use the latter coordinates and better because F' and the expansion of the V_{12} and V_{12}' terms can be included. The approximate internal functions will therefore be constructed from linear combinations of functions.

$$H_{n_-}(\alpha_-+ka)H_{n_+}(\alpha_++la) \qquad (6)$$

where H_n is the nth harmonic oscillator function (modified to be periodic in 2π) and $k, l=0, +1$, or -1 with $a=2\pi/3$. The operations of C_{3v}^- can alter only the first factor and those of C_{3v}^+ only the last factor. For a given value of n^- (or n^+) there are three functions and for a given set of n_- and n_+ there are nine product functions.

TABLE V. Characters and species of free rotor functions under C_{3v}.

	E	$2C_3$	$3\sigma_v$	
$m=0$	1	1	1	A_1
$m=3n$	2	2	0	A_1+A_2
$m\neq 0, 3n$	2	−1	0	E

The reduction of the three functions $H_n(\alpha+ka)$ for a given value of n for the group C_{3v} is well known and is illustrated in Table I (last line). If n is even, the species are A_1+E and if n is odd, they are A_2+E. The species for the nine product functions will be the direct product of the three functions in C_{3v}^- with the three in C_{3v}^+. These are given in Table IV.

For sufficiently high barriers V_1, each value of the pair n_-, n_+ gives a ninefold degenerate level, which would split into the four components shown in the general case. For sufficiently high barriers the coupling terms between rotation and internal torsion should not destroy this ninefold degeneracy, as can be seen by thinking of the internal torsion as a vibration with negligible tunneling between the three minima of each methyl group. The effect of the terms in F' and V_{12}' is to prevent the high-barrier levels for which $n_-\neq n_+$ from coalescing into pairs ($n_-=n'$, $n_+=n''$ and $n_-=n''$, $n_+=n'$) to give 18-fold degenerate levels.

There is an intermediate situation in which not all the high-barrier extra degeneracy is lost on lowering the barrier somewhat. If the term in F' and therefore the difference between F_x and F_z can be neglected, as well as V_{12}', and if for the moment the terms coupling internal and over-all rotation are set aside, the Hamiltonian has a still higher symmetry than group I because it is invariant to $\alpha_1\rightarrow-\alpha_1$ and separately to $\alpha_2\rightarrow-\alpha_2$ which are equivalent to $\alpha_+\rightarrow-\alpha_-$ and $\alpha_+\rightarrow\alpha_-$, respectively. The resulting group can be considered as the ordinary Four group V acting on the rotational coordinates θ, ϕ, γ times a new group III acting on α_1 and α_2 (or α_- and α_+). The group III contains 72 operations, cannot be written as the direct product of two smaller groups, and is isomorphous with a certain permutation group on the six hydrogens. It is therefore a subgroup of the symmetric group of degree 6. Its character table has been published.[8] It has four nondegenerate species which reduce to A_1A_1 or A_2A_2 of I. There is one doubly degenerate species which reduces to $A_1A_2+A_2A_1$. Finally there are four quadruply degenerate species which reduce to EE, EE, A_1E+EA_1, A_2E+EA_2, respectively.

TABLE VI. Species of free internal rotation functions under $C_{3v}^-\times C_{3v}^+$.

$m_-=m_+=0$	A_1A_1
$m_-=0$, $m_+=3n$	$A_1A_1+A_1A_2$
$m_-=3n$, $m_+=0$	$A_1A_1+A_2A_1$
$m_-=0$, $m_+\neq 3n$, 0	A_1E
$m_-\neq 3n$, 0, $m_+=0$	EA_1
$m_-=m_+=3n$	$A_1A_1+A_1A_2+A_2A_1+A_2A_2$
$m_-=m_+\neq 3n$, 0	EE
$m_-=3n'\neq m_+=3n'$	$A_1A_1+A_1A_2+A_2A_1+A_2A_2$
$m_-=3n'\neq m_+=3n$	$A_1A_1+A_1A_2+A_2A_1+A_2A_2$
$m_-=3n$, $m_+\neq 3n$, 0	A_1E+A_2E
$m_-\neq 3n$, 0, $m_+=3n$	EA_1+EA_2
$m_-\neq 3n$, $0\neq m_+\neq 3n'$, 0	$2EE$

Application of group III to the representation formed by the high-barrier functions of Eq. (6) shows that the ground torsional state will have (for this approximation) three components of degeneracies 1, 4, and 4 while the first excited state would have five components of degeneracies 2, 4, 4, 4, 4. These components should be split from one another on lowering the barrier sufficiently.

When the terms coupling internal and external rotation are introduced by perturbation theory, it often turns out that only the second-order terms are of importance. A study of these shows that they conform to the higher symmetry III whereas the first-order perturbations do not. Therefore, in the fairly common case where odd-order perturbation terms can be neglected, as well as F' and V_{12}', moderately low barriers will split the ground state into a triplet and the first excited torsional state into a quintet, rather than all the way to a quartet and an octet.

TABLE VII. Characters for species of C_3.

	E	C_3 ($w=-\frac{1}{2}+\frac{1}{2}\sqrt{-3}$)	C_3^2
A	1	1	1
E_a	1	w	w^2
E_b	1	w^2	w

[8] D. E. Littlewood, *The Theory of Group Characters* (Oxford University Press, New York, 1950), p. 275.

TABLE VIII. Calculation of statistical weights.

C^-C^+	EE	EC_3	EC_3^2	$2C_2E$	$2C_2C_3$	$2C_2C_3^2$	$3\sigma_vE$	$3\sigma_vC_3$	$3\sigma_vC_3^2$
$\chi_C{}^-{}_E\chi_C{}^+{}_E$	4	−2	−2	−2	1	1	0	0	0
±	+	+	+	+	+	+	−	−	−
$\Pi(2s_m+1)$	2^6	2^2	2^2	2^2	2^1	2^1	2^3	2	2
$g_C{}^-g_C{}^+$	1	1	1	2	2	2	3	3	3
Term	256	−8	−8	−16	32	32	0	0	0

These splittings of the energy levels should be reflected in the splitting of the pure rotational spectra and in fact triplets have been observed for dimethyl ether[1] and dimethyl silane[2] whereas quartets have been seen in acetone.[3]

Zero Barrier Case

If all the potential energy terms are neglected as well as the coupling between internal and over-all rotation, the internal wave function becomes[9]

$$\exp(im_-\alpha_-)\exp(im_+\alpha_+) \qquad (7)$$

in which the quantum numbers m_-, m_+ are positive or negative integers or zero. If also $F'=0$, the energy depends only on $m_-{}^2+m_+{}^2$. Consequently, the degeneracy (in this approximation) can be $1(m_-=m_+=0)$, $4(m_-=0,\ m_+\neq 0$ or $m_-\neq 0,\ m_+=0)$, $4(m_-=m_+\neq 0)$, or $8(m_-\neq m_+,\ m_-\neq 0,\ m_+\neq 0)$.

From the way in which α_- transforms under $C_{3v}{}^-$, the characters for the functions

$$\exp(\pm im_-\alpha_-)$$

can be found and the species under $C_{3v}{}^-$ written down (see Table V). These results apply to either m_-, giving species of $C_{3v}{}^-$, or to m_+, giving species of $C_{3v}{}^+$. Consequently, the species under I for any level are as given in Table VI.

Splitting of Low Barrier Levels

Introduction of a small barrier and the other omitted terms in H can split up part of the degeneracy exhibited above. However, the double degeneracy of EA_1, etc., and the quadrupole degeneracy of EE cannot be further split no matter how accurately the problem is solved. Hence, the eightfold level of Table VI with symmetry $2EE$ could split into two fourfold levels, whereas the eightfold level with $m_-=3n\neq m_+=3n'$ can split into eight components.

The introduction of the term in F' makes $F_x\neq F_z$ and thereby splits apart the component levels in separate rows of Table VI connected by brackets. The introduction of V_1 and V_{12} with the neglect of F' and V_{12}' leads to the symmetry of group III and to the retention of some degeneracy as discussed previously. A small barrier and the addition of F' will split A_1 from A_2 and the component levels in separate rows thus destroying all the extra degeneracy.

STATISTICAL WEIGHTS

To obtain the spin degeneracies and hence the statistical weights, the subgroup of group I consisting of those rotations which are equivalent to a simple interchange of equivalent nuclei should be used.[10] This group (called group II) omits C_{2z} and hence half the elements of group I. The result is a group of 18 elements isomorphous with $C_{3v}{}^-\times C_3{}^+$.

Table VII gives the characters for the group C_3. The relationship between the species of C_{3v} and those of its subgroup C_3 is

$$A_1\rightarrow A, \qquad A_2\rightarrow A, \qquad E\rightarrow E_a+E_b \qquad (8)$$

For protons, the over-all wave functions for acetone or dimethyl ether must be of species A_2A since $C_{31}{}^mC_{32}{}^{m'}$ always interchanges an even number of pairs but C_{2z} interchanges three pairs. For deuterons, the required species is A_1A.

To determine the statistical weights of a level whose total wave function, exclusive of nuclear spin, is of species $\Gamma i\Gamma j$ (e.g., A_2E) of the group $C_{3v}{}^-\times C_{3v}{}^+$ (group I), the set of over-all wave functions formed by multiplying the function of species $\Gamma i\Gamma j$ by all possible spin functions is reduced on the group II ($C_{3v}{}^-\times C_3{}^+$). The required weight is the number of times the proper species (A_2A for $(CH_3)_2CO$ or A_1A for $(CD_3)_2CO$) appears in the reduction. What is desired is therefore (from the standard formula),

$$n_k=(1/g)\sum_C g_C\chi_C{}^{(k)*}\chi_C \qquad (9)$$

where n_k is the desired weight, g is the number of elements in group II (18), g_C is the number of elements in the class C, $\chi_C{}^{(k)}$ is the character for class C of species k of group II, this being A_2A or A_1A as noted above, χ_C is the character for the reducible representation formed by those total wave functions which have symmetry $\Gamma i\Gamma j$ except for their spin factors.

[9] For $V_1=V_{12}=V_{12}'=0$, the Hamiltonian is invariant to the operations of $C_{\infty v}{}^+\times C_{\infty v}{}^-$ since $\alpha_1\rightarrow\alpha_1+\delta$ (δ arbitrary) is a symmetry operation. This group has species of dimensions 1, 2, and 4. However, if $F'=0$ and the terms in Q_x and Q_z vanish, the symmetry is still higher since $\alpha_1\rightarrow-\alpha_1$ independently of α_2, etc. Here the species must be of dimensions 1, 4, or 8.

[10] E. Bright Wilson, Jr., J. Chem. Phys. 3, 276 (1935).

But every class C of group II is a product C^-C^+ of classes from C_{3v}^- and C_3^+ so $g_C=g_{C^-}g_{C^+}$, from the smaller groups. Further $\chi_C^{(k)*}=\chi_{C^-}{}^{(k-)}\chi_{C^+}{}^{(k+)}=\pm 1$ depending on whether the operation C^-C^+ interchanges an even or an odd number of pairs of H nuclei (not D).

The character χ_C is found as follows. The spin factors lead to a reducible representation whose character for a given operation C^-C^+ is equal to the number of spin functions left unaltered by the permutation equivalent to C^-C^+, because any permutation which sends one spin function into another contributes zero to the diagonal sum or character. The number left unchanged is[11]

$$\prod_m (2s_m+1)_{C^-C^-} \tag{10}$$

where, for a given operation C^-C^+, the nuclei are divided into sets such that members of a given set are permuted among themselves but not with members of other sets and s_m is the total spin of one of the equivalent nuclei in the mth set. This character for the spin part needs to be multiplied by the character, for C^-C^+, of the rest of the wave function, which by hypothesis is χ_C for $\Gamma i\Gamma j$, or

$$\chi_{C^-}{}^{\Gamma i}\chi_{C^+}{}^{\Gamma j}, \tag{11}$$

The whole formula for the statistical weight is therefore:

$$(1/g)\sum_{C^-}\sum_{C^+}\pm g_{C^-}g_{C^+}\chi_{C^-}{}^{\Gamma i}\chi_{C^+}{}^{\Gamma j}\prod_m (2s_m+1)_{C^-C^+} \tag{12}$$

where the $(\pm)$ is assigned to a term C^-C^+ as described above. Note that the characters $\chi_{C^-}{}^{\Gamma i}\chi_{C^+}{}^{\Gamma j}$ are those of species under group I even though the sum is over classes of group II.

[11] L. D. Landau and E. M. Lifshitz, *Quantum Mechanics Non-Relativistic Theory* (Addison-Wesley Publishing Company, Reading, Massachusetts, p. 385.

TABLE IX. Nuclear spin statistical weights.

Species[a]	6H	6D	8H	Species[a]	6H	6D	8H
A_1A_1	6	66	36	A_2E	6	56	12
A_1A_2	6	66	36	EA_1	4	64	16
A_1E	2	72	20	EA_2	4	64	16
A_2A_1	10	55	28	EE	16	176	64
A_2A_2	10	55	28				

[a] The species of the wave function without the spin factor.

For example, consider the statistical weight for a level of acetone whose wave functions, exclusive of nuclear spin, are of species EE under $C_{3v}^-\times C_{3v}^+$. The necessary quantities are given in Table VIII by classes.

The statistical weight for the EE species is therefore the sum over the last row divided by $h(=18)$, or 16. Similar calculations can be made for each species, with results summarized in Table IX. This table also includes, under column "8H," the molecule $(CH_3)_2SiH_2$. Here only plus signs enter the formula above because now all operations interchange even numbers of pairs of hydrogens. Further the quantity

$$\prod_m (2s_m+1)$$

shown in the table is multiplied by 4 for all classes except the last three, where the factor is 2. This arises because the two H nuclei on Si are not permuted except by the last three classes, in which they are simply interchanged.

In acetone or dimethyl either, the $A\leftrightarrow B_x$ rotational transitions will have components with statistical weights 6:2:4:16 while the $B_z\leftrightarrow B_y$ transitions would have weights 10:6:4:16, for the A_1A_1, A_1E, EA_1 and EE internal torsional levels (CH_3 groups). In the case of dimethyl ether only triplets are obtained but they were observed[1] to have statistical weights in accordance with a superposition of the A_1E and EA_1 lines.

Electronic Transitions of Rare Earth Ions in the Infrared Region

G. MANDEL, R. P. BAUMAN, AND E. BANKS

Department of Chemistry, Polytechnic Institute of Brooklyn, New York

(Received February 1, 1960)

The $^2F_{7/2}$←$^2F_{5/2}$ transition of the cerous ion has been observed in solid solutions of cerium(III) fluoride in cadmium fluoride. The band center is at about 2250 cm^{-1}, in good agreement with the free-ion value of 2253.0 cm^{-1}. The crystal field splitting of the band appears to be enhanced by the effect of the interstitial fluoride ions which compensate for the excess positive charge of Ce^{3+} in Cd^{2+} positions. Addition of NaF, which eliminates the interstitial fluoride ions, decreases the splitting. Praseodymium and neodymium ions in CdF_2 also showed absorption bands.

THE ground state of the cerous ion, Ce^{3+}, is a $^2F_{5/2}$ state, the companion $^2F_{7/2}$ state lying 2253.0 cm^{-1} above this[1] as a consequence of the rather large spin-orbit coupling. Attempts to observe the forbidden transition between these two levels have been unsuccessful in the past, probably because the apparent intensity is decreased by the inhomogeneity of a powdered sample.

During the course of a search for color centers,[2] solid solutions of cerous fluoride in cadmium fluoride were prepared. The CdF_2 was prepared by solution of $CdCO_3$ in concentrated aqueous ammonia, followed by precipitation of CdF_2 from the filtrate with aqueous HF. The precipitate was washed with boiling concentrated hydrofluoric acid. CeF_3 was prepared by reduction of ceric ammonium nitrate with hydrogen peroxide, followed by treatment, as above, with aqueous HF. Single crystals of various compositions were grown by slow cooling from the melt (1120°C) in a graphite crucible under a helium atmosphere. The crystals were sliced, then polished to reduce scattering losses. Infrared spectra were obtained on a Perkin-Elmer Model 21 double-beam spectrometer (unflushed), a Model 137 (Infracord) double-beam spectrometer (flushed with nitrogen), and a Model 112 single-beam, double-pass spectrometer with CaF_2 prism (flushed). Lattice constants were determined with a Norelco recording high-angle diffractometer. These measurements, coupled with density determinations, showed that the Ce^{3+} ions occupied lattice sites and the excess F^- ions occupied interstitial positions.[2]

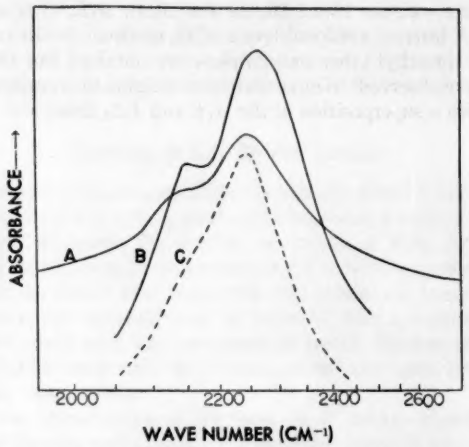

FIG. 1. Infrared absorbance of solid solutions of CeF_3 in CdF_2. *A*: 1 mole % CeF_3; *B*: 2 mole % CeF_3; *C*: 2 mole % CeF_3+2 mole % NaF.

Single crystals, about 1 mm thick, showed a strong, moderately broad absorption band between 2100 and 2400 cm^{-1} (Fig. 1. This appeared to consist of three peaks when scanned on a double-beam spectrometer without flushing; later spectra obtained on single-beam and double-beam instruments flushed with nitrogen showed the band to comprise two peaks, the apparent splitting of the stronger band having been caused by atmospheric CO_2.

A number of mechanisms were considered as possible sources of the observed absorption bands. Triple bonds or allene-type structures are known to absorb in this region, but these were ruled out on the basis of the known composition and crystal structure. Since the absorption due to Cd-F and Ce-F vibrations falls below 900 cm^{-1},[2] and no binary combination bands are observed above 900 cm^{-1}, it is extremely unlikely that a ternary combination could appear with such intensity. The possibility that the absorption could be attributed to a Ce-O or Cd-O vibration was also considered, but was ruled out on the basis of previous experiments,[2] which had shown that oxide is lost from the crystals when CdF_2 is melted in graphite crucibles, with the formation of carbon monoxide and cadmium vapor. In the same work, it was found that sulfide ion could go into limited solid solution in CdF_2, with the production of a strong yellow color. However, the introduction of sulfide in the absence of cerium did not affect the absorption in the infrared region.

Since the new absorption bands follow Beer's law for changing Ce^{3+} concentration, it was thought to be extremely unlikely that the absorption could be at-

[1] R. J. Lang, Can. J. Research **14A**, 127 (1936).
[2] M. Rubenstein and E. Banks, J. Electrochem. Soc. **106**, 404–409 (1959).

tributed to the accidental incorporation of other impurities. As a further check of the possibility that the band might be of vibrational origin, samples of CdF_2 and LaF_3 were prepared and investigated. These samples showed no absorption in this spectral region. Since the masses, radii, and charges of Ce^{3+} and La^{3+} are essentially identical, one would expect vibrational motions in which they were involved to lead to nearly the same absorption spectra. Since La^{3+} has a "rare gas" electronic structure, the absence of absorption in these samples suggests strongly that the spectrum is electronic in nature. Samples prepared from commercially purified raw materials, without repurification, showed an apparent quenching of the band, which is compatible with the idea that the band originates in an electronic transition. The position of the absorption peak agrees very well with the predicted value for the forbidden "spin-reversal" transition.[1]

An additional possibility for an electronic transition was the introduction of metastable "trapping states" into the energy gap of CdF_2 as a result of the addition of Ce^{3+}. Such states might be partially filled during exposure to room light, and emptied by the absorption of infrared. Although the sharpness of the observed peaks (at room temperature) was not favorable to this hypothesis, a test was made. A crystal was exposed to approximately monochromatic 2250 cm^{-1} radiation for 24 hr, by placing it behind the exit slit of the monochromator. This produced no detectable change in absorption intensity, although one would have expected the band to be significantly bleached if it had originated in a metastable state.

On the basis of the above arguments, it was concluded that the observed absorption spectrum was indeed due to an electronic transition from the ground state of Ce^{3+}, probably the $^2F_{7/2}$←$^2F_{5/2}$ transition.

The splitting of the band increases with increasing CeF_3 concentration, as would be expected from crystal field splitting caused by interstitial fluoride ions. As the number of interstitial fluorides is reduced by the addition of NaF, the splitting decreases. Cooling the crystal with a stream of cold nitrogen gas (bubbled through liquid nitrogen) narrowed the bands without revealing additional structure.

Electron paramagnetic resonance measurements by Low[3] have shown the field around the gadolinium ion in a solution of GdF_3 in CaF_2 to be cubic. If one assumes the same to be true for solutions in CdF_2, which also has the cubic fluorite structure, each of the electronic levels of the Ce^{3+} should be split.[4] As many as six bands might thus be expected, of which only one is forbidden by the selection rules of the octahedral double group. No evidence for more than two components has been found. At room temperature the apparent splitting for a 2 mole % solution of CeF_3 in CdF_2 is about 110 cm^{-1} (2264 and 2155 cm^{-1}); this apparent splitting increases by about 10 cm^{-1} (2264 and 2146 cm^{-1}) as the bands become narrower at lower temperatures, probably owing solely to the variation in overlap rather than to an actual shift in band positions. The apparent quenching of the band by trace impurities probably resulted from increased splitting, causing a decrease in peak intensities.

TABLE I. Position of absorption peaks in solid solutions of PrF_3 and NdF_3 in CdF_2.

Ion	Conc. (wt %)	Wave number
Pr^{3+}	4.5	6200
		5900
		5050
		4400
		2323
		2163
		1740
		1575
		1450
Nd^{3+}	5.1	3920
		2195
		2095
		2022
		1948
		1910
		1820
		1739
		1600

The transition violates the selection rules $\Delta S=0$ and $\Delta L=\pm 1$, but the large splitting between the levels of the doublet shows that these quantum numbers are not valid. The angular momentum, J, is a valid quantum number and the transition is allowed under the rule $\Delta J=0, \pm 1$. The transition is considered to be forbidden because it violates LaPorte's rule, $g \leftrightarrow u$, $g \leftrightarrow g$, $u \leftrightarrow u$. The observed integrated intensity indicates an oscillator strength for the band of 2×10^{-6}. This is in good agreement with the predicted[5] intensity of 10^{-6} for transitions of this type.

Preliminary examination of praseodymium and neodymium fluorides in cadmium fluoride revealed the bands listed in Table I. No absorption in this region was observed for lanthanum or ytterbium ions.

Note added in proof. Since the submission of this manuscript to the Journal, we have learned that P. P. Feofilov [Optika i Spektroskopiya **6**, 150 (1959)] has observed these transitions in CaF_2–CeF_3 solid solutions. The spectra shown are more complex than ours, which is attributable to the presence of oxide in the CaF_2. In view of the known difference in the chemistry of CdO and CaO in contact with carbon, the presence of oxide in Feofilov's crystals and its absence in ours is easily understood.

[3] W. Low, Ann. N. Y. Acad. Sci. **72**, 69–126 (1958).
[4] H. Bethe, Ann. Phys. (5) **3**, 133 (1929).
[5] L. F. Broer, C. J. Gorter, and J. Hoogschagen, Physica **11**, 231 (1944).

Structure of the Complex Ion in Aqueous Solutions of Zirconyl and Hafnyl Oxyhalides†

GEORGE M. MUHA AND PHILIP A. VAUGHAN

School of Chemistry, Rutgers, The State University, New Brunswick, New Jersey

(Received February 19, 1960)

X-ray scattering by aqueous solutions of $MOX_2 \cdot 8H_2O$ (M = Zr and Hf, X = Cl and Br) can be explained if one assumes the existence of a complex $[M_4(OH)_8(H_2O)_{16}]X_8$. The metal atoms in this complex are arranged in a square and are held together by double OH bridges along each edge. In addition, each metal atom is bound to four additional water molecules in such a manner that the configuration about the metal is a square Archimedes antiprism. The halogen ions are not bound directly to the metal. They do, however occupy definite positions in the complex, and are presumably held in place by electrostatic forces. The structure is very similar to that which has been found in the crystalline oxyhalides.

INTRODUCTION

SEVERAL studies[1–10] of various physicochemical properties of aqueous solutions of zirconyl salts indicate that the zirconium species exists in some type of condensed complex. Although there has been some disagreement as to the size and distribution of the polymeric species, the extensive investigations of Zr(IV) and Hf(IV) solutions made by Kraus and Johnson[8–10] with the ultracentrifuge indicate that over a wide range of concentration and acidity the solutions are monodisperse with a degree of polymerization of three or four. A study of crystalline $ZrOCl_2 \cdot 8H_2O$ by x-ray diffraction[11] has revealed that the zirconyl species in this compound is tetrameric and can best be described by the formula $[Zr_4(OH)_8 \cdot 16H_2O]^{8+}$. It is possible although by no means certain, that this ion exists in aqueous solution.

In this paper we present the results of a study of this problem by means of x-ray diffraction by aqueous solutions of $ZrOCl_2 \cdot 8H_2O$, $ZrOBr_2 \cdot 8H_2O$, $HfOCl_2 \cdot 8H_2O$, and $HfOBr_2 \cdot 8H_2O$.

EXPERIMENTAL

The compounds $ZrOCl_2 \cdot 8H_2O$ and $ZrOBr_2 \cdot 8H_2O$ were prepared by repeated recrystallization of technical grade $ZrOCl_2 \cdot 8H_2O$ from 6*M* HCl or HBr. The compounds $HfOCl_2 \cdot 8H_2O$ and $HfOBr_2 \cdot 8H_2O$ were prepared by hydrolyzing the corresponding tetrahalides with 6*M* HCl or HBr. The tetrahalides were prepared from hafnium dioxide.[12]

X-ray diffraction curves were obtained from solutions of the following approximate concentrations: 2, 1.5, 1, and 0.5 molal $HfOCl_2$; 2 molal $HfOBr_2$, $ZrOCl_2$, and $ZrOBr_2$. More information concerning these solutions is given in Table I. The densities were determined at ambient room temperature by the pycnometer method. Because these solutions show time-dependent phenomena,[1,2] the samples were allowed to stand at least 18 but not more than 28 hr before use

The instrument used to obtain the diffraction curves was a Philips Electronics diffractometer; however, two different techniques were used. Most of the data for the $HfOCl_2$ and $HfOBr_2$ solutions were obtained with Mo$K\alpha$ radiation by a transmission method in which monochromatization was achieved by a curved quartz crystal after diffraction. The samples were held in cells, each of which was made by cementing together a sandwich arrangement consisting of two pieces of 0.003-in. thick Mylar film separated by a spacer. The spacers were made of Mylar or polyethylene of thickness chosen to give approximately maximum diffraction intensity at zero angle. To provide rigidity, the cells were cemented to an aluminum block, which had a hole cut in it to allow the passage of x rays. The sample was loaded into the cell with a hypodermic syringe.

The above method did not give good results when it was applied to $ZrOCl_2$ and $ZrOBr_2$ solutions because of fluorescence. The $K\beta$ lines of zirconium are only slightly shorter than Mo$K\alpha$ and enough spurious radiation got through the monochromator so that interpretation was difficult and uncertain. Therefore, Cu$K\alpha$ radiation was used, and, because of high absorption, the measurements were made by reflection. Since the curved-cyrstal monochromator was designed for the transmission method, monochromatization was achieved with balanced filters. The filters consisted of 0.001-in. thick Ni foil and a suspension of finely divided Co powder in a collodion film with a density of approxi-

† We wish to thank the Titanium Alloy Manufacturing Division of the National Lead Company for the financial support given to one of us (G.M.M.) in the form of the Meredith Fellowship.

[1] R. Ruer, Z. anorg. Chem. **43**, 282 (1905).
[2] F. P. Venable and D. H. Jackson, J. Am. Chem. Soc. **42**, 2531 (1920).
[3] M. Adolf and W. Pauli, Kolloid-Z. **29**, 173 (1921).
[4] H. T. S. Britton, J. Chem. Soc. **127**, 2120 (1925).
[5] G. Jander and K. F. Jahr, Kolloid-Beih. **43**, 295 (1936).
[6] R. E. Connick and W. H. Reas, J. Am. Chem. Soc. **73**, 1171 (1951).
[7] B. A. J. Lister and L. A. McDonald, J. Chem. Soc. **1952**, 4315.
[8] K. A. Kraus and J. S. Johnson, J. Am. Chem. Soc. **75**, 5769 (1953).
[9] J. S. Johnson, K. A. Kraus, and R. W. Holmberg, J. Am. Chem. Soc. **78**, 26 (1956).
[10] J. S. Johnson and K. A. Kraus, J. Am. Chem. Soc. **78**, 3937 (1956).
[11] A. Clearfield and P. A. Vaughan, Acta Cryst. **9**, 555 (1956).
[12] W. S. Hummers, S. Y. Tyree, and S. Yolles, *Inorganic Synthesis* (McGraw-Hill Book Company, Inc., New York, 1953), Vol. IV, p. 121.

mately 24 mg/cm² of Co. The absorption spectra of several pieces of Co filter were compared with the absorption spectrum of the Ni foil, and the piece which gave best balancing at 1.398 A ($CuK\beta_1$) was used in the diffraction measurements. The balancing method was essentially that described by Soules, Gordon, and Shaw.[13] The cell used for these experiments consisted of a block of polystyrene which had a 2.2- × 1.5- × 0.5-cm hole milled into it; the hole was covered with a thin (0.0002-in.) film of collodion. The cell was filled through a small hole in the side of the block by means of a hypodermic syringe. The data obtained by this method are not considered as satisfactory as those obtained with the crystal monochromator, particularly since diffraction at values of s ($s=4\pi\lambda^{-1}\sin\theta$; 2θ is the angle of diffraction) greater than 8 A^{-1} could not be obtained.

With both of the above techniques, the diffracted intensity was measured with a scintillation counter and pulse-height analyzer. In order to ensure that diffraction was measured against a constant total flux of incident x rays, the primary beam was continuously monitored. A piece of aluminum foil was placed in the beam, which diffracted a portion of the incident radiation into a Geiger counter. The count rate at the monitor was adjusted by means of pinhole and foils to 150-200 counts per sec, a region in which the count rate was found to be linear. By means of a relay, the Geiger counter controlled the diffracted-beam detector so that the latter was allowed to count only during the time it took the monitor to accumulate a predetermined number (usually 25 600) of counts. The diffracted beam was measured at fixed settings, and at least 2500 counts were registered at each setting. This monitor arrangement was checked by the statistical method used by Gilliam and Dole[14] and was found to give good reproducibility over a period of 4 days. As a further precaution against nonrandom errors, the measurements were alternated in such a way that no two consecutive points on the experimental curves were obtained within 2 hr of each other.

TABLE I. Data on $HfOCl_2$, $HfOBr_2$, $ZrOCl_2$, and $ZrOBr_2$ solutions.

Reference code	Compound	Molality	Density g/cm³
HC20	$HfOCl_2$	2.04	1.412
HC15	$HfOCl_2$	1.48	1.322
HC10	$HfOCl_2$	1.01	1.232
HC05	$HfOCl_2$	0.50	1.124
HB20	$HfOBr_2$	1.99	1.503
ZC20	$ZrOCl_2$	2.04	1.259
ZB20	$ZrOBr_2$	2.00	1.356

[13] H. Soules, P. Gordon, and W. Shaw, Rev. Sci. Instr. **27**, 12 (1953).
[14] E. Gilliam and D. Dole, J. Sci. Inst. **30**, 429 (1953).

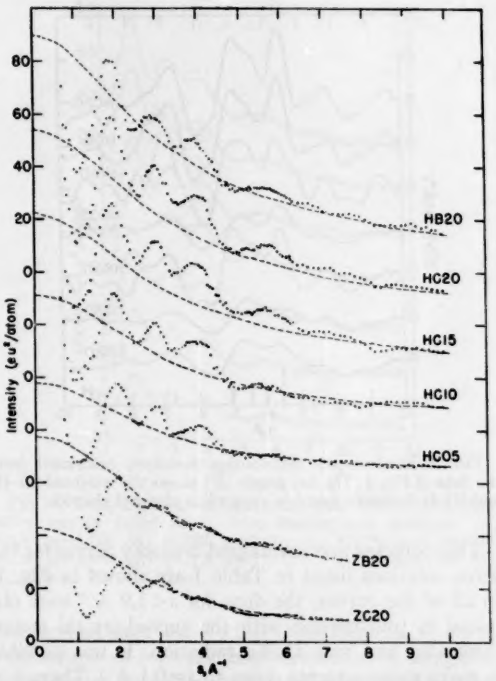

FIG. 1. Experimental data. The curves are labeled according to the code given in Table I. The dots represent the experimental points and the dashed curves are the atomic scattering curves.

Before the scattering curves were constructed, the following corrections were made to the experimentally measured intensities.

(1) The non-x-ray background was subtracted. This was measured every two hours during each run.

(2) The cell scattering was subtracted. This was obtained by measuring the scattering curve of the cell before it was filled with solution. In the transmission method, the cell scattering was multiplied by the absorption factor for the filled cell before subtraction.

(3) In the transmission method, the numbers obtained after the above corrections were divided by the absorption and volume factor, which is given by $\sec\theta\exp(-\mu t\sec\theta)$, in which μ is the linear absorption coefficient, t is the cell thickness, and 2θ is the angle of diffraction. The value of μt was calculated from transmission measurements on the full and empty cells in the primary beam.

(4) The intensities were then divided by the polarization factors, which are given by $(1+\cos^2 2\theta)/2$ for the balanced-filter method and[15] $(1+\cos^2 2\theta\cos^2 2\alpha)/(1+\cos^2 2\alpha)$ for the crystal-monochromator method. In these expressions 2θ is the angle of diffraction for the solution, and α is the Bragg angle for the monochromator crystal.

[15] L. Azaroff, Acta Cryst. **8**, 701 (1955).

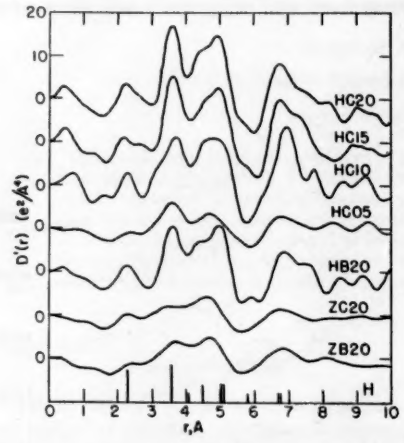

FIG. 2. Electron-pair distribution functions calculated from the data of Fig. 1. The bar graph (H) shows the weighted Hf–Hf and Hf–O distances found in crystalline zirconyl chloride.

The corrected and normalized intensity curves for the seven solutions listed in Table I are shown in Fig. 1. In all of the curves, the data for $s<1.9$ A^{-1} were obtained in transmission with the curved-crystal monochromator and with Cu$K\alpha$ radiation. It was possible to make measurements down to $s=0.1$ A^{-1}. There is a large concentration-dependent peak in the region of $s=0.4$ A^{-1} which is not shown in Fig. 1 since it is very large compared to the high-angle scattering. It does not arise from intramolecular scattering and will not be discussed in this paper. The intensity was measured at intervals of 0.063 A^{-1} in s for $s<6.3$ A^{-1} and at double this interval at higher angles.

STRUCTURE DETERMINATION

To normalize the corrected relative intensities, we used the method suggested by Krogh-Moe[16] and Norman.[17] The normalization constant is given by

$$K=\left(\int_0^{s_m} s^2 I_{at}(s)ds-2\pi^2\rho_0^2 V/N\right)\Big/\int_0^{s_m} s^2 I_{obs}(s)ds, \quad (1)$$

in which $s=(4\pi/\lambda)\sin\theta$, $I_{obs}(s)$ is the observed relative intensity function, ρ_0 is the mean electron density in the scattering sample, V/N is the volume per atom in the scattering sample, s_m is the maximum value of s and $I_{at}(s)$ was computed from the relation[18]

$$I_{at}(s)=\sum_i x_i f_i^2(s)+[1+(2h\sin^2\theta)/\lambda^2 mc]^{-2}\sum_i x_i S_i(s), \quad (2)$$

in which $f_i^2(s)$ and $S_i(s)$ are, respectively, the coherent and incoherent scattering intensities for an atom of type i, and x_i is the corresponding atom fraction. We used the atomic scattering amplitudes $f_i(s)$ given by Thomas and Umeda,[19] incoherent scattering factors for oxygen and chlorine given by Compton and Allison[20] and incoherent scattering factors for hafnium, zirconium, and bromine were calculated by a method described by Bewilogua.[21] The integrals in Eq. (1) were evaluated by means of a planimeter, and the values of ρ_0 and V/N were computed from the densities and compositions of the solutions. The curves for $KI_{obs}(s)$ are given in Fig. 1 with the corresponding functions $I_{at}(s)$ (dotted lines).

The scattering curves were first analyzed by the radial distribution method. Thus,

$$4\pi r^2 D'(r)=4\pi r^2[D(r)-\rho_0^2]$$
$$=(2rN/\pi V)\int_0^\infty s[KI_{obs}(s)-I_{at}(s)]\sin srds, \quad (3)$$

in which $D(r)$ is the radial distribution function for electron pairs which are not in the same atom. The functions $D'(r)$ for the seven solutions are given in Fig. 2. The Fourier integrals were computed by approximating them as sums, and, of course, there is an upper cutoff s_m.

The major peaks on the radial distribution functions are roughly the same as the metal-metal and metal-oxygen distances found in crystalline zirconyl chloride octahydrate,[11] as can be seen from the bar graph in Fig. 2; and a theoretical molecules scattering curve for the ion $[Hf_4(OH)_8\cdot 16H_2O]^{8+}$ was computed. For this trial structure the ion was assumed to have D_{4h} symmetry with metal-metal distances of 3.57 A and metal-oxygen distances of 2.24 A. These distances are the same as those in crystalline $ZrOCl_2\cdot 8H_2O$[11] and coincide with the first two peaks on the radial distribution functions.

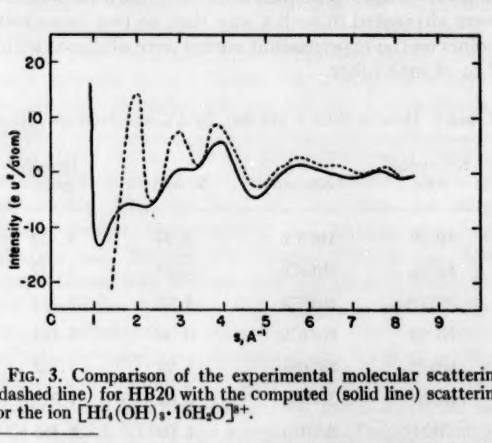

FIG. 3. Comparison of the experimental molecular scattering (dashed line) for HB20 with the computed (solid line) scattering for the ion $[Hf_4(OH)_8\cdot 16H_2O]^{8+}$.

[16] J. Krogh-Moe, Acta Cryst. **9**, 951 (1956).
[17] N. Norman, Acta Cryst. **10**, 370 (1957).
[18] R. W. James, *The Optical Principles of the Diffraction of x-rays* (G. Bell and Sons. Ltd., London, 1950), Chap. IX.
[19] L. H. Thomas and K. Umeda, J. Chem. Phys. **26**, 293 (1957).
[20] A. Compton and S. Allison, *X-rays in Theory and Experiment* (D. Van Nostrand Company, Inc., Princeton, New Jersey, 1935), p. 278.
[21] L. Bewilogua, Phys. Zeit. **32**, 740 (1931).

The antiprism arrangement about each hafnium was made as symmetrical as possible. The intensity curve is not sensitive to small changes in the oxygen positions and no further changes were made. The molecular scattering (per atom), given by

$$I_m(s) = (n/N) \sum_i \sum_j f_i f_j \, (\sin sr_{ij}/sr_{ij}), \qquad (4)$$

is shown in Fig. 3 compared with the corresponding experimental function for solution HC20, which is given by

$$I_e(s) = KI_{obs}(s) - I_{at}(s). \qquad (5)$$

In (4) n/N is the ratio of ions of $[Hf_4(OH)_8 \cdot 16H_2O]^{8+}$ to atoms computed from the composition of the solution. It is obvious that the curves do not agree very well, although agreement improves at the higher angles. To investigate the source of this disagreement, a Fourier transform of the difference between the theoretical and experimental curves was computed; and this is shown in Fig. 4. Obviously there are some important distances at about 4.6 and 7.3 A which are not accounted for by the ion $[Hf_4(OH)_8 \cdot 16H_2O]^{8+}$.

Because of the charge on the complex hafnyl tetramer, it would certainly exert a large attractive force on chloride ions; and it seems reasonable that these may occupy specific sites in the neighborhood of the ion. In the crystal, the chloride ions occupy two different sites. The first of these is approximately in the plane which contains two diagonally opposed Zr atoms and is perpendicular to the plane of the square Zr arrangement. These chlorides are at distances of approximately 4.6 A(1), 7.2 A(2), and 9.1 A(1) from the Zr atoms. The second site is approximately in the plane which is the perpendicular bisector of an edge of the Zr square, and is at distances of 4.5 A(2) and 7.1 A(2) from Zr atoms. Examination of Fig. 4 indicates that the latter site is more favorable; moreover, in the case of isolated zirconyl complexes there are eight of these

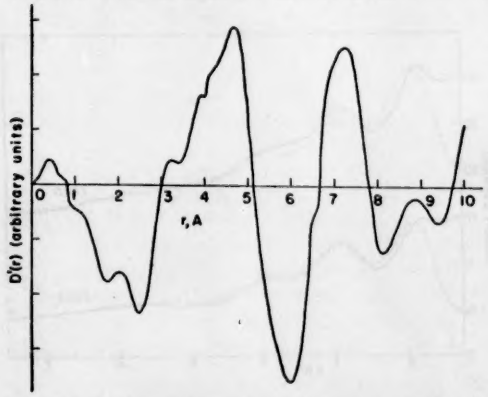

FIG. 4. Electron-pair distribution function calculated from the difference between the experimental and theoretical curves shown in Fig. 3.

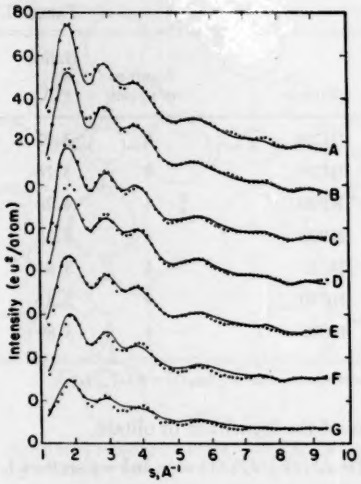

FIG. 5. Comparison of experimental data (dots) with theoretical curves (solid lines) from least-squares analyses. (A) HB20, $\alpha=1.00$; (B) HB20, $\alpha=0.60$; (C) HC20, $\alpha=1.00$; (D) HC20, $\alpha=0.60$; (E) HC15, $\alpha=1.00$; (F) HC10, $\alpha=1.00$; (G) HC20, $\alpha=1.00$.

sites around each ion. To test these ideas $I_m(s)$ curves were computed for various combinations of occupancy of these sites, and good agreement with the first three peaks on the experimental curve was obtained only when the chlorides were placed in the second of the sites described above. The same result was obtained in the case of the 2*m* hafnyl bromide solution.

To refine further the halide positions, molecular scattering curves were computed for twenty-five different models for both the bromide (HB20) and chloride (HC20), in which the halide positions were varied. The best of these was selected on the basis of agreement with the positions, shapes, and heights of the first three peaks of the experimental curves. It was found, however, that agreement between theoretical and experimental scattering curves was somewhat worse at the higher angles ($s>6$ A^{-1}) by inclusion of the halides, particularly for the bromide. Thus it appears that a temperature factor should be included in the atomic scattering factors for the halides.

The final parameters were determined by a least-squares method. The equation used was

$$kI_{obs}(s) = I_c(s) \exp(-g \sec\theta), \qquad (6)$$

in which k is an empirical scale factor, $\exp(-g \sec\theta)$, an empirical correction for the absorption factor, $I_{obs}(s)$ is the experimental intensity, and $I_c(s)$ is the sum of the theoretical atomic and molecular intensities, which is assumed to be a function of the halide coordinates x and y (see Fig. 7) and the parameter B in the temperature factor $\exp(-B\lambda^{-2} \sin^2\theta)$ applied to the halide scattering factors. We use the Taylor's series

TABLE II. Results of least-squares analyses.

Sample	Number of cycles	Halide Parameters x(A)	z(A)	B(A^{-1})	g	k	α	Standard deviation[a]	Initial μl
HC20	8	3.77	3.66	6.7	1.015	0.251	1.00	0.045	1.285
HC20	4	3.76	3.67	2.9	1.403	0.245	0.60	0.048	1.285
HB20	4	4.28	3.36	18.5	0.0629	1.120	1.00	0.060	2.415
HB20	4	4.25	3.37	10.6	0.0629	1.120	0.60	0.024	2.415
HC15	4	3.84	3.66	6.8	2.21	0.079	1.00	0.047	1.045
HC10	4	3.81	3.66	6.8	2.09	0.092	1.00	0.103	0.756
HC05	4	3.89	3.66	5.8	2.24	0.082	1.00	0.099	0.815

[a] Root-mean-square value of $[I_{obs}(s)-I_c(s)]/I_c(s)$.

expansion of the logarithm to obtain

$$\{[I_{obs}(s)-I_c^0(s)]/I_c^0(s)\}=-\ln k-g\sec\theta+[1/I_c(s)]\times\{[\partial I_c(s)/\partial x]\Delta x+[\partial I_c(s)/\partial y]\Delta y+[\partial I_c(s)/\partial B]\Delta B\} \quad (7)$$

which is linear in the five variables $\ln k$, g, Δx, Δy, and ΔB. In this expression, $I_c^0(s)$ is the intensity computed from the initial coordinates. Attempts were also made to include in the least-squares procedure an additional parameter α, which represents the average fractional occupancy of the halide sites. It was found, however, that the correlation between α and B was so large that the procedure did not converge. The least-squares analysis was carried out with 63 points from the smoothed experimental curves in the interval $s=1.6$ to 9.5 A^{-1}. The results of the analysis for the five hafnyl halide solution is summarized in Table II, and comparisons of the final computed curves with the experimental data are shown in Fig. 5. For the $2m$ solutions, analyses were carried out with $\alpha=1.00$ and $\alpha=0.60$. Acceptable results were obtained in both cases, although the result was somewhat better with hafnyl bromide for $\alpha=0.60$. The final coordinates of all of the atoms in the complex are given in Table III. The chloride parameters are those determined with the data obtained with the $2m$ solutions.

Least-squares analyses were not made with the data obtained with the zirconyl halide solutions. Fig. 6 gives a comparison of the experimental curves with calculated intensity based on the parameters found for the corresponding hafnyl solutions.

TABLE III. Final parameters for complex hafnyl halide ions. Point group D_{4h}.

Atoms	Point symmetry of position	Coordinates[a] (x, y, z) in A
4 Hf	$2m$	1.78, 1.78, 0
8 O_1	m	2.11, 0, 2.11
8 O_2	m	2.65, 2.65, 2.16
8 O_3	m	4.02, 1.66, 0
8 Cl	m	3.77, 0, 3.66
8 Br	m	4.26, 0, 3.37

[a] See Fig. 7.

DISCUSSION

A drawing of the structure is shown in Fig. 7. The degree of agreement between experimental and calculated intensities indicates very strongly that this is the predominant species in the concentration range of the hafnyl halides which we studied. For the zirconyl halide solutions, the agreement is not as good. In particular, the experimental curves lie considerably above the calculated curve for s less than 2 A^{-1}, although the general features of the two curves are similar for higher angles. This suggests that there may be more highly polymerized species in the zirconyl halide solutions. The longer distances in these species may give rise to additional scattering in the low-angle region. Kraus and Johnson[9,10] found that high polymers were present at lower pH's for zirconyl than for hafnyl solutions.

The shortest halogen-oxygen distances are 2.84, 3.24, and 4.01 A for the chloride and 2.95, 3.32, and 3.75 A for the bromide. Although the 2.84- and 2.95-A

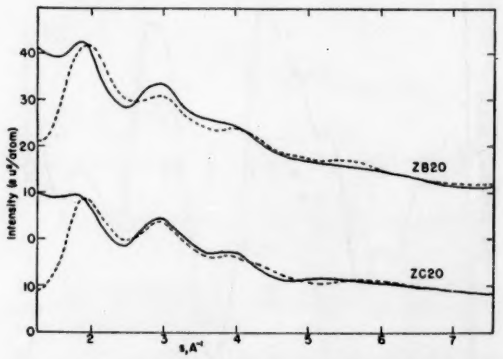

FIG. 6. Comparison of experimental data (dashed lines) for ZB20 and ZC20 with theoretical curves (solid lines) obtained with least-squares parameters found for corresponding hafnyl solutions.

distances are probably too short, they could be increased by small displacements of the oxygen atoms. Since the diffraction curve is insensitive to small variations of the oxygen position, no attempt was made to do this.

Because of the strong correlation of the occupancy factor α with the thermal parameter B, it is difficult to make definite conclusions concerning the average number of chloride ions attached to a hafnyl complex in the hafnyl chloride solution. In the case of the bromide, the agreement with the experimental curve is better for $\alpha = 0.6$ than for $\alpha = 1.0$. That bromide is more weakly bound to the complex than chloride is also indicated by the larger thermal parameter B for the bromide. The type of halide binding indicated by this investigation provides a qualitative explanation for the low rate of electromigration of the zirconium species[7] and the low chloride activity[8] in solutions of zirconyl chloride.

The "absorption" correction parameter g is rather large for the chloride solutions (see Table II); in some cases it is more than twice as large as the experimentally determined value of μt. This is a reflection of the fact, which is obvious from an inspection of Fig. 1, that the experimental scattering curves lie somewhat above the atomic scattering curves for values of s less than 5 A^{-1}. Although experimental errors in the measurement of μt might contribute to this, any source of error which would affect the average slope of the experimental curve would be included in the correction factor $\exp(-g \sec\theta)$. For example, nonuniformity in sample thickness and errors in incoherent and coherent scattering factors could have this effect. It should be noted that comparatively large values of g will produce only small changes in the slope of the curve since the values of $\sec\theta$ were in the interval 1.00–1.18 for the points used in the least-squares analysis.

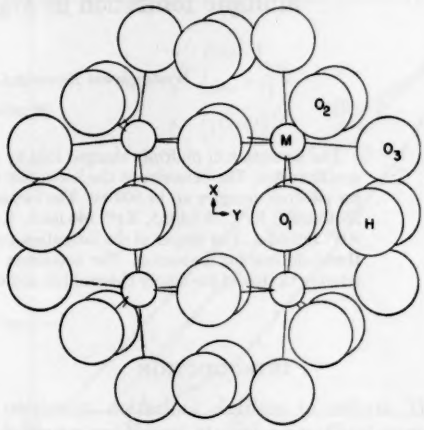

FIG. 7. Structure proposed for ion in hafnyl and zirconyl halide solutions studied in this work. M: metal; O: oxygen; H: halide.

Multiple Ionization in Argon and Krypton by Electron Impact

R. E. Fox

Westinghouse Research Laboratories, Pittsburgh 35, Pennsylvania

(Received February 4, 1960)

The formation of multiply charged ions by electron impact in argon and krypton is studied with a mass spectrometer. The behavior of the ionization cross section as a function of electron energy is investigated for electron energies up to 600 ev. The ionization potentials in ev are determined to be as follows: Kr^{2+} 38.45±0.1, Kr^{3+} 75.6±0.5, Kr^{4+} 146.6±2, Kr^{5+} 217.5±10, Kr^{6+} 350±10, Ar^{2+} 43.4±0.3, Ar^{3+} 84.8±0.5, Ar^{4+} 150.0±5. The shapes of the ionization curves near threshold are studied and discussed in terms of the threshold law for ionization. The maximum cross sections for each multiply charged ion is determined relative to that of the singly charged ion and compared to data obtained by previous investigators.

INTRODUCTION

THE studies of multiple ionization in helium and xenon by electron impact have been reported previously.[1] The work reported here is a continuation of those studies on argon and krypton. The studies were made with a 90° sectored field mass spectrometer capable of utilizing the retarding potential difference method (RPD)[2] for obtaining ionization by essentially monoenergetic electrons. The experimental procedures were the same as those reported for helium and xenon. Focusing for the ions was obtained by varying either the accelerating voltages, or the magnetic field, or both. The ion current as a function of electron energy was observed for the different ions. It was possible to make measurements for electron energies up to 800 ev.

It is apparent that instrumental effects are very difficult to eliminate from ionization probability curves taken with a mass spectrometer. It is felt that some of the points raised in this paper need further investigation. Since, however, there is no forseeable opportunity to continue these investigations and in view of the interest expressed in the obtained data, a decision was reached to submit this work for publication.

EXPERIMENTAL RESULTS

1. Krypton

The ionization curves for Kr^+, Kr^{2+}, and Kr^{3+} were obtained by using the RPD method with monoenergetic electrons. The Kr^{4+}, Kr^{5+}, and Kr^{6+} curves were obtained with the conventional electron energy spread.

The ion current near the ionization threshold for Kr^+ and for Kr^{2+} is shown in Fig. 1. The ionization for Kr^+ is observed to follow a linear threshold law. The break in the Kr^+ curve occurs at 0.6 ev above threshold, marking the onset of ionization to the $^2P_{\frac{1}{2}}$ state of the ion. The amount of tailing at the threshold is an indication of the energy spread of the electron beam. The study of this curve has been reported previously[3] in greater detail and is reported here merely to indicate the magnitude of the electron energy distribution.

Curve *b* in Fig. 1 is the ionization obtained for Kr^{2+}. The energy scale has been determined, as for all the krypton multiply charged ions, from the comparison of the Kr^+ appearance potential to the ionization potential obtained from spectroscopic data. The data do not appear to follow a simple power law.[4] There is an apparent linear onset followed by two shallow maxima on an ascending curve. The upper portion of the curve has been fitted by two linear segments though the break is an indefinite one. There are four points, however, in each portion to determine the linear segments. The spectroscopically determined energy levels are indicated by the arrows. There is reasonably good agreement between the breaks in the curve and the spectroscopic energy levels with the exception of $^1D_2$ state. In this region, however, there is considerable structure which does not appear to be instrumental in origin. Possibly this is indicative of autoionization in this region.

It has been proposed from theoretical considerations[5] that near threshold the ionization should follow the law $I_+ = CE^n$ where C is a constant of proportionality, E is the electron energy in excess of the ionization energy, and n is the degree of ionization. On the basis of this consideration, the data for Kr^{2+} has been replotted in Fig. 2 where $[I(Kr^{2+})]^{\frac{1}{2}}$ has been plotted vs the electron energy. The points should fit a straight line which extrapolates to the ionization potential. Except for the departure in the 40–41 ev region, the points lie on a straight line. This line, however, extrapolates to an ionization potential of 37.86 ev which is not in good agreement with the spectroscopic value of 38.56. Since the Kr^+ data was used to correct the energy scale it is difficult to understand how the energy scale can be in error by more than 0.1 ev. On the other hand, the plot of the ion current (I_+) vs the electron energy in Fig. 1(b)

[1] R. E. Fox, *Advances in Mass Spectrometry*, edited by S. D. Waldron (Pergamon Press, London, 1959), p. 397 ff.

[2] R. E. Fox, W. M. Hickam, D. J. Grove, and T. Kjeldaas, Rev. Sci. Instr. **26**, 1101 (1955).

[3] R. E. Fox, W. M. Hickam, and T. Kjeldaas, Phys. Rev. **89**, 555 (1953).

[4] This curve is in reasonably good agreement with a previously published curve by Hickam, Fox, and Kjeldaas, Phys. Rev. **96**, 63 (1954) in which the data points were made to fit linear segments intersecting at the spectroscopic energy levels.

[5] S. Geltman, Phys. Rev. **102**, 171 (1956).

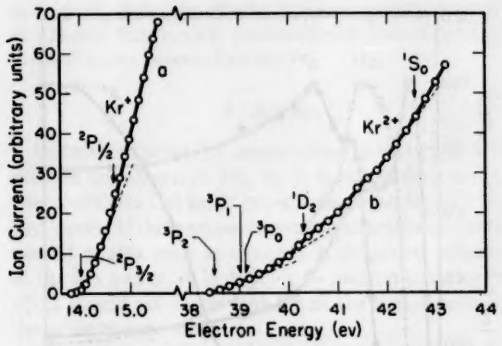

FIG. 1. Ionization by the RPD method near threshold for (a) Kr^+ and (b) Kr^{3+}. The electron energy scale was determined by correcting the Kr^+ appearance potential to the spectroscopically determined ionization potential. The arrows indicate the excited states of the ions determined spectroscopically.

yields a value of 38.48 ev for the ionization potential in satisfactory agreement with the spectroscopic value.

The data for Kr^{3+} is shown in Fig. 3. Curve 1 shows the ion current $I(Kr^{3+})$ plotted as a function of the electron energy. The energy scale has been corrected from the Kr^+ data. Here linear segments have been used to fit the data and yield an ionization potential of 75.5 ev in excellent agreement with the spectroscopic value of 75.46 ev. The linear plot of Kr^{3+} (curve 1) exhibits a break at 80 ev and a second break at about 84 ev. It is not possible to correlate these breaks with any known energy states of the ion. In curve 3 the cube root of the ionization $[I(Kr^{3+})]^{\frac{1}{3}}$ has been plotted in accordance with the theory. The linear extrapolation of the straight line fit to the data points yields the low value of 71.8 ev for the ionization potential. In curve 2 the square root of the ionization $[I(Kr^{3+})]^{\frac{1}{2}}$ has been plotted as a function of the energy. The data also fits a straight line in the initial portion but yields an ionization potential of 73.5 ev.

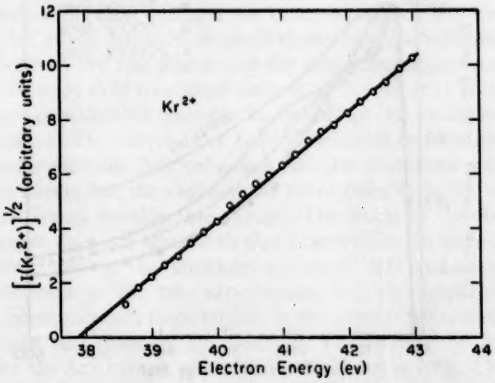

FIG. 2. $[I(Kr^{3+})]^{\frac{1}{2}}$ is plotted as a function of electron energy. The straight line fit to the data points does not yield the spectroscopic ionization potential of 38.56 ev.

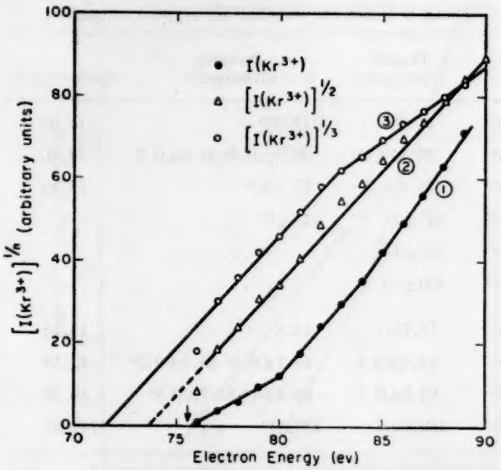

FIG. 3. Curve 1, $I(Kr^{3+})$ is plotted as a function of electron energy; curve 2, the square root of the ion current is plotted vs electron energy; curve 3, the cube root of the ion current is plotted vs electron energy. The extrapolations of the straight lines fitted to the square and cube root plots do not yield the spectroscopic ionization potential indicated by the arrow. The energy scale was determined by a slight correction of the Kr^+ data to fit the spectroscopic data. The data was obtained by the RPD method.

In Fig. 4 are shown the initial portions of the ionization curves for Kr^{4+}, Kr^{5+}, and Kr^{6+}. These curves were taken without using the RPD method. It is not possible to fit these data with straight lines by plotting the data as $[I(Kr^{n+})]^{1/n}$ where n is the appropriate degree of ionization.

The ionization potentials for the ions of krypton are summarized in Table I. The values shown are the averages of two runs and the errors assigned are a little larger than the differences obtained from the two values. There is good agreement between the values obtained in this work and the earlier work of Tate and Smith,[6] as well as with the values obtained from spectro-

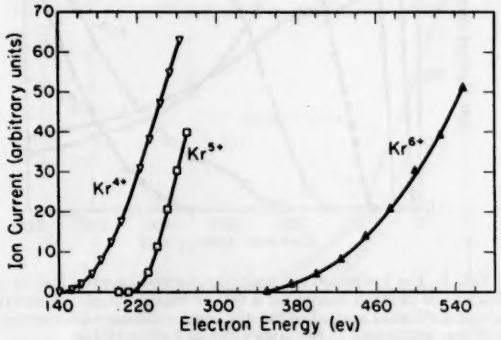

FIG. 4. Threshold ionization as a function of electron energy for Kr^{4+}, Kr^{5+}, and Kr^{6+}. The RPD method was not employed.

[6] J. T. Tate and P. T. Smith, Phys. Rev. 46, 773 (1934).

TABLE I. Ionization potentials for krypton and argon.

	Present investigator	Previous investigator	Spectroscopic
Kr^{+}	14.00[a]	13.94[b]	14.00
Kr^{2+}	38.45±.1	38.9±0.5[b] 38.6±0.2[c]	38.56
Kr^{3+}	75.6±.5	77.4±2[b]	75.46
Kr^{4+}	147±2	145±5[b]	...
Kr^{5+}	218±10	...	...
Kr^{6+}	350±10	...	...
Ar^{+}	15.76[a]	15.8	15.76
Ar^{2+}	43.4±0.3	44.1±0.5[d] 43.6±0.2[e]	43.38
Ar^{3+}	84.8±0.5	88.4±1[d] 83.7±0.5[e]	84.28
Ar^{4+}	150.0±5	259±3[d]	144.07

[a] Used as standard to calibrate energy scale.
[b] Tate and Smith.[4]
[c] Dibeler, Mohler, and Reese, J. Research Natl. Bur. Standards **38**, 617 (1947).
[d] W. Bleakney.[7]
[e] Dorman, Morrison, and Nicholson, J. Chem. Phys. **31**, 1335 (1959).

scopic data.[7] A value of about 143.5 ev for Kr^{4+} is listed by Herzberg.[8] Moore[7] does not list a value for this ion and states that the spectrum has not been sufficiently analyzed.

The ionization curves for the ions of krypton for electron energies up to 600 ev are shown in Fig. 5. All curves with the exception of Kr^{5+} and Kr^{6+} have been normalized to 100 at their maximum cross sections. The

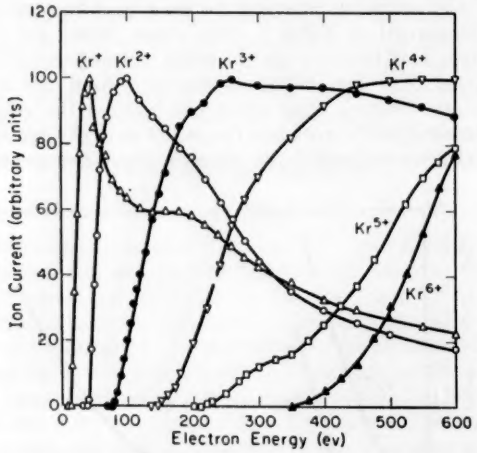

FIG. 5. The ionization for multiply charged krypton ions as a function of electron energy for a 600-ev energy range. All curves except Kr^{6+} were normalized to the same maximum ion current. Kr^{6+} was normalized to the same value as Kr^{5+} at 600 ev.

[7] C. E. Moore, *Atomic Energy Levels*, Natl. Bur. Standards Circ. No. **467**, Vol. 2 (1952).
[8] G. Herzberg, *Atomic Spectra and Atomic Structure* (Dover Publications, New York, 1944).

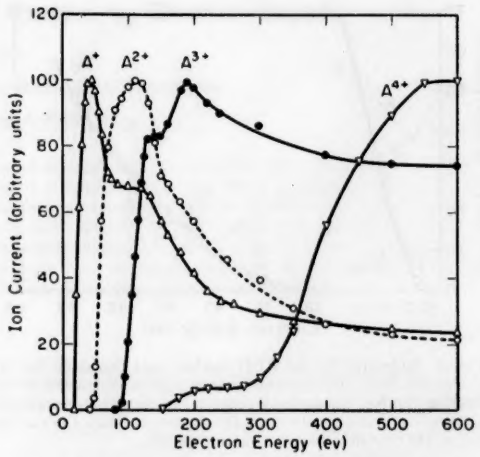

FIG. 6. Ionization curves for Ar^{+}, Ar^{2+}, Ar^{3+}, and Ar^{4+} as a function of electron energy over a 600-ev energy range. The curves were normalized to have the same maximum intensity.

relative magnitudes at the maxima are listed in Table II. It was not possible to reach the maximum cross section for Kr^{6+}. This curve was normalized to have the same magnitude as Kr^{5+} at 600 ev.

The over-all shape of the curves remained constant when the ions were focused either by changing the magnetic field or the ion-accelerating voltages. There was some lack of reproducibility especially at the higher energies with changing ion source parameters such as focusing electrode voltages and the auxillary magnetic field used for aligning the electron beam. The second maximum in Kr^{+} persisted although not always with the same intensity relative to the first maximum. This shape does not agree with that obtained by Tate

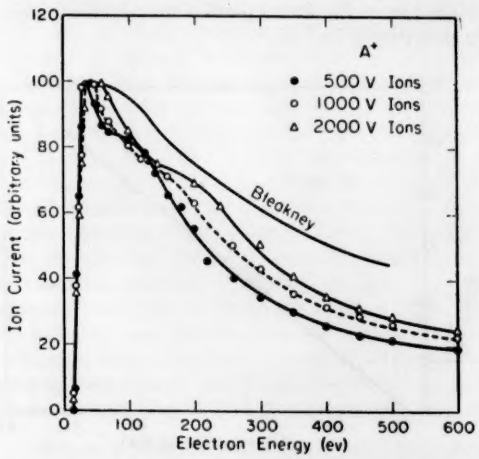

FIG. 7. Ionization of Ar^{+} as a function of electron energy for ions having different kinetic energies. The curve with no points is that obtained by Bleakney.

and Smith, their data showing no evidence of the second maximum. This second maximum was also observed in the Xe^+ curve reported earlier.[1]

2. Argon

Ionization curves for argon taken without the RPD method are shown in Fig. 6. It is noted that the Ar^+ curve exhibits the same general shape as the Kr^+ and Xe^+ curve. If these secondary maxima are due to instrumental effects such as changes in collection efficiency of the ion source, it is difficult to understand why this effect should not be evident for all the ions observed in the same energy range.

Some of the difficulty in obtaining meaningful data with a mass spectrometer is illustrated in Fig. 7. Here is shown the ionization curve for Ar^+ for three different ion energies obtained by keeping the conditions in the

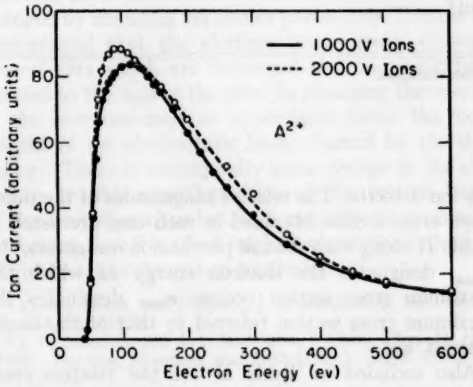

FIG. 8. Ionization of Ar^{2+} as a function of electron energy for ions having different kinetic energies.

ion source constant, with the possible exception of changes in the stray magnetic field from the main magnet resulting from changes demanded by different ion-accelerating voltages, in order to refocus the ion. This effect, however, is small since magnetic shielding between the ion source and the main magnet reduces this stray field to a small amount. It is seen that there are considerable changes in the shape of ionization curves. The curves have been normalized to have the same maxima. Not only does the first maximum shift in energy but the shape of the curve from 75 to 200 ev undergoes considerable change. The shape of the Ar^+ curve does not agree with that observed by Bleakney.[9] Not only is the structure at about 100 ev energy different in the two experiments, but the amplitude decreases much more rapidly in the present experiment than that observed by Bleakney. For example, at 250 ev the Ar^+ current observed by Bleakney is 70%. This change was not as pronounced in the curve for Ar^{2+},

[9] Walter Bleakney, Phys. Rev. **36**, 1303 (1950).

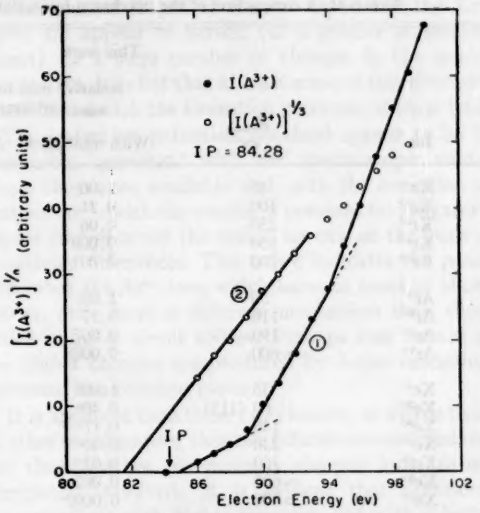

FIG. 9. Curve 1, the ionization of Ar^{3+} as a function of electron energy. The cube root of the ion current is plotted in curve 2. The straight line fit to the data points in curve 2 does not yield the spectroscopic ionization potential designated by the arrow.

shown in Fig. 8, although there seems to be a slight energy shift in the position of the maximum.

The ionization of Ar^{3+} near the threshold, taken with the RPD method, is shown in Fig. 9. Curve 1 shows the ion current plotted as a function of electron energy. The energy scale has been corrected from a comparison of the observed ionization potential of Ar^+ to the spectroscopically determined ionization potential. In this curve the data have been fitted with linear segments and yield an ionization potential of 84.6 ev as compared to the spectroscopic value of 84.28 ev. Curve 2 shows the cube root of the ion current plotted vs the electron energy. The straight line fit through

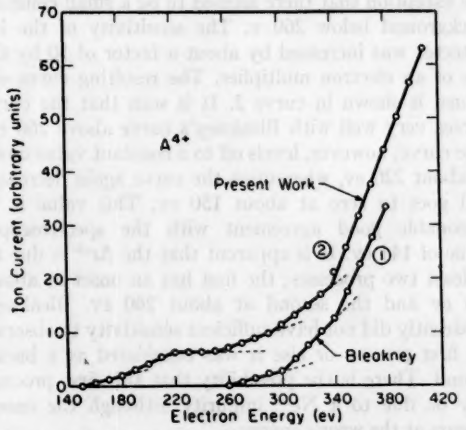

FIG. 10. The ionization of Ar^{4+} as a function of electron energy. Curve 1 shows previous results by Bleakney. Curve 2 shows present results obtained with increased detector sensitivity.

TABLE II. A comparison of the maximum ionization probabilities for multiply charged ions of Xe, Kr, and Ar.

	This work			Previous work	
		Relative max ion intensity σ_{max} (arbitrary units)			
Ion	$E_{\sigma max}$ ev	With multiplier	No multiplier[a]	$E_{\sigma max}$ ev	Relative[a] σ_{max} (arbitrary units)
Kr^+	45	1.00	1.00	50	1.00[b]
Kr^{2+}	100	0.21	0.095	90	0.13[b]
Kr^{3+}	250	0.06	0.012	~300	0.017[b]
Kr^{4+}	550	0.008	0.0005	...	0.0018[b]
Kr^{5+}	~780	0.001	...	...	...
Ar^+	50	1.00	1.00	50	1.00
Ar^{2+}	110	0.17	0.07	120	0.10[c] 0.11[d]
Ar^{3+}	190	0.007	0.001	~200	0.005[c]
Ar^{4+}	~600	0.0008	0.00009	...	0.0007[c]
Xe^+	35	1.00[e]	1.00		1.00[b]
Xe^{2+}	60 (115)	0.40[e]	0.18		0.16[b]
Xe^{3+}	135	0.17[e]	0.05		0.05[b]
Xe^{4+}	230	0.06[e]	0.009		0.01[b]
Xe^{5+}	360	0.02[e]	0.003		0.004[b]
Xe^{6+}	~600	0.002[e]	0.00015		
Xe^{7+}	>600	0.0002[e]			

[a] These values are obtained by dividing the current ratios by the appropriate number of charges.
[b] Tate and Smith.[6]
[c] Bleakney.[9]
[d] Stevenson and Hipple.[10]
[e] Fox.[1]

the initial points extrapolates to an ionization potential of 81.5 ev which is not in agreement with the spectroscopic value.

A list of the ionization potentials for argon is given in Table I, where the values are the averages of two determinations with the exception of Ar^{4+} which is based on a single determination.

A very interesting comparison of the Ar^{4+} curve is shown in Fig. 10. The curve obtained by Bleakney[9] is shown yielding an ionization potential of 258 ev. In the present experiment the first runs obtained showed a remarkable agreement with Bleakney's curve with the exception that there seemed to be a small constant background below 260 v. The sensitivity of the ion detector was increased by about a factor of 10 by the use of an electron multiplier. The resulting curve obtained is shown in curve 2. It is seen that the curve agrees very well with Bleakney's curve above 260 ev. The curve, however, levels off to a constant value down to about 220 ev, whereupon the curve again decreases and goes to zero at about 150 ev. This value is in reasonable good agreement with the spectroscopic value of 144 ev. It is apparent that the Ar^{4+} is due to at least two processes; the first has an onset at about 150 ev and the second at about 260 ev. Bleakney apparently did not have sufficient sensitivity to observe the first process or else it was considered as a background. There is the possibility that this first process may be due to a Ne^{2+} impurity although the onset appears at the wrong energy.

The ionization curves for krypton and argon were observed with and without an electron multiplier as the ion detector. The relative magnitudes of the maximum cross section obtained in each case are listed in Table II along with data of previous investigators.[6,9,10] $E_{\sigma_{max}}$ designates the electron energy at which the maximum cross section occurs. σ_{max} designates the maximum cross section referred to that of the singly charged ion.

Also included in Table II are the relative cross sections of the multiply charged ions of xenon taken without a multiplier. The data taken with the multiplier have been previously reported.[1]

For the data taken without the multiplier, the ions strike the collector with essentially zero energy (<3ev) since both the ion source and ion collector are at ground potential. For the data taken with the multiplier the energy of the ions striking the first dynode depends upon the ionic charge since the potential of the first dynode is held constant with respect to the ion source. The differences in the two cases would presumably be due to the dependence of the secondary electron coefficient as a function of kinetic energy and charge. Since the first dynode was 3000 ev above ground, the energy of the singly charged ions striking the first dynode was 3000 ev.

DISCUSSION

The ionization probability curves for multiply charged ions have yielded conflicting results which are not readily resolved. These data on Kr and Ar, as well as previous data on Xe[1] obtained with the use of monoenergetic electrons, indicate that linear threshold

[10] D. P. Stevenson and J. A. Hipple, Phys. Rev. 62, 237 (1942).

law fits the observed data better than the appropriate higher-power law predicted from theoretical considerations. Recent experiments by Krauss, Reese, and Diebeler[11] and by Morrison *et al.*[12] on the multiply charged ions of the rare gases produce results which are in apparent agreement with the theory.[3] However, in both these experiments the electron beam possessed a very large energy spread (~2 ev) although it is not clear why this should be important at these energies. It is seen from Figs. 2, 3, and 9 that the appropriate root of the ion current plotted against the electron energy can be made to fit a linear curve. These curves however, do not yield the proper appearance potentials. This effect which is also evident from the data of Morrison *et al.*,[12] has also been observed by Diebeler *et al.*

The shapes of the ionization probability curves over large energy ranges (600 ev) appear to be open to some question since some of the observed structure can be changed by changing ion source parameters. It must be remembered that the electron beam passes through several slits which are immersed in a magnetic field parallel to the axis of the slits. In changing the energy of the electrons over an appreciable range, the focal lengths of the electrostatic lenses formed by the slits change. There is undoubtedly some change in the size and/or possible spatial position of the electron beam in the ionization chamber. It is not easy to determine the extent that this effect might have on the collection efficiency of the slit system for the ions.

[11] Krauss, Reese, and Diebeler, J. Research Natl. Bur. Standards **63A**, 201 (1959).

[12] J. D. Morrison and A. J. Nicholson, J. Chem. Phys. **31**, 1320 (1959); Dorman, Morrison, and Nicholson, J. Chem. Phys. **31**, 1335 (1959).

The unusual shapes of the Ar^+ curve and the Kr^+ curve did appear to persist (to a greater or smaller extent) for a large number of changes in the source parameters. It is felt that at least some of this structure is associated with the ionization processes of these ions.

The ionization potentials obtained appear to be in reasonable agreement with the spectroscopic values where they were available and, with the exception of that for Ar^{4+}, with the results of previous investigators. Figure 10 points out the reason for this on the basis of sensitivity differences. This curve indicates the possibility that the Ar^{4+} ions, which have an onset at about 260 ev, arise from a different mechanism than those which onset at about 150 ev. Perhaps ions formed at the higher energies are produced by Auger cascading, discussed in a previous paper.[1]

It is apparent from these experiments, as well as those of other investigators, that the difficulties in determining the threshold law for multiply charged ions are not completely resolved. It is evident that additional investigations with higher precision and with a better understanding of the ion source behavior are necessary before some of the difficulties can be satisfactorily answered.

The values for the appearance potentials obtained in this work are in good agreement with those spectroscopic ionization potentials which have been determined. The values for the relative maximum ionization probabilities are in reasonably good agreement with those obtained by previous investigators. Further investigations on the shapes of ionization probability curves over large energy ranges will be necessary before the true shapes can be known with a large degree of confidence.

Flow Adaptation of the Isotopic Dilution Method for the Study of Ionic Hydration

H. W. BALDWIN* AND H. TAUBE

George Herbert Jones Laboratory, University of Chicago, Chicago, Illinois

(Received January 21, 1960)

A method is described for rapid mixing and sampling in the application of the isotopic dilution technique to the study of ionic hydration. The behavior of solutions of various salts has been compared with that of solutions containing a hydrated cation of known formula, namely $Cr(H_2O)_6^{+++}$. The holdback of water per ion of Al^{+++} is the same (within 0.4 molecules of H_2O as that of Cr^{+++}, and $t_{\frac{1}{2}}$ for the exchange of $Al(H_2O)_6^{+++}$ with H_2O is >0.02 sec. at 25°. $t_{\frac{1}{2}}$ for the exchange of water between Ni^{++} (aq) or Fe^{+++} (aq) and solvent is less than 0.02 sec.

THE isotopic dilution technique for determining the number of water molecules bound in aquo cations in aqueous solution has thus far been applied successfully[1] only to $Cr(H_2O)_6^{+++}$. The feature which more than any other limits the scope of the method is the time taken between mixing the O^{18} enriched water with the solution of the salt to be studied and sampling the solvent to determine its isotopic composition. Thus far only batch operating procedures have been used, the two solutions being mixed by pouring, and sampling being accomplished by withdrawing water vapor by vacuum distillation. It is difficult in a batch operation of this kind to reduce the time between mixing and sampling to much less than a minute, a time which is long compared to the half-time for the exchange of the hydration water of many cations with solvent.

By using a flow technique it is possible to reduce greatly the time between mixing and sampling. In this paper we describe the adaptation we have made of the flow method to the problem at hand, and the results obtained applying the method to several cations. The method is not yet a dependably absolute one, but by calibrating it with an ion of known formula and kinetic behavior such as $Cr(H_2O)_6^{+++}$ some definite conclusions have been reached about the hydration of other cations.

METHOD

The apparatus used for mixing and sampling the solutions is shown in Fig. 1. The solution of salt in ordinary water, and water enriched in O^{18} separately enter the mixing chamber. The combined solution flows through a short length of capillary, then issues into the gas space, and finally disappears below the surface of *n*-pentane cooled to −78°C. Sampling of the solvent is accomplished by evaporation from the combined stream in transit, dry N_2 being used to conduct the water vapor to a collecting trap. Thus the time between mixing and sampling is the time required for the solution to flow from the mixing chamber to the surface of the *n*-pentane.

Experiments were conducted with two sets of apparatus. The mixing chambers differed only slightly in dimensions for the two, and the major difference was in the means used for impelling the solutions. In the first series of experiments, the solutions were driven from the reservoirs by gas pressure, but in the later series by pistons actuated by a mechanical drive. The change to the mechanically driven pistons was made because it was felt that the tendency for the streams to pulse, or alternate in flow would be less with it than with the other apparatus. However, the performance of the second apparatus did not prove to be superior to the earlier. But it was somewhat more versatile because with it we were able conveniently to vary the rate of solution flow over a wider range.

The mixing chambers were of conventional design, the separate streams entering the chambers tangentially and the combined stream then leaving in a direction perpendicular to the plan defined by the feed tubes. Some dimensions for the mixing chamber used for the second series of experiments are recorded herewith, more as a warning to other experimenters who may be interested, than as a recommendation (as the results to be described indicate, mixing was probably not complete in the experiments done with the second apparatus). A lucite block was used, and inlet tunnels were drilled 0.41 mm in diam. The exit tunnel was drilled 0.92 mm in diam, and was fitted with a stainless steel tube 0.95 mm o.d., 0.64 mm i.d. The steel tube was not forced quite to the height of the orifices of the inlet tunnels but a length of ca 1 mm was left to provide a mixing chamber of larger diameter than the exit tube. The distance traversed by the stream of solution before it entered the quenching liquid was about 2 cm.

The dry N_2 used as carrying gas was obtained by boiling liquid N_2. The rate of flow was controlled by the rate at which heat was supplied to the storage Dewar, and was measured by a flow meter. The temperature of the N_2 was controlled by electric heaters.

The data needed for the determination of water holdback by the salt in the mixed solution are: (a) the chemical composition of the salt solution before mixing, (b) the isotopic composition of the O^{18} enriched water, and the water in the salt solution before mixing, (c) the isotopic composition of the solution after complete exchange of hydration water with solvent, and (d) the

* Present address: Department of Chemistry, University of Western Ontario, London, Ontario.

[1] J. P. Hunt and H. Taube, J. Chem. Phys. **19**, 602 (1951).

isotopic composition of the solvent in the solution after mixing but before exchange has taken place.

The data called for under (a) are obtained without difficulty. The data called for under (b) and (c) were obtained by evaporating water from the liquids in question, and equilibrating the water obtained with CO_2. Relatively large quantities of water (ca 50 mg) were collected for these analyses, and the distillation was carried out to approximate equilibrium conditions. Successive samples of vapor were removed from 15 ml of liquid placed in a large volume, time being allowed between sampling to allow equilibrium to be established. Allowance was made for the isotope fractionation on distillation ($d \ln O^{16}/d \ln O^{18} = 1.008$ *vide infra*).

Some difficulty in isotopic analysis of the mixed solution collected at the end of the run was encountered in early experiments in which petroleum ether was used as quenching liquid, and this difficulty was also met in the determinations required under (d). Some components of the petroleum ether were carried over into the CO_2 and resulted in spurious readings of the isotopic composition of the CO_2. This difficulty was readily eliminated by changing to pure *n*-pentane as the quenching liquid, although the cause of the difficulty was not so readily recognized.

The chief problems arise in the determinations required for (d). The amount of distillate water which is collected for a reasonable expenditure of O^{18} enriched water is small (in a typical experiment 4 mg for 30 ml of enriched water). An obvious consequence of the small sample size is the liability of the distillate to isotopic contamination by water adhering to the glass surface to which the sample is exposed. A systematic study of the magnitude of the effects arising from the source was made, and the procedure was modified by seasoning the trap and other containers with water of nearly the isotopic composition of that expected for the distillation. Even without this precaution, these effects were not serious and they are eliminated by this step of the procedure.

In determining the isotopic composition of water by equilibrating it with CO_2,[2] the relative amounts of the two substances must be known, unless the liquid is used in large excess. For samples of water as small as those collected in each run, the amount of water relative to that of the CO_2 must be known accurately, because there is considerable isotopic dilution of the water by the CO_2. The direct determination of the water by weighing is difficult to make with sufficient accuracy, and a procedure was adopted which is in effect equivalent to determining the amount of water by isotopic dilution.[3] The sample of water is equilibrated first with a known amount of CO_2 of known isotopic composition close to that of the liquid. This CO_2 is removed for isotopic analysis, and a second sample is introduced, the same in amount and of known isotopic composition differing widely from that of the first sample. The ratios of the intensities for $CO^{16}O^{16}$ compared to $CO^{16}O^{18}$, initial and final, for each of the two samples of CO_2 serve to fix the initial isotopic composition of the sample of water distilled. The equation which relates the atom fraction of O^{18} in the water (N) to the isotopic ratios determined in the CO_2 is

$$N = ({}^1R_e K + 1)^{-1} + \left[\frac{({}^1R_e K + 1)^{-1} - ({}^2R_e K + 1)^{-1}}{({}^2R_e + \tfrac{1}{2})^{-1} - ({}^2R_o + \tfrac{1}{2})^{-1}}\right] [({}^1R_e + \tfrac{1}{2})^{-1} - ({}^1R_o + \tfrac{1}{2})^{-1}]$$

where K is the equilibrium constant for the exchange reaction

$$H_2O^{18} + CO_2{}^{16}{}_{gas} = H_2O^{16} + CO^{16}O^{18}$$

(and is 2.080 at 20°).[4] The symbols R represent the intensity ratios $CO^{16}O^{16}/CO^{16}O^{18}$, the left superscripts 1 and 2 designate the first and second samples of CO_2, and the right subscripts o and e designate before and after equilibration. This equation is derived making an extension of that of Dostrovsky and Klein.[5]

The precision of the method can be gauged by the results of two series of experiments herewith reported. Within each series, 4 identical samples were used, each

TABLE I. Isotopic Fractionation in Evaporation from the Flowing Stream. (Temperature of liquid, 22–24°, rate of liquid flow, 22.5 ml/min, temp of N_2 = 44°; apparatus No. 2).

Atom % O^{18} in liquid	Atom % O^{18} in evaporated liquid
0.2130	0.2058
	0.2059
	0.2059
Mean	0.2059

$d \ln H_2O^{16}/d \ln H_2O^{18} = 1.034$

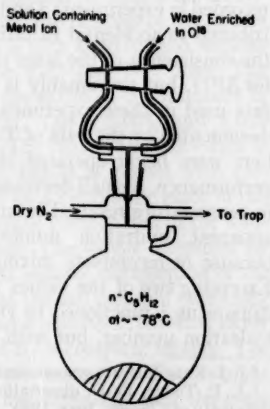

FIG. 1. Apparatus for rapid mixing and isotopic sampling of solvent.

[2] M. Cohn and H. C. Urey, J. Am. Chem. Soc. **60**, 679 (1938).
[3] This method was suggested in the course of a discussion of the problem of analysis with H. R. Hunt.
[4] H. C. Urey, J. Chem. Soc. **1947**, 562.
[5] I. Dostrovsky and F. S. Klein, Anal. Chem. **24**, 414 (1952).

TABLE II. Attempts to determine hydration number using apparatus no. 1 (nitrate salts, temp 23°).

No.	Cation	Molality		Rate of flow ml/min	Atom % O^{18} before mixing		Atom % O^{18} in solution		Hyd No.
		Before mixing	After mixing		Solvent H_2O	Enriched H_2O	Flowing stream	After exchange	
1[a]	Cr(III)	2.23	0.77	20.0[b]	0.2622	2.9843	1.469	1.377	5.5
2[a]	Cr(III)	2.23	0.79	23.5	0.2622	1.9843	1.466	1.377	5.2
3	Cr(III)	2.23	1.03	19.2	0.2703	2.0739	1.453	1.268	8.4
4	Cr(III)	2.23	1.05	18.7	0.2703	2.0739	1.452	1.260	8.6
5	Al(III)	2.56	0.73	26.4	0.2622	1.9843	1.585	1.471	6.5
6	Al(III)	2.59	0.65	27.8	0.2703	2.0739	1.728	1.623	6.2
7	Al(III)	2.59	0.61	26.5	0.2703	2.0739	1.734	1.651	5.3
8	Al(III)	2.61	0.91	26.5	0.2703	2.0739	1.586	1.466	5.7
9	Al(III)	2.61	0.92	25.6	0.2703	2.0739	1.582	1.449	6.1
10	Ni(II)	2.2	1.0	25.0	0.2703	2.0739	1.090	1.079	...

[a] Isotopic analysis by BrF_3. All others by double equilibration.
[b] With this apparatus, a flow rate of 25 ml/min corresponds to a time between mixing and quenching of 2.4×10^{-3} sec.

sample being approximately 5 mg by weight. The values of N calculated for the samples of the one series were 1.1791, 1.1789, 1.1795, and 1.1773 atom % O^{18}, and for the other 0.6664, 0.6667, 0.6670, 0.6641 atom % O^{18}.

Having determined the isotopic composition of the water distilled from the stream as outlined above, allowance must also be made for the isotopic fractionation which takes place on evaporation. This fractionation factor ($d\ln H_2O^{16}/d\ln H_2O^{18}$) has been reported[1] to be 1.009 ± 0.001 in rapid low-pressure distillation from a pot of liquid, and this value is close to that measured in the present work for the same type of process (1.008 ± 0.001). When evaporation takes place from the flowing stream, isotopic fractionation is much more marked. Table I presents the results obtained in a series of experiments corresponding as closely as possible to the conditions used for the determination of hydration numbers.

A series of experiments undertaken to study the factors that may affect the fractionation factor on evaporation (rate of liquid flow varied from 15 to 42 ml/min, temp of N_2 gas 44° or 64°, rate of N_2 flow varied by a factor of 2) gave values of $d\ln H_2O^{16}/d\ln H_2O^{18}$ ranging from 1.026 to 1.035, but showed no systematic variation with the variables introduced. In fact, the variability observed can be attributed largely to the contamination of the samples by spurious masses derived from the organic solvent which in this series was petroleum ether (in the series of Table I, done later, pure *n*-pentane was used as the quenching liquid).

In the earliest experiments, an attempt was made to do the isotopic analyses by oxidizing the water with BrF_3. Reasonable results were obtained in the first analyses, but the results became progressively worse as we continued to use the apparatus. The difficulty was with memory effects, and these become serious when water is distilled through a metal vacuum line through which BrF_3 is also distilled. The experience of others[6,7] has shown that the BrF_3 method can in fact be used for the analysis of water, but contact of the water vapor with the line must be restricted to the reaction chamber, and only a slight excess of BrF_3 can be used.[7] Unfortunately, this information came to our notice too late to be of use to us.

RESULTS AND DISCUSSION

The results of the experiments done with the gas-driven apparatus are shown in Table II, and those done with the mechanically-driven unit in Table III.

Some conclusions of a semiquantitative nature are indicated by the data of Table II obtained with Apparatus 1. Holdback of water by Cr^{3+} is demonstrated, reasonably close to the value of 6.0 expected for the ion.[1] Of the 4 values recorded for Cr^{3+} only the first two should be considered. The higher values recorded in experiments 3 and 4 can probably not be attributed to accidental variation (in this connection note the consistency of the large number of values measured for Al^{3+}), but presumably is a result of the lower flow rate used in these experiments. As is more completely documented by the data of Table III, the mixing chambers were being operated close to a critical level of performance. A small decrease in flow rate, or a decrease in temperature resulted in unreasonable values for the apparent hydration number of Cr^{3+}, presumably because of incomplete mixing under these conditions. Excepting two of the values for Cr^{3+}, it appears that Apparatus 1 functioned to yield absolute values of the hydration number, but with considerable imprecision.

[6] J. J. Katz (private communication).
[7] A. P. Tudge, Ph.D. dissertation, Department of Chemistry, University of Chicago, June, 1959.

TABLE III. Attempts to determine hydration number using Apparatus 2[a] (at 23°, solutions acidified).

No.	Salt	Molality		Rate of flow ml/min^{-1}	Atom % O^{18} before mixing		Atom % O^{18} in solution		Hyd no.
		Before mixing	After mixing		Solvent	Enriched water	Flowing stream	After exchange	
1	$Cr(NO_3)_3$	2.39	1.14	30.0	0.2076	1.6949	1.132	1.005	8.0
2	$Cr(NO_3)_3$	2.39	1.13	30.0	0.2076	1.6949	1.0835	1.004	6.6
3	$Cr(NO_3)_3$	2.39	1.14	30.0	0.2076	1.6949	1.086	1.005	6.5
4	$Al(NO_3)_3$	2.36	1.11	15.5	0.2075	1.6786	1.175	0.993	11.2
5	$Al(NO_3)_3$	2.36	1.10	15.5	0.2075	1.6916	1.238	0.994	14.1
6	$Al(NO_3)_3$	2.41	1.13	22.7	0.2126	1.6803	1.089	0.996	7.2
7	$Al(NO_3)_3$	2.41	1.12	22.7	0.2126	1.6803	1.056	0.995	5.7
8	$Al(NO_3)_3$	2.41	1.13	22.7	0.2132	1.6623	1.074	0.991	6.8
9	$Al(NO_3)_3$	2.41	1.13	22.7	0.2132	1.6623	1.078	0.993	6.8
10	$Al(NO_3)_3$	2.37	1.11	30.0	0.2075	1.6949	1.078	1.002	6.4
11	$Al(NO_3)_3$	2.37	1.11	30.0	0.2075	1.6949	1.075	1.002	6.3
12	$Al(NO_3)_3$	2.37	1.12	30.0	0.2075	1.6949	1.074	1.001	6.3
13	$Al(NO_3)_3$	2.37	1.14	30.0	0.2075	1.6949	1.073	1.000	6.2
14	$Fe(ClO_4)_3$	2.0	1.1	30.0	0.2069	1.702	1.030	1.067	...
15	$Fe(ClO_4)_3$	2.0	1.1	30.0	0.2069	1.702	1.028	1.070	...
16	$Fe(ClO_4)_3$	2.0	1.1	30.0	0.2069	1.702	1.036	1.069	...
17	$Ni(NO_3)_2$	2.0	1.1	30.0	0.2080	1.702	0.928	0.988	...
18	$Ni(NO_3)_2$	2.0	1.1	30.0	0.2080	1.702	0.969	0.988	...

[a] Flow rate of 30 ml/min corresponds to an interval of 3.4×10^{-2} sec between mixing and sampling.

We conclude from the data that the hydration number of Al^{3+} is 6 ± 0.5, and that the half-time for the exchange between $Al(H_2O)_6^{3+}$ and H_2O is greater than 2×10^{-2} sec. Ni^{2+} shows no significant hold-back, and the half-time for the exchange of water between Ni^{2+} (aq) and solvent is less than 10^{-2} sec at 25°.

The data obtained with Apparatus 2 and reported in Table III do not admit of as direct an interpretation as do those for Apparatus 1. The results obtained in Experiments 14 to 18 of Table III at once show a curious anomaly. For all of them, the relation of the figures in the 8th and 9th columns is such as to suggest *negative* hydration numbers for the Fe^{3+} and Ni^{2+} ions. The effect is fairly consistent, the ratios of the numbers in question being 1.036, 1.051, 1.031, 1.064, and 1.020 for Experiments 14 to 18. The reason for this effect is not known with certainty, but it is known with certainty that it is not caused by a systematic error in the value measured for the isotopic composition of the solution after complete exchange. The values computed by taking account of the initial isotopic composition of the solution, and the dilution of the salt solution on mixing agree quite closely with those observed. It seems likely that the effects are caused by incomplete mixing. The velocity of the liquids is low enough so that laminar flow is obtained; and it is not impossible that the more viscous salt solution is slightly concentrated at the surface of the flowing stream.

If the data are treated by assuming that the mean of the ratios recorded in the previous paragraph is a measure of the anomaly for all the experiments, and if this is applied as a correction factor to all the data, the values for hydration number recorded in the last column are calculated. The fact that a value for n close to the known value of 6.0 for Cr^{3+} (aq) is observed, indicates that this procedure is approximately justified; or stated conversely, the data indicate that Fe^{3+} and Ni^{2+} hold back approximately six less water molecules than does Cr^{3+}.

In Experiments 5–13 reasonably consistent values for the hydration number of Al^{3+} are observed, and the comparison with the results for Cr^{3+} shows that the holdback for Al^{3+} is very nearly the same as for Cr^{3+}, in agreement with the conclusion from the data of Table II. The results of Experiments 4 and 5 indicate incomplete mixing of the solution at the lower flow rate. If for example, alternate slugs of liquid pass down the tube, there will be more evaporation from the saltfree liquid containing the excess H_2O^{18}, and high values of holdback are simulated. A number of experiments were also done at 4°C. These in many cases also gave results corresponding to unreasonably large

holdback. They are not reported in detail, and serve only to confirm our belief that Mixing Chamber II also operated close to a critical mode.

The high values of the fractionation factor observed on evaporating from the flowing stream deserve some comment. For an evaporation process in which each molecule which leaves the liquid is removed from the system, and in which exchange equilibrium between the body of the liquid and the surface film is maintained, a maximum fractionation factor of $(18/16)^{\frac{1}{2}} \times 1.008 = 1.066$ (the first factor arises from the mobility of the H_2O^{16} compared to H_2O^{18}, and the second is the equilibrium fractionation factor) would be measured. In ordinary vacuum distillation from a pot, equilibrium between the surface film and the liquid may not be maintained, and the process may correspond closely to skinning off successive layers of liquid. In the flowing steam, it is possible that equilibrium between the surface film and the body of the liquid is better maintained by turbulence in the stream, than is the case when distillation takes place from bulk, quiescent liquid.

ACKNOWLEDGMENT

This work was supported in its initial stages by the Office of Naval Research and later by the U. S. Atomic Energy Commission. We are indebted to E. L. King for clarification on several points in this paper.

THE JOURNAL OF CHEMICAL PHYSICS VOLUME 33, NUMBER 1 JULY, 1960

Dielectric Behavior and Crystal Structure of Ethyl and Vinyl Stearate*

MARTIN G. BROADHURST† AND EDWIN R. FITZGERALD

Department of Physics, The Pennsylvania State University, University Park, Pennsylvania

(Received January 28, 1960)

Measurements of the real (ϵ') and imaginary (ϵ'') components of the complex dielectric constant have been made on ethyl and vinyl stearate and on mixtures of ethyl stearate in *n*-heneicosane at temperatures from +60° to −80°C and over a frequency range from 100 to 50 000 cps. A relaxation dispersion region, which was similar in shape and position for all samples, occurred below 0°C for the frequency range considered here. The magnitudes of the dispersions were found to be greater the more quickly the samples were frozen, and very much reduced for samples crystallized from acetone. Annealing of the solid samples at temperatures as low as 20 centigrade degrees below the freezing points resulted in a gradual decrease in polarization. Cooling curve data was obtained in order to supplement the above work. The results suggest that the molecular rotations involved in the observed solid state dispersions are associated with metastable crystal structures and that, in particular, the decrease in polarization with time is due to a gradual transformation in parts of the sample from a vertical to a tilted crystal structure.

I. INTRODUCTION

THE dielectric properties of long-chain organic compounds have received much attention both experimentally and theoretically, and attempts have been made to correlate observed long-chain behavior with crystal structures and dipolar motions. In particular, many esters, both as pure solids[1–4] and in solid paraffin solutions,[5–6] exhibit one or more dielectric relaxation dispersions. These dispersion effects have been observed to be strongly dependent on the rate at which samples are frozen, on the sample storage time, and on the amount of mechanical working undergone by the sample. Orientation polarization in solid esters has previously been attributed to motions of molecules that freeze with their dipoles out of the dipolar plane.[7]

Although there have been no previous dielectric data reported for vinyl stearate, ethyl stearate has been the subject of extensive study. Malkin[8] found that ethyl stearate was polymorphic and occurred in both an α form where the carbon chains are perpendicular to the plane formed by the end groups, and a β form where the carbon chains are tilted with respect to the end group plane. Baker and Smyth[9] studied the dielectric properties of ethyl stearate and reported no molecular rotation below the vertical-tilted transformation temperature ($\approx$25°C). Pelmore,[10] however, found that a solid mixture of ethyl stearate in hexadecane exhibited dielectric dispersion. Dryden and Dasgupta[3] found a

* Based in part on a thesis submitted by Martin G. Broadhurst in partial fulfillment of the requirements for the Ph.D. degree Pennsylvania State University, 1959.

† Present address: Dielectrics Section, National Bureau of Standards, Washington, D. C.

[1] R. W. Crowe and C. P. Smyth, J. Am. Chem. Soc. **73**, 5401 (1951).

[2] J. S. Dryden and H. K. Welsh, Australian J. Sci. Research **A4**, 616 (1951).

[3] J. S. Dryden and S. Dasgupta, Trans. Faraday Soc. **51**, 1661 (1955).

[4] J. S. Dryden, J. Chem. Phys. **26**, 604 (1957).

[5] W. Jackson, Proc. Roy. Soc. (London) **A150**, 197 (1935).

[6] R. T. Meakins, Australian J. Sci. Research **A2**, 405 (1949).

[7] R. W. Crowe, J. D. Hoffman, and C. P. Smyth, J. Chem. Phys. **20**, 550 (1952).

[8] T. Malkin, Trans. Faraday Soc. **29**, 977 (1933).

[9] W. O. Baker and C. P. Smyth, J. Am. Chem. Soc. **60**, 1229 (1938).

[10] D. R. Pelmore, Proc. Roy. Soc. (London) **A172**, 502 (1939).

relaxation loss peak in ethyl stearate at room temperature with a maximum at 10^7 cps.

In the present work, the dielectric properties of ethyl stearate and vinyl stearate are reported for temperatures between +50°C and −80°C and for frequencies from 100 to 50 000 cps. In the same frequency and temperature range, dielectric data are also reported for a 10% mixture of ethyl stearate in normal heneicosane. The mixture was thought to be of particular interest since the dimensions of the heneicosane lattice[11] appear to be identical with the lattice dimensions of ethyl stearate in the vertical form.

II. DETERMINATION OF THE COMPLEX DIELECTRIC CONSTANT

The complex dielectric constant can be written as the sum of a real and imaginary part $\epsilon^*=\epsilon'-\epsilon''$. The ordinary dielectric constant $\epsilon'=C/C_0$ and loss factor $\epsilon''=G/\omega C_0$ are determined from bridge measurements of the capacitance C and the conductance G of the dielectric cell containing the sample. C_0 is the measured capacitance of the empty dielectric cell and $\omega=2\pi\times$ frequency. The capacitance and conductance were measured using a Leeds and Northrup model 1554 capacitance and conductance bridge, modified as described previously[12] to accommodate the capacitance-conductance values of the dielectric cell. Frequencies from 100 to 50 000 cps were obtained from a Hewlett-Packard model 202 low frequency oscillator with the frequency standardized by means of a Hewlett-Packard model 100 low frequency standard. The frequency is considered accurate to within ±0.1%.

The samples were measured in a Fitzgerald-Miller combination dielectric cell.[13] This cell is a parallel-plate guarded electrode condenser type for use with both solid and liquid samples. Dielectric constant measurements of benzene and toluene using the above bridge and cell combination were found to be within ±0.5% of the standard values.[12] The capacitance of the empty cell C_0 was measured over a temperature range from −50° to +100°C. The value of C_0 was found to vary linearly with temperature and changed by approximately 0.01 $\mu\mu$f per centigrade degree. A 0.5 $\mu\mu f$ discontinuity was found to occur between 20° and 24°C probably because of a phase transition in the Teflon gasket which seals the cell. The error in ϵ' in that region is still considered to be no greater than 1%.

All data were taken with the cell immersed in a constant temperature bath[12] designed for use with the dielectric cell. The inner compartment containing the cell and bath liquid is surrounded by a cooling chamber that contains dry ice or liquid nitrogen during low-temperature measurements. Two 350-w immersion heaters in the inner compartment are controlled by a thermostat that is also immersed in the bath liquid. A small motor driven propeller provides continual agitation of the bath liquid and the temperature of the bath was found to remain constant to within ±0.25°C.

Sample temperatures were measured to within ±0.25°C using an iron-constantan two-junction thermocouple inserted into the cell to within 0.05 in. of the sample. By comparison with a standard thermocouple, calibrated by the National Bureau of Standards, the thermocouple used here was found to be accurate to within ±0.1°C. For all measurements, one half-hour was allowed, after the cell reached a desired temperature, for the sample to achieve thermal equilibrium.

The limit of error in the measurement of the capacitance (and hence the dielectric constant ϵ') is ±1%. The conductance measurements are accurate to within ±1% or 0.0001 mhos, whichever is larger, so that for small values of the loss factor ϵ'' at low frequencies, the error in ϵ'' may be considerably greater than 1%.

III. DETERMINATION OF COOLING AND HEATING CURVES

Cooling and heating curve measurements were obtained by placing approximately 3 g of liquid sample, heated to about 10 centigrade degrees above the melting point, in a 5-cc test tube filled with the fine brass turnings. A two-junction iron-constantan thermocouple (No. 30 B and S gauge wire) was located in the center of the sample and the test tube was placed in an insulated metal container that in turn was immersed in a water bath. The water temperature was regulated so that the ambient temperature in the air space immediately surrounding the test tube changed by about 0.2°C per min. The emf between the sample junctions and the reference junctions (kept at 0°C), was measured by means of a potentiometer. Sample temperatures were measured every minute and the ambient temperature was read (by means of a second thermocouple) every 2 to 3 minutes.

IV. MATERIALS STUDIED

The vinyl stearate and ethyl stearate were furnished in the form of a fine white precipitate by the United States Department of Agriculture, Agricultural Research Service.[14,15] The ethyl stearate (CH_3—CH_2—OCO–$C_{17}H_{35}$) contained less than 0.3% stearic acid and had a saponification value of 180.0 (theoretical value 179.5). The vinyl stearate (CH_2—CH—OCO—$C_{17}H_{35}$) was prepared commercially from purified stearic acid by direct vinylation and crystallized from three volumes of acetone. Its iodine number was 80.0 (theoretical value 81.7). The heneicosane (n—$C_{21}H_{44}$) was prepared by the Applied Science Laboratories of State College, Pennsylvania. The material was received in

[11] W. M. Mazee, Rec. trav. chim. **67**, 197 (1947).
[12] S. G. Turley, Doctoral thesis, The Pennsylvania State University, 1957.
[13] E. R. Fitzgerald and R. M. Miller, J. Colloid Sci. **8**, 149 (1952).
[14] The samples were prepared by W. S. Port of the Eastern Utilization Research Branch of the Agricultural Research Service of the U.S.D.A., Philadelphia, Pennsylvania.
[15] E. R. Fitzgerald, J. Chem. Phys. **32**, 771 (1960).

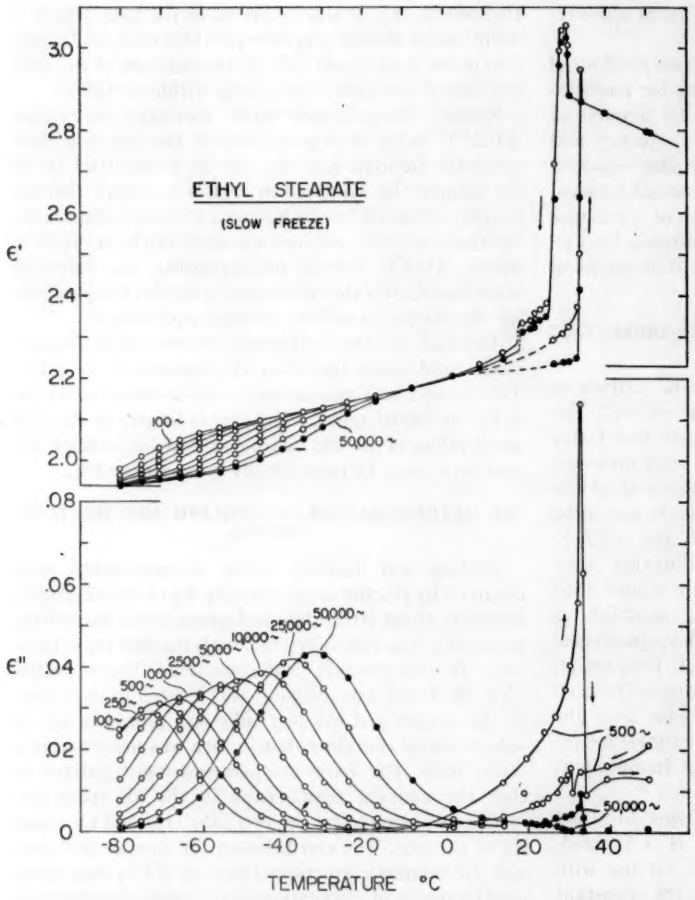

FIG. 1. Variation of the dielectric constant ϵ' and loss factor ϵ'' in ethyl stearate as a function of temperature for a slowly frozen sample at the frequencies shown.

two batches, both of which consisted of the middle cuts of a fractionation through a 100 theoretical plate column. Gas chromatography studies supplied with the samples indicated that both batches were at least 99% pure. Samples were prepared for dielectric measurements by placing the melted material in the cell and allowing it to solidify between the fixed condenser plates. The ethyl stearate was mixed with n—$C_{21}H_{44}$ by shaking the two substances together for several hours at 50°C.

Ethyl stearate was found to solidify at 30.9°C and, with further cooling, to undergo a solid-solid transition at 25.5°C. During the solid-solid transition the ethyl stearate changed from a transparent to a cloudy white substance, which gradually formed large clear crystals after standing for several weeks. A reverse solid-solid transition is not evident in heating curves and melting occurs at 33.3°C. Slow recrystallization of ethyl stearate from acetone produces large clear monclinic crystals. The observed properties are consistent with previous work on ethyl stearate.[16]

The vinyl stearate solidifies at 30.3°C as a cloudy white solid that is similar in appearance to the low temperature form of ethyl stearate. Further cooling produces no change in the appearance of the material, but upon standing, the vinyl stearate changes into a fluffy white powder, in contrast to the behavior of ethyl stearate. The melting occurs around 32°C. The n-heneicosane freezes at 39.8°C and undergoes a transition at 29.2°C. The material remains more transparent than the esters. The solid-solid transition is reversible and the melting and freezing points coincide.

V. EXPERIMENTAL RESULTS

Dielectric Measurements

The dielectric data consist of values of the dielectric constant and loss factor for frequencies of 100, 250, 500,

[16] T. Malkin, J. Chem. Soc. (London) **1931**, 2796.

1000, 2500, 5000, 10 000, 25 000, and 50 000 cps. Measurements at each of these frequencies were made at various temperatures over the range from −80° to +60°C. For the ethyl and vinyl stearate, data were recorded for temperature intervals of approximately 5°, while for the paraffin and the ethyl stearate-paraffin mixtures, 10° intervals were sufficient to determine the shape of the dielectric curves. All samples were extremely unstable at temperatures down to 20 centigrade degrees below the freezing point. In this region the measurements were strongly time dependent, and the resulting values cannot be considered as representing equilibrium conditions. At temperatures outside the time-dependent range the values recorded were obtained after the samples had reached thermal equilibrium, and in all cases measurements were made for both increasing and decreasing temperatures in order to check the reproducibility of the data. In some cases, where particularly small values of the loss factor were found at low frequencies, a lack of precision has made

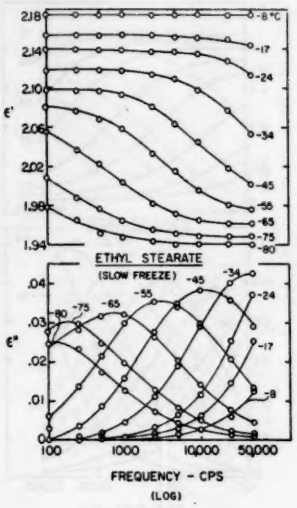

FIG. 2. Variation of the dielectric constant ϵ' and loss factor ϵ'' in ethyl stearate as a function of frequency for a slowly frozen sample at the temperatures shown.

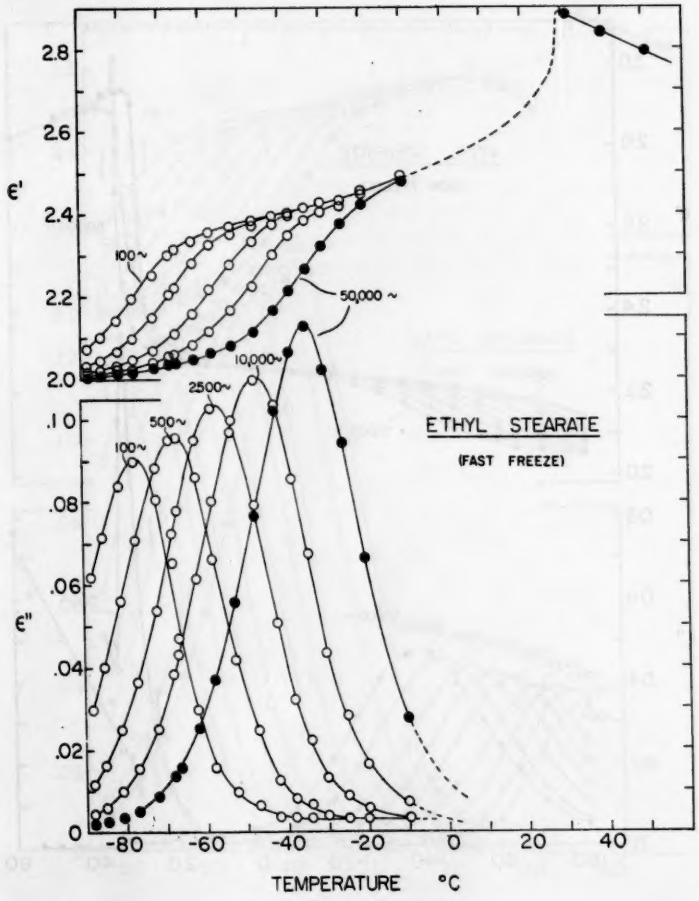

FIG. 3. Variation of the dielectric constant ϵ' and loss factor ϵ'' in ethyl stearate as a function of temperature for a quickly frozen sample at the frequencies shown.

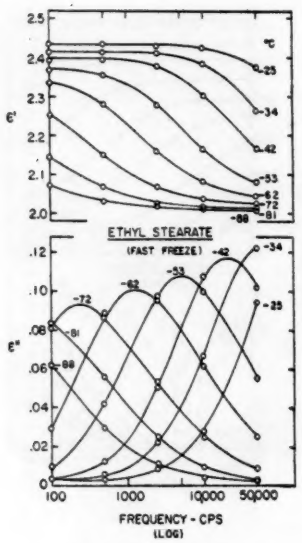

FIG. 4. Variation of the dielectric constant ϵ' and loss factor ϵ'' in ethyl stearate as a function of frequency for a quickly frozen sample at the temperatures shown.

it necessary to omit the results for one or more of the lowest frequencies.

The dependence of the dielectric properties on the freezing rate of the sample was found to be of particular interest and consequently; two sets of data—one for a slow and one for a fast freeze—were taken for each sample. For a slow freeze, the samples were allowed to cool slowly through the freezing point over a period of 24 hr or more. For the fast freeze the samples were cooled at the rate of about 1°/min from 10 deg above their freezing points to 30 deg or more below their freezing points, at which temperature the data were usually quite stable and reproducible. Measurements around the freezing points were not taken for quickly frozen samples due to the strong time dependency of the dielectric properties there.

The dielectric properties of a slowly frozen sample of ethyl stearate are plotted against temperature in Fig. 1 and against frequency in Fig. 2. A small dispersion was found below 0°C for the frequencies considered here. The instability and time dependency of the properties

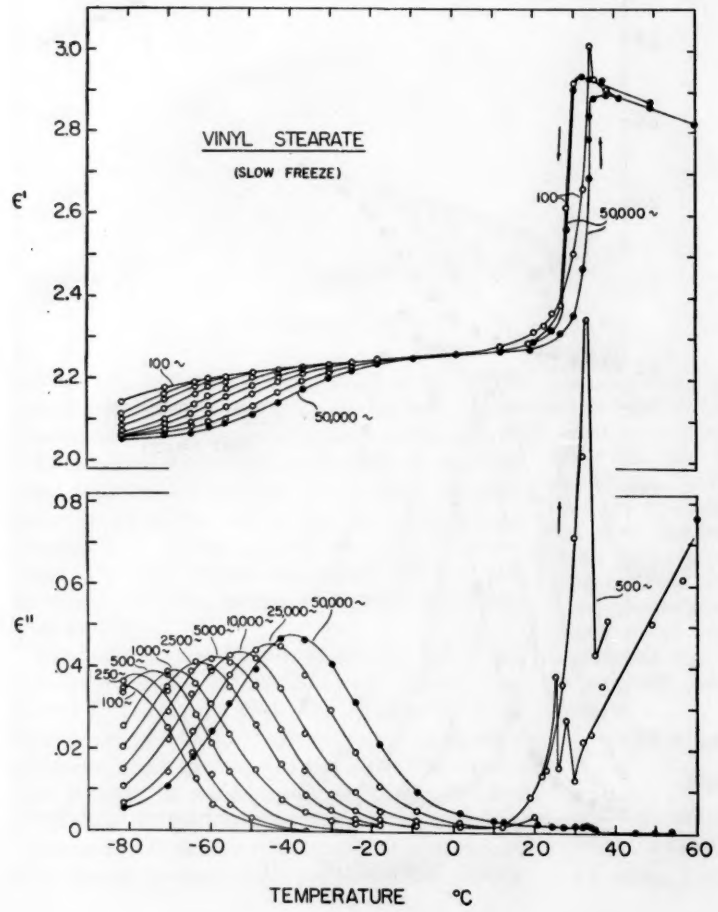

FIG. 5. Variation of the dielectric constant ϵ' and loss factor ϵ'' in vinyl stearate as a function of temperature for a slowly frozen sample at the frequencies shown.

just below the freezing point are shown by discontinuities in the curves in that region. The jumps in ϵ' are due to extra-long time delays between readings.

The quickly frozen sample of ethyl stearate gave the data shown in Figs. 3 and 4 plotted against temperature and frequency, respectively. A dispersion was found to occur at approximately the same place as with the slowly frozen sample but the loss peaks were nearly three times the height of the slow freeze peaks. A sample frozen at a medium rate (not shown) was found to give dispersion peaks intermediate in height between the slow and the fast freeze peaks.

Vinyl stearate behaved very much like ethyl stearate in its dielectric properties. A dispersion region was found at approximately the same place for both the slowly (Figs. 5 and 6) and the quickly (Figs. 7 and 8) frozen samples. Furthermore, these peaks were found to be of approximately the same height for both ethyl and vinyl stearate, for corresponding freezing rates.

The results of slow and fast freezing rates on the

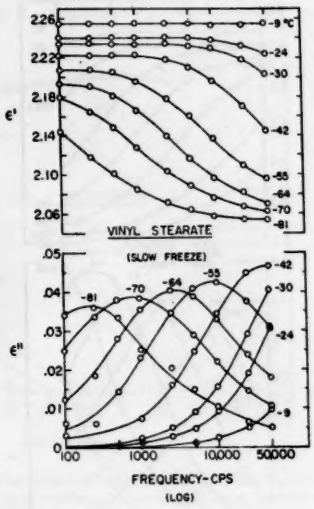

FIG. 6. Variation of the dielectric constant ϵ' and loss factor ϵ'' in vinyl stearate as a function of frequency for a slowly frozen sample at the temperatures shown.

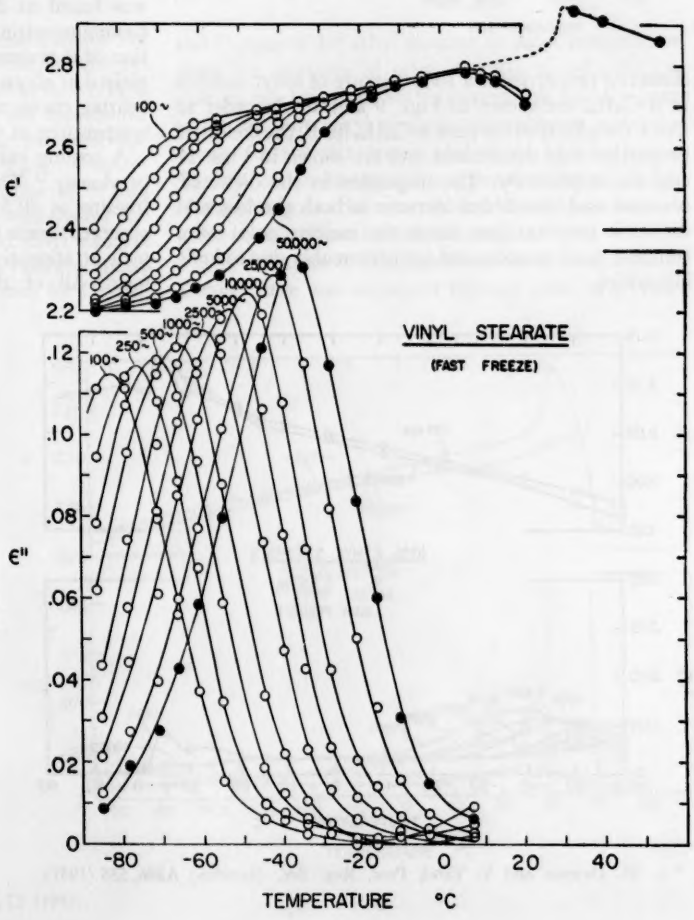

FIG. 7. Variation of the dielectric constant ϵ' and loss factor ϵ'' in vinyl stearate as a function of temperature for a quickly frozen sample at the frequencies shown.

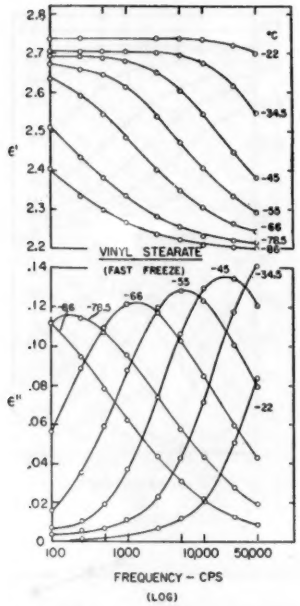

FIG. 8. Variation of the dielectric constant ϵ' and loss factor ϵ'' in vinyl stearate as a function of frequency for a quickly frozen sample at the temperatures shown.

dielectric properties of a 10% mixture of ethyl stearate in n-$C_{21}H_{44}$ are shown in Figs. 9 and 10. In order to check the effects of the pure n-$C_{21}H_{44}$ itself, the dielectric properties were determined and are shown in Figs. 11 and 12, respectively. The dispersion in the dielectric constant and the sudden increase in both the loss and dielectric constant just below the melting point were common to all samples and are presumably due to ionic impurities.

In order to measure the effect of careful crystallization from a solvent, ethyl stearate was allowed to crystallize slowly at room temperature from an acetone solution. The resulting laminar crystals were about 2 mm on a side, $\frac{1}{2}$ mm thick and were of the same form as the paraffin crystals studied by Dawson and Vand.[17] The crystals were then compressed between the capacitor plates and ϵ' and ϵ'' were determined over the temperature range from 25° to −60°C. Due to irregularities in the surface of the compressed sample only the loss tangent (ϵ''/ϵ'), which is independent of sample size and density, can be considered significant. Fig. 13 shows the loss tangent as a function of temperature for the recrystallized sample of ethyl stearate. The loss tangent curves for the quickly and slowly frozen samples of ethyl stearate are included in Fig. 13 for comparison.

VI. COOLING CURVES

The cooling and heating curves for ethyl stearate are shown in Fig. 14. The sample was found to supercool slightly and to freeze at 30.9°C. A solid-solid transition was found at 25.5°C with a large amount of supercooling occurring. The heating curve showed no indication of a reverse solid-solid transition and the sample melted at about 33.3°C. A very slight disruption in the heating curve can be seen at approximately the same temperature at which the sample froze.

A cooling curve for vinyl stearate has been shown previously.[15] The sample supercooled slightly before freezing at 30.5–30.6°C. No solid-solid transition was observed down to 18°C, but the sample was found to melt at approximately 32°C, indicating a second solid form. All of the vinyl stearate samples measured

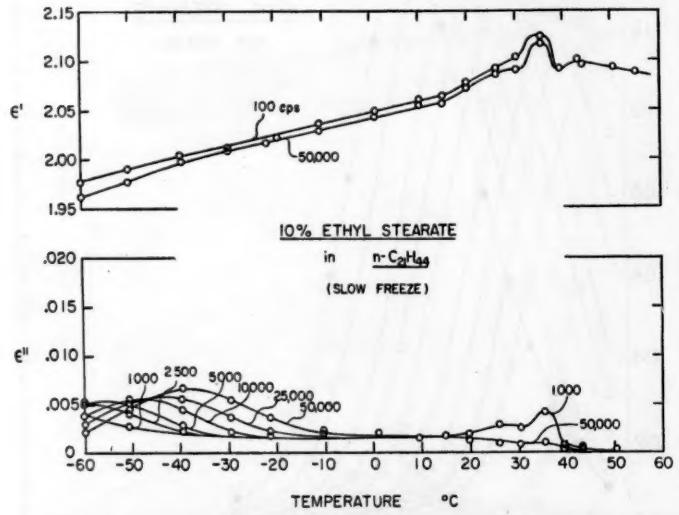

FIG. 9. Variation of the dielectric constant ϵ' and loss factor ϵ'' in a 10% mixture of ethyl stearate in n-$C_{21}H_{44}$ as a function of temperature for a slowly frozen sample at the frequencies shown.

[17] L. M. Dawson and V. Vand, Proc. Roy. Soc. (London) **A206**, 555 (1951).

exhibited a slight disruption in the cooling curve at 32.6°C while in the liquid state.

Fig. 15 shows the heating and cooling curves for pure n-$C_{21}H_{44}$. The sample supercooled slightly and froze at 39.8°C. A solid-solid transition at 29.2°C was not preceded by any supercooling. The heating curve shows the solid-solid transition to be reversible and the melting and freezing points coincide in temperature.

A mixture of 10% ethyl stearate in n-$C_{21}H_{44}$ gave the cooling curve in Fig. 16. Freezing occurs at 38.6–38.7°C, or about 1.1 centigrade degrees below the freezing point of n-$C_{26}H_{44}$ (calculated value is 1.2 centigrade degrees). The ethyl stearate lowered the solid-solid transition temperature 3.8 centigrade degrees to 25.4°C. Heating curves showed both the solid-solid and liquid-solid transitions to be reversible.

VII. ANALYSIS OF THE RESULTS

The apparent activation energy for dipole rotation was calculated using the relationship[18]

$$T\tau = \tau_0 \exp(Q_D/RT),$$

where τ_0 is a constant, τ is the relaxation time of the dipole and Q_D is the apparent molar activation energy. Using a mean relaxation time, τ_m defined as $\tau_m = 1/2\pi f_m$ where f_m is the frequency at which the loss factor maximum occurs at temperature T_m, we have approximately (for a small range in T_m), $-\ln f_m = Q_D/RT_m +$ constant. Thus, from the slope of $-\ln f_m$ vs $1/T_m$, Q_D can be determined. Values of Q_D for the slow and fast freezes of both ethyl and vinyl stearate were all 12.7 kcal/mole (0.55 ev). This value compares favorably with the 13 kcal/mole obtained by Dryden and Dasgupta[3] for ethyl stearate at room temperature. Since for mixtures of ethyl stearate in n-$C_{21}H_{44}$, the shift in the loss peak with temperature was the same as for the pure ethyl stearate, the apparent activation energy for the mixtures is also about 12.7 kcal/mole. The activation energy Q_D is approximately the height of the energy barrier over which a dipole must move in order to contribute to the polarization.

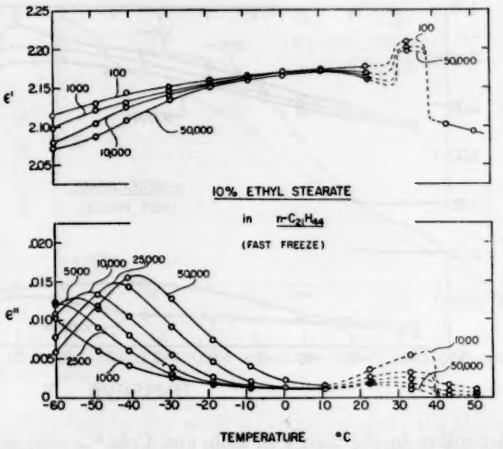

FIG. 10. Variation of the dielectric constant ϵ' and loss factor ϵ'' in a 10% mixture of ethyl stearate in n-$C_{21}H_{44}$ as a function of temperature for a quickly frozen sample at the frequencies shown.

The deviation of the dispersion curves from a simple Debye curve was examined through plots of ϵ' vs ϵ''.

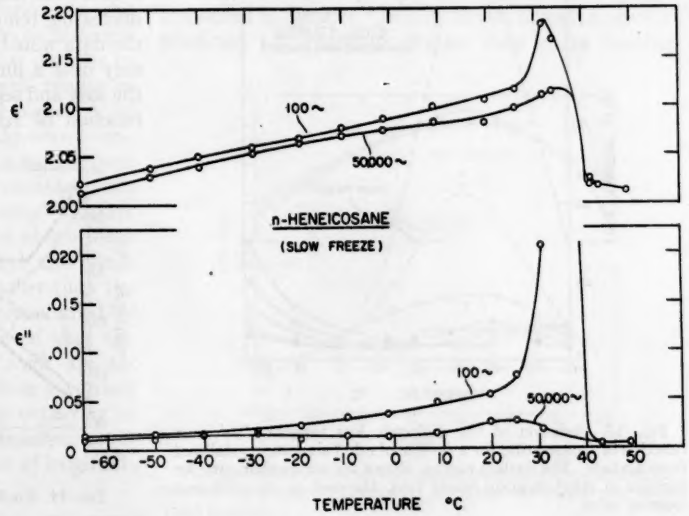

FIG. 11. Variation of the dielectric constant ϵ' and loss factor ϵ'' for n-$C_{21}H_{44}$ as a function of temperature for a quickly frozen sample at the frequencies shown.

[18] W. Kauzmann, Revs. Modern Phys. **14**, 12 (1942).

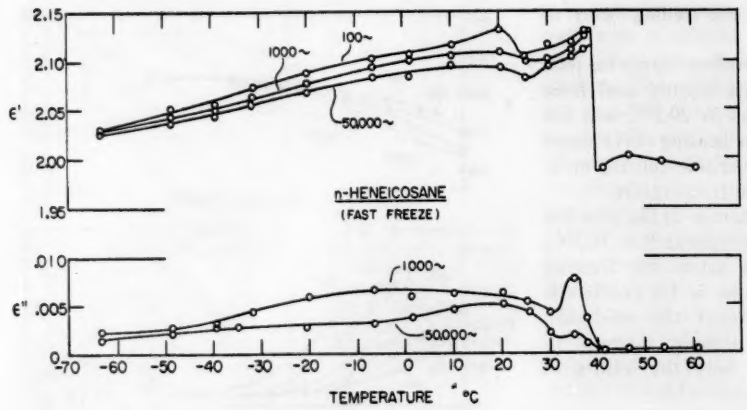

FIG. 12. Variation of the dielectric constant ϵ' and loss factor ϵ'' for $n-C_{21}H_{44}$ as a function of temperature for a slowly frozen sample at the frequencies shown.

According to the theory of Cole and Cole,[19] a plot of ϵ' vs ϵ'' for a Debye dispersion results in a curve which is a complete half circle. If the dispersion curves are broader than Debye curves, then the ϵ' vs ϵ'' plot results in a circular arc that is less than a half circle. Setting the angle between the ϵ' axis (abscissa) and radius drawn to ϵ_∞ (the first intersection of the arc with the abscissa) equal to $\pi\alpha/2$ then the parameter α, is a measure of the deviation of the dispersion from a simple Debye dispersion in which $\alpha=0$. In this case the data fits approximately a modified Debye dispersion of the form

$$\epsilon^*=\epsilon_\infty+\{(\epsilon_0-\epsilon_\infty)/[1+(i\omega\tau_0)^{1-\alpha}]\}.$$

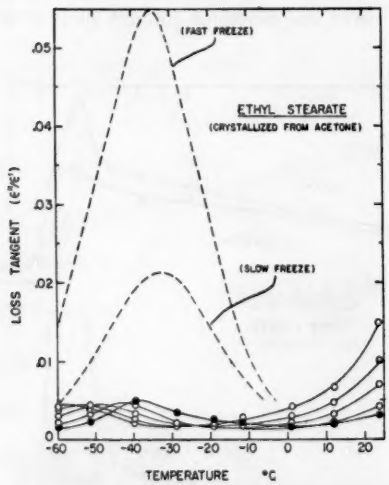

FIG. 13. Variation of the dielectric loss tangent ϵ''/ϵ' as a function of temperature for a sample of ethyl stearate crystallized from acetone. The dashed curves, shown for comparison, are for samples of ethyl stearate frozen from the melt at two different freezing rates.

[19] K. S. Cole and R. H. Cole, J. Chem. Phys. **9**, 341 (1941).

The low temperature dispersions reported here gave $\alpha=0.39$, indicating that the deviations from a Debye dispersion were the same in ethyl and vinyl stearate and in the ethyl stearate-paraffin mixture.

The broadness of experimental dispersion curves has previously been attributed either to two or more discrete relaxation times or to a continuous distribution of relaxation times. It was thought to be instructive here to examine the nature of the continuous distribution function $\psi(\tau)$ using the empirical approximation of Williams and Ferry[20] for the inversion of the equations

$$\epsilon'=\epsilon_\infty+\int_{-\infty}^{\infty}\psi(\tau)/(1+\omega^2\tau^2)d\ln\tau,$$

and

$$\epsilon''=\omega\int_{-\infty}^{\infty}\psi(\tau)/(1+\omega^2\tau^2)d\ln\tau.$$

Since the heights of the loss maxima decreased with decreasing temperatures for the esters considered here, the data would not superpose and $\psi(\tau)$ could be found only over a limited frequency range. Figure 17 shows the first and second approximations to the distribution function of relaxation times for the quickly frozen

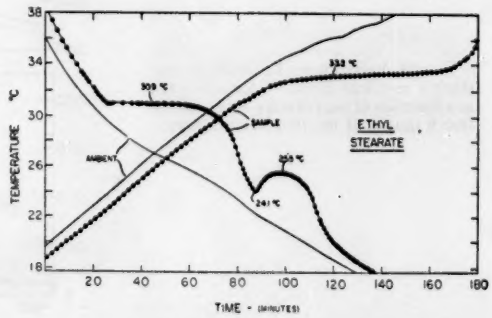

FIG. 14. Cooling and heating curves for ethyl stearate.

[20] M. L. Williams and J. D. Ferry, J. Polymer Sci. **11**, 169 (1953).

sample of vinyl stearate. The shape of the curve is typical of those obtained at different freezing rates for both ethyl and vinyl stearate.

VIII. DISCUSSION

It is generally agreed that the type of molecular motion that gives rise to dielectric dispersion in solid long-chain hydrocarbons occurs only in regions of crystalline disorder. This conclusion is consistent with the fact that the dispersion is greatly reduced in carefully crystallized samples. Arnold and Meakins,[21] have also found that cold working greatly increases dispersion in long-chain ethers and that annealing reduces the dispersion. Similar annealing effects were observed in the present work on ethyl and vinyl stearate where a pronounced decrease with time occurred in ϵ' for quickly frozen samples when they were heated to within 20 centigrade degrees of their melting points.

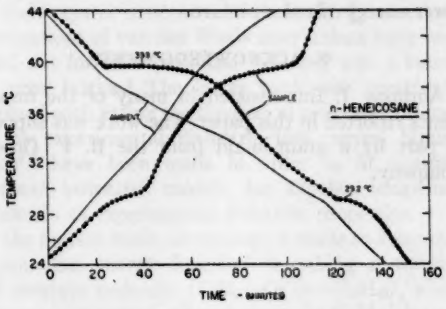

FIG. 15. Cooling and heating curves for $n-C_{21}H_{44}$.

From their work on long chain esters, Crowe, Hoffman, and Smyth[7] concluded that variations in the polarization with freezing rate were due to different degrees of a particular type of longitudinal disorder in the crystal in which rapid crystal growth results in some molecules freezing into the crystal planes in an inverted position. Part of the basis for the above conclusion was the observation that once a sample was frozen, its dielectric properties remained constant with time. The time effects found here in ethyl stearate are not necessarily inconsistent with the above ideas of longitudinal disorder since both ethyl and vinyl stearate tend to form tilted structures rather than the vertical structures found in the longer esters studied by the above authors. However, it is believed that the time effects observed in this present work are associated with a gradual transformation from a vertical to a tilted structure with no polarization occurring in the tilted form and with the amount of polarization in the vertical form governed by the amount of longitudinal disorder.

[21] J. W. Arnold and R. J. Meekins, Trans. Faraday Soc. **51**, 1667 (1955).

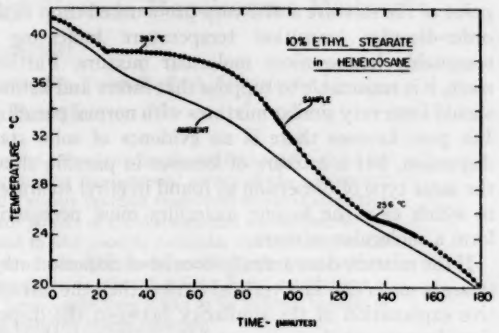

FIG. 16. Cooling curve for a mixture of 10% ethyl stearate in $n-C_{21}H_{44}$.

Although further work is needed to verify the above possibility, there is some indirect evidence for its validity. When ethyl stearate was solidified from acetone into large single crystals in a presumably perfect tilted structure, the solid state dispersion was very much less than for samples cooled from the melt into a less perfect structure. Dilatometer studies[22] have shown that after quenching a sample of ethyl stearate to 15°C, and then heating it to room temperature, the density continued to increase with time at room temperature indicating that the transformation to the stable low temperature tilted structure is gradual and need not occur completely at the usual vertical-tilt transformation temperature.

The results of mixture measurements were quite similar to those for pure ethyl stearate with the apparent polarization in the mixture being about one tenth that for the pure ester. It appears at first that the mixture actually consists of groups of ethyl stearate crystals suspended in paraffin. Cooling curves, however, show a predicted 1.1 centigrade degrees drop in the freezing

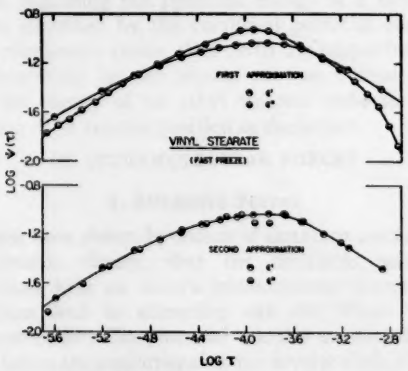

FIG. 17. The first and second approximation of the distribution function of relaxation times $\psi(\tau)$ for a quickly frozen sample of vinyl stearate.

[22] A. J. Bur, this Laboratory (unpublished data).

point of the mixture and a very pronounced drop in the order-disorder transition temperature indicating a reasonably homogenious molecular mixture. Furthermore, it is reasonable to suppose that esters and ketones should form very similar mixtures with normal paraffins. For pure ketones there is no evidence of solid state dispersion, but a mixture of ketones in paraffin shows the same type of dispersion as found in ethyl stearate,[23] in which case the ketone molecules must necessarily form a molecular mixture.

If the mixture does actually consist of dispersed ethyl stearate molecules in a vertical lattice, then the alternative explanation of the similarity between the dispersions in pure ethyl stearate and the mixture is that the molecules that contribute to the polarization in pure ethyl stearate are themselves located in a vertical lattice—i.e., that rotation occurs only in those parts of the sample which have been frozen into a vertical structure.

Although as yet unverified, the above possibility might provide a convenient tool for explanation of long-chain behavior. For instance, the lack of rotation in solid acids and ketones might well be due to the high stability of the nonrotating tilted structure for these compounds.

[23] R. J. Meakins, Australian J. Sci. Research **A2**, 405 (1949).

IX. CONCLUSIONS

A dielectric relaxation dispersion region exists in solid ethyl and vinyl stearate and in mixtures of ethyl stearate in *n*-heneicosane, at temperatures from −80° to −35°C for frequencies from 100 to 50 000 cps.

The dispersion results from polarization associated with changes in the orientation of dipolar molecules about their long-chain axis. The amount of polarization is very much dependent on the way in which the solid samples are formed, being greatest when the samples are frozen quickly from the melt and least when the samples are slowly crystallized from a solvent. Annealing of a sample within about 20 centigrade degrees of its melting point caused the polarization to decrease with time. The polarization in these long-chain esters seems to be associated with metastable crystal structures and it is suggested that polarization is present in those parts of the sample that are frozen into a vertical structure and absent from those parts that are transformed into the lower energy tilted structure.

X. ACKNOWLEDGMENTS

Anthony J. Bur assisted in many of the measurements reported in this paper. The work was supported in part by a grant-in-aid from the B. F Goodrich Company.

Theoretical Dielectric Behavior of an Ethyl Stearate-Heneicosane Mixture*

MARTIN G. BROADHURST†

Department of Physics, The Pennsylvania State University, University Park, Pennsylvania

(Received January 28, 1960)

The variation in potential energy with position for an ethyl stearate molecule rotating rigidly about its chain axis in a heneicosane lattice has been found by evaluating the potential energy of the component atoms at 18 angular positions of the molecule. The potential energy function considered involves attractive van der Waals terms in the inverse sixth, eighth, and tenth powers of the distance and an exponential repulsive term. The resulting potential energy curve was used to find possible molecular motions, and calculations of the predicted dielectric relaxation dispersion were made. The model predicts only two positions available to the ethyl stearate molecule and hence only one dielectric relaxation time. Exact calculations of the dielectric properties of a mixture of ethyl stearate in heneicosane were found to be difficult because of the extreme sensitivity of the results to slight errors in the assumed energy function.

I. INTRODUCTION

SEVERAL attempts have been made to correlate the physical behavior of long-chain carbon compounds with their crystal structure and molecular interactions. Investigations of van der Waals interactions have been carried out for solid paraffins,[1–3] soaps,[4] and a ketone in a urea lattice.[5] The latter work was specifically concerned with fitting the theoretical molecular interactions to experimental dielectric loss curves. Similar studies[6,7] have been made in order to fit assumed rotational potential models for dipolar long-chain compounds to experimental dielectric properties.

In the present work, an attempt is made to determine the potential energy function describing a rotating ethyl stearate molecule (C_2H_5—OCO—$C_{17}H_{35}$), which is located in a nonpolar heneicosane (n-$C_{21}H_{44}$) lattice, and to thereby predict the dielectric properties of the system. Such a calculation could be expected to yield information not only on the molecular behavior of long-chain compounds but also on the limitations of the calculation as a theoretical tool.

II. CRYSTAL STRUCTURE

The structure of n-heneicosane is shown in Figs. 1 and 2 and the important dimensions are given in Table I. The values of the cell dimension are those given by Müller[2] for a general 20–30-carbon paraffin. Müller's values agree with those found by Mazee for n-$C_{21}H_{44}$[8] and are given to one more significant figure. The distance between crystal layers was taken as 3.3 A instead of the more generally accepted 4.0 A, in order that the long cell dimension as calculated from the repeat distance along the chain would agree with the x-ray long spacing.[9] It was found that the use of 4.0 A would not greatly alter the results. Although the carbon-carbon bond length of 1.54 A is generally agreed to be accurate to the third place, the other bond lengths and angles given in Table I are probably accurate only to ±2%. It is assumed on the basis of reported measurements[10] that replacing a paraffin molecule by an ester molecule (which has the same length and structure) does not affect the cell dimensions of the pure paraffin lattice. The lattice molecules are considered to be fixed in their equilibrium positions and it is also assumed that, as a dipolar molecule moves rigidly from one angular position to another, the rotation occurs about an axis (fixed with respect to the lattice) which is parallel to the carbon chain and bisects the carbon-carbon bonds. On the basis of the above model one can calculate, for any angular position of an ethyl stearate molecule, the distances between the individual atoms of that molecule and the atoms in the surrounding lattice. Assuming the potential energy of a molecule can be described by the combined potential energies of its component atoms, then given the proper interaction potentials for the atoms, one can compute the potential energy of an ethyl stearate molecule as a function of its angular position in the lattice.

III. INTRAMOLECULAR FORCES

1. Attractive Forces

It has been shown by means of quantum mechanical perturbation theory, that the multipole moments associated with an atom's instantaneous charge configuration lead to attractive van der Waals forces between atoms. The potential energies associated with these forces are proportional to the inverse sixth, eighth, and tenth powers of the distance between interacting atoms for the dipole-dipole, dipole-quadrapole, and

* Based in part on a thesis submitted by Martin G. Broadhurst in partial fulfillment of the requirements for the Ph.D. degree, Pennsylvania State University, 1959.

† Present address: Dielectrics Section, National Bureau of Standards, Washington, D. C.

[1] A. Müller, Helv. Phys. Acta **9**, 627 (1936).
[2] A. Müller, Proc. Roy. Soc. (London) **154**, 624 (1936).
[3] A. Müller, Proc. Roy. Soc. (London) **178**, 227 (1941).
[4] V. Vand and J. H. DeBoer, Proc. Honinkijke Ned. Akad. Van Wetenschappen **50**, 273 (1947).
[5] J. I. Lauritzen, Jr., J. Chem. Phys. **28**, 118 (1958).
[6] H. Frohlich, *Theory of Dielectrics* (The Clarendon Press, Oxford, 1958), 2nd ed.
[7] J. D. Hoffman, J. Chem. Phys. **20**, 541 (1952).
[8] W. M. Mazee, Rec. trav. chim. **67**, 197 (1947).
[9] A. E. Smith, J. Chem. Phys. **21**, 2229 (1953).
[10] A. Müller, Proc. Roy. Soc. (London) **A120**, 437 (1928).

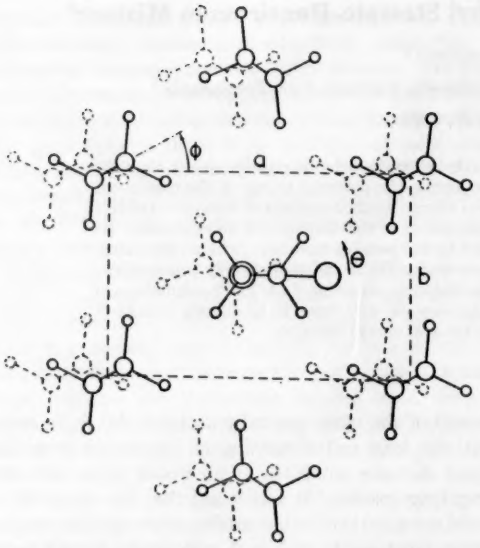

FIG. 1. Top view showing the assumed crystal structure of ethyl stearate (center molecule) in normal $C_{21}H_{44}$. The **a** and **b** dimensions are shown by the dashed square and the positions of the molecules in an adjacent layer are shown by dashed molecules. Small circles are hydrogen atoms, medium circles are carbon atoms, and the large circles represent the two oxygen atoms. Dimensions are given in Table I. The ethyl stearate molecule is shown at $\theta=0°$.

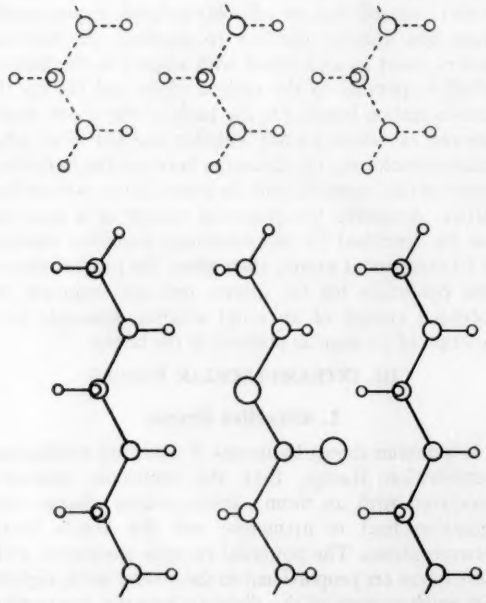

FIG. 2. Side view of the assumed crystal structure of ethyl stearate (center molecule) in normal $C_{21}H_{44}$. The dashed molecules are in an adjacent layer. The small circles represent hydrogen atoms, the medium circles represent carbon atoms, and the large circles represent oxygen atoms.

quadrupole-quadrupole interactions, respectively. The interactions of a group of atoms are conveniently independent[11] and the potentials are therefore additive.

The largest potential term arises from the dipole-dipole interaction and is given by

$$V=-(2/3r^6)\sum_j\sum_k[(\mu_{0j})^2(\mu_{0k}')^2/(E_j+E_k'-E_0-E_0')] \tag{1}$$

where r is the separation distance between atoms 1 and 2, μ_{0j} is the dipole moment associated with the mixing of energy states 0 and j for atom 1, and E_j and E_0 are the energies of the excited state j and the ground state 0. The primed terms refer to molecule 2. If the excited states are localized in a very narrow energy range so that E_j-E_0 can be approximated by a single term $\Delta_1(\Delta=h\nu_m$, the energy of maximum absorption) then Eq. (1) simplifies to the London approximation,[11]

$$V=-(3\alpha_1\alpha_2/2r^6)(\Delta_1\Delta_2/\Delta_1+\Delta_2),$$

where $\alpha_1=2\sum_j(\mu_{0j})^2/3\Delta_1$ is the quantum mechanical polarizability of atom 1.

TABLE I. Molecular and crystal dimensions used in the calculations of interatomic distances in a heneicosane lattice containing an ethyl stearate molecule (Figs. 1, 2).

Description	Dimension
a axis	7.426 A
b axis	4.956 A
Repeat distance along carbon chain	2.54 A
Distance between layers	3.3 A
H—C—H angle	109° 30′
C—C—C and C—O—C angle	110° 30′
C—H bond length	1.12 A
C—C and C—O bond lengths	1.54 A
C=O bond length	1.22 A
Setting angle ϕ	30°

Owing to the shorter range of the inverse eighth and tenth power terms, a less exact approximation, derived by Margenau[12] for the interaction between two like harmonic oscillators, can be used in the form

$$V=-\tfrac{3}{4}(\alpha^2h\nu/r^6)-\tfrac{15}{4}[\alpha^3(h\nu)^2/fe^2r^8]$$
$$-\tfrac{315}{32}[\alpha^4(h\nu)^3/f^2e^4r^{10}],$$

where α is the polarizability, ν is the natural frequency of oscillation, h is Planck's constant, e is the electronic charge, f is the number of oscillating electrons and r is the separation distance. It is noted that the inverse sixth power terms in both expressions are the same for like molecules. The combined attractive potential

[11] F. London, Trans. Faraday Soc. **33**, 8 (1937).
[12] H. Margenau, Revs. Modern Phys. **11**, 1 (1939).

function used here is

$$V=-\tfrac{3}{2}(\alpha_1\alpha_2\Delta_1\Delta_2/r^6\Delta_1\Delta_2)-\tfrac{1}{4}\tfrac{5}{}(\bar{\alpha}^3\bar{\Delta}^2/f\bar{e}^2r^8)$$
$$-\tfrac{3}{3}\tfrac{1}{2}\tfrac{5}{}(\bar{\alpha}^4\bar{\Delta}^3/f^2\bar{e}^4r^{10}) \quad (2)$$

where the bars indicate that the quantities are averaged over the two interacting atoms. The above expression can be evaluated if the polarizabilities and absorption energies are known.

The polarizabilities are most easily determined from refractive index measurements on homologous series of carbon compounds. Assuming validity of the Lorenz-Lorentz equation $P=(n^2-1)M/(n^2+2)\rho=4\pi N_A\alpha/3$ where P is the refractivity, n the index of refraction, M the molecular weight, ρ the density, N_A Avogadro's number, and α the polarizability, one can arrive at a consistent set of values for the polarizabilities of atoms such that when the values are added together in the proper ratios, one can obtain the total polarizability of the whole molecule.

TABLE II. Assumed polarizabilities for chemically bound atoms.

Atom	Polarizability (α) (cm^3)
—H	0.438×10^{-24}
	0.955×10^{-24}
—O—	0.651×10^{-24}
=O	0.876×10^{-24}

The values for α determined in the above way, which were used in the present work, are given in Table II. It should be mentioned that, instead of assuming the atoms to be the force centers, one could alternatively treat the bonds as being the centers of the van der Waals forces. Müller[2] has found fair agreement between the two methods in his work with paraffins.

The electronic absorption energies are more difficult to find than the polarizabilities. For the present work only approximate values were assumed from absorption and ionization data. For n-paraffins ultraviolet absorption occurs above $\nu=6$ ev$/h$,[13] (h=Planck's constant). For H_2 the absorption decreases rapidly above $\nu=10$ ev$/h$[14] so that one might conclude that the proper value of Δ for bound hydrogen lies between 6 and 10 ev. Since methane[15] is more easily ionized than H_2[16] it is reasonable to conclude that the absorption associated bound carbon is of slightly lower energy than that of hydrogen. Since ethers react much like n-paraffins to ultraviolet light[13] one could choose the same value of α for the ethoxy oxygen as for carbon. For the carbonyl oxygen, which possesses localized electrons, one can reasonably take Δ as 5.6 ev corresponding to the absorption of acids.[13] The above assumed values of Δ are listed in Table III.

TABLE III. Assumed absorption energies for chemically bound atoms.

Atom	Absorption energy (Δ) (ev)
—H	9.0
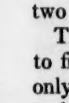	8.0
—O—	8.0
=O	5.6

The coefficients of Eq. (2), which can be rewritten as $V=-Cr^{-6}-C'r^{-8}-C''r^{-10}$, can now be evaluated, and the results are given in Table IV.

2. Repulsive Forces

When two atoms are close enough that their electron shells begin to overlap, they experience the onset of a very sharply increasing potential energy. This potential energy is best represented by an exponential term of the form $C'''e^{-br}$.[12] Due to the short range of the repulsive forces only the hydrogen-hydrogen and hydrogen-carbonyl oxygen interactions are important. That is, the chain carbons are never close enough to neighboring molecules to experience a significant repulsion.

For the hydrogen-hydrogen interaction, one can employ directly the expression obtained by Müller[11] from compressibility data on normal paraffins, where he found that $C'''\exp(-br)=2.75\times10^3\exp(-5\times10^{10}r)$ ev, where r is in meters. No such expression is available for the hydrogen-carbonyl oxygen interaction, but due to the similarity between repulsive potentials for various compounds,[16] and the relative unimportance of the hydrogen-oxygen interaction in comparison to the more numerous hydrogen-hydrogen pairs, a rough

TABLE IV. Constants used for calculating the potential energy of an atom due to the presence of a second atom from the expression: $V=-Cr^{-6}-C'r^{-8}-C''r^{-10}+C'''e^{-br}$.

Type of interaction	C (ev A^6)	C' (ev A^8)	C'' (ev A^{10})	C''' (ev)	b (m^{-1})
(H)—(H)	1.294	1.775	1.28	2.75×10^3	5.0×10^{10}
(H)—(C)	2.66	2.54	1.10	...	...
(C)—(C)	5.47	4.63	1.26	...	...
(=O)—(H)	1.99	1.125	0.284	1.0	4.6

[13] A. Gillian and E. S. Stern, *Electronic Absorption Spectroscopy* (Edward Arnold Publishers, Ltd., London, 1954).
[14] K. Walanabe and C. Y. Inn, J. Opt. Soc. Am. **43**, 32 (1958).
[15] E. V. Condon and H. Odishaw, *Handbook of Physics* (McGraw-Hill Book Company, Inc., New York, 1958).
[16] K. S. Pitzer, *Quantum Chemistry* (Prentice-Hall, Inc., Englewood Cliffs, New Jersey, 1953).

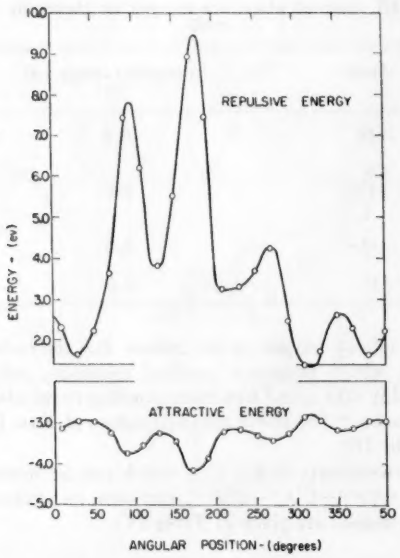

FIG. 3. Theoretical repulsive and attractive potential energies for ethyl stearate in $n-C_{21}H_{44}$ as a function of angular position.

value of $10^3\exp(-4.6\times10^{10}r)$ ev was thought to be satisfactory. The above values for C''' and b are included in Table IV.

3. Electrostatic Forces

Dipole-induced dipole interactions between the ester group and neighboring hydrogens, dipole-dipole interactions between neighboring C–H dipoles, and hydrogen bonding between the carbonyl oxygen and neighboring C–H groups are all possibly important interactions. Direct calculations,[17] however, show that the above electrostatic forces can be reasonably neglected for the system considered here.

IV. FINAL DISTANCE AND POTENTIAL CALCULATIONS

Due to symmetry, only 20 atoms of the ethyl stearate molecule were needed for the distance calculations. All lattice atoms close enough to contribute 1.0% or more of the contribution of the closest atom pairs were considered (up to 7 A for the attractive and up to 4 A for the repulsive calculations). Hand calculations of $\sum e^{-br}$ and computer calculations of $\sum r^{-6}$, $\sum r^{-8}$, and $\sum r^{-10}$ were made at each of 18 angular positions of the ethyl stearate molecule, from $\theta=10°$ (Fig. 1) to $\theta=350°$. The summation is over all similar atom pairs. The above summations were multiplied by the appropriate coefficients from Table IV and the resulting attractive and repulsive potential energy functions were found as shown separately in Fig. 3 and combined in Fig. 4. It is apparent that the height of the smallest barrier in Fig. 4, is larger than the 0.55-ev (12.7-kcal/mole) activation energy determined experimentally for a 10% mixture of ethyl stearate in *n*-heneicosane.[18] A rough correction was made in the most sensitive and most uncertain constant C''' for hydrogen-hydrogen interactions by decreasing it from 2.75×10^3 to 1.57×10^3 ev. The results of that change are shown in Fig. 5.

[17] M. G. Broadhurst, Doctoral thesis, The Pennsylvania State University, 1959.

V. THEORETICAL DIELECTRIC DISPERSION CURVES

By means of the detailed calculations of Hoffman and co-workers,[19–21] one can use Fig. 5 to calculate the low-frequency dielectric dispersion in the theoretical ethyl stearate-heneicosane mixture. In the present case only wells 1 and 4 are accessible to ethyl stearate molecules in sufficient numbers to affect the polarization. Consequently, the equations describing the change in the numbers of dipolar molecules in the various wells, reduce to

$$dN_4/dt=K_8N_1-K_7N_4,$$
$$dN_1/dt=-K_8N_1+K_7N_4, \qquad (3)$$

where N_1 and N_4 are the numbers of dipoles per unit volume of sample in wells 1 and 4, respectively, and the K's represent the probability per second of a transition shown in Fig. 5. The K's can be evaluated from $K=A\exp(-\Delta E/kT)$, where A is the number of times per second that a dipole strikes the barrier involved in a transition, ΔE is the energy difference between the bottom of the well from which a molecule originates to the top of the barrier over which it passes, k is Boltzmann's constant, and T is the absolute temperature. Fitting a given well to a harmonic oscillator potential

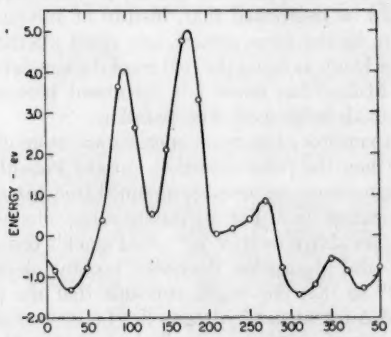

FIG. 4. Theoretical total potential energy of ethyl stearate in $n-C_{21}H_{44}$ as a function of angular position.

[18] M. G. Broadhurst and E. R. Fitzgerald, J. Chem. Phys. **32**, (1960), preceding paper, this issue.

[19] J. D. Hoffman and H. G. Pfeiffer, J. Chem. Phys. **22**, 132 (1954).

[20] J. D. Hoffman and B. M. Axilrod, J. Research Natl. Bur. Standards **54**, 357 (1955).

[21] J. D. Hoffman, J. Chem. Phys. **23**, 1331 (1955).

enables one to calculate an approximate value for A from the expression $A=(1/2\pi)(K^1/I)^{\frac{1}{2}}$, where K^1 is the force constant, and I is the moment of inertia of an ethyl stearate molecule about its long axis. For wells 1 and 4 of Fig. 5, A is approximately 2.2×10^{-14}/sec, and $K_7=7.5\times10^5$, $K_8=2.7\times10^5$ at $T=230°$K.

The solutions to Eqs. (3) are

$$N_1=C_{11}+C_{12}\psi$$

$$N_2=C_{41}-C_{12}\psi,$$

where $\psi=\exp(-t/\tau)$, the C's are constants, and $-1/\tau$ is the nonzero root of the secular equations formed from Eqs. (3). If a weak electric field is applied to the sample and suddenly removed, the polarization decays according to the expression,

$$P(t)=P\exp(-t/\tau).$$

By use of the Boltzmann distribution law and appropriate boundary conditions one finds the average polarizability of the above system to be

$$\alpha=C_{11}C_{41}\mu^2/3kTN^2,$$

where μ is the dipole moment, N is the number of dipoles per unit volume, T is the absolute temperature and k is Boltzmann's constant. The above equations have been simplified by using $+30°$ and $-30°$ as the positions of wells 1 and 4 rather than $+30°$ and $-50°$. Making the approximation $C_{41}/N\approx1$ and $C_{11}/N\approx(-V/kT)$, one finds that $\alpha\approx\exp(-V/kT)\mu^2/3kT$. Using $V=0.02$ ev (the difference between the minima of wells 1 and 4 in Fig. 5), $\mu=1.3$ debyes,[22] $N=1.6\times10^{22}$/cm^3, $\tau=1/(K_7+K_8)=0.98\times10^{-6}$ sec, one finds that $\alpha\approx6.3\times10^{-24}$/cm^3.

The theoretical dispersion curves can now be evaluated from the expressions

$$\epsilon''=4\pi N\alpha\kappa[\chi\omega\tau/(1+\chi^2\omega^2\tau^2)],$$

$$\epsilon_s-\epsilon_\infty=4\pi N\kappa\alpha,$$

where κ and χ are correction terms for the difference between the applied field and the field at the dipole. For the Lorentz field,

$$\kappa=(\epsilon_\infty+2)/9=0.44 \qquad (\epsilon_\infty\approx2.0)$$

$$\chi=(\epsilon_s+2)/(\epsilon_\infty+2)=\epsilon_s/4+\tfrac{1}{2}.$$

Thus,

$$\epsilon_s=2.56$$

and

$$\epsilon''=0.56[6.7\times10^{-6}f/(1+4.5\times10^{-11}f^2)],$$

where f is the frequency of oscillation of the applied field. The resulting dispersion involves a single Debye loss peak of height 0.28 with a 150-kc maximum at $-43°$C.

VI. DISCUSSION

On the basis of x-ray measurements by Müller[2] the setting angle (the angle between the plane of the carbon atoms in a molecule and the **a** cell direction) was assumed to be 30° (Fig. 1). A simple check can be made on the potential energy curves (Figs. 4 and 5) since the equilibrium position of the ethyl stearate molecule (which corresponds to the position of the deepest energy well) should be at $\theta=-30°$. The deepest well is located at $-50°$ indicating a probable error in the setting angle given by Müller.[2] The correct setting angle could be found by repeating the calculations at different assumed setting angles until the position of the deepest well for ethyl stearate agrees with the assumed angle. The correction should not, however, produce any large changes in the curve of Fig. 4. Well 4 is seen to have a negative energy as it must have for a stable crystal structure.

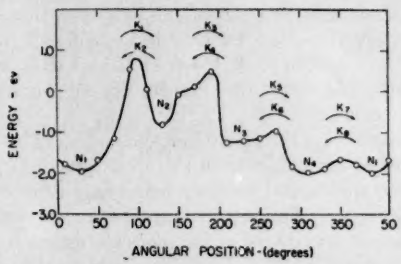

FIG. 5. Total potential energy of ethyl stearate in $n-C_{21}H_{44}$ as a function of angular position. For this curve the coefficient of the repulsive energy has been reduced from 2.75×10^3 to 1.57×10^3 ev for better agreement with experimental data.

The actual height and position of the dielectric dispersion curves as calculated from the energy curve is extremely sensitive to slight changes in the potential function (especially the repulsive potential), so that exact predictions of the dielectric properties are not possible. Similarly the broadness of the actual measured dispersion curves[18] is not correctly predicted from the model used here. It seems unlikely that this broadness could be the result of the superposition of two or more single Debye curves since it would be difficult to reasonably alter the calculations enough to account for more than one relaxation time.

Furthermore, the present model gives no prediction of a second dispersion region that has been found at microwave frequencies in many long chain esters,[23,24] and can reasonably be expected to be present in ester-paraffin mixtures also. The high-frequency dispersion has a low activation energy (about 0.2 ev) indicating transitions over a very low energy barrier. It might be argued that the coefficient of the repulsive energy term C''' should be lowered even further than was done in Fig. 5 so that transitions between wells 1 and 4 could account for the high-frequency dispersion and

[22] R. W. Sillers, Proc. Roy. Soc. (London) **A169**, 66 (1938).

[23] J. S. Dryden and H. K. Welsh, Australian J. Sci. Research **A4**, 616 (1951).

[24] J. S. Dryden and S. Dasgupta, Trans. Faraday Soc. **51**, 1611 (1955).

well 3 might be lowered enough to account for the low-frequency dispersion. Further decrease in C''', however, results in making well 1 deeper than well 4 which is incompatible with the known crystal structure of heneicosane.

It seems that the actual long-chain system has rather important deviations from the ideal behavior assumed for the model, and possible inaccuracies are evident. For instance, the lattice molecules might well shift position as an ethyl stearate molecule moves from one well to another. All such effects would tend to smooth out the potential energy curve and might be the cause of dispersion broadening or even of separate dispersion regions.

It is interesting to note that the calculations carried out here apply equally well to the relaxation dispersion in pure ethyl stearate provided that one assumes a vertical structure. In a preceding paper,[18] it was shown experimentally that the relaxation dispersions in both ethyl stearate and ethyl stearate heneicosane mixtures are very similar and it was suggested that rotation occurs only in parts of the material that have been frozen into a metastable vertical structure. Further, the molecular motions predicted here for the ethyl stearate-heneicosane mixture would not be hindered by the field of the dipole layer of an ethyl stearate lattice. Such a lattice has a net moment in the $\theta=0°$ direction (Fig. 1) and would tend to lower the barrier between the $\theta=+30°$ and $-50°$ wells.

In conclusion, it seems clear that the behavior of polar long-chain molecules in a vertical structure is controlled primarily by attractive van der Waals forces and by repulsive overlap forces. Although the attractive forces are dominant when the molecules are occupying a low-energy equilibrium position, the repulsive forces largely determine the shapes and sizes of the potential energy barriers. At least two positions are low enough in energy to accommodate the dipolar molecules and transitions can occur between these positions. The molecular exchange between the low-energy wells, which are separated by about 80°, gives rise to electric polarization under the influence of a weak applied field. An ideal rigid lattice model cannot adequately predict the shape or position of the dielectric dispersion curves due to the extreme sensitivity of the results to slight errors in the energy function and to departures of actual long-chain crystals from the assumed ideal behavior. But the model does furnish general information necessary to understand the molecular basis for the dielectric behavior of long chain compounds.

VII. ACKNOWLEDGMENTS

The author is grateful to Professor Edwin R. Fitzgerald for his assistance and support of this work. Mrs. Roñald Althouse, Mrs. Thomas Zielinsky, and Mrs. Martin Broadhurst performed many of the calculations. Financial support was due in part to a grant-in-aid from the B. F. Goodrich Company.

On the Presence of NaOH in Crystalline NaCl

DUMAS A. OTTERSON

Lewis Research Center, National Aeronautics and Space Administration, Cleveland, Ohio

(Received February 15, 1960)

The alkalinity of NaCl crystals from various sources are reported with the method of its determination. Melt-grown crystals are usually more alkaline than natural rock salt. The alkalinity may vary in a melt-grown crystal. The alkalinity appears in melted salt, probably as a result of hydrolysis which produces NaOH and possibly by a reaction capable of liberating chlorine.

INTEREST has recently been shown in the contamination of melt-grown sodium chloride crystals by sodium hydroxide.[1-3] Research on the ductility of melt-grown single crystals of NaCl at the Lewis Research Center has prompted a study of this impurity and the ways in which it is introduced into the NaCl. This paper reports the preliminary results.

C. R. Johnson[4] presented evidence as early as 1935 in which the alkalinity of sodium chloride was increased upon melting in air. Burkhard and Corbett[5] measured the water absorbed and the hydrogen chloride liberated by molten alkali chlorides and found that more water was absorbed than could be accounted for by assuming the following hydrolysis:

$$Cl^- + H_2O \rightarrow OH^- + HCl.$$

Etzel and Patterson[6] and Rolfe[2] have shown by absorption spectroscopy that differences exist in the amounts of OH^- present in various samples of alkali halides although quantitative values were not reported. Hacskaylo and Otterson[7] determined the alkalinity in x-irradiated NaCl by measuring the color change of an acid-base indicator. In this case, however, the alkalinity was due predominantly to the presence of "free sodium."

In the present work, the method of Hacskaylo and Otterson is modified to increase the accuracy of the alkalinity measurement in the low-concentration region. In view of the identification of the alkali present in NaCl as NaOH[2,6] the results will be reported here as NaOH.

PROCEDURE

All water used was redistilled from an alkaline permanganate solution. The first portions of this distillation were discarded. This method should produce a water that is free from all weak acids, weak bases, and their salts. All pipetting was done using a rubber bulb in order to reduce contamination with CO_2. The color reagent was 0.02% *p*-nitrophenol in redistilled water.

The well-cleaned color cell was rinsed with the color reagent. The cell was filled with color reagent and its absorbancy measured at 415 mμ. This procedure was repeated until several subsequent readings were the same. A clean 10-ml volumetric flask was rinsed in a similar manner until a rinsing gave the same absorbancy reading as above. The flask was filled with color reagent and the absorbancy reading was made and recorded. The sample (usually 0.20 g) was dissolved in the color solution remaining in the flask. The solution was diluted to mark with color reagent, mixed, and the absorbancy measured. The difference between the last two readings, hereafter referred to as the absorbancy change, was a measure of the alkalinity increase due to the sample.

A calibration curve was made by measuring the color change upon addition of suitable aliquots of 0.002 *N* NaOH to 50 ml of color reagent. This NaOH was made by diluting 0.1 *N* NaOH which was standardized against potassium hydrogen iodate using bromcresol purple as an indicator. Figure 1 was the calibration curve obtained using color reagent containing 0, 2, or

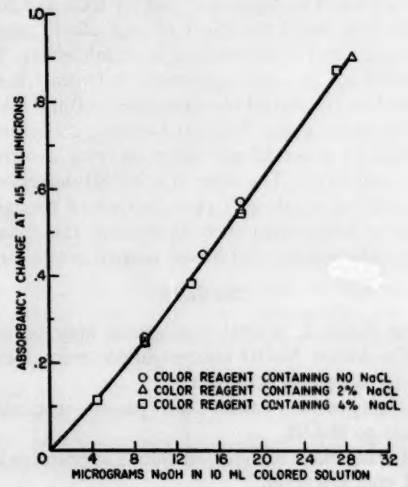

FIG. 1. Calibration curve.

[1] H. W. Etzel and J. G. Allard, Phys. Rev. Letters **2**, 452 (1959).
[2] J. Rolfe, Phys. Rev. Letters **1**, 56 (1958).
[3] W. D. Compton, Phys. Rev. **107**, 1271–5 (1957).
[4] C. R. Johnson, J. Phys. Chem. **39**, 791 (1935).
[5] W. J. Burkhard and J. D. Corbett, U. S. Atomic Energy Commission, ISC **929**, 30 (1957); Chem. Abstracts **52**, 17904a (1958).
[6] H. W. Etzel and D. A. Patterson, Phys. Rev. **112**, 1112 (1959).
[7] M. Hacskaylo and D. A. Otterson, J. Chem. Phys. **21**, 552 (1953).

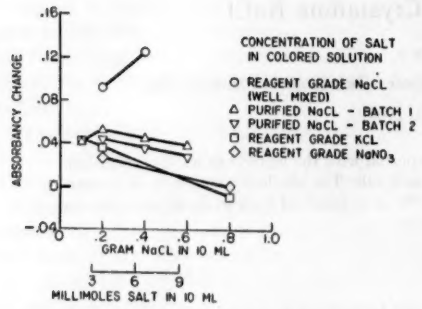

FIG. 2. Color change caused by adding salt.

4% NaCl. None of the points were more than 0.5 μg away from the curve suggesting that the NaCl did not alter the shape of the curve. Beer's law is obviously not obeyed; however, in the part of the curve with the greatest curvature, the maximum error that would result if a calibration point were ignored is less than a microgram.

One should note that the above calibration does not correct for any absorbancy change due to addition of pure NaCl. Figure 2 shows the absorbancy change obtained due to varying amounts of reagent grade NaCl, KCl, $NaNO_3$, and purified NaCl. Purified NaCl was precipitated by adding ethanol to 200 ml of a 95% saturated water solution of NaCl. In order to obtain a sufficiently pure product, it was necessary to discard the precipitate obtained upon adding the first 50 ml of ethanol and to use that obtained upon adding the following 100 ml. The fact that reagent grade NaCl produced an absorbancy change much greater than the other three salts suggested it contained NaOH. In the case of the other three salts, the absorbancy change was inversely proportional, in general, to the amount of salt added. This suggested that for KCl, and $NaNO_3$, and purified NaCl the effect of any alkali present is quite small and is covered up by a salt effect. This is confirmed by the good agreement between the values obtained for the NaOH concentration (9.0 and 8.5 ppm) of the reagent grade NaCl at two salt concentrations (0.2 and 0.4 g per 10 ml) after applying a correction for the salt effect. The error of a NaOH determination is thought to be about 2 ppm in view of the possible sources of error mentioned above and the consistent results obtained for well-mixed reagent grade samples.

RESULTS

From Table I, several conclusions may be drawn.

1. The lowest NaOH concentrations were found in naturally occurring rock salt.

2. Melt-grown crystals can possess considerable amounts of NaOH.

3. Melting NaCl in moist air causes an increase in the NaOH concentration.

TABLE I. Concentration of NaOH in NaCl.

Description of NaCl sample	Concentration of NaOH, ppm
Well-mixed reagent grade	8, 8, 8, 9
Reagent grade melted in stream of moist air for 2 hr	98, 83, 89, 77
Reagent grade melted in open air overnight	226, 328
Harshaw melt-grown single crystals	7, 11, 3, 9, 4, 10, 11, 5, 3, 3, 3, 5, 9, 16, [a](20, 18), 9, 6, 15, (12, 15, 9)
Single crystals purchased from the Optovac Company as OH^- free	4, (0, 2, 2, 1), (3, 5), (5, 7), (3, 3, 4), (7, 6)
Single crystals purchased from the Optovac Company as containing OH^-	(14, 84, 82, 12, 16, 14, 19, 17, 31, 35, 34), (14, 16, 50, 12, 16, 15, 18, 30, 48), (40, 12, 21, 21, 40, 24, 28, 38, 20), 130
Cone end of melt purchased from the Semi-elements Company	(4, 3, 3)
Heel end of melt purchased from the Semi-elements Company	(3, 3)
Windsor Mine, Ontario, Canada, Morton Salt Company	1, 0, 1, −1, 2
Grand Saline Mine, Texas Morton Salt Company	0, 1, 1, 1, [b]8, 4
Natural rock salt (unknown origin)	−1, 1, 4, [b]8, 2

[a] All values in parentheses are on samples from the same crystal.
[b] Outer surface of crystal included.

4. In melt-grown crystals, the alkalinity is not necessarily homogeneous.

Most of the single crystals currently being studied at various laboratories have been grown from the molten salt. The alkalinity of such crystals probably depends on the amount of contact made between the hot salt and those components of moist air that are capable of reacting with it. Water, as mentioned above, is one of these components. Oxygen is another component that appears to be capable of reacting with molten NaCl. This is suggested by recent work of this laboratory in which free chlorine was detected in the effluent gases when dry oxygen was passed over molted NaCl in a platinum boat which was inside a Vycor tube. The test consisted in adding acidified *o*-tolidine[8] to a dilute NaOH solution through which these gases had bubbled. Such a reaction might account for the results of Burkhard and Corbett[5] mentioned in the Introduction. Since natural rock salt crystals have most probably never been melted, the low NaOH concentration reported is to be expected.

[8] M. Hacskaylo, D. A. Otterson, and P. Schwed, J. Chem. Phys. **21**, 1434 (1953).

In general, a sample of NaCl indicated in Table I to be from a particular source was from a single melt; Harshaw crystal might have come from two different melts. In view of the wide variation in results from these samples, the assumption that crystals from a given melt all have the same degree of purity is not necessarily valid. An effort will be made to study the effects of the OH^- concentration on the mechanical properties of NaCl and to study the factors that cause the formation of free chlorine.

THE JOURNAL OF CHEMICAL PHYSICS VOLUME 33, NUMBER 1 JULY, 1960

Primary Processes in the Gaseous Photolysis of Polyatomic Molecules. I. Biacetyl

JEAN T. DUBOIS

Aeronautical Research Laboratory, Wright-Patterson Air Force Base, Ohio

(Received February 10, 1960)

The application of photochemical information to the characterization of primary processes is discussed; the selection of proper experimental conditions is of crucial importance in order to avoid ambiguous or misleading interpretations of such data. As an example, the existing data on the photolysis of biacetyl in the range λ 4358–3660 A is analyzed. The treatment indicates the presence of a single process with an activation energy $E=13\,300$ cal/mole and a frequency factor $\nu=1.5\times10^{13}$ sec^{-1}.

GENERAL

THE usual photochemical experiment calls for the detection and analysis of as many of the products and intermediates as the analytical tools at hand will permit; this is done under various conditions of wavelength, temperature, pressure, and absorbed radiation intensity. In principle, if all the products are quantitatively obtained, a probable mechanism can be evolved for the case under consideration. From such a mechanism the quantum yield of the primary step, i.e., of the intramolecular energy redistribution which results in products, can be calculated. This method in general does not permit a characterization of the primary process for polyatomic molecules in terms of a frequency factor an and activation energy. The reasons for these failures are that generally the primary quantum yields, obtained as described above, are greatly distorted by vibrational stabilization of the dissociating molecule with pressure, and because the effective temperature of the reaction cannot be calculated unless the reacting molecules are sufficiently complex.[1] Thus, if it were possible to photolyze a substance under the conditions, that (a) the pressure is low enough to minimize vibrational stabilization, and (b) the molecule is sufficiently complex to allow its vibrational energy to relax rapidly to a Maxwell-Boltzman distribution during the lifetime of the molecule, then the rate constant for the primary step could be obtained directly from the primary quantum yields, according to the equation

$$k_d=[\phi/(1-\phi)][k_i+(1/\tau_0)], \qquad (1)$$

where ϕ is the primary quantum yield, k_i is the probability of internal conversion, and τ_0 is the natural lifetime of the excited level. The effective vibrational temperature[1] for such a reaction is given by the equation

$$T_{\text{vib}}=T_x+[(\nu-\nu_0)/C_{\text{vib}}], \qquad (2)$$

where T_x is the experimental temperature of the vapor, ν_e is the absorbed frequency, ν_0 is the energy difference between the lowest vibrational levels of the ground state and the fluorescent state, and C_{vib} is the vibrational heat capacity of the molecule.

A conventional Arrhenius plot of $\log k$ vs $1/T_{\text{vib}}$ yields directly the frequency factor and the activation energy involved.

Photolysis at pressures which are low enough to fulfill condition (a) are extremely difficult to carry out with accuracy. The question of how complex a polyatomic molecule should be in order that its relaxation to a Maxwell-Boltzman distribution takes place during its lifetime is yet to be answered. Thus condition (b) is difficult to define. Fortunately, when a molecule contains very little or no excess (over thermal) vibrational energy in its excited state, as is achieved by exciting near the 0–0 transition, the pressure effect on the primary quantum yield ϕ is negligible and the effective temperature becomes the experimental temperature of the vapor. An Arrhenius diagram of $\log k$ vs $1/T_x$ should under these conditions characterize the reaction. Multiple, simultaneous, energy-dependent processes would be indicated by intersecting linear segments on the Arrhenius diagram. Thus, under the condition of low vibrational content in the excited state, the primary process can be defined regardless of the pressure or of the complexity of the molecule.

[1] M. Boudart and J. T. Dubois, J. Chem. Phys. **23**, 223 (1955).

TABLE I. Rates of photolysis of biacetyl at λ 4358 A.

tx°C	$\phi_{av.}$[a]	log kd	$1/Tx \cdot 10^3$
29[b]	0.001	3.78	3.31
75	0.010	4.78	2.87
100	0.042	5.42	2.68
125	0.115	5.89	2.51
145	0.195	6.16	2.39
198	0.408	6.62	2.12

[a] Averaged data of Sheats and Noyes.[3,4]

[b] Because of a small intensity effect at this λ and t, this point is not used in computing the slope of the Arrhenius plot; its position on the diagram, however is indicated by a question mark (?).

BIACETYL AT λ 4358 A

The foregoing is applied to the photolysis of biacetyl because this molecule is typical of a large class of such reactions; there also exist a great deal of reliable quantitative data on this system, and comparison of the process when the 0–0 transition is excited can be made with that at shorter wavelengths.

The spectrum of biacetyl has been studied.[2] Although the 0–0 transition to the first singlet excited state ($I'Au$) is well defined in the crystal at 20°K, its value in the gas phase at 300°K is only roughly estimated at 22 500 cm^{-1}. Systematic studies of the photochemistry and the fluorescence of biacetyl at λ4385 A and λ3660 A have been reported.[3–5] At the longer wavelength, pressure has no effect on either the photolysis or the fluorescence. These results indicate, as expected, that this wavelength excites only the lowest vibrational levels of the first singlet excited state. Measurements of the ratio of phosphorescence to fluorescence[6] at λ4358 A and λ3660 A also suggest that the internal conversion process is independent of wavelength and that the minimum value of the probability of internal conversion is 6×10^6 sec^{-1}.

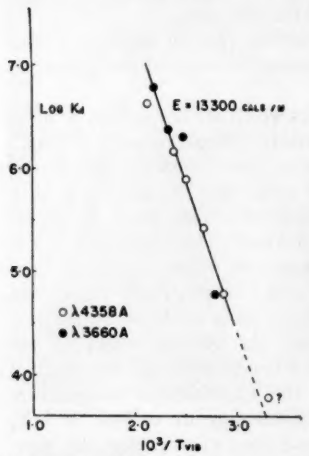

FIG. 1. Arrhenius diagram for the photolysis of biacetyl molecules excited to the $I'Au$ level. For λ 4358 A, the vibrational excitation is purely thermal and T_{vib} is the same as T experimental.

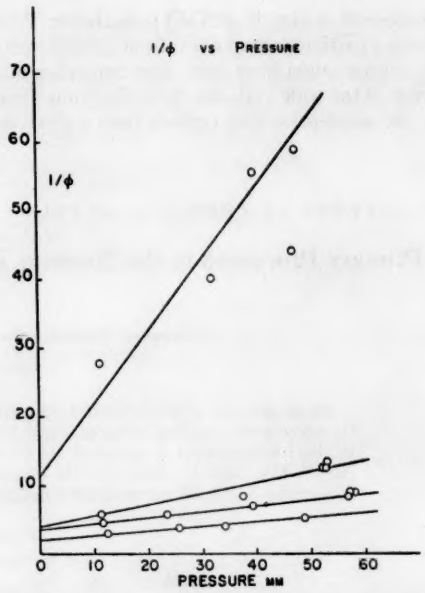

FIG. 2. Extrapolation of the inverse of the experimentally determined primary quantum yields of biacetyl photolysis to zero pressure.

When τ_0 in Eq. (1) is taken as 10^{-5} sec[6], the rate constants obtained are shown in Table I. From these and the experimental temperature, a frequency factor $\nu=1.5\times10^{13}$ and an activation energy $E=13\,300$ cal/mole are calculated (see Fig. 1).

TENTATIVE CORRELATION OF BIACETYL PHOTOLYSIS AT λ 3660 A

In biacetyl at λ3660 A, vibrational stabilization plays an important role. This is shown by the decrease of the primary yield with pressure and the corresponding increase in fluorescence.[3–5] This process is a stepwise degradation of vibrational energy with pressure, and its analytical form[1] is such that the function $1/\phi$ plotted against pressure is linear at low pressures (see Fig. 2). Thus, the true primary quantum yields of

TABLE II. Rates of photolysis of biacetyl at λ 3660 A.

tx°C	$\phi_{lim.}$[a]	log kd	$1/T_{vib.} \cdot 10^3$
29	0.088	4.78	2.79
75	0.25	6.30	2.48
100	0.28	6.37	2.33
124	0.5	6.78	2.20
198[b]	...	...	...

[a] Data of Sheats and Noyes[3,4] corrected for vibrational stabilization.

[b] Data at this temperature are insufficient for extrapolation to $\phi_{lim.}$

[2] J. W. Sidman and D. S. McClure, J. Am. Chem. Soc. **77**, 6461 (1955).

[3] G. F. Sheats and W. A. Noyes, Jr., J. Am. Chem. Soc. **77**, 1421 (1955).

[4] G. F. Sheats and W. A. Noyes, Jr., J. Am. Chem. Soc. **77**, 4532 (1955).

[5] J. Heicklen, J. Am. Chem. Soc. **81**, 3863 (1959).

[6] H. Okabe and W. A. Noyes, Jr., J. Am. Chem. Soc. **79**, 801 (1957).

biacetyl at λ3660 A (in the absence of collisions) can be obtained by extrapolation to zero pressure. These results are given in Table II.

It may be questioned whether biacetyl is complex enough for a vibrational temperature to be defined according to Eq. (2). It is, however, interesting to note the results of such an analysis. The rate of the primary process at λ3660 A is given by

$$k_d=\nu \exp\left\{-\frac{E}{R[T_x+(\nu_e-\nu_0)/C_{\text{vib}}]}\right\} \qquad (3)$$

where E and ν have their usual significance, and the other symbols have been defined. If the primary process at this wavelength is the same as at λ4358 A, ν and E are determined, and Eq. (3), when solved for C_{vib}, gives $C_{\text{vib}}=78$ cm^{-1}. From this, T_{vib} for all the data at λ3660 A is calculated and recorded in Table II. The Arrhenius diagram obtained by plotting the log$k$ against $1/T_{\text{vib}}$ is shown in Fig. 1, superimposed on that for the data at λ4358 A. The congruence of the two plots would, of course, be expected if any significance were attached to vibrational temperatures for a molecule such as biacetyl, provided that a unique primary process were representative of the range of wavelengths in question. Thus, it seems as for the case of even simpler systems,[7] that an effective vibrational temperature does describe the system. It remains to explain the abnormally high heat capacity (ca 3.5 times the maximum theoretical heat capacity at constant volume for a molecule of 12 atoms) which results from this treatment. Errors in the choice of k_i or τ_0 would affect neither the activation energy nor the vibrational heat capacity. C_{vib}, however, depends on accurate knowledge of the 0–0 transition.

A general way to obtain the vibrational heat capacity, the activation energy and the frequency factor for any intramolecular energy transfer process is to solve Eq. (3) for three sets of data (corrected for vibrational stabilization) at three different wavelengths, provided that the range of wavelengths chosen corresponds to absorption to a single electronic excited state. A previous suggestion that C_{vib} can be obtained from the horizontal displacement of curves obtained when log$k$ is plotted against the inverse of the experimental temperature[8] is only meaningful for specified narrow ranges of temperature. In the interest of clarifying further the picture of intramolecular energy transfer processes, measurements should be made under conditions where the ranges of thermal and optical excitation energies overlap.

[7] G. Herzberg, *Spectra of Diatomic Molecules* (D. Van Nostrand Company, Inc., Princeton, New Jersey, 1950), 2nd ed., Chap. IV, p. 204.

PHOTOLYSIS AT SHORTER WAVELENGTHS

Accurate experimental data for biacetyl photolysis also exist at λ3130, 2804, 2654, 2537, and 2380 A,[9] but the number of low-pressure points at these wavelengths is not sufficient for a reasonable extrapolation of $1/\phi$ against pressure. It would be of great interest to obtain the necessary data at these wavelengths because there is chemical evidence that not one, but two simultaneous primary processes contribute to the photodissociation of biacetyl,[10]

$$CH_3COCOCH_3 \rightarrow 2CH_3CO$$

$$\text{or} \rightarrow CH_3COCH_3+CO.$$

Furthermore, upon absorption of radiation λ3130 A and shorter, the $^1\Pi'Au$ state of biacetyl becomes excited[2] and may very well lead to the second postulated process. It is known that steps of the type $B_n+B \rightarrow B_0+B$[5,6,11] where the subscripts "n' and '0" refer to vibrationally active and inactive levels, respectively, are a first approximation only and do not represent properly the cascade process which occurs in the system. A detailed calculation of this cascade degradation of vibrational energy is not possible at this time. However, its influence on photolysis is understood and may be accounted for in the manner described.

[8] B. Stevens, J. Chem. Phys. **24**, 488 (1956).

[9] W. A. Noyes, Jr., G. B. Porter, and J. E. Jolley, Chem. Revs. **56**, 49 (1956).

[10] W. E. Bell and F. E. Blacet, J. Am. Chem. Soc. **76**, 5332 (1959).

[11] J. Heicklen and W. A. Noyes, Jr., J. Am. Chem. Soc. **81**, 3858 (1959).

Conduction Electrons in Sodium Tungsten Bronze*

JOSEPH M. KELLER

Institute for Atomic Research and Department of Physics, Iowa State University, Ames, Iowa

(Received March 1, 1960)

The vanishing of the Knight shift of Na^{23} in sodium tungsten bronze is interpreted in terms of an inverted conduction band.

SODIUM tungsten bronzes are nonstoichiometric crystals, with the chemical formula Na_xWO_3, $0.3<x<1.0$. The structure is nearly cubic[1]; if a W atom is at the center of a cube, the O atoms are at the face centers, and the Na atoms occupy corners. WO_3 is an insulator (with noncubic structure), but each Na atom appears to provide one nearly free conduction electron in the bronze.[2]

Barnes, Hultsch, and Jones[3] have measured the nuclear magnetic resonance of Na^{23} in sodium tungsten bronze over a range of sodium concentration from $x=0.56$ to $x=0.89$ and find no Knight shift. This implies a negligible concentration of conduction electrons at the Na positions. A possible explanation for this fact lies in the assumption that the conduction band is one arising from W orbitals and that it is "inverted," i.e., that the bottom of the band occurs at maximum rather than minimum value of the wave vector $\mathbf{k}$.

To the extent that the bonding in WO_3 is ionic, additional electrons would be most strongly attracted to positions of the positively charged W ions and repelled by the negative O ions. So, from an atomic standpoint, one would expect the electrons liberated from the Na to occupy W orbitals (perhaps $6s$). In the crystal, these will be combined into bands of Bloch functions, whose form and energy will be affected by the other atoms. If one assumes that the most important effect is coulomb repulsion by the O ions, and if (for simplicity) one calculates the dependence of energy E on $\mathbf{k}$ by the "tight binding" approximation,[4] one gets the usual result except with a reversal of sign:

$$E=E_0+\gamma(\cos k_x a+\cos k_y a+\cos k_z a),$$

where γ is a positive constant. Here a is the lattice parameter.

According to this result, zero wave number indicates the maximum energy of the band, and the minimum energy occurs for $k=(\pm\pi/a, \pm\pi/a, \pm\pi/a)$. (These 8 points are all equivalent to a single point in the reduced zone.) Now a wave function with this wave number is a real function that must change sign in going from one unit cell of the crystal to the next. If its extreme value occurs at the W sites, it will have nodes at the Na sites, and, in fact, every place on the planes midway between W atoms. Of course, only one electron in the crystal can have exactly the prescribed wave number. But electrons with nearby wave numbers must have correspondingly small densities at the Na nuclei.

Sienko[5] has recently proposed an alternative explanation for the vanishing of charge density at the Na positions, based on angular rather than translational symmetry. Sienko suggests that the conduction band is formed from the twofold degenerate $5d$ orbitals of W, which should have nodes in the directions of the nearest Na atoms. This model requires that mixing of other than d states in the crystal wave functions be slight, which is reasonable, at best, only for special k values. On the other hand, the twofold degeneracy of the d bands makes departure from some particular k value less serious than in the author's model.

If the conduction electrons are repelled by O ions, as assumed by the author, then one would expect the lowest-energy d orbitals of W in the tungsten bronzes to be the threefold degenerate d orbitals, whose nodes are in the direction of the O atoms and not toward the Na positions.

G. C. Danielson (in a private communication) has pointed out that the present proposal predicts a vanishing Knight shift also at the oxygen positions in sodium tungsten bronze and that a test of these ideas would be provided by measuring the nuclear magnetic resonance of O^{17} in bronzes containing some of this isotope.

Another, probably more feasible, experiment of measuring the nuclear magnetic resonance of the W has been proposed by R. G. Barnes (private communication). This experiment would not test my hypothesis directly, but would distinguish between s and d orbitals on W. A large Knight shift would imply that the conduction electrons have a largely s character about the W positions, and then it seems difficult to understand the vanishing Knight shift of Na except on the basis of translational nodes in the wave functions. A vanishing Knight shift would indicate angular nodes in these wave functions, in support of Sienko's hypothesis.

* This work was performed in the Ames Laboratory of the U. S. Atomic Energy Commission.

[1] J. H. Ingold and R. C. DeVries, Acta Met. **6**, 736 (1958).

[2] W. R. Gardner and G. C. Danielson, Phys. Rev. **93**, 46 (1954).

[3] R. G. Barnes, R. A. Hultsch, and W. H. Jones, Bull. Am. Phys. Soc. Sec. II, **4**, 166 (1959).

[4] N. F. Mott and H. Jones, *The Theory of the Properties of Metals and Alloys* (Dover Publications, New York, 1958), p. 68.

[5] M. J. Sienko, J. Am. Chem. Soc. **81**, 5556 (1959).

Infrared Studies of Crystal Benzene. IV. Absolute Intensities

WILLIS B. PERSON AND CHARLES A. SWENSON

Department of Chemistry, State University of Iowa, Iowa City, Iowa

(Received January 21, 1960)

The intensity of the absorption due to ν_{20} at 1036 cm^{-1} in solid benzene at −170°C has been measured relative to the intensity of this band measured with the same benzene film in the liquid phase at 25°C. From this ratio and from the value for the absolute intensity of ν_{20} in liquid benzene reported by Hisatsune and Jayadevappa, a value of 670±90 darks for the absolute intensity of ν_{20} in solid benzene has been obtained. Using the relative intensity measurements reported earlier, the absolute intensities of all the gas-phase-allowed fundamentals have been estimated. All the intensities in the crystal are lower than the values in the liquid phase, but the behavior of the bands at 1036 and 1480 cm^{-1} is not too abnormal. However, the intensities of the fundamentals at 687 and 3060 cm^{-1} decrease markedly from the gas-phase values, the former by a factor greater than two, the latter by a factor of seven. Thus, it is concluded that the interactions in the solid which cause the intensity to change are quite specifically limited to these two normal modes. Analysis of the data using the isotope intensity sum rules modified for use with crystals reveals that the intensity changes observed are much greater than those expected due to simple distortion of the norma coordinates by the crystal field.

INTRODUCTION

IN an earlier paper[1] we have reported the intensities of benzene fundamentals relative to the E_{1u} fundamental, ν_{20}, at 1036 cm^{-1}. These measurements showed that large intensity changes occurred when the benzene molecules condense from the gas to the solid phase, even though the changes in frequency are quite small. As interesting as these results may be, no real attempt can be made to understand them until we know just which fundamental is different in the solid. Thus, we must make some attempt to measure the *absolute* intensities of these fundamentals in the polycrystalline samples.

The experimental difficulties connected with absolute intensity measurements in solid firms are formidable. All the errors in measuring the integrated absorbance **Bnl** which were discussed in our first paper[1] are possible. However, the problem of measuring the path length is even more difficult. Indeed, this problem is almost insurmountable. We made several attempts to solve it, finally resorting to an old technique: the sample is contained in a liquid cell and frozen down—we hope without changing the value of the concentration per unit area, *nl*. From a measurement of the integrated absorbance and knowledge of **B** in the liquid, we were able to get a fairly reliable estimate of the absolute intensity of the 1036 cm^{-1} band, ν_{20}. From the values of the relative intensities which we reported earlier,[1] we can then determine approximate absolute intensities for all the band observed in a thin film of solid benzene. The results of these measurements are reported below.

EXPERIMENTAL PART

Much of the experimental procedure was the same as described earlier[1] for the measurement of the relative intensities. The spectra were obtained using the same Perkin-Elmer Model 12c double-pass prism spectrometer described earlier.[1] The procedure used in order to obtain the intensity has also been described before,[1] and the error analysis there applies also to the absolute intensity measurements here. The error in our knowledge of *nl* will be discussed separately.

The main difference in procedure was in sampling. In order to be able to estimate the value of *nl* with any reliability, the following procedure was adopted. A small fixed liquid cell was built from two CsBr windows 25- × 16- × 5-mm, separated by a spacer made of amalgamated silver foil which was nominally 2 μ thick. The outer window was drilled and attached to a stainless steel filling block by amalgamated spacers. The details of construction are shown in Fig. 1. This cell was clamped to the brass cooling block of a conventional cold cell by means of screws through the filling block. The cell length was adjusted by varying the pressure on the screws. The final cell was about 10 μ in length. On the bottom of the outer jacket of the cold cell was a large hole through which the liquid cell could be filled with a hypodermic syringe in the usual way. The metal adapters on the filling plate *F* were then closed with Teflon plugs as usual. The hole in the outer jacket of the cold cell was then covered with a large aluminum plate, $3\frac{1}{4}$ in. square, which was sealed to the glass with Apiezon "Q" wax. The cold cell could then be evacuated. However, in order to prevent the Teflon plugs from popping out and thus causing the benzene sample to be lost, the cell was cooled before evacuation. Liquid nitrogen was poured into the inner container and the temperature of the sample was reduced to the point where the benzene froze. Then the cell was evacuated slowly and the liquid nitrogen replenished as needed. In this way the temperature of the sample could be reduced to about −170°C, when evacuation was as complete as possible.

In order to determine *nl*, the following procedure was adopted. We measured the integrated absorbance

[1] C. A. Swenson and W. B. Person, J. Chem. Phys. **32**, 56 (1960), Part II of this series.

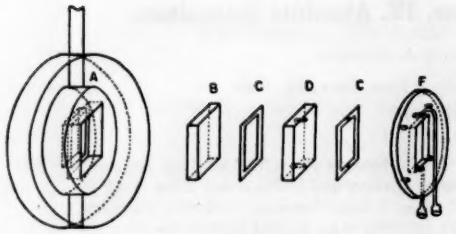

FIG. 1. Detail of the assembly of the fixed liquid cell for intensity measurements. A: cooling block and radiation shield; B: CsBr window; C: amalgamated silver spacers; D: drilled CsBr window; F: stainless steel plate, showing the hypodermic needles used for filling.

Bnl of the 1036 cm^{-1} band for a liquid film in the cell. Then, without moving the cell, we rapidly cooled and evacuated it until we got a solid film. We then measured the intensity of the absorption of this band in the solid. *We then made the assumption that the nl product remained constant during the process of freezing.* We thus determined the ratio of the intensity of this band in the solid to the intensity of the same band in the liquid. From the measurements of Hisatsune and Jayadevappa[2-4] on the absolute intensity of this band in liquid benzene, we are then able to determine the absolute intensity of the 1036 cm^{-1} fundamental in the solid.

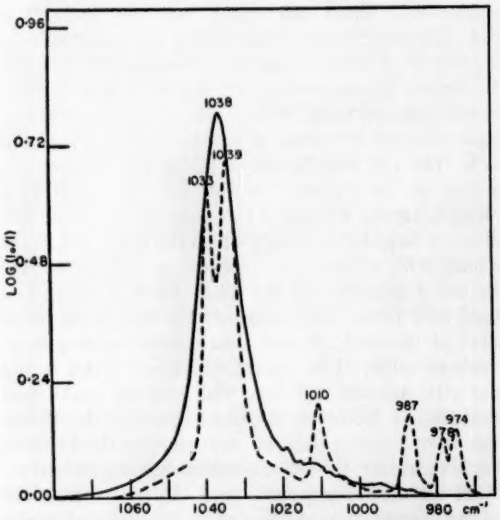

FIG. 2. Comparison of the spectrum of ν_{20} in liquid benzene to that in solid benzene at −160°C; —— liquid benzene; ------ solid benzene.

[2] I. C. Hisatsune and E. S. Jayadevappa, J. Chem. Phys. **30**, 848 (1959).
[3] E. S. Jayadevappa, Ph.D. thesis, Kansas State University, 1959.
[4] I. C. Hisatsune and E. S. Jayadevappa, J. Chem. Phys. **32**, 565 (1960).

Subsequent measurements of the temperature dependence of the intensities of these bands in solid benzene[5,6] indicate that our assumption that *nl* does not change is probably reasonably correct.

Some ambiguity is introduced into this procedure by the unsymmetrical shape of the 1036 cm^{-1} band in the liquid state.[4] The wing of this band on the low-frequency side is rather extended, and the whole band is distorted by the increased absorption in the low-frequency wing. We believe that this is due to the absorption in the liquid state due to the induced infrared bands at 1010, 987, and 975 cm^{-1} in the solid spectrum.[1] Thus, in comparing the intensity of the 1036 cm^{-1} band in the liquid to that in the solid, we should try to separate out the intensity of the induced bands. This has been done graphically, by drawing in the low-frequency wind so that the band appears to be symmetrical, as described by Hisatsune and Jayadevappa.[4]

TABLE I. Ratio of the intensity of ν_{20} in liquid benzene to the intensity in crystal benzene ($t = -170°C$).

Expt.	Ratio
1	1.58±0.09
2	1.32±0.06
3	1.98±0.06
4	1.35±0.15
5	1.60±0.11
6	1.94±0.15
	Av 1.63±0.22

RESULTS

Figure 2 shows a comparison between the spectra of ν_{20} at 1036 cm^{-1} in the liquid phase and in the solid phase for the same film of liquid benzene, obtained as described above. We see that the intensity of this band in liquid benzene is somewhat greater than the intensity in solid benzene, primarily because of the more extended wings of the band in the liquid. Also, the absorption on the low-frequency side in the liquid phase is apparent.

In Table I, the ratio of the intensity of this band in the liquid phase to the intensity of this band in the solid phase is shown for a number of measurements. We see that the average deviation from the mean for all these measurements is only about twice the average deviation found in the three spectra comprising each individual determination (see Part II[1] for a description of the experimental procedures and estimates of the latter average deviation). Part of the scatter in these data comes about because of the ambiguity in the measurement of the intensity of ν_{20} in the liquid state, which we discussed above. Actually the observed scatter from the mean is about the same order as the scatter

[5] D. Olsen, Ph.D. thesis, State University of Iowa, 1960.
[6] J. Fordemwalt, Ph.D. thesis, State University of Iowa, 1960.

observed in our relative intensity measurements, and is approximately the order of the estimated experimental errors.[1] Thus, *assuming that the nl product remains constant as the liquid is condensed to the solid at* −170°C, this scatter probably represents the error in our absolute intensity.

The data in Table I have been selected somewhat. In measuring this liquid-solid intensity ratio, the band shape for this 1036 cm^{-1} band in solid benzene sometimes changed its appearance. We believe this was due to partial orientation of the solid film as it froze between the two CsBr windows. Experiments showing this effect were discarded and the solid-liquid intensity ratio was measured only for solid films whose spectra were similar to those observed on films formed by use of the spray technique.

The absolute intensity of ν_{20} in the solid phase has been calculated using our value for the liquid-solid intensity ratio shown in Table I and the value of the intensity of ν_{20} in the liquid phase found by Hisatsune and Jayadevappa.[2] The absolute intensities of the other infrared-active fundamentals in solid benzene have been calculated from this value and the relative intensity values reported earlier.[1] The absolute intensity values for these four gas-phase-allowed fundamentals in all three phases are shown in Table II.

TABLE II. Comparison of the absolute intensities of the gas-phase-allowed fundamental vibrations of benzene in the three phases.

Phase	ν_{11} (687 cm^{-1})	ν_{20} (1036 cm^{-1})	ν_{19} (1480 cm^{-1})	ν_{18}[a] (3060 cm^{-1} doublet)
Gas[b] A_g[c]	8780	880	1300	5980
Liquid[d] A_l[c]	8970	1090	1910	4440
Solid[e] A_s[c]	3500[f]±650	670±90	1200±300	950±200

[a] This is the sum of the intensities of the two components of the Fermi doublet, at 3036 and 3092 cm^{-1}.
[b] Data from H. Spedding and D. H. Whiffen, Proc. Roy. Soc. (London) **A238**, 245 (1956).
[c] Units are cm^{-1} cm^2/mM (darks).
[d] Data from Hisatsune and Jayadevappa[4] (no wing correction applied).
[e] This research (t=−170°C).
[f] This includes the intensity of the 705 cm^{-1} band.

DISCUSSION

The measurements reported earlier[1] on the relative intensities of bands in crystal benzene led us to expect remarkable changes in the intensities of the gas-phase-allowed fundamentals of benzene. The results shown in Table II thus come as no shock. The changes in ν_{19} and ν_{20} from the liquid phase to the solid phase are indeed remarkable enough, showing a decrease in intensity of about 50%. By a most peculiar coincidence the intensities of these two bands are about the same in the solid phase as they are in the gas phase. However, if we may consider the behavior of these bands to be "normal," we see immediately that the behavior of ν_{18}, at 3000 cm^{-1}, and to a lesser extent, of ν_{11}, at 687 cm^{-1}, is most abnormal. The C—H stretching frequency, in particular, shows a decrease in intensity from the gas phase *by a factor of seven*. This occurs in spite of the fact that the frequency shift is very small.[1]

As Hisatsune and Jayadevappa point out,[4] the behavior of intensity exhibited by ν_{19} and ν_{20} on condensation from the gas phase to the liquid phase is more or less in agreement with the equation of Polo and Wilson[7] which takes into account the effect due to the changed dielectric constant of the medium surrounding the absorbing molecule. Thus, the behavior of these bands from gas to liquid may indeed be "normal." We should expect that this effect should be about the same in the solid as in the liquid phase, for there is not a marked change in the index of refraction of benzene in going from liquid to solid. Thus, some other effect apparently becomes dominant in determining the intensity of the band in the solid state.

One possible explanation for this change might be a distortion of the normal vibrations in the solid state. This presumably results in the appearance in the spectrum of the solid of bands such as the B_{1u} vibration at 1010 cm^{-1} which do not appear in the gas phase. Thus, distortion of the normal vibrations in the solid *might* result in a decrease in intensity of the E_{1u} fundamental with a resulting increase in intensity of the induced bands. However, this seems rather unlikely, as we have discussed earlier,[1] due to the small change in the frequencies going from gas phase to the solid phase. Also, the induced bands in the liquid are probably even more intense than these bands in the solid phase, and so it would seem that the change in normal coordinates from liquid to solid should thus not be very great. However, if such distortion of the normal coordinates were to occur, the intensities of the bands observed for solid benzene would be related to the intensities of these bands in the isolated molecules by the sum rules first developed by Crawford for isotopically substituted molecules.[8]

Crawford gave two relations which should hold:

$$\sum_1^F = \sum_a (I_{1a}/\omega_{1a}^2) = 4\pi^2 \sum_x p_{1k}^x p_{1j}^x (F^{-1})^{kj} \qquad (1)$$

and

$$\sum_1^G = \sum_a I_{1a} = \sum_x p_{1k}^x p_{1j}^x G_1^{kj}. \qquad (2)$$

Here I_{1a} is essentially the integrated absorption coefficient, **A** (multiplied by the universal constants); p_{1k}^x is the derivative of the x component of the dipole moment, **p**, with respect to the kth internal coordinate R^k (in practice, the kth symmetry coordinate); $(F^{-1})^{kj}$ is the kj term of the inverse force constant matrix;

[7] S. R. Polo and K. Wilson, J. Chem. Phys. **23**, 2376 (1955).

[8] B. Crawford, Jr., J. Chem. Phys. **20**, 977 (1952).

TABLE III. Intensity sum rule for crystal benzene.

Band	Intensity
Gas	
ν_{11} (671)	8780
ν_{20} (1036)	880
ν_{19} (1480)	1300
ν_{18} (3060)	5980
	ΣI_{1a}=16 940
Solid (t=−170°)	
ν_{11} (687 region)	3500
ν_{17} (975)	70
? (987)	40
ν_{12} (1010)	50
ν_{20} (1036)	670
ν_{15} (1148)	100
ν_{19} (1478)	1200
ν_{18} (3036±3090)	950
ν_{13} (3067)	200
	ΣI_{2a}=6780

G_1^{kj} is the kj component of the inverse kinetic energy matrix G. The subscript 1 designates a particular isotopic molecule.

In the case of isosopically substituted molecules, the F matrix is the same as for the normal molecule, although the G matrix is different. Thus, Eq. (1) states that the intensity sum on the left-hand side will be invariant under isotopic substitution, since the $p_{1k}{}^z$'s are the same and F is the same. However, if we use these relations in comparing the spectrum of a molecule in the crystal with that of an isolated molecule then we must reexamine these rules. First let us consider the $p_{1k}{}^z$'s ($\equiv[\partial p^z/\partial R^k]_1$). In applying these rules, we assume that these terms are the same for the molecule in the crystal as they are for the isolated molecule. (This is the "oriented gas" approximation.) The benzene molecule is not distorted appreciably in the crystal[9]; therefore, the G matrix, which depends only on the geometry, will be the same as the G matrix for the isolated molecule. However, the F matrix may be different, because the restoring forces for certain distortions of the molecule will be different due to the presence of the neighboring molecules. Thus, the normal coordinates of the isolated molecule will be distorted because of the change in the F matrix so that we get the new normal coordinates of the crystal.

As a result of this analysis, it is obvious that the intensity sum rule (1) used with isotopically substituted molecules is not correct for the case of the crystal, and the appropriate intensity sum rule for comparing intensities of the crystal to those of the isolated molecule is the "G-sum rule" given by Eq. (2). In the present example, the summation should be carried out over all the *ungerade* fundamental frequencies.

[9] E. G. Cox, D. W. J. Cruickshank, and J. A. S. Smith, Proc. Roy. Soc. (London) **A247**, 1 (1958).

From the absolute intensities given in Table II and from the intensity ratios reported in Table III of Part II,[1] we have calculated the intensities for the *ungerade* fundamental frequencies. These are presented in Table III. It is obvious that the intensity sum for these bands in the crystal is far too small. The obvious conclusion is that the $\partial p^z/\partial R_k$'s are different for the molecule in the crystal, and, as we stated above, the observed changes in intensity are definitely not due to a distortion of the normal coordinates alone.

These results were obtained from a sample at a temperature of −170°C. Preliminary results[5] show that there is a considerable decrease in intensity as the temperature decreases. However, we feel sure that this temperature effect will certainly not account for the differences observed in the intensity of ν_{18}, for example, in the different phases.

Finally, we should examine the assumption that nl remains constant. We have estimated the effect on the cell length, l, due to cooling from room temperature to liquid nitrogen temperature to be negligible, and Olsen[5] has verified experimentally that the cell length is the same within the experimental error of ±1.5 μ. Thus, the variation in nl will be due entirely to the variation in density with temperature. Solid benzene is considerably more dense than liquid benzene (d= 1.02 at −3°C compared with d=0.879 for liquid benzene at 25°C), and the density at liquid-nitrogen temperatures is somewhat greater than at 0°C. Thus if nl changes, the calculated value of B which we report in Table II is *too high*, possibly by 30%. Since these values are already much lower than the values reported for the liquid benzene, the failure of our assumption of a constant value for nl will result in an even greater discrepancy between the values in the solid and in the other phases.

Other errors have been discussed earlier.[1] For the reasons given there, we believe that the errors in the measured values of the integrated intensities of bands in the solid phase are probably of the order of 10 to 20%. The error due to resolution would tend to make our values of **B** too low, but the error due to reflection would tend to make **B** high. We conclude that these errors will have little effect on the results reported here. The decrease in the intensities of ν_{11} and ν_{18} from the liquid to the solid phase is an extension of a trend noted by Hisatsune and Jayadevappa in their measurements in liquid benzene, when the values for these bands are compared with the gas-phase values.[4]

ACKNOWLEDGMENTS

Financial support by the Office of Ordnance Research, U. S. Army, is gratefully acknowledged. It is a pleasure to acknowledge the many helpful discussions and correspondence with Dr. R. M. Hexter, Professor D. A. Dows, and Professor I. C. Hisatsune.

Casimir Coefficients and Minimum Entropy Production

R. E. NETTLETON

Mineral Products Division, National Bureau of Standards, Washington, D. C.

(Received February 15, 1960)

The rate equations obeyed by scalar relaxation parameters in a liquid are extended to include inertial terms in the form of second-order time derivatives, and the relations containing these terms are then written formally as first-order equations by treating first-order time derivatives as additional parameters. The resulting equations are interpreted thermodynamically as phenomenological relations containing anti-symmetric Casimir coefficients, and this interpretation leads, with application of the Onsager-Casimir reciprocity theorem, to an additional set of phenomenological equations which reduces to those used in an earlier relaxation theory when inertial effects are neglected. In this way, earlier formulas for the bulk viscosity and high-frequency bulk modulus are recovered unchanged. It is also shown why Prigogine's minimum entropy production theorem should no longer hold when one considers inertial effects.

INTRODUCTION

IT has been recognized that the decay of small fluctuations in the variables determining the macroscopic state of a system will obey linear differential equations of first order in the time only if no attempt is made to describe changes which occur over exceedingly short time intervals. When short times are to be considered, second-order time derivatives appear, representing what we shall call "inertial effects." This has been demonstrated by Kästner,[1] who started with the Kramers equation for the phase space distribution function of a system interacting weakly and impulsively with a heat bath and derived a set of second-order differential equations for the state variables. If the latter equations are averaged over a small interval of time, the high-frequency Fourier components of the motion, which make the main contribution to the inertial terms, will average to zero, and the time-averaged variables will approximately obey first-order equations such that evolution of the system in time is determined by specifying the values of the variables at some instant, but not their time derivatives. The time-averaged states which evolve in this way are analogous to what Landau and Lifshitz[2] have called states of "incomplete equilibrium."

Since the phenomenological equations of irreversible thermodynamics are of first order,[3] it would appear at first that these equations neglect inertial effects and consequently describe only states of incomplete equilibrium. However, two examples have been given to show that the usual formulation of the theory of irreversible processes can be made to include inertial terms if one employs the mathematical device of reducing a second-order differential equation to a pair of equations of first order. In the first of these examples, Meixner has shown,[4] for the particular case of a system of dipoles rotating about fixed axes, that inertial effects may be introduced implicitly into a system of first-order differential equations through the introduction of variables the elimination of which leads to equations of second order in time. The variables eliminated in this way have opposite symmetry with respect to time reversal from the remaining variables, to which they are linked by phenomenological coefficients obeying the anti-reciprocity theorem of Casimir (footnote reference 3, p. 216). It has been shown,[5] similarly, that inertial effects in heat conduction may be treated by supposing that the energy flux vector depends on a vector parameter, antisymmetric with respect to time reversal, which in turn obeys a linear relaxation equation.

The foregoing examples, which link in the same relaxation equation variables of opposite time-reversal symmetry, violate the principle that the steady state, approached by the system when some of the variables are held fixed, should be a state of minimum entropy production. This has been pointed out by Callen[6] who argues that the Casimir coefficients all vanish. The Callen treatment, however, does not appear to account for inertial effects, since the independent variables he uses are all components of the quantum mechanical density matrix and do not include time derivatives of these components. In the present treatment we shall use the time derivatives of internal state variables, along with the variables themselves, to specify a non-equilibrium state and shall link all these parameters in a system of first-order linear relaxation equations formally analogous to that introduced by Meixner.[4] This set of first-order equations reduces, at low frequencies, to a set used in an earlier paper[7] to describe the relaxation of the parameters giving the distribution of molecules among a discrete set of vibrational-rotational and configurational states, and thus we shall obtain here a more general basis for the latter equations, as well as a new derivation of an expression pre-

[1] S. Kästner, Ann. Physik **458**, 82 (1959).
[2] L. D. Landau and E. M. Lifshitz, *Statistical Physics* (Addison-Wesley Publishing Company, Inc., Reading, Massachusetts, 1958), p. 377.
[3] S. R. DeGroot, *Thermodynamics of Irreversible Processes* (North-Holland Publishing Company, Amsterdam, 1951), see Chap. II.
[4] J. Meixner, Z. Physik **149**, 624 (1957).
[5] R. E. Nettleton, Phys. Fluids **3**, 216 (1960).
[6] H. B. Callen, Phys. Rev. **105**, 360 (1957).
[7] R. E. Nettleton, J. Acoust. Soc. Am. **31**, 557 (1959).

viously employed[7,8] to calculate the bulk viscosity in a liquid. A general expression for the rate of entropy change in the presence of inertial effects will be derived, from which it will be seen why the steady state is not, under these circumstances, the state which minimizes the rate of entropy production.

RELAXATION EQUATIONS

Consider an infinite, homogeneous liquid. The system to be described is a small region in this liquid just large enough for the application of statistics to the molecules therein. Internal states of this system are specified by N independent scalar parameters $\zeta_i (i=1, \cdots, N)$, and for concreteness we shall discuss a model in which each molecule can be in one of N states plus the ground state (the latter denoted by index $i=0$), ζ_i being the fractional number of molecules in state i. In particular, the states may be the various vibrational-rotational levels of a molecule and the energy levels occupied by a molecule in a given potential well determined by interaction with neighboring molecules.

In thermal and mechanical equilibrium, the ζ_i can be calculated from the partition function as functions $\zeta_i^0 (i=1, \cdots, N)$ of the mass density ρ and temperature T. When a small fluctuation from this equilibrium state occurs, the ζ_i will relax toward the values ζ_i^0 determined by the local density and temperature—a fact which we can express by a system of equations

$$\dot{\zeta}_i = \sum_j L_{ij}\xi_j + \sum_{j,k} L_{ijk}\xi_j\xi_k + \cdots,$$

$$\xi_i \equiv \zeta_i - \zeta_i^0, \qquad (i=1, \cdots, N) \tag{1}$$

where a dotted symbol denotes a substantive time derivative, and the eigenvalues of the matrix L_{ij} are negative. If the nonlinear terms in (1) are neglected, the solutions will relax to equilibrium with a set of characteristic times which are the reciprocals of the eigenvalues of the coefficient matrix. As an example we can consider a liquid in which ζ_i and ζ_j are the fractional occupation numbers of two different states of a molecular vibration. If $nZ^{(r)}$ is the frequency of r-ple collisions per unit volume, n being the molecular number density, $P_{ij}^{(r)}$ is the probability, evaluated for equilibrium, that in an r-fold collision at least one molecule makes a transition to or from state i when it is given that prior to the collision at least one of the molecules is in state j, and ν_{ij}, which may be positive or negative, is the mean number of transitions to state i under these circumstances, then approximately,

$$L_{ij} = \sum_r r Z^{(r)} [P_{ij}^{(r)} \nu_{ij} - P_{j0}^{(r)} \nu_{j0}] \tag{2}$$

and similarly for the other $L_{ijk}\ldots$.[9]

In the example just given, Eq. (1) will not obtain until a molecule has suffered several collisions. In fact until a molecule in state i has had time to make at least one collision, no changes can occur and $\dot{\zeta}_i = 0$. We can express this formally for the general case by writing in place of (1) the equations

$$(\partial\dot{\zeta}_i/\partial t) + \mathbf{u}\cdot\nabla\dot{\zeta}_i = -(1/\tau_i')\dot{\zeta}_i + \sum_j (L_{ij}/\tau_i')\xi_j + \cdots (i=1, \cdots, N). \tag{3}$$

Equations (3) state the fact that a fluctuation $\xi_i \neq 0$ does not instantaneously change the numbers ζ_i, but rather affects initially only the "accelerations" $\partial\dot{\zeta}_i/\partial t$. If the motion has no Fourier components of very high frequency, the acceleration terms may be neglected, and we recover Eq. (1). At times $\leq \tau_i'$, the state of the system depends on the independent variables $\dot{\zeta}_i$ as well as on ρ, T, and the ξ_i.

THERMODYNAMIC INTERPRETATION

For a given choice of parameters ζ_i and a given model of the internal relaxation mechanisms of the system, we can calculate the coefficients L_{ij} and τ_i' in Eqs. (3)—an example of such a calculation being given by Eq. (2). We shall now rewrite (3) in the form of a first-order rate equation linear in the ξ_i and in the new variable $\eta_i \equiv \dot{\zeta}_i$ and then examine the consequences of assuming that the terms in the right-hand member, which in first approximation will be linear in the ξ_i and η_i, are thermodynamic forces conjugate to the "fluxes" $\dot{\xi}_i$ and $\dot{\eta}_i$, respectively—a procedure applied in earlier papers[7,8,10] on transport coefficients. The new thermodynamic forces will take the form

$$\Phi_i \equiv \sum_j \alpha_{ij}(\rho, T)\xi_j + \sum_{j,k} \alpha_{i,j,k}(\rho, T)\xi_j\xi_k + \cdots,$$

$$\Psi_i \equiv -(1/\gamma_i\tau_i')\eta_i \tag{4}$$

where the coefficients $\alpha_{ij}(\rho, T)$, $\alpha_{i,j,k}$, $\gamma_i(\rho, T)$ are to be determined in such a way that Eqs. (3) assume the form

$$\dot{\eta}_i = \gamma_i\Psi_i + \sum_j \tilde{\omega}_{ij}(\rho, T)\Phi_j \qquad (i=1, \cdots, N). \tag{5}$$

If Ψ_i is to be interpreted as a force conjugate to the flux $\dot{\eta}_i$, while Φ_i is a force conjugate to $\dot{\xi}_i$, then we must have (footnote reference 3, p. 14)

$$T^{-1}\Phi_i = \partial\sigma/\partial\xi_i, \qquad T^{-1}\Psi_i = \partial\sigma/\partial\eta_i, \tag{6}$$

[8] R. E. Nettleton, Phys. Fluids **2**, 256 (1959).

[9] Since ζ_j is the probability that a molecule chosen at random is in state j, the probability that in a group of r molecules at least one is in state j is approximately $r\zeta_j$. The frequency of r-fold collisions per molecule in which there is a transition to or from i is then $\Sigma_j Z^{(r)} P_{ij}^{(r)} r\zeta_j$ and thus, neglecting nonlinear terms $n\dot{\zeta}_i = \Sigma_r \Sigma_j n r Z^{(r)} \nu_{ij} P_{ij}^{(r)} r\zeta_j$. When $\zeta_j = \zeta_j^0$, the rates all vanish, and thus we can replace ζ_j with ξ_j in this expression and then set $\xi_0 = -\Sigma_{j>0}\xi_j$, obtaining the linear terms in the right-hand member of Eq. (1).

[10] R. E. Nettleton, Trans. Soc. Rheol. (to be published); this paper contains a concise summary of the approach of footnote references 7 and 8.

where σ is the entropy per molecule, which is given, accordingly by the Gibbs equation by

$$Td\sigma=du-(P/n)ds+\sum_i\Phi_i d\xi_i+\sum_i\Psi_i d\eta_i. \quad (7)$$

Here P is the thermodynamic pressure, $s=(\rho-\rho_0)/\rho_0$ the condensation, ρ_0 being a fixed value, and u is the internal energy per molecule. From (7) we find at once that the Helmholtz free energy per molecule $A=u-T\sigma$ obeys the equation

$$dA=-\sigma dT+(P/n)ds-\sum_i\Phi_i d\xi_i-\sum_i\Psi_i d\eta_i. \quad (8)$$

The condition that dA be a perfect differential requires that

$$\partial\Phi_i/\partial\xi_j=\partial\Phi_j/\partial\xi_i \qquad (i,j=1,\cdots,N)$$

which implies

$$\alpha_{ij}=\alpha_{ji}, \qquad \alpha_{ijk}=\alpha_{jik} \quad (9)$$

assuming the coefficients to be symmetrized, which may be done without loss of generality, so that

$$\alpha_{ijk}=\alpha_{ikj}, \qquad L_{ijk}=L_{ikj}. \quad (10)$$

Having established the restrictions (9) and (10), we shall proceed to calculate the α_{ij} and α_{ijk} before going on to consider other consequences of Eqs. (6)–(8). Comparison of Eqs. (3) and (5) shows that

$$\sum_k\tilde{\omega}_{ik}\alpha_{kj}=L_{ij}/\tau_i' \qquad (i,j=1,\cdots,N). \quad (11)$$

Equation (11) will not determine all the coefficients $\tilde{\omega}_{ij}$ and α_{ij} without further physical conditions, and so in the present paper it will be assumed that

$$\alpha_{ij}=-(1/\tilde{\omega}_i\tau_i)\delta_{ij}, \quad (12)$$

where δ_{ij} is the Kronecker delta, $\tau_i=-(L_{ii})^{-1}$; $\tilde{\omega}_i$ will be discussed later. This is equivalent to assuming that a rate equation will depend on two different variables ξ_i and ξ_j only if it depends on both the associated forces Φ_i and Φ_j and not on one of them alone. This assumption, together with Eq. (11), gives

$$\tilde{\omega}_{ij}=-L_{ij}\tilde{\omega}_j\tau_j/\tau_i'. \quad (13)$$

In a similar fashion,

$$\sum_m\tilde{\omega}_{im}\alpha_{mjk}=L_{ijk}/\tau_i'. \quad (14)$$

Equations (9), (10), and (14) determine the α_{ijk} and those L_{ijk} for which j or k is $<i$, when it is assumed that the L_{ijk} for j, k both $\geq i$ can be calculated from collision theory. This procedure corresponds to the usual practice of using the principle of detailed balance to determine the probability that a molecule will gain vibrational energy in a collision when the probability of deexcitation is determined from quantum mechanics.[11] Detailed balance can here be used to determine L_{ij} for $j<i$ if the L_{ij} for $j>i$ are known.

In addition to Eq. (9), we can obtain another important result from (8). When Φ_i and Ψ_i are known, Eq. (8) may be used to calculate derivatives of A to all orders with respect to ξ_i and η_i. Thus we can obtain Taylor expansions for the thermodynamic functions, in which the terms in A quadratic in the η_i (linear terms being absent) assume the form $(\frac{1}{2})\sum_j[(\eta_j)^2/\gamma_j\tau_j']$.

A third significant consequence of Eqs. (5) and (7) is that they enable us to write down the rate equation for $\dot{\xi}_i$. Since $\dot{\eta}_i$ depends on the thermodynamic force Φ_j conjugate to the flux $\dot{\xi}_j$, it follows from the Onsager-Casimir reciprocity theorem that $\dot{\xi}_j$ must depend on for force Ψ_i conjugage to $\dot{\eta}_i$. Since Ψ_i and Φ_j are, respectively, odd and even with respect to time reversal, the coefficient relating $\dot{\xi}_j$ to Ψ_i must be the negative of that relating $\dot{\eta}_i$ to Φ_j. Thus we can write down at once,

$$\dot{\xi}_i=-\sum_j\tilde{\omega}_{ji}\Psi_j+\Gamma_i b, \quad (15)$$

where $b\equiv\nabla\cdot\mathbf{u}$ is the divergence of the Eulerian flow velocity. The significance of the term in Γ_i is found by examining the limit of (15) for the case of a sound wave of infinite angular frequency. From the equation of mass continuity, $b\doteq-\dot{s}$, so that during passage of a wave with $\exp(i\omega t)$ time dependence, $b=-i\omega s$, while $\dot{\xi}_i=i\omega\xi_i$. From Eq. (3) it is established that $\eta_i\to0$ as $\omega\to\infty$, so that in the limit ζ_i is fixed at $\zeta_{i,0}$, the value about which it oscillates. With these considerations, the limit of Eq. (15) as $\omega\to\infty$ yields

$$\Gamma_i=s^{-1}\lim_{\omega\to\infty}[\zeta_i^{\rho}(\rho T)-\zeta_{i,0}]=(\partial\zeta_i^{\rho}/\partial s)+(1/\alpha_\infty)(\partial\zeta_i^{\rho}/\partial T), \quad (16)$$

where

$$\alpha_\infty\equiv\lim_{\omega\to\infty}[s/\Delta Te^{i\omega t}],$$

ΔT being the amplitude of oscillation of T. The expression $\alpha_\infty=\rho C_i/T\alpha_p B_t$ has been obtained elsewhere (footnote reference 5), where α_p and B_t are, respectively, the cubical expansion coefficient and isothermal bulk modulus, and C_i is the vibrational-rotational specific heat per gram.

It should be noticed that terms linear in the forces Φ_i have not been included in Eq. (15), which is at first surprising, since Φ_i is conjugate to $\dot{\xi}_i$. However, if such terms were included, a fluctuation in one of the variables ξ_j would instantaneously cause $\dot{\xi}_i$ to be different from zero which contradicts the inertial principle that a time of the order τ_i' will be required to establish nonzero rates of relaxation. Nevertheless, $\dot{\xi}_i$ does effectively depend on Φ_i at low frequencies. In the broad fre-

[11] Compare R. N. Schwartz and K. F. Herzfeld, J. Chem. Phys. 22, 767 (1954).

quency range satisfying $0 \leq \omega \ll (\tau_i')^{-1}$ for all i, we can neglect $\dot{\eta}_i$ in (5) and set

$$\Psi_i = -\sum_j (\tilde{\omega}_{ij}/\gamma_i)\Phi_j. \tag{17}$$

On substituting this result into (15), we have

$$\dot{\xi}_i = \sum_j \Lambda_{ij}\Phi_j + \Gamma_i \nabla \cdot \mathbf{u} [\omega \ll (\tau_i')^{-1} \text{ for all } i] \tag{18}$$

where

$$\Lambda_{ij} = \sum_k \tilde{\omega}_{ki}\tilde{\omega}_{kj}/\gamma_k = \Lambda_{ji}. \tag{19}$$

Equation (18) shows that when the inertial terms $\dot{\eta}_i$ may be neglected, the thermodynamic equations are identical in form with equations previously derived[7] to describe compressional relaxation in liquids. At these frequencies the $\dot{\xi}_i$ are linear combinations of the forces Φ_i, and the Onsager reciprocal relations hold among the coefficients.

A second low-frequency form of Eq. (15) may be written which permits us to evaluate the γ_i. In the limit $\omega \to 0$, sound wave propagation is adiabatic[12] and also $\dot{\zeta}_i \cong \dot{\xi}_i^0 = (\partial \zeta_i^0/\partial s)_\sigma \dot{s}$ where subscript σ denotes the adiabatic derivative. Under these conditions (15) assumes the form

$$\Gamma_i = \sum_j [\tilde{\omega}_{ji}/\gamma_j \tau_j'](\partial \zeta_j^0/\partial s)_\sigma. \tag{20}$$

Equation (20) may be solved for the coefficients γ_i. However, if the solution of (20) fails to satisfy the condition $\gamma_i > 0$ for all i, which we shall see is required to make the rate of entropy production positive definite, it might then prove necessary to modify Eq. (12).

In the earlier relaxation theory[7] it was shown that one could calculate the bulk viscosity through a coupling between the pressure and Eq. (18). In the present treatment, we refer to Eq. (15) and observe that since $\dot{\xi}_i$ depends on the antisymmetric force $-\nabla \cdot \mathbf{u}$ with coefficient $-\Gamma_i$, then by the Casimir antireciprocity theorem, the trace $\tilde{P}$ of the pressure tensor depends on $n\Phi_i$ with coefficient Γ_i. Thus

$$\tilde{P} = P^0(\rho, T) + n\sum_i \Gamma_i \Phi_i, \tag{21}$$

where P^0 is the pressure calculated from equilibrium statistical mechanics. At low frequencies ($\omega \to 0$), we set $\Psi_i = (1/\gamma_i \tau_i')(\partial \zeta_i^0/\partial s)_\sigma \nabla \cdot \mathbf{u}$ in (17) and solve for Φ_i to obtain

$$\Phi_i = -\sum_j (\tilde{\omega}_{ij}^{-1}/\tau_j')(\partial \zeta^0/\partial s)_\sigma \nabla \cdot \mathbf{u} (1 \leq i \leq N; \omega \to 0), \tag{22}$$

where $\tilde{\omega}_{ij}^{-1}$ is the reciprocal matrix to $\tilde{\omega}_{ij}$. Substitution of (22) into (21) yields for the bulk viscosity η_0 the expression

$$\eta_0 = n\sum_{i,j} (\tilde{\omega}_{ij}^{-1}/\tau_j')\Gamma_i(\partial \zeta_j^0/\partial s)_\sigma. \tag{23}$$

On substituting for Γ_i from (20), we obtain from (23) the expression

$$\eta_0 = n\sum_j [\gamma_j(\tau_j')^2]^{-1}[(\partial \zeta_j^0/\partial s)_\sigma]^2. \tag{24}$$

From Eq. (13), we have

$$\tilde{\omega}_{ij}^{-1} = -\tau_j' L_{ij}^{-1}/\tilde{\omega}_i \tau_i$$

which on substitution into (23) gives

$$\eta_0 = -n\sum_{i,j} (L_{ij}^{-1}/\tilde{\omega}_i \tau_i)\Gamma_i(\partial \zeta_j^0/\partial s)_\sigma. \tag{25}$$

It has been found in earlier calculations of η_0 that Eq. (23), specialized for the case $N=1$, gives good results, provided

$$\tilde{\omega}_i = \Gamma_i/\epsilon_i \tau_i \qquad (i = 1, \cdots, N), \tag{26}$$

where ϵ_i is the energy difference between level i and the ground level [compare footnote reference 5, Eq. (26)]; and the rather crude arguments used to justify (26)[13] can be carried over unchanged to the present treatment. Insofar as (26) is valid, we can use it to eliminate $\Gamma_i/\tilde{\omega}_i \tau_i$ from (25) and obtain

$$\eta_0 = -n\sum_{i,j} \epsilon_i L_{ij}^{-1}(\partial \zeta_j^0/\partial s)_\sigma. \tag{27}$$

When (25) is specialized to the case $N=1$, for which $L_{11} = -(\tau_1)^{-1}$, we recover precisely the expression used in the previous computations.[7]

MINIMUM ENTROPY PRODUCTION

If Eq. (7) is used to calculate $\dot{\sigma}$, and we substitute from (5) and (15) for the fluxes $\dot{\eta}_i$ and $\dot{\xi}_i$, then the irreversible part of the entropy production is (omitting contributions from shear relaxation and heat conduction calculated in footnote references 5 and 8)

$$\dot{\sigma}_{\text{irrev}} = T^{-1}\sum_j \gamma_j(\Psi_j)^2 = T^{-1}\sum_j \{(\dot{\xi}_j)^2/[\gamma_j(\tau_j)^2]\}. \tag{28}$$

Obviously, the minimum of $\dot{\sigma}_{\text{irrev}}$ occurs when all $\dot{\zeta}_i = 0$ ($i = 1, \cdots, N$), so that when inertial terms are taken into account, the minimum entropy production consistent with any set of constraints not specifying constant rates $\dot{\zeta}_i$ is zero—the value obtained at the initial in-

[12] K. F. Herzfeld and T. A. Litovitz, *Absorption and Dispersion of Ultrasonic Waves* (Academic Press, Inc., New York, 1959); see p. 30.

[13] R. E. Nettleton, J. Appl. Phys. **29**, 204 (1958); see Eq. (65).

stant, before any of the internal irreversible processes have begun to run. Thus we can clearly understand why the introduction of Casimir coefficients which has been made in Eqs. (5) and (15) should not be consistent with the theorem (footnote reference 3, p. 196 ff) that the entropy production is a minimum in the steady state which the system approaches after some time. The latter theorem can hold only after all effects of inertial terms have disappeared, i.e., when Eq. (22) is valid.

DISCUSSION

Equations (5) and (15) exemplify the general method by which inertial terms may be incorporated into the treatment of scalar relaxation processes in liquids[14] in such a way that the rate equations may be given a thermodynamic interpretation—without modifying the usual formulation of irreversible thermodynamics[3] in which the force-flux equations involve only first-order time derivatives of the variables. Such a thermodynamic interpretation has been accomplished by treating first-order time derivatives as state variables and by recognizing certain terms in the rate equations as forces coupled to the remaining terms by antisymmetric Casimir coefficients.

This Casimir-type coupling establishes a clear logical connection between the relaxation model, from which Eqs. (3) and (5) are derived, and the system of equations (18) which have been introduced in earlier papers[7,15] to calculate the bulk viscosity and acoustic absorption in liquids.

The latter equations could be justified only approximately from the model and were applied (footnote reference 7) in the limit $\omega\rightarrow\infty$ for which they are not valid because of the presence of inertial effects. However, we have now been able to show, using Eq. (15), that on taking the limit $\omega\rightarrow\infty$ in (18) we arrive at the correct result, $\xi_i=-\Gamma_i s$, and thus expressions previously obtained[7] for the high-frequency bulk modulus are still valid. It has also been possible to justify Eq. (27), which was used in earlier papers to calculate bulk viscosity, without using an additional completely arbitrary assumption made previously (footnote reference 7, Eq. 14) about the relation between $(\partial\zeta_1^0/\partial s)_e$ and the Γ_i—an assumption which may well be invalid.

[14] *Note added in proof.* Recent results, to be discussed in a subsequent publication, indicate that Eq. (15) should be modified for the case of vibration-rotational relaxation in a moderately dense gas, although the basic idea that ζ_i should be an independent state variable is retained. The present treatment should be limited to liquids.

[15] R. E. Nettleton, Phys. Rev. **108**, 631 (1957).

Simple Configuration Interaction Wave Functions. III. Three-Electron Atomic System: An Analytic Study

MILOS MACHACEK* AND CHARLES W. SCHERR

Department of Physics, The University of Texas, Austin, Texas

(Received January 25, 1960)

An analytical study of the ^2S ground state of lithium like ions employing Slater-type orbitals to form the open-shell function $(1s1s'2s)$ and the angularly correlated configuration-interaction functions $(1s1s'2s)+\lambda 1s(2p)^2$ and $(1s1s'2s)+\lambda 2s(2p)^2$ has been made. Expressions for the wave function parameters and energy values in terms of the nuclear charge Z have been obtained. These are asymptotic expansions for large Z, but they reproduce numerically obtained results for small Z with sufficient accuracy to be useful for many purposes. An unusual result is that, for large Z, the computed energy values are lowest if the orbitals $1s$ and $1s'$ are allowed to have complex orbital exponents.

INTRODUCTION

IN the first two papers of the present series a numerical study[1] and an analytical study[2] of the two-electron atomic systems were carried out employing the same approximate wave functions in the two papers. In the fourth paper of this series,[3] a report will be made of a numerical study of the three-electron atomic system about a nucleus of charge Z employing the following two normalized approximate wave functions:

$$\psi=(1+\lambda)^{-\frac{1}{2}}\{N[1s(1)1s'(2)2s(3)+1s'(1)1s(2)2s(3)]+(\lambda/\sqrt{3})[1s''(1)2p_0(2)2p_0(3)+1s''(1)2p_1(2)2p_{-1}(3)+1s''(1)2p_{-1}(2)2p_1(3)]\}, \quad (1a)$$

and

$$\psi=(1+\lambda)^{-\frac{1}{2}}\{N[1s(1)1s'(2)2s(3)+1s'(1)1s(2)2s(3)]+(\lambda/\sqrt{3})[2s''(1)2p_0(2)2p_0(3)+2s''(1)2p_1(2)2p_{-1}(3)+2s''(1)2p_{-1}(2)2p_1(3)]\}, \quad (1b)$$

each with a doublet spin function. The present paper investigates the same problem analytically. We work throughout in atomic units[4] so that the Hamiltonian for the three-electron atom of nuclear charge Z is

$$-\tfrac{1}{2}\nabla_1^2-\tfrac{1}{2}\nabla_2^2-\tfrac{1}{2}\nabla_3^2-(Z/r_1)-(Z/r_2)-(Z/r_3)+r_{12}^{-1}+r_{13}^{-1}+r_{23}^{-1}. \quad (2)$$

The normalized radial portions of the atomic orbitals in Eq. (1) are

$$R_{10}=2\zeta^{\frac{3}{2}}(1+x)^{\frac{1}{2}}\exp[-\zeta(1+x)r]; \quad (3.1)$$

$$R_{10}'=2\zeta^{\frac{3}{2}}(1-x)^{\frac{1}{2}}\exp[-\zeta(1-x)r]; \quad (3.1')$$

$$R_{10}''=2(\zeta v)^{\frac{3}{2}}\exp(-\zeta vr); \quad (3.1'')$$

$$R_{20}=\tfrac{2}{3}\sqrt{3}(\zeta w)^{5/2}r\exp(-\zeta wr); \quad (3.2)$$

$$R_{20}''=\tfrac{2}{3}\sqrt{3}(\zeta w'')^{5/2}r\exp(-\zeta w''r); \quad (3.2'')$$

$$R_{21}=\tfrac{2}{3}\sqrt{3}(\zeta y)^{5/2}r\exp(-\zeta yr). \quad (3.3)$$

We retain the notation of II wherever possible; in particular, subscripts c, o, and a refer to closed-shell, open-shell, and angularly correlated, respectively. As a further notation, we let a subscript infinity sign on a parameter indicate that the parameter is a limiting value for large z. The use of these subscripts indicates specifically an optimized quantity.

COMPLEX ORBITAL EXPONENTS

The customary usage in the past has been to choose the orbital exponents to be real. This restriction overlooks an entire available domain of parameter space. The investigation of the general case of complex orbital exponents in wave functions of the form of Eq. (1) will perhaps most satisfactorily be handled by numerical techniques, and accordingly, we leave the general problem for possible consideration in future papers of this series. In the present series-within-a-series where we try to see how far a nonnumerically oriented analysis may be carried, a fortunate circumstance has enabled us to investigate with encouraging results a small portion of the complex-parameter domain at no cost in effort at all. In the present problem no further analysis is needed to extend the domain of x to include pure imaginary values of x also, once the analysis for x real is completed. If x is pure imaginary then the $1s$ and $1s'$ orbitals are each other's complex conjugates, and the wave function, Eq. (1), is its own complex con-

* Portion of a thesis submitted to the Department of Physics, The University of Texas, in partial fulfillment of the requirements for the Master of Arts degree.

[1] J. N. Silverman, O. Platas, and F. A. Matsen, J. Chem. Phys. **32**, 1402 (1960).

[2] C. W. Scherr and J. N. Silverman, J. Chem. Phys. **32**, 1407 (1960). Hereafter referred to as II.

[3] O. Platas and F. A. Matsen (to be published). Hereafter referred to as IV.

[4] Lengths in units of the Bohr radius, a_0, and energies in units of e^2/a_0.

jugate, that is, real. Thus, whether x is real or imaginary, we may write for the variational energy,

$$\int d\tau\psi^* H\psi = \int d\tau\psi H\psi = E(x^2, p_i), \quad (4)$$

and obtain the identical energy expression in either case. We have indicated specifically that E is a function of p_i (the other parameters in the problem) and x^2. Thus it is only necessary to note that positive values of x^2 correspond to real orbital exponents, and negative values of x^2 to our special case of complex orbital exponents. The complex orbital exponent is significant, not a mere phase factor; as is shown below, it is necessary for systems with large Z in order to obtain a lower energy value than can be obtained from Eq. (1) when its orbital exponents are required to be real.

In the sections that follow, the equations have been obtained using x real. Since the normalization is different in the two cases, the equations may differ by a factor from the corresponding equations for x imaginary, though of course, the final energy expressions are the same.

OPTIMIZATION

It is well known[5] that the energy of atomic wave functions such as Eq. (1) above may be written as

$$E = S(T\zeta^2 + V\zeta),$$

where S, T, and V are independent of ζ, and S is some over-all normalization factor. Then E optimized with respect to ζ is given by

$$E = -V^2/(4T/S); \qquad \zeta = -V/2T. \quad (5)$$

If we further optimize with respect to the other parameters of the problem, p_i, we obtain[5] for each p_i

$$2(T/S)(\partial V/\partial p_i) - V[\partial(T/S)/\partial p_i] = 0. \quad (6)$$

When we refer to Eq. (6) in the text, we insert a parenthetic indication of the variable to be used for p_i.

CLOSED SHELL $(1s)^2 2s$

Here λ and x are zero. If we define

$$a = w + 1, \quad (7)$$

then we have

$$T = 1 + \tfrac{1}{6}(a-1)^2 - 32(4a-3)(a-1)^5 a^{-8}; \quad (8)$$

$$V_Z = -\tfrac{3}{2} - \tfrac{1}{2}a + 64(2a+3)(a-1)^5 a^{-8}; \quad (9)$$

$$V_e = (\tfrac{5}{8}) - 128(a-1)^5(a+2)^{-4}a^{-7}P_0(a) + (a-1)a^{-5}P_1(a) - 44(a-1)^5 a^{-7}; \quad (10)$$

$$N^{-1} = S = 1 - 192(a-1)^5 a^{-8}; \quad (11)$$

where

$$P_0(a) = 3a^3 + 24a^2 + 32a + 16, \quad (12)$$

$$P_1(a) = 2a^4 + 2a^3 - 8a^2 + 7a - 2, \quad (13)$$

[5] E. Hylleraas, Z. Physik **54**, 347 (1929).

TABLE I. Closed-shell limiting parameters and energies.

w_{cc}	ζ_{cc}/Z	E_{cc}/Z^2	
0.425107436	0.993649472	−1.12347980	A minimum
1.97705686	0.357693182	−0.545190862	A maximum
3.93932482	0.409809597	−0.743322377	A minimum

and

$$V = V_e + ZV_Z. \quad (14)$$

When these terms were substituted into Eq. (6) ($p_i = a$) a rational function of the form

$$A(a)Z + B(a) = 0 \quad (15)$$

was obtained. For large Z Eq. (15) becomes

$$A(a)Z \approx 0. \quad (16)$$

Equation (16) was readily solved, and has only three positive roots. These roots are tabulated in Table I, along with their corresponding ζ values and energies. We wrote

$$w_c = w_{cc}(1+\epsilon), \quad (17)$$

where w_{cc} refers to the first entry in Table I. The w expression Eq. (17) was substituted into the terms of Eqs. (8)–(11) and all expressions were expanded neglecting terms fourth order and higher in ϵ. In this way Eq. (6) ($p_i = \epsilon$) was made amenable to solution, yielding for the condition on ϵ that

$$(0.62361612\epsilon - 1.1690943\epsilon^2)Z + 0.63262761 - 1.6221746\epsilon + 1.1922960\epsilon^2 = 0. \quad (18)$$

Note that the constant term in the coefficient of Z has vanished,[6] so that ϵ goes to zero with large Z. In fact it follows from Eq. (18) that for large Z

$$\epsilon_c \approx -1.0144504/Z. \quad (19)$$

If, instead of Z, we express ϵ_c in terms of ζ_c, we obtain

$$\epsilon_c \approx -1.0080081/\zeta_c. \quad (19')$$

Expansion solutions similar to Eq. (18) were found[7] for ζ_c and for E_c. Some results are displayed in Table II, together with some numerical values[8] for comparison.[9]

[6] A direct consequence of Eq. (16).

[7] Because of the probably limited interest in these expansions, we do not present them here. They are available in mimeographed form upon request.

[8] R. P. Hurst, J. D. Gray, G. H. Brigman, and F. A. Matsen, Mol. Phys. **1**, 189 (1958).

[9] Note that the authors of IV and of footnote reference 8 used the energy itself directly as their criterion of the selection of parameter values, and necessarily obtained only four or five significant figures in their parameters, since they carried eight figures in the energy calculations.

TABLE II. Closed-shell parameters and energies.

Z		3	4	5	10	50	∞
ζ_c/Z	Present paper	0.89745	0.92169	0.93594	0.96456	0.98780	0.993649472
	Footnote reference 8	0.89881	0.92048	0.93518	0.96443	0.98760[a]	0.9934[b]
w_c	Eqs. (16) and (22)	0.22454	0.28952	0.32245	0.37847	0.41636	0.425107436
	Footnote reference 8	0.23724	0.29496	0.32524	0.37889	0.41644[a]	0.4258[b]
E_c/Z^2	Present paper	−0.82430	−0.89224	−0.93401	−1.025250	−1.1032962	−1.12347980
	Footnote reference 8	−0.82421	−0.89266	−0.93399	−1.025249	−1.1032964[a]	−1.1223[b]

[a] Computed for us by Oscar Platas.
[b] By extrapolation as described in the text.

TABLE III. The α_{inp}

	α_{3np}				α_{4np}						α_{5np}				
$p \backslash n$	0	1	2	3	0	1	2	3	4	5	0	1	2	3	4
0	1				−3	4					3	2			
1	28	−24	3		−84	296	−178	24			84	−8	−42	6	
2	70	−168	84	−8	−210	1568	−2296	1008	−139	4	210	−308	−168	168	−17
3	28	−168	210	−56	−84	1400	−4396	4032	−1204	104	84	−392	84	420	−140
4	1	−24	84	−56	−3	188	−1528	3024	−1666	224	3	−62	120	168	−182
5			3	−8			−50	360	−436	56			6	6	−44
6									−11	−4					−1

TABLE IV. Open-shell parameters and energies.

Z		3	4	5	10	50
ζ_0/Z	Present paper	0.8874	0.9150	0.9314	0.9633	0.9878
	Footnote reference 8	0.8943	0.9193	0.9342	0.9641	...
w_0	Eqs. (29) and (32)	0.2787	0.3153	0.3373	0.3813	0.4165
	Footnote reference 8	0.2382	0.2957	0.3257	0.3787	...
x_0^2	Eq. (31)	0.0483	0.0351	0.0271	0.0112	−0.00146
	Footnote reference 8	0.0526	0.0378	0.0286	0.0121	...
E_0/Z^2	Present paper	−0.82667	−0.89255	−0.93486	−1.02541	−1.10330
	Footnote reference 8	−0.82707	−0.89266	−0.93490	−1.02541	...

TABLE V. Open-shell limiting parameters and energies.

w_{c0}	x_{c0}^2	ζ_{c0}/Z	E_{c0}/Z^2	
0.4252924	−0.0045242553	0.9937801	−1.1235050	The minimum at A[a]
2.0637905	−0.1855960	0.3265241	−0.4448136	The maximum at B[a]
2.8941240	0.5289878	0.4915486	−0.8554477	The minimum at C[a]

[a] Refer to Fig. 1.

OPEN SHELL $N(1s1s'2s+1s'1s2s)$

Here λ is zero. We found the explicit expressions for N, T, and V_Z as functions of a and x^2:

$$N^{-1}=S=2+2(1-x^2)^3-48(a-1)^5(1-x^2)^3F$$
$$-6(a-1)^5F^2P_2(a,x^2); \quad (20)$$

$$T=(a^2-2a+7)[1+(1-x^2)^3]+2x^2-2x^2(1-x^2)^3$$
$$+8(1-x^2)^3(a-1)^5(5x^2-4a+3)F$$
$$-(a-1)^5F^2P_3(a,x^2); \quad (21)$$

$$V_Z=-(a+3)[1+(1-x^2)^3]$$
$$+16(1-x^2)^3(2a+3)(a-1)^5F$$
$$+2(a-1)^5F^2P_4(a,x^2), \quad (22)$$

where

$$F=8(a^2-x^2)^{-4},$$

and

$$P_i(a,x^2)=a^s\sum f_{in}(a)(x/a)^{2n}; \quad (23)$$

$$f_{in}(a)=\sum\alpha_{inp}a^p. \quad (24)$$

The α_{inp} are listed in Table III. Instead of obtaining V_e in the form above, we wrote it as a function of w and x, and in order to proceed, wrote

$$w_0=w_{cc}(1+\epsilon). \quad (25)$$

Then we expanded the energy expression neglecting terms fourth order and higher in ϵ as before, and neglecting terms third order and higher in x^2.[7] [E equals $E(x^2)$, cf. Eq. (4).]

When the expanded energy expression was inserted into Eq. (6) ($p_i=x^2$) there resulted a linear equation in x_0^2, so that x_0^2 as a function of ϵ was obtained immediately.[7] In order to avoid some tedious algebra, we simplified the expression for x_0^2 by using its limiting form for large Z,

$$x_0^2\approx\frac{33.278794-0.97676416Z}{36.466666+210.53910Z}. \quad (26)$$

Note that for Z larger than about 34, x_0^2 is negative.

In order to be certain that the negative x_0^2 was not an artifact of our truncations, we computed the E of Eq. (5) via the unexpanded energy expressions, Eqs. (20)–(22), for the infinite Z case, and constructed the contour diagram of the energy, shown in Fig. 1. The dashed ordinate at $x^2=0$ indicates the closed-shell energies. The diagram is constructed for infinite Z, but ought to be qualitatively correct even for the small Z values. The principal difference for the small Z values is that the location of the $x^2=0$ ordinate has moved to the left slightly, but enough, so that the root at A is now in the region of positive x^2. It is this minimum at A which is reported by IV and by others.[8] For large $Z(Z>\sim34)$ root A is to the left of the $x^2=0$ ordinate, and the only minimum for real x, other than for $x=0$, is the local root at C.

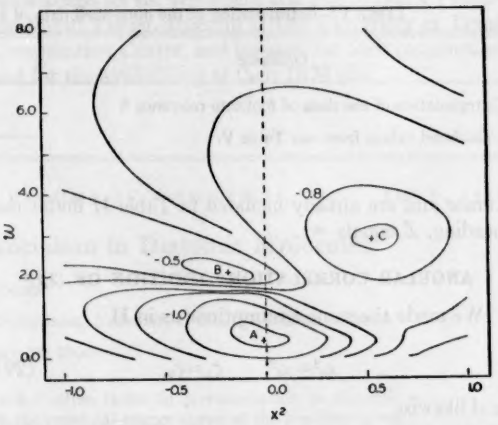

FIG. 1. A contour diagram of the reduced energy, E/Z^2, ($\lambda=0$, Z infinite, and ζ optimized) as a function of x^2 and w. The contours are in steps of 0.1, except for the broken contour at -0.65 and for the innermost contour to the root C at -0.85.

We expanded Eq. (26) in powers of Z^{-1}:

$$x_0^2\approx-0.0046393481+0.15886824Z^{-1}+\cdots, \quad (27)$$

which compares quite well with the data of footnote reference 8, both in slope and in negative intercept when their x_0^2-values are plotted against Z^{-1}. In view of this agreement, we inserted Eq. (27) into the energy expression directly, so that upon applying Eq. (6) ($p_i=\epsilon$), we obtained

$$\epsilon_0=0.00045155-1.0346380Z^{-1}+\cdots. \quad (28)$$

The small differences between the constant terms in these two equations and the appropriate entries in Table V are reflections of the inadequacies of the expansions. In order to obtain ζ_0 and E_0, we inserted these parameter values into Eqs. (20)–(22), and into the expansion for V_e, and used Eq. (5). Some results are displayed in Table IV, together with some numerical values[8] for comparison.[9]

We conclude this section with a discussion of the limiting parameters and energy values listed in Table V. The tabular entries were computed directly from the exact (i.e., unexpanded) expressions in Eqs. (20)–(22) and from their derivatives via simultaneous solution of Eq. (6) ($p_i=\epsilon$, $p_i=x^2$). The entries in Table V are thus exact for Eq. (1).[10] We plotted the numerical open-shell data of footnote reference 8 as a function of Z^{-1} and, by drawing straight lines through the points, extrapolated the data to infinite Z. The results are shown in Table VI. Since we have a point at Z equals 50 for the closed-shell case (computed for us by Oscar Platas), the extrapolations are somewhat more ac-

[10] On the other hand, the exact solution of the Hamiltonian, Eq. (2), for infinite Z is the zero-order perturbation value, $E_{cc0}/Z^2=-1.125$. Note the inherent inadequacy of Eq. (1). This point is being investigated further.

TABLE VI. Extrapolation of the open-shell data of footnote reference 8 to infinite Z using Z^{-1} as the abscissa.

Ordinate	ζ_0/Z	w_0	x_0^2	E_0/Z^2
Extrapolation of the data of footnote reference 8	0.9938	0.428	−0.0040	−1.120
Calculated values from our Table V.	0.99378	0.4253	−0.00452	−1.1235

curate and are already included in Table II under the heading, Z equals ∞.

ANGULAR CORRELATION: ADDITION OF $(2p)^2$

We made the same assumptions as in II

$$x_a^2 \approx x_0^2; \qquad \zeta_a \approx \zeta_0, \tag{29}$$

and likewise

$$w_a \approx w_0, \tag{30}$$

and worked with the limiting values of these parameters.

We have from Eq. (1a)

$$\begin{aligned} H_{12} = {} & 64\zeta y^5(1-x^2)^{\frac{1}{2}} w^{5/2} v^{\frac{1}{2}} N \times \\ & -(1+y+x)^{-2}(w+y)^{-3}(1+w+2y+x)^{-6} \\ & \times (1+v-x)^{-3} P_5(x) \\ & -(1+y-x)^{-2}(w+y)^{-3}(1+w+2y-x)^{-6} \\ & \times (1+v+x)^{-3} P_5(-x) \\ & +[7(1+y)^2-3x^2][(1+y)^2-x^2]^{-2}(1+y)^{-5}(v+w)^{-4}, \end{aligned} \tag{31a}$$

TABLE VII. Angularly correlated parameters and energies.

		Extrapolated from footnote reference (3)	Present paper: Open-shell	Present paper: Closed-shell[a]
Eq(1a)	y	1.561	1.566898	1.566489
	v	0.240	0.2350117	0.2348502
	$(\lambda Z/N)^2$	0.03953	0.03950661	0.03901580
	$(\lambda\zeta/N)^2$		0.03901668	0.03852183
	$\lambda\zeta$		0.1070629	0.1068630
	ϵ_2	0.0207[b]	0.020715070	0.020634688
Eq(1b)	y		1.543061	1.542586
	w''		0.4016077	0.4013412
	$(\lambda Z/N)^2$		0.04379481	0.04326582
	$(\lambda\zeta/N)^2$		0.04325170	0.04271804
	$\lambda\zeta$		0.1127237	0.1125330
	ϵ_2		0.022754444	0.022666735

[a] Tabulated here for reference. The proper comparison is with the open-shell values.

[b] That is, the improvement in the open-shell energy. This quantity was varying so slowly that it seems likely it was at its limiting value at $Z=10$ already, which is the quantity reported here.

and from Eq. (1b)

$$\begin{aligned} H_{12} = {} & 64\sqrt{3}\zeta y^5(1-x^2)^{\frac{1}{2}} w^{5/2} w''^{5/2} N \times \\ & -(1+y+x)^{-2}(w+y)^{-3}(1+w+2y+x)^{-6} \\ & \times (1+w''-x)^{-4} P_5(x) \\ & -(1+y-x)^{-2}(w+y)^{-3}(1+w+2y-x)^{-6} \\ & \times (1+w''+x)^{-4} P_5(-x) \\ & +[7(1+y)^2-3x^2][(1+y)^2-x^2]^{-2}(1+y)^{-5}(w''+w)^{-5}, \end{aligned} \tag{31b}$$

where

$$\begin{aligned} P_5(x) = {} & 49(1+w+2y+x)^3 \\ & -27(1+w+2y+x)^2(1-w+x) \\ & -21(1+w+2y+x)(1-w+x)^2+15(1-w+x)^3. \end{aligned} \tag{32}$$

For large Z

$$H_{11} \approx -1.1235050Z^2, \tag{33}$$

and using Eq. (1a)

$$H_{22} \approx \zeta^2(y^2+\tfrac{1}{2}v^2) - \zeta Z(y+v); \tag{34a}$$

using Eq. (1b)

$$H_{22} \approx \zeta^2(y^2+w''^2) - \zeta Z(y+\tfrac{1}{2}w''). \tag{34b}$$

Proceeding as in II, we maximized the second-order perturbation approximation to the energy,

$$\epsilon_2 = H_{12}^2/(H_{11}-H_{22}), \tag{35}$$

which must here be done simultaneously for y and v (or w''). This is equivalent to solving

$$2(H_{11}-H_{22})(\partial H_{12}/\partial p_i) + H_{12}(\partial H_{22}/\partial p_i) = 0 \tag{36}$$

for $p_i = y$ and $p_i = v$(or w''). The solutions were found by the use of a program written for the IBM 650. We found that the data of IV (for Z equals 7 through 10) fitted to a straight line when plotted against Z^{-1}, and we used this observation to extrapolate their results to infinite Z. Their agreement with our results (see Table VI) is a good indication of the reliability of both our results and those of Platas and Matsen. The calculations were also carried out for the closed-shell case, using the appropriate ζ and w values. The results of this section are presented in Table VII.

ACKNOWLEDGMENTS

We wish to express our gratitude to Oscar Platas for making his results available to us prior to publication, and particularly for performing a number of numerical calculations for us. We would also like to thank Professor David Young, Director of The University of Texas Computation Center, and his staff for their cooperation and for the availability of their IBM 650.

THE JOURNAL OF CHEMICAL PHYSICS VOLUME 33, NUMBER 1 JULY, 1960

Some Neglected Subcases of Predissociation in Diatomic Molecules*

R. S. MULLIKEN

Laboratory of Molecular Structure and Spectra, Physics Department, University of Chicago, Chicago, Illinois

(Received February 26, 1960)

The theoretically to be expected effects of the Franck-Condon factor in predissociation in diatomic molecules are examined qualitatively for cases in which the potential-energy curve of the predissociating electronic state crosses that of the predissociated state at an internuclear distance r_c near or less than the equilibrium distance r_e of the latter state. It is shown that the incidence of predissociation as a function of the vibrational and rotational quantum numbers v and J should be quite different in such cases than in the more familiar cases where $r_c > r_e$. Various subcases of Herzberg's cases *a*, *b*, *c* depending on the relation of r_c to r_e are specified and designated. Some probable examples of known predissociations where $r_c < r_e$ are discussed. The need for further quantitative studies is emphasized.

INTRODUCTION

HERZBERG in his extensive 1931 article,[1] in discussing the predissociation of a stable by a less stable or unstable electronic state of a diatomic molecule, distinguished four cases (*a*, *b*, *c*, *d*) differing in the relative positions of the potential curves of the two electronic states. In all these cases, the potential curve of the electronic state which causes the predissociation (let us here call it state *B*) crosses that of the stable state (say, *A*); see Fig. 1. In cases *b*, *a*, and *c*, respectively, the dissociation asymptote of state *B* (below which predissociation can in no event occur) lies above, approximately at, or below the crossing point of curves *A* and *B*. In his 1931 article, Herzberg distinguishes a fourth case *d*, but, in his book,[2] he treats this as a variety of case *c*. It differs from the usual case *c*, where the interatomic distance at the crossing point, say r_c, is larger than the equilibrium distance r_e of state *A*, in that now $r_c < r_e$. However, $r_c < r_e$ can also occur in cases *a* and *b*. Since the relation of r_c to r_e has some rather important effects on predissociation, it appears desirable to distinguish the three possibilities $r_c < r_e$, $r_c \approx r_e$, $r_c > r_e$ by adding a superscript $-$, *i*, or $+$, respectively, to the case letters *a*, *b*, *c*. For example, the usual case *c* with $r_c > r_e$ becomes case c^+, while Herzberg's 1931 case *d* becomes case c^-.

Cases c^i and c^- have proved to be of particular interest in a study by P. G. Wilkinson and the writer of some unconventional examples of predissociation in N_2, and the present paper is devoted mainly to a discussion of these cases. (Herzberg[1,2] has discussed case c^- only very briefly.) A further situation[1,2] in which predissociation occurs when the potential curves of states *A* and *B* do not cross but only come close to each other should also be kept in mind. In this situation, one may distinguish three cases which may conveniently be called b^0, a^0, and c^0, according as the dissociation asymptote of state *B* lies above, approximately at, or below the bottom of the potential curve of state *A*. (The choice of the bottom of the *A* curve is arbitrary, but some arbitrary choice is necessary since an r_e does not now exist.) The several cases and subcases described above are illustrated in Fig. 1.

In all cases, the occurrence (or strength) of predissociation depends to an important degree on the rotational quantum number (say, J) and the vibrational quantum number (v), for reasons based on the Franck-Condon principle.[3] As Herzberg has shown, predissociation in case b^+ or a^+ should set in at lower and lower J values as v increases. Similarly, in case c^+, it should become strong at lower and lower J values as v increases; however, because of tunneling, its onset (especially for molecules of low reduced mass) should not be as completely sudden as in case b^+. In both cases,

* This work was assisted by the Geophysics Research Directorate of the Air Force Cambridge Research Center, Air Research and Development Command, under contract with the University of Chicago.

[1] G. Herzberg, Ergeb. exakt. Naturwiss. **10**, 207 (1931).

[2] G. Herzberg, *Molecular Spectra and Molecular Structure. I. Spectra of Diatomic Molecules* (D. Van Nostrand Company, Inc., Princeton, New Jersey, 1950), 2nd ed., pp. 405–434, 442–443, 448–450.

[3] See especially Figs. 186 and 191 of footnote reference 2 (cf. also Figs. 185, 188–189, 190).

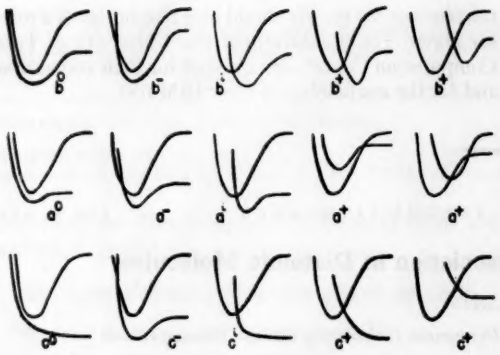

FIG. 1. The three cases for predissociation of state A of a diatomic molecule by a state B and the four subcases of each. (Two rather different examples are shown for the last subcase of each case.) The curves shown are schematic. The ordinate in each is the potential energy U, and the abscissa is the internuclear distance r.

predissociation continues at J values above the onset value.

Quantum-mechanically, the probability of predissociation (that is, of radiationless transition from a given level v, J of state A to an equal-energy unbound state of equal J of state B) is approximately proportional to the product of (1) a Franck-Condon factor

$$\int \Psi_A^{J,v}(r)\Psi_B^{J}(r)dr,$$

where r is the internuclear distance, and (2) an electronic-rotational factor.[2] $\Psi_A^{J,v}(r)$ is the vibrational wave function of quantum number v for the rotational state J of state A, and $\Psi_B^J(r)$ the corresponding continuum wave function of state B; the form of each depends little on J, but the integral of their product depends rather strongly on J. The Franck-Condon factor is governed by the relative positions and forms of the potential curves of states A and B. The electronic-rotational factor depends on the electronic wave functions of the two states and, in general, on the J value. In *homogeneous* predissociation, the electronic-rotational factor has no important dependence on J, in *heterogeneous* predissociation, it contains a factor $J(J+1)$.

If states A and B have the same electron spin, homogeneous predissociation occurs only if the two states are of identical electronic species, while heterogeneous predissociation occurs if and only if their Λ values differ by ± 1. Usually, however, if states A and B are of identical species, they interact so strongly that, instead of homogeneous predissociation, two new potential curves result. Nevertheless, a familiar and apparently authentic example of homogeneous predissociation involving states of identical species exists in the predissociation of the state $C\ ^3\Pi_u$ of N_2 by another $^3\Pi_u$ state of N_2.[4]

If states A and B differ in spin, predissociation should, in general, be much weaker than if they are alike in spin. Homogeneous predissociation now occurs between states of identical Ω value and type, and heterogeneous predissociation between states where Ω values differ by ± 1. In applying these statements to states with weak (Hund's case *b*) spin-orbit coupling, for which Ω values have no direct meaning, one must think in terms of corresponding states with strong (case *a* or case *c*) spin-orbit coupling. Thus, for example, a $^3\Sigma_g^-$ state functions like two states, one with $\Omega=0_g^+$, the other with $\Omega=1_g$, and can predissociate either a $^1\Sigma_g^+$ state ($\Omega=0_g^+$) or a $^1\Pi_g$ state ($\Omega=1$), and can do so both homogeneously and heterogeneously in either case, but with the homogeneous effect presumably much the stronger. But a $^3\Sigma_g^-$ state can predissociate a $^1\Sigma_g^-$ state ($\Omega=0_g^-$) only heterogeneously, since 0_g^+ and 0_g^- states do not interact.

As already stated, the probability of predissociation is approximately proportional to a product of two factors. Of these, the electronic-rotational factor for any particular states A and B should usually be nearly a constant in homogeneous predissociation, but nearly a constant times $J(J+1)$ in heterogeneous predissociation. The constant may be small or large depending on the detailed nature of states A and B. The electronic-rotational factor will not now be further considered, since the problem to be examined here is one which is governed by the Franck-Condon factor.

SUBCASES c^+, c^-, AND c^i

The internuclear distance r_c at which the $U(r)$ curves of two states A and B intersect (cf. Fig. 1), if they do, plays a decisive role for the Franck-Condon factor. This can be seen[2,3] by drawing *effective* potential energy curves $V^J(r)$ obtained by adding the rotational kinetic energy function $[hJ(J+1)/8\pi^2\mu cr^2$, in spectroscopic units, $cm^{-1}]$ to $U(r)$, also in cm^{-1}, for each of the two states A and B. Every such pair of $V(r)$ curves intersects at the same r value r_c independently of J. This can be seen in Figs. 2 and 3. In these figures, the $U(r)$ curve of state A has been drawn as a Morse curve with constants approximately like those for an N_2 state of rather small dissociation energy.

The intersections coincide (or nearly coincide) in energy with actual energy levels of state A only for particular values of J and v. To illustrate a case c^+ situation, the *right-hand side* of Fig. 2 has the $V^{14}(r)$ curves of states A and B crossing at an energy which coincides with that of the $v=1$, $J=14$ energy level of state A, and the $V^{74}(r)$ curves crossing at an energy nearly equal

[4] G. Büttenbender and G. Herzberg, Ann. der Physik (5) **21**, 577 (1935). R. S. Mulliken, in *The Threshold of Space* (Pergamon Press, London, 1959), Ed. M. Zelikoff, note on states 11 and 15, on p. 176.

to that of the level $v=0$, $J=74$. [The lower left-hand side of Fig. 2 and the left side of Fig. 3 illustrate case c^- (see below).] The J values at which crossings occur at energies coinciding with those of actual rotation-vibrational levels may be called *critical J values*, and the corresponding energies may be called *critical energies*. In general, there is one critical J value for each of several v values. In the case c^+ example in Fig. 2, however, there are only two critical J values, for $v=1$ and 0; these may be called J_1 and J_0 ($J_1=14$ and $J_0=74$).

The significance of the critical J value for any given value of v may be seen by a consideration of Franck-Condon factors for J values below, at, and above the critical value. To illustrate, Fig. 3 shows parts of Fig. 2 on an enlarged scale, with the addition of the $V^{20}(r)$ curves for states A and B. Then, in Fig. 4, the $v=1$ vibrational wave functions $\Psi_A{}^J(r)$ of state A and the equal-energy continuum wave functions $\Psi_B{}^J(r)$ of state B (from the integral of whose product the Franck-Condon factor is obtained) are sketched[5] for case c^+ for the critical J value 14. It is seen that there is a considerable overlap (shaded area) between Ψ_A and Ψ_B at this J and energy.

It will be noted that *classically*, predissociation to B from $v=1$ of A should not occur below $J=14$ for case c^+ in Fig. 3, since for $J<14$ the crossing point of the $V^J(r)$ curves of states A and B forms an energy barrier higher than the energy of $v=1$ for $J<14$. In Fig. 3, this barrier is clearly shown for $J=0$, but a barrier, of decreasing height as J increases, exists also for each higher J value until $J=14$. As can be seen, however, from an estimation of relative values of the Franck-Condon factor, obtained by making a sketch, similar to Fig. 4, of the overlapping vibrational $\Psi_A{}^{v=1}$, J and equal-energy continuum $\Psi_B{}^J$ wave functions,[6] appreciable predissociation must occur by penetration of

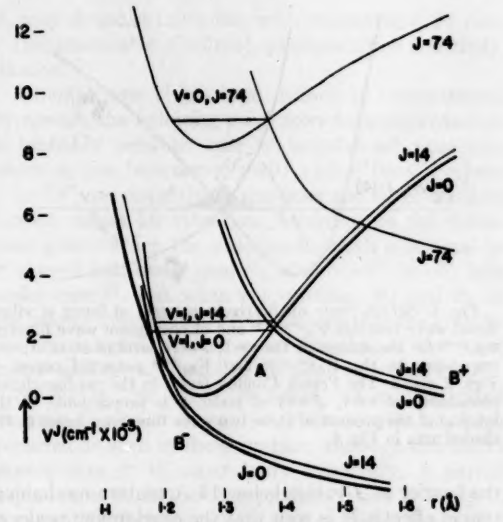

FIG. 2. Potential Curves $V^J(r)$ and some low vibrational levels (horizontal lines) for a stable state A and curves $V^J(r)$ for a predissociating state B, to illustrate the predissociation cases c^+ (at right, B^+ curves) and c^- (at left, B^- curves). Heavy curves, $J=0$; light curves, $J=14$ and $J=74$ (the critical J values for $v=1$ and $v=0$, respectively). The $U(r)$ curve for state A is a Morse curve corresponding to the parameter values $B_0=1.5$, $\omega_e=1500$, $D=10\,000$ cm^{-1}, similar to those for a rather loosely bound state of N_2.

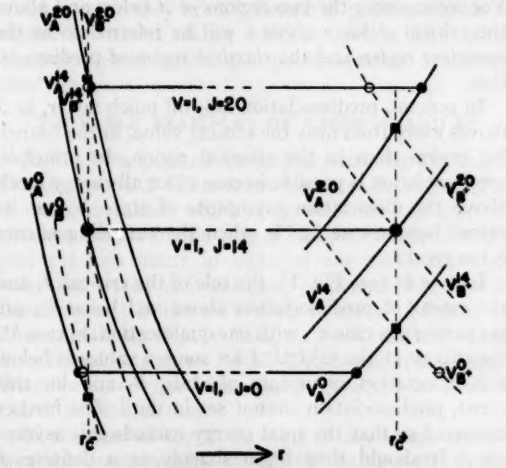

FIG. 3. Enlargement of regions around the critical J value ($J=14$) for the two predissociations shown in Fig. 2 (case c^- at left, case c^+ at right). Portions of the $V^J(r)$ curves of the predissociated state (A, full lines) and the predissociating states (B^+ or B^-, dashed lines) are shown. The horizontal lines indicate the heights of the $v=1$ energy level of state A for $J=0$, 14, and 20; the filled circles at the ends of each horizontal line mark the turning points for classical vibration. The open circles mark the turning points for the classical motion of a pair of atoms colliding along one of the B state $V^J(r)$ curves with a total energy equal to that of the $v=1$ state A vibrational level having the same energy. The small black squares mark the points of intersection of $V^J(r)$ curves of states A and B; all are at $r=r_c$, for each of the two cases c^+ and c^-.

[5] In drawing $\Psi_A{}^{v=1,J=14}$ and $\Psi_B{}^J$ for $E=E_A(v=1, J=14)$ in Fig. 4, the following familiar quantum-mechanical considerations have been taken into account, although no attempt has been made to make the wave functions quantitatively accurate. (1) Each wave function necessarily has a *point of inflection* at the r value (here r_c) at which the classical motion for the given potential curve (here $V_A{}^{14}$ or $V_B{}^{14}$) would have a turning point. (2) The wavelength λ for each wave function, insofar as it can be defined, obeys the de Broglie relation $\lambda=h/\mu v$, where $\mu v=[E-V(r)]^{\frac{1}{2}}/\mu^{\frac{1}{2}}$, μ being the reduced mass (here $7m_H$ if we are thinking of N_2). (3) The absolute values of Ψ_B can, for our purposes, be chosen arbitrarily, provided the height of the first maximum of Ψ_B is taken the same for other J and E values if comparisons are made with these. (This proviso characterizes an approximation which ceases to be a good one if the energy is altered strongly.)

[6] As we move from $J=0$ through $J=14$ to $J=20$ and beyond, for $v=1$ in Fig. 3, the classical turning points (black circles) for the vibration on $V_A{}^J(r)$ move toward increasing r, while those (open circles) for $V_B{}^J(r)$ move toward decreasing r. This is true both at the high r and at the low r sides of $V_A{}^J(r)$, and for the two predissociating states B (the one for case c^+, the other for case c^-) whose potential curves are shown in Figs. 2 and 3. *At* $J=14$ (for $v=1$), the V_A and V_B turning points coincide. Case c^- differs characteristically from case c^+ in that in the former the Franck-Condon integral normally contains considerable negative as well as positive overlap contributions.

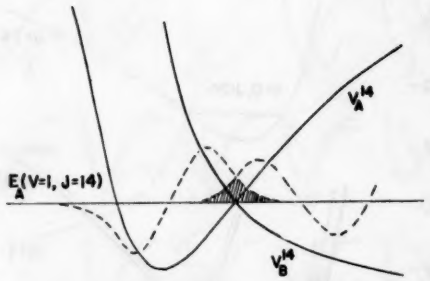

FIG. 4. Sketch (only qualitatively correct) of forms of vibrational wave function $\Psi_A^{v=1,J=14}$ and of continuum wave function $\Psi_{B^+}^{J=14}$ for the energy of the $v=1$, $J=14$ level of state A, corresponding to the $V_A^{v=1,J=14}$ and $V_{B^+}^{J=14}$ potential curves of Figs. 2 and 3. The Franck-Condon factor in the predissociation probability at $v=1$, $J=14$ of state A is proportional to the integral of the product of these two wave functions, hence to the shaded area in Fig. 4.

the barrier at J values below 14 (quantum-mechanical tunnel effect). It is seen that the overlapping peaks of Ψ_A and Ψ_B draw apart, so that the Franck-Condon factor decreases, moderately rapidly below $J=14$. Further consideration, for example of $\Psi_A{}^v=1$, $J=20$ and $\Psi_B{}^J=20$ for the same energy, indicates that the Franck-Condon factor (hence the predissociation probability) reaches a maximum somewhat above $J=14$, then falls off rather slowly at higher J values. For convenience the two regions of J below and above the critical J for a given v will be referred to as the *tunneling region* and the *classical region* of predissociation.

In general, predissociation falls off much faster, as J moves away from near the critical value, in the tunneling region than in the classical region, In principle, predissociation is possible in case c^+ for all energy levels above the dissociation asymptote of state B, but its extent becomes negligible when the tunneling barrier is too great.[7]

In case b^+ (see Fig. 1), the role of the critical J, and the extent of predissociation above and below it, are the same as in case c^+, with one qualification: in case b^+, the energy at the critical J for some v values is below the dissociation asymptote of state B, and in, this event, predissociation cannot set in until J is further increased so that the total energy exceeds this asymptote.[7] It should then begin sharply at a definite J value.

In case c^- (left-hand side of Figs. 2 and 3), the situation is quite different in some ways than in case b^+, or than in case c^+ to which it is most closely related. If one draws $V(r)$ curves (See Figs. 2 and 3), one now finds that, with increasing v, the critical J value *increases* instead of decreasing as in cases b^+ and c^+. Moreover, one sees on making sketches similar to Fig. 4 that the tunneling region is now above and the classical region below the critical J, the reverse of what is true in case c^+. However, because of the necessarily much smaller angle of intersection of curves A and B in case c^- than in case c^+ (See Figs. 2, 3), the tunnel effect should characteristically be much more persistent than in case c^+, so that predissociation may be expected to remain fairly strong for some distance above as well as below the critical J.

As already stated, the foregoing characteristics of case c^- can be seen by drawing $V(r)$ curves. However, the difference between cases c^+ and c^- can be brought out more clearly by another kind of diagram. Let the rotational kinetic energy of state B *at the point of intersection* of the A and B $U(r)$ curves of either case be called $B_eJ(J+1)$, where $B_e=h/8\pi^2c\mu r_e^2$ using cm^{-1} units. For state A, the total energy for any vibrational and rotational state is given by

$$E_A{}^{v,J}=A_v+B_vJ(J+1)-DJ^2(J+1)^2+\cdots, \quad (1)$$

where $A_v=E_A{}^0+\omega_0v-x_0\omega_0v^2+\cdots$, and B_v changes slowly (usually decreases) with increasing v. The term in D may be neglected for present purposes since it is usually very small.

Let us then plot $E^{v,J}=A_v+B_vJ(J+1)$ for state A for each of several values of v, as ordinate, against $J(J+1)$ as abscissa. One has then a series of sloping straight lines (Fig. 5). Let us now plot on the same diagram the energy $E_B{}^J(r_e)=U_B(r_e)+B_eJ(J+1)$, of state B at r_e, also against $J(J+1)$ as abscissa. This

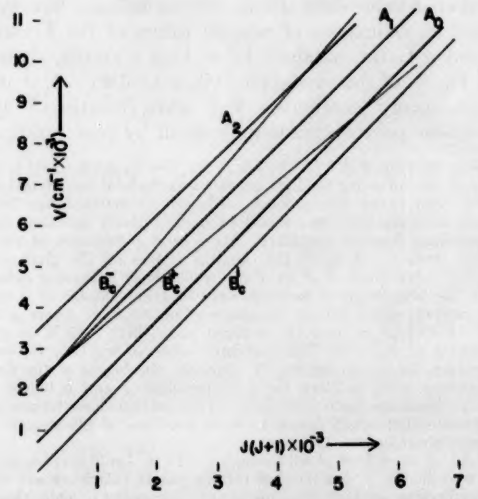

FIG. 5. Loci [cf. Eq. (1)] of rotation-vibration energy levels for state A of Fig. 2 for $v=0$, 1, and 2 as functions of $J(J+1)$; marked A_0, A_1, and A_2. Further, energy of state B at r_e as function of $J(J+1)$ for cases c^+, c^-, and c^i, of Fig. 2 (marked $B_e{}^+$, $B_e{}^-$, and $B_e{}^i$, respectively). The state A lines should bend down very slightly at large J due to a term $-DJ^2(J+1)^2$, but the effect is too small to be visible in the J range shown here. Critical J values are shown at $J=14$ for $v=1$ and $J=74$ for $v=0$ in case c^+, and at $J=14$ for $v=1$ and $J=67$ for $v=2$ in case c^-.

[7] Allowance must here also be made when $J>0$ for the occurrence at large r values of a hump in the $V^J(r)$ curve of state B, increasing in height with J (cf. Fig. 188 in footnote reference 2).

also is a straight line, of *smaller* slope than for state A if $B_v > B_e$ (as is true, if v is not too large, in cases b^+ and c^+, where $r_e > r_e$), but of *steeper* slope than for state A if $B_v < B_e$ ($r_e < r_e$; case c^-). Both cases are illustrated in Fig. 5, using A_v, B_v, U_B, and B_e values corresponding to the A and B potential curves of Figs. 2 and 3.

On this sort of diagram, the critical J values appear as points of intersection of the $E_B{}^J(r_e)$ line with the $E_A{}^{v,J}$ lines. For at each such intersection point, the energy of a particular vibrational and rotational level (v, J) of state A is equal at $r = r_e$ to that of state B for this same J value; which means that the $V(r)$ curves of states A and B for that J value intersect at the position of a vibrational level of state A. This is precisely the condition which determines the critical J values as a function of v in Figs. 2 and 3.

Referring to Fig. 5, one sees immediately that the critical J decreases with increasing v in case c^+, but that in case c^- it *increases* with increasing v. With the particular illustrative forms used for the case c^+ A and B curves in Figs. 2 and 3, predissociation should be especially strong in the classical region above and to some extent in the upper part of the tunneling region just below $J = 74$ for $v = 0$, and $J = 14$ for $v = 1$. For $v > 1$, where now the critical J no longer exists in case c^+ (it is evident from Fig. 5 that the critical value of $J(J+1)$ would be negative), predissociation should occur for all J values, but with a Franck-Condon factor which decreases with increasing v and J.

In a similar way for case c^- (Figs. 2, 3, and 5), predissociation should be especially strong near and *below* (and by tunneling, above) $J = 14$ for $v = 1$, and near and below certain higher J values obtainable for $v > 1$ from Fig. 5 or its extension to higher v and J values. For $v = 0$, where now the critical J no longer exists [the critical value of $J(J+1)$ being negative], predissociation should occur only by a tunnel effect, decreasing with increasing J from $J = 0$. However, as already mentioned above, predissociation by tunneling should be more important and should persist over a wider range of J values in case c^- than in case c^+.

Consideration of the case intermediate between cases c^+ and c^-, case c^i (cf. Fig. 1), where r_e is close to r_e of state A, throws light on both these cases, as well as being of interest for itself. In Fig. 5, the lowest slanting line represents $B_e J(J+1)$ for case c^i. It is seen that usually this line will intersect the $B_v J(J+1) - D J^2(J+1)^2 + \cdots$ lines, even for $v = 0$, only at very high J values, since B_v (especially B_0) is only a little smaller than B_e and the term in D is very small unless J becomes very large or state A is unusually weakly bound. Even though a critical J may be too high to be obtained by ordinary methods of spectroscopic excitation, it is easily seen, by sketching (as in Fig. 4) Ψ_A for $v = 0$, and Ψ_B for the same energy, for $J \geq 0$, that the Franck-Condon factor integral should be fairly large for all J values for $v = 0$. It can also be seen that this factor, although remaining somewhat independent of J, may decrease fairly fast with increasing v. In case c^i (for practicable J values), predissociation is entirely classical.

Although *case* c^i has been defined as characterized by $r_e \approx r_e{}^A$, the following *much more inclusive definition* is probably sensible: case c^i includes all situations where r_e lies between $r'(v=0)$ and $r''(v=0)$, where r' and r'' are respectively the inner and outer classical turning points for vibration. According to the definitions given earlier, the situation in which r_e is equal to r' of $v = 0$ falls under case c^-, while $r_e = r''$ $(v=0)$ falls under case c^+. But when one considers Ψ_A and Ψ_B at (or below) the energy of $v = 0$, it is seen that the Franck-Condon integral is much more like that of the strict case c^i with $r_e = r_e{}^A$ than like the usual case c^+ or c^-.

So far as the writer is aware, no authenticated example of case c^- or case c^i predissociation has been reported as such in the literature, although one might expect case c^- to occur fairly frequently. A partial explanation might be that predissociation is likely to occur with sufficient strength over so wide a range of J values that emission bands from states subject to case c^- or case c^i predissociation are likely not to be observed in emission, although they *should* occur in absorption. However, in a paper to be published by P. G. Wilkinson and the writer, some probable examples of case c^- and case c^i predissociation in emission in N_2 are discussed; the fact that they are observed can be understood because they are attributed to predissociation of singlet by triplet states, which (together with other factors) should make the predissociation relatively very weak.

PROBABLE EXAMPLES OF CASES c^- AND b^0

As has been pointed out to the writer by Dr. A. E. Douglas, some of the emission bands of Si_2 and of CN^+ show phenomena[8] which may well involve case c^- predissociation. In the case of the $f\,{}^1\Sigma^+$ state of CN^+, perturbations occur in some of the $v = 0$ and $v = 1$ rotational levels, also accidental predissociation ($J = 18$ lines missing) in the $v = 1$ level. In the $v = 2$ levels, all lines are missing from levels up to $J = 7$, and, in $v = 3$, all lines from levels up to $J = 13$. This behavior is qualitatively in agreement with what is expected for a weak case c^- predissociation.

In the case of the $L\,{}^3\Pi_u$ state of Si_2, bands are observed only from what is believed to be $v = 0$. In the ${}^3\Pi_0$ and ${}^3\Pi_1$ sublevels, all lines from levels of low J values are missing, but higher J lines are observed. This behavior is of the kind expected for case c^- predissociation. At still higher J values, there is a falloff or breakoff of the usual type, explainable by a second, case c^+ or b^+, predissociation or predissociations. In the ${}^3\Pi_2$ sublevel, which is lowest (the ${}^3\Pi$ is an inverted one), lines of low J are observed, while those in the range 16–40 are missing, after which lines are observed

[8] Si_2: A. E. Douglas, Can. J. Phys. **33**, 801 (1955). CN^+: A. E. Douglas and P. M. Routly, Astrophys. J. **119**, 303 (1954).

up to $J=55$. This behavior agrees qualitatively with what is expected for case c^- predissociation with a critical J of perhaps about 35. For the $^3\Pi_1$ and $^3\Pi_0$ levels, what is observed seems to be in agreement with what might be expected for case c^- predissociation with a lower critical J. Although, in case c^-, the critical J should increase with increasing v, so that the case c^- predissociation probably would disappear for $v>0$ of $L\,^3\Pi_u$ of Si_2, the absence of observed bands with $v>0$ can be understood as a result of the second, case c^+, predissociation, whose critical J is fairly large for $v=0$. It is reasonable to suppose that the critical value of $J(J+1)$ is negative for $v>0$ for this predissociation, so that all rotational levels are predissociated.

In Herzberg's book,[9] the predissociation observed by Grabe and Hulthén[10] in certain AlH bands is cited as an example of case c^-. Reference to the original paper shows, however, that, although the authors considered this possibility, they concluded quite definitely that this predissociation corresponds to what is here called case b^0. In AlH, a sharp breakoff above $J=10$ of $v=0$ in one $^1\Sigma^+$ state, called $^1\Sigma^{**}$, with a potential curve similar to the upper curve in case b^0 of Fig. 1, is attributed to homogeneous predissociation by a second $^1\Sigma^+$ state, called $^1\Sigma^*$, with a curve similar to the lower curve in case b^0 of Fig. 1. In AlD, no corresponding predissociation is observed, a fact which is understandable in terms of a much smaller Franck-Condon factor, hence a much smaller tunneling effect, due to the larger reduced mass of AlD.

[9] See footnote reference 2, p. 432.
[10] B. Grabe and E. Hulthén, Z. Physik **114**, 470 (1939).

CONCLUSION

Although the present paper elucidates qualitatively the expected characteristic differences between cases such as c^- and c^+, it also indicates strongly a need for a systematic quantitative study of the magnitude of the Franck-Condon factor in predissociation as a function of v, J, the forms of the A and B potential curves for various cases, and the reduced mass μ. Such a study should include the cases a^0, b^0, c^0 of Fig. 1, in view of their relevance to the question of the rate of excitation of colliding atoms (for example, of rare gas atoms in a shock tube) to excited and ionized molecular and thence often also atomic states.

ACKNOWLEDGMENT

The author is indebted to Dr. S. Sundaram for valuable assistance with the figures.

THE JOURNAL OF CHEMICAL PHYSICS VOLUME 33, NUMBER 1 JULY, 1960

Near-Infrared Absorption Spectra of Ortho- and Para-H_2O in Solid Xenon and Argon

JAY A. GLASEL*

Department of Chemistry, University of Chicago, Chicago, Illinois

(Received December 7, 1959)

The near-infrared absorption spectra of H_2O trapped in solid argon and xenon have been studied at 20°K. The spectra, taken at concentrations of H_2O to matrix of 1:600, exhibit structure which is analyzed in terms of the known rotational and vibrational constants of the H_2O molecule. The results show that in solid xenon and argon matrices, the monomer H_2O exists as two modifications, one of which is rotating in its ground vibrational state. The theoretical intensities for the spectral bands of H_2O gas at 20°K are calculated and shown to agree with the bands observed in H_2O-xenon. The changes in the observed intensities for other matrices are discussed. The changes in the spectra of the films when they are warmed to 35°K are shown and discussed.

I. INTRODUCTION

EXTENSIVE studies have been made of the polymeric species of H_2O in various solid matrices at low temperatures.[1,2] In the experiments described in this paper, these studies have been extended to include the previously unreported spectrum of H_2O-xenon near 2.7 μ, and the changes in the 2.7-μ bands of H_2O-xenon and H_2O-argon with time at temperatures of 20° and 35°K. The bands due to the monomer are shown to derive from the expected vibration-rotation spectra of the two spin modifications of H_2O.

II. EXPERIMENTAL

Mixtures of the rare gases with water were obtained by placing Linde or Airco research-grade gases in Pyrex flasks having extension fingers containing water. During an experiment the finger was cooled to a temperature such that the ratio of the vapor pressure of ice to the known pressure of the gas gave a mole ratio

* Present address: University of California, School of Science and Engineering, La Jolla, California.
[1] M. Van Thiel, E. O. Becker, and G. C. Pimentel, J. Chem. Phys. **27**, 486 (1957).
[2] E. Catalano and D. E. Milligan, J. Chem. Phys. **30**, 45 (1959).

of water to gas of 1:600. The mixture was then condensed slowly onto a sapphire window cooled to 20°K.[3] The temperature of the extension was lowered slowly to keep the mole ratio approximately constant. The sapphire window was contained in an optical cell which was fitted into a Beckman DK-1 double-beam spectrophotometer. The spectrophotometer was calibrated using the 2.7-μ water-vapor bands. The whole instrument was flushed continuously with dry nitrogen to remove traces of atmospheric-water bands. Scattering by the films was not appreciable in the 2.7-μ region.

III. OBSERVATIONS

The results of the experiments are given in Table I, and illustrated in Figs. 1 and 2. In several repeated experiments the sharp peak c, at 3724 cm^{-1} in H_2O-argon, could not be observed in H_2O-xenon. However, a small shoulder on the high-frequency side of peak d is observable in the H_2O-xenon spectra. The doublet, a, b, at 3737, 3758 cm^{-1} in H_2O-xenon changed as shown in Fig. 1 upon remaining at 20°K for the times indicated. The behavior was similar to that of H_2O-argon. In this case, however, the peaks lost intensity much more rapidly.

In another experiment, which is not shown, a film of H_2O-argon was warmed to 35°K, and then recooled to 20°K. The intensity of the doublet peaks was reduced, as was that of peak c, at 3724 cm^{-1}. This experiment was repeated with H_2O-xenon, and the results are illustrated in Fig. 2. Besides the reduction of the doublet peaks, a shift in the wavelength of the strong peak d, at 3686 cm^{-1}, is noticeable.

TABLE I. Observed spectra and intensity behavior.

H_2O-argon		Behavior on standing at 20°K or warming to 35°K
λ ($m\mu$)	$\bar{\nu}$ (cm^{-1})	
2654	3768	Decrease slowly
2668	3748	Decrease rapidly
2685	3724	Decrease slowly
2711	3689	Increase slowly
2750	3636	Increase slowly
2851	3508	Increase slowly
H_2O-xenon		
2661	3758	Decrease slowly
2676	3737	Decrease rapidly
2702	3686	Decrease slowly
2768	3613	Decrease slowly
2792	3582	Decrease slowly
2826	3539	Increase slowly
2840	3521	Increase slowly
2891	3459	Increase slowly
3006	3327	Increase slowly

[3] Further description of the apparatus to be published in this journal.

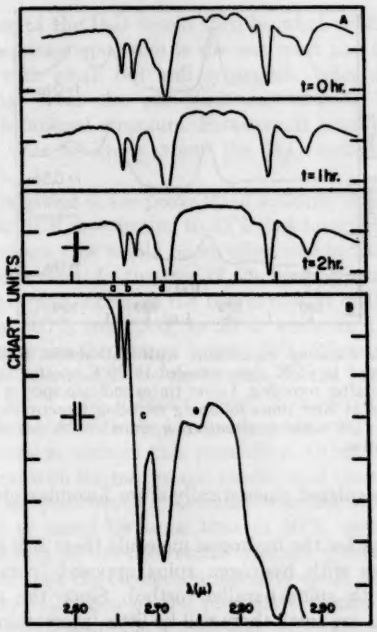

FIG. 1. Typical experiments: (A) film of H_2O-xenon at 20°K standing for the indicated times after deposition. Spectrophotometer on I/I_0 scale with no magnification. (B) film of H_2O-argon 1 hr after deposition. Spectrophotometer on I/I_0 scale with an electronic magnification factor of 10. Resolution sacrificed slightly to reduce noise level.

From the appearance of the spectra it is evident that three general phenomena must be interpreted: (1) the presence of the doublet peaks (these are not observed in H_2O-nitrogen at the same temperature and concentration[1]); (2) the apparent absence of peak c in H_2O-xenon; and (3) the behavior of the peaks upon warming the mixtures to 35°K or allowing them to stand for several hours at 20°K.

IV. INTERPRETATION

The asymmetric-top molecule, H_2O, has low moments of inertia which manifest themselves in large rotational constants.[4] The observed spectral positions of the levels of low rotational number are given in Table II.[5] The observed lines to be interpreted below are those of the ν_3 vibration of the H_2O monomer. This vibration is characterized by an antisymmetric eigenfunction. The 0_0 wave number is at 3757 cm^{-1} for this vibration. The observed levels agree very well with

[4] G. Herzberg, *Infrared and Raman Spectra* (D. Van Nostrand Co., Inc., Princeton, New Jersey, 1945), p. 308.
[5] J. R. Nielsen, Phys. Rev. **62**, 422 (1942).

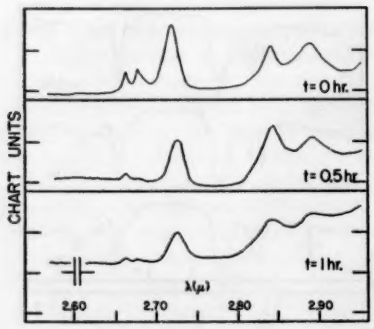

FIG. 2. Warming experiment with H_2O-xenon. First trace: film warmed to 35°K then recooled to 20°K spectra taken immediately after recooling. Lower traces indicate spectra of same film taken at later times following recooling. Spectrophotometer on $\log_{10} I_0/I$ scale (concentration units) with no electronic magnification.

those calculated theoretically from formulas given by Wang.[6]

Just as for the hydrogen molecule there will be H_2O molecules with hydrogen spins opposed (para), and those with spins parallel (ortho). Since the nuclear moments are small there will be little interaction of the two states with each other, and uncatalyzed conversion will be slow compared with experimental times. The percentage of para molecules in the equilibrium mixture at 300° and 20°K for H_2O is 25.00 and 37.02%, respectively.[7] This may be compared with 25.10 and 99.82% for the H_2 molecule.[8]

The effect of these two modifications on the spectra of H_2O at low temperatures is illustrated in Fig. 3. The lowest rotational number the para modification can reach in the ground vibrational state is $J_\tau = 0_0$. For ortho-H_2O the lowest state is $J_\tau = 1_{-1}$. The allowed transitions to the first vibrational state of the antisymmetrical vibration ν_3 are shown in this figure, and listed in Table II. The table also gives the positions of the allowed transitions from the central *minimum* which corresponds to $\bar{\nu}_3$. In the case of the para molecule, even at 20°K there will be a nonnegligible population in the first rotational level, 1_0, of the lowest vibrational state. For ortho molecules the rotational levels 1_{-1} and 1_{+1} will be populated in the lowest vibrational state.

For mixtures of ortho and para molecules the spectra at low temperatures consist of peaks at $\bar{\nu}_3 \pm 5$ cm^{-1}, $\bar{\nu}_3 \pm 23$ cm^{-1}, $\bar{\nu}_3 + 42$ cm^{-1}, $\bar{\nu}_3 + 46$ cm^{-1}, and $\bar{\nu}_3 + 53$ cm^{-1}. The theoretical intensities of these peaks have been calculated, and are listed in Table II in arbitrary units. To obtain those values the intensities calculated by Nielsen for equilibrium water vapor at 300°K were taken and an appropriate Boltzmann factor applied to convert the intensities to 20°K. Nielsen's calculated intensities include statistical weight effects and agree well with the observed intensities at 300°K. The intensities listed in Table II are therefore those for H_2O gas at 20°K consisting of 25.00% para and 75.00% ortho molecules.

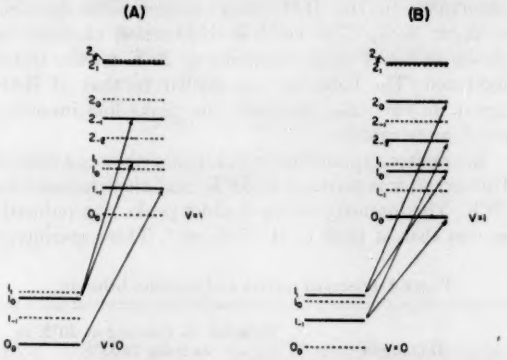

FIG. 3. Theoretically allowed transitions for (A) para molecules, and (B) ortho molecules. Spacings of rotational levels from each vibrational level are proportional to actual energy spacings.

TABLE II. Allowed transitions for ortho- and para-H_2O, and theoretical intensities for the gas at 20°K. Each rotational level J is split into $2J+1$ nondegenerate sublevels characterized by a pseudoquantum number τ.

Modification	$J_\tau' - J_\tau$	Difference from $\bar{\nu}_3$[a] $\bar{\nu}$	λ (mμ)	Intensity
para	$1_{-1}-0_0$	+23 cm^{-1}	(15 mμ)	5.7
	$1_{+1}-1_0$	+5	(3.3)	0.3
	$2_{-1}-1_0$	+42	(28)	0.5
ortho	0_0-1_{-1}	−23	(−15)	7.6
	1_0-1_{+1}	−5	(−3.3)	2.6
	$2_{-2}-1_{-1}$	+46	(31)	10.0
	2_0-1_1	+53	(35)	1.9

[a] 0_0 at 3757 cm^{-1}.

The predicted intensities and band spacings agree satisfactorily with the intensities and spacings observed in H_2O-xenon. The high-frequency component of the doublet (*a*) is therefore identified with the strong peak $\bar{\nu}_3 + 46$ cm^{-1}. The component *b*, observed at a frequency 21 cm^{-1} less than this is identified with the para-molecule absorption at $\bar{\nu}_3 + 23$ cm^{-1}. These two peaks represent the *R* branch of the spectrum. The $Q(\Delta J = 0)$ branch is represented by the weak peak which forms the shoulder of the broad peak *d* at 3686 cm^{-1}. Peak *d* has been studied by Pimentel and his coworkers and assigned to the dimer of H_2O. The peak at $\bar{\nu}_3 - 23$ cm^{-1} will be hidden by this dimer peak. The shift of peak *d* shown in Fig. 2 when the amount of monomer decreases is further proof of this assignment.

[6] S. Wang, Phys. Rev. **34**, 243 (1929).
[7] C. C. Stephenson and H. O. McMahon, J. Chem. Phys. **7**, 614 (1939).
[8] A. Farkas, *Orthohydrogen, Parahydrogen and Heavy Hydrogen* (Cambridge University Press, New York, 1935), p. 14.

A loss of the monomer components $\bar{\nu}_3 \pm 5$ cm^{-1} or $\bar{\nu}_3 - 23$ cm^{-1} will shift the dimer peak to the red from its initial position.

A change in the absolute value of vibrational frequencies from matrix to matrix is common for this type of experiment. It is illustrated by the changes in the spectra of the ν_3 vibration in going from the xenon matrix to the argon matrix. The doublet peaks *a*, *b* observed in H_2O-argon are at distances 24 and 44 cm^{-1} from the strong peak *c* at 3724 cm^{-1}. Within the error of the measurement this is exactly what is predicted if the doublet is associated again with the *R* branch of the rotational structure of the vibration. The peak at 3724 cm^{-1} is therefore identified as the *Q* branch. The peak at $\bar{\nu}_3 - 23$ cm^{-1} which would lie at 3705 cm^{-1} is still covered by the broad peak *d*. The positions of the peaks in H_2O-argon are therefore essentially those of the peaks of H_2O-xenon, taking into account a shift of ν_3 towards the blue by an amount of 10 cm^{-1}.

In H_2O-argon, however, the intensity ratios do not fit those of H_2O gas at 20°K. For instance, the ratio of the total intensity of the *Q* branch to the peak representing $\bar{\nu}_3 + 23$ cm^{-1} is observed to be approximately 6:1 whereas the theoretical ratio is 1:4. As mentioned previously the doublet peaks do not appear in the H_2O-nitrogen mixtures.

If one posits that the rare gases have actually crystallized into their normal face-centered-cubic lattices as hard spheres, the size of the largest interstitial holes which may contain the H_2O may be calculated. This calculation gives a value of 1.84 A for the diameter of the holes in xenon, and 1.58 A for argon. The size of the H_2O molecule is over 2.00 A as determined by various physical methods.[9] Even though the hole would appear to be too small in both cases it must be remembered that the outer charge clouds of the surrounding rare-gas molecules present a highly symmetrical electric field to a molecule trapped in such a hole, and would not necessarily affect the rotational motion of the molecule until the hole becomes so small that the inner charge cores of the surrounding molecules begin to take effect. The lattice parameter of the nitrogen face-centered-cubic lattice, which exists below 35°K, is 5.67 A[10] or about the same size as the argon lattice. However, the nitrogen molecules are not spherical, and it is possible that the interstitial holes are so asymmetric in this case as to prevent the unhindered rotational motion of the H_2O. The general effect on the spectrum of the H_2O would then be what is observed, viz., the xenon spectrum is the one most like the gas, argon, with small but still symmetric holes deviates somewhat from the gas spectrum, and N_2 has no visible rotational structure. However, it is not possible at this time to know where the H_2O molecules are trapped.

The behavior of the peaks upon allowing the films to stand at 20°K or warming to 35°K has several possible explanations. One would be an effect due to the ortho-para conversion. In the case of the hydrogen molecule the conversion increases the concentration of the para form by 300% from 300° to 20°K while for the H_2O para molecules the change is only 50%. The change in the spectrum should be an increase in the peak *b*, at $\bar{\nu}_3 - 23$ cm^{-1}. The opposite effect is observed. These facts combined with the previously mentioned slowness of conversion exclude this possibility. Other explanations deal with the nature and condition of the trapping sites. The spectrum of H_2O-xenon after the material is allowed to stand for some time at 20°K corresponds more closely to the theoretical intensity pattern. This indicates that the changes in intensity could be caused by a crystallization of the previously strained glassy matrix which results in a more ordered environment in which the trapped molecules are situated. The resulting spectrum could then be expected to more closely approximate the gas spectrum.

The behavior of D_2O may be expected to be similar to H_2O with a difference only in the moments of inertia and the statistical weights of the various levels. However, HDO has no ortho-para modifications, and so its behavior would follow that of a molecule which had all the rotational levels allowed to it.

V. CONCLUSIONS

The spectrum of H_2O trapped in a solid xenon matrix at 20°K displays a spectrum which closely approximates the gas spectrum of a mixture of 75% ortho and 25% para H_2O at 20°K. The intensities of the various lines of the spectrum change depending on whether argon, xenon, or nitrogen is used as a matrix, and in particular the rotational structure due to the *R* branch disappears for nitrogen matrix. Other than a constant shift of the frequency of vibration the rotational spacings are constant from argon matrix to xenon matrix. In a given matrix the intensity pattern of the lines changes with the condition of the matrix.

VI. ACKNOWLEDGMENTS

The author wishes to thank Professor J. E. Mayer for many illuminating and pertinent discussions. The work was supported by a grant from the U. S. Atomic Energy Commission.

[9] J. Jeans, *Dynamical Theory of Gases* (Dover Publications, New York), 4th ed.

[10] Crystal data taken from R. W. G. Wyckoff, *The Structure of Crystals* (Reinhold Publishing Corporation, New York, 1931); and R. W. G. Wyckoff, *Crystal Structures* (Interscience Publishers, Inc., New York, 1959).

Antiferromagnetic Coupling and Covalent Bonding in Almost Totally Ionic Salts*

THOMAS R. WAITE†

Gates and Crellin Laboratories of Chemistry, California Institute of Technology, Pasadena, Califrnia

(Received December 23, 1959)

Anderson has recently presented an analysis of antiferromagnetic coupling in salts. His results are derived and extended by an alternate, more physical method. The problem of antiferromagnetism in salts is the problem of spin-spin coupling between two magnetic cations separated by an intervening anion. A linear three-ion array (in the presence of the rest of the crystal) is considered from the viewpoint of molecular orbital theory. In anticipation of electron-electron correlation, and in order to associate each electron spin with only one cation, the molecular orbitals are relocalized. Configuration interaction is small and may be treated by perturbation theory. The perturbation matrix is defined in terms of this representation rather than as a real physical part of the Hamiltonian. The cation-cation spin coupling terms appear as isolated, additive perturbing terms. The expansion parameter is the percent covalent character of the anion-cation bond. Coupling is antiferromagnetic for cations with from five to eight d electrons. Parameters may be estimated from (1) crystal field splittings and/or (2) hyperfine interaction between magnetic electrons and anion nuclei. The perturbed ground state wave function is reduced to a single Slater determinate involving nonorthogonal one electron wave functions, thereby revealing the physical cause of the coupling. Since no cation-cation coupling occurs in zero order with localized orbitals, the spin functions can be constructed from eigenfunctions of the individual cation spin operators using Clebsch-Gordon series. The coupling energy is of the form $K_{ij}\mathbf{S}_i\cdot\mathbf{S}_j$ where $\mathbf{S}_i$ is the total vector spin of cation i in the zero-order representation.

I. INTRODUCTION

THERE are a large number of ionic salts which, although paramagnetic at high temperatures, undergo transitions at low temperatures such that their magnetic susceptibilities are constant or decreasing with further decrease in temperature. The high-temperature susceptibilities of these antiferromagnetic substances follow the Curie-Weiss law with negative Curie temperatures. It has been established by neutron diffraction that at low temperatures the spins of the magnetic ions are aligned alternatively spin up and spin down.[1] The spin coupling is remarkable in that it appears to be greatest for magnetic cations separated by an intervening anion.[2]

These phenomena may be accounted for semiquantitatively by assuming that the crystal consists of a system of weakly coupled ions each of which is almost in an eigenstate of its spin operator $\mathbf{S}_i$ and that the coupling between ions is a perturbation of the form

$$\sum_{i,j} J_{ij}\mathbf{S}_i\cdot\mathbf{S}_j. \tag{1}$$

The sum extends over all pairs of cations which share a nearest-neighbor anion. Equation (1) with the assumption of otherwise independent cation spins is merely a convenient prescription for generating an energy-level spectrum whose spin dependence is similar to that of the real crystal.

Anderson[3] has recently presented an analysis of antiferromagnetism based on a hypothetical set of Bloch wave functions presumed to be exact solutions of the problem of the single d electron in the presence of the full diamagnetic lattice. Anderson anticipates electron-electron correlation and relocalizes these functions by the Wannier method.[4] This unitary transformation introduces off-diagonal elements in the one-electron Hamiltonian. The many-particle problem is solved by perturbation theory using second quantization formalism. Perturbations arise from e^2/r_{ij} terms and from the off-diagonal elements of the one-electron Hamiltonian. By comparing the computed spectrum with that of Eq. (1), Anderson finds

$$J_{ij}\approx 2N^{-2}[(10/3)(Dq)^2U^{-1}-G], \tag{2}$$

where N is the number of unpaired electrons per cation, $10\,Dq$ is the crystal field splitting, U is the activation energy for electrical conductivity and G is a ferromagnetic coulomb exchange term.

These results are obtained here and the inherent approximations are investigated from purely local considerations using a physically clear molecular orbital theory with configuration interaction. The simplification is achieved with no loss in accuracy. The many-electron wave function containing all of the information in Eq. (2) is reduced to a single Slater determinant. It is emphasized that the anion electron-bonding orbitals must be understood before the magnitude of the d-electron interaction is explicable. Spin polarization of the anion is examined more thoroughly.

II. METHOD OF ATTACK

Most theoretical attempts to compute antiferromagnetic coupling energies begin by a perturbation method. This seems appropriate since the spin coupling energies are an extremely small part of the total crystal energy. The difficulty arises in attempting to construct the eigenfunctions of the zero-order Hamiltonian, that

* Contribution No. 2538.

† National Science Foundation Post Doctoral Fellow (on leave of absence from Bell Telephone Laboratories).

[1] C. G. Shull and J. S. Smart, Phys. Rev. **76**, 1256 (1949).

[2] C. G. Shull, W. A. Strauser, and E. O. Wollan, Phys. Rev. **83**, 333 (1951).

[3] P. W. Anderson, Phys. Rev. **115**, 2 (1959).

[4] G. H. Wannier, Phys. Rev. **52**, 191 (1937).

is, the Hamiltonian of the entire crystal omitting the spin coupling energies of Eq. (1). In fact, no such zero-order Hamiltonian exists. It is not a specific small piece of the Hamiltonian which gives the coupling. It is rather the very large terms which have small differences depending on the structure of the spin part of the properly antisymmetrized many-electron wave functions. Therefore, the best one can hope to do is construct a complete set of many-electron wave functions such that:

(1) The correct total Hamiltonian in this representation may be separated into a diagonal matrix and a lesser perturbing matrix.

(2) The cation-cation spin coupling energies appear as isolated terms in the perturbation matrix so that they are not overwhelmed by errors in evaluating the larger crystal energies.

(3) The set of zero-order wave functions is clearly and simply defined so that the matrix elements can be evaluated at least approximately. The perturbation is undefined until the representation is *completely* specified.

The major interactions of a d electron on a cation in the antiferromagnetic crystal are: (1) interactions with the ion on which it is located; (2) potential due to rest of crystal; (3) covalent bonding interactions with adjacent anions; and (4) interactions with other cations which are covalently bonded to the same anion. The anion-cation bonding must be included in the zero-order representation in order to insure the three desired properties.

To simplify the problem, it is desirable to consider as few ions as possible. The three-ion array cation-anion-cation in the electrostatic field of the rest of the crystal is considered here from the viewpoint of molecular orbital theory. This is essentially a self-consistent field approximation to the *entire* crystal. In Sec. XIII it is proven that the errors in this approximation are of high order in the percent covalent character.

A complete set of Slater determinants can be constructed from the three-centered molecular orbitals. Diagonalizing the Hamiltonian is the familiar configuration interaction. As Pople[5] has shown, and in analogy with Anderson,[3] one can anticipate electron-electron correlation and initially relocalize the molecular orbitals. Configuration interaction is then small and can be analyzed by perturbation theory.

Although the perturbation formalism is based on "exact" molecular orbitals, approximate orbitals are presented in order to identify leading terms in the perturbation series and to make the discussion more physical. The details of the present analysis will apply only to cations of the first transition series with from five to eight d electrons. The cations will be assumed to form a simple cubic lattice with one anion lying midway between each nearest-neighbor cation pair. Each cation is surrounded by an octahedron of six anions. Nearest-neighbor octahedral complexes share one anion corner.

[5] J. A. Pople, Quart. Rev. (London) **11**, 273 (1957).

III. ONE CATION AND NEAREST ANIONS

The pertinent molecular orbitals are understood most simply by considering first the familiar octahedral complex of one cation plus six anions and then two such octahedra which share an anion corner. The molecular orbitals for a single octahedron are well known from the study of complex ions and crystal field theory.[6,7] The d-like orbitals are illustrated in Fig. 1. The electrostatic field of the anions raises the energy of the d_γ electrons (orbitals pointing toward the anions) above that of the d_ϵ electrons (orbitals pointing between the anions).

The s and p electrons on each anion partake of a small amount of covalent character spreading out onto the d_γ orbitals of cation A. By the exclusion principle the d_γ electrons are forced into an antibonding mixture of d_γ and anion orbitals. From symmetry alone, Van Vleck[6] has shown that these orbitals are of the form

$$\psi(z^2, E_\theta) \approx (1-\alpha^2)^{\frac{1}{2}}\psi(d_{z^2}) - \alpha(\tfrac{1}{12})^{\frac{1}{2}}\{2(f_3+f_6)-(f_1+f_4+f_2+f_5)\}$$
$$\psi(x^2-y^2, E_\theta) \approx (1-\alpha^2)^{\frac{1}{2}}\psi(d_{x^2-y^2}) - \tfrac{1}{2}\alpha(f_1+f_4-f_2-f_5), \quad (3)$$

where the f_i are a mixture of anion s and p orbitals with the positive lobe pointing toward the cation. Ions 1 and 4 are on the x axis; 2 and 5 on the y axis; and 3 and 6 on the z axis. The d_ϵ orbitals are not involved in bonding. (In the present approximation π bonding is neglected.) The antibonding causes a further separation in the d_γ and d_ϵ energies which will be referred to as "the antibonding part of the crystal field splitting." In the first transition series, the splitting is not often

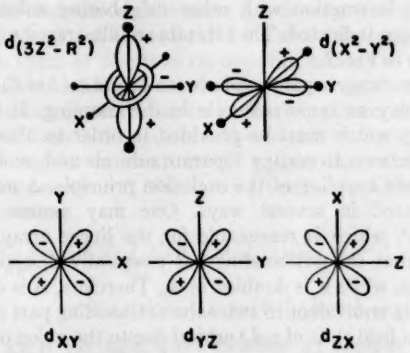

FIG. 1. Cation d orbitals appropriate to octahedral symmetry. Antibonding anion components indicated.

[6] J. H. Van Vleck, J. Chem. Phys. **3**, 807 (1935).

[7] For reviews and bibliographies see: J. S. Griffith and L. E. Orgel, Quart. Rev. **11**, 381 (1957); W. Moffitt and C. J. Ballhausen, Ann. Rev. Phys. Chem. **7**, 107 (1956).

large enough to cause a violation of Hund's rule of maximum multiplicity. The orbital angular momentum is completely quenched.

It is convenient to define the coefficient of the p orbital of the anion on the positive z axis, in Eq. (3) as λ [this p orbital is contained in f_3 of Eq. (3)], and define the fraction covalent character of the anion-cation bond as $(\lambda)^2$. Shulman and Jaccarino[8] have estimated the fraction covalent bonding in transition metal fluorides from measurements of magnetic electron-fluorine nucleus hyperfine interaction. Tinkham[9] has made similar estimates using solutions of transition elements in zinc fluoride. The results indicate $\lambda^2 \approx$ 0.02 to 0.06.

IV. TWO CATIONS AND NEAREST ANIONS

Consider two octahedral ion complexes with a common z axis sharing one anion on the z axis.[10] The $\psi(z^2, E_g)$ electrons of both cations are spread out onto the intervening anion. Strong spin-dependent interaction of these d_{z^2} electrons occurs. Only the d orbitals, as modified by the presence of anion s and p electrons, are considered. Mixing of orbitals, other than the d_{z^2} and anion s and p orbitals, will be considered negligible due to symmetry or distance. The three central ions are labeled: cation A, anion X, and cation B.

By symmetry alone, the pertinent molecular orbitals are approximately

$$\phi_1 \approx (1-2\lambda_s'^2)^{\frac{1}{2}}\psi_X(2s)+\lambda_s'[\psi_A(d_{z^2})+\psi_B(d_{z^2})]$$

$$\phi_2 \approx (1-2\lambda'^2)^{\frac{1}{2}}\psi_X(2p)+\lambda'[\psi_A(d_{z^2})-\psi_B(d_{z^2})]$$

$$\phi_3 \approx N_+[\psi_A(z^2, E_g)+\psi_B(z^2, E_g)]$$
$$\approx N_+[\psi_A(d_{z^2})+\psi_B(d_{z^2})-2\lambda_s\psi_X(2s)]$$

$$\phi_4 \approx N_-[\psi_A(z^2, E_g)-\psi_B(z^2, E_g)]$$
$$\approx N_-[\psi_A(d_{z^2})-\psi_B(d_{z^2})-2\lambda\psi_X(2p)], \quad (4)$$

where interaction with other neighboring anions has not been indicated. The orbitals are illustrated qualitatively in Fig. 2.

The energy separation between ϕ_3 and $\phi_4(\Delta \equiv E_4 - E_3)$ will play an important role in the coupling. It is the energy which must be provided in order to allow the d_{z^2} electrons to occupy separate orbitals and avoid the absolute coupling of the exclusion principle. Δ may be estimated in several ways. One may assume that $\lambda^2 \gg \lambda_s^2$, which is reasonable for the linear array, and note that the antibonding has essentially disappeared from ϕ_3 while it is doubled in ϕ_4. Therefore, Δ is qualitatively equivalent to twice the antibonding part of the crystal field shift of a d_{z^2} orbital due to the anion on the positive z axis. The symmetry of d_{z^2} is really $(2z^2-x^2-y^2)$ and the crystal field shift is due to all six anion neighbors. Anions on the z axis have weight $(2)^2$, those on the x and y axis weight $(1)^2$. Therefore, Δ is about $\frac{2}{3}$ the antibonding part of the crystal field splitting. This argument is identical to that used by Anderson[3] in evaluating the matrix elements which in his theory play a role similar to Δ. The antibonding energy is related to the bonding energy so that Δ is about the same magnitude as the covalent contribution to the anion-cation bond energy.

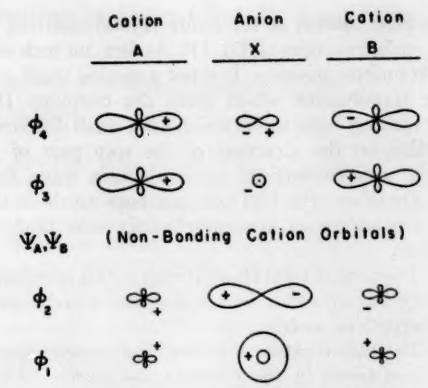

FIG. 2. Approximate molecular orbitals for linear array: cation-anion-cation.

Alternatively, one may compare the expectation of the Hamiltonian for one electron in ϕ_3 to that for one electron in ϕ_4. Very crude estimates using Madelung potentials to approximate the crystal potential, etc., give $(\lambda^2-\lambda_s^2)\times 20$ ev. One may expect Δ to be about 0.5 to 1.0 ev.

V. MOLECULAR ORBITALS

The discussion of the molecular orbitals above has been only approximate. It is now assumed that each of the valence and magnetic electrons is in a molecular orbital satisfying

$$H_k\phi_k = E_k\phi_k$$
$$H_k = -\hbar^2/2m\nabla_k^2 + V_k(r_k), \quad (5)$$

where V_k is the potential acting on the electron in ϕ_k. It is made up of three parts: (1) potential due to the ion cores of the central ions, (2) electrostatic potential of the rest of the crystal, and (3) self-consistent field due to the other $2n+3$ valence and magnetic electrons. Four of the lower-lying orbitals ($k=1$ to 4) may be identified with the ϕ_k of Sec. IV. Other molecular orbitals may be identified with the localized nonbonding d orbitals. In determining the self-consistent potential, ϕ_1, ϕ_2, and ϕ_3 of Eq. (4) and Fig. 2 are assumed to be doubly occupied. The self-consistent field for H_4 is taken identical to that for H_3. The other $2n-2$ magnetic electrons are taken to be in the singly occupied cation d orbitals other than the d_{z^2} orbitals. Variation in the number of electrons is permitted by

[8] R. G. Shulman and V. Jaccarino, Phys. Rev. **108**, 1219 (1957).
[9] M. Tinkham, Proc. Roy. Soc. (London) **A236**, 549 (1956).
[10] In the crystal all anions are shared by other cations. In so far as the assumed octahedral symmetry prevails the result would be the same on any other axis.

allowing the number of other singly occupied d orbitals to vary. In the first transition series this is equivalent to the assumption that each cation has from 5 to 8 d electrons (in some special cases 4 or 9 electrons might be included).

In addition to Eq. (5) it is assumed that the ϕ_k are orthogonal to one another and to the ion-core wave functions which are themselves assumed to be stationary states of the system. It is not in general possible to satisfy these assumptions. There are precise analytical methods of avoiding this difficulty. One may construct for all the electrons on the central ions that complete set of orthogonal one-electron wave functions which permits the best possible description of the ground state by a single Slater determinant. The spin-orbitals method of Löwdin[11] would be appropriate. That method would lead to results identical in form to those presented here with physically similar parameters.

VI. LOCALIZED MOLECULAR ORBITALS

In Sec. IV it was shown that the energy separating ϕ_3 and ϕ_4 is about 0.5 to 1.0 ev. In a naive aufbau, ϕ_3 would be doubly filled and ϕ_4 empty. However, when Slater determinants are constructed and configuration interaction considered one finds the state with ϕ_4 doubly filled (and ϕ_3 empty) strongly mixed with the ground state. The e^2/r_{ij} exchange integrals are approximately 8 ev [Slater orbital and Eq. (4)]. This large electron-electron repulsion energy may be recovered by introducing localized molecular orbitals and insisting that they be singly occupied.[3,5] Configuration interaction is then small (of the order λ^4) and may be analyzed approximately by a perturbation series. It is the attempt to recover some of the molecular orbital energy Δ by a little double occupation of ϕ_3 which causes the antiferromagnetism.

The most convenient choice of localized orbitals is

$$\psi_1=\phi_1; \qquad \psi_2=\phi_2$$
$$\psi_3=(\tfrac{1}{2})^{\frac{1}{2}}(\phi_3+\phi_4)$$
$$\psi_4=(\tfrac{1}{2})^{\frac{1}{2}}(\phi_3-\phi_4). \tag{6}$$

The relocalized wave functions are illustrated qualitatively in Fig. 3. Other nonbonding molecular orbitals are equivalent to the localized nonbonding d orbitals. ψ_3 and ψ_4 are not eigenfunctions of H_3 and H_4 but they satisfy the important equation

$$[H_3(\mathbf{r}_3)+\mathrm{H}_4(\mathbf{r}_4)]\psi_3(\mathbf{r}_3)\psi_4(\mathbf{r}_4)=(E_3+E_4)\psi_3(\mathbf{r}_3)\psi_4(\mathbf{r}_4)$$
$$-\Delta/2[\psi_3(\mathbf{r}_3)\psi_3(\mathbf{r}_4)+\psi_4(\mathbf{r}_3)\psi_4(\mathbf{r}_4)]. \tag{7}$$

Clearly, a zero-order ground state described by localized orbitals will have Hamiltonian matrix elements of order Δ connecting it to the so called ionic excited states.

[11] Per-Olov Lowdin, Phys. Rev. 97, 1475 (1955).

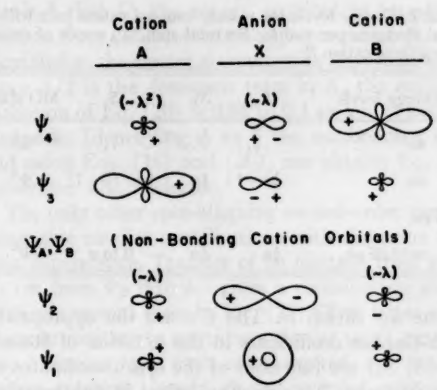

FIG. 3. Relocalized molecular orbitals for linear array: cation-anion-cation.

These relocalized orbitals (given octahedral symmetry in the obvious manner) are similar to Anderson's localized Bloch waves.[3] The wave functions of Eq. (6) are, however, a somewhat better description of the system because the self-consistent fields of the localized d electrons have been considered in their construction.

VII. GROUND STATE

The zero-order ground state orbital configuration may be written down immediately in terms of localized molecular orbitals

$$\Psi_0=\Psi_X\Psi_A\Psi_B\psi_3\psi_4$$
$$\Psi_X=\psi_1\psi_1\psi_2\psi_2, \tag{8}$$

where Ψ_A is the product of one-electron wave functions[12] for unpaired d electrons, other than d_{z^2}, on cation A. Ψ_B is the same for cation B.

In order to obtain the ground-state spin configuration, it is sufficient to note that the coupling between magnetic electrons on the same ion is very strong involving energies of the order of 1 ev, while the coupling between spins of electrons on opposite cations is very small of the order of a few hundredths of an electron volt. The energy levels for the lowest-lying states are as shown in Table I. The combination of two such systems each of angular momentum $n/2$ to form a system of angular momentum S is uniquely given by the Clebsch-Gordan series

$$\chi^0(S, S_z)=\chi_X(0,0)\sum_{S_{zA}}C(n/2, n/2; S; S_{zA}, S_z-S_{zA})$$
$$\times\chi_A(n/2, S_{zA})\chi_B(n/2, S_z-S_{zA}), \tag{9}$$

where χ_X is the spin wave function of angular momentum zero for the doubly filled orbitals; χ_A is the unique eigenfunction of the A cation spin operators $\mathbf{S}_A$ and $\mathbf{S}_{zA}$ with eigenvalues $n/2$ and S_{zA}. The χ_B are

[12] In the case of 6 or 7 d electrons per cation orbital degeneracy occurs (which will be removed by distortion in any real case) and Ψ_A (or Ψ_B) may be a sum of products of d orbitals.

TABLE I. Energy levels for weakly coupled cation pair with n unpaired electrons per cation. S=total spin, S_A=spin of cation A, S_B=spin of cation B.

Energy levels	S_A	S_B	S	MO state
≡	...	...	...	Ψ'
≡	$\frac{1}{2}n-1$	$\frac{1}{2}n$	1 to $(n-1)$	Ψ°
~3 ev				
≡ }0.05 ev	$\frac{1}{2}n$	$\frac{1}{2}n$	0 to n	Ψ°

the same for cation B. The C's are the appropriate Clebsch-Gordan coefficients in the notation of Rose.[13] The $\chi^0(S, S_z)$ are functions of the spin coordinates of all the electrons. No difficulty arises in constructing these functions in terms of the individual electron spin coordinates. However, their explicit form will not be required for the computations.

The lowest lying zero-order states are

$$\Phi^0(S, S_z)=\mathfrak{A}\{\Psi^0\chi^0(S, S_z)\}, \tag{10}$$

where Ψ^0 and χ^0 are given by Eqs. (8) and (9). $\mathfrak{A}$ is the antisymmetrizing operator and may be written as

$$\mathfrak{A}=N\sum_P(-1)^pP, \tag{11}$$

where P is an operator permuting the labels of the electrons; p is the order of P; N is the normalization constant; and the sum extends over all permutations.

VIII. PERTURBATION FORMALISM

The correct total Hamiltonian is completely symmetric in the coordinates of all the electrons. It commutes with $\mathfrak{A}$ and may be considered to act directly upon Ψ^0. With this interpretation matrix elements involving the ground state may be computed using

$$H=\sum_k H_k+\sum_{i>j}e^2/r_{ij}-\sum_{i,j}V_{ij}(\mathbf{r}_j), \tag{12}$$

where the H_k are the one-electron Hamiltonians of Eq. (5). The V_{ij} are the self-consistent potentials included in the V_k of Eq. (5).

The expectation of the Hamiltonian for the lowest zero-order states is given by

$$\langle\Phi^0(S, S_z)\mid H\mid\Phi^0(S, S_z)\rangle$$
$$=E^0+\sum_{i,j}\langle P_{ij}\{\Psi^0\chi^0(S, S_z)\}\mid e^2/r_{ij}\mid\Psi^0\chi^0(S, S_z)\rangle, \tag{13}$$

where P_{ij} permutes the coordinates of electron i and j. The sum extends over all electron pairs, except those occupying the same molecular orbital. The energy E^0 defined by Eq. (13) is independent of S and S_z.

[13] (a) M. E. Rose, *Elementary Theory of Angular Momentum* (John Wiley & Sons, Inc., New York, 1957); (b) E. U. Condon and G. H. Shortly, *The Theory of Atomic Spectra* (Cambridge University Press, New York, 1935).

The terms not included in E^0 are defined to be the first-order perturbation to the zero-order ground state energy. The diagonal elements of the perturbation matrix for excited configurations may be defined similarly. The off-diagonal elements of the perturbation matrix may be defined as the off-diagonal elements of the total Hamiltonian.

IX. FIRST-ORDER PERTURBATION

Terms in the sum in Eq. (13) for which one of the electrons is on the anion give no spin-alligning effect. Terms in which both of the electrons are on the same cation are the familiar atomic exchange effects first analyzed by Slater.[14] They are responsible for coupling the n unpaired d electrons of each cation to form a system of spin $n/2$ (Table I).

Terms in Eq. (13) involving electrons on opposite cations introduce a direct spin-spin coupling between the cations. Taking advantage of the symmetry between cations, there are

$$-G'=-2\sum_i\langle\chi^0(S, S_z)\mid P_{ij}\mid\chi^0(S, S_z)\rangle$$
$$\times\langle\Psi_A(\cdots\mathbf{r}_i\cdots)\psi_4(\mathbf{r}_j)\mid e^2/r_{ij}\mid$$
$$\times P_{ij}\{\Psi_A(\cdots\mathbf{r}_i\cdots)\psi_3(\mathbf{r}_j)\}\rangle$$
$$-\langle\chi^0(S, S_z)\mid P_{kl}\mid\chi^0(S, S_z)\rangle$$
$$\times\langle\psi_3(\mathbf{r}_k)\psi_4(\mathbf{r}_l)\mid e^2/r_{kl}\mid\psi_3(\mathbf{r}_l)\psi_4(\mathbf{r}_k)\rangle. \tag{14}$$

Terms involving electrons neither of which is in ψ_3 or ψ_4 are negligible. P_{ij} acting on χ^0 is to be interpreted as permuting the spin coordinates of two electrons on opposite cations. The sum extends over all unpaired electrons in Ψ_A. By comparing Eq. (18) with Fig. 3, it is clear that the terms in the sum are of order λ^4 times atomic d-orbital exchange integrals. The term involving ϕ_3 and ϕ_4 is of order λ^4 times the sum of atomic coulomb integrals which partially cancel but whose total effect is of order λ^4 times 15 ev. These are by no means negligible. Anderson,[3] using less explicit expressions for localized Bloch waves, estimates this type of coupling to be of order ϵ^4 times atomic exchange integrals, where ϵ is the amplitude of the anion p orbital in the localized Bloch function

All of the spin matrix elements in Eq. (17) are identical. In Appendix I their value is shown to be

$$\langle\chi^0(S)\mid P_{kl}\mid\chi^0(S)\rangle=(1/n^2)[S(S+1)-n]$$
$$=\tfrac{1}{2}+(2/n^2)\mathbf{S}_A\cdot\mathbf{S}_B, \tag{15}$$

where $\mathbf{S}_A$ and $\mathbf{S}_B$ are the total spins of cations A and B.

The entire first-order perturbation is of the form

$$F-(2G/n^2)\mathbf{S}_A\cdot\mathbf{S}_B, \tag{16}$$

where F and G are independent of the spin alignment. G is the same as G' of Eq. (17) with the spin coefficients

[14] J. C. Slater, Phys. Rev. **34**, 1293 (1929).

omitted. It is one or two hundredths of an electron volt in magnitude and positive, favoring ferromagnetism.

X. SECOND-ORDER PERTURBATIONS

The most important one-electron excitations which contribute to the cation-cation spin coupling are those which carry a magnetic electron on one cation into an already singly occupied d orbital on the other cation. The most important excited states are

$$\Phi^i=\mathfrak{A}\{\Psi^i\chi^i(S, S_z)\}$$

$$\Psi^1=\Psi_X\Psi_A\Psi_B\psi_3\psi_3$$

$$\Psi^2=\Psi_X\Psi_A\Psi_B\psi_4\psi_4$$

$$\chi^1(S, S_z)=\chi_X(0, 0)\chi_{k1}(0, 0)$$
$$\times\sum_{S_{zA}}C[\tfrac{1}{2}(n-1), \tfrac{1}{2}(n-1); S; S_{zA}, S_z-S_{zA}]$$
$$\chi_A^-[\tfrac{1}{2}(n-1), S_{zA}]\chi_B^-[\tfrac{1}{2}(n-1), S_z-S_{zA}], \quad (17)$$

where χ_A^- is the spin state for the $n-1$ unpaired electrons on cation A (χ_B^- is the same for cation B) and $\chi_{k1}(0, 0)$ is the spin state for the electron pair in the now doubly occupied d orbital.

By the orthogonality of the molecular orbitals and by Eqs. (7), (10), and (17), one obtains

$$\langle\Phi^1(S)\mid H\mid\Phi^0(S)\rangle=\langle\chi^1(S)\mid\chi^0(S)\rangle\{\Delta/2$$
$$+\sum_i\langle\Psi_B(\cdots r_j\cdots)\psi_3(r_k)$$
$$\times\mid e^2/r_{kj}\mid\Psi_B(\cdots r_k\cdots)\psi_3(r_j)\rangle\}. \quad (18)$$

The sum extends over all unpaired d electrons in Ψ_B. The energy coefficients in the sum are of order λ^2 times atomic exchange integrals. Other terms of order λ^4 arising from the fact that the self-consistent fields were defined in terms of the ϕ's have been dropped. Symmetries of the spin functions have been used to eliminate certain terms and simplify others.

The spin term is evaluated in Appendix II. It is given by

$$\langle\chi^1(S)\mid\chi^0(S)\rangle=[1/(2n^2)\{n(n+1)-S(S+1)\}]^{\frac{1}{2}}$$
$$=[\tfrac{1}{4}-1/n^2\mathbf{S}_A\cdot\mathbf{S}_B]^{\frac{1}{2}}, \quad (19)$$

where S_A and S_B refer to the ground state Φ^0.

The perturbation Φ^2 is identical with that due to Φ^1 and their total effect is

$$-2K^2/U(\tfrac{1}{4}-1/n^2\mathbf{S}_A\cdot\mathbf{S}_B), \quad (20)$$

where K is the energy coefficient in Eq. (18) and U is the energy separation between Φ^1 and Φ^0. Direct computation using free ion Slater orbitals and Eqs. (6), (7) and (17) indicates that $U\approx 15$ ev. Anderson[3] has shown that polarization effects in the solid reduce this to about 5 or 10 ev. He points out, in agreement with Morin,[15] that U, the energy required to transfer a d electron from cation A to an adjacent cation B, can be identified as the electrical conduction activation energy. Since $\Delta/2$ is the dominant term in K, the entire perturbation of Eq. (20) is 0.01 to 0.1 ev and is antiferromagnetic. Identifying Δ as $\frac{3}{2}$ the antibonding energy and using Eqs. (16) and (20), one obtains Eq. (2) in agreement with Anderson.[3]

The only other spin-alligning second-order perturbations give smaller contributions with the same $\mathbf{S}_A\cdot\mathbf{S}_B$ spin dependence. Transfer of an electron from Ψ_A into Ψ_4 (or from Ψ_B into ψ_3) gives a contribution identical with the second term in Eq. (18). Two types of two-electron excitations contribute similar small terms: (1) two electrons from each anion excited, one onto each cation entering already singly occupied orbitals; (2) one magnetic electron from each cation excited into the same higher-lying molecular orbital. Coulombic exchange terms with electrons in doubly filled orbitals and ion cores give a small correction to the one electron excitations above.

Excited spin states with the ground state molecular orbital configuration (Table I) contribute only terms of order λ^3.

Spin-dependent perturbations arise because of excited states in which an electron from a doubly filled anion orbital ψ_i is excited into an unfilled molecular orbital ϕ_E. If ϕ_E and ψ_i have the same symmetry with respect to reflection in the plane perpendicular to the three-ion axis, the perturbation is ferromagnetic. If they have opposite symmetry the perturbation is antiferromagnetic. The spin dependence is in each case $\mathbf{S}_A\cdot\mathbf{S}_B$. The magnitude of the energy coefficients is

$$\mid\sum_i\langle\psi_j(A)\phi_E(1)\mid e^2/r_{1A}\mid\psi_j(1)\psi_i(A)\rangle\mid^2V_{E,i}^{-1},$$

where the sum extends over all singly occupied orbitals ψ_j on cation A, and $V_{E,i}$ is the orbital excitation energy. The effect is not entirely negligible, but if symmetric and antisymmetric orbitals with similar matrix elements occur in pairs they will tend to cancel. These results are derived in Appendix III.

The mixing of molecular orbitals with the same reflection symmetry can only produce anion spin polarization in concentric shells. Coulomb exchange energy is least if the cations both have spin parallel to the spin of the outermost polarization shell. When the molecular orbitals have opposite reflection symmetry, mixing permits a non symmetric polarization. The two halves of the polarized anion must have opposite spin, therefore, exchange energy is least when the cations have opposite spin.

XI. PHYSICAL INTERPRETATION

As usual there is no single interpretation of quantum mathematics which makes the physical phenomenon

[15] F. J. Morin, *Semiconductors*, edited by N. Hannay (Reinhold Publishing Company, New York, 1959), pp. 600–631.

completely clear. Some understanding of antiferromagnetic coupling can be obtained by examining the perturbed many-electron wave functions. The lowest set becomes

$$\Phi(S, S_z) \approx \Phi^0(S, S_z) - K/U[1/(2n^2)\{n(n+1) - S(S+1)\}]^{\frac{1}{2}} \times \{\Phi^1(S, S_z) + \Phi^2(S, S_z)\}. \quad (21)$$

The system is degenerate in S_z.

The state $\Phi^0(S)$ represents the state of lowest energy for fixed S under the constraint that electrons singly occupy orthogonal, localized molecular orbitals. The mixing in of higher states is, in a sense, the effect of relaxing the constraint and lowers the energy. The effect on the one-electron orbitals is seen best by noting (proof in Appendix II) that

$$\mathfrak{A}\{\Psi^1\chi^0(S, S_z)\} = [1/(2n^2)\{n(n+1) - S(S+1)\}]^{\frac{1}{2}} \times \mathfrak{A}\{\Psi^1\chi^1(S, S_z)\}. \quad (22)$$

If we use Eq. (22) we find that the perturbed state Eq. (21) becomes

$$\Phi(S, S_z) \approx \mathfrak{A}\{[\Psi^0 + K/U(\Psi^1 + \Psi^2)]\chi^0(S, S_z)\}. \quad (23)$$

When we neglect terms of order $(K/U)^2$ and recall the simple form of the spatial wave function, this reduces to:

$$\Phi(S, S_z) \approx \mathfrak{A}\{\Psi_X\Psi_A\Psi_B[\psi_3 + K/U\psi_4] \times [\psi_4 + K/U\psi_3]\chi^0(S, S_z)\} \quad (24)$$

which is a single Slater determinant. Eq. (24) when reexpressed in terms of the molecular orbitals ϕ_k presents a solution of the antiferromagnetic coupling problem in terms of the alternant orbitals of Löwdin.[16] Direct application of the original Löwdin method to the ϕ_k does not readily lead to Eq. (24) because it fails to take advantage of the unique nature of the zero-order spin configurations and the smallness of K/U. As pointed out qualitatively by Löwdin[16] and by Anderson,[3] the antiferromagnetic coupling arises because electrons on opposite cations lower their energy by occupying nonorthogonal orbitals. They recover some of the molecular orbital energy Δ.

It should be emphasized that the bracketed term in Eq. (24) contains parts which are completely symmetric in the pair of electrons in the overlapping orbitals. The symmetric parts vanish under the antisymmetrizing operation. The extent to which this occurs depends on S. The normalization constant in $\mathfrak{A}$ will depend on S, also.

Although the perturbed state of Eq. (21) is definitely not an eigenfunction for the spins of the individual cations, it seems that Eq. (24) is. This has been achieved only by further clouding the definition of "electrons on cation A" and, therefore, the "spin of cation A."

The perturbed one-electron orbitals in Eq. (24) differ from ψ_3 and ψ_4 (Fig. 3) by having less of the antibonding anion p character by an amount K/U [(K is a measure of the antibonding energy, U is a measure of the electron-electron repulsion energy gained if ψ_3 and ψ_4 are mixed so as to completely eliminate the antibonding effect)]. The new orbitals lie lower in energy by K^2/U, including electron-electron repulsion. Since these orbitals are not orthogonal; they can be occupied only to the extent that the two electrons in ψ_3 and ψ_4 have opposite spin.

It is clear that the coupling between the two electrons in ψ_3 and ψ_4 is antiferromagnetic. The strong coupling of each of these electrons to the other unpaired electrons on its own ion acts to couple *all* of the spins on one ion antiferromagnetically to *all* of the spins on the other ion. This may be related to the mathematics through the symmetries of the spin functions. All of the magnetic electrons on cation A, including the one in ψ_3, are strongly coupled into a spin function $\chi_A(n/2, S_{zA})$ which is totally symmetric in the spin coordinates of all these electrons (due to e^2/r_{ij} terms). The same is true of cation B. But the pair of electrons in ψ_3 and ψ_4 can lower their energy by spreading out into nonorthogonal molecular orbitals. This can be achieved only to the extent that $\chi^0(S, S_z)$ is antisymmetric in that pair. This effect is small and does not destroy the original symmetry of χ_A and χ_B. Any antisymmetry for the pair of electrons in ψ_3 and ψ_4 must be matched by antisymmetry in every pair of electrons when one is taken from each of the two cations. Thus all of the electrons are coupled.

Another interpretation is possible. Excitation of both of the d_{z^2} electrons into the bonding orbital ϕ_3 corresponds to a weak covalent bond between the cations (extending across the anion). This configuration, which is not orthogonal to the zero-order ground state Φ^0, introduces a little more than half of the antiferromagnetic coupling due to Φ^1 and Φ^2 considered above. The remainder of that coupling (nearly half) comes from the excited configuration corresponding to double occupation of the antibonding orbital ϕ_4 (with ϕ_3 empty). This configuration is not orthogonal to Φ^0 either and its amplitude in the perturbed ground state is such as to "remove double occupation of ϕ_4" from Φ^0. The perturbation clearly increases bonding between the cations (occupation of ϕ_3) and reduces antibonding (occupation of ϕ_4). The remarks in Sec. IV relate the cation-cation bonding energy Δ to the anion-cation bonding. This bond formation is inhibited by the very large electron-electron repulsion U (which was the original reason for using the relocalized ψ's in the zero-order ground state). Bonding is still favorable to the extent Δ/U but can occur only insofar as the spin part of the wave function is antisymmetric in the appropriate electron pair.

[16] Per-Olov Löwdin, Phys. Rev. **97**, 1509 (1955).

XII. HIGHER-ORDER PERTURBATIONS

Third-order perturbations due to the above states are not completely negligible. Terms of order $\lambda'^2\Delta$ and λ'^4 times atomic exchange integrals (reduced by the square of an energy ratio somewhat less than one) appear in third order. The number of excited configurations may be large enough to make the effect important. Furthermore, λ' may be larger than λ. The third-order perturbation will be considered in a subsequent publication.

It should be emphasized that terms of order λ^4 will appear in all orders of perturbation theory. Each of the localized molecular orbitals will be perturbed by higher molecular orbitals localized in the same region. This local effect will be of order zero in λ. Connecting with other states will introduce spin-dependent terms of order λ^4. These perturbations will be small only if the zero order set of localized one-electron orbitals make possible a good description of one octahedral complex in the electrostatic field of the rest of the crystal by means of a single Slater determinant. There is little reason to believe that the localized Bloch waves would satisfy this condition, particularly since Anderson[3] has proven that the one electron picture using the *exact* Bloch waves is very inadequate. The present method suffers from this to a lesser degree, but could be improved by an even more local beginning which still included the anion-cation bonding.

XIII. ANTIFERROMAGNETIC CRYSTAL

The three-centered Hamiltonian with the electrostatic field of the rest of the crystal differs from the correct crystal Hamiltonian only in that most of the electrons are replaced by their self-consistent fields. These other electrons are assumed to occupy localized orbitals on other ions similar to those considered above. In principle, one could construct Slater determinants for the entire crystal and consider configuration interaction. In analogy with the above results, configuration interaction would delocalize the electrons only to the order Δ^2/U. Anderson[3] has proven this by showing that because of electron-electron repulsion the Bloch functions are a better zero-order representation after localization.

Electrons on adjacent ions overlap the central ions introducing corrections to the exchange terms in the second order perturbations above, these are clearly of higher order in the percent covalent character. Therefore, in agreement with Anderson,[3] the entire crystal spin energy is a sum of pair coupling energies to the accuracy with which the three-centered problem has been considered.

XIV. CONCLUSIONS

The physical cause of the coupling in ionic salts is related to the small amount of anion cation covalent bonding. The anion valence electrons form weak covalent bonds with each of their neighboring cations, spreading out into their d_γ orbitals. The d_γ electrons are forced (by the exclusion principle) into antibonding orbitals which overlap the anion. The d_γ electrons on two cations which share an anion neighbor have enhanced interaction. Spin-alligning energies of second-order in the covalent character of the anion-cation bond arise. A term G due to direct e^2/r_{ij} exchange is ferromagnetic. A second term arises because the d_γ orbitals can combine so as to reduce the antibonding energy Δ. But this is opposed by electron-electron repulsion energies of order U. The effect occurs only to the extent Δ/U. The net energy reduction is of order Δ^2/U. These energetically most favorable orbitals are not orthogonal, and may be used only to the extent that the d_γ electrons on neighboring cations have opposite spins. Antiferromagnetism is favored.

Both coupling terms ($\Delta^2/U-G$) vanish when no unpaired d_γ electrons are present. The experimental data indicates that the coupling is somewhat weaker in such salts, but not negligible. Consider the antiferromagnetic transition temperatures: FeF_3 (394°K); CrF_3 (80°K); $LaFeO_3$ (750°K); $LaCrO_3$ (320°K). Trivalent chromium has no d_γ electrons, yet its coupling in salts is 20 to 50% that of the equivalent iron salts. Either π bonding, anion polarization (as described at the end of Sec. X) or the higher-order perturbations are responsible. A formalism similar to that presented here would relate a one-electron description of π bonding to the spin coupling.

By purely local arguments, it is proven, in agreement with Anderson,[3] that (1) through second order in the percent covalent character, the entire crystal spin energy may be written as a sum of pair coupling energies, and (2) the dominant pair-coupling term is of the form $\mathbf{S}_i\cdot\mathbf{S}_j$. Anderson's result is extended to show that this is true of anion polarization, also.

The limitation on the accuracy with which one can evaluate the matrix elements is the difficulty in formulating and solving the one electron problem for the three central ions in the electrostatic field of the rest of the crystal. The range of magnitude estimates of the matrix elements presented above indicate that J_{ij} is about $0.01/n^2$ to $0.1/n^2$ ev favoring antiferromagnetism. This suggests transition temperatures in the range 100° to 1000°K in agreement with the experimental data. More quantitative computations may be made on the basis of the physical identification of the matrix elements in terms of crystal field splittings and electrical conduction activation energies. Anderson[3] has analyzed a number of salts from this viewpoint and finds fair agreement with the experimental data.

ACKNOWLEDGMENTS

The ideas for this work arose as a result of the author's association with members of the chemical physics research group at Bell Telephone Laboratories. Their efforts in obtaining, correlating, and interpreting experimental data on resonance, optical, and transport

TABLE II.

k	1	2	3	4	5	6	7	8	9	10	11
(s_1+s_2)	0	1	0	0	0	1	1	1	1	1	1
(s_A+s_B)	0	1	1	1	1	0	0	0	1	1	1
$(s_1+s_2+s_A+s_B)$	0	0	1	1	1	1	1	1	1	1	1
$(S_A^z+S_B^z)$	S	S	$S+1$	S	$S-1$	$S+1$	S	$S-1$	$S+1$	S	$S-1$

phenomena in antiferromagnetic salts rank as major contributions to the understanding of these materials.

The author has benefited from discussions with R. G. Shulman, C. Iddings, H. M. McConnell, F. J. Morin, P. W. Anderson, A. Liehr, and C. A. Englebrecht.

APPENDIX I

The evaluation of the spin term in Eq. (14) may be accomplished by substituting from Eq. (9). The analysis for $S_z=0$ proceeds as follows (other values of S_z give identical results):

$$\langle\chi^0(S)\mid P_{kl}\mid\chi^0(S)\rangle=\sum_{M_A}\sum_{M_A'}C(n/2,n/2;S;M_A,-M_A)C(n/2,n/2;S;M_A',-M_A')$$
$$\times\langle\chi_A(n/2,M_A')\chi_B(n/2,-M_A')\mid P_{kl}\{\chi_A(n/2,M_A)\chi_B(n/2,-M_A)\}\rangle \quad \text{(A1)}$$

where k and l refer to electrons on opposite cations. Other than this, it does not matter which electrons because χ_A is symmetric in its n electrons (same for χ_B). In order to perform the permutation operation it is necessary to separate off electron k from χ_A and electron 1 from χ_B. This may be done in a unique manner using Clebsch-Gordan[17] coefficients for combining a system of spin $\frac{1}{2}$ with a system of $(n-1)/2$. The matrix elements in Eq. (A1) then become the sum of products of matrix elements for the simpler systems which are obviously zero or one. The result

$$\langle\chi_A(n/2,M_A')\chi_B(n/2,-M_A')\mid P_{kl}\{\chi_A(n/2,M_A)\chi_B(n/2,-M_A)\}\rangle$$
$$=2/n^2(n/2-M_A)(n/2+M_A)\delta_{M_A,M_A'}+1/n^2(n/2+M_A)(n/2-M_A+1)\delta_{M_A-1,M_A'}$$
$$+1/n^2(n/2-M_A)(n/2+M_A+1)\delta_{M_A+1,M_A'} \quad \text{(A2)}$$

Substituting in Eq. (A1) and using a well-known recursion relation for Clebsch-Gordan coefficients[18] the summation may be performed and one obtains Eq. (15).

APPENDIX II

The spin configurations for the excited states are best classified in the representation in which $(\mathbf{s}_1+\mathbf{s}_2)$, $(\mathbf{s}_A+\mathbf{s}_B)$ and $(\mathbf{S}_A+\mathbf{S}_B)$ are diagonal. $(\mathbf{s}_1+\mathbf{s}_2)$ is the spin operator for a pair of anion electrons in the ground state. $(\mathbf{s}_A+\mathbf{s}_B)$ is the spin of an electron pair one taken from cation A one from cation B. $\mathbf{S}_A$ is the spin of the $n-1$ unpaired electrons left on cation A. $\mathbf{S}_B$ is the same for cation B. The states required are labeled as shown in Table II.

The only states of importance in the present analysis have $\mathbf{S}_A=\mathbf{S}_B=\frac{1}{2}(n-1)$ and $(s_1+s_2+s_A+s_B)=0$ or 1.

Projecting $\chi^0(S,0)$ on this representation:

$$\chi^0(S)=K_1(S)\chi^1(S)+K_3(S)\chi^3(S)+K_5(S)\chi^5(S). \quad \text{(A3)}$$

The coefficient $K_1(S)$ is the only one required here and it is evaluated most readily by noting that

$$\langle\chi^0(S)\mid P_{AB}\mid\chi^0(S)\rangle=1-2K_1^2 \quad \text{(A4)}$$

where P_{AB} permutes the pair of electrons separated off from cation A and cation B. Equating this to the result of Appendix I one obtains Eq. (19) (since $K_1=\langle\chi^1\mid\chi^0\rangle$).

Note that Eq. (22) of Sec. XI may be proven by substituting from Eq. (A3) into the left-hand side of Eq. (22). Because χ^3 and χ^5 are symmetric in the electron pair in the doubly occupied orbital, the corresponding terms vanish under $\mathbf{A}$.

APPENDIX III

The perturbation of the state $\Phi^0(S,0)$ by excited orbital configurations in which an anion electron from doubly occupied ψ_i has been excited into ϕ_E is given by:

$$-\sum_k\mid\langle\chi^k(S)\mid P_{1A}+\tau(E,i)P_{1B}\mid\chi^0(S)\rangle\sum_j\langle\psi_j(\mathbf{r}_A)\phi_E(\mathbf{r}_1)\mid e^2/r_{1A}\mid\psi_j(\mathbf{r}_1)\psi_j(\mathbf{r}_A)\rangle\mid^2V_{E,i}^{-1} \quad \text{(A5)}$$

[17] E. U. Condon and G. H. Shortly, footnote reference 13(b), p. 76.
[18] M. E. Rose, footnote reference 13(a), p. 44.

The sum on k extends over all spin states compatible with the excited orbital configuration. The sum on j extends over all singly occupied orbitals on cation A (ψ_3 and Ψ_A). P_{1A} permutes the excited anion electron with an unpaired electron of cation A. P_{1B} is the same for cation B. $V_{E,i}$ is the orbital excitation energy. $\tau(E, i)$ is plus or minus one depending on whether the symmetry of ϕ_E with respect to reflection in the plane perpendicular to the three ion axis is the same or opposite to that of ψ_i. It arises because every exchange term with an electron on cation A is matched by an exchange term with cation B of the same magnitude and equal or opposite sign depending on the relative symmetry of ϕ_E and ψ_i.

By the closure property:

$$\sum_k |\langle \chi^k(S) | P_{1A}+\tau(E,i)P_{1B} | \chi^0(S)\rangle|^2 = \langle \chi^0 | (P_{1A}+\tau P_{1B})^2 | \chi^0\rangle$$
$$=2[1+\tau(\tfrac{1}{2}-K_1^2)]$$
$$=2\{1+\tau[\tfrac{1}{4}+(1/n^2)\mathbf{S}_A\cdot\mathbf{S}_B]\}. \quad \text{(A6)}$$

The second step in Eq. (A6) has been performed by writing out that part of the wave function of Eq. (A3) which refers to the four unique electrons and by performing the operations explicitly. The remarks in Sec. X follow from Eqs. (A5) and (A6).

THE JOURNAL OF CHEMICAL PHYSICS VOLUME 33, NUMBER 1 JULY, 1960

Frequency Spectrum for a Two-Dimensional Lattice*

JACOB NEUBERGER†‡ AND ROBERT D. HATCHER

Washington Square College, New York University, New York

(Received January 18, 1960)

The methods of lattice dynamics are applied to a study of the frequency distribution function $f(\nu)$ of a two-dimensional model of a monatomic crystal. It is shown that if the interaction of the atoms of the lattice is of short range such that next-nearest neighbor interactions are much weaker than nearest neighbor interactions, the function $f(\nu)$ can be expressed in terms of elliptic integrals of the first kind. These functions are calculated for a particular choice of the ratio of the interaction constants which had previously been discussed in the literature by approximate numerical methods. This gives some evidence that the numerical scheme for obtaining $f(\nu)$, based on a comparatively small spanning of wave-vector space which is used extensively in more complicated crystal models, is adequate provided that ν is a fairly smooth function of the wave vector.

I. INTRODUCTION

THE calculation of the frequency distribution function $f(\nu)$ for crystals of simple structure by the methods of lattice dynamics has been investigated by many authors.[1] The resultant specific heats show marked deviations from calculations based on the Debye continuum model, especially in the low temperature region. Since the evaluation of $f(\nu)$ presents mathematical difficulties for realistic crystal models, most investigations have been based on idealized one-, two-, and three-dimensional periodic structures. For many of those cases, numerical calculations based on a finite subdivision of wave-vector space are necessary to obtain $f(\nu)$. A serious question arises as to the accuracy of this scheme since calculations are based on a negligible number of points when compared to the total number of wave vectors which are of order 10^{23}. We therefore investigate here the behavior of $f(\nu)$ for a special two-dimensional model from two points of view. The numerical scheme for finding $f(\nu)$ for this model has been obtained by others.[2,3] On the other hand, by suitably generalizing a method first given by Montroll,[4] we are able to obtain $f(\nu)$ by means of an analytic calculation. Thus, a continuous wave-vector distribution can lead to a direct evaluation of $f(\nu)$ for the aforementioned model. This is shown

* The research reported in this paper has been sponsored by the Electronics Research Directorate of the Air Force Cambridge Research Center, Air Research and Development Command under contract.

† Now at Rutgers University, Newark, New Jersey.

‡ Much of the material included in this paper was used in a Ph.D. dissertation at New York University (1958).

[1] M. Born and K. Huang, *Dynamical Theory of Crystal Lattices* (Oxford University Press, New York, 1954), Chap. V.

[2] M. Blackman, Proc. Roy. Soc. (London) **A148**, 365, 384 (1935).

[3] E. Montroll, J. Chem. Phys. **10**, 218 (1942).

[4] E. Montroll, J. Chem. Phys. **15**, 575 (1947).

in Sec. II. The comparison between these two calculations and an evaluation of the significance of the results are given in Sec. III.

II. DERIVATION OF $f(\nu)$

Consider a two-dimensional square lattice of N^2 identical atoms. Following the principles of small oscillation theory,[5] the potential energy of the displaced lattice up to next-nearest neighbor interactions becomes

$$V=\tfrac{1}{2}\alpha[\sum_{l,m=1}^{N}(u_{l+1,m}-u_{l,m})^2+(v_{l,m+1}-v_{l,m})^2]$$
$$+\tfrac{1}{4}\beta[\sum_{l,m=1}^{N}(u_{l+1,m+1}-u_{l,m}+v_{l+1,m+1}-v_{l,m})^2$$
$$+(v_{l,m}+u_{l+1,m-1}-u_{l,m}-v_{l+1,m-1})^2] \quad (1)$$

where α, β are the nearest and next-nearest neighbor interaction constants and $u_{l,m}$, $v_{l,m}$ represent the x and y components of the displacement of the l, mth atom. For the resultant equations of motion we consider the customary solution of the form

$$u_{l,m}=A\exp\{i[\omega t-(\phi_1 l+\phi_2 m)]\}$$
$$v_{l,m}=B\exp\{i[\omega t-(\phi_1 l+\phi_2 m)]\}$$

with $\phi_i=2\pi k_i/N$, k_i being an integer such that $-N/2<k_i\leq N/2$ due to the Born-von Karman boundary conditions. Nontrivial solutions demand the vanishing of the determinant of the coefficients of A and B in the equation of motion:

$$\begin{vmatrix}\mu\omega^2-2\alpha(1-c_1)-2\beta(1-c_1c_2) & 2\beta(1-c_1^2)^{\frac{1}{2}}(1-c_2^2)^{\frac{1}{2}}\\ 2\beta(1-c_1^2)^{\frac{1}{2}}(1-c_2^2)^{\frac{1}{2}} & \mu\omega^2-2\alpha(1-c_2)-2\beta(1-c_1c_2)\end{vmatrix}=0 \quad (2)$$

where $c_i=\cos\phi_i$.

Each of the two solutions of ω^2 of (2) can take on N^2 values corresponding to N choices for both ϕ_1 and ϕ_2. Thus the number of possible frequencies is $2N^2$ equal to the number of degrees of freedom of the lattice. Treating ϕ as a continuous variable (N^3 is of the order of 10^{23}) we see that the number of modes of vibration associated with a closed region in (ϕ_1, ϕ_2) space is proportional to the area of the region. Thus if $L(\nu_k)$ represents the total number of frequencies less than some ν_k we have

$$L(\nu_k)=(N^2/4\pi^2)\int_R\int d\phi_1 d\phi_2 \quad (3)$$

where R denotes the region in (ϕ_1, ϕ_2) space for which $\nu^2(\phi_1, \phi_2)$ as given by (2) is less than ν_k^2. Hence the number of frequencies between ν and $\nu+d\nu$ is given by[4]

$$f(\nu)=(N^2/4\pi^2)(\partial/\partial\nu)\int_R\int d\phi_1 d\phi_2. \quad (4)$$

Equation (4) can only be computed in analytic form if ω^2 is a simple function of ϕ_1, ϕ_2. Montroll[4] carried through the calculation for the special case when $\beta/\alpha=\frac{1}{2}$ which implies a potential decreasing as r^{-2}. A case of more general interest occurs when β/α is sufficiently small such that all terms in $(\beta/\alpha)^2$ and higher order can be ignored. This implies a very short-range interaction which is usually assumed in more complicated three-dimensional crystal models. Thus for β/α small (2) becomes

$$[\mu\omega^2-2\alpha(1-c_1)-2\beta(1-c_1c_2)]$$
$$\times[\mu\omega^2-2\alpha(1-c_2)-2\beta(1-c_1c_2)]=0. \quad (5)$$

Letting $\lambda=\omega^2$ and $\gamma=\beta/\alpha$ the two branches have solution

$$\lambda_1=(2\alpha/\mu)[1-\cos\phi_1+\gamma(1-\cos\phi_1\cos\phi_2)], \quad (6)$$
$$\lambda_2=(2\alpha/\mu)[1-\cos\phi_2+\gamma(1-\cos\phi_1\cos\phi_2)]. \quad (7)$$

Since the two branches differ only by an interchange of ϕ_1 and ϕ_2 the subsequent discussion will be restricted to the λ_1 solution. Letting $g_1^2=\lambda_1/\lambda_{1\,\max}=(\nu_1/\nu_{1\,\max})^2$ where $\lambda_{1\,\max}=(4\alpha/\mu)(1+\gamma)$, Eq. (6) takes the form

$$2g_1^2(1+\gamma)=1-\cos\phi_1+\gamma(1-\cos\phi_1\cos\phi_2). \quad (8)$$

It will be noted that

$$\begin{aligned}&\max\ g_1^2=1, && \text{at } (\pi,0)\\ &\min\ g_1^2=0 && \text{at } (0,0)\\ &\text{saddle pt } g_1^2=1/(1+\gamma) && \text{at } (\pi,\pi)\\ &\text{saddle pt } g_1^2=\gamma/(1+\gamma) && \text{at } (0,\pi)\\ \text{and}\quad &g_1^2=\tfrac{1}{2} && \text{at } (\tfrac{1}{2}\pi,\phi_2). \end{aligned} \quad (9)$$

Contour lines of constant frequency are shown in Fig. 1 where the intersections with the axes are indicated rather than the exact shape of a line. Since g_1 is an even function of ϕ_1 and ϕ_2, the discussion can be restricted to a quadrant of ϕ_1, ϕ_2 space. Thus (4) becomes

$$f(\nu)=(N^2/\pi^2)(\partial/\partial\nu)\int_{R'}\int d\phi_1 d\phi_2. \quad (10)$$

We now break up R' into four regions as shown in Fig. 2 such that

$$\begin{aligned}&0\leq g_1^2\leq\gamma/(1+\gamma) && \text{for } R_a;\\ &\gamma/(1+\gamma)\leq g_1^2\leq\tfrac{1}{2} && \text{for } R_b;\\ &\tfrac{1}{2}\leq g_1^2\leq 1/(1+\gamma) && \text{for } R_c;\\ &1/(1+\gamma)\leq g_1^2\leq 1 && \text{for } R_d.\end{aligned}$$

[5] H. Goldstein, *Classical Mechanics* (Addison-Wesley Press, Reading, Massachusetts, 1951), p. 318 ff.

For R_a the ϕ_2 intercept of a typical contour line is at $\phi_2=\cos^{-1}\{[(1+\gamma)(1-2g_1^2)-1]/\gamma\}$. Letting f_a be the frequency distribution in R_a and ν_m the maximum frequency, and noting that $\partial/\partial\nu=(1/\nu_m)(\partial/\partial g_1)$, (10) becomes for R_a

$$f_a(g_1\nu_m)=(N^2/\pi^2\nu_m)(\partial/\partial g_1)\left[\int_0^{\psi(g_1)}d\phi_2\int_0^{\Omega(g_1\phi_2)}d\phi_1\right] \quad (11)$$

where $\cos\Omega=(1+\gamma)(1-2g_1^2)/(1+\gamma\cos\phi_2)$ and $\cos\psi=[(1+\gamma)(1-2g_1^2)-1]/\gamma$. On setting $u=\cos\phi_2$ and differentiating, (11) becomes

$$f_a(g_1\nu_m)=\frac{4N^2g_1(1+\gamma)}{\pi^2\nu_m\gamma}\int_\eta^1\frac{du}{[(1-u)(u-\eta)(u+1)(u-\xi)]^{\frac{1}{2}}} \quad (12)$$

where

$$\eta=[(1+\gamma)(1-2g_1^2)-1]/\gamma$$

and

$$\xi=-[(1+\gamma)(1-2g_1^2)+1]/\gamma.$$

The roots of the integrand of (12) are in the order

$$1>\eta>-1>\xi.$$

This integral may be found in a standard table of integrals[6] and yields

$$f_a(g_1\nu_m)=\frac{4N^2g_1}{\pi^2\nu_m(\gamma)^{\frac{1}{2}}}\left(\frac{1+\gamma}{1-2g_1^2}\right)^{\frac{1}{2}}K(\delta_a) \quad (13)$$

where

$$\delta_a=\left[g_1^2\left\{\frac{1-g_1^2(1+\gamma)}{\gamma(1-2g_1^2)}\right\}\right]^{\frac{1}{2}} \quad (14)$$

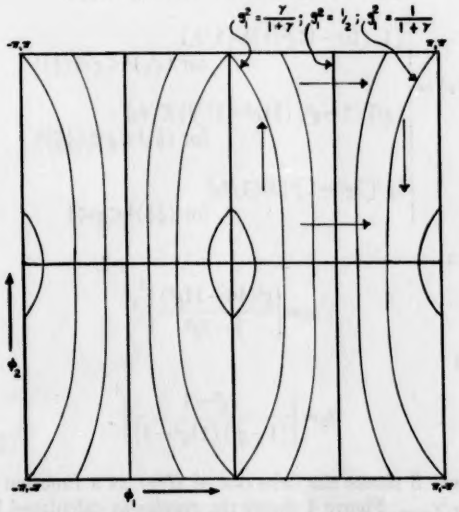

FIG. 1. Frequency contour lines showing their intersections with the ϕ_1, ϕ_2 axes. The curves are not meant to show the exact behavior of g_1 as related to ϕ_1, ϕ_2. The arrows indicate the direction in which frequency increases.

[6] B. Pierce, *A Short Table of Integrals* (Ginn and Company, Boston, Massachusetts, 1929), 3rd ed., p. 70.

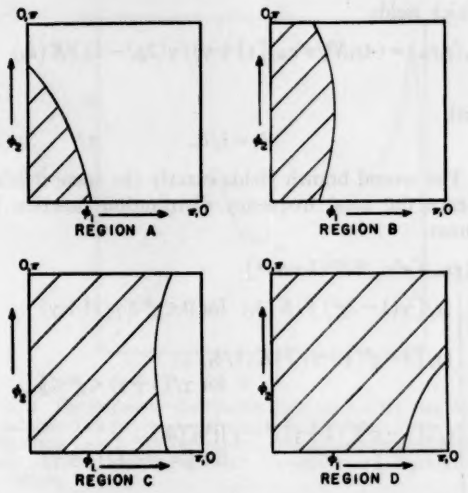

FIG. 2. The four regions over which $f(\nu)$ is calculated. Note that in region A contour lines cut the ϕ_1, ϕ_2 axes, in regions B and C the $\phi_2=0$ and π axes, and in region D the $\phi_2=0$ and $\phi_1=\pi$ axes.

and $K(\delta_a)$ is the complete elliptic integral of the first kind defined by

$$K(\delta_a)=\int_0^{\pi/2}\frac{d\theta}{(1-\delta_a^2\sin^2\theta)^{\frac{1}{2}}};\qquad \delta_a^2<1.$$

For region b we have

$$f_b(g_1\nu_m)=\frac{N^2}{\pi^2\nu_m}\frac{\partial}{\partial g_1}\int_0^{\pi}d\phi_2\int_0^{\cos^{-1}[(1+\gamma)(1-2g_1^2)]/[(1+\gamma\cos\phi_2)]}d\phi_1. \quad (15)$$

Following the same procedure as above, we obtain

$$f_b(g_1\nu_m)=(4N^2/\pi^2\nu_m)\{(1+\gamma)/[1-g_1^2(1+\gamma)]\}^{\frac{1}{2}}K(\delta_b) \quad (16)$$

where

$$\delta_b=1/\delta_a. \quad (17)$$

For region c, (15) still applies but the roots appear in different order. The result is

$$f_c(g_1\nu_m)=\frac{4g_1N^2}{\pi^2\nu_m}\left\{\frac{1+\gamma}{(1-g_1^2)[(1+\gamma)g_1^2-\gamma]}\right\}^{\frac{1}{2}}K(\delta_c) \quad (18)$$

where

$$\delta_c^2=\frac{\gamma(2g_1^2-1)}{(1-g_1^2)[(1+\gamma)g_1^2-\gamma]}. \quad (19)$$

For region d we have

$$f_d(g_1\nu_m)=\frac{N^2}{\pi^2\nu_m}\frac{\partial}{\partial g_1}\left\{\pi^2-\int_{\cos^{-1}[-(2g_1^2-1)]}^{\pi}\times\cos^{-1}\left[\frac{[\gamma-2g_1^2(1+\gamma)+1-\cos\phi_1]}{\gamma\cos\phi_1}\right]d\phi_1\right\} \quad (20)$$

which yields

$$f_d(g\nu_m) = (4g_1N^2/\pi^2\nu_m)[(1+\gamma)/\gamma(2g_1^2-1)]^{\frac{1}{2}}K(\delta_d) \tag{21}$$

with

$$\delta_d = 1/\delta_c. \tag{22}$$

The second branch yields exactly the same relation. Hence the total frequency distribution function becomes

$$f(g\nu_m)[\pi^2\nu_m/8N^2(1+\gamma)^{\frac{1}{2}}] = \begin{cases} \{g/[\gamma(1-2g^2)]^{\frac{1}{2}}\}K(\delta_1) & \text{for } 0<g^2<\gamma/(1+\gamma) \\ \{1/[1-g^2(1+\gamma)]^{\frac{1}{2}}\}K(1/\delta_1) & \text{for } \gamma/(1+\gamma)<g^2<\frac{1}{2} \\ g/\{[1-g^2][(1+\gamma)g^2-\gamma]\}^{\frac{1}{2}}K(\delta_2) & \text{for } \frac{1}{2}<g^2<1/(1+\gamma) \\ \{g/[\gamma(2g^2-1)]^{\frac{1}{2}}\}K(1/\delta_2) & \text{for } 1/(1+\gamma)<g^2<1 \end{cases} \tag{23}$$

with

$$\delta_1^2 = (g^2/\gamma)\{[1-g^2(1+\gamma)]/(1-2g^2)\}$$

and

$$\delta_2^2 = \gamma/(1-g^2)\{(2g^2-1)/[g^2(1+\gamma)-\gamma]\}.$$

Since the elliptic integral $K(k)$ has the properties[7]

$$K(k) = \tfrac{1}{2}\pi(1+\tfrac{1}{8}k^2)$$

for k small

and

$$K(k) = \ln[4/(1-k^2)^{-\frac{1}{2}}]$$

for k near 1, we find from (23) that for low frequencies

$$f(g\nu_m) = (4g/\pi\nu_m)[(1+\gamma)/\gamma]^{\frac{1}{2}} \tag{24}$$

or that the frequency distribution is a linear function of the frequency in agreement with the Debye continuum theory. Also, it is noted that $f(g\nu_m)$ shows logarithmic infinities as g approaches $1/(1+\gamma)$ or $\gamma/(1+\gamma)$ which are also the saddle points of g in wave-vector space. This is in complete agreement with the general theory of Van Hove[8] and Montroll[9] which predicts infinities in the frequency distribution function for all frequencies which correspond to saddle points in wave-vector space.

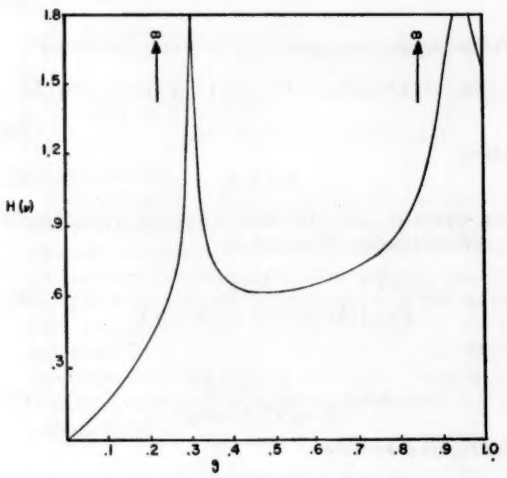

FIG. 3. The frequency distribution function

$$H(\nu) = [\pi^2\nu_m f(g\nu_m)]/N^2 8(11)^{\frac{1}{2}}$$

vs $g = \nu/\nu_m$ as calculated here.

[7] E. T. Whittaker and G. N. Watson, *Modern Analysis* (Cambridge University Press, New York, 1920), p. 522.

III. COMPARISON WITH PREVIOUS CALCULATIONS

The frequency distribution for the two-dimensional lattice studied above has been calculated by numerical (i.e., nonanalytical) methods by Blackman[2] and Montroll[3] for the special case when $\gamma = 0.1$.[10] Thus (23), which is based on the approximation that γ^2 is ignored, can adequately be applied for that case. Letting

$$H(\nu) = \frac{\pi^2\nu_m f(g\nu_m)}{N^2 8(11)^{\frac{1}{2}}}$$

which is proportional to $f(\nu)$, (23) becomes

$$H(\nu) = \begin{cases} [g/(1-2g^2)^{\frac{1}{2}}]K(\delta_1) & \text{for } 0<g<(\frac{1}{11})^{\frac{1}{2}} \\ [1/(10-11g^2)^{\frac{1}{2}}]K(1/\delta_1) & \text{for } (\frac{1}{11})^{\frac{1}{2}}<g<(\frac{1}{2})^{\frac{1}{2}} \\ \{g/[(1-g^2)(11g^2-1)]^{\frac{1}{2}}\}K(\delta_2) & \text{for } (\frac{1}{2})^{\frac{1}{2}}<g<(\frac{10}{11})^{\frac{1}{2}} \\ \{g/[2g^2-1]^{\frac{1}{2}}\}K(1/\delta_2) & \text{for } (\frac{10}{11})^{\frac{1}{2}}<g<1 \end{cases}$$

with

$$\delta_1 = \left\{\frac{g^2(10-11g^2)}{1-2g^2}\right\}^{\frac{1}{2}}$$

and

$$\delta_2 = \left\{\frac{2g^2-1}{(1-g^2)(11g^2-1)}\right\}^{\frac{1}{2}}. \tag{25}$$

Figure 3 shows the behavior of $H(\nu)$ as a function of $g = \nu/\nu_{max}$. Figure 4 shows the results as calculated by

[8] L. Van Hove, Phys. Rev. **89**, 1189 (1953).
[9] E. Montroll, Am. Math. Monthly **61**, 7II, 46 (1954).
[10] In both the works cited in footnotes 2 and 3, Eq. (1) is written in form $\frac{1}{2}\beta'$ etc. Thus the choice $\beta'/\alpha = 1/20$ given there corresponds to $\beta/\alpha = 1/10$ in the notation used here.

Blackman and Montroll where the function

$$\nu_m G(\nu) = \int_{\nu}^{\nu+\Delta\nu} f(\nu)\,d\nu$$

is plotted vs ν/ν_m. In the region where $f(\nu)$ is finite $G(\nu)\sim f(\nu)$ and thus $H(\nu)$, whereas $G(\nu)$ will have finite maxima for the infinities of $f(\nu)$. It will be noted that the frequency distribution function as calculated here agrees very closely with Blackman's numerical work, both as to the position of the maxima and the shape of the curve. Montroll's results based on the moment-trace approximation differ somewhat because of a wide spread of the first maximum of $f(\nu)$. The reason for this discrepancy is not clear. Thus the close agreement between the numerical and analytic scheme for obtaining $f(\nu)$ gives some evidence for the validity of the subdivision of wave-vector space into large regions containing of the order of 10^{20} values of the wave vector. If the approximate positions of the maxima of $f(\nu)$ are known from an analysis of the saddle points of ν in wave-vector space, even a rough scanning of the rest of the spectrum should be adequate. This is especially important for more complicated systems where the numerical scheme is the only method available for the calculation of $f(\nu)$.

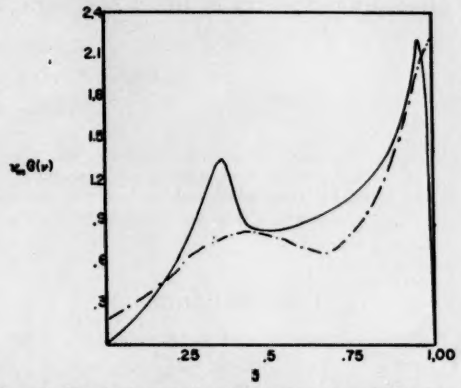

FIG. 4. The frequency distribution function $\nu_m G(\nu)$ (see text for definition) vs $g=\nu/\nu_m$ as calculated by Blackman (——) and by Montroll (-·-·). The vertical scale was adjusted such that the largest maxima coincide for both Montroll's and Blackman's calculations.

Absorption Spectra of Solid Methane, Ammonia, and Ice in the Vacuum Ultraviolet*

K. DRESSLER† AND O. SCHNEPP‡

National Bureau of Standards, Washington 25, D. C.

(Received December 2, 1959)

The vacuum ultraviolet spectra of solid ammonia and ice are found to be shifted to higher frequencies relative to the corresponding vapor spectra by 7000 cm^{-1}. The effects of hydrogen bonding in the ground states of these solids, and the nature of repulsive interactions possible in the excited states are discussed. In methane, which forms a pure van der Waals solid, the spectra of gas and solid are found to be very similar.

I. INTRODUCTION

WATER, ammonia, and methane form a series of hydride molecules whose bonds decrease in polarity in the order in which they are listed here. Parallel with this decrease in bond polarity, their power to form hydrogen bonds decreases, and as a consequence the sublimation energies of the crystals are considerably affected. The sublimation energy of ice is 12.2 kcal/mole, that of ammonia 6.5 kcal/mole, and that of methane 2.2 kcal/mole. Of these totals it has been estimated[1] that hydrogen-bonding interactions account for about 9 kcal/mole in ice and about 4 kcal/mole in ammonia, the balance representing binding of the van der Waals type. Solid methane is a pure van der Waals solid.

We have investigated the absorption spectra of these three substances in the vacuum ultraviolet region in pure solid phases at low temperatures and compared these spectra with those of the vapors. We shall describe our experimental results and discuss the spectra of the three solids briefly in terms of their relationship to the hydrogen-bonding properties of the solids and the nature of the molecular electronic transitions from which they arise.

II. EXPERIMENTAL

The apparatus employed here has been described elsewhere.[2] A massive copper tube was used to admit the vapors into the vacuum chamber of the cryostat in which the cold lithium fluoride window was situated. The tube was kept at room temperature over its entire length to prevent freezing of the material in it. The absorption spectra were observed in transmission through the cold window on which the solid deposits were formed. A conventional hydrogen discharge and a condensed discharge through xenon[3] were used as light sources.

Absorption coefficients were determined from estimates of layer thicknesses and measurements of the intensity ratios I/I_0. Microdensitometer tracings were used, and the exposure times necessary to produce equal plate density, at the wavelength of interest, through layers of varying thicknesses, served as measures of I/I_0. A wide variety of exposure times and film thicknesses (0.01–30 μ in the case of methane and ice) were used. The transmitted intensity at the long-wavelength side of the onset of absorption showed that light scattering had no detectable effect in the layers investigated here. The film thicknesses were estimated by measuring the amount of gas deposited and assuming a reasonable geometry of deposition. The large possible errors in the absolute determination of absorption coefficients (see Table I) are primarily due to the uncertainty in the estimates of film thicknesses. The relative errors within the group of substances investigated are expected to be smaller, since the same assumptions have been made in every case.

Liquid helium and liquid nitrogen served as refrigerants. Temperatures intermediate between 77°K and room temperature were maintained for short periods of time by allowing the Dewar to warm up slowly from lower temperatures. Copper-constantan thermocouples, soldered into a hole in the lithium fluoride window and to the copper frame holding it by means of Wood's metal served for temperature measurements.

The crystal structure of methane is a well-known cubic one.[4] Solid methane was formed in our experiments by deposition of the gas at 4.2°K. Ammonia, when frozen from the liquid phase, also forms a cubic crystal,[5] whereas recently two noncubic structures have been found[6] when the solid was formed from the vapor by rapid deposition on a cold surface below 125°K. The same investigators found that deposition above 125°K, or annealing of the low-temperature deposit at

* This research was performed under the National Bureau of Standards Free Radicals Research Program, supported by the Department of the Army. It was supported in part by the Office of Ordnance Research.

† Guest scientist from the Department of Chemistry, The Catholic University of America, Washington 17, D. C. Present address: Princeton University Observatory, Princeton, New Jersey.

‡ On leave from the Department of Chemistry, Israel Institute of Technology, Haifa, Israel.

[1] L. Pauling, *The Nature of the Chemical Bond* (Cornell University Press, Ithaca, New York, 1939), pp. 281, 284.

[2] O. Schnepp and K. Dressler (unpublished).

[3] Y. Tanaka, J. Opt. Soc. Am. **45**, 710 (1955).

[4] H. H. Mooy, Proc. K. Akad. Wetensch. Amsterdam **34**, 550 (1931).

[5] H. Mark and E. Pohland, Z. Krist. **61**, 532 (1925); Proc. K. Akad. Wetensch. Amsterdam **33**, 447, 814 (1930).

[6] F. A. Mauer and H. F. McCurdie, reported at the Am. Crystallographic Assoc. meeting at Milwaukee, Wisconsin, June, 1958.

or above this temperature, resulted in the known cubic structure. We have deposited ammonia vapor at 125°K, and at 77°K in different experiments, but all spectral observations were made at 77°K. The crystal structures of ice including those obtained by deposition from the vapor on cold surfaces at various temperatures have been the subject of numerous investigations,[7] e.g., deposits formed above 173°K are reported to be purely hexagonal, those formed at 77°K to be amorphous. We have deposited water vapor at 175°K and at 77°K. The former type of deposit was cooled to 77°K prior to the spectral observations, and it is assumed to have hexagonal crystal structure whereas the latter type of deposit is assumed to be amorphous.

The methane used was of research grade (at least 99.0% purity). The gas was passed through a liquid-nitrogen trap before it was deposited, but volatile impurities were not removed by that procedure. A test for oxygen impurity by means of the vacuum ultraviolet absorption spectrum of the methane sample in the gas phase set an upper limit of 0.2% for the possible oxygen content. The spectral investigation of the solid was consequently limited to thin enough films which would not show absorption due to small amounts of impurities. Cylinder ammonia was purified by vacuum distillation, and only the middle fraction was retained. Distilled water was degassed by pumping at room temperature. Both ammonia and water vapor were deposited without passing through a cold trap.

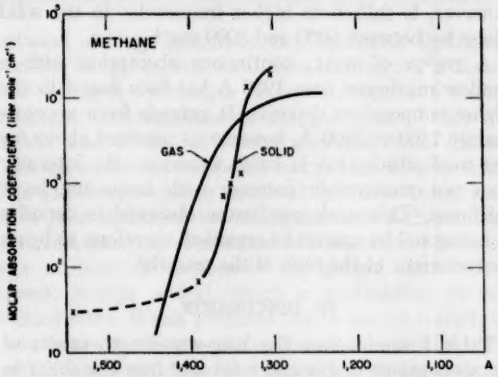

FIG. 1. Molar absorption coefficient of solid methane as a function of wavelength. The dashed part of the curve, which connects experimental points X, was obtained using thick films and may be due to absorption by small amounts of impurities. The gas-phase plot is based on footnote reference 8 and is given for comparison.

III. RESULTS

The absorption spectra of solid methane, ammonia, and ice consist of strong continua which are marked on the long-wavelength side by steeply rising absorption coefficients. We present our results in Figs. 1–3 where we have plotted the absorption coefficients of the investigated solids as a function of wavelength. The corresponding gas-phase plots have been adopted from the work of Watanabe, Zelikoff, and Inn[8] and are given for comparison. The absorption coefficients of the solids have been estimated as described in the preceding section.

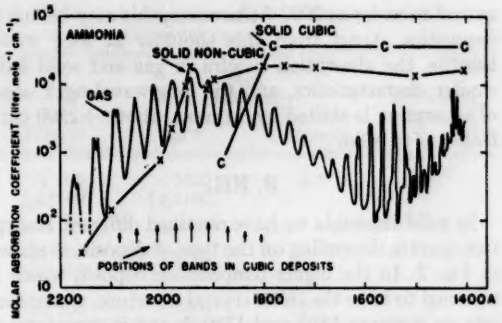

FIG. 2. Molar absorption coefficients of solid ammonia deposited at 175°K (experimental points C) and at 77°K (experimental points X). Arrows indicate the positions of nine broad bands observed in some of the deposits (see text). The gas-phase plot is adopted from footnote reference 8.

A. CH_4

Solid methane is characterized by a strong absorption continuum which rises very steeply between approximately 1390 and 1310 A (see Fig. 1). Towards longer wavelengths, a region of weak absorption appears to

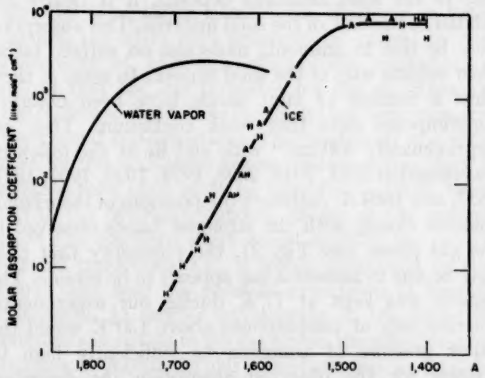

FIG. 3. Molar absorption coefficient of ice. Experimental points H and A represent values obtained using deposits which are assumed, respectively, to have hexagonal crystal structure and to be amorphous. The vapor-phase plot is based on footnote reference 8 and is given for comparison.

[7] P. G. Owston, Advances in Phys. 7, 171 (1958); M. Blackman and N. D. Lisgarten, Advances in Phys. 7, 189 (1958). Earlier references are given in these two papers.

[8] K. Watanabe, M. Zelikoff, and E. C. Y. Inn, Geophysical Research Papers No. 21, Geophysics Research Directorate, Air Force Cambridge Research Center, Cambridge, Massachusetts, 1953. Earlier references are given in this paper. See also K. Watanabe, J. Chem. Phys. 22, 1564 (1954).

extend to as far as 2000 A; however, this may be due to impurities. Apart from this shoulder at long wavelengths, the absorption spectra in gas and solid have similar characteristics, and the long-wavelength onset of absorption is shifted by, at most, about $+2500$ cm^{-1} from gas to solid.

B. NH_3

In solid ammonia we have obtained different absorption spectra depending on the type of deposit, as shown in Fig. 2. In the higher-temperature deposit, which is assumed to have the cubic crystal structure, absorption sets on between 1880 and 1780 A and is very intense and uniform below 1780 A. In the deposit formed at 77°K, the long-wavelength onset of absorption is marked by a very intense and comparatively narrow absorption band at 1940 A, which has a half-intensity width of 20 A. This band is followed to shorter wavelengths by uniformly strong absorption. Experiments using a xenon light source which emits a good continuum in the wavelength region 2100 to 1500 A showed for both types of ammonia deposits that the absorption intensity remains remarkably uniform below about 1800 A. In one experiment the deposit formed at 77°K was subsequently cooled to 4.2°K; no change was observed, however, in the width of the band at 1940 A nor in any other region of the spectrum.

In the higher-temperature deposits a region of weak, continuous absorption has been observed to extend from the long-wavelength onset of strong absorption up to approximately 2100 A. The intensity of this absorption, however, is not increased with growing layer thickness, and although it is believed that it is due to the solid ammonia deposits, it is clearly not related to the bulk of the solid material. This absorption may be due to ammonia molecules on surface rather than volume sites of the solid deposit. In some of these films a number of faint bands have been observed superimposed onto that weak continuum. They are approximately 400 cm^{-1} wide and lie at the following wavelengths: 2083, 2049, 2008, 1974, 1939, 1907, 1871, 1837, and 1804 A. Although the positions of these bands coincide closely with the strongest bands observed in the gas phase (see Fig. 2), the possibility that they may be due to ammonia gas appears to be remote. The deposit was kept at 77°K during our experiments, whereas only at temperatures above 130°K would the vapor pressure of ammonia be sufficiently high to account for the observed absorption. As described above for the weak continuum, the extinction in these bands appears to be unrelated to the layer thickness, and the origin of the bands may be similar to that of the continuum.

Our results are in agreement with an earlier investigation of the absorption spectrum of crystalline ammonia in the near ultraviolet by Prikhotko,[9] who reports that solid films, between 1 and 28 mm thick, are transparent above 2116 A and that they show only weak absorption between that wavelength and 2000 A.

C. H_2O

No difference has been detected between the absorption spectra of the two types of ice formed by deposition of water vapor at 175° and at 77°K. Figure 3 shows the rapid increase of the absorption coefficients of ice between 1700 and 1500 A. Our results for the thickest films agree well with those obtained in an earlier investigation of relatively thick ice layers by Cassel[10] who found the "long-wavelength limit" of absorption near 1670 A in a layer estimated to be 3–4 μ thick. The absorption spectra of vapor and solid have similar shapes, the long-wavelength onset of absorption, however, is shifted to higher frequencies in the solid phase by between 6000 and 8000 cm^{-1}.

A region of weak, continuous absorption with a shallow maximum near 1950 A has been found in the higher-temperature deposits. It extends from approximately 1800 to 2100 A, however as reported above for the weak absorption in cubic ammonia, the intensity does not measurably increase with increasing layer thickness. This weak continuum observed in deposits of hexagonal ice cannot be regarded, therefore, as being characteristic of the bulk of the material.

IV. DISCUSSION

Table I summarizes the long-wavelength onsets of the absorptions in gas and solid and lists the shifts in wave-number units and in kcal per mole.[11] In both water and ammonia the spectra undergo a considerable shift to greater energies in going from gas to solid, and possible reasons for these shifts shall be examined below.

Blue shifts of molecular spectra in solutions have been attributed[12] to hydrogen-bonding effects of the solvent and are indicative of electronic transitions involving nonbonding electrons in the ground state. It is argued that the electronic charge density shifts from the periphery of the molecule toward the interior during a transition from a nonbonding to an antibonding orbital. The ground-state orbital is in such a case strongly perturbed by the hydrogen-bonding solvent molecules and its energy thereby lowered. The excited state orbital is stabilized less or not at all. On the other hand, the effect of hydrogen bonding on transitions from a bonding orbital in the ground state to an antibonding orbital in the excited state is expected to be just the opposite since the charge density now shifts

[9] A. Prikhotko, Acta Physicochim. U.R.S.S. **12**, 559 (1940).

[10] E. J. Cassel, Proc. Roy. Soc. (London) **A153**, 534 (1936).

[11] "Long-wavelength onset of absorption" has been chosen as the wavelength where I/I_0 equals $1/e$ in 0.15 mm atm of gas, or in a layer of solid 0.15 μ thick, corresponding to a molar absorption coefficient of approximately 1500 cm^{-1}.

[12] See for example G. J. Brealey and M. Kasha, J. Am. Chem. Soc. **77**, 4462 (1955), and footnote reference 13.

[13] G. C. Pimentel, J. Am. Chem. Soc. **79**, 3323 (1957).

TABLE I. Summary of long-wavelength onsets of absorption in the gas (in 0.15 mm atm) and the solid (in a film approximately 0.15 μ thick). For ammonia the data are listed for cubic and for noncubic deposits.

Substance	Gas		Solid		Shift (Solid-gas)		H-Bonding energy
	λ(A)	$\tilde{\nu}$(cm^{-1})	λ(A)	$\tilde{\nu}$(cm^{-1})	cm^{-1}	kcal/mole	kcal/mole
CH_4	1380	72 500	1350 (±20)	74 100 (±1100)	+1600 (±1100)	4.5	0
NH_3	2130	46 900	1860 (±40)	53 800 (±1200)	+6900 (±1200)	20	3.9
			1990 (±40)	50 300 (±1000)	+3400 (±1000)	10	?
H_2O	1760	56 800	1570 (±30)	63 700 (±1200)	+6900 (±1200)	20	9

outward during excitation causing more hydrogen bonding in the excited state than in the ground state.

The longest-wavelength absorption spectra of water, ammonia, and methane in the gas phase[8,14] are all diffuse and consist of strong continua, with diffuse band structure superimposed in the case of ammonia. The electronic orbitals involved in these transitions have been discussed by Mulliken[15] and Walsh.[16] The ammonia bands are attributed to a transition of a lone-pair nonbonding electron in the ground state to an atomic 3*s*-type orbital, which is nonbonding, in the excited state. Walsh proposes that a second transition contributes to the gas absorption, and he ascribes the continuum of ammonia as well as that of water vapor to a transition of a lone-pair nonbonding electron in the ground state to an antibonding orbital in the excited state, which is repulsive. On the basis of this interpretation the considerations outlined in the preceding paragraph are consistent with the direction of the observed spectral shifts to higher energies in solid ammonia and ice. The magnitude of a shift caused by hydrogen bonding is ordinarily expected to be at most equal to the hydrogen bonding energy of the ground state,[17] or 3.9 kcal/mole for ammonia and 9 kcal/mole for water.[1] The observed shifts are considerably larger than these amounts which can be attributed to the lowering of the ground-state energy in the solid.

An additional contribution to spectral shifts which are caused by the effects of hydrogen bonding is expected owing to the Franck-Condon principle, as has been pointed out by Pimentel.[13] Electronic transitions which cause a decrease in the hydrogen bonding energy will be accompanied by a corresponding increase in equilibrium intermolecular distances, and as a result the strongest transitions will involve the excitation of lattice vibrations.

In the case of water and ammonia it is possible that still another effect contributes to the repulsive intermolecular interactions in the electronically excited states. The H–N–H angle of NH_3 and the O–H distance of H_2O are both reported to increase considerably accompanying the electronic transitions under consideration here. This change in geometry could give rise to a situation in which the excited-state molecule in its equilibrium configuration cannot easily be accommodated in the ground-state lattice site. The hydrogen atoms in their new positions in excited H_2O might approach their nearest lattice neighbors closely enough to give rise to repulsive interactions. However, in both molecules, the effect may primarily be caused by the displacement of hydrogen atoms into excited-state positions that are less favorable for the maintenance of the hydrogen-bond links in which they were engaged in the ground state positions. The magnitude of a shift caused by this additional loss of binding energy during excitation may once more be expected to be at most equal to the hydrogen bonding energy of the ground state.[18] The described effect would apply to the purely electronic transitions, i.e., it would contribute to the spectral shift near the onset of absorption at longest wavelengths. At shorter wavelengths, in the region of maximum absorption in the gas phase, the simultaneous excitation of intramolecular vibrations has to be con-

[14] S. W. Leifson, Astrophys. J. **63**, 73 (1926).
[15] R. S. Mulliken, J. Chem. Phys. **3**, 506, 517 (1935).
[16] A. D. Walsh, J. Chem. Soc. **1953**, 2260, 2296. See also W. C. Price, J. P. Teegan, and A. D. Walsh, Proc. Roy. Soc. (London) **A201**, 600 (1950).
[17] If each molecule contributes two nonbonding electrons to the formation of hydrogen bonds, the loss of one of them due to excitation may actually produce a shift corresponding to only one-half of the hydrogen-bonding energy of the ground state.
[18] If the hydrogen-bonding energy is visualized as being localized in individual H-bond links, each such link engages two molecules, and the total number of H bonds in which one molecule participates represents twice the amount of H-bonding energy per molecule, e.g., in hexagonal ice the ground-state molecule is engaged in four H-bond links, representing a total energy of about 18 kcal/mole. One-half of this amount is affected by the inward shift of the negative charge density associated with the excitation of one of the nonbonding electrons. The other half is affected by the displacement of the positive charge density associated with the two hydrogen nuclei.

sidered. This will primarily change the positive charge distribution associated with the hydrogen nuclei and thereby modify the effect due to the change of molecular geometry. It should also be noted that the additional loss of binding energy attributed here to the change of geometry would be accompanied by a further increase of the shift due to the intermolecular Franck-Condon effect.[13]

In solid methane the observed spectral shift is small. This is consistent with the expected absence of strong intermolecular interactions of the type described above. The shape of the molecule is effectively spherical, and the observed spectrum has been ascribed[15] to a transition of a bonding electron of the ground-state configuration to an atomic 3*s*-type orbital in the excited state. It is doubtful whether the shift listed in Table I is real, since the estimates of film thicknesses introduce a large possible error. Depending on the steepness of the potential surface associated with the repulsive excited state, a small shift to higher energy may be attributed to the effect of the intramolecular Franck-Condon principle in combination with thermal depopulation of low-lying vibrational levels in the ground state. It should be noted that we have compared the absorption coefficients of the solid at 4.2° K with those of the gas at 300°K, since no data on the gas absorption at low temperatures seem to be available.

No explanation can be offered for the absorption band observed in the noncubic ammonia deposits at 1940 A. The band and the adjacent continuum may represent the same spectral transition as the one observed in the cubic deposits at shorter wavelengths. Alternately it might be due to a symmetry-forbidden transition which becomes allowed in crystals of lower than cubic symmetry. The weak bands and continua which were observed in some of the ammonia and ice deposits (see Sec. III) and the conditions for their appearance need to be further confirmed and investigated.

V. ACKNOWLEDGMENTS

We gratefully acknowledge illuminating discussions with Professor V. Griffing. We wish to thank Professor G. C. Pimentel for valuable comments and Dr. H. P. Broida, who made this work possible, for his guidance and encouragement.

THE JOURNAL OF CHEMICAL PHYSICS VOLUME 33, NUMBER 1 JULY, 1960

Valence Structure of the Higher Borides

WILLIAM N. LIPSCOMB, *Department of Chemistry, Harvard University, Cambridge 38, Massachusetts*
AND
DOYLE BRITTON, *Department of Chemistry, University of Minnesota, Minneapolis 14, Minnesota*

(Received February 15, 1960)

An attempt is made to systematize the valence orbital structures of the boron frameworks in MB_2, MB_4, MB_6, MB_{12}, $B_{12}C_3$, and elementary boron.

INTRODUCTION

ATTEMPTS to bridge the gaps between localized chemical bonds and delocalized molecular orbitals with the use of semilocalized multicentered orbitals have effected an increase in the understanding of boron hydrides.[1] In the more open polyhedral frameworks, three-center bonds have been helpful, but in the closed or nearly closed molecular or ionic polyhedra, molecular orbitals have provided a simpler interpretative approach. It has been hoped since the early stages of these studies that an approach to the valence theory of intermetallic compounds might be suggested. Here, one such approach is explored in applications to the structures of the higher borides, which contain sheets of boron atoms or more complex three-dimensional arrays.

Specifically the approach may be outlined as follows:

(a) The boron framework is isolated into polyhedra which are connected to each other by localized bonds, occasionally with the use of multicentered orbitals.

(b) The molecular orbitals of the individual polyhedra are investigated.

(c) Electrons are transferred from the more electropositive element to the boron framework until the bonding orbitals are filled.

(d) Excess valence electrons on the metal atoms are regarded as metallic in character and should lead to metallic optical and electric properties.

It is difficult to defend this procedure as a new one or, even less, as a general one applicable to all intermetallic compounds. In the borides themselves, this procedure was inferred in the group theoretical arguments[2] relating to the B_6 octahedral arrangements, and was studied in detail[3] independently in CaB_6. A somewhat similar discussion[4] has been given previously for $B_{12}C_3$, in which vacant p orbitals of the central C atom of the linear C_3 group are required to conjugate with the remainder of the structure. Also the simpler rhombohedral form of boron has an understandable valence structure,[5] but seems widely at variance with the apparent[4] valence structure of tetragonal boron.

The metalliclike properties of some of these compounds, the range of compositions, and their formation often from metals of different groups of the periodic table suggest that, in general, completely closed valence shells are not to be expected except for certain idealized compositions. Hence, we shall attempt to reduce the discrepancy between electron-pair numbers and orbital numbers insofar as possible, or chemically reasonable. In addition we shall try to indicate which structures correspond to filled orbitals, so that those structures which do not will be suggested as having an excess or deficiency of electrons, with corresponding electrical properties. Finally we hope to unify the discussion among the different boride structures insofar as this is possible at present. We realize that, at best, our discussion of the different structures is a bit uneven, but feel that an attempt at a unified presentation is worthwhile.

MB_2, MB_6, AND MB_4

The compound most nearly approaching a closed-shell structure of the known MB_2 compounds is probably MgB_2. Similarly, CaB_6 is the closed-shell prototype of the MB_6 structures. The similarity of the valence orbitals of the intermediate structure[6] MB_4 to these two leads us to suggest, as we shall indicate below, that the closed-shell form is the MgB_4 structure in spite of the present limitations[7] of this phase to the rare earths,[8] Th, and U. When atoms with more than two electrons are present in the MB_2 and MB_6 structures the electrical and optical properties are much more marked.[9]

If M forms a $2+$ ion the B_2^{2-} framework in MB_2 is completely isoelectronic with that of graphite, and partial transfer of these electrons back to M^{2+} would

[1] W. N. Lipscomb, Advances in Inorganic and Radio Chemistry (Academic Press, New York, 1959), Vol. 1, p. 117.
[2] W. H. Eberhardt, B. L. Crawford, Jr., and W. N. Lipscomb, J. Chem. Phys. **22**, 985 (1954).
[3] H. C. Longuet-Higgins and M. de V. Roberts, Proc. Roy. Soc. (London) **A224**, 336 (1954).
[4] H. C. Longuet-Higgins and M. de V. Roberts, Proc. Roy. Soc. (London) **A230**, 110 (1955).
[5] L. V. McCarty, J. S. Kasper, F. H. Horn, B. F. Decker, and A. E. Newkirk, J. Am. Chem. Soc. **80**, 2592 (1958); also B. F. Decker and J. S. Kasper, Acta Cryst. **12**, 503 (1959).
[6] A. Zalkin and D. H. Templeton, Acta Cryst. **6**, 269 (1953).
[7] However, see M. E. Jones and R. E. Marsh, J. Am. Chem. Soc. **76**, 1434 (1954); and J. Russell, R. Hirst, F. A. Kanda, and A. J. King, Acta Cryst. **6**, 870 (1953) for evidence concerning MgB_4.
[8] B. Post, D. Moscowitz, and F. W. Glaser, J. Am. Chem. Soc. **78**, 1800 (1956).
[9] M. v. Stackelberg and F. Neumann, Z. physik. Chem. **B19**, 314 (1932).

complete the description. It is relevant to $M^{2+}B_6^{2-}$ that there have been two independent discussions[2,3] of the internal orbitals of a B_6^{2-} octahedral arrangement with single bonds external to the octahedron. The seven internal bonding molecular orbitals of B_6^{2-} require seven pairs, and the external six orbitals prepared for bonding with similar orbitals from other octahedra require one electron in each, thus accounting for the 20 available electrons per B_6^{2-}.

In the MB_4 structure there are two octahedral B_6 groups and four single B atoms in trigonal sp^2 bonding to other boron atoms. Hence we take M_4B_{16} as our unit for discussion. Each B_6 octahedron requires 14 electrons for internal bonds and six more as its share of electron pairs in the six external bonds, thus requiring a total of 20 electrons per octahedron or a total of 40 electrons for two octahedra. The four additional B atoms are bonded in pairs, as in ethylene, and would require four per B_2 group to bind the pair and four more per B_2 group as its share of the electron pairs in the external orbitals for bonding to octahedra, or a total of 16 for all four B atoms of this kind. Thus a total of 56 electrons is required per unit cell, a total which would be provided nicely by the 16 B atoms and the $4M^{2+}$ ions.

UB_{12} AND ZrB_{12}

The geometrical coordination of boron atoms around a central Zr has been discussed previously.[10,11] However, we wish to emphasize that this structure can be regarded as an array of B_{12} groups and metal atoms in the NaCl arrangement. The B_{12} polyhedron is of symmetry O_h and can be called a cube-octahedron [Fig. 1(a)]. Whereas earlier studies[2-4] had based boron hydride molecules or ions on the icosahedron, octahedron, or tetrahedron, or on their fragments, this polyhedron as well as the recently discovered B_8 arrangement[12] in B_8Cl_8 and the B_{10} arrangement[13] in $B_{10}H_{10}^{2-}$ are relatively new in boron chemistry.[13a] Each of the B atoms in the B_{12} group is bonded to a B atom of another B_{12} group, and the Zr atoms lie in the interstices outside of the B_{12} groups.

If one considers the external bonds here as normal single covalent bonds the question of the bonding arrangement in the group arises. A simple LCAO molecular-orbital approach gives a reasonable answer to this question. A convenient choice for the atomic orbitals is the unhybridized set of an s and three p orbitals with the p_x orbital on each atom tangential to the sphere circumscribing the polyhedron and pointing toward the triangular faces, the p_y orbital also tangential, pointing toward the center of the square faces, and the p_z orbital radially directed [Fig. 1(b)]. A consideration of the character table for the point group O_h to which this polyhedron belongs leads to the following representations for the molecular orbitals:

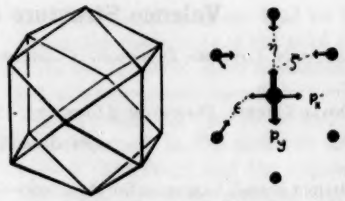

(a) (b)

FIG. 1. (a) The B_{12} polyhedron. (b) Arrangement of the atomic orbitals and the important interactions.

	s	p_x	p_y	p_z
A_{1g}	x			x
A_{1u}				
A_{2g}			x	
A_{2u}		x		
E_g	x		x	x
E_u		x		
F_{1g}		x	x	
F_{1u}	x	x	x	x
F_{2g}	x	x		x
F_{2u}	x		x	x.

The s and p_z orbitals can be hybridized to form one set of orbitals pointing primarily outward, which can be used to form the external bonds, and which will henceforth be ignored here, and one set pointing primarily inward. There are four different interactions possible between sp orbitals on different atoms. Call the resonance integral for the interaction between nearest neighbors α, second-nearest neighbors β, third-nearest neighbors γ, and fourth-nearest neighbors δ. Upon solving the secular determinant the following energy levels are found:

A_{1g}:	$H_0+4\alpha+2\beta+4\gamma+\delta$	bonding
E_g:	$H_0-2\alpha+2\beta-2\gamma+\delta$	antibonding
F_{1u}:	$H_0+2\alpha \quad -2\gamma-\delta$	bonding
F_{2g}:	$H_0 \quad -2\beta \quad +\delta$	antibonding
F_{2u}:	$H_0-2\alpha \quad +2\gamma-\delta$	antibonding.

In a similar fashion, considering only the p_z orbitals with the resonance integral ϵ between nearest neighbors and ignoring all others, since they are very small, one finds

A_{2u}:	$H_0+4\epsilon$	bonding
E_u:	$H_0-2\epsilon$	antibonding
F_{1g}:	$H_0-2\epsilon$	antibonding
F_{1u}:	H_0	nonbonding
F_{2g}:	$H_0+2\epsilon$	bonding.

[10] F. Bertaut and P. Blum, Compt. rend. **229**, 666 (1949).
[11] B. Post and F. W. Glaser, J. Metals 631 (1952).
[12] R. A. Jacobson and W. N. Lipscomb, J. Chem. Phys. **31**, 605 (1959).
[13] W. N. Lipscomb, A. R. Pitochelli, and M. F. Hawthorne, J. Am. Chem. Soc. **81**, 5833 (1959).
[13a] Asymmetric units of three different unit cells of $M_2B_{10}H_{10}$ salts contain $2B_{10}H_{10}^{-2}$ (B. R. Penfold and W. N. Lipscomb, study in progress); conceivably, another possibility is $B_{20}H_{20}^{-4}$, perhaps formed in D_{2d} symmetry from $2B_{10}H_{10}^{-2}$, decaborane-like ions held together by 4 three-center bonds.

Finally, considering the p_y orbitals with resonance integrals ζ between nearest neighbors, and η between second-nearest neighbors, and ignoring all others one finds:

A_{2g}:	$H_0-4\zeta+2\eta$	antibonding
E_g:	$H_0+2\zeta+2\eta$	bonding
F_{1g}:	$H_0 \quad -2\eta$	antibonding
F_{1u}:	$H_0+2\zeta$	bonding
F_{2u}:	$H_0-2\zeta$	antibonding.

It can be seen that the bonding orbitals will accomodate 13 pairs of electrons. Since the 12 borons have 36 electrons of which 12 are needed for the external bonds one more pair must be supplied by the metal atom. Therefore the group should be written as B_{12}^{2-} if all of the bonding orbitals are filled with electrons. If the order of the magnitudes of the resonance integrals is estimated as $\epsilon>\zeta>\eta>\alpha>\beta>\gamma>\delta$ then the decreasing order of the bonding orbitals is

(p_z)	F_{1u}:	H_0	nonbonding
(sp)	F_{1u}:	$H_0+2\alpha-2\gamma$	
(p_y)	F_{1u}:	$H_0+2\zeta$	
(p_x)	F_{2g}:	$H_0+2\epsilon$	
(p_y)	E_g:	$H_0+2\zeta+2\eta$	
(p_z)	A_{2u}:	$H_0+4\epsilon$	
(sp)	A_{1g}:	$H_0+4\alpha+2\beta+4\gamma+\delta$	lowest state.

The highest bonding orbital is a triplet level as is the next higher orbital which is nonbonding; therefore, it is exceedingly likely that the doubly negative ion is formed within this three-dimensional framework.

There are several sets of orbitals with the same symmetry. Hence a more thorough treatment should consider the shifting of their relative energies by the possible interactions between levels. There are two reasons why this refinement seems unnecessary in this approximation. The first is that it is apparent from inspection of a model of the polyhedron that all the resonance integrals other than the ones listed must be small, so that their inclusion would not shift the energy levels significantly. The second is that the levels in which the shifts would matter the most are the three F_{1u} levels. To a first approximation the interactions of these levels would leave the middle level unchanged, and still bonding, and the highest orbital would be changed from nonbonding to slightly antibonding. The conclusions reached above would therefore not be altered.

It is of interest to note that a choice of atomic orbitals of p_y as above and three sp^2, one directed externally, would give the same result if the sp^2 orbitals were viewed as forming 8 localized three-center bonds in the triangular faces and the p_y's were treated as above.

The relation, shown in Fig. 2, of the geometrical structures of the cube-octahedron to the more compact icosahedron, suggests two interesting aspects of these boron arrangements. Although both B_{12} arrangements would *a priori* seem to be good candidates for $B_{12}H_{12}^{2-}$ ions, it seems likely that the cube-octahedron would

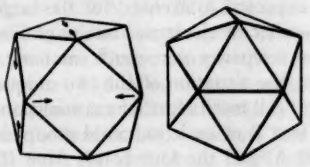

(a) (b)

FIG. 2. (a) The small distortions of the B_{12} cube-octahedron which are required to convert it to the icosahedron (b) are shown by the small arrows.

probably be unstable with respect to the small displacements that would lead it to adopt the icosahedral arrangement. On the other hand, the cube-octahedron arrangement is quite probably stabilized by the interactions of the highest filled oritals of the B_{12} groups with the d^2sp^3 orbitals of the Zr atom. The arrangement would thus lead to a closed shell for $M^{2+}B_{12}^{2-}$, and to a partial transfer of electrons back to M^{2+} from the boron orbitals. It might then be expected that ZrB_{12} has two electrons per ZrB_{12} in excess of the closed shells. The physical properties[14] of ZrB_{12} are consistent with this assumption of excess electrons in ZrB_{12}.

BORON

The simpler[5] rhombohedral form of boron has boron-boron bonds among atoms of icosahedra only. Half of the boron orbitals external to the icosahedra are involved in two-center bonds, and half are in three-center bonds, all between different icosahedra. Thus each B_{12} is "prepared" for bonding by placement of one electron in each orbital to be used in a two-center bond, and by placement of one electron per 1.5 boron orbitals of the borons involved in the three-center bonds. Ten electrons are then required from each B_{12} group for the external bonds to other icosahedra, thus leaving 26 electrons for the intraicosahedral bonds of each B_{12}. These 26 electrons just fill the bonding intraicosahedral molecular orbitals. This valence structure was recognized by Decker and Kasper.[5]

The complex rhombohedral form of boron[15] is, at present, an unsolved structure.

Tetragonal boron[16] presents a difficult interpretive problem[4] in the framework of these assumptions. There are four B_{12} icosahedra, and two additional boron atoms (B_t) per unit cell, furnishing a total of 150 electrons. Preparation of each B_t to form four bonds requires eight electrons for $2B_t$, preparation of the B_{12} for external bonds requires 48 electrons for B_{12}, and assignment of 26 electrons inside each B_{12} requires 104 electrons, thus requiring a total of 160 electrons per unit cell, 10 more than the number available. Hoard *et al.*, found strong indications of approximately $\frac{3}{4}$ additional boron-atom impurity per unit cell. This

[14] G. V. Sampsonov and L. Y. Markovskii, Uspek. Khim. **25**, 190 (1956).

[15] D. E. Sands and J. L. Hoard, J. Am. Chem. Soc. **79**, 5582 (1957).

[16] J. L. Hoard, S. Geller, and R. E. Hughes, J. Am. Chem. Soc. **73**, 1892 (1951); J. L. Hoard, R. E. Hughes, and D. E. Sands, J. Am. Chem. Soc. **80**, 4507 (1958).

excess can hardly be expected to account for the large discrepancy in the number of electrons, but might be involved if the actual discrepancy were much smaller.

In tetragonal boron the situation of the two unique boron atoms B_t per unit cell merits further examination. The B_t—B distance, to a B of an icosahedral group, is very short, about 1.60 A, and the four bonds from B_t are greatly flattened from a regular tetrahedral configuration such that the B—B_t—B angle is 135°. Let B_t be initially unhybridized, and choose p_z along the c axis, and p_x and p_y in the bc plane but oriented at 45° with respect to b and c, respectively, so that p_x and p_y almost point toward the closest boron atoms of the four icosahedra bonded to B_t. At this short distance the overlap integral of p_x on B_t with a parallel p orbital on the nearest B of the B_{12} group is 0.30, greater than that for π–π overlap in C_2H_4. Even the p_z orbital of the B of B_{12}, which is perpendicular to the B—B_t bond and therefore 23.5° away from the direction of p_z of B_t, has an overlap integral very nearly equal to that for π–π in C_2H_4. Therefore, these p orbitals of B_t must interact strongly with the p orbitals on closest atoms of the four B_{12} groups, and therefore with some of the quadruply degenerate U_u levels[4] of the B_{12} groups which are the highest filled levels if we assign 26 electrons to each B_{12} group. A simplified description of the x, y interactions is obtained by replacing the icosahedral U_u levels by a single p orbital in the xy plane (Fig. 3).

We now approximate a bonding scheme for tetragonal boron. Bonds to the B_t at the center of the unit cell can be a five-center bond, involving the four sp bonds interacting with the $2s$ orbital, and two three-center bonds, along x involving an sp, p_x on B_t, and sp, and, similarly, along y involving an sp, p_y, and sp. The five-center bond does not interact with the highest filled levels inside the icosahedra, but the two three-center bonds interact so strongly that we propose that the electron pair of the appropriate icosahedral U_u level fills each corresponding three-center bond: the interaction of these three-center bonds with icosahedral levels result in an infinite string of interactions along x or along y, but parallel strings do not interact, nor do perpendicular strings, and the highest filled level could be considered as corresponding to bonding in pairs of these two localized molecular orbitals. At least this much bonding is required in order to ensure that the resulting bonding orbitals are at least as stable as the other U_u icosahedral levels themselves. Thus two of the 26 electrons of an icosahedral level also fill a three-center bond about B_t in these xy interactions. Before we discuss the slightly weaker π_z interactions of B_t with the icosahedra let us recount the bonding electrons per unit cell:

$4B_{12}$	internal bonding	104
$4B_{12}$	external bonding to other B_{12}	40
$2B_t$	five-center bonds	4
		148.

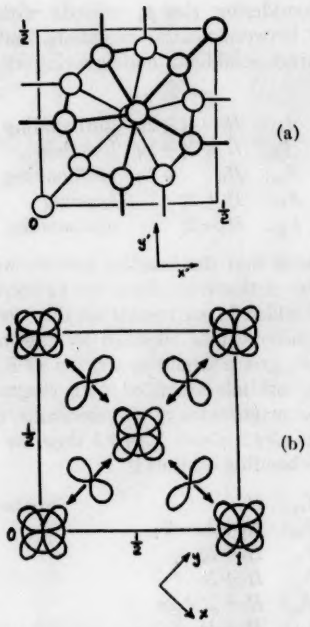

FIG. 3. (a) One quarter of the unit cell of tetragonal boron. (b) Full unit cell, in which B_{12} has been replaced by a single π orbital with two sp bonds pointing outward represented by arrows. The π_z orbital of the B_t at the origin and center are omitted, but π_x and π_y and the bonding $2s$ orbitals are shown.

Of the 104 electrons in internal bonds, 96 are in bonds between B's inside icosahedra and eight occupy the levels which interact strongly with B_t. We are left, at this stage, with an excess of two electrons. If the interactions of a different U_u level with p_z of B_t were just as strong we could require bonding of a similar type between a p_z of B in B_{12} to p_z of B_t, but only along one direction x or y, because there are only half as many p_z's on B_t as there are icosahedra. On the other hand these interactions are weaker, though still comparable with the usual π–π interactions in double bonds, than those in the x, y directions, and it may well be that these remaining two electrons are indeed required to help bond, on the average, the approximately $\frac{3}{4}$ B impurity, probably along p_z of somewhat less than half of the B_t's. These excess electrons added to those of the impurity atom would give it a total of about six electrons, thus requiring it to share two from the molecular orbitals, in addition to those required to bond more directly to B_t along the z direction. It would thus be most informative to examine experimentally the ranges of permissible impurities of both B and C in this tetragonal phase, before a precise electron count is claimed for this structure. Nevertheless, reduction of the apparent discrepancy to a very small number of electrons per unit cell does follow from this examination of the very strong interactions of the two unique boron atoms with the four icosahedra in the unit cell of tetragonal boron.

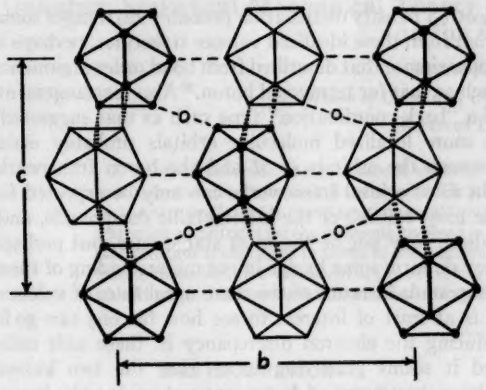

FIG. 4. A conceivable structure for boron, related as hexagonal closest packing is related to simple cubic packing of icosahedra in the known simpler rhombohedral modification. The space group is D_{2h}^{17}–*Cmcm* with $a=4.7$ A, $b=9.3$ A, and $c=7.8$ A. The five heavier-lined icosahedra are at $a=0$, and the four lighter ones are centered on the plane $a=\frac{1}{2}$. Half of the boron atoms of each icosahedron are involved in three-center bonds which lie very nearly in the c glide planes at $b=\frac{1}{4}$ and $\frac{3}{4}$ relative to the centers of symmetry indicated by circles. Three-center bonds are indicated by dotted lines, and single bonds by dashed lines.

$B_{12}C_3$

Little can be added to the earlier discussion[4] of B_{12} icosahedra and linear C_3 chains in $B_{12}C_3$.[17] If 26 electrons are required inside each icosahedron, 12 electrons for the 12 outward pointing boron orbitals, and six for the six orbitals pointing away from each C_3 group, only four electrons remain for bonding the central C atom to the outer two of each C_3 group. Single σ bonds along the C—C—C axis would use up these, thus leaving the π orbitals of the central C vacant for conjugation with the bonds from C to B. At least we may add that the eight π electrons of the $B_3{\equiv}C{-}C{-}C{\equiv}B_3$ unit can be formed into reasonable molecular orbitals which are doubly degenerate and increasing in energy, and, since they are based upon only one hybrid orbital from each B, they can be made orthogonal to the remaining orbitals of the structure. It may be that these orbitals are filled by varying amounts in different samples, since there is a rather large range[14,16,18] from 4 to 26 atom % of C in the structure.

AlB_{12}, AlB_{10}, AND B

A critique of the aluminum boride phases has recently been published[19] along with the identification of a new compound AlB_{10}. The general problems presented by these phases are rather formidable. It is easy to formulate a three-dimensional structure for α-AlB_{12} ($a=10.16$ A, $c=14.28$ A, D_4^4–$P4_12_12$) based upon 16 AlB_{12} in a unit cell which is a superlattice of the cubic UB_{12} or ZrB_{12} structure. Unfortunately the density of the crystal requires 14.4 AlB_{12} in the unit cell, and hence a defect structure is plausible. Similarly, it is easy to formulate an orthorhombic structure for AlB_{10} ($a=8.88$ A, $b=9.10$ A, $c=5.69$ A, C_{2v}^{12}–*Bb2m*, C_{2v}^{16}–*Bbm2* or D_{2h}^{17}-*Bbmm*) based upon four AlB_{10} in C_{2v}^{16}-*Bbm2*. Unfortunately the density of the crystal requires 5.20 AlB_{10} in the unit cell, and, although an excess structure could occur, it is surely not possible (except statistically) to have six Al in the unit cell. Both of these structures are based upon the principles outlined above, that boron polyhedra are joined to other boron polyhedra or atoms, and that the Al occur in the vacancies.

A survey of these problems, and of the relations between the other aluminum borides and boron suggests that a principle of boron chemistry different from presently known principles may occur here. Kohn *et al.*[19] suggest the identity of the unit cells of monoclinic[20] AlB_{12} ($a=8.50$ A, $b=10.98$ A, $c=9.40$ A, $\beta=110°54'$) and rhombohedral elemental boron[15] ($a=10.12$ A, $\alpha=65°28'$), and Parthé and Norton[21] had earlier made "monoclinic AlB_{12}" from 99% pure B. Similar close relations may be noted here between the unit cells of α-AlB_{12} ($a=10.16$ A, $c=14.28$ A) and a new form[22] of boron ($a=10.12$ A, $c=14.14$ A), and also between β-AlB_{12}[23] ($a/\sqrt{2}=8.88$ A, $c/2=5.09$ A) and tetragonal boron ($a=8.73$ A, $c=5.03$ A).

A simple hypothesis that correlates all of these problems is that Al substitutes for B in these structure types. Whether it does so at random or in certain preferred positions is not clear in each instance, but the space group indications are rather in favor of preferred positions if, indeed, there is any merit in these correlations. This hypothesis, moreover, provides a reasonable basis for understanding the "anomalous" densities of AlB_{12} and AlB_{10}. In AlB_{12} the 14.4 formula weights per unit cell corresponds to 187 atoms only a few percent less than the 192 atoms which would be required for 16 $(B, Al)_{12}$ groups, or eight $(B, Al)_{10}$ plus eight $(B, Al)_2$ groups, an assumption which would nicely account for the cleavage on (201). In AlB_{10} the almost unreasonable number of 5.2 formula weights in space groups requiring multiples of four corresponds to 57 atoms, within a few percent of 56, which could arise from four $(B, Al)_{14}$ groups, or four $(B, Al)_{12}$ plus four $(B, Al)_2$, or four $(B, Al)_{10}$ plus eight $(B, Al)_2$, etc. The partial or complete ordering of Al in these structures would make them similar to, but not identical to, the corresponding boron phases, and would stabilize the valence structures by removal of the

[17] G. S. Zhdanov and N. G. Sevastyanov, Compt, rend. acad. sci. U.R.S.S. **32**, 432 (1941); H. K. Clark and J. L. Hoard, J. Am. Chem. Soc. **65**, 2115 (1943).

[18] A. H. Silver and P. J. Bray, Bull. Am. Phys. Soc. Ser. II, **2**, 387 (1957).

[19] J. A. Kohn, G. Katz, and A. A. Giardini, Z. Krist. **111**, 53 (1958–59).

[20] F. Halla and R. Weil, Z. Krist. **101**, 435 (1939).

[21] E. Parthé and J. T. Norton, Z. Krist. **110**, 167 (1958).

[22] C. P. Talley, B. Post, and S. LaPlaca, Conference on Boron, U. S. Army Signal Research and Development Laboratory, Fort Monmouth, New Jersey, September 18–19, 1959.

[23] St. v. Náray-Szabó, Z. Krist. **94**, 367 (1936).

degeneracy of the valence levels of the icosahedra or other polyhedra.

The covalent radius of B is[24] 0.88 A, or a bit smaller, and that of Al is 1.26 A. An Al—Al distance would probably greatly distort the structures, but the Al—B distance of 2.0 A is at least within the range of B—B distances found in boron hydrides and borides. Hence, limited substitution of B by Al would not be unreasonable from the point of view of interatomic distances. The apparent order introduced into the present controversies over the existence of higher Al, B phases, their relations to the boron structures, and the understanding of the unit cell and density measurements would seem to justify an approach to structure determinations based upon the hypothesis of limited partial substitution of Al for B, and may suggest directions in which to look for new types of phases in the Al, B system.

Finally, the simpler rhombohedral form[5] of boron corresponds to a cubic close packing of icosahedra, and hence it is a very natural suggestion that a corresponding structure may exist based upon hexagonal close packing. Such a structure, suggested in Fig. 4, has not yet been discovered. Just as the rhombohedral form has lower than cubic symmetry, this suggested form has lower than hexagonal symmetry because the icosahedron is less symmetric than a sphere. This structure may be one of the unidentified phases noted recently by Hoard and Newkirk.[25] The bond angle distortions, shown best by this particular projection, are quite comparable with those in simple rhombohedral boron.

DISCUSSION

Two modifications of the electron density undoubtedly occur in these idealized valence structures, but we feel that such changes would not modify the extent to which the orbitals are filled. First the final electron density distribution probably rearranges somewhat from these idealized valence structures, perhaps to approximate that described from bond order arguments, such as that for tetragonal boron.[26] Also rearrangements of a "back coordination" type such as that suggested[27] in more localized molecular orbitals probably occur between the orbitals of M and the boron framework. The filled orbital frameworks can only be expected for the most saltlike of the intermetallic compounds, and, indeed, may not be the most stable ones, but perhaps they do form some bridge in our understanding of these compounds in terms of the more usual rules of valence. It is at least of interest to see how far one can go in reducing the electron discrepancy in these unit cells, and it seems gratifying to us that the two known valence structures of boron are not as greatly inconsistent as was thought previously.

A further study is suggested of polyhedral approaches to valence structures, with the addition of topological rules somewhat like those formulated[28] for the boron hydrides, but generalized to other types of semilocalized molecular orbitals. Finally, the extension to structures like those of the lower borides[29] requires a much more detailed examination of the $M-M$ interactions, and the extension to other classes of intermetallic compounds may involve placement of atoms inside polyhedra with due regard for orbital symmetries.

ACKNOWLEDGMENTS

We wish to acknowledge support of this research by the Office of Naval Research and the Office of Ordnance Research. It is a pleasure to acknowledge conversations on the Al, B system with K. Eriks and N. Yannoni, who also had thought of the substitution of Al for B in the AlB_{12} structure.

[24] L. Pauling, *Nature of the Chemical Bond* (Cornell University Press, Ithaca, New York, 1940), 2nd ed., p. 179.
[25] J. L. Hoard and A. E. Newkirk, J. Am. Chem. Soc. **82**, 70 (1960).
[26] L. Pauling and B. Kamb, Z. Krist. **112**, 472 (1959).
[27] H. C. Longuet-Higgins, Quart. Revs. **11**, 121 (1957).
[28] R. E. Dickerson and W. N. Lipscomb, J. Chem. Phys. **27**, 212 (1957).
[29] R. Kiessling, Acta Chem. Scand. **4**, 209 (1950).

Quantum Statistical Mechanical Theory of the Rate of Exchange Chemical Reactions in the Gas Phase*

TSUNENOBU YAMAMOTO†
Department of Chemistry, University of Oregon, Eugene, Oregon

(Received December 22, 1959)

A theory of the reaction rate of simple exchange reactions in the gas phase is developed on the basis of the quantum-statistical mechanical theory of linear irreversible processes due to Kubo *et al.* A formal expression for the rate coefficient is found near the equilibrium point. A number of relations are derived concerning the scattering amplitudes for the collisions involved in the above reactions. By making use of these relations, the rate constant is expressed in terms of the reaction cross sections in a way which coincides with that known from a more intuitive collisional approach. Since no *ad hoc* assumptions are made, the present theory can be said to provide a statistical mechanical foundation for the collision theory in the particular case discussed.

I. INTRODUCTION

COLLISION-theoretical approaches[1] have made a remarkable contribution to the theory of reaction rates in its earlier stage of development. Since the decade beginning around 1930, a more refined theory, the absolute reaction rate theory of Eyring and others,[2] has been developed. As is well known, the very simplicity and usefulness of the Eyring theory come from the ingenious replacement of considerations on the dynamical aspects of the reaction mechanisms by those on the equilibrium properties of the so-called activated complexes. Now, in order to improve the Eyring theory, it seems to be necessary to return again to collisional approaches, because they are quite powerful in attacking essentially dynamical problems such as chemical reactions. Indeed, some important investigations have recently been carried out in the spirit of the collision theory, i.e., Tayler and Datz[3] measured the reaction cross sections to disclose the reaction mechanism of the chemical reaction $K+HBr \rightarrow KBr+H$ from the experimental side, whereas Eliason and Hirschfelder[4] have formulated a general theory for bimolecular reactions in the gas phase from the theoretical side.

A new approach is presented in the present paper and worked out in the case of simple exchange chemical reactions in the gas phase. It is not a collisional approach in the usual sense, but an application of the general statistical mechanical theory of irreversible processes recently established by R. Kubo *et al.*[5] and by H. Mori.[6] However, the essential parts of the present calculation are carried out on the basis of scattering theory and the final expression for the rate constant is given in terms of reaction cross sections. It should be emphasized that due attention is paid to the nondiagonal as well as diagonal elements of the density matrix which describes the motion of the chemically reacting system toward the equilibrium point. On the contrary, the previous collisional approaches have taken into account only the diagonal aspects of the motion, relying from the outset on a stochastic equation, instead of the Schrödinger equation, to follow the motion of the system. In this respect, the present theory stands on a more firm foundation than any previous collisional or kinetic theoretical approach to reaction rate theory.

Chemical reactions, considered as irreversible processes, are not linear, whereas the statistical mechanical theory of irreversible processes, mentioned before, applies to linear cases only. We are not in a position, therefore, to consider all aspects of our problem at the present stage of the theory; for example, an important point which has to be given up is the derivation of the phenomenological equations of chemical kinetics from the statistical mechanical standpoint. The considerations of the present paper will be confined to the structure of the rate constants, which can be investigated even in the frame of a linear theory. The reason for this is the experimentally well-known fact that reaction rate constants are essentially constant in a large number of chemical reactions so long as the temperature and the pressure of the system are kept constant.[7] There is then no reason to hesitate to evaluate the rate constants in any state near equilibrium, where the phenomenological reaction-rate equations become linear and where the general statistical mechanical theory of linear irreversible processes can at once be applied to the evaluation of the

* This work was supported in part by a research grant from the National Science Foundation.

† On leave from the Department of Chemistry, Faculty of Science, University of Kyoto, Japan.

[1] L. S. Kassel, *The Kinetics of Homogeneous Gas Reactions* (The Chemical Catalog Company, Inc., New York, 1932); R. Fowler and E. A. Guggenheim, *Statistical Thermodynamics* (Cambridge University Press, New York, 1952), Chap. XII.

[2] S. Glasstone, K. Laidler, and H. Eyring, *The Theory of Rate Processes* (McGraw-Hill Book Company, Inc., New York, 1941).

[3] E. H. Tayler and S. Datz, J. Chem. Phys. **23**, 1711 (1955).

[4] M. A. Eliason and J. O. Hirschfelder, J. Chem. Phys. **30**, 1426 (1959).

[5] R. Kubo, J. Phys. Soc. Japan **12**, 570 (1957); R. Kubo, M. Yokota, and S. Nakajima, *ibid.* **12**, 1203 (1957). The first paper refers to irreversible processes which occur under external forces, whereas the second one, on which the present theory is based, refers to processes which proceed under thermodynamical driving forces.

[6] H. Mori, J. Phys. Soc. Japan **11**, 1029 (1956). Another formulation was given by M. S. Green, J. Chem. Phys. **20**, 1281 (1953) and by T. Yamamoto, Progr. Theoret. Phys. **10**, 11 (1953).

[7] For example, K. J. Laidler, *Chemical Kinetics* (McGraw-Hill Book Company, Inc., 1950), Chap. I.

rate constants.[8,9] Once a molecular-theoretical expression is thus found for a rate constant near equilibrium, it may be supposed to hold for any state, however far from equilibrium, unless the particular case happens to fall outside of the range of the experimental fact referred to previously. In Sec. II of the present paper we develop a statistical mechanical formulation of linear chemical reactions in general, along the lines outlined before. In particular, the rate coefficient is given a formal expression which can easily be related to the conventional reaction-rate constant. The transformation of the rate coefficient into a more practical form is the main concern of the following sections, where we confine ourselves to the discussion of a particular case, namely, simple exchange reactions in the gas phase. In Sec. III we study the quantum-mechanical properties of the scattered waves describing the chemically reacting collisions. Various new relations are found among the scattering amplitudes, which are derived after the method of Glauber and Schomaker[10] in their theory on electron diffraction. We shall have frequent occasion to apply them in the next section, IV, where the general formulation given in Sec. II is applied to the foregoing example. No approximations or assumptions are adopted to simplify the calculation, except a reasonable, but conventional, definition which is introduced for specifying the molecular species involved. The rate coefficient is expressed in terms of reaction cross sections. A typical property of so-called gross variables in the theory of irreversible processes is made clear through the calculation given in Sec. IV. Section V is concerned with the derivation of the relation between the rate coefficient and the rate constant and our final expression is found for the latter quantity. Some considerations based on classical mechanics are outlined in the Appendix.

II. STATISTICAL MECHANICAL FORMULATION FOR CHEMICAL REACTIONS NEAR EQUILIBRIUM

We now present a statistical mechanical formulation for linear chemical reactions, that is, for chemical reactions near their equilibrium points. Formally speaking, the application of the general formalism for irreversible processes by Kubo *et al.*[5] can be made straightforwardly to chemical reactions, nothing new being needed methodologically. Thus we may confine ourselves here to a brief outline of the formalism and to a statement of the required results.

Let us consider a homogeneous chemical reaction of the following type

$$\nu_1 A_1+\nu_2 A_2+\cdots \rightleftarrows \nu_1' B_1+\nu_2' B_2+\cdots, \qquad (2.1)$$

where the ν's are the so-called stoichiometric coefficients and those with a prime are counted positive and those without a prime negative. Suppose the whole system is in a nonequilibrium state which involves $\langle N_1\rangle$ molecules of A_1, $\cdots$, and $\langle M_1\rangle$ molecules of B_1, $\cdots$. When the state is sufficiently near the true equilibrium—this situation is always assumed throughout the present paper—we may assume that the system is in a state of partial equilibrium in the sense that all degrees of freedom other than the number of molecules of each species have already reached their equilibrium distributions. We can then assign a value of the free energy to this nonequilibrium state. Indeed, the thermodynamics of irreversible processes postulates that the Gibbs relation holds all the way to the true equilibrium state. Namely, the change of free energy due to the motion of the system toward equilibrium is assumed to be given by

$$d(\Delta\Omega)=\sum\mu_i d\langle\Delta N_i\rangle+\sum\mu_j' d\langle\Delta M_j\rangle \qquad (2.2)$$

in the present situation of constant temperature and volume.[9] Here Ω is the Helmholtz free energy, the μ's are chemical potentials and Δ means the deviation from the equilibrium value. Introducing the chemical affinity[11]

$$\mathfrak{A}=-\sum\nu_i\mu_i-\sum\nu_j'\mu_j', \qquad (2.3)$$

we can write Eq. (2.2) as

$$d(\Delta\Omega)=-\mathfrak{A}d\langle\Delta N\rangle \qquad (2.4)$$

with

$$\langle\Delta N\rangle=\langle\Delta N_1\rangle/\nu_1=\cdots=\langle\Delta M_1\rangle/\nu_1'=\cdots.$$

According to Kubo *et al.*[5] the above consideration is interpreted in the language of statistical mechanics as follows. The partial equilibrium state, the free energy of which changes according to Eq. (2.4), can be described by a kind of generalized canonical ensemble

$$\rho(t)=\exp\beta\{\Omega(t)-H_T+\mathfrak{A}(t)\Delta N\}. \qquad (2.5)$$

Here $\beta=1/kT$, H_T is the Hamiltonian of the total system and ΔN denotes the quantum mechanical operator corresponding to the number of molecules of any species A_i (or B_j) divided by ν_i (or ν_j'). It is not difficult to prove (2.4) from (2.5). $\mathfrak{A}$ is supposed to be a small quantity of first order, because the state under consideration is assumed to be sufficiently near equilibrium. We may then expand Eq. (2.5) in a power series with respect to $\mathfrak{A}$. Retaining up to the second-

[8] I. Prigogine, P. Outer, and A. Herbo, J. Phys. & Colloid Chem. **52**, 321 (1948).

[9] I. Prigogine, *Etude Thermodynamique des Phénomènes Irréversibles* (Dunod, Paris, 1947), Chap. II; or De Groot, *Thermodynamics of Irreversible Processes* (North-Holland Publishing Company, Amsterdam, 1951), Chap. IX.

[10] R. Glauber and V. Schomaker, Phys. Rev. **89**, 667 (1953).

[11] Th. De Donder and P. van Rysselberghe, *Thermodynamic Theory of Affinity* (Stanford University Press, Stanford, California, 1936), Chaps. IV and V.

order terms, we have

$$\rho=\exp[\beta(\Omega-H_T)]+\exp[\beta(\Omega_0-H_T)]\mathfrak{A}\int_0^\beta d\lambda \times\exp(\lambda H_T)\Delta N\exp(-\lambda H_T) +\exp[\beta(\Omega_0-H_T)]\mathfrak{A}^2\int_0^\beta d\lambda\int_0^\lambda d\lambda' \times\exp(\lambda H_T)\Delta N\exp[-(\lambda-\lambda')H_T]\Delta N\exp[-\lambda' H_T]. \tag{2.6}$$

The normalization condition for $\rho(t)$ determines the deviation of the free energy from its equilibrium value, Ω_0, with the result

$$\Delta\Omega=-\tfrac{1}{2}\mathfrak{A}^2\int_0^\beta d\lambda\langle\Delta N\Delta N(i\hbar\lambda)\rangle \tag{2.7}$$

where $\langle\ \ \rangle$ means to take the average over

$$\rho_0=\exp\beta(\Omega_0-H_T),$$

and

$$\Delta N(i\hbar\lambda)=\exp(-\lambda H_T)\Delta N\exp(\lambda H_T).$$

Furthermore, the expectation value of ΔN is obtained from Eq. (2.6):

$$\langle\Delta N\rangle=\mathfrak{A}\int_0^\beta d\lambda\langle\Delta N\Delta N(i\hbar\lambda)\rangle. \tag{2.8}$$

Comparing Eqs. (2.7) and (2.8), we finally obtain

$$\Delta\Omega=-\tfrac{1}{2}\mathfrak{A}\langle\Delta N\rangle \tag{2.9}$$

which is equivalent to Eq. (2.4).

Again according to the thermodynamics of irreversible processes, the driving force for the flow $d\langle\Delta N\rangle/dt$ is given by $-\partial\Delta\Omega/\partial\langle\Delta N\rangle$ which is equal to $\mathfrak{A}$ by Eq. (2.4). Thus we should expect that the linearized rate equation for the chemical reaction Eq. (2.1) is written

$$d\langle\Delta N\rangle/dt=G\mathfrak{A}, \tag{2.10}$$

G being called the rate coefficient.[8,9] The statistical mechanical derivation of Eq. (2.10) is straightforward. We retain the zeroth- and first-order terms in the expansion (2.6) to follow the motion of $\rho(t)$ by the Schrödinger equation. Then the deviation $\Delta N(t+\Delta t)$ at a later time $t+\Delta t$ can at once be written down. If the magnitude of Δt can be chosen such that it is long enough in a microscopic sense so that the correlation function

$$\int_0^\beta d\lambda\langle\dot{N}\dot{N}(t+i\hbar\lambda)\rangle$$

decays to zero in a period much shorter than Δt, and such that it is still short enough in a macroscopic sense so that $[\langle\Delta N\rangle(t+\Delta t)-\langle\Delta N\rangle(t)]/\Delta t$ can be supposed to give $d\langle N\rangle(t)/dt$ macroscopically, then the rate equation, (2.10), is derived together with the formal expression for the rate coefficient:

$$G=\int_0^{\Delta t}dt\int_0^\beta d\lambda\langle\dot{N}\dot{N}(t+i\hbar\lambda)\rangle, \tag{2.11}$$

where $\dot{N}=d\Delta N/dt=(1/i\hbar)[N, H_T]$. Incidentally, the statement that the state of the system on the way toward the true equilibrium state is always represented by a density matrix with the form Eq. (2.5) is the most essential assumption in the theory by Kubo *et al.*[5] In some cases some degrees of freedom other than the number of molecules of each species might not be in their equilibrium distributions. However, if the deviation from equilibrium is not large, it is still possible to include the accompanying relaxation processes by modifying Eq. (2.5). We shall not consider this point any further. The assumption of the time interval Δt with the properties referred to above will be discussed at the end of the section.

The number operator N may be defined by an appropriate projection operator which characterizes any molecular species involved in Eq. (2.1). However, in the case of gas-phase reactions, it is more convenient to define one projection operator for each side of Eq. (2.1), say O_α and O_γ. O_α corresponds to a situation in which there exist $|\nu_1|$ free molecules of A_1, $|\nu_2|$ free molecules of A_2, $\cdots O_\gamma$ has an analogous meaning. Since $N_1=|\nu_1|\sum O_\alpha, \cdots$, $M_1=\nu_1'\sum O_\gamma, \cdots$, we have

$$\dot{N}=-\sum\dot{O}_\alpha=\sum\dot{O}_\gamma. \tag{2.12}$$

The summation should be carried out over all possible combinations of particles which can just make up $|\nu_1|$ molecules of A_1, $|\nu_2|$ molecules of A_2, $\cdots$ and therefore also ν_1' molecules of B_1, ν_2' molecules of B_2, $\cdots$. The number of such combinations is clearly given by

$$n=\binom{\langle N_1\rangle}{|\nu_1|}\binom{\langle N_2\rangle}{|\nu_2|}\cdots+\binom{\langle M_1\rangle}{\nu_1'}\binom{\langle M_2\rangle}{\nu_2'}\cdots. \tag{2.13}$$

The rate coefficient G is expressed in terms of O_α by

$$G=n\int_0^{\Delta t}dt\int_0^\beta d\lambda\langle\dot{O}_\alpha\dot{O}_\alpha(t+i\hbar\lambda)\rangle. \tag{2.14}$$

Here we have replaced the double summation, which should have appeared, by a single summation and then by a simple multiplication by n, because the cross terms vanish upon being averaged over the equilibrium ensemble. Needless to say, this simplification just corresponds to the neglect of the effect of multiple scatterings, which may be ignored in the case of simple reactions in the gas phase such as those discussed below. G, given by Eq. (2.14), is now concerned simply with the subsystem consisting of $|\nu_1|$ molecules of A_1, $|\nu_2|$ molecules of A_2, $\cdots$, or of ν_1' molecules of B_1, ν_0' molecules of B_2, $\cdots$, the rest of the system being omitted completely.

H. Nakano has shown in his theory of the electrical conductivity in metals[12] that the double integration in Eq. (2.14) can be carried out formally if we introduce the representation which diagonalizes the Hamiltonian of the subsystem, H, and if the energy spectrum is a continuum. The result is

$$G=(\beta n\pi\hbar/Z)\sum_{k,k'}\exp(-\beta E_k)|(k\mid \dot{O}_\alpha\mid k')|^2\delta(E_k-E_k'), \tag{2.15}$$

where k (or k') specifies an individual eigenstate of H, E_k (or E_k') is its eigenvalue, and Z is the partition function. Since we have no interest in the motion of the subsystem after Δt, it is regarded as an open system, and as a result, the eigenfunctions which are to be used in calculating $(k\mid O_\alpha\mid k')$ should be the scattering-theoretical steady-state solutions of H. As regards the magnitude of Δt, it has to be far greater than the mean duration time of collisions, otherwise we could not eliminate Δt from Eq. (2.14) to get Eq. (2.15). On the other hand, Δt need not necessarily be shorter than the mean free time of the molecules because, as was already stated, perturbing effects from outside of the subsystem would have a tendency to cancel each other. Thus, we may reasonably assume that a time interval with the required properties exists in many gas-phase reactions. The expression (2.15) will be the starting point of the following sections.

III. SOME RELATIONS BETWEEN SCATTERING AMPLITUDES

The purpose of this section is to prepare, mathematically, for the discussion in the next section, especially to establish some relations between scattering amplitudes in the case of the chemical reactions of the type

$$\mathrm{A+BC}\rightleftarrows\mathrm{AB+C}, \tag{3.1}$$

where an atom A reacts with a diatomic molecule BC to produce a diatomic molecule AB and an atom C. This section will be concerned only with the purely quantum-mechanical, in particular, scattering-theoretical aspects of the reaction.

A state which corresponds to the left- or right-hand side of Eq. (3.1) is characterized by $(\mathbf{k},\alpha)$ or $(\mathbf{p},\gamma)$, respectively, where $\mathbf{k}$ or $\mathbf{p}$ means the propagation vector of atom A or C relative to the center of mass of molecule BC or AB, respectively, and α or γ specifies the internal quantum state of free A and free BC or free AB and free C, respectively.[13] An incident wave has either the form

$$\Phi(\mathbf{k},\alpha)=\exp(i\mathbf{k}\cdot\mathbf{r})\phi(\alpha), \tag{3.2}$$

or the form

$$\Phi(\mathbf{p},\gamma)=\exp(i\mathbf{p}\cdot\mathbf{s})\phi(\gamma), \tag{3.3}$$

where $\phi(\alpha)$ and $\phi(\gamma)$ denote the eigenfunctions of the internal states of A and BC and AB and C, respectively, and $\mathbf{r}$ and $\mathbf{s}$ are the relative coordinates of A and C with respect to the centers of mass of BC and AB, respectively. The corresponding energies are given by

$$E(k,\alpha)=(\hbar^2k^2/2M_\alpha)+E(\alpha), \tag{3.4}$$

$$E(p,\gamma)=(\hbar^2p^2/2M_\gamma)+E(\gamma), \tag{3.5}$$

with

$$M_\alpha=\frac{M_\mathrm{A}(M_\mathrm{B}+M_\mathrm{C})}{M_\mathrm{A}+M_\mathrm{B}+M_\mathrm{C}}\quad\text{and}\quad M_\gamma=\frac{M_\mathrm{C}(M_\mathrm{A}+M_\mathrm{B})}{M_\mathrm{A}+M_\mathrm{B}+M_\mathrm{C}}, \tag{3.6}$$

M_A, M_B, and M_C being the masses of A, B, and C, respectively.

The scattering-theoretical steady-state solutions of H are denoted by $\Psi(\mathbf{k},\alpha)$ and $\Psi(\mathbf{p},\beta)$, the asymptotic forms of which are well known[14]: when $r=|\mathbf{r}|$ is sufficiently large and $r_\mathrm{BC}<r_0$,[15] we have

$$\Psi(\mathbf{k},\alpha)\cong\Phi(\mathbf{k},\alpha)+\sum_{\alpha'}f(\mathbf{k},\alpha\mid\mathbf{k}',\alpha')[\exp(ik'r)/r]\phi(\alpha'), \tag{3.7}$$

$$\Psi(\mathbf{p},\gamma)\cong\sum_{\alpha''}f(\mathbf{p},\gamma\mid\mathbf{k}'',\alpha'')[\exp(ik''r)/r]\phi(\alpha''), \tag{3.8}$$

where $\mathbf{k}'$ and $\mathbf{k}''$ are propagation vectors in the direction $\mathbf{r}$ and their magnitudes k' and k'' are determined by

$$E(k,\alpha)=E(k',\alpha'),\qquad E(p,\gamma)=E(k'',\alpha''). \tag{3.9}$$

On the other hand, when $s=|\mathbf{s}|$ is sufficiently large and $r_\mathrm{BA}<r_0$, we have

$$\Psi(\mathbf{k},\alpha)\cong\sum_{\gamma'}f(\mathbf{k},\alpha\mid\mathbf{p}',\gamma')[\exp(ip's)/s]\phi(\gamma'), \tag{3.10}$$

$$\Psi(\mathbf{p},\gamma)\cong\Phi(\mathbf{p},\gamma)+\sum_{\gamma''}f(\mathbf{p},\gamma\mid\mathbf{p}'',\gamma'')[\exp(ip''s)/s]\phi(\gamma''), \tag{3.11}$$

where $\mathbf{p}'$ and $\mathbf{p}''$ have the same direction as $\mathbf{s}$ and their magnitudes p' and p'' are determined by

$$E(k,\alpha)=E(p',\gamma'),\qquad E(p,\gamma)=E(p'',\gamma''). \tag{3.12}$$

[12] H. Nakano, Progr. Theoret. Phys. **15**, 77 (1956); **17**, 145 (1957).
[13] The motion of the center of mass of A+BC or AB+C can be omitted without loss of generality.
[14] N. F. Mott and H. S. W. Massey, *Theory of Atomic Collisions* (Oxford University Press, New York, 1949), 2nd ed., Chap. VIII.
[15] The value of r_0 is so chosen that, for $r_\mathrm{BC}>r_0$ and $r_\mathrm{BA}>r_0$, all the relevant $\phi(\alpha)$ and $\phi(\gamma)$ vanish.

The mathematical properties of scattered waves in reacting systems have been fully investigated in the theory of nuclear reactions,[16] where the so-called scattering matrix plays the central role. This matrix concerns partial waves with a definite angular momentum and not scattered waves as a whole, so that the formal properties of scattering amplitudes have been left less unknown. The relations among scattering amplitudes which are derived below have a close relation with the well-known properties of the scattering matrix.

Glauber and Schomaker[10] have found some interesting relations concerning scattering amplitudes in the case of elastic scattering. In particular, they have generalized the optical theorem in scattering theory to the case of nonforward scattering. Their theory is extended here to include more general scattering, reacting as well as inelastic, which occurs in the reacting system under consideration.

Let us consider two scattered waves $\Psi(\mathbf{k}, \alpha)$ and $\Psi(\mathbf{k}', \alpha')$ with $E(k, \alpha) = E(k', \alpha')$. From the Schrödinger equation we have

$$\Psi^*(\mathbf{k}', \alpha') H\Psi(\mathbf{k}, \alpha) - \Psi(\mathbf{k}, \alpha) H\Psi^*(\mathbf{k}', \alpha') = 0. \quad (3.13)$$

Here H is the Hamiltonian of the system A+BC or AB+C and its kinetic energy part associated with the nuclear motion is given by[17]

$$-(\hbar^2/2M_\alpha)\Delta_r - (\hbar^2/2M')\Delta_{r_{BC}}$$

or

$$-(\hbar^2/2M_\gamma)\Delta_s - (\hbar^2/2M'')\Delta_{r_{BA}} \quad (3.14)$$

with

$$M' = M_B M_C/(M_B + M_C)$$

and

$$M'' = M_A M_B/(M_A + M_B).$$

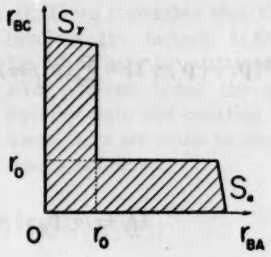

FIG. 1. Schematic illustration of the domain of integration in Eq. (3.15).

Now we integrate Eq. (3.13) over the domain shown schematically in Fig. 1. The boundaries S_α and S_γ are defined by $r = R = \text{const}$, and $s = S = \text{const}$, respectively. The integral can be converted into surface integrals, of which only two have nonvanishing values, so that we obtain

$$M_\alpha^{-1}\int \{\Psi^*(\mathbf{k}', \alpha')(\partial/\partial r)\Psi(\mathbf{k}, \alpha) - \Psi(\mathbf{k}, \alpha)(\partial/\partial r)\Psi^*(\mathbf{k}', \alpha')\}_{r=R} d\Omega_r d\mathbf{r}_{BC}$$

$$+ M_\gamma^{-1}\int \{\Psi^*(\mathbf{k}', \alpha')(\partial/\partial s)\Psi(\mathbf{k}, \alpha) - \Psi(\mathbf{k}, \alpha)(\partial/\partial s)\Psi^*(\mathbf{k}', \alpha')\}_{s=S} d\Omega_s d\mathbf{r}_{BA} = 0, \quad (3.15)$$

where the vectors $\mathbf{r}$ and $\mathbf{s}$ on the left-hand side are integrated over the spheres $r = R$ and $s = S$, respectively. If we let R and S be sufficiently large, the values of the surface integrals can be evaluated by making use of the asymptotic forms (3.7) and (3.10) for $\Psi(\mathbf{k}, \alpha)$. Thus we find the following result: if $E(k, \alpha) = E(k', \alpha')$,

$$(1/2i)\{f(\mathbf{k}, \alpha \mid \mathbf{k}', \alpha') - f^*(\mathbf{k}, \alpha \mid \mathbf{k}', \alpha')\} = \sum_{\alpha''}(k''/4\pi)\int f^*(\mathbf{k}', \alpha' \mid \mathbf{k}'', \alpha'') f(\mathbf{k}'', \alpha'' \mid \mathbf{k}, \alpha) d\Omega_{k''}$$

$$+ \sum_\gamma (p/4\pi)\int f^*(\mathbf{k}', \alpha' \mid \mathbf{p}, \gamma) f(\mathbf{p}, \gamma \mid \mathbf{k}, \alpha) d\Omega_p. \quad (3.16)$$

Here we have anticipated the symmetry relations Eqs. (3.21) and (3.22). Especially when $\mathbf{k} = \mathbf{k}'$ and $\alpha = \alpha'$, we obtain the optical theorem[18]

$$(k/4\pi)\sigma(\mathbf{k}, \alpha) = \mathrm{Im} f(\mathbf{k}, \alpha \mid \mathbf{k}, \alpha). \quad (3.17)$$

In the same way, we can derive the following relations: If $E(k, \alpha) = E(p, \gamma)$,

$$(1/2i)\{f(\mathbf{p}, \gamma \mid \mathbf{k}, \alpha) - f^*(\mathbf{p}, \gamma \mid \mathbf{k}, \alpha)\} = \sum_{\alpha'}(k'/4\pi)\int f^*(\mathbf{p}, \gamma \mid \mathbf{k}', \alpha') f(\mathbf{k}', \alpha' \mid \mathbf{k}, \alpha) d\Omega_{k'}$$

$$+ \sum_{\gamma'}(p'/4\pi)\int f^*(\mathbf{p}, \gamma \mid \mathbf{p}', \gamma') f(\mathbf{p}', \gamma' \mid \mathbf{k}, \alpha) d\Omega_{p'}; \quad (3.18)$$

[16] For example, see J. M. Blatt and V. F. Weisskopf, *Theoretical Nuclear Physics* (John Wiley & Sons, New York, 1952), Chap. X.

[17] To simplify the discussion, we do not refer to the electronic motion at all. However, this does not necessarily imply the necessity of introducing an approximation on the nuclear motion such as the adiabatic approximation.

[18] For example, see, L. D. Landau and E. M. Lifshitz, *Quantum Mechanics, Nonrelativistic Theory* (Addison-Wesley Publishing Company, Inc., Reading, Massachusetts, 1958), Chaps. XIV and XV.

if $E(p,\gamma)=E(p',\gamma')$,

$$(1/2i)\{f(\mathbf{p},\gamma\mid\mathbf{p}',\gamma')-f^*(\mathbf{p},\gamma\mid\mathbf{p}',\gamma')\}=\sum_{\gamma''}(p''/4\pi)\int f^*(\mathbf{p}',\gamma'\mid\mathbf{p}'',\gamma'')f(\mathbf{p}'',\gamma''\mid\mathbf{p},\gamma)d\Omega_{p''}$$
$$+\sum_{\alpha}(k/4\pi)\int f^*(\mathbf{p}',\gamma'\mid\mathbf{k},\alpha)f(\mathbf{k},\alpha\mid\mathbf{p},\gamma)d\Omega_k; \quad (3.19)$$

and

$$(p/4\pi)\sigma(\mathbf{p},\gamma)=\mathrm{Im}\,f(\mathbf{p},\gamma\mid\mathbf{p},\gamma). \quad (3.20)$$

Furthermore, we can obtain the symmetry relations of the scattering amplitudes, again following Glauber and Schomaker's method.[10] Only the results will be listed below.

$$f(\mathbf{k},\alpha\mid\mathbf{k}',\alpha')=f(-\mathbf{k}',\alpha'\mid-\mathbf{k},\alpha)=f(\mathbf{k}',\alpha'\mid\mathbf{k},\alpha), \quad (3.21)$$

$$M_\gamma^{-1}f(\mathbf{k}\cdot\alpha\mid\mathbf{p},\gamma)=M_\alpha^{-1}f(-\mathbf{p},\gamma\mid-\mathbf{k},\alpha)$$
$$=M_\alpha^{-1}f(\mathbf{p},\gamma\mid\mathbf{k},\alpha) \quad (3.22)$$

$$f(\mathbf{p},\gamma\mid\mathbf{p}',\gamma')=f(-\mathbf{p}',\gamma'\mid-\mathbf{p},\gamma)=f(\mathbf{p}',\gamma'\mid\mathbf{p},\gamma). \quad (3.23)$$

Here we have used the inversion symmetry of the Hamiltonian to obtain the third form in each of the above relations.

IV. CALCULATION OF THE RATE COEFFICIENT

The formal expression (2.15) for the rate coefficient is now worked out for the special case (3.1) by utilizing the relations concerning the scattering amplitudes obtained in the preceding section. We shall not find it necessary to adopt any new approximations to obtain the final results, except for a simplifying convention on the definition of O_α.[19] This operator is defined as follows:

$$(\mathbf{r}_{BC},\mathbf{r}\mid O_\alpha\mid\mathbf{r}_{BC}',\mathbf{r}')$$
$$=D^-(r_{BC}-r_0)D^+(r-R)\delta(\mathbf{r}_{BC}-\mathbf{r}_{BC}')\delta(\mathbf{r}-\mathbf{r}') \quad (4.1)$$

where

$$D^-(r_{BC}-r_0)=1, \quad \text{if} \quad r_{BC}<r_0,$$
$$0, \quad \text{if} \quad r_{BC}>r_0, \quad (4.2)$$

and

$$D^-+D^+=1. \quad (4.3)$$

R is a constant which is assumed to be large enough to allow us to use the asymptotic forms for the Ψ's if $r>R$. Generally speaking, O_α should be given a more physical definition. But so long as the temperature is not very high, as is the case under ordinary conditions, the purely geometrical definition Eq. (4.1) is just sufficient for the particular reaction under consideration, for the dissociated states of molecules AB or BC make no appreciable contribution to the value of the rate constant because of their high energies.

The matrix elements of O_α can be calculated straightforwardly in the Ψ representation from Eq. (4.1) and (3.7) through (3.12). One of the results may be written down here:

$$(\mathbf{k},\alpha\mid O_\alpha\mid\mathbf{k}',\alpha')=\delta(\mathbf{k}-\mathbf{k}')\delta_{\alpha,\alpha'}-[1/(2\pi)^2](1/ik)\{\pi\delta(\bar{k}-k)-[i/(\bar{k}-k)]_P\}f(\mathbf{k}',\alpha'\mid\bar{\mathbf{k}},\alpha)\exp[i(\bar{k}-k)R]$$
$$+[1/(2\pi)^2](1/ik')\{\pi\delta(\bar{k}'-k')+[i/(\bar{k}'-k')]_P\}f^*(\mathbf{k},\alpha\mid\mathbf{k}',\alpha')\exp[-i(\bar{k}'-k')R]$$
$$+[1/(2\pi)^3]\sum_{\alpha''}\{\pi\delta(k''-k''')-[i/(k'''-k'')]_P\}\int f^*(\mathbf{k},\alpha\mid\mathbf{k}'',\alpha'')f(\mathbf{k}''',\alpha''\mid\mathbf{k}',\alpha')d\Omega_{k''}\exp[i(k'''-k'')R] \quad (4.4)$$

where

$$\bar{\mathbf{k}}=(\bar{k}/k)\mathbf{k}, \qquad \bar{\mathbf{k}}'=(\bar{k}'/k')\mathbf{k}',$$
$$E(\bar{k}',\alpha')=E(k'',\alpha'')=E(k,\alpha),$$
$$E(\bar{k},\alpha)=E(k''',\alpha'')=E(k',\alpha'). \quad (4.5)$$

$\mathbf{k}''$ and $\mathbf{k}'''$ have the same direction and $[\ ]_P$ means to take the principal value. Equation (4.4) is full of singularities. It is those singularities associated with the principal value terms that make nonvanishing contributions to the final result, as will be seen just below. The properties of gross variables in general have been discussed on many occasions[20] but still remain obscure because of the lack of accurate calculations in

[19] The statistical mechanical theory developed in Sec. II does not always need an exact definition for O_α; such a theory is always concerned with so-called gross variables in order to obtain phenomenological relations.

[20] For example, Van Kampen, Physica **20**, 603 (1954).

practical cases. Equation (4.4) is a typical example of this important problem.

The matrix elements of $\dot{O}_\alpha$ are given by

$$(\mathbf{k}, \alpha \mid \dot{O}_\alpha \mid \mathbf{k}', \alpha') = (i\hbar)^{-1}\{E(k', \alpha') - E(k, \alpha)\}(\mathbf{k}, \alpha \mid O_\alpha \mid \mathbf{k}', \alpha'), \quad (4.6)$$

etc. If we remember that the expression (2.15) for G involves the factors, $\delta(E(k', \alpha') - E(k, \alpha))$, etc., Eq. (4.6) may be evaluated in the limits, $E(k', \alpha') \to E(k, \alpha)$, etc. Using the symbol $\Rightarrow$ instead of the equality sign, and omitting the factors whose absolute magnitudes are equal to unity, we can write down the results as follows:

$$(\mathbf{k}, \alpha \mid \dot{O}_\alpha \mid \mathbf{k}', \alpha') \Rightarrow [1/i(2\pi)^2](\hbar/M_\alpha)\{f(\mathbf{k}, \alpha \mid \mathbf{k}', \alpha') - f^*(\mathbf{k}, \alpha \mid \mathbf{k}', \alpha')\}$$
$$- \sum_{\alpha''}[\hbar k''/(2\pi)^3 M_\alpha]\int f^*(\mathbf{k}, \alpha \mid \mathbf{k}'', \alpha'')f(\mathbf{k}'', \alpha'' \mid \mathbf{k}', \alpha')d\Omega_{k''} \quad (4.7)$$

which is alternatively written, using Eq. (3.16), as

$$\Rightarrow \sum_{\gamma''}[\hbar p''/(2\pi)^3 M_\alpha]\int f^*(\mathbf{k}, \alpha \mid \mathbf{p}'', \gamma'')f(\mathbf{p}'', \gamma'' \mid \mathbf{k}', \alpha')d\Omega_{p''}; \quad (4.8)$$

$$(\mathbf{k}, \alpha \mid \dot{O}_\alpha \mid \mathbf{p}, \gamma) \Rightarrow [1/i(2\pi)^2](\hbar/M_\gamma)f^*(\mathbf{k}, \alpha \mid \mathbf{p}, \gamma)$$
$$+ \sum_{\gamma''}[\hbar p''/(2\pi)^3 M_\gamma]\int f^*(\mathbf{k}, \alpha \mid \mathbf{p}'', \gamma'')f(\mathbf{p}'', \gamma'' \mid \mathbf{p}, \gamma)d\Omega_{p''}, \quad (4.9)$$

which, using Eq. (3.18), is in turn rewritten as

$$\Rightarrow [1/i(2\pi)^2](\hbar/M_\gamma)f(\mathbf{k}, \alpha \mid \mathbf{p}, \gamma) - \sum_{\alpha''}[\hbar k''/(2\pi)^3 M_\gamma]\int f^*(\mathbf{k}, \alpha \mid \mathbf{k}'', \alpha'')f(\mathbf{k}'', \alpha'' \mid \mathbf{p}, \gamma)d\Omega_{k''}; \quad (4.10)$$

and finally

$$(\mathbf{p}, \gamma \mid \dot{O}_\alpha \mid \mathbf{p}', \gamma') \Rightarrow \sum_{\alpha''}[\hbar k''/(2\pi)^3 M_\gamma]\int f^*(\mathbf{p}, \gamma \mid \mathbf{k}'', \alpha'')f(\mathbf{k}'', \alpha'' \mid \mathbf{p}', \gamma')d\Omega_{k''}. \quad (4.11)$$

Now we can proceed to the calculation of the rate coefficient. It consists of four terms:

$$G = g(\alpha, \alpha) + g(\alpha, \gamma) + g(\gamma, \alpha) + g(\gamma, \gamma), \quad (4.12)$$

where, for instance,

$$g(\alpha, \alpha) = (\beta n \pi \hbar/Z)\sum_{\alpha, \alpha'}\int d\mathbf{k}d\mathbf{k}' \exp[-\beta E(k, \alpha)] \mid (\mathbf{k}, \alpha \mid \dot{O}_\alpha \mid \mathbf{k}', \alpha') \mid^2 \delta(E(k, \alpha) - E(k', \alpha')). \quad (4.13)$$

It is an easy matter to prove that

$$g(\alpha, \alpha) = g(\gamma, \gamma)$$

and

$$g(\alpha, \gamma) = g(\gamma, \alpha). \quad (4.14)$$

From Eqs. (4.7), (4.8), and (4.10) we have

$$g(\alpha, \alpha) = (\beta n \pi \hbar/Z)[1/i(2\pi)^5](\hbar^4/M_\alpha^2 M_\gamma)\sum_{\alpha, \alpha', \gamma}\int d\mathbf{k}d\mathbf{k}'d\mathbf{p} \exp[-\beta E(k, \alpha)]$$
$$\times \delta(E(k, \alpha) - E(k', \alpha'))\delta(E(k, \alpha) - E(p, \gamma))\{f(\mathbf{k}, \alpha \mid \mathbf{k}', \alpha') - f^*(\mathbf{k}, \alpha \mid \mathbf{k}', \alpha')\}f(\mathbf{k}, \alpha \mid \mathbf{p}, \gamma)f^*(\mathbf{p}, \gamma \mid \mathbf{k}', \alpha')$$
$$- [\beta n \pi \hbar/Z(2\pi)^6](\hbar^3/M_\alpha M_\gamma)^2 \sum_{\alpha, \alpha', \alpha'', \gamma}\int d\mathbf{k}d\mathbf{k}'d\mathbf{k}''d\mathbf{p} \exp[-\beta E(k, \alpha)]$$
$$\times \delta(E(k, \alpha) - E(k', \alpha'))\delta(E(k, \alpha) - E(k'', \alpha''))\delta(E(k, \alpha) - E(p, \gamma))$$
$$\times f(\mathbf{k}, \alpha \mid \mathbf{k}', \alpha')f^*(\mathbf{k}', \alpha' \mid \mathbf{p}, \gamma)f^*(\mathbf{p}, \gamma \mid \mathbf{k}'', \alpha'')f(\mathbf{k}'', \alpha'' \mid \mathbf{k}, \alpha). \quad (4.15)$$

In the same way we can find from Eq. (4.10) an analogous expression for $g(\alpha, \gamma)$ which can be written as follows:

$$g(\alpha,\gamma)=(\beta n\hbar/2Z)[1/(2\pi)^3](\hbar/M_\gamma)^2\sum_{\alpha,\gamma}\int d\mathbf{k}d\mathbf{p}\exp[-\beta E(k,\alpha)]$$
$$\times\delta(E(k,\alpha)-E(p,\gamma))f(\mathbf{k},\alpha\,|\,\mathbf{p},\gamma)f^*(\mathbf{k},\alpha\,|\,\mathbf{p},\gamma)-g(\alpha,\alpha). \quad (4.16)$$

Thus we obtain

$$G=[\beta n\hbar/(2\pi)^3Z](\hbar/M_\gamma)^2\sum_{\alpha,\gamma}\int d\mathbf{k}d\mathbf{p}\exp[-\beta E(k,\alpha)]\delta(E(k,\alpha)-E(p,\gamma))\,|f(\mathbf{k},\alpha\,|\,\mathbf{p},\gamma)\,|^2, \quad (4.17)$$

which can be written either as

$$G=[\beta n/(2\pi)^3Z]\sum_\alpha\int d\mathbf{k}\exp[-\beta E(k,\alpha)](\hbar k/M_\alpha)\sigma_r(\mathbf{k},\alpha), \quad (4.18)$$

or as

$$G=[\beta n/(2\pi)^3Z]\sum_\gamma\int d\mathbf{p}\exp[-\beta E(p,\gamma)](\hbar p/M_\gamma)\sigma_r(\mathbf{p},\gamma), \quad (4.19)$$

with

$$\sigma_r(\mathbf{k},\alpha)=\sum_{\gamma;E(k,\alpha)=E(p,\gamma)}(M_\alpha p/M_\gamma k)\int|f(\mathbf{k},\alpha\,|\,\mathbf{p},\gamma)\,|^2d\Omega_p \quad (4.20)$$

and

$$\sigma_r(\mathbf{p},\gamma)=\sum_{\alpha;E(p,\gamma)=E(k,\alpha)}(M_\gamma k/M_\alpha p)\int|f(\mathbf{p},\gamma\,|\,\mathbf{k},\alpha)\,|^2d\Omega_k. \quad (4.21)$$

The σ_r's may be called the total reaction cross sections. Of course, the alternatives Eqs. (4.18) and (4.19) for G come from the symmetry relation (3.24) of the scattering amplitudes, or from the principle of detailed balancing.[21]

V. EXPRESSIONS FOR THE RATE CONSTANTS

This section will be concerned with the relation between the rate coefficient, Eqs. (4.18) or (4.19), and the forward and backward rate constants, k_f and k_b. As is well known, the phenomenological rate equation for the reaction (3.1) is described by

$$d\langle N_{AB}\rangle/dt=V^{-1}\{k_f\langle N_A\rangle\langle N_{BC}\rangle-k_b\langle N_{AB}\rangle\langle N_C\rangle\}, \quad (5.1)$$

V being the volume of the system. The linearized form of Eq. (5.1), which should be compared with Eq. (2.10), is found by expanding Eq. (5.1) near the equilibrium point and by retaining only the first order terms with respect to the deviation $\langle\Delta N_{AB}\rangle$. The result is expressed as

$$d\langle N_{AB}\rangle/dt=k_f(\beta\langle N_A\rangle^0\langle N_{BC}\rangle^0/V)\,\mathcal{A}. \quad (5.2)$$

Here, to calculate the chemical affinity $\mathcal{A}$, we have assumed the system is an ideal gas consisting of two kinds of monatomic molecules A and C and two kinds of diatomic molecules BC and AB. $\langle\ \rangle^0$ means the equilibrium value. Comparing Eq. (5.2) with Eq. (2.10), we obtain the required relation

$$k_f=VG/\beta\langle N_A\rangle^0\langle N_{BC}\rangle^0. \quad (5.3)$$

Substituting Eq. (4.18) into Eq. (5.3) and using the value $\langle N_A\rangle^0\langle N_{BC}\rangle^0+\langle N_{AB}\rangle^0\langle N_C\rangle^0$ for n, we finally find the expression for k_f in terms of the reaction cross sections:

$$k_f=[(2\pi)^3Z_a]^{-1}\sum_\alpha\int d\mathbf{k}$$
$$\times\exp[-\beta E(k,\alpha)](\hbar k/M_\alpha)\sigma_r(\mathbf{k},\alpha), \quad (5.4)$$

where Z_a is the partition function of a free A and a free BC per unit volume with neglect of the contribution from the translational motion of A+BC as a whole, i.e., the product of three factors: internal partition function of A, internal partition function of BC, and translational partition function of a free particle of mass M_a. The backward rate constant is obtained by dividing Eq. (5.4) by the equilibrium constant, or more symmetrically, we can use Eq. (4.20) with the result:

$$k_b=[(2\pi)^3Z_\gamma]^{-1}\sum_\gamma\int d\mathbf{p}$$
$$\times\exp[-\beta E(p,\gamma)](\hbar p/M_\gamma)\sigma_r(\mathbf{p},\gamma). \quad (5.5)$$

The results Eqs. (5.4) and (5.5) for the rate constants just coincide with those given by the more intuitive theory based on a kinetic or collisional method

[21] Work cited in footnote 18.

under the assumption of equilibrium distribution of the reactant molecules among their internal as well as translational degrees of freedom.[4] Thus we can conclude that the kinetic method provides the practically exact result for rate constants in the particular case discussed, if the system is near equilibrium and if multiple scattering can be ignored. Although we have studied only a particularly simple class of reactions, the present theory may be extended without any difficulty to more general binary chemical reactions in the gas phase.

VI. ACKNOWLEDGMENTS

The author is deeply grateful to Professor Terrell L. Hill, University of Oregon, for his encouragement, many suggestions, and stimulating discussions in the course of this work, and for reading the manuscript. He is also much obliged to Professor J. L. Powell, University of Oregon, who gave him valuable suggestions concerning the discussion of Sec. III, and to Professor Nobuhiko Saito, Waseda University, for his continued interest in the work. He wishes to express his appreciation for the hospitality of the Department of Chemistry, University of Oregon.

APPENDIX

A classical theory of reaction rates is outlined here. The starting point of the discussion is the expression (2.14) for G. Before entering the classical discussion, it will be more convenient to rewrite Eq. (2.14) in another form. Namely, the double integration can be carried out formally and we obtain

$$G=-(n/i\hbar)\langle[O_a, O_\gamma(\Delta t)]\rangle \tag{A.1}$$

where $[\ ,\ ]$ means the commutator and we have replaced $O_a(\Delta t)$ by $-O_\gamma(\Delta t)$. Now, in order to calculate G classically, we may replace the commutator by the corresponding Poisson bracket:

$$G_c=-n\langle\{O_a, O_\gamma(\Delta t)\}\rangle. \tag{A2}$$

To make the discussion simpler, we here redefine O_a as follows:

$$O_a=D^-(r_{BC}-r_0). \tag{A3}$$

O_γ is given an analogous definition. Then Eq. (A2) can be expressed at once as

$$G_c=(\beta n/Z)\langle \dot{r}_{BC}\delta(r_{BC}-r_0)O_\gamma(\Delta t)\rangle. \tag{A4}$$

The rate constant, k_f, is found from Eq. (5.3):

$$k_f=(1/Z_a)\langle \dot{r}_{BC}\delta(r_{BC}-r_0)O_\gamma(\Delta t)\rangle. \tag{A5}$$

This result shows that k_f is the flow rate of the fluid corresponding to the equilibrium ensemble, which goes up from the reactant valley, over the barrier and down to the product valley. This interpretation for k_f has been well known since Marcelin and was the starting point in many previous theories on reaction rates.

Effect of Pressure on the *M* Center in Alkali Halide Crystals*

S. MINOMURA AND H. G. DRICKAMER

Department of Chemistry and Chemical Engineering, University of Illinois, Urbana, Illinois

(Received February 18, 1960)

The effect of pressure to 52 800 atm has been measured on the *M* band in NaCl, KCl, KBr, and KI, and on the R_2 and *N* bands in KCl. In general, the band peak shifts to higher frequency with increasing pressure for all bands. At the phase transition from fcc to sc there is a blue shift in KCl, but a red shift in KBr and KI. It is suggested that the shift corresponds to a balance between contraction and polarizability effects. From an Ivey-type relation, it would seem that the *M* center is somewhat less compressible than the *F* center.

There is a marked increase in intensity of the *M* center in the potassium halides in going through the phase transition from the fcc to the sc lattice.

INTRODUCTION

THE effect of pressure on the *M* band produced by x-ray irradiation in four alkali halides (NaCl, KCl, KBr, and KI) and on the R_2 and *N* bands in KCl has been studied to as high as 52 800 atm. The R_1, R_2, and *M* centers may be produced as the first products of the coagulation of *F* centers by irradiating with *F* light for a time in the order of minutes and according to Seitz' model[1] are associated, respectively, with a union of an *F* center and a vacant negative-ion site, another *F* center, and a pair of vacancies of opposite sign. A modification of the Seitz' model of the *M* center wherein a positive-ion and an electron occupy an aggregation of two pairs of vacancies of opposite sign was proposed by Knox.[2] It was suggested by Seitz that the *N* center should be associated with a unit containing three negative-ion vacancies.

There have been previous investigations of the effect of pressure on the *F* bands in several alkali halides[3–6] and on the *M* band in LiF[5] and in LiCl.[6] It has been found that the peaks of the *F* and *M* bands shift to higher frequency with increasing density, and the rate of change in the frequency of the *F* band with density is greater by a factor 1.7 to 2.3 than that predicted from Ivey's relation[7] as long as no phase transition occurs. This indicates that the compressibility in the neighborhood of the *F* center is greater by this factor than that in the bulk crystal.

The following subjects have been discussed in the present study: (1) the rate of change in the frequency of the *M* band with density in four alkali halides, particularly the difference in their rates in three potassium halides, (2) the difference in the rates for the *M*, R_2, *N*, and *F* bands in KCl, and (3) intensity effects.

EXPERIMENTAL PROCEDURE

The crystals obtained from the Harshaw Chemical Company were cleaved to be about $3\times5\times\frac{1}{2}$ mm. These were irradiated with x rays at a distance of about 25 mm for a time ranging from 7 to 26 hrs. The x-ray apparatus was observed at 40 kv and 25 ma with tungsten target. The crystals were then irradiated with *F* light from a Beckman DUR for about 20 min.

A high-pressure cell with a piston of $\frac{1}{8}$ in. diam was used for the spectral measurements. The high-pressure optical system and the techniques have been described previously,[8] except that a RCA 7102 photomultiplier was used. The results were confirmed by a check run for each compound.

RESULTS

Typical spectra are shown for KCl and KI in Figs. 1 and 2. The R_2 and *N* bands can be observed in KCl on the higher and the lower frequency sides of the *M* band, respectively, although they were very weak. The peak heights of the *M* band in the high-pressure phase, the CsCl (sc) structure, are greater by a factor of 2 in KCl, 3 in KBr, and 3.4 in KI than those in the face centered cubic (fcc) structure. In all cases, however, after returning to the fcc structure from the high-pressure phase the peak heights were less than the original heights in this structure.

The peaks of the *M* bands in the four alkali halides and those of the R_2 and *N* bands in KCl shift to higher frequencies with increasing pressure except during a phase transition. The change in the frequency of the peak of the *M* band ($\Delta\nu=\nu-\nu_0$) with pressure is plotted in Fig. 3; ν_0 is the frequency of the peak of the *M* band at atmospheric pressure. The results are also plotted as $\log(\nu/\nu_0)$ vs $\log(\rho/\rho_0)$ in Fig. 4, where ρ/ρ_0 is the fractional change in density according to Bridgman.[9] The rates of change in the frequency of the *M* band with fractional density are almost identical in the three potassium halides. However, the discontinuities at the phase transitions are different. That is, the *M*

* This work was supported in part by a U. S. Atomic Energy Commission contract, Chemical Engineering project 5.

[1] F. Seitz, Revs. Modern Phys. **26**, 7 (1954).
[2] R. S. Knox, Phys. Rev. Letters **2**, 87 (1959).
[3] E. Burstein, J. J. Oberly, and J. W. Davisson, Phys. Rev. **85**, 729 (1952).
[4] I. S. Jacobs, Phys. Rev. **93**, 993 (1954).
[5] W. G. Maish and H. G. Drickamer, J. Phys. Chem. Solids **5**, 328 (1958).
[6] R. A. Eppler and H. G. Drickamer, J. Chem. Phys. **32**, 1418 (1960).
[7] H. F. Ivey, Phys. Rev. **72**, 341 (1947).
[8] R. A. Fitch, T. E. Slykhouse, and H. G. Drickamer, J. Opt. Soc. Am. **47**, 1015 (1957).
[9] P. W. Bridgman, Proc. Am. Acad. Arts Sci. **76**, 1 (1945).

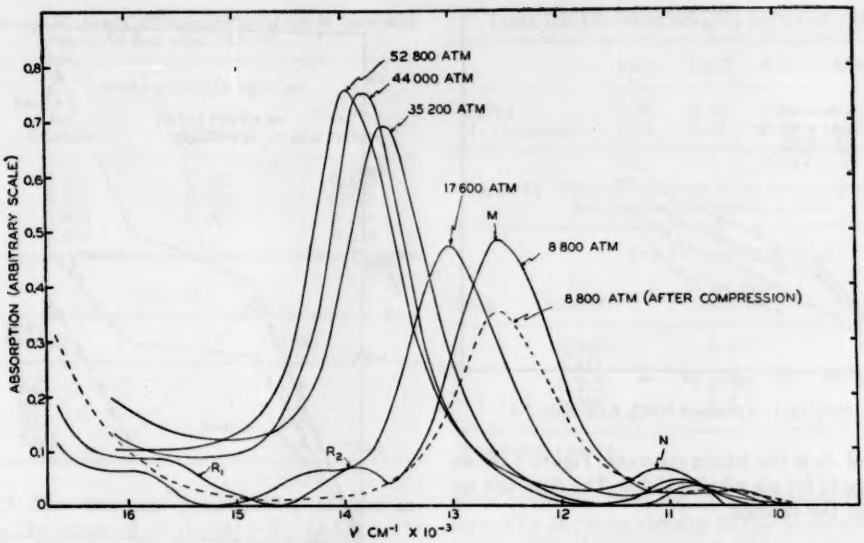

FIG. 1. Absorption vs wave number KCl.

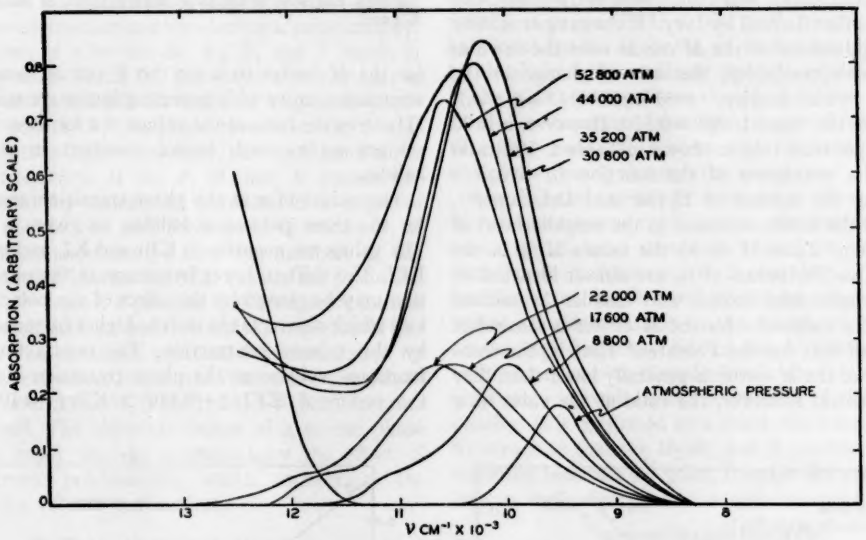

FIG. 2. Absorption vs wave number KI.

band in KCl shifts to a higher frequency, but the *M* bands in KBr and KI shift to a lower frequency with increasing density; also KI shows a greater red shift than KBr. The rate of change in the frequency of the *M*, R_2, *N*, and *F* bands in KCl with fractional density is compared in Fig. 5. The R_2 band cannot be resolved in the sc structure, but the absorption coefficient in the frequency range where the R_2 should be located is much greater than that before the phase transition. The *N* band shifts to a lower frequency with increasing density at the phase transition; on the other hand, the *M* and *F* bands shift to higher frequencies.

DISCUSSION

A. Frequency Shifts

If for the *M* center one accepts as a zeroth approximation, the model consisting of a particle in a box, $\log E_m$ should be proportional to $\log A_0$, where E_m is the frequency of the peak of the *M* band at atmospheric

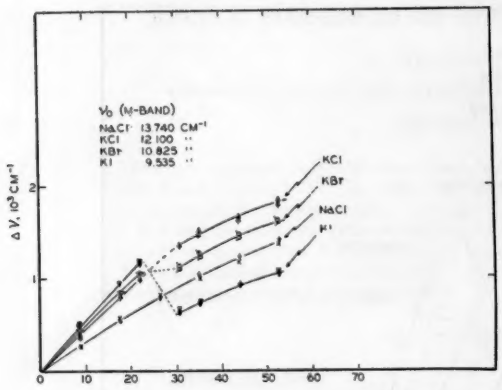

FIG. 3. Shift ($\Delta\nu$) vs pressure NaCl, KCl, KBr, KI.

pressure and A_0 is the lattice constant. Figure 6 shows $\log E_m$ vs $\log A_0$ for six alkali halides. The data can be expressed by the relation

$$E_m A_0^{1.56} = 26.0 \text{ (ev A}^2\text{)},$$

which is, except for a slight difference in the coefficient, the same as that derived by Ivey.[7] If the compressibility in the neighborhood of the M center were the same as the bulk compressibility, the rate of change in the frequency with density, $x = \partial \log(\nu/\nu_0)/\partial \log(\rho/\rho_0)$, should have the value $1.56/3 = 0.520$. However, x is 20 to 60% larger than this, as shown in Table I. The ratio also permits evaluation of the function $f_M = \partial \ln R/\partial \ln A$, (using the method of Eppler and Drickamer[6]), where R is the lattice constant in the neighborhood of the M center.[6] Table II shows the values of f_M in the fcc structure. The values of f_M are almost identical in the three potassium halides and smaller in sodium chloride. The value of x for the M center is somewhat smaller than that for the F center.[6] That is, the compressibility of the M center is generally lower than that of the F center. However, the ratio of the value of x for the M center to x for the F center increases and approaches unity with increasing lattice constant. Table III shows the ratio of the values of x for these two color centers x_M/x_F with lattice constant in five alkali halides.

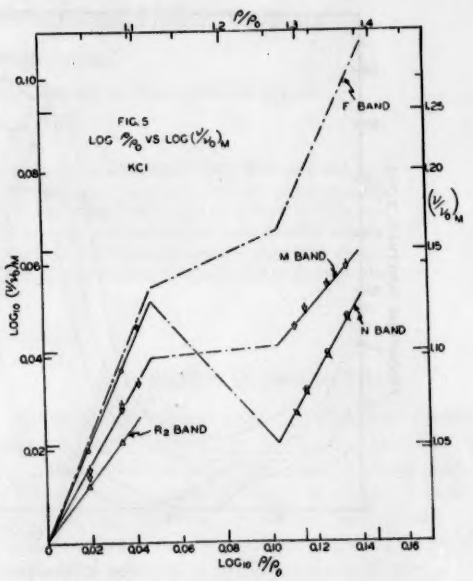

FIG. 5. $\text{Log}_{10}\nu/\nu_0$ vs $\log_{10}\rho/\rho_0$: KCl F band, M band, N_1 band, R_2 band.

The values of x at the phase transition are different for the three potassium halides, as given in Table I. The values are negative in KBr and KI, and positive in KCl. The shift to lower frequency at the phase transition may be caused by the effect of the polarization of ions which contracts the shift to higher frequency caused by the volume contraction. The contraction in the fractional volume at the phase transition increases in the order of KCl (-0.110) > KBr(-0.105) > KI-

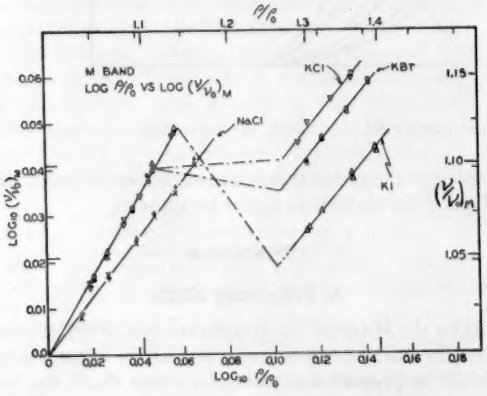

FIG. 4. $\text{Log}_{10}\nu/\nu_0$ vs $\log_{10}\rho/\rho_0$ NaCl, KCl, KBr, KI.

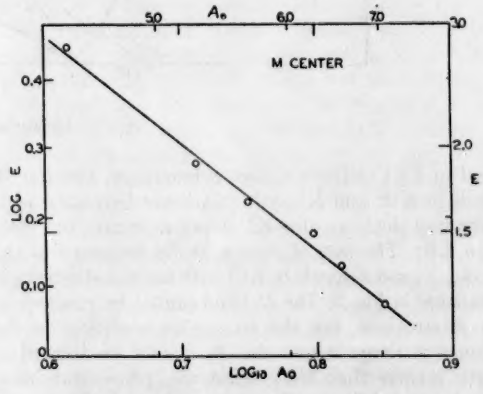

FIG. 6. $\text{Log}E_m$ vs $\log A_0$ for the M center.

TABLE I. The rate of change in the frequency of the M band with density in four alkali halides.

	$x=\partial\log(\nu/\nu_0)/\partial\log(\rho/\rho_0)$		
Crystals	fcc structure	At the phase transition	sc structure
KCl	0.813	0.077	0.543
KBr	0.850	−0.092	0.543
KI	0.850	−0.665	0.543
NaCl	0.633	...	0.633

TABLE II.

Crystals	f_M(fcc)
KCl	1.6
KBr	1.6
KI	1.6
NaCl	1.2

TABLE III. The values of x_M/x_F and lattice constants.

	LiCl	NaCl	KCl	KBr	KI
x_M/x_F	0.20	0.49	0.58	0.77	0.81
A_0 (Angstrom)	5.14	5.62	6.28	6.58	7.06

TABLE IV. The rate of change in the frequency of M, R_2, N, and F bands with density in KCl.

	$x=\partial\log(\nu/\nu_0)/\partial\log(\rho/\rho_0)$		
Bands	fcc structure	At the phase transition	sc structure
M	0.813	0.077	0.543
R_2	0.633	...	...
N	1.102	−0.547	0.872
F[a]	1.208	0.207	1.005

[a] See footnotes 5 and 6.

(−0.085).[9] The electronic polarizability of ions increases in the order of I^- (6.16) > Br^-(4.13) > Cl^- (3.00) > K^+ (0.97) in units of 10^{-24} cm³.[10] The algebraic values of x for the three potassium halides could be accounted for by the difference of the above two effects, the volume contraction and the electronic polarizability.

The values of x for the M, R_2, N, and F bands in KCl are given in Table IV. The value of x increases in the order of $F>N>M>R_2$ bands as long as no phase transition occurs. At the phase transition the F and M bands shift to higher frequency, but the N band shifts to lower frequency. If the F, M, and N centers are approximated by models of particles in a negative vacancy, and in two and three pairs of vacancies of opposite sign, respectively; then the numbers of the first neighboring ions to the color centers are 6 positive ions in the F center, 8 positive and 8 negative ions in the M center, and 11 positive and 11 negative in the N center. The electronic polarizability contributed by the nearest neighbors ions to the color centers increases in the order of $N(43.67)>M(31.76)>F(5.28)$ in units of 10^{-24} cm³. The algebraic values of x at the phase transition could thus be accounted by the effect of the electronic polarizability which counteracts the effect of the volume contraction.

B. Changes of Peak Heights

The peak heights of the M bands in the three potassium halides increase by a factor of 2 to 3.4 across the phase transition from the fcc structure to the sc structure. The M-center density in the sc structure should increase by a factor of about 1.25 than that in the fcc structure according to Bridgman's compressibility data. If the oscillator strength times the M-center density is proportional to the peak height times the half width for the M center, as derived for the F center by Smakula,[11] the oscillator strength of the M center in the high-pressure phase should be greater than that in the low-pressure phase by a factor of over 1.6. On the other hand, M centers may be formed from F centers in passing through the transition.

The R_2 band can not be resolved in the sc structure, but the absorption coefficient in the frequency range where the R_2 band should be located is much greater than that in the fcc structure. It could be ascribed to the broadening of the R_2 band caused by interaction with lattice imperfections, or to the enhancement of a tail on the high-frequency side of the M band associated with transitions to discrete levels above the first excited state, as well as to the increase of the R_2-center density. It is confirmed by a check run returning to the fcc structure that the M, R_2, and N centers can be considerably bleached by going through the phase transition in both directions.

ACKNOWLEDGMENTS

S. Minomura wishes to acknowledge helpful discussions with K. B. Keating, A. S. Balchan, and J. C. Zahner.

[10] C. J. F. Böttcher, Rec. trav. chim. **62**, 325, 503 (1943).

[11] A. Smakula, Z. Physik **63**, 762 (1930).

Letters to the Editor

THE Letters to the Editor section is subdivided into three parts entitled Communications, Comments and Errata, and Notes. These three sections are all subject to the same limitations on length. The textual material of each Letter is limited to a number of words equal to 950 minus the following: (a) 200 words for each average-sized figure; (b) 50 words for each displayed equation; (c) 7 words for each line of table including headings and horizontal rulings. No proof will be sent to the authors of "Communications" and "Comments and Errata." Proof will be sent to the authors of "Notes." The publication charge for Letters is $30 per page, with a minimum of $30 per Letter. If honored, the Institution will be entitled to 100 reprints without covers. See issues of May–September, 1957, for descriptions of categories.

Communications

Far Infrared Spectrum of Trimethylene Oxide

ALFRED DANTI,* W. J. LAFFERTY, AND R. C. LORD

Spectroscopy Laboratory, Massachusetts Institute of Technology, Cambridge 39, Massachusetts

(Received April 25, 1960)

FOR an understanding of the structure and force field of the cyclobutane molecule, a knowledge of the energy levels of the ring-puckering vibration is helpful. Unfortunately, this vibration is not infrared active in either a D_{4h} or D_{2d} structure, nor has it been reported in the Raman spectrum. It is infrared active, however, in the closely related molecule trimethylene oxide (*TMO*), in which one of the CH_2 groups of cyclobutane has been replaced by the isoelectronic and almost isobaric oxygen atom.

As part of a more general study of the vibrational spectrum of *TMO*, we have measured the far infrared absorption of the vapor.[1] No appreciable absorption was found in the range 40–70 cm^{-1}. Above 80 cm^{-1} a broad region of absorption was observed with several strong, sharp peaks whose frequencies in cm^{-1} (and relative absorbances) were 89.8 (1.0), 118.3 (1.0), 128.9 (0.9), 147.6 (0.44), 154.9 (0.35), and 161.8 (0.30). In addition, strong absorption was measurable at 105 and 139.0 cm^{-1}, but the presence of peaks at these points is uncertain because of masking by the very strong water-vapor lines at 104.68 and 139.00 cm^{-1}. A broad, weak band without sharp peaks was found in the range 250–300 cm^{-1}, but no other vapor absorption was detected at frequencies below 600 cm^{-1}. Two very weak bands have been observed in the liquid state on a double-beam instrument at about 390 and 410 cm^{-1}.

There is little doubt that the strong absorption peaks arise from the puckering vibration of *TMO*. Vibrational transitions for this mode should give rise to bands with the sharp, intense Q branches characteristic of type-C bands.[2] Since the vibration is expected to be rather anharmonic whether the ring is planar or not, the observation of numerous Q branches is not surprising. Their frequencies and relative intensities should be useful in the evaluation of the potential function for puckering of the *TMO* ring as well as in the interpretation of certain complexities in the spectrum above 600 cm^{-1}.

W. D. Gwinn and associates[3] have interpreted the results of their extensive microwave studies of *TMO* to mean that the potential function has a central barrier whose height is so low that all vibrational levels lie above it. The resultant anharmonicity should lead to nonuniform separation of the levels and thus to the appearance of several Q branches in the infrared spectrum. We believe that the Q-branch frequencies are to be interpreted on this basis, and that they represent successive transitions starting from the levels $v=0, 1, 2, 3$, etc. The observed intensities are somewhat stronger for the transitions from the higher levels than would be expected from the Boltzmann factors alone, but as Gwinn and co-workers point out, the higher transitions have larger matrix elements which partially compensate for the low Boltzmann factors.

The energy levels inferred from the series of Q branches (including one at 139 cm^{-1}) lead to the prediction of a series of first-overtone bands ($\Delta v=2$) at 208.1, 247.2, 267.9, 286.6, 302.5, and 316.7 cm^{-1}. These will be of type A with much weaker Q branches than the fundamentals and thus could give rise to the weak, structureless absorption found in the range 250–300 cm^{-1}. Second overtone frequencies ($\Delta v=3$) are calculated at 337.0, 386.2, 415.5, 441.5, and 464.3 cm^{-1}. The pair of doubtful bands observed in the liquid at 390 and 410 may be the second and third of these. The liquid spectrum was investigated below 380 cm^{-1} only with a single-beam instrument. Since it is difficult to detect broad weak bands with such instruments, the last two might have been missed because of low intensity.

In an earlier interpretation of the Q-branch series, one of us[4] put forward an alternative explanation of these peaks involving a considerably higher barrier of the order of 450 cm^{-1}. In view of the intensity data given above (which were not available previously) and especially of the microwave results of Gwinn and coworkers, the earlier interpretation is now regarded as unsatisfactory. Further confirmation of the present interpretation is being sought in the near infrared spectrum of *TMO* and in the far infrared spectrum of *TMO* $-d_6$.

We are indebted to Professor Gwinn and Sunney Chan for communication of their microwave results and interpretation prior to publication, to Dr. I. Nakagawa for calculation of vibrational energy levels in various

models of *TMO*, and to the United States Air Force and the National Science Foundation for financial assistance of this work.

* Present address: Chemical and Petroleum Research Laboratory, Carnegie Institute of Technology, Pittsburgh 13, Pennsylvania.

[1] Instrumentation and procedures used have been described by R. C. Lord and T. K. McCubbin, Jr., J. Opt. Soc. Am. **47**, 689 (1957); and by A. Danti and R. C. Lord, J. Chem. Phys. **30**, 1310 (1959).

[2] R. F. Zürcher and Hs. H. Günthard, Helv. Chim. Acta **38**, 849 (1955).

[3] Sunney I. Chan, John Zinn, and William D. Gwinn, J. Chem. Phys., **33**, 295 (1960).

[4] R. C. Lord, general lecture, Fourth European Molecular Spectroscopy Conference, Bologna, Italy, September, 1959.

Double Minimum Vibration in Trimethylene Oxide

SUNNEY I. CHAN,* JOHN ZINN,† AND WILLIAM D. GWINN

Department of Chemistry, University of California, Berkeley 4, California

(Received April 25, 1960)

PREVIOUS reports on trimethylene oxide have indicated that the molecule has a four-membered ring which is essentially planar.[1-3] The potential function for the ring-puckering motion was actually found to contain a small barrier in the planar configuration, with the lowest vibrational level only slightly above the top of the barrier.

The existence of the hump in the potential function was firmly established by the nature of the vibration-rotation interaction. The experimentally determined rotational constants when plotted vs the quantum number of the ring-puckering vibration exhibited a peculiar zigzagging variation. This zigzagging phenomenon was shown to arise as a result of the double minimum nature of the potential function. This potential function may be taken to be an harmonic oscillator perturbed by a hump. Since harmonic oscillator wave functions for the odd vibrational levels contain nodes at the planar configuration, the barrier gives rise to a much larger perturbation for the even levels than for the odd ones.

The zigzagging nature of the rotation constant variation was fairly well reproduced with a potential function of the form $\frac{1}{2}kz^2+c\exp-\beta z^2$, where k, c, and β are parameters which were adjusted in the calculations to fit the data.[4] It was later found necessary to steepen the walls of the potential well in order to explain the general curvature and other, finer details of the rotational constant variation. This was done by the addition of an appropriate quartic term to the above potential function.

At this time, we were most fortunate to learn about the extensive far infrared studies of Alfred Danti, W. J. Lafferty, and R. C. Lord on trimethylene oxide.[5] The results of their work are reported in the accompanying Letter to the Editor. Their far infrared data provide strong conclusive evidence for a steeper potential well than that of an harmonic oscillator. With the use of their data, we further refined our calculations to yield the following potential function for the ring-puckering vibration. This potential function, $V_{cm^{-1}}=9\,145z^2+301\,540z^4+130.2\exp-196.7z^2$, has been found to best fit both the far infrared and our microwave vibration-rotation interaction. In this expression, z is the out-of-plane vibrational displacement of the ring atoms from the hypothetical average plane defined by the planar ring. An effective reduced mass of 71.3 amu has been assumed.

That this potential function gives a nearly perfect fit to the vibration-rotation interaction can be seen in Fig. 1, where the experimental and calculated rotational constants are plotted versus the vibrational quantum number for the largest rotational constant. The agreement is better than 1 Mc.

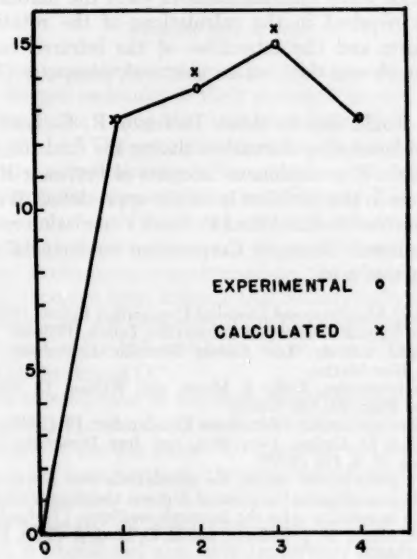

FIG. 1. Comparison of experimental and calculated rotational constants for different vibrational levels.

The first 10 energy levels in this potential function are: 141.29, 211.41, 329.85, 456.40, 595.06, 742.09, 896.75, 1 058.0, 1 225.9, and 1 398.0 cm^{-1}. The height of the barrier restricting the puckering vibration is calculated to be 30 cm^{-1}. The ground vibrational level is 11.1 cm^{-1} above the top of this barrier. The calculated far infrared transitions are listed in Table I together with their calculated relative absorbances. Except for the fundamental, the calculated values are in excellent agreement with those reported by Danti, Lafferty, and Lord.

TABLE I. Frequencies and intensities of far infrared transitions.

Transition	Calculated Frequency cm^{-1}	Calculated Relative absorbance	Danti, Lafferty, and Lord[a] Frequency cm^{-1}	Danti, Lafferty, and Lord[a] Relative absorbance
0–1	70.1	0.46	89.8	1.0
1–2	118.4	(1.0)	118.3	1.0
2–3	126.6	0.89	128.9	0.9
3–4	138.7	0.69	(139.0)	...
4–5	147.0	0.46	147.6	0.44
5–6	154.7	0.28	154.9	0.35
6–7	161.2	0.16	161.8	0.30
7–8	167.9	0.08	...	...
8–9	172.1	0.04	...	...

[a] See footnote reference 4.

In the above calculations, the energy matrix was set up using the first 20 harmonic oscillator wave functions as basis functions. The Hamiltonian was diagonalized, and the resulting transformation matrix was then applied to the z, z^2, and z^4 matrices in the harmonic oscillator wave function basis to yield the matrix elements required in the calculations of the rotational constants and the intensities of the infrared bands. This work was done on an electronic computer (IBM 701).

We would like to thank Professor R. C. Lord for several interesting discussions during the final stages of this work. The continuous interests of Professor Rollie J. Myers in this problem is deeply appreciated. We are also indebted to the Alfred P. Sloan Foundation and to the California Research Corporation for financial support of this work.

* Kaiser Aluminum and Chemical Corporation Fellow, 1958–59. National Science Foundation Cooperative Fellow, 1959–60.
† Present address: Los Alamos Scientific Laboratory, Los Alamos, New Mexico.

[1] Jose Fernandez, Rollie J. Myers, and William D. Gwinn, J. Chem. Phys. **23**, 758 (1955).
[2] William D. Gwinn, Discussions Faraday Soc. **19** (1955).
[3] William D. Gwinn, John Zinn, and Jose Fernandez, Bull. Phys. Soc. II, **4**, 153 (1959).
[4] For a given barrier height, the calculations were found to be relatively insensitive to the value of β. β was therefore arbitrarily chosen to be equal to α for the harmonic oscillator, $[(4\pi^2\mu\nu_0)/h]$.
[5] Alfred Danti, W. J. Lafferty, and R. C. Lord, J. Chem. Phys. **33**, 294 (1960).

Mass Spectrometric and Infrared Emission Investigation of the Vapor Species in the B-S System at Elevated Temperatures*

ARMIN SOMMER, PATRICK N. WALSH, AND DAVID WHITE

Cryogenic Laboratory, Department of Chemistry, The Ohio State University, Columbus 10, Ohio

(Received April 18, 1960)

THE similarity of chemical properties of oxygen and sulfur suggests that the variety of vapor species found in the B-O system at elevated temperatures[1–3] might also be observed in the B-S system. As B-S compounds are more volatile than their B-O analogs, investigation of their structural and thermodynamic properties is greatly facilitated. This is of considerable importance, at least as far as structure determinations are concerned, because it may be possible from a more complete spectroscopic study of the B-S system to justify certain assumptions which were necessitated in the B-O system.[4]

The reaction between ZnS(s) and B(s) at 700–900°C in graphite refractories has been used to prepare the vapor species studied here. The starting materials were degassed separately before use by heating *in vacuo*.

The vapor species resulting from the foregoing reaction were identified with a Model 12-101 Bendix time-of-flight mass spectrometer.[5] From the variation of ion intensity with electron energy, the boron-containing species resulting from primary ionization were identified as $B_2S_3^+$, $B_2S_2^+$, BS_2^+, and, as a minor constituent, $B_2S_2O^+$, which probably arises from reaction with the small amount of background oxygen. The identification of BS_2^+ as a primary species is not unequivocal. Its intensity seems too high for it to be a fragment, but its ionization potential seems anomalous, being 3 to 4 ev higher than those of the aforementioned molecules. B^+ and BS^+ were also observed, but these were clearly fragmentation products.

It was not possible to relate the ion intensities to the equilibrium partial pressures with any degree of reliability because they varied with time. This probably resulted from lack of chemical equilibrium in the solid-solid mixture and from variations in the activity of the solids as materials vaporized. All that can be said is that, estimating the relative ionization cross sections as $Zn:BS_2:B_2S_2:B_2S_3::1:1.5:2:2$,[6] the relative partial pressures of these species, under typical operating conditions were in the ratio 30:1:2:8. The stability of BS_2 is interesting if real, as the corresponding species has not been observed in the B-O system, though its existence has been inferred from spectroscopic evidence.[3]

The infrared emission of the vapors resulting from the reaction between Zn(s) and B(s) was measured in the range 650–3500 cm^{-1} using the furnace and spectroscopic equipment previously described.[4] NaCl optics were used throughout. At a temperature of approximately 1000°C, three emission bands were observed when boron of natural isotopic abundance was used. The band maxima occurs at 1314, 1215, and 993 cm^{-1}, the latter being difficult to establish because of its width and low intensity. When a sample containing 96% B^{10} was examined under similar conditions, the corresponding maxima occurred at 1361, 1252, and 1052 cm^{-1}.

These data can be interpreted readily by analogy with the spectra of B_2O_3 and B_2O_2.[4] The two highest frequency bands most probably arise from B=S stretchings and are therefore assigned to B_2S_3 and B_2S_2.

If, as seems likely from consideration of the corresponding vibrations of B_2O_3 and B_2O_2,[4] the highest frequency band is due to B_2S_3, the magnitude of the isotope shift, 47 cm^{-1}, strongly suggests that the molecular symmetry is identical with that of B_2O_3. On assignment of the 1215 cm^{-1} band to B_2S_3, one finds that the observed isotope shift is exactly equal to that predicated by the Teller-Redlich product rule for the asymmetric B═S stretch (Σu^+) of linear B_2S_2 (S═B—B═S). However, *cis* and *trans* forms, of symmetry C_{2v} and C_{2h}, respectively, cannot be eliminated as possibilities. The lowest observed frequency probably arises from a B—S stretch. The isotopic shift appears larger than might be expected for the asymmetric stretch in B_2S_3 (by analogy with B_2O_3), but this might be due in part to the presence of BS_2. Kaskan and Millikan[3] observed a strong band of BO_2 in the region of the single-bond stretch of B_2O_3. The observed emission frequencies and isotope shifts do not agree entirely with those assigned to $B_2S_3(g)$, by Greene and Margrave.[7] In view of the unexpected complexity of the vapor phase observed in our investigation, it is possible that their assumption that the species giving rise to their spectrum was only B_2S_3 may not be justified.

The ratios of partial pressures determined mass-spectrometrically as described earlier have been employed in conjunction with some preliminary Knudsen effusion data to calculate the heats of formation of the gaseous boron sulfides. Graphite of spectroscopic purity was used for the effusion cells. A distinct dependence of evaporation rate on orifice area was noted, as might be expected for a solid-solid reaction; data obtained with the smallest orifice to evaporating surface area ratio were used in the calculations. Free-energy functions of the boron sulfides were estimated with the aid of the fragmentary spectroscopic data given here; those of ZnS(s), B(s), and Zn(g) were taken from standard tables.[8,9]

The derived heats of formation (ΔH_0^0) of $B_2S_3(g)$, $B_2S_2(g)$, and $BS_2(g)$ are -11, 18, and 13 (all ± 10) kcal $mole^{-1}$, respectively. These lead to 125 and 100 kcal $mole^{-1}$ for the B═S and B—S bond energies, respectively.[10] Whether BS_2 is actually a reaction product is still not certain. However, it is interesting to note that its atomization energy is very nearly equal to the sum of the single and double bond energies given. The same is true of BO_2, if the heat of reaction given by Kaskan and Millikan[3] is correct.

The authors would like to thank Dr. David E. Mann of the National Bureau of Standards for many helpful discussions.

* This work was supported by the Chemistry Branch of the Office of Naval Research, Washington, D. C. A more complete account of this work will be reported at a later date.

[1] M. G. Inghram, R. F. Porter, and W. A. Chupka, J. Chem. Phys. **25**, 498 (1956).

[2] W. A. Chupka and J. Berkowitz, presented at the 135th Meeting of the American Chemical Society, Boston, Massachusetts, April, 1959.

[3] W. E. Kaskan and R. C. Millikan, private communication J. Chem. Phys. (to be published).

[4] D. White, D. E. Mann, P. N. Walsh, and A. Sommer, J. Chem. Phys. **32**, 481 (1960); **32**, 488 (1960).

[5] Details of the furnace and the performance of the Bendix spectrometer will be reported shortly in connection with another investigation in this laboratory.

[6] These values were estimated by comparison with total vapor compositions determined in Knudsen effusion experiments.

[7] F. T. Greene and J. L. Margrave, J. Am. Chem. Soc. **81**, 5555 (1959).

[8] D. R. Stull and G. C. Sinke, "Thermodynamic properties of the elements" (American Chemical Society, Washington, D. C.), 1956.

[9] J. L. Margrave, in "High temperature—a tool for the future" (Stanford Research Institute, Menlo Park, California), 1956.

[10] The B—B bond energy was taken as 115 kcal $mole^{-1}$, as in B_2O_2.

The Production of Vibrationally Excited S_2 in the Isothermal Flash Photolysis of S_2Cl_2

W. D. McGRATH

Department of Chemistry, The Queen's University of Belfast, Belfast, North Ireland

(Received May 2, 1960)

IT has recently been shown that vibrationally excited oxygen molecules in their electronic ground states are produced during the flash photolysis of O_3, ClO_2, and NO_2.[1,2] The analogous molecule S_2 has been observed spectroscopically in the gas-phase photolysis of various sulfur compounds such as H_2S and CS_2, but in no case was any vibrational excitation observed when the photolysis was carried out under isothermal conditions. Preliminary experiments on the photolysis of S_2Cl_2, reported here, indicate that vibrationally excited S_2 molecules are produced during the decomposition, and that these S_2* molecules show a stability comparable to that of O_2*.

An investigation of the flash photolysis of S_2Cl_2 was undertaken primarily to see if the SCl radical could be detected in the gas phase. No spectrum of this radical has so far been reported, although Sowden and Davidson,[3] using the matrix-isolation technique at 77°K have observed an absorption peak at 2370 A when S_2Cl_2 is photolyzed and have tentatively ascribed this to trapped SCl radicals. In the work reported here, it was unfortunately not possible to investigate the region below 3100 A, because of absorption by residual S_2Cl_2 and deposited sulfur.

Commercial S_2Cl_2 was purified by distillation *in vacuo* and its purity checked by comparison of its ultraviolet spectrum with that published by Koch.[4] The spectra were photographed on a large Littrow-type spectrograph (Hilger E478) using a quartz reaction vessel giving a path length of 50 cm and a flash energy of 2000 joules. When a mixture of S_2Cl_2 and nitrogen, mixture ratio 1/100, is flashed, two band systems are seen in absorption 30 μsec after the flash. One of these has been identified as part of the $^3\Sigma_g^- \rightarrow {}^3\Sigma_u^-$ system of S_2,

with values of v'' from 5 up to 12. Measurements on the band heads agree well with those obtained in emission, tabulated by Pearse and Gaydon.[5] The other system consists of broad, rather diffuse bands degraded to the red, and is tentatively attributed to the S_2Cl radical. Details of this spectrum are given in Table I.

TABLE I.

Band head (λ in A)	Intensity (visual estimate)	Description
4417.0	1	
4340.0	1	
4325.0	2	
4253.0	2	
4236.5	6	diffuse
4189.0	3	
4150.0	8	diffuse
4069.0	10	broad, diffuse
4008.5	6	fairly sharp
3996.5	6	fairly sharp
3979.0	6	fairly sharp
3953.0	1	
3912.5	10	sharp, broad band

Examination of the spectrum described above shows that it is unlikely to be due to a simple diatomic absorber such as SCl, since there is no apparent regularity in the vibrational intervals ΔG. Neither do the measurements check with any impurity which could possibly be present, such as SO, SO_2, or H_2S. It would seem, therefore, that the only absorbing species capable of being responsible for the spectrum are S_2Cl and SCl_2. The latter possibility can be ruled out, since its spectrum is identical with that of S_2Cl_2, so we may assume that the spectrum given in Table I is that of S_2Cl.

When no inert gas is used and pure S_2Cl_2 is flashed, none of the bands listed in Table I appears; instead, a very extensive S_2 spectrum is obtained with values of v'' up to 14. The complex appearance of the rotational structure of these bands is indicative of the high temperature attained in the photolysis.

Assuming that S_2Cl is the absorber, the initial photolytic cleavage is most probably

$$S_2Cl_2 \xrightarrow{h\theta} S_2Cl + Cl \cdots. \quad (1)$$

Also, since the spectrum does not appear unless a large amount of inert gas is present, it is likely that the S_2Cl_2 radical is initially formed in an unstable state. It could conceivably break down in two ways: (a) to give S_2Cl; or (b) to SCl and S. The possibility that S_2^* may be formed by decomposition (a) is not great, since the change is bond length is very small. If decomposition according to (b) occurs, the S atom so produced could further react by

$$S + S_2Cl_2 \rightarrow S_2^* + SCl_2 \cdots. \quad (2)$$

This reaction is 51 kcal/mole exothermic for ground-state S atoms, which is more than sufficient to account for the maximum vibrational excitation observed, since $v''=12$ for S_2 corresponds to 25 kcal/mole. Also this is the same type of reaction which has been shown to produce vibrationally excited molecules in other photolytic reactions.[1,2]

Other reactions similar to (2) could possibly be responsible for S_2^* production, e.g., if the S atom attacks S_2Cl or SCl_2. Reaction with S_2Cl is not likely to be important under the conditions used because of its relatively small concentration compared with that of S_2Cl_2. Reaction with SCl_2, however, could become important in the later stages of the reaction when the concentration of SCl_2 becomes appreciable. This reaction is 32 kcal/mole exothermic, which is still sufficient to account for the observed excitation of the S_2^*.

[1] W. D. McGrath and R. G. W. Norrish, Proc. Roy. Soc. (London), **A242**, 265 (1957).
[2] F. J. Lipscomb, R. G. W. Norrish, and B. A. Thrush, Proc. Roy. Soc. (London) **A233**, 455 (1956).
[3] R. G. Sowden and N. Davidson, J. Am. Chem. Soc. **78**, 1291 (1956).
[4] H. P. Koch, J. Chem. Soc. **1949**, 394.
[5] R. W. B. Pearse and A. G. Gaydon, *The Identification of Molecular Spectra* (Chapman and Hall, Ltd., London, 1950).

Rotational Isomerism Involving the 2-3 Carbon-Carbon Bond of the 1-Alkenes

L. A. HARRAH AND D. W. MAYO*

Physics Division, Materials Laboratory, Wright Air Development Division, Air Research and Development Command, Wright-Patterson Air Force Base, Ohio

(Received April 27, 1960)

THE first member of the homologous series of 1-alkenes capable of possessing rotational isomers is 1-butene. Past investigations[1-5] of this olefin have failed to establish the presence of nonequivalent conformations, although Kilpatrick and Pitzer[6] postulated their existence.

We have reexamined the infrared spectrum of 1-butene with the aim of making a complete vibrational assignment. As a result of this investigation and additional studies of other members of this unsaturated series, we wish to report that the behavior of two absorption bands observed in the KBr region of the spectrum of the 1-alkenes suggests that 1-butene very likely does exist at room temperature as two pairs of *nonequivalent* isomers.

In general, the 1-alkenes were obtained as "highest-purity" samples from the American Petroleum Institute. The spectra were recorded with Perkin-Elmer instruments, models 112 and 321, employing KBr and CsBr prisms, respectively. The wave numbers of the two bands studied are listed in Table I.

The 1-alkenes possess two bands of medium intensity near 630 and 550 cm^{-1}, with the exception of propene,

TABLE I. The infrared frequencies of the ethylenic twisting vibrations of the 1-alkenes.

	Wave number (cm^{-1}) Form I	Form II
propene	578	
1-butene	552	636
1-pentene	552	634
1-hexene	552	634
1-heptene	552	634
1-octene	552	633
1-nonene	552	632
1-decene	551	633
1-undecene	551	634
1-dodecene	552	633
1-tridecene	552	634
1-tetradecene	552	633
1-pentadecene	552	634
1-hexadecene	552	634

which has only a single, intense, type "*C*" band at 578 cm^{-1}. This latter band has been assigned to the ethylenic twisting vibration.[7,8] A comparison of the variation in intensity of the 630 and 550 cm^{-1} bands with that of the 730 cm^{-1} methylene absorption band as chain length increases, however, shows that *both* bands must arise from terminal group vibrations. As no other end-group fundamental would be expected to occur in this region, the presence of rotational isomers is indicated. In this connection the envelope of the band occurring near 550 cm^{-1} strongly resembles the previously mentioned type "*C*" band exhibited by propene.

In order to establish unambiguously the presence or absence of rotational isomers, the infrared spectra of several of the 1-alkenes have been recorded with the aid of a low-temperature cell of our own design, to be described elsewhere. In every case studied, the transition of the 1-alkene into the crystalline phase was accompanied by the disappearance of the 550 cm^{-1} band, while the 630 cm^{-1} band showed a corresponding increase in intensity. In several instances the formation of a glass (in which both isomeric forms persisted) occurred if the sample temperature was lowered too quickly or if small amounts of impurities were present. This effect was particularly evident in the higher members of the series where complete crystallization could be obtained only with difficulty. Both bands appeared to intensify slightly as the olefin was cooled, but the same peak absorbance ratio was maintained within the experimental accuracy (see Table II). The energy difference between the two forms is thus very nearly zero in the liquid.

TABLE II. Temperature dependence of the intensity ratio A_{552}/A_{634} for 1-hexene.

Temperature (°K)	A_{552}/A_{634}
290	0.331±0.01
243	0.325±0.01
208	0.342±0.01

On the basis of the above evidence the 630 and 550 cm^{-1} bands have been tentatively assigned to the ethylenic twisting vibration of two conformational isomers which arise by rotation of the vinyl group about the 2–3 carbon-carbon bond. The envelope of the 550 cm^{-1} band indicates that the isomer to which it belongs is a nearly planar modification of the molecule. An examination of Stuart and Briegleb models suggests that steric interference is least when the alkyl group is rotated approximately ±30° (form I) and ±90° (form II) from the plane of the extended *trans* configuration (see Fig. 1). The disappearance of the 550 cm^{-1} band from the spectrum of the crystalline phase therefore establishes form II as the preferred solid-state isomer.

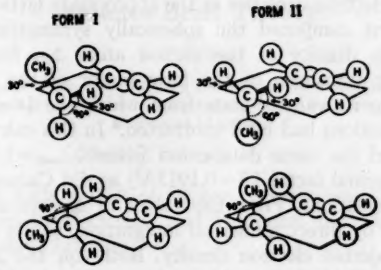

Thermodynamic calculations, vibrational assignments, and the synthesis of appropriate isotopic derivatives are now in progress.

* Present address: Department of Chemistry, Massachusetts Institute of Technology, Cambridge, Massachusetts.

[1] K. W. F. Kohlrausch and W. Stockmair, Z. physik. Chem. (Leipzig) **B29**, 292 (1935).
[2] M. Bourguel and L. Piaux, Bull. Soc. chim. France **2**, 1958 (1935).
[3] R. S. Rasmussen and R. R. Brattain, J. Chem. Phys. **15**, 120 (1947).
[4] J. G. Aston, G. Szasz, H. W. Woolley, and F. G. Brickwedde, J. Chem. Phys. **14**, 67 (1946).
[5] N. Sheppard, J. Chem. Phys. **17**, 74 (1949).
[6] J. E. Kilpatrick and K. S. Pitzer, J. Research Natl. Bur. Standards **73**, 163 (1946).
[7] P. Torkington, J. Chem. Phys. **17**, 1279 (1949).
[8] R. C. Lord and P. Venkateswarlu, J. Opt. Soc. Am. **43**, 1079 (1953).

Comments and Errata

Comments on Carpenter's Paper "Density of the Bonding Electrons in Diamond"

JAMES A. IBERS
Shell Development Company, Emeryville, California

(Received April 4, 1960)

RECENTLY Carpenter[1] obtained what he described as "the best experimentally derived view of a

chemical bond yet presented." In this note we suggest that Carpenter on the basis of his calculations could not have distinguished overlap of electrons of adjacent atoms from chemical bonding, where by "bonding" we mean redistribution of electrons among the atoms.

Carpenter's Fig. 3, the significant one for our purposes, is the projection of electron density of the valence electrons of carbon atoms in diamond onto the plane formed by a and [011]. This Fourier projection was based on experimental structure factors from which the contributions of the 1s electrons, as determined from the contributions of these electrons to the form factor of carbon,[2] had been subtracted.

To compare with this projection, we prepared electron density maps by superimposing *isolated* carbon atom electron densities at the appropriate lattice sites. We first computed the spherically symmetric outer electron density of the carbon atom $\Delta\rho_3$ from the Fourier transform of the form factor of the carbon atom in its valence state from which the 1s electron contributions had been subtracted.[2] In this calculation we used the same data cutoff $[(\sin\theta/\lambda)_{max}=1.65\text{A}^{-1}]$ and thermal factor ($B=0.1913\text{A}^2$) as did Carpenter in his calculations. From the values of $\Delta\rho_3$ we also obtained, by direct numerical integration, values of $\Delta\rho_2$, the projected electron density. Both $\Delta\rho_3$ and $\Delta\rho_2$ are given in Table I. From these data we obtained by laying down the densities at the lattice sites of diamond and summing: (1) a section of the three-dimensional density function through the central and two lower atoms of Carpenter's Fig. 3; and (2) the two-dimensional projected electron density. Both of these maps show similar features. Although the section provides more information, we show in Fig. 1 that the projection for it may be compared directly with Carpenter's Fig. 3. The agreement between our projection and Carpenter's is complete in over-all detail. (There are some numerical differences, but these are to be expected, for Carpenter's calculation is based on experimental structure factors and ours, in effect, on calculated structure factors.) Note that the density at the center of a bond is over twice that at the same distance from an atom but midway between bonds. Note particularly that along the perpendicular bisector of the bond the electron density rises to a slight maximum at the center of the bond. These are some of the features which Carpenter took to indicate bonding. It is clear, of course, that these features on our projection cannot be interpreted in terms of bonding i.e., in terms of a redistribution of electrons), for our projection is derived by the simple superposition of *isolated* atoms. Since Carpenter's calculation does not permit a separation of this overlap from the effects of bonding, we contend that he is not justified in claiming that he has obtained a view of a chemical bond.

TABLE I. Outer electron density of the carbon atom and its projection.

r(A)	$\Delta\rho_3(e/\text{A}^3)$	$\Delta\rho_2(e/\text{A}^2)$
0	1.72	2.2
0.1	1.46	2.1
0.2	1.13	2.0
0.3	1.22	1.9
0.4	1.40	1.8
0.5	1.27	1.5
0.6	1.00	1.2
0.7	0.77	0.9
0.8	0.56	0.7
1.0	0.26	0.3
1.2	0.11	0.1_5
1.4	0.05	0.0_4
1.6	0.01	0.0_1

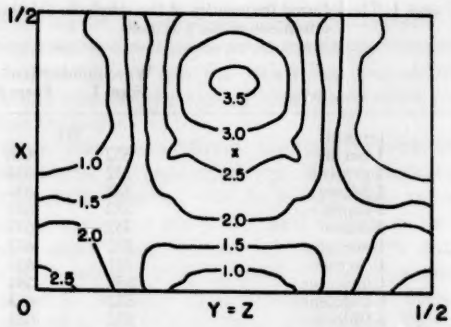

FIG. 1. Projection of the outer electron density in diamond. (The numbers refer to values of projected density in e/A².)

[1] G. B. Carpenter, J. Chem. Phys. **32**, 525 (1960).
[2] R. McWeeny, Acta Cryst. **4**, 513 (1951); Acta Cryst. **7**, 180 (1954).

Density of the Bonding Electrons in Diamond

G. B. CARPENTER

Metcalf Chemical Laboratories, Brown University, Providence 12, Rhode Island

(Received April 14, 1960)

IN 1950 Brill[1] calculated the usual difference synthesis for diamond: the difference between the electron density (in projection) derived from observed structure factors and that derived from theoretical structure factors for spherical carbon atoms. This difference synthesis appeared to show distinct evidence for slight movement of electrons into the bonds. The interpretation of my recent calculations[2] assumed implicitly that the improvements made since 1950 in the form factor of carbon and the temperature factor would not drastically affect Brill's conclusion. The calculation of Ibers[3] now shows this assumption to have been wrong. In fact, a new difference synthesis, with the new values, shows no region with density larger than 1.0

electron/A², and at this point my earlier[2] Fig. 3 shows a density of about 4.5; Ibers'[3] figure shows about 3.5 electrons/A². Thus the shift of electrons into bonds is so small as to be of doubtful significance.

Consequently, the conclusion must now be that while my Fig. 3 presents[2] the best experimentally derived *view* of a chemical bond, there is in this view no convincing evidence for a movement of electrons from the distribution expected from isolated spherical carbon atoms.

Brill[4] has just presented a revised discussion of this problem with a somewhat different emphasis.

[1] R. Brill, Acta Cryst. **3**, 333 (1950).
[2] G. B. Carpenter, J. Chem. Phys. **32**, 525 (1960).
[3] J. A. Ibers, preceding letter.
[4] R. Brill, Z. Elektrochem. **63**, 1088 (1959).

Remarks on Doubly Excited States of the Negative Atomic Hydrogen Ion

E. Holøien

Institute of Theoretical Physics, University of Oslo, Oslo, Norway

(Received May 4, 1960)

A REPORT of a search on bound states (metastable?) in the quasidiscrete region of the H^- spectrum is given in a previous communication.[1] A bound $(3p^2)^3P$ state is found, but since this state is subject to autoionization, the result is of minor importance. The investigation has been made of the lowest states of the series $(2pnp)^3P$, $(3dnd)^3D$, etc., which according to Wu do not undergo autoionization.[2] Meanwhile, Dr. Geltman has directed my attention to the fact that the latter series $(3dnd)^3D$, $(4fnf)^3F$, etc., are actually capable of autoionization.[3]

The purpose of this note is to point out this evidence. In the case of H^- where $Z=1$, the spin-orbit interaction is negligible. The approximation may then be treated in the LS-coupling scheme. This implies that the parity must be unchanged, $\Delta L=0$, and $\Delta S=0$. Radiationless transitions into the adjacent continuum (autoionization) can thus take place, such as:

A. $(3dnq)^{1,3}L \rightarrow (1skq)^{1,3}L$ or $(2pk(q+1))^{1,3}L$, where $q=L$ $(L=2,3,\cdots)$ and $n \geqq L+1$. It is to be noted that the state $(3d^2)^3D$ does not exist according to the exclusion principle.

B. $(4fnq)^{1,3}L \rightarrow (2pkq)^{1,3}L$ or $(3dk(q+1))^{1,3}L$, where $q=L$ $(L=3,4,\cdots)$ and $n \geqq L+1$.

Similarly, it can be shown that the series $(mxnq)^{1,3}L$, where $x=4,5,\cdots$, $m=x+1$, $q=L \geqq x$, and $n \geqq L+1$, are subject to autoionization.

The only states that escape autoionization are the series $(2pnq)^{1,3}L$ where $q=L$ $(L=1,2,\cdots)$ and $n \geqq L+1$. Furthermore, it is evident that they cannot be metastable even if they are bound, since they will decay by dipole transitions to lower states (lifetimes of order $10^{-7}-10^{-8}$ sec). Obviously, no metastable quasidiscrete state can exist in H^-. The $(2p^2)^3P$ state, which is the lowest one of the nonautoionization series, is probably bound and may be regarded as the initial level for dipole transition to the $(1s2p)^3P$ state (also probably bound) giving an ordinary spectrum line (sharp).

[1] E. Holøien, J. Chem. Phys. **29**, 676 (1958).
[2] T. Y. Wu, Phys. Rev. **66**, 293 (1944).
[3] S. Geltman (private communication).

Improved Molecular Orbitals and the Valence Bond Theory

A. C. Hurley

Division of Chemical Physics, Commonwealth Scientific and Industrial Research Organization, Fishermen's Bend, Melbourne, Australia

(Received February 25, 1960)

THE state $B\,^1\Sigma_u^+$ of H_2 has recently been investigated by Huzinaga[1] and Phillipson and Mulliken[2] with a wave function

$$\Theta_1^0 = 2^{-\frac{1}{2}}\{|\sigma_g\bar{\sigma}_u'| + |1\sigma_u'\bar{\sigma}_g|\}, \tag{1}$$

where

$$\sigma_g = 2^{-\frac{1}{2}}n_g(a+b), \qquad \sigma_u' = 2^{-\frac{1}{2}}n_u'(a'-b').$$

Here a, b and a', b' are hydrogenic $1s$ functions with orbital exponents ζ and $\zeta'(\pm\zeta)$.

The latter authors minimized the energy with respect to variations of ζ, ζ'. Their results (*loc. cit.*, Table I) imply that for large nuclear separations both ζ and ζ' tend to 0.6875 and that the wave function (1) leads on dissociation to a proton and the closed shell ion $H^-(1s)$.[2]

The true behavior of the function (1) on dissociation is more complicated than this and is of some interest, since it provides the simplest example of the relationship between improved molecular orbital functions and the valence bond theory.

The function (1) may be expressed in the form

$$\Theta_1^0 = \lambda_I\Psi_I - \lambda_C\Psi_C, \tag{2}$$

where

$$\Psi_I = \{4(1+t^2)\}^{-\frac{1}{2}}\{|a\bar{a}'| + |a'\bar{a}| - |b\bar{b}'| - |b'\bar{b}|\}, \tag{3}$$

$$\Psi_C = \{4(1-t^2)\}^{-\frac{1}{2}}\{|a\bar{b}'| + |b'\bar{a}| - |a'\bar{b}| - |b\bar{a}'|\}, \tag{4}$$

and $\lambda_I = 2^{-\frac{1}{2}}n_g n_u'(1+t^2)^{\frac{1}{2}}$, $\lambda_C = 2^{-\frac{1}{2}}n_g n_u'(1-t^2)^{\frac{1}{2}}$, with

$$t = \int aa'dv = \int bb'dv.$$

The functions Ψ_I and Ψ_C are normalized for infinite nuclear separation.

From Eqs. (2), (3), and (4) we see the relationship of the function (1) to the valence bond theory. The

term Ψ_I is the usual ionic function $2^{-\frac{1}{2}}\{|\, a\bar{a}\,| - |\, b\bar{b}\,|\}$, except that the closed-shell ion $H^-(1s)^2$ has been replaced by the open-shell ion $H^-(1s\ 1s')$. If this were the only term in Eq. (2) the optimum values of the parameters for large nuclear separations would be[3] $\zeta=1.0392$, $\zeta'=0.2832$.

The second term in Eq. (2) is of a novel type. For $\zeta=\zeta'$, it vanishes and we have the usual purely ionic wave function. For $\zeta\pm\zeta'$, Ψ_C is unaltered by replacing a' by $a''=a'-\alpha a$, and b' by $b''=b'-\alpha b$, where α is chosen so that

$$\int aa''dv=\int bb''dv=0.$$

It is now easily seen that Ψ_C describes two neutral hydrogen atoms; one in the $1s$ state and the other in the $2s$ state. Admittedly a'' and b'' are not exact hydrogenic $2s$ functions, but for optimum values of ζ, ζ' they are very accurate approximations.[4] Indeed, for $\zeta=0.9590$, $\zeta'=0.2807$, Ψ_C gives $E(\infty)=-0.6199$ (a.u.) in place of the accurate dissociation limit of $B\,'\Sigma^+_u$ (-0.625 a.u.). This is the most important case since, if λ_I and λ_C in Eq. (2) are varied to minimize the total energy, then as $R\to\infty$, $\lambda_I\to 0$, $\lambda_C\to 1$. Such a calculation is equivalent to a molecular orbital calculation based on Θ_1 and $\Theta_2=2^{-\frac{1}{2}}|\{\ \sigma_g'\bar{\sigma}_u\,|+|\,\sigma_u\bar{\sigma}_g'\,|\}$.

From Eq. (2) we see that the function (1) leads on dissociation to a combination of the ionic and covalent states in the ratios $\lambda_I^2/\lambda_C^2=(1+l^2)/(1-l^2)$. For large nuclear separations the total energy $E(\Theta_1)$ is given by

$$E(\Theta_1)=\tfrac{1}{2}q^2(1-\tfrac{1}{2}s)-q(1-\tfrac{1}{8}s-\tfrac{1}{32}s^2-\tfrac{5}{32}s^3)-\frac{1+s^3}{2R}+\Delta, \tag{5}$$

where $q=\zeta+\zeta'$, $s=4\zeta\zeta'(\zeta+\zeta')^{-2}$ and Δ falls off exponentially as the nuclear separation $R\to\infty$.

Neglecting Δ in Eq. (5) and minimizing $E(\Theta_1)$ with respect to variations of ζ, ζ' (i.e., q, s) we find that for $R=\infty$, $\zeta=1.0305$, $\zeta'=0.2121$ and that the approach to these asymptotic values is determined by the equations

$$s=0.5662+1012\ \ (1888R-21{:}4),$$

and

$$q=(36-4s-s^2-5s^3)\ \ (32-16s).$$

Since when Δ is neglected, Eq. (5) is symmetrical in ζ and ζ', these results apply also to the function Θ_2. Indeed as $R\to\infty$, Θ_1 and Θ_2 become degenerate. By examination of the leading term in Δ it has been shown that for very large separations ($R\approx 100$ a.u.) $E(\Theta_1)<E(\Theta_2)$, as is the case for the small separations considered by Phillipson and Mulliken.[2] However, it is possible that for intermediate values of $R(\approx 10$ a.u.) $E(\Theta_2)<E(\Theta_1)$. This would involve a discontinuous change in the optimum values of ζ and ζ'. Such behavior appears likely on physical grounds, since for $R\approx 10$, $\zeta\approx 1.03$ $\zeta'\approx 0.21$ the function Θ_1 contains one nonbonding orbital (σ_g) and one antibonding orbital (σ_u') whereas Θ_2 contains a bonding orbital (σ_g') and a nonbonding orbital (σ_u).

From the above discussion it is clear that the good results obtained from the wave function (1)[1,2] at the equilibrium nuclear separation are largely attributable to the improved description of the dissociation products.

The author is indebted to Dr. Phillipson and Professor Mulliken for a stimulating discussion.

[1] S. Huzinaga, Progr. Theoret. Phys. **20**, 15 (1958).
[2] P. E. Phillipson and R. S. Mulliken, J. Chem. Phys. **28**, 1248 (1958).
[3] H. Shull and P. Löwdin, J. Chem. Phys. **25**, 1035 (1956).
[4] H. Preuss, Z. Naturforsch. **10**, 267 (1955).

Effect of Deuterium Substitution on the Lifetime of the Phosphorescent Triplet State of Naphthalene*

H. Sternlicht and H. M. McConnell†

Gates and Crellin Laboratories of Chemistry,‡ California Institute of Technology, Pasadena 4, California

(Received May 13, 1960)

In a communication with the above title, Hutchison and Mangum[1] have reported that the replacement of protons by deuterons in naphthalene increases the phosphorescent lifetime of this substance from 2.1 sec to 16.9 sec at the temperature of boiling N_2. One of us (McC) suggested[1] to Professor Hutchison that (a) the isotope effect might conceivably arise from nuclear hyperfine interactions and (b) if so, there should be a dependence of the phosphorescent lifetime on molecular orientation in the magnetic field, since the proton hyperfine interaction is known to be strongly anisotropic. Suggestion (a) would appear to be farfetched indeed, in view of the weakness of such hyperfine interactions ($\sim$100 Mc) relative to spin-orbit matrix elements[2] ($\sim$10 000 Mc). In fact, we can give no order-of-magnitude calculation justifying (a). However, the hyperfine interaction *can* mix singlets and triplets, and the ratio of the phosphorescence lifetimes $(\tau_D/\tau_H)\sim 8.1$ *is* of the same order of magnitude as the predicted ratio of average square nuclear magnetizations $\gamma_H^2 I_H(I_H+1)/\gamma_D^2 I_D(I_D+1)=16$, where γ_H, γ_D are the magnetogyric ratios. Moreover, a detailed analysis shows that suggestion (b) above is *not* correct, so that the observed[1] independence of τ_H and τ_D on orientation does not eliminate the possibility of the nuclear hyperfine effect. This analysis indicates that when the rate of paramagnetic relaxation ($\sim 1/T_1$) among the electron and nuclear spin states of the phosphorescent triplet state is large compared to the phosphorescence rate ($1/\tau_H$, $1/\tau_D$) itself—which is almost certainly the case at liquid air temperatures—then τ_H, τ_D are independent of the spin state representation (hence independent of orientation and applied field strength). The analysis is

based on the conventional notion that τ_H, τ_D are determined by the first-order singlet component of the triplet state.[2] The independence of τ_H, τ_D on orientation and field strength is also expected if spin-orbit interaction is responsible for the mixing.

We wish to thank Professor Clyde Hutchison for many helpful discussions concerning this problem.

* Sponsored by the National Science Foundation, the United States Public Health Service, and the Office of Ordnance Research, United States Army.
† Alfred P. Sloan Fellow.
‡ Contribution No. 2582.
[1] C. A. Hutchison, Jr., and B. W. Mangum, J. Chem. Phys. **32**, 1261 (1960).
[2] D. S. McClure, J. Chem. Phys. **20**, 682 (1952).

Absorption Spectra of $MnCl_2$ and $MnBr_2$

J. W. Stout

Institute for the Study of Metals and Department of Chemistry, University of Chicago, Chicago, Illinois

(Received March 29, 1960)

RECENTLY Pappalardo[1] has reported measurements of the optical absorption spectra of $MnCl_2$ and $MnBr_2$ in the range 15 000–30 000 cm^{-1}. He interpreted the observed spectra by considering the Racah[2] parameters, B and C, the covalency parameter,[3] $\epsilon = 1 - \cos^2 \Psi$, and a cubic ligand field parameter, Dq, as adjustable parameters chosen to fit the experimental results. He concluded that, for $MnCl_2$, $\epsilon = 0.03$, and obtained in the crystal values of the Racah parameters which are different from those needed to fit the energy levels of the free gaseous ion. If one sets $\epsilon = 0$, to calculate the energy levels of the free Mn^{++} ion, then the calculated energy spacings from the ^6S ground level to the various quartet levels, using Pappalardo's B and C values, are less than those observed by amounts ranging from 0.3 to 4.2×10^3 cm^{-1}.

In the interpretation of the absorption spectrum[4] of MnF_2 we employed a different procedure, which takes the energy levels of the free Mn^{++} ion as a starting point and uses only two adjustable parameters, ϵ and Dq, to fit the observations. The positions of the levels $^4A_{1g}(^4G)$, $^4E_g(^4G)$, $^4E_g(^4D)$, and $^4A_{2g}(^4F)$ depend only on the covalency parameter ϵ whereas the $^4T_{1g}$ and $^4T_{2g}$ levels are also affected by the ligand field parameter Dq. It is the purpose of this letter to point out that the observed spectra of $MnCl_2$ and $MnBr_2$ may also be satisfactorily interpreted in this fashion.

The calculated and observed positions of the various quartet levels in $MnCl_2$ and $MnBr_2$ are given in Table I. In calculating the positions of the energy levels the energy matrices given in Table VI of the MnF_2 paper[4] have been used. The calculations have been carried only to the first order in ϵ; that is, terms in ϵ^2 of the diagonal elements and in ϵ of off-diagonal elements (except when combined with Dq) have been ignored. Although the inclusion of the higher order terms in ϵ would be, in some cases, numerically significant for $MnCl_2$ and $MnBr_2$, we do not believe that there is theoretical justification for regarding ϵ as more than a first-order correction and so have arbitrarily neglected the terms in ϵ^2. Pappalardo[1] experimentally observed considerable structure in the various absorption bands, probably arising from different vibrations associated with the electronic transitions as well as, in some cases, splittings by the crystalline field of trigonal symmetry (the point symmetry at the Mn^{++} ion is D_{3d} in $MnCl_2$ and $MnBr_2$). This latter effect should be small for the $^4A_{1g}$ and ^4E_g levels and for these levels we have listed in Table I the lowest frequency strong absorption observed by Pappalardo at 78°K. For the $^4T_{1g}$ and $^4T_{2g}$ levels, where the trigonal field has a first order effect, we have listed the weighted center of the observed bands. In view of the uncertainties introduced by the neglect of the vibrational energies and the trigonal field splittings, the agreement of the calculated and observed positions of the levels is satisfactory. In particular, the positions of the $^4A_{1g}$ and the two ^4E_g levels, whose shift from the free-atom values is calculated only from the adjustable parameter ϵ, is adequately accounted for. The values of ϵ required, 0.13 for $MnCl_2$, 0.15 for $MnBr_2$, and 0.064 for MnF_2[4] lie in an order that is reasonable from a chemical point of view.

TABLE I. Comparison of calculated and observed[1] spectra of $MnCl_2$ and $MnBr_2$.

	Wave number in 10^3 cm^{-1}			
	$MnCl_2$		$MnBr_2$	
Upper-state designation	$\epsilon = 0.13$ Calc	$Dq = 0.83$ $\times 10^3$ cm^{-1} Obs	$\epsilon = 0.15$ Calc	$Dq = 0.94$ $\times 10^3$ cm^{-1} Obs
$^4T_{1g}(^4G)$	17.9	18.5	16.5	...
$^4T_{2g}(^4G)$	22.6	22.0	21.5	21.65
$^4A_{1g}(^4G)$	23.5	23.59	23.0	23.084
$^4E_g(^4G)$	24.0	23.825	23.6	23.35
$^4T_{2g}(^4D)$	27.8	26.75	27.2	26.52
$^4E_g(^4D)$	28.1	28.065	27.4	27.505
$^4T_{1g}(^4P)$	31.3	...	31.6	...
$^4A_{2g}(^4F)$	34.2	...	32.8	...
$^4T_{1g}(^4F)$	42.2	...	42.1	...
$^4T_{2g}(^4F)$	42.2	...	42.3	...

There is an error in the lower of the two eigenfunctions listed by the $^4E_g(^4D, ^4G)$ matrix on p. 714 of footnote reference 4. The asterisks, indicating reversed spin, should be on v in the first term and on u in the second, rather than on ξ and η.

This research was supported in part by the Office of Naval Research.

[1] R. Pappalardo, J. Chem. Phys. **31**, 1050 (1959).
[2] G. Racah. Phys. Rev. **62**, 438 (1942); **63**, 367 (1942); **76**, 1352 (1949).
[3] S. Koide and M. H. L. Pryce, Phil. Mag. **3**, 607 (1958).
[4] J. W. Stout, J. Chem. Phys. **31**, 709 (1959).

Validity and Consequences of Schreinemakers' Theorem on Ternary Distillation Lines

[J. Chem. Phys. **31**, 308 (1959)]

A. E. KORVEZEE

Laboratory of Physical Chemistry, Technological University, Delft, Netherlands

AND

J. L. MEYERING

Philips Research Laboratories, N. V. Philips' Gloeilampenfabrieken, Eindhoven, Netherlands

(Received April 25, 1960)

THE number (9) has been moved in printing to the set of calculated x values on p. 310. It should indicate the differential equation in the second footnote on p. 309. Equation (9) was cited by O. Redlich [J. Chem. Phys. **31**, 314 (1959)].

Microwave Spectrum of Acetyl Cyanide

[J. Chem. Phys. **31**, 882 (1959)]

LAWRENCE C. KRISHER

Columbia Radiation Laboratory, Columbia University, New York 27, New York

(Received April 27, 1960)

AN incorrect conversion factor from Mc to cal/mole has been used. The first paragraph of p. 887 should read "a reasonable value for the barrier would be 1210±30 cal/mole." In Table V, p. 886, the values for V_3 should be 1212, 1214, 1226, 1204 rather than the reported 1271, 1273, 1285, 1263. Since this was a final conversion, no other results in the paper are affected. The erroneous result has also been reported in the review paper by C. C. Lin and J. D. Swalen [Revs. Modern Phys. **31**, 841 (1959)].

Notes

Explanation of the Nonadditivity of Bond Lengths

HENRY A. BENT

School of Chemistry, Institute of Technology, University of Minnesota, Minneapolis, Minnesota

(Received February 22, 1960)

BOND lengths may sometimes show marked deviations from simple additivity. For example, one-half the sum of the carbon-carbon and fluorine-fluorine distances in ethane and fluorine, respectively, is 0.17 A greater than the observed C–F distance in carbon tetrafluoride.

$CH_3—CH_3$ $\quad 1.54 \div 2 = 0.77$

$:\ddot{F}—\ddot{F}:$ $\quad 1.44 \div 2 = 0.72$

$CF_3—\ddot{F}:$	C–F Distances (in A)	1.49 Predicted 1.32 Observed
$CH_3—\ddot{F}:$		1.39 Observed

Similar foreshortenings have been reported in other cases.[1]

Noting that the foreshortenings occurred most frequently for bonds joining atoms that differ in electronegativity, Schomaker and Stevenson proposed the following empirical rule for predicting bond lengths[1]:

$$r_{ab} = r_a + r_b - 0.09 \mid x_a - x_b \mid .$$

It is the purpose of this communication to suggest a possible explanation for this rule and to point out certain instances where the rule does not apply.

For example, the rule predicts no difference for the C—F bond length in carbon tetrafluoride and methyl fluoride, whereas the actual difference in bond length is 50% of the electronegativity correction for the C—F bond. It may also be noted that, were repulsions between the fluorine atoms the important factor operating, the C—F bond in carbon tetrafluoride would be expected to be longer than the C—F bond in methyl fluoride, whereas the C—F bond in carbon tetrafluoride is actually the shorter of the two, by 0.07 A. This foreshortening may be ascribed to a change in hybridization of the carbon atom. From symmetry, carbon must use four equivalent sp^3 orbitals in CF_4, while in CH_3F the large difference in electronegativity between hydrogen and fluorine causes the carbon atom to concentrate its s character preferentially in the C—H bonds at the expense of the C—F bond, which therefore becomes richer in p character from the carbon side and longer.[2] Evidence that atoms tend to concentrate their s character in orbitals directed toward weakly electronegative groups (unshared electrons are regarded as electrons in a bond to an atom of vanishing electronegativity) is provided by the bond angles in such compounds as OX_2. For $X = CH_3$, H, and F, the XOX angles are 111°, 105°, and 103.2°, respectively.[3,4] In the NX_3 series the corresponding angles are 109°, 106°46′, and 102°30′.[4,5] Further examples are cited by Mellish and Linnett. Evidence that atom hybridization affects bond lengths, as well as bond angles, bond length increasing with increasing p character, has been summarized recently by Brown.[6]

A purely formal extension of the Schomaker-Stevenson rule leads to the wrong conclusion regarding the relative bond lengths in CF_4 and CH_3F. Since hydrogen

is less electronegative than fluorine, the effective electronegativity of the carbon atom toward fluorine in CH_3F is less than the effective electronegativity of the carbon atom toward fluorine in CF_4; i.e., the electronegativity difference between CH_3 and F is greater than that between CF_3 and F; hence, the subtractive term in the Schomaker-Stevenson rule should be larger and the C–F distance shorter in CH_3F than in CF_4, contrary to observation.

It is natural to consider whether the explanation offered above for the foreshortening of the C—F bond in methyl fluoride compared to that in carbon tetrafluoride is also applicable to the deviations from simple additivity considered by the Schomaker-Stevenson rule.

Is it possible, for example, that the fluorine atom, in passing from F_2 to CF_4, rehybridizes in such a way as to shorten its effective covalent radius? Qualitatively, yes. In F_2, the fluorine atom is joined to an atom that is highly electronegative. Consequently, most of the *s* character of the fluorine atom in F_2 is captured by the unshared electrons. In CF_4, however, the bonding orbital tilts down steeply toward fluorine. This increases the demand made by the bonding electrons for *s* character from the fluorine atom, and as the fluorine atom rehybridizes to meet this demand the bond to carbon becomes richer in *s* character from the fluorine side and shorter. Whether or not this explanation can account quantitatively for the relatively large observed deviations from additivity is a matter that we hope to investigate more fully at a later date.

[1] V. Schomaker and D. P. Stevenson, J. Am. Chem. Soc. **63**, 37 (1941).

[2] Admittedly, from the *fluorine side*, the H_3C—F bond is richer in *s* character than the F_3C—F bond (owing to the difference in electronegativity of carbon toward fluorine in these two compounds); however, unless the effective covalent radius of fluorine is much more strongly hybridization dependent than that of carbon, this will be of only secondary importance so far as the C—F bond length is concerned, since the initial perturbation (the change from CF_4 to CH_3F) is a perturbation *on carbon*.

[3] L. E. Sutton, editor, "Tables of Interatomic Distances and Configuration in Molecules and Ions," Special Publication No. 11, The Chemical Society, Burlington House, W.1, London, 1958.

[4] J. A. Ibers, and V. Schomaker, J. Phys. Chem. **57**, 699 (1953).

[5] C. E. Mellish and J. W. Linnett, Trans. Faraday Soc. **50**, 657 (1954). See also, V. Schomaker and Chia-Si Lu, J. Am. Chem. Soc. **72**, 1182 (1950).

[6] M. G. Brown, Trans. Faraday Soc. **55**, 694 (1959). See, also, C. C. Costain and B. P. Stoicheff, J. Chem. Phys. **30**, 777 (1959).

Some Thermal Data for Bi_2Te_3

G. F. Bolling

Crystallogenic Section, Metallurgy Department, Westinghouse Research Laboratory, Pittsburgh, Pennsylvania

(Received March 14, 1960)

RECENTLY, some thermal experiments have been performed on Bi_2Te_3. The results of these experiments are discussed here.

Latent Heat of Fusion. I. The first method of determination was similar to that devised by Oelsen *et al.*[1] Above a calorimeter, shown in Fig. 1, a vertical tube furnace containing argon was arranged to swing over the copper can from a position away from the calorimeter and from this furnace a container filled with Bi_2Te_3 was dropped into the can. This container was made from thin-walled graphite surrounded by a double wall of thin stainless-steel sheet filled with Vycor wool. A fine thermocouple was centered in the Bi_2Te_3.

The method of measurement depends upon developing a steady-state heat transfer to the calorimeter during freezing and during this process the temperatures of the charge T and of the calorimeter θ are measured. Under steady-state the total change in θ from the beginning to the end of freezing is due only to latent heat. The result for Bi_2Te_3 is the average of seven runs using two different masses of charge. As a check, the values of L were obtained for Zn(99.999%) and for Al(99.999%) which had previously been accurately determined by this method,[2] i.e.,

L kcal/mole

	Zn	Al	Bi_2Te_3
Present work	1.69±0.04	2.65±0.02	29.7±0.2
Oelsen et al.[2]	1.70±0.01	2.63±0.03	

II. The second method of determination was a variation of the drop technique.[3] A capsule consisting of a boron nitride container sealed in a welded, stainless-steel can was heated in the furnace, (controlled within ±2°C), and dropped into the calorimeter with the copper can in position II. The dry can was then capped and pushed into position I in the calorimeter. Heat losses due to splashing, evaporation, and boiling within the confines of the copper can were eliminated in this manner when water entered the can.

θ was measured both before dropping the capsule and after equilibrium was reached in the calorimeter for several runs from various furnace temperatures in the range 500° to 640°C. A plot of total heat content vs temperature is discontinuous at the melting point, 586°C, and runs made in this vicinity at intervals of 5°C or less provided a good extrapolation. After standard corrections the latent heat was obtained as $L=28.4(\pm 0.8$ estimated) kcal/mole. No change was observed in the weight of each component of the capsule, and there was no sign of reaction between the Bi_2Te_3 and the BN or the stainless steel after all the runs.

III. Assuming that solid Bi_2Te_3 is completely ordered at the melting point, the entropy of fusion was calculated[3] and compared to the measured quantities:

ΔS_f	calculated	33.55±1.65	cal/mole °C.
ΔS_f	drop method	33.1 ±0.9	cal/mole °C
ΔS_f	cooling method	34.6 ±0.2	cal/mole °C.

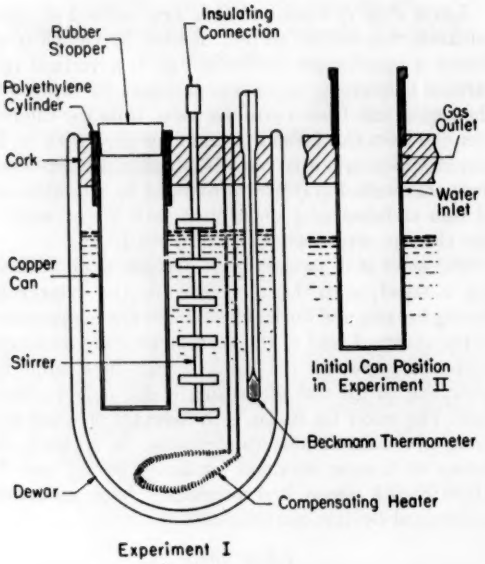

FIG. 1. The calorimeter.

The agreement among the three values is good. However, the agreement between the measured values is not within the precision involved. This can be understood, because the cooling method yields high values for a poor thermal conductor where there is difficulty in achieving the steady state. On the other hand, the drop method tends to yield low values.

The average experimental value of the latent heat of fusion is

$$L=29.0\pm1.0 \text{ kcal/mole}=36.2\pm1.25 \text{ cal/g}.$$

Specific Heat. The drop technique was used in the same calorimeter to determine the specific heat C_p of Bi_2Te_3. The charge was sealed in a Vycor capsule which was heated to different temperatures in the vertical tube furnace. The total heat content was then measured between a specific temperature in the range 100–550° and 28.3°C. An identical empty Vycor capsule was given the same treatment in order to obtain the heat content of the capsule.

From the difference between the two curves the following equation, numerically accurate within ±2%, was determined for the specific heat:

$$C_p=36.0_0+1.30_5\times10^{-2}T-3.11_5\times10^{-5}T^2 \text{ cal/°K/mole}.$$

This work was supported by the U. S. Department of Navy, Bureau of Ships.

[1] W. Oelsen, K. H. Rieskamp, and O. Oelsen, Arch Eisenhuttenw. **26**, 253 (1955).
[2] W. Oelsen, O. Oelsen, and D. Thiel, Z. Metallk. **46**, 555 (1955).
[3] O. Kubaschewski and E. Ll. Evans, *Metallurgical Thermochemistry* (Butterworths Scientific Publications, Ltd., London, 1951), pp. 170–177.

On the Existence of Polyoxides of Hydrogen*

SIDNEY W. BENSON

Chemistry Department, University of Southern California, Los Angeles 7, California

(Received February 22, 1960)

THERE has been considerable discussion in the past few years concerning the existence and isolation of the higher homologues of H_2O_2, such as H_2O_3 and H_2O_4.[1,2] The claims by the Russian workers[1] to have isolated such polyoxides have been effectively refuted by recent experiments.[2] It is therefore of some interest to consider the possible existence of these compounds from other points of view.

Benson and Buss[3] have demonstrated that the law of additivity of bond enthalpies is obeyed to within a few kcal even when species of vastly different electronegativities are bonded to the same atom. Thus it is possible from their values quoted for the O—H and O—O bonds to deduce $\Delta H_f^0(H_2O_3)=-11$ kcal and $\Delta H_f^0(H_2O_4)=+10.5$ kcal. The values obtained using only the thermal data for H_2O and H_2O_2 yields $\Delta H_f^0(H_2O_3)=-7$ kcal and $\Delta H_f^0(H_2O_4)=+18.1$ kcal and are probably to be preferred.[4] In either case one sees that H_2O_4 is unstable with respect to disproportionation into $2HO_2$ radicals[5] by some 6.5 to 14 kcal. However H_2O_3 is stable with respect to a split into $OH+HO_2$ radicals, but only by some 17 to 21 kcal. Either value for the instability of H_2O_4 is such as to render its existence extremely doubtful. The split into free radicals would require no nuclear shifts and would thus be expected to occur without any activation energy.[6]

The values for H_2O_3, however, suggest that although it might decompose readily at temperatures above 0°C there is a chance of finding it at much lower temperatures. Unfortunately, the methods which have been proposed for obtaining it can be shown to lead to situations where other products would be kinetically favored. Thus, the reaction of H atoms with O_3 at low temperatures[1] is sufficiently exothermic that the favored products would be be $OH+O_2$ and not the hoped-for intermediate HO_3.[7] The only alternative method of synthesis, which is production of comparable quantities of HO and HO_2 radicals in the same vessel (e.g., by the photolysis of H_2O_2), is not expected to yield appreciable quantities of H_2O_3. The reason for this is that under conditions where these radicals could be produced in comparable quantities, the competing processes $HO+H_2O_2\rightarrow H_2O+HO_2$ and $HO+HO_2\rightarrow H_2O+O_2$ would tend to keep the yield of H_2O_3 very low. This would be further aggravated by the secondary attack of the radicals on the H_2O_3, which would also tend to keep its stationary concentration extremely low.[8]

The weight of the thermodynamic and kinetic evidence thus suggests that H_2O_4 cannot exist, while H_2O_3,

which might exist at low temperatures, cannot be made by any methods thus far suggested.

* This work was supported by a grant from the U.S. Atomic Energy Commission.

[1] Kobozev, Nekrasov, and Eremin, Zhur. Fiz. Khim. **30,** 2580 (1956); Kobozev, Skorokhodov, Nekrasov, and Makarova, Zhur. Fiz. Khim. **31,** 1843 (1957); **32,** (I) 87 (1958).

[2] J. G. Marshall and P. V. Rutledge, Nature **174,** 2013 (1959); P. A. Giguère and D. Chin, J. Chem. Phys. **31,** 1685 (1959).

[3] S. W. Benson and J. H. Buss, J. Chem. Phys. **29,** 546 (1958).

[4] In obtaining a value for O—O (Ref. 4) the data for organic peroxides and hydroperoxides have probably been weighed more heavily than they deserve.

[5] Using $\Delta H_f(HO_2) = +2$ kcal and $\Delta H_f(OH) = +8$ kcal.

[6] Since the proponents of H_2O_4 have suggested its occurrence from the reverse process, $2HO_2 \rightarrow H_2O_4$, any activation energy would be prohibitively large at the low temperatures used. Note that H_2O_4 is close to unstable with respect to a split into $2OH+O_2$.

[7] It is possible to show from bond energy considerations that HO_3 is unstable with respect to decomposition into $HO+O_2$ and thus not a utilizable intermediate.

[8] A simple kinetic treatment shows that the maximum possible concentration of H_2O_3 formed from $OH+HO_2$ would be less than about five times the concentration of the HO_2 radical itself. This neglects the fact that radical attack on H_2O_3 leads to a chain via $HO_3 \rightarrow HO+O_2$.

Limitations of the Reflected-Shock Technique for Studying Fast Chemical Reactions

THEODORE A. BRABBS, STEVEN A. ZLATARICH, AND FRANK E. BELLES

Lewis Research Center, National Aeronautics and Space Administation, Cleveland, Ohio

(Received February 26, 1960)

USE of the region behind a reflected shock wave for chemical kinetic studies presupposes that the temperature is known. Three easily measured properties are available from which the temperature can be calculated with one-dimensional theory: incident Mach number M_s, reflected Mach number M_{rs} (defined in each case as wave velocity divided by sound speed at initial conditions), or reflected shock pressure p_5. Two previous articles have dealt with the validity of such calculations for the case of argon. Strehlow and Cohen[1] used measured M_{rs} to compute temperatures 300–500°K lower than those computed from measured M_s. Skinner[2] measured p_5 and found it to give temperatures only 30–50°K lower than those calculated from M_s. It was believed that further information bearing on this point might be derived from simultaneous measurements of all three properties, also in argon.

The shock tube used is made of $2\frac{1}{2}$-in. i.d. stainless-steel tubing, with a 15-ft expansion section and a $5\frac{1}{2}$-ft driver. Incident and reflected shock velocities were measured with two Berkley time-interval meters adjusted to different trigger sensitivities and operated by miniature piezoelectric pressure transducers.[3] Pressures were measured with a SLM[4] transducer placed 6 in. from the end plate. This pickup, which has the property of static response, was calibrated by means of a dead-weight gauge. The p_5 measurements were taken from photographs of oscilloscope traces and, owing to finite line widths and a slight ringing of the pickup, they contain an uncertainty of about 2%.

Both incident and reflected shock velocities were measured over two regions in the shock tube, in separate experiments. The near region had two probes located 6 and 10 in. from the end plate, while the far region had the probes 6 and 25 in. from the end plate. The greatest uncertainty existed in measurements taken of the velocity of the fast-moving incident shock as it traversed the 4 in. of the near position; it was about 1%.

Figure 1 shows all the data plotted in terms of M_s against the ratio $P_{51}(p_5/p_1$, where the initial pressure p_1 was 150 mm Hg in all cases). The dashed curve is simply the ideal one-dimensional relation between P_{51} and M_s. The other two curves show P_{51} computed from measured M_{rs} against simultaneously measured M_s for the near and far regions. If the reflection were ideal, all three curves would coincide. However, that the curve for the far region lies closer to theory than that for the near region, and that both lie below the ideal, could be explained by a deceleration near the back wall, followed by the measured acceleration. Such a phenomenon is predicted by Mark[5] for argon between $M_s = 1.4$ and 2.8. Since most of the data are not in this Mach number region, the shock speed variations herein encountered must be a result of another phenomenon.

The measured values of P_{51} are denoted by crosses in Fig. 1; these are pressures corresponding to the vertical rise of the oscilloscope trace when the reflected shock passes the pickup. It can be seen that these measured P_{51}'s fall essentially on the curve for reflected shock pressures calculated from the far position

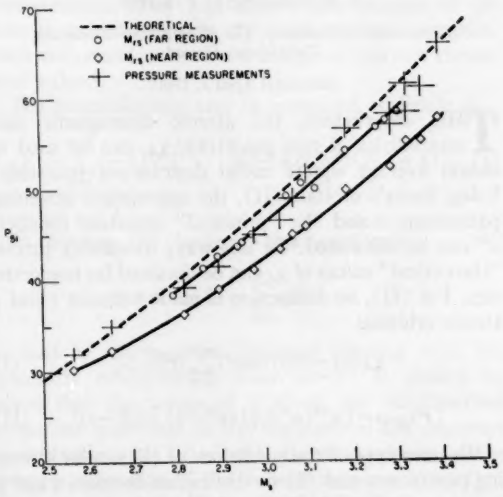

FIG. 1. P_{51} values for argon calculated from M_s, M_{rs} (near region), M_{rs} (far region) and pressure measurements.

velocities, even though the pressure pickup was at the near position. This concord between the pressure measured at the 6-in. position and the far-position reflected-shock speed indicates that the wave, as it passed the SLM pickup, was traveling at a speed near this average value. This would mean that the pressure, as well as the shock speed, depends upon the location selected to make the measurement. The departures of measured P_{61}'s from the ideal, when translated to temperature, were averaged for M_s ranges 2.5–3.0 and 3.0–3.5 and amounted to about 40° and 60°K respectively, just as Skinner concluded.

Following the initial pressure jump, the traces show a continued slow rise, such as Skinner described. At 500 μsec after the jump, many of the traces indicated a pressure slightly larger than that expected for an ideal reflection.

In conclusion, it appears that the values of both M_{rs} and p_5 depend upon the position selected to record the measurement. It is believed that reaction temperatures derived from pressure measurements are better than those from M_{rs} measurements, because the pressure reflects the time-temperature history over the region in question.

[1] R. A. Strehlow and A. Cohen, J. Chem. Phys. **30**, 257 (1959).
[2] G. B. Skinner, J. Chem. Phys. **31**, 268 (1959).
[3] Made by us, using Clevite Corporation's PZT-5 crystal elements.
[4] Purchased from Kistler Instrument Company, Model No. 680.
[5] Herman Mark, "The interaction of a reflected shock wave with the boundary layer in a shock tube," NACA TM 1418 (1958).

Quantum-Mechanical Approximations to Chemical Systems*

R. E. Glick and D. F. Kates

Department of Chemistry, The Florida State University, Tallahassee, Florida

(Received April 7, 1960)

THE observables, the atomic diamagnetic susceptibilities of rare gases (I), χ_A, can be used to obtain average square radial distribution functions.[1] Using Slater's orbitals (II), the appropriate screening parameters s and the "principal" quantum numbers n^* can be calculated.[1] In this way, reasonably precise "theoretical" values of χ_A can be obtained for isoelectric ions. For (II), no distinction is made between s and p atomic orbitals.

$$\chi_A=(-e^2N/6mc^2)\sum_{n^*}\langle r^2\rangle_{n^*}, \qquad \text{(I)}$$

$$\langle r^2\rangle_{n^*}=[n^{*2}(n^*+\tfrac{1}{2})(n^*+1)]/(Z-s)^2. \qquad \text{(II)}$$

We have applied the conditions of (1) similar screening parameters and (2) no distinction between s and p electrons to the calculation of the molecular susceptibility of ethylene. Condition (1) is quite easily met, but condition (2) requires that the description of the electrons for the carbon-carbon bond must not be the usual $\sigma(sp^2)$ and π atomic orbitals but must be, for example, two equivalent sp^3 atomic orbitals inclined at one-half the tetrahedral angle from a line joining the carbon atoms and in a plane perpendicular to the molecular plane—the "bent-bond" structure for ethylene.[2] Using such orbitals and the variation method of Guy and Tilleiu[3] for the calculation of molecular susceptibilities, we have determined the theoretical value for the diamagnetic susceptibility of ethylene, χ_M, to be -20.48×10^{-6}. This would yield better agreement with the experimental values for ethylene-type molecules.[3]

There appears to be some arbitrariness as to which function is more appropriate in the description of the properties of a substance as ethylene. The σ–π structure would seen more appropriate in the description of the ultraviolet spectra of ethylene, while the "bent-bond equivalent orbital (EO)" approach seems preferable in this instance.

But is there indeed a question of arbitrariness? We believe not. We suggest that both representations are correct and for frequencies associated with electronic excitation the molecule appears to have an electron distribution approximated by σ–π, but over the longer time of molecular vibration-rotation the EO description more exactly represents the electron distribution.

Thus it is suggested that a "resonance" description of ethylene is required, as part of the zero-point character of the molecule, with the σ–π electron orbital description appropriate for high frequency experiments and the EO for lower frequencies, i.e., for most "chemically" important phenomena. An extension to similar chemical systems can be made.

* Support by a grant from the Research Corporation is gratefully acknowledged.
[1] J. C. Slater, Phys. Rev. **32**, 349 (1928); **38**, 57 (1930).
[2] J. A. Pople, Quart. Rev. **11**, 273 (1957).
[3] J. Guy and J. Tillieu, Compt. rend. **242**, 1279 (1956); J. Chem. Phys. **24**, 1117 (1956).

Mass-Spectrometric Study of the Osmium-Oxygen System*

R. T. Grimley, R. P. Burns, and Mark G. Inghram

Department of Physics, University of Chicago, Chicago, Illinois

(Received April 13, 1960)

WITH the exception of the osmium and ruthenium tetroxides, the existence of platinum metal oxides in the vapor phase has been a matter of conjecture.[1] In addition, reliable thermodynamic data for either the solid or gaseous platinum metal oxides are virtually nonexistent. Based on the limited information available, Brewer[1] has predicted that, at temperatures in excess of 1500°K and 1 atm oxygen, the M_xO and

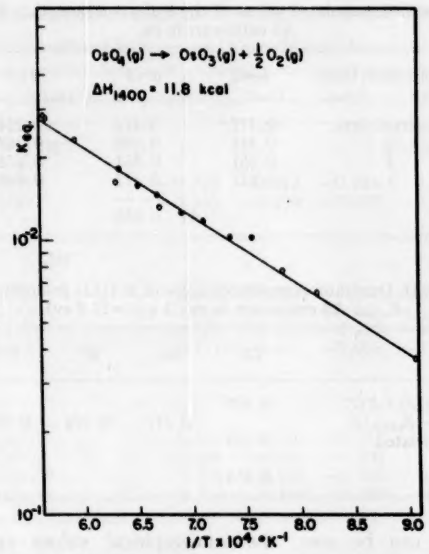

FIG. 1. Equilibrium constant, $K = P_{O_2} P_{O_3}^2 / P_{O_3O_4}$ (pressures in atmospheres) as a function of $1/T \times 10^4 °K^{-1}$.

M_xO_2 gaseous suboxides would be the only important species in the osmium-oxygen system. This paper presents the results of a study of the osmium-oxygen system.

The mass spectrometer and associated experimental techniques have previously been described,[2] with the exception that a gas-inlet system was added to permit admission of oxygen within the Knudsen cell at controlled pressures. The internal liner of the cell, which contained the sample of finely powdered Johnson, Matthey spectroscopic osmium, was made of Morganite alumina,[3] while the cell itself was fabricated from molybdenum.

In the temperature range 1100–1750°K, the main ionic species produced from the vapor effusing from the Knudsen cell were OsO_3^+ and OsO_4^+ with approximate appearance potentials of 12.3±1 and 12.6±1 ev. The ion-intensity ratio of OsO_3^+ to OsO_4^+ was a function of the oxygen pressure and the temperature, thus confirming the presence of at least two stable osmium oxide molecules in the vapor phase. Taking into account the appearance potentials, we ascribe these ions to simple ionization of OsO_3 and OsO_4.

At higher temperatures (>1700°K) there is evidence to support the existence of a stable OsO_2 molecule. The intensity of the OsO_2 species is $\leq 1/1000$ of the OsO_3 intensity. Under the conditions of this study, no other lower oxide species, as suggested by Brewer, could be detected.

A plot of the equilibrium constants vs $1/T$ for the reaction $OsO_4(g) \rightarrow OsO_3(g) + \frac{1}{2}O_2(g)$ is given in Fig. 1. The circles represent values determined at an average oxygen pressure of 3.5×10^{-5} atm, whereas the solid data points were taken at an average oxygen pressure of 1.2×10^{-5} atm. The invariance of the equilibrium constant over a threefold change in oxygen pressure would tend to indicate that equilibrium had been established in the gas phase reaction. The $\Delta H_T°$ ($T = 1400°K$) for the reaction was found to be 11.8±1 kcal/mole.

A more complete study of the platinum metals-oxygen systems will appear in forthcoming publications.

* Supported in part by the Office of Ordnance Research, U. S. Army, and in part by the National Science Foundation.

[1] L. Brewer, Chem. Revs. **52**, 1 (1953).

[2] M. G. Inghram and J. Drowart, "Mass spectroscopy applied to high temperature chemistry," appearing in *Proceedings of an International Symposium on High Temperature Technology at Asilomar, California* (McGraw-Hill Book Company, Inc., New York, 1959), p. 219ff.

[3] Morganite Incorporated, Long Island City, New York.

Some Remarks on the Electron Affinity of Atomic Lithium*

E. HOLØIEN

Institute of Theoretical Physics, University of Oslo, Norway

(Received March 9, 1960)

AN earlier report quoted an roughly made approximation of the electron affinity of atomic lithium.[1] So far, this quantity has not been measured in the laboratory. Unfortunately, the method of photodetachment does not appear to be as applicable to Li^- as to many of the heavier negative ions.[2]

From a theoretical point of view, however, it is possible to compute the affinity with a precision limited by the extremely hard numerical work.

In Lithuania, Jucys *et al.* have recently computed $EA(\mathrm{Li}) = 0.462$ ev when using Hartree-Fock solutions in a three-configurational approximation with amending configurations $1s^22p^2$ and $2s^22p^2$.[3] The purpose of this note is to reinvestigate the semiempirical computations and consider the results in light of this new theoretical value.[4]

The extrapolations may be expressed explicitly as

$$J_n(Z) = \sum_{k=1}^{n+1} (-1)^{k+1} \binom{n+1}{k} (1+kZ^{-1})^{n-2} J(Z+k), \quad (1)$$

provided $n \geqq 2$.

In this way, the physically significant series

$$J_n(Z) = \sum_{i=0}^{n} c_i Z^{2-i}$$

is used as extrapolation formulas starting with the quadratic extrapolation when $n = 2$.[5] It should be noted that the values of $J(Z+k)$ are the observed ionization potentials of the members of the sequence isoelectronic with Li^- ($Z = 3$). Recent revisions of the spectroscopic data of the helium sequence show that the figures given by Moore for the beryllium sequence are by no means all significant.[6] It has therefore been

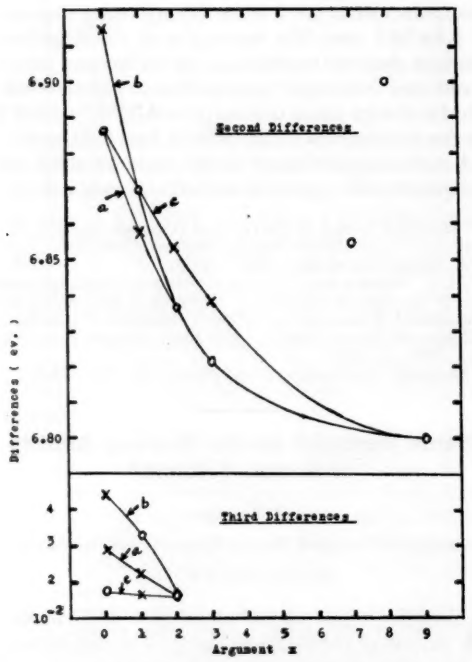

FIG. 1. Second and third differences of $J(Z+k)$. Circles and crosses denote observed and corrected data, respectively.

found helpful to check the empirical data for smoothness and possibly correct them before extrapolation. Unfortunately no observed value for Ne^{6+} is available.[6] As the starting point, we have plotted the second and third differences of $J(Z+k)$:

$$\Delta^m J(x)=\sum_{i=0}^{m}(-1)^i\binom{m}{i}J(6+x-i), \qquad (2)$$

with $m=2$ and 3, respectively (Fig. 1).

The differences can be smoothed in three possible ways denoted by the curves *a*, *b*, and *c*. Two points (circles, $x=7$ and 8) derived from data of multiply ionized atoms of the sequence appear to be quite incorrect and have been omitted. When smoothed, the third differences give almost straight lines. Results obtained from extrapolations of observed and corrected data to Li^- are condensed in Table I.

The average value at the maximum ($n=3$) is $EA(\mathrm{Li})=0.476$ ev. We shall not deal here with the validity of this result but merely consider a value of equal magnitude extrapolated from data of the berylliumlike series.

$$E(Z)=(-1.25Z^2+1.559274Z-0.8260-0.2800Z^{-1})$$

a.u. This series has been deduced empirically from the best results obtained by Jucys *et al.* for Be-like atoms.[7] The extrapolated values are given in Table II.

TABLE I. Extrapolated values of the ionization potential of Li^-. All entries are in ev.

Extrapolated from	$n=2$	$n=3$	$n=4$
Observed data	0.377	0.412	0.224
a	0.341	0.409	0.363
b	0.461	0.561	0.472
c	0.377	0.412	0.348
		Av 0.476	

TABLE II. Quadratic extrapolated value of $EA(\mathrm{Li})$ from $E(Z)-E_{\mathrm{exptl}}$. All entries are in ev (1 a.u.=27.2 ev).

	Li^-	Be	B^+	C^{2+}
$E_{\mathrm{exptl}}(\mathrm{Li})-E(Z)$	0.339			
$E(Z)-E_{\mathrm{exptl}}(Z)$		0.317	0.576	0.922
Extrapolated	0.139			
$EA(\mathrm{Li})$	0.478			

As can be seen, the semiempirical values agree fairly well with each other and also with the theoretical one. This makes it plausible that $EA(\mathrm{Li})$ is actually about the magnitude of 0.48 ev, rather than 0.74 ev as previously expected.[8]

* Work supported by grant from the Norwegian Research Council for Science and Humanities.

[1] E. Holøien, Nature **183,** 173 (1959).
[2] L. M. Branscomb and S. J. Smith, J. Research Nat. Bur. Standards **55,** 165 (1955).
[3] A. Jucys and T. Strocktyte, Lietuvos TSR Mosklu Akad. Darbai **B1,** 17 (1958).
[4] H. O. Pritchard, Chem. Revs. **52,** 529 (1953); S. Geltman, J. Chem. Phys. **25,** 782 (1956).
[5] D. Layzer, M. N. **114,** 692 (1954).
[6] G. Herzberg, and H. R. Moore, Can. J. Phys. **36,** 1293 (1959). C. E. Moore, Natl. Bur. Standards Circ. No. 467 (1949), Vol. I.
[7] G. G. Hall, lecture at International Summer Institute in Quantum Chemistry, Skogshem, Sweden (1959).
[8] B. L. Moiseiwitsch, Proc. Phys. Soc. (London) **A67,** 25 (1954).

On Excited Bound States of Negative Atomic Ions*

E. HOLØIEN

Institute of Theoretical Physics, University of Oslo, Norway

(Received March 9, 1960)

RECENTLY, particular attention has been paid to the existence of probably excited bound states in the H^- spectrum.[1] As is well known, the H^- controls the continuous opacity for the visible spectra of the sun and similar, cooler stars, and this problem is thus of current astrophysical interest.

Apart from the continuum, the energy spectra of negative ions consist, in general, of discrete states lying below and imbedded in the continuum of the

TABLE I. Extrapolated detachment potentials of excited states. All entries are in ev (1 ev=8066 cm^{-1}).

States	$n=2$	$n=3$	$n=4$	$n=5$
H^-				
$(1s2p)^3P$	−0.228	+0.012	−0.024	−0.206
$(1s2s)^3S$	−0.245	−0.196	−0.308	−0.534
He^-				
$(1s^22p)^2P$	−0.193	+0.083	+0.211	−0.208
$(1s^23p)^2P$	−0.062	+0.019	+0.075	+0.011
$(1s^22s)^2S$	−0.528	−0.360	−0.201	−0.221
$(1s^23s)^2S$	−0.171	−0.102	−0.055	−0.359
Li^-				
$(1s^22p^2)^1D$	−0.623	−0.030	+0.367	−0.230
$(1s^22p^2)^1S$	−0.609	−0.191	−0.800	...
$(1s^22s2p)^3P$	−0.399	−0.296	−0.700	...
$(1s^22s2p)^1P$	−0.845	−0.443	−0.402	−0.496

parent neutral atoms. Obviously the latter quasi-discrete states (doubly excited states) occur most frequently bound in the negative ion structure, but, owing to their spontaneous decay through radiationless transitions into the adjacent continuum (with the exception of a few nonautoionization states which also can be metastable), the interest is focused mainly on the former singly excited states. In the case of H^- so far only the 2^3S and 2^1S states have been considered by quantum computations based on the variational principle. If bound in H^- these states will be metastable, but the results predict, however, unbound states.[2] Meanwhile, there still remains the question whether these states become bound when more flexible eigenfunctions, taking into account the electronic correlation, are used. Extensive research in the future could be devoted to clearing up this problem.

The purpose of the present note is to report semiempirical results obtained for some singly excited states of the three lightest negative atomic ions. Although the values derived by semiempirical methods are extremely sensitive to small errors in observed data, they may be of great interest in connection with the interpretation of electronic collisions with atoms. The same extrapolation formulas as given in reference 3 are used. It is noticed that the values of $J(Z+k)$ for the excited states yield the differences between the ground-state ionization potentials and the excitation potentials, and are similarly checked for smoothness and corrected if necessary. The results are condensed in Table I. The values obtained, being qualitatively correct, may be regarded as very encouraging in the current search for bound states in the spectra of H^-, He^-, and Li^-. As can be seen, they predict the H^- 2^3S state unbound consistent with the performed quantum computations.[2] On the other hand, this preliminary semiempirical analysis predicts a bound P state of $H^-(1s2p^3P)$, which is very interesting in view of recent results obtained for p-wave scattering of slow electrons by hydrogen atoms.[4] In fact, the extrapolations made here are based on observed data of the first members of the isoelectronic sequence. Correctly, the first three parameters $c_j(j=0, 1, \text{and } 2)$ of the extrapolation formulas have to be determined from asymptotic behavior of the sequences. This gives a source of error, the size of which can be estimated. As an example, we have done this in the case of the H^- 2^3P state by considering the series

$$J(Z)=\sum_{j=0}^{4} c_j Z^{2-j},$$

where the values of c_j are determined by a procedure similar to that of Johnson and Rohrlich.[5] The results are $J(Z)=(3.3875Z^2-6.120Z+1.880+0.622Z^{-1}+0.312Z^{-2})$ ev, which for $Z=1$ gives a positive detachment potential of 0.095 ev. The previously mentioned error seems to be small in this case.

Moreover, as the predicted detachment potentials indicate, there may occur excited bound states such as probably He^- $(1s^22p)^2P$, $Li^-(1s^22p^2)^1D$ and possibly $He^-(1s^23p)^2P$, the latter very uncertain in view of probable large errors in the observed excitation potentials. The lifetimes of these states, including the H^- triplet P state, are essentially limited by the allowance of dipole transitions to lower configurations. In the case of H^- the transition $(1s2p)^3P-(1s^2)^1S$ can take place where the final level is the stable ground state, whereas for the He^- and Li^- the final levels are unbound states which disintegrate spontaneously.

Obviously, the lifetimes shall be of order 10^{-8} sec. In conclusion, it will be mentioned that all observed data are taken from Moore.[6]

* Work supported by grant from the Norwegian Research Council for Science and Humanities.

[1] I. Fischer-Hjalmars, Arkiv. Fysik. **16**, 4, 33 (1959); B. Bederson, H. Malamud, and J. Hammer, Bull. Am. Phys. Soc. Ser. II **2**, 172 (1957); R. T. Brackmann and W. L. Fite, Phys. Rev. **112**, 1157 (1958).

[2] T. Y. Wu, Phys. Rev. **89**, 629 (1953). C. R. Lowry and R. Present, Astrophys. J. **125**, 611 (1957).

[3] Reference here to first note.

[4] B. H. Bransden, A. Dalgarno, T. L. John, and M. J. Seaton, Proc. Phys. Soc. (London) **71**, 877 (1958).

[5] H. J. Johnsen and F. Rohrlich, J. Chem. Phys. **30**, 1608 (1959).

[6] C. E. Moore, Natl. Bur. Standards Circ. No. 467 (1949), Vol. I.

Flash-Absorption Spectroscopy of Free Radicals in Shock Waves*

R. M. IKEDA†

Gibbs Laboratory, Harvard University, Cambridge 38, Massachusetts

(Received March 4, 1960)

FLASH-absorption spectroscopy has been applied to radicals other than OH in reactions initiated by

shock waves. A shock tube was constructed of rectangular brass tubing of $1\frac{5}{8}\times5\frac{5}{8}$-in. inside dimensions. The driver section was 5 ft long and the experimental section was 14 ft, with quartz windows and platinum resistance velocity gauges near the downstream end. A rectangular plug could be inserted to allow use of the reflected wave. The continuum flash lamp consisted of 1-mm tungsten electrodes spaced 3 cm apart and encased loosely in a 2-mm quartz capillary. A 60-joule discharge in O_2 (6.3 cm pressure) produced a short-duration, (2 μsec) uniform continuum in the ultraviolet. The lamp was triggered by a velocity gauge with a preset delay for any time after the passage of the shock. A Bausch and Lomb medium quartz spectrograph recorded the spectra.

Experiments were performed with mixtures of 10 and 20% SO_2 in argon with the hope of seeing the spectrum of the SO radical. Instead, at temperatures above 3100°K, the SO_2 bands were replaced immediately by a continuum in the 2900 A region. The bands later reappeared after a time interval which increased with the temperature.

A similar observation has been explained by Norrish[1] on the basis of a reversible thermal process, $SO_2 \rightleftarrows SO_2^*$, and, hence, the reappearance of the SO_2 bands might be caused by a cooling of the gas behind the shock. Since such cooling seems unlikely to be hydrodynamic in nature, the most reasonable explanation is the dissociation of SO_2 into SO and O radicals ($\Delta H=130$ kcal). At 3400°K, the extent of dissociation required for the cooling is about 2% and, to account for the cooling rate of the gas behind the shock as indicated by the reappearance of the SO_2 bands, the dissociation rate constant must be $(0.09\text{–}2.0)\times10^{13}e(-130000/RT)$.

Other SO bands at 2370, 2340, and 2310 A were observed, but the apparatus sensitivity prevented quantitative measurements.

Experiments were also performed using an 8.1/3.1/88.8, $C_2H_2/O_2/Ar$ mixture. Observations behind the reflected shock wave at 5350° and 5700°K showed that the 4389 A C_2 band, the 3900 A CH band and a diffuse absorption at about 4000 A (ascribed to C_3[2]) were sufficiently intense for quantitative study.

Data on the change in absorption with time for these three bands at 5350°K and 5700°K are presented in Figs. 1 and 2. The concentrations of CH and C_2 increase at the same rate to constant values which are independent of temperature. The rate of increase also appears to be temperature independent. The concentration of the diffuse band appears to increase logarithmically with time. The rate of increase is not strongly temperature dependent ($E_{act}\leqq100$ cal), but at the higher temperature the concentration is decreased by a factor of five, indicating that the step producing this species is exothermic with respect to some other reaction to the extent of 230 kcal.

Preliminary experiments on the pyrolysis of CH_4 and C_2H_2 have also shown intense C_2 and diffuse spectra.

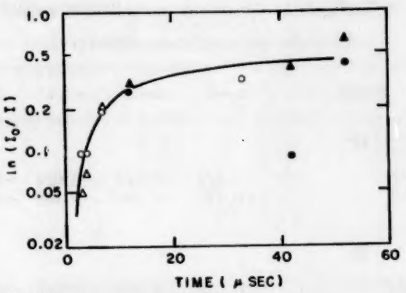

FIG. 1. Concentration in arbitrary units vs time for CH(△) and C_2(○) absorption. Filled points are experiments at 5700°K., open points, at 5350°K.

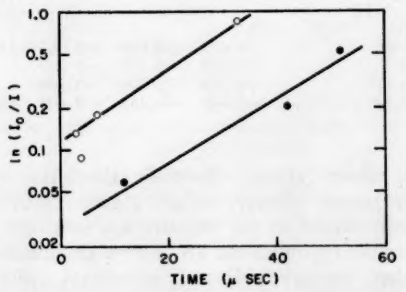

FIG. 2. Concentration vs time for diffuse absorption (possibly C_3). Filled points are experiments at 5700°K, open points at 5350°K.

The author would like to express his appreciation to the National Science Foundation for a Post Doctoral Fellowship and to Professor G. B. Kistiakowsky for many helpful discussions.

* This research was supported by the Office of Naval Research.

† Present address: Film Department, Experimental Station, E. I. du Pont de Nemours and Company, Wilmington, Delaware.

[1] R. G. W. Norrish and A. P. Zeelenberg, Proc. Roy. Soc. (London) **A240**, 293 (1957).

[2] N. H. Kiess and H. P. Broida, Can. J. Phys. **34**, 1471 (1956).

Calculation of Equilibrium Constants for Several Isotope Exchange Reactions Involving N_2O_4*

E. U. MONSE

Department of Chemistry, Rutgers, The State University, Newark, New Jersey

(Received February 24, 1960)

THE exchange of N^{15} between oxy-compounds of nitrogen has been studied for more than 20 years, and equilibrium constants for a number of exchange reactions have been calculated from spectroscopic data.[1] Constants for reactions involving N_2O_4 could not be calculated, since the assignment of the fundamental vibrational frequencies from the N_2O_4 spectrum was

TABLE I. Observed and calculated fundamental frequencies of N_2O_4 and NO_2 in cm^{-1}.

Molecule	$N_2^{14}O_4^{16a}$	$N_2^{14}O_4^{16b}$	$N_2^{15}O_4^{16b}$	$N_2^{14}O_4^{18b}$	$N^{14}O_2^{16c}$	$N^{15}O_2^{16c}$	$N^{14}O_2^{18b}$
ν_1	1380	1379.0	1355.5	1342.4	1357.8	1342.5	1309.5
ν_2	809	804.4	795.4	771.9	756.8	747.1	727.2
ν_3	265	267.3	265.8	254.4	1665.5	1628.0	1633.7
ν_4	...	50[d]	50.0	47.1			
ν_5	1712	1715.5	1676.7	1684.2			
ν_6	481	480.5	476.6	458.8			
ν_7	442	...	431.6	434.5			
ν_8	666	...	647.0	660.1			
ν_9	1748	1749.8	1711.3	1715.6			
ν_{10}	385	386.2	385.6	365.0			
ν_{11}	1261	1261.4	1247.5	1214.3			
ν_{12}	750	748.9	739.4	720.9			

[a] Observed, reference 2.
[b] Calculated, this paper.
[c] Zero-order frequencies, reference 4.
[d] Calculated, reference 2.

uncertain. Recently, I. C. Hisatsune reported a frequency assignment, which is supported by the agreement between the calculated and observed values of the specific heat and entropy of the solid molecule.[2] Using this assignment, calculations of the partition function ratios of isotopic N_2O_4 molecules have been made, and equilibrium constants for several exchange reactions between N_2O_4 and other molecules have been tabulated.

The fundamental frequencies for the planar vibrations of the isotopic molecules $N_2^{15}O_4^{16}$ and $N_2^{14}O_4^{18}$ have been obtained via the F and G matrices, together with the spectroscopic values of the force constants for a modified valence force field, as given by Hisatsune for the planar vibrational modes.[2] The values used for the interatomic distances and the O—N—O bond angle were those determined by Smith and Hedberg.[3] The frequencies of the nonplanar vibrations were calculated by application of the Teller-Redlich product rule to the observed frequencies of $N_2^{14}O_4^{16}$.

In Table I the observed and calculated frequencies of N_2O_4 are listed, as well as the frequencies of NO_2 reported by Arakawa and Nielsen.[4] The calculated frequencies for the planar vibrations of $N_2^{14}O_4^{16}$ and $N_2^{15}O_4^{16}$ agree with the values previously obtained by Hisatsune,[2] who pointed out that, since the number of force constants equals the number of the planar vibrations, the agreement of observed and calculated frequencies of $N_2^{14}O_4^{16}$ is good. New investigations of the $N_2^{15}O_4^{16}$ molecule confirm the values in Table I within experimental error.[5]

In Table II the equilibrium constants for nitrogen and oxygen isotope exchange reactions among N_2O_4, NO_2, and NO at different temperatures are listed. They were calculated from the frequencies of Table I, and frequencies for NO reported by Gillette and Eyster,[6] using the method of Bigeleisen and Mayer.[7]

The figures above the double bar refer to $1/n \ln s/s'f$, where f is the ratio of the partition functions and s' and s are the symmetry numbers of the heavy and light molecule; n is the number of N or O atoms, respectively, in each molecule. The figures below the double bar are the equilibrium constants for the exchange reactions between the species listed in the left column and the species listed in the top row of the tables. Values >1 mean a concentration of the heavy isotope in the species listed in the left column.

TABLE II. Equilibrium constants for nitrogen and oxygen exchange.

Nitrogen exchange	N_2O_4	NO_2	NO	Temperature in °K
$1/n \ln s/s'f$	0.1546	0.1244	0.0750	263.1
	0.1328	0.1074	0.0655	293.1
	0.0930	0.0759	0.0476	373.1
N_2O_4	(1.000)	1.031	1.083	263.1
		1.026	1.070	293.1
		1.017	1.046	373.1
NO_2		(1.000)	1.051	263.1
			1.043	293.1
			1.029	373.1

Oxygen exchange	N_2O_4	NO_2	NO	Temperature in °K
$1/n \ln s/s'f$	0.1146	0.1031	0.1097	263.1
	0.0976	0.0884	0.0958	293.1
	0.0672	0.0616	0.0696	373.1
N_2O_4	(1.000)	1.012	1.005	263.1
		1.009	1.002	293.1
		1.006	0.998	373.1
NO_2		(1.000)	0.993	263.1
			0.993	293.1
			0.992	373.1

It may be noted that the magnitude of the equilibrium constant for the exchange of N between N_2O_4 and NO is large. The difficulty of its measurement has been discussed in a previous paper.[8] Combining N_2O_4

and NO leads to the formation of N_2O_3 and, further, a two-phase system consisting of +2- and +4-nitrogen contains four different species: NO, NO_2, N_2O_3, and N_2O_4 in each phase. Every one of these species participates in isotopic exchange with every other, and so far it is not possible to evaluate the contributions of all the individual exchange reactions.

The equilibrium constant for exchange of N between N_2O_4 and NO_2 at 293.1°K agrees with the value of 1.023 estimated by Begun from separation experiments in a bubble cap-column,[9] and also with the results obtained by Kuhn, Narten, and Thuerkauf from a Rayleigh distillation of N_2O_4.[10] The equilibrium constant extrapolated from their experiments is 1.018, which is in fairly good agreement with the calculated value.

I am gratefully indebted to Professor W. Spindel of Rutgers University and Professor T. I. Taylor of Columbia University for stimulating discussions and continual interest in this work, and to Professor I. C. Hisatsune of Kansas State University for making his data available before publication. I also wish to thank Paul Tag for his help in many of the calculations.

* Supported in part by a grant from the U. S. Atomic Energy Commission.

[1] E. Leifer, J. Chem. Phys. **8**, 301 (1940); W. Spindel, *ibid.* **22**, 1271 (1954).
[2] I. C. Hisatsune, Scientific Report No. 1, 1959, AFCRC-TN-59-453, Department of Chemistry, Kansas State University, Manhattan, Kansas.
[3] D. W. Smith and K. Hedberg, J. Chem. Phys. **25**, 1282 (1956).
[4] E. T. Arakawa and A. H. Nielsen, J. Mol. Spectroscopy **2**, 413 (1958).
[5] G. M. Begun and W. H. Fletcher (private communication).
[6] R. H. Gillette and E. H. Eyster, Phys. Rev. **56**, 1113 (1939).
[7] J. Bigeleisen and M. Göppert-Mayer, J. Chem. Phys. **15**, 261 (1947).
[8] E. U. Monse, W. Spindel, L. N. Kauder, and T. I. Taylor, J. Chem. Phys. **32**, 1557 (1960).
[9] G. M. Begun, J. Chem. Phys. **25**, 1279 (1956).
[10] Kuhn, Narten, and Thürkauf, Helv. Chim. Acta **42**, 1433 (1959).

Infrared and Raman Spectra of C_2Br_3D

JAMES R. SCHERER, J. C. EVANS, AND JOHN OVEREND

Chemical Physics Research Laboratory, The Dow Chemical Company, Midland, Michigan

(Received March 10, 1960)

DURING an investigation of the potential function for a series of substituted bromoethylenes, it was found that although vibrational-frequency data were available in the literature for the majority of these molecules there appeared to be no information on tribromo-ethylene-*d*. To provide this information, we have prepared this compound and have measured its vibrational spectrum.

The compound was prepared by bubbling C_2D_2, generated by action of D_2O on CaC_2, into liquid bromine. The excess Br_2 was then distilled off, and the remaining $C_2Br_4D_2$ was added to the degenerated CaC_2–D_2O slurry. This was stirred vigorously for about 6 hr and then distilled, giving about a 90% yield of C_2Br_3D containing less than 0.5% C_2Br_3H.

The infrared spectrum was measured with a grating spectrometer[1] designed by L. W. Herscher. The 385 cm^{-1} infrared band was measured with a modified Perkin-Elmer 12C spectrometer equipped with CsBr prism. The Raman spectra were measured with a Hilger photoelectric recording instrument using 4358 A excitation and the linear dispersion was 6 A/mm. Depolarization measurements were made[2] and corrected for convergence error.[3] These spectra are tabulated in Table I.

Aided by calculations, which will be described in a subsequent communication, and by the spectra and assignments of the related molecules trichloroethylene-*d*[4], tribromoethylene,[5] and tetrabromoethylene,[6] the

TABLE I. Infrared and Raman spectra of liquid C_2Br_3D.[a]

Infrared observed peaks (cm^{-1})	Raman observed peaks (cm^{-1})	Polarization	Assignment
3237 (vvw)			$\nu_1+\nu_2$
3064 (vvw)			$2\nu_2$
2920 (vvw)			$\nu_1+\nu_{10}$
2850 (vvw)			$\nu_1+\nu_{11}+\nu_{12}$
2297 (s)	**2292** (m)	*p*	$\nu_1(a')$
2280 (m)	2275 sh	*p*	$\nu_2+\nu_4$
1805 (vvw)			$\nu_2+\nu_7$
1768 (vvw)			$\nu_2+\nu_8$
1730 (vvw)			$\nu_3+\nu_4$
1574 (w)	**1571** (m)	*p*	Fermi resonance
1529 (w)	**1525** (c)	*p*	ν_2, $2\nu_4(a')$
1384 (vvw)			$\nu_4+\nu_{10}$
1219 (vw)			$2\nu_{10}$
1180 (vvw)			$\nu_3+\nu_7$
1153 (vvw)			$\nu_4+\nu_{11}$
1140 (vvw)			$\nu_3+\nu_8$
1119 (vvw)			$\nu_3+\nu_{12}$
1065 (ww)			$\nu_3+\nu_9$, $\nu_5+\nu_{13}$
1009 (vvw)			$\nu_4+\nu_7$
994 (w)	990 (vw)	?	$\nu_{10}+\nu_{11}$
988 (w)			$2\nu_6$
953 (s)	**954** (m)	*p*	$\nu_5(a')$
913 (w)			$\nu_5+2\nu_9$, $\nu_5+\nu_7+\nu_8$
856 (vvw)			$\nu_7+\nu_{10}$, $\nu_5+\nu_{12}$
831 (ww)			C_2Br_3H impurity
792 (m)			$\nu_5+\nu_9$
775 (vs)	**773** (vw)		$\nu_4(a')$
752 (w)			$2\nu_{11}$, $\nu_{10}+\nu_{12}$
730 (vvw)			$\nu_6+\nu_7$
715 (vvw)			$\nu_9+\nu_{10}$
703 (vvw)	707 (vw)		C_2Br_3H impurity
678 (s)	**676** (vw)	?	$\nu_3(a')$
669 (w) sh			$\nu_6+\nu_8$, CO_2?
609 (s)	**610** (vw)	*Dp*?	$\nu_{10}(a'')$
586 (vvw)			$\nu_4-\nu_8$, $\nu_{10}+\nu_{12}-\nu_8$
564 (vvw)			$\nu_{11}+\nu_{12}$, $\nu_8+\nu_{11}$
534 (vvw)			$3\nu_8$
518 (vvw)			$\nu_7+\nu_9+\nu_{12}$
493 (ms)	495 (m)	*p*	$\nu_6(a')$
385 (ms)	387 (vw)	*Dp*?	$\nu_{11}(a'')$
	238 (vs)	*p*	$\nu_7(a')$
	218 (vw)	*p*	$C_2Br_4D_2$ impurity or $2\nu_9$
	182 (w)	*p*	$\nu_8(a')$
	169 (s)	*Dp*	$\nu_{12}(a'')$
	115 (s)	*p*	$\nu_9(a')$

[a] w=weak, m=medium, s=strong, v=very; sh=shoulder; p=polarized, Dp=depolarized.

assignment was straightforward. If we use the Evans-Bernstein assignment for C_2Br_3H, the observed product rule values $(\Pi\nu_i(H)/\nu_i(D))$ for the a' planar and a'' nonplanar modes are 1.976 and 1.332.[7] These compare favorably with the theoretical values of 1.986 and 1.401.

[1] L. W. Herscher, Spectrochim. Acta **11**, 901–8 (1959).
[2] J. T. Edsall and E. B. Wilson, Jr., J. Chem. Phys. **8**, 124 (1938).
[3] D. H. Rank and R. E. Kagarise, J. Opt. Soc. Am. **40**, 89 (1950).
[4] H. J. Bernstein, Can. J. Research **B28**, 132 (1950).
[5] J. C. Evans, H. J. Bernstein, Can. J. Chem. **33**, 1171–82 (1955).
[6] D. E. Mann, J. H. Meal, and E. K. Plyler, J. Chem. Phys. **24**, 1018 (1956).
[7] The unperturbed values of ν_1 and ν_2 in C_2Br_3D were taken to be about 2290 and 1550 cm^{-1}. The assumed molecular dimensions were $r_{CC}=1.31$ A, $r_{CBr}=1.90$ A, $r_{CH}=1.07$ A, CCH=121.5°, and CCBr=123°.

Induced Q Branch in the Vibration-Rotation Spectrum of HCl Pressurized with Ar

GEORGE C. TURRELL,* H. VU, AND B. VODAR

Centre National de la Recherche Scientifique, Laboratoire des Hautes Pressions à Bellevue (Seine-et-Oise), France

(Received March 21, 1960)

A NUMBER of observations of the vibration-rotation spectra of polar diatomic gases pressurized with nonpolar gases have been made in this laboratory.[1] The principal effect which has been observed is the appearance of a strong Q branch in the fundamental vibration-rotation band of the polar molecule. At moderate densities the intensity of the Q branch appears to be proportional to the density of each component of the mixture, indicating that the breakdown in the usual selection rule, $\Delta J=\pm 1$, is the result of heterogeneous binary collisions.

The systems in which the polar gas is a hydrogen halide and the nonpolar molecule is an inert gas (other than helium) lend themselves to an expecially simple theoretical treatment. In these cases the coupling of the angular momentum of the diatomic rotor to that of the collision pair is small. Furthermore, if it can be assumed that the heterogeneous interaction is governed by an effective spherical potential, the wave function for the internal degrees of freedom of the system can be written in terms of the usual rigid-rotor, harmonic-oscillator approximation. The effect of an angularly dependent interaction potential has been investigated by Galatry.[2]

By taking matrix elements of the total dipole moment of a collision pair with respect to rigid-rotor, harmonic-oscillator wave functions, it is easily found that the only terms which contribute to a Q branch are those arising from induction by the quadrupole moment of the diatomic molecule and from the effect of molecular overlap.[3] If an exp-4 model is assumed for the induced dipole moment of a pair, an equation for the integrated intensity of the Q branch can be derived following the method developed by Van Kranendonk[4] for the absorption induced in hydrogen by foreign gases. An earlier treatment by Galatry[2] of the electrostatic interactions in a collision pair neglected the possible effects of the overlap moment.

The preliminary experimental work of Vu and Vodar[5] on the spectra of HCl–Ar mixtures has been repeated in order to obtain a quantitative measurement of the Q branch intensity as a function of pressure and temperature. Unfortunately, the integrated intensities of the Q branches are very difficult to estimate because of overlapping by the P and R branches. However, approximate values of the extinction coefficients at the maxima have been measured and are presented in Table I. These data were obtained by measuring $\log(I_0/I)$ from the spectra and subtracting the effect of overlapping of the first few rotational lines of the P and R branches. This effect was estimated by assuming Lorentz shapes for nearby rotational lines, combined with measurements of their widths and heights. The resulting corrected values of $\log(I_0/I)$ at the Q branch maxima yielded approximately straight lines when plotted against the density of argon, up to about sixty Amagats. The values of κ_{exp} given in Table I were obtained from the slopes of these plots.

An elementary treatment of the collision broadening of the induced Q branch in polar–nonpolar gas mixtures has been carried out,[3] which yields the following approximate expression for the extinction coefficient at the maximum:

$$\kappa=(\pi^3/Mc)\,(m/2\pi kT)^{\frac{1}{2}}n_p n_n \times[(3\alpha^2/2\sigma^4)Q'^2 I_q+8e^2\lambda^2\rho\sigma^3 I_0], \quad (1)$$

where

$$I_q=\int_0^\infty \exp[-V(x)/kT]x^{-5}dx,$$

and

$$I_0=\int_0^\infty \exp[-2\sigma(x-1)/\rho-V(x)/kT]x^2dx.$$

M is the reduced mass of the rotor and m is that of the collision pair; n_p and n_n are the numbers of polar and nonpolar molecules per unit volume, respectively; Q' is the derivative of the quadrupole moment of the polar molecule with respect to its internuclear distance. The interaction is described by a potential function of the

TABLE I. Extinction coefficients[a] and bandwidths of induced Q branches in HCl-Ar mixtures.

T(°K)	κ_q	κ_0	κ_{exp}	δ_0 (cm^{-1})
163	0.24	51	58	28
293	0.12	23	20	37

[a] Extinction coefficients are in units of 10^{-4} cm^{-1} $Amagats^{-2}$.

Lennard-Jones (6–12) type, where $x=r/\sigma$ and the constants σ and ϵ are estimated from the usual combining laws for polar–nonpolar gas mixtures.[6,7] The polarizability of the inert gas is represented by α; ρ and λ are the overlap parameters defined by Van Kranendonk.[4] The range parameter ρ is taken to be $0.145\,\sigma$, as proposed by Van Kranendonk for hydrogen mixtures. The value of $\lambda=8.5\times10^{-2}$ is chosen to provide the best fit to the experimental data. The temperature dependence then indicates the success of the assumed relation, $\rho=0.145\sigma$.

The quantities κ_q and κ_0 in Table I represent the relative importance of quadrupole and overlap induction [based on the first and second terms in braces in Eq. (1), respectively, with $Q'\approx1.3\times10^{-18}$ esu-cm]. It is apparent that the effect of quadrupole induction is negligible and that the observed induced Q branch can be attributed to angularly independent terms in the overlap moment.

In principle, an independent determination of ρ can be made from the width (at half-height) of a Q branch produced by the overlap moment. The bandwidth is given approximately by[3]

$$\delta_0=(2/\pi c)\,(2kT\ln 2/2^{1/6}\rho\sigma m\pi)^{\frac{1}{2}}. \qquad (2)$$

Hence, it is proportional to the square root of the absolute temperature and is independent of pressure, in agreement with the qualitative conclusions of Van Kranendonk.[4] Taking $\rho=0.145\sigma$, as before, yields the bandwidths δ_0 given in Table I. These values provide a good fit to the observed Q branches.

* Guggenheim Fellow, 1958–59. Present address: Department of Chemistry, Howard University, Washington 1, D. C.

[1] Coulon, Oksengorn, and Vodar, Compt. rend. **239**, 964 (1954); R. Coulon, thesis, Paris, 1958, J. Recherches Centre nat. recherche sci. (Paris) **45**, 305 (1958); H. Vu, thesis (Paris), in preparation; B. Vodar, Proc. Conf. Mol. Spectroscopy (London, 1958) and Proc. Roy. Soc. (London) (to be published).

[2] L. Galatry and B. Vodar, Compt. rend. **240**, 1072 (1955); L. Galatry, thesis (Paris, 1958), J. Recherches Centre nat. recherche sci. (Paris) **46**, 43 (1959).

[3] G. C. Turrell, J. Recherches Centre nat. recherche sci. (Paris) (to be published).

[4] J. Van Kranendonk, thesis, Amsterdam, 1952; and Physica **24**, 347 (1958).

[5] H. Vu and B. Vodar, Compt. rend. **248**, 2082 (1959).

[6] J. O. Hirschfelder, C. F. Curtiss, and R. B. Bird, *Molecular Theory of Gases and Liquids* (John Wiley & Sons, Inc., New York, 1954), p. 222.

[7] For HCl-Ar mixtures, $\sigma=3.35$ A and $\epsilon/k=215°$.

Note on the Internal-Rotation Barrier in Ethanic Compounds

MARTIN KARPLUS*

Noyes Chemical Laboratory, University of Illinois, Urbana, Illinois

(Received September 15, 1959)

ALTHOUGH chemists have long been aware of the barriers to internal rotation that are present in ethanic compounds, there does not exist a complete understanding of their properties. From the relative invariance of the magnitude of the barrier in a number of related compounds of the form $CH_3CH_nX_{n-3}$ (X= H, F, Cl, Br), it has been suggested that a single interaction makes the major contribution.[1] In this note we give some evidence for believing that the deviations from perfect pairing, which have the desired property of being insensitive to substituents, are not an important factor in the potential barrier.

In 1939, Eyring *et al.*[2] first gave a valence-bond treatment of the rotational barrier in ethane. Their calculation, which indicated that the eclipsed configuration was the stable one (in disagreement with recent experimental data[3]), is not valid because of the primitive approximations used for the evaluation of the necessary molecular integrals. Since, even today, a complete quantum-mechanical treatment of the barrier is extremely difficult, we attempt to determine the reliability of the theoretical results reported here by reference to some NMR and ESR measurements of electron-nuclear coupling.

As described previously,[4] a nonionic valence-bond calculation of the ground state of the HCC'H' fragment model for ethane has been performed for a number of values of the HCC'/CC'H' dihedral angle ϕ. All of the five possible spin-pairing structures were included. Details of the method used and the approximations involved are given in I.[4] In Table I are listed the values obtained for the difference in energy δE between the complete wave function and the perfect-pairing structure ($E\sim300$ kcal). Since the energy of the perfect-pairing structure is independent of the relative orientation of the methyl groups in ethane,[5] the barrier height E_b can be estimated from the results in Table I by summing over the appropriate terms[6] ($E_b=-3[\delta E(180°)+2\delta E(60°)-\delta E(0°)-2\delta E(120°)]$). This leads to the value $E_b=0.05$ kcal. Its small magnitude when compared with the experimental value of ~3 kcal indicates that deviations from perfect pairing make only a negligible contribution to the barrier.

TABLE I. HCC'H' Fragment model exchange integrals and energy.

	Dihedral angle ϕ			
	0°	60°	120°	180°
δE (kcal)	−0.3950	−0.3187	−0.3210	−0.4160
$[C_{b1}, C_{a1}]$(kcal)	−5.7918	−1.0151	−1.3876	−6.5369
$[C_{a1}, A]$(kcal)	−87.689	−87.689	−87.689	−87.689

To obtain a criterion for the validity of the calculation, we consider the valence-bond structures involved. Of the four structures other than the one with perfect pairing only two [$\psi_1=(A,\,B)(C_{a1},\,C_{a2})(C_{b1},\,C_{b2})$ and $\psi_2=(A,\,B)(C_{a1},\,C_{b1})(C_{a2},\,C_{b2})$ of I][7] make a first-order contribution to the barrier, with ψ_2 the more important of the two. Restricting the discussion to the function ψ_2 and employing a perturbation approach to

simplify the argument, we find that the coefficient c_2 of ψ_2 in the ground-state wave function is given by the expression

$$c_2=[C_{b1}, C_{a1}]/[4(C_{a1}, A)-2(C_{b1}, C_{a1})], \quad (1)$$

and the energy contribution δE_2 by

$$\delta E_2=-3[C_{b1}, C_{a1}]^2/[8(C_{b1}, C_{a1})-16(C_{a1}, A)] \quad (2)$$

where $[C_{a1}, A]$ and $[C_{b1}, C_{a1}]$ are exchange integrals defined in I. The only ϕ-dependent term is the integral $[C_{b1}, C_{a1}]$ between the carbon orbitals directed toward the hydrogens H and H'. Its values, which are given in Table I with those for $[C_{a1}, A]$, essentially determine the barrier. Although the integral $[C_{b1}, C_{a1}]$ is difficult to evaluate accurately and was obtained by a two-electron approximation in the present calculation, comparison with NMR and ESR data suggests that the result is of the correct order of magnitude. Both the proton-proton coupling constant[8] observed in the NMR spectrum of ethanic compounds and the proton hyperfine splitting[9] found in the ESR spectrum of the ethyl radical are largely determined by the value of the coefficient c_2. Recent experiments[10] show that the theoretical magnitudes of these quantities are approximately correct; at worst, they are too small by a factor of 2. From a comparison of Eqs. (1) and (2) we see that for c_2 increased by a factor of 2, the energy δE_2 would be larger by a factor of $\sim$4. This would increase the barrier contribution of the deviations from perfect pairing to $\sim$0.2 kcal, which is still only a small fraction of the total.[11]

Another consideration that enters into the comparison with the coupling constant calculation is its dependence on an average excitation energy.[12] Although an exact choice of such an energy is difficult to make except by a complete variation-perturbation treatment,[13] comparison with other results[14] indicates that the value used (9 ev) is not wrong by more than a factor of two. Also, the calculation of hyperfine splittings in the ESR spectra are *independent* of any such average excitation energy value.

Because of the approximate nature of the model, the considerations of this note cannot completely exclude the possibility that deviations from perfect pairing cause the rotational barrier in ethanic compounds. However, the combination of experimental and theoretical results presented here make it most unlikely that these deviations yield a major contribution.[15]

The author would like to express his thanks to Professor E. Bright Wilson, Jr., and Professor H. S. Gutowsky for helpful discussion.

[*] Alfred P. Sloan Foundation Fellow.
[1] E. Bright Wilson, Jr., Advances in Chem. Phys. **2**, 367 (1959).
[2] Gorin, Walter, and Eyring, J. Am. Chem. Soc. **61**, 1876 (1939).
[3] R. S. Wagner and B. P. Dailey, J. Chem. Phys. **26**, 1588 (1957).
[4] M. Karplus, J. Chem. Phys. **30**, 11 (1959); referred to as I.
[5] See reference 1.
[6] The neglect of the structures that would occur if the entire ethane molecule were being considered causes a negligible change in the result.
[7] In I, ψ_1 and ψ_2 are interchanged in Eq. (6).
[8] See reference 4.
[9] M. Karplus (unpublished calculation). See also A. D. McLachlan, Mol. Phys. **1**, 233 (1958), for a somewhat more empirical approach.
[10] For the ESR results see B. Smaller and M. S. Matheson, J. Chem. Phys. **28**, 1169 (1958); and W. Gordy and C. G. McCormick, J. Am. Chem. Soc. **78**, 3243 (1956). For the NMR results we refer to data of E. J. Corey (private communication) and N. Sheppard, Proc. Chem. Soc. **1959**, 266.
[11] Accurate measurements of the coupling constants between vicinal protons structurally fixed at 0°, etc., would be useful here.
[12] M. Karplus, Revs. Modern Phys. **32**, 455 (1960).
[13] T. P. Das and R. Bersohn, Phys. Rev. **115**, 897 (1959); M. J. Stephen, Proc. Roy. Soc. (London) **A243**, 274 (1957).
[14] N. F. Ramsey, Phys. Rev. **91**, 303 (1953).
[15] Since this note was submitted, there has appeared a paper by G. M. Harris and F. W. Harris [J. Chem. Phys. **31**, 1450 (1959)] which apparently uses the identical valence-bond method (with somewhat different approximations for the integrals) to obtain a barrier of 7.5 kcal. Publication of the note was delayed to make possible a comparison of the two calculations. Unfortunately, the data available on the Harris and Harris function are insufficient for a detailed comparison. However, an estimate of the coupling constant with their function (on the assumption of orthogonal orbitals) yields a result that is nearly independent of the angle ϕ, in disagreement with experiment.

Second-Order Perturbation Energy of the Two-Electron Atom

CHARLES W. SCHERR

Department of Physics, The University of Texas, Austin, Texas

(Received December 16, 1959)

THE conventional second-order perturbation energy ϵ_2 for the ground state of the two-electron atom is given by

$$\epsilon_2=\sum_{i\neq 0} H_{0i}^2/(E_0-E_i). \quad (1)$$

The H_{0i} represent the electron interaction integrals between the zero-order wave function ψ_0 and the terms ψ_i of the first-order wave function. In terms of normalized hydrogenlike atomic wave functions, u_{nlm},

$$\psi_i=\sum_m [u_{n_1lm}(\mathbf{r}_1)u_{n_2l-m}(\mathbf{r}_2)+u_{n_2l-m}(\mathbf{r}_1)u_{n_1lm}(\mathbf{r}_2)] \times(-1)^{l+m}[2(1+\delta_{n_1,n_2})(2l+1)]^{-\frac{1}{2}}.$$

In the course of another investigation not yet completed, a number of the H_{0i} were evaluated, and it was felt it would be worthwhile to extend the analysis to evaluate ϵ_2 via Eq. (1) directly.[1] A complete analysis was not possible, but it is believed that the entire contribution to ϵ_2 from the terms corresponding to doubly bound states (40.0%), to singly ionized states composed from u_{nlm} with $l=0$ and with $l=1$ (40.8%), and to doubly ionized states composed from u_{nlm} with $l=0$ (10.5%) has been obtained. These account for over 91% of ϵ_2, leaving the remaining portion to come mostly from doubly ionized states constructed from continuum wave functions with higher l values. The

TABLE I. The doubly bound terms.

ψ_i	$\Sigma H_{0i}^2/\Delta E$	ψ_i	$\Sigma H_{0i}^2/\Delta E$	ψ_i	$\Sigma H_{0i}^2/\Delta E$
$1sns$	0.0591625942				
$2sns$	0.0012483900	$2pnp$	0.0022706268		
$3sns$	0.0001107459	$3pnp$	0.0002055833	$3dnd$	0.000001193
$4sns$	0.0000231706	$4pnp$	0.0000432559		
$5sns$	0.0000071761	$5pnp$	0.0000134285		
$6sns$	0.0000027983				
$7sns$	0.0000012713				
Subtotal	0.0605561463		0.0025328945		0.000001193
Remainder by extrapolation	0.00000163		0.00001120		0.00000041
Total	0.06055778		0.00254409		0.00000160

TABLE II. The singly ionized terms.

ψ_i	$\int dk H_{0i}^2/\Delta E$	ψ_i	$\int dk H_{0i}^2/\Delta E$
$1sks$	0.051840565		
$2sks$	0.003044215	$2pkp$	0.0049768794
$3sks$	0.000799603	$3pkp$	0.0013699273
$4sks$	0.000323741	$4pkp$	0.0005620037
$5sks$	0.000162659	$5pkp$	0.0002839630
$6sks$	0.000093176		
$7sks$	0.000058317		
Subtotal	0.056322276		0.0071927734
Remainder by extrapolation	0.0001749		0.0005607
Total	0.0564972		0.0077535

TABLE III. Summary.

Contribution to ϵ_2 from doubly bound states	0.06310347
Contribution to ϵ_2 from singly ionized states	0.0642507
Contribution to ϵ_2 from doubly ionized states constructed from hydrogenic continuum functions with l equals zero	0.0165692
Total	0.1439234
ϵ_2 as computed by Hylleraas and Midtdal[a]	0.1576575
Difference	0.0137341

[a] See reference 1.

results are tabulated in Tables I–III. The numbers are the total contributions to ϵ_2 of the group of ψ_i, symbolized by the heading to the left of each entry. Thus, for example, $1sns$ indicates a summation over the contributions of all doubly bound ψ_i constructed from a $1s$ hydrogenic orbital and an ns hydrogenic orbital; $1sks$ indicates an integration over the contributions of all singly ionized ψ_i constructed from a $1s$ hydrogenic orbital and a hydrogenic continuum function corresponding to wave number k.

I should like to thank R. E. Knight for his assistance with the numerical calculations, and for an independent check on part of the analysis. The calculations were performed on an IBM 650 located at the Computing Center of The University of Texas.

[1] See E. Hylleraas and J. Midtdal, Phys. Rev. **109**, 1013 (1958), for an evaluation of ϵ_2 by a variational-perturbation method.